Drug resistance mechanisms of FGFR-driven cancers

Yasmine Eugénie Djamila Tanner

Submitted in partial fulfilment of the requirements for the degree of

Doctor of Philosophy

2018

Queen Mary University of London
Barts and the London School of Medicine and Dentistry
Barts Cancer Institute, Centre for Tumour Biology
Charterhouse Square, London, EC1M 6BQ

Declaration of authorship

I, Yasmine Tanner, confirm that the research included within this thesis is my own work or that where it has been carried out in collaboration with, or supported by others, that this is duly acknowledged below and my contribution indicated. Previously published material is also acknowledged below.

I attest that I have exercised reasonable care to ensure that the work is original, and does not to the best of my knowledge break any UK law, infringe any third party's copyright or other Intellectual Property Right, or contain any confidential material.

I accept that the College has the right to use plagiarism detection software to check the electronic version of the thesis.

I confirm that this thesis has not been previously submitted for the award of a degree by this or any other university.

Signature: Yasmine Tanner

Date: 26th of October 2018

Abstract

The fibroblast growth factor (FGF) signalling pathway contributes to the regulation of a variety of cellular functions, affecting differentiation, migration, proliferation, and survival. Unsurprisingly, cancer cells can hijack this pathway for growth or survival advantages, through alterations in ligands, receptors or regulatory molecules. Sequencing consortia have highlighted how mutation, amplification, translocation or loss of elements in the FGF signalling network can contribute to tumourigenesis, and the pathway is a major clinical target. Many FGF receptor (FGFR) driven cancers develop resistance against commonly used receptor tyrosine kinase (RTK) targeted therapeutics and dissection of the mechanisms that underlie this, both in the cancer cell, and also via stromal crosstalk in the tumour microenvironment, is of utmost importance to the development of therapeutic approaches to treat FGFR-driven cancers. In this work, I focus on the mechanisms of FGF deregulation and the impact of stromal cells. I aim to identify the implications of FGFR2 aberrations on gastric and endometrial cancer, and FGFR1 aberrations on lung cancer. Furthermore, I aim to dissect the mechanisms by which targeted cells may develop drug resistance both in two-dimensional (2D) and in a more physiomimetic three-dimensional (3D) co-culture model.

It was established that cancer cells with FGFR aberrations were sensitive towards FGFR inhibitors such as PD173074 (PD), AZD4547 (AZD) and BGJ398 (BGJ). Cancer cells could be killed with increasing concentration of these drugs and exhibited sensitivity to FGFR inhibitors by decreased p-AKT and p-ERK signalling. However, with prolonged exposure to FGFR inhibition, certain cells began to acquire resistance in 2D. To study drug resistance in a more physiomimetic environment, cells were grown alone or co-cultured with fibroblasts and treated with FGFR inhibitors PD, AZD or BGJ and imaged using fluorescent live cell imaging. These cultures were then fixed, paraffin embedded and immuno- or Haematoxylin and Eosin (H&E) stained. To study the emergence of drug resistance in 3D with and without stromal support, cells were seeded into Alvetex® scaffolds and treated with increasing concentrations of BGJ until resistant populations were observed via confocal fluorescence

microscopy. Cancer cells grown in co-culture with fibroblasts acquired resistance faster than monoculture cells. Significantly regulated genes between resistant and parental mono- and co-culture cells were identified using ribonucleic acid sequencing (RNA-Seq) and bioinformatics. The majority of significantly regulated pathways in *FGFR2*-amplifed gastric cancer cells, were metabolic pathways including retinol metabolism, starch and sucrose degradation, which was mainly driven by sucrase-isomaltase (SI) and aldolase B (ALDOB), resulting in glucose generation. Targets were then modified using different approaches such as knockdown, overexpression and drug treatments to observe how this affects resistance of FGFR-driven cancers. Blockade of ALDOB resulted in lower cell numbers within 2D cultures in drug-resistant gastric cancer cells, possibly by slowing down cell growth rather than inducing cell death. However, the effect of glucose or sucrose on cells is possibly through a SI-independent manner. When analysing gene expression in cells grown on 2D *versus* 3D substrates, expression levels varied considerably, and this underlines the importance of investigating biological processes in a physiomimetic *in vivo*-like setting.

Drug resistance in cancer is an increasing issue for successful therapy and a number of interesting targets have been identified in *FGFR2*-amplified gastric cancer that could be responsible for drug resistance towards FGFR inhibitors. With stromal support, cancer cells acquired resistance faster, which highlights the influence of fibroblasts and the extracellular matrix (ECM) environment on resistance. It was shown that sugar metabolism plays a substantial part in resistance, together with the retinol pathway. Possibly, these genes and pathways are intertwined, ultimately aiding cancer cells to grow in presence of inhibition via cytoprotective mechanisms and also generation of metabolites to ensure sustained proliferation of cells. The importance of these genes and pathways need to be further evaluated. Therefore, drug combination therapy could be the pivotal way forward to hinder cancer cells from rewiring their pathways to overcome drug inhibition.

Acknowledgements

I want to address my sincerest gratitude to my supervisor, Richard Grose, for giving me the opportunity to do my PhD in his fantastic group and the continuous support and guidance through this PhD. I want to say thanks to you for this great experience and also your patience during the writing up process. I consider myself extremely lucky with a supervisor like you - I could not have imagined a better one. Many thanks also to my second supervisor Pedro Cutillas for suggestions and advice during my PhD. I would further like to thank Hefin Jones and Ai Nagano for help and analysis of bioinformatics data. I would like to acknowledge support from the Barry Reed/Arthur Morris Fund for enabling me to do my PhD and funding my studentship. It has been a great pleasure to meet and interact with benefactors at charity events and I am grateful for this experience. Furthermore, I would like to thank George Elia for help with histopathology, Deborah Buckle for running the lab, Steven Lim for help with FACS and Linda Hammond for support and advice with the microscopes.

I can not thank the FGF Forever group enough. It has changed quite a bit over time but I would like to mention in particular the constant members Ed, Abigail and Natasha. I am forever grateful to you for all the scientific and non-scientific talks and other things that matter in life, for all the suggestions and help. I am honoured to have been part of such a fantastic group and I think Richard has a great sense choosing people. Many thanks also to Lucia and Ekaterina former and current lab members for great conversations in the lab. Many thanks also to former group member Abbie for the advice and motivation and who has been there at the start of my PhD and now also at the end of my PhD back in Switzerland. I am sure we will all remain friends also beyond the PhD and BCI.

I have met some truly amazing and kind people during this time and this experience would not have been the same without the fantastic people at this institute. I want to thank the whole PhD office and Tumour Biology lab for this exciting time, for the support and laughter they brought to my life every day. In particular, I would like to mention in addition to the FGF group, Ketan, Prabhu, Caroline, Claire, Banu,

Michelle, my amazing former desk neighours Bakhouche and Zareen, Abiruph, Kunal, Paul, Viola and Neil for making this one of the best time of my life. Special thanks to Viola for our great and productive writing retreat in Munich. I also want to thank Gabriela, Rachel, Michael and Beta and many others in the lab who have given me advice and helped me and sparked interesting conversations. The presence and the interactions with all these people and occasional after work drinks has made the long days turning into nights and weekends at BCI fun and more enjoyable and I hope that we will still keep in touch in the future and reminisce about our time at BCI.

I also want to express my gratitude to my dear friends in London, especially Sara and Alix, that I am so happy I have met. Finding friends like you made the last years worthwile. Big thanks also to my friends in Switzerland and all over the world, especially Emma, I want to thank you for your friendship even across an ocean and the time difference. I would like to say thanks to my friends, who have accompanied me in this life now for a long time, Hanna, Susana, Anina, Madeleine for being there, for their understanding and support. Furthermore, I would like to thank my new co-workers who without knowing have made the, from times to times, difficult period of writing up more enjoyable and contributed with great laughs to lighten the sleepless writing nights during this time.

I will be forever grateful to Prabhu and Ketan who I know I can always count on. Big thanks to Prabhu who has been an amazing friend and helped me with so many necessary and unnecessary flat moves. I could not write this without saying thanks to Ketan who was there all along and has shown me relentless support not just with flat moves but with all kinds of things no matter how big or little. I want to thank you for all the times you helped me, for our long stimulating conversations and discussions, all the treats and taking me for little breaks or a pint to take my mind of experiments. Thank you so much for making me laugh and cheering me up. I am very grateful that I have met you and for all the good memories.

Last but not least my deepest and sincerest gratitude to my family. Ich möcht mi ganz herzlich bi euch bedanke, mine Eltere Rolf und Rosa und Bruederherz Marat, für all die Unterstützig wo ich vo euch beko ha die Zit und mis ganze Läbe. Es isch ame sehr schwierig gsi und es isch umso schöner gsi vo euch die Unterstützig zbeko und dass ihr an mich glaubet wenn ich ha wölle ufge. Ich ha euch alli unglaublich gärn. Ich möcht mi ganz bsunders bi mine Eltere Rolf und Rosa bedanke, denn ohni euch wäre ich nit wo ich bi und wär nit die Person wo ich hütt bi. Danke wird nie gnueg si. Ich widme die Arbeit euch.

А это, мам, для тебя. Я так благодарна, что у меня есть такая мама, как ты. Ты мой источник вдохновения, ведь ты столько добилась в своей жизни, и я восхищаюсь твоей смелостью и силой воли. Ты сделала меня тем человеком, которым я являюсь сегодня. И ты не только моя мать, но и мой пример для подражания и моя лучшая подруга. Я тебя очень люблю.

Table of Contents

List of Figures

List of Tables

Abbreviations

2D	Two-dimensional
3D	Three-dimensional
ABC	ATP-binding cassette
ADC	Adenocarcinoma
ADH	Alcohol dehydrogenases
AFM	Atomic force microscope
AFP	Alpha-fetoprotein
AKT	Protein kinase B
ALDH	Aldehyde dehydrogenase
ALDOB	Aldolase B
ALK	Anaplastic lymphoma kinase
AML	Acute myeloid leukaemia
ALL	Acute lymphoblastic leukaemia
APS	Ammonium persulphate
ARVC	Arrhythmogenic right ventricular cardiomyopathy
ASC	Adipose derived stem cells
ATP	Adenosine trisphosphate
ATRA	*all-trans* retinoic acid
AZD	AZD4547
BCL2	B-cell lymphoma 2
BGJ	BGJ398
BICC1	Bicaudal C homolog 1
Bp	Base pairs
BRAF	Serine-threonine protein kinase b-raf
BSA	Bovine serum albumin
CAF	Cancer-associated fibroblasts
CAGE	Cap analysis of gene expression
CBL	Casitas B-lineage lymphoma
CCRT	Concurrent chemoradiotherapy
cDNA	Complementary DNA

CDK	Cyclin-dependent kinases
CML	Chronic myeloid leukaemia
c-MYC	Cellular homologue of v-MYC
CRABP	Cellular retinoic acid-binding protein isoforms
CRBP	Cellular retinol-binding proteins
CREB	cAMP response element-binding protein
COSMIC	Catalogue of somatic mutations in cancer
CRISPR	Clustered regulatory interspaced short palindromic repeats
DAG	Diacylglycerol
DAPI	4', 6-diamidino-2-phenylindole
DHAP	Dihydroxyacetone phosphate
DMEM	Dulbecco's modified Eagle's medium
DMSO	Dimethyl sulphoxide
DNA	Deoxyribonucleic acid
DNMT	DNA methyltransferase
DOX	Doxorubicin
DSB	Double strand break
DTT	Dithiothreitol
DUSP6	Dual specificity phosphatase 6
ECL	Enhanced chemiluminescence
ECM	Extracellular matrix
EDTA	Ethylenediaminetetraacetic acid
EGFR	Epidermal Growth Factor Receptor
EIF4EBP	Eukaryotic translation initiation factor 4E binding protein
EMS	Eosinophilic myeloproliferative syndrome
EMT	Epithelial to mesenchymal transition
ER	Endoplasmic reticulum
ERK	Extracellular signal regulated kinase
ErbB	Erythroblastic leukaemia viral oncogene
ETD	Electron transfer dissociation
F-1-P	Fructose 1-phosphate

FA	Formic acid
FACS	Fluorescence activated cell sorting
FBP	Fructose 1,6-bisphosphate
FBS	Foetal bovine serum
FGF	Fibroblast growth factor
FGFR	Fibroblast growth factor receptor
FGFRL1	Fibroblast growth factor receptor-like 1
FHF	FGF homologous factors
FRS2	Fibroblast growth factor receptor substrate 2
Fs	Frameshift
FSC	Forward scatter
g	Gravitational force
G3P	Glyceraldehyde 3-phosphate
GAB1	GRB2-associated binder-1
GAS	Gamma-activated site
gDNA	Genomic DNA
GFP	Green fluorescent protein
GIST	Gastrointestinal stromal tumour
GITC	Guanidinium isothiocyanate
Glc	Glucose
GLC7	Serine/threonine-protein phosphatase PP1-2
GRB2	Growth factor receptor-bound protein 2
GWAS	Genome wide association studies
GSEA	Gene Set Enrichment Analysis
H&E	Haematoxylin-eosin
HCC	Hepatocellular carcinoma
HDAC	Histone deacetylase
HER2	Human epidermal growth factor 2
HFF2	Human foreskin fibroblast 2
HKII	Hexokinase II
HPV	Human papilloma virus

HR	Homologous repair
HS	Heparan sulphate
HSC70	Heat shock chaperone 70
HSPG	Heparan sulphate proteoglycans
HTS	Higher throughput screening
Ig	Immunoglobulin
IP3	Inositol 1, 4, 5 trisphosphate
IPA	Ingenuity pathway analysis
JAK	Janus kinase
kDa	Kilodalton
K-RAS	Kirsten-rat sarcoma viral oncogene homologue
LB	Luria Broth
LCC	Large cell carcinoma
MAPK	Mitogen activated protein kinase
MEK	MAPK kinase
MEM	Modified Eagle's medium
MET	Mesenchymal to epithelial transition
MKP3	MAPK phosphatase 3
MMP	Matrix metalloproteinases
MS	Mass spectrometry
mTOR	Mammalian target of rapamycin
mTORC	mTOR complex
MTT	(4,5-dimethylthiazol-2-yl)- 2,5-diphenyl tetrazolium bromide
MTS	3-(4,5-dimethylthiazol-2-yl)-5-(3-carboxymethoxyphenyl)-2-(4-sulfophenyl) -2H-tetrazolium)
MTX	Methotrexate
MPSS	Massively parallel signature sequencing
NAF	Normal-activated fibroblasts
NGS	Next generation sequencing
NSCLC	Non-small cell lung cancer
p16	Cyclin-dependent kinase inhibitor 2A

PAH	Polynuclear aromatic hydrocarbons
p-AKT	Phospho-AKT
PANDA	Peptide ANalysis and Database Assembly
PBS	Phosphate buffered saline
PCA	Principal component analysis
PCBP1	Poly(rC)-binding protein 1
PCL	Polycaprolactone
PCR	Polymerase chain reaction
PD	PD173074
PDAC	Pancreatic ductal adenocarcinomas
PDGFRβ	Platelet derived growth factor receptor beta
PDK1	Phosphoinositide-dependent kinase 1
p-ERK	Phospho-ERK
PEP	Phosphoenolpyruvate
PET	Polyethylene terephthalate
PFA	Paraformaldehyde
P-FRS2	Phospho- FRS2
PH	Pleckstrin homology
PH3	Phosphorylated Histone H3
PHLDA	Plekstrin homology like domain A
PI	Propidium iodide
PI3K	Phosphoinositide 3-kinase
PI3Kα	Phosphoinositide 3-kinase alpha
PI3Kβ	Phosphoinositide 3-kinase beta
PI3Kδ	Phosphoinositide 3-kinase delta
PI3Kγ	Phosphoinositide 3-kinase gamma
PIK3CA	Phosphoinositide 3-kinase catalytic subunit alpha
PIK3CB	Phosphoinositide 3-kinase catalytic subunit beta
PIK3CD	Phosphoinositide 3-kinase catalytic subunit delta
PIK3CG	Phosphoinositide 3-kinase catalytic subunit gamma
PIK3R1	Phosphoinositide 3-kinase regulatory subunit 1

PIK3R2	Phosphoinositide 3-kinase regulatory subunit 1
PIK3R3	Phosphoinositide 3-kinase regulatory subunit 1
PIP2	Phosphatidylinositol (4, 5) bisphosphate
PIP3	Phosphatidylinositol (3, 4, 5) trisphosphate
PIWI	P-element-induced wimpy testis
PIWIL1	Piwi-like protein 1
PLCγ	Phospholipase C gamma
PPAR	Peroxisome proliferator-activated receptor
PS	Polystyrene
pSite	PhosphoSite
PTB	Phosphotyrosine-binding
PTEN	Phosphatase and tensin homologue
RA	Retinoic acid
RAR	Retinoic acid receptors
RAF	Rapidly accelerated fibrosarcoma
RAS	Rat sarcoma
RBD	RAS-binding domain
RBP	Retinol binding protein
REG	Regenerating islet-derived
RFP	Red fluorescent protein
RIN	RNA Integrity Number
RIPA	Radioimmunoprecipitation assay
RMA	Robust multi-array average
RNAi	RNA interference
RNA-Seq	RNA sequencing
RPKM	Reads Per Kilobase Million
RT	room temperature
RTK	Receptor tyrosine kinase
RXR	Rexinoid receptors
S6K	Ribosomal S6 kinase
SAGE	Serial analysis of gene expression

SCC	Squamous cell carcinoma
SCCHN	Squamous cell carcinomas of the head and neck
SSC	Side scatter
SCLC	Small cell lung cancer
SEF	Similar expression to FGF
SEM	Standard error of the mean
SH2	Src homology-2
SH3	Src homology-3
SH3BP4	SH3 binding protein 4
SHP2	SH region 2-containing protein tyrosine phosphatase 2
SI	Sucrase-Isomaltase
siRNA	Short interfering RNA
SLC45A3	Solute Carrier Family 45, Member 3
SMA	Smooth muscle actin
SNP	Small nucleotide polymorphism
SOS	Son of sevenless
SPRED1/2	Sprouty-related enabled/ vasodilator-stimulated phosphoprotein homology 1/2 domain
SPRY	Sprouty
STAT	Signal transducer and activator of transcription
TACC1/3	Transforming acidic coiled-coil 1/3
TBST	Tris-buffered saline Tween20
TCA	Tricarboxylic acid
TGF	Transforming growth factor
TNF	Tumour Necrosis Factor
TNSA	Tobacco-specific N-nitrosamines
TSC	Tuberous sclerosis complex
UT	Untreated
UV	Ultra violet
VEGFR	Vascular endothelial growth factor receptor
ZNF	Zinc finger nucleases

Chapter I

Introduction

1.1 Fibroblast growth factors (FGF) and FGFR signalling

Fibroblast growth factor (FGF) signalling plays critical roles in cellular crosstalk, proliferation, survival and migration (Tanner and Grose, 2016). It is essential during development and aberrant signalling can result in developmental defects (Coumoul and Deng, 2003).

FGFs are small signalling molecules, which bind to receptor tyrosine kinases, FGF receptors (FGFR). In addition to receptor-based signalling, FGFRs can also directly migrate into the nucleus and exert their functions (Coleman et al., 2014). There are 22 members of the FGF family with sizes ranging between 17-34 kDa (Ornitz and Itoh, 2001). FGF11-14, also known as FGF homologous factors (FHF), share substantial structural identity with FGF family members, however are usually not considered true family members as they remain intracellular and therefore do not bind known FGFRs (Olsen et al., 2003). FGFs share homologous core regions but diverge in C- and N-termini. Most FGF family members, except FGF1 and 2, incorporate an N-terminal signal sequence peptide to be secreted via the endoplasmic reticulum (ER) and Golgi-dependent secretory pathways. FGF1 and FGF2 are secreted via an ER-Golgi-independent pathway (Mignatti et al., 1992). FGFs often signal between epithelium and mesenchyme in a paracrine manner and are expressed in almost all tissues, where they mediate essential cellular functions during embryonic development, homeostasis, metabolism and repair (Carter et al., 2015). When FGFs, in combination with heparan sulphate (HS), bind to an extracellular immunoglobulin domain of the receptor, dimerisation of the receptor is induced, followed by transphosphorylation of the kinase domain and recruitment of adaptor proteins to phosphotyrosine residues, leading to the activation of downstream signalling cascades (Furdui et al., 2006; Turner and Grose, 2010) **(Figure 1.1)**. There are seven signalling FGFRs encoded by four *FGFR* genes, *FGFR1-FGFR4*. FGFRL1 (also known as FGFR5) lacks kinase activity and might therefore be involved in negative regulation (Sleeman et al., 2001). FGFR1-4 all consist of three extracellular domains (D1-D3), a transmembrane and a cytoplasmic domain (Beenken and Mohammadi, 2009).

D1 is thought to be responsible for regulating receptor signalling via auto-inhibition, whilst D2 and D3 are crucial for ligand specificity and D3 can be alternatively spliced, leading to FGFRb and FGFRc isoforms for FGFR1-3.

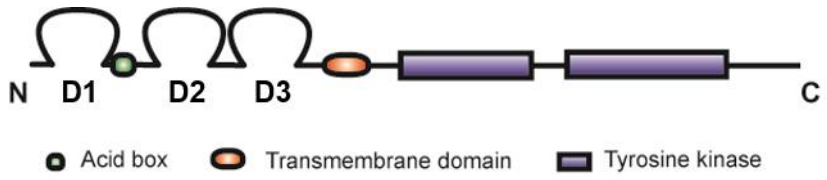

Figure 1.1. Schematic representation of FGFR.
N, N terminus; C, C terminus

1.2 FGF, FGFR and HS complex

FGF signals are ubiquitously expressed in development, homeostasis and disease; therefore a tight regulation of the pathway is essential. Canonical FGFs have a high affinity for heparin and form tight bonds with heparin/heparan sulphate proteoglycans (HSPGs), to regulate specificity and affinity for FGFRs but also limit diffusion through the extracellular matrix (ECM) (Beenken and Mohammadi, 2009; Matsuo and Kimura-Yoshida, 2013; Ornitz, 2000; Sarrazin et al., 2011; Yayon et al., 1991). HS is a highly sulphated polysaccharide that consists of 50-150 basic disaccharide repeats of uronic acid and D-glucosamine units (Bernfield et al., 1999). HSPGs play a crucial role in the formation of the FGF:FGFR:HS complex (Lindahl and Höök, 1978). Their appearance is similar to a sulphated saccharide chain that has acidic properties (Gambarini et al., 1993). For interaction with FGFs or FGFRs, the length of the molecule is important and, upon binding to FGF/FGFR, a conformational change is induced in the HS saccharide. FGFRs harbour highly conserved heparin-binding residues in the Immunoglobulin II loop (Schlessinger et al., 2000). However, in FGFs such residues are very diverse (Bellosta et al., 2001). Thus, for the ideal activity of FGFs, different lengths of chains and HS sulphation patterns are necessary, which have an effect on FGF:FGFR interaction and are thought to activate FGFR signalling (Gambarini et al., 1993).

1.3 FGF signalling pathways

1.3.1 FGFR activation

Fibroblast signalling begins with the formation of a ternary complex with two 1:1:1 FGF, FGFR and HS molecules forming a functional signalling complex composed of a symmetrical dimer (Plotnikov et al., 2000; Schlessinger et al., 2000). The complex formation allows transphosphorylation of specific tyrosine residues of the intracellular kinase domains **(Figure 1.2)**. The activated receptor recruits scaffolding or signalling molecules containing phosphotyrosine-binding src-homology 2 (SH2) domains which, thus activate further signal transducers and trigger downstream signalling cascades (Anderson et al., 1990; Moran et al., 1990; Pawson et al., 1993). Studies to further elucidate signalling cascades have typically involved FGFR1, revealing the existence of seven tyrosines that can be phosphorylated. From these tyrosine residues Tyr^{653}, Tyr^{654} are essential for the catalytic activity of the receptor while Tyr^{463}, Tyr^{583}, Tyr^{585}, Tyr^{730}, Tyr^{766} are thought to serve as recognition sites for scaffolding proteins for downstream signalling (Mohammadi et al., 1996).

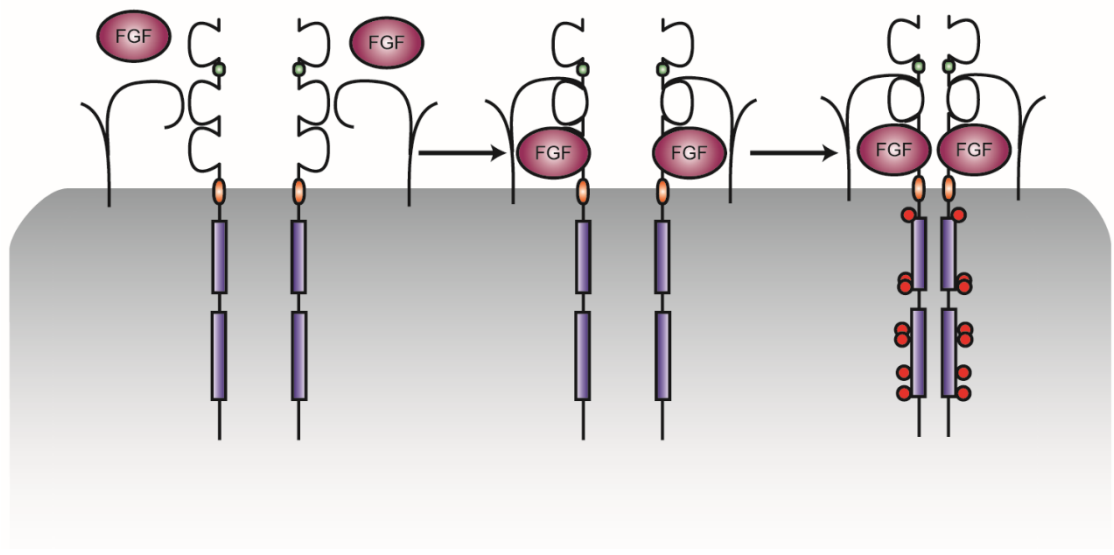

Figure 1.2. Canonical FGFR activation.
The classical model of FGFR activation involves the formation of a symmetrical complex composed of two HS chains, both ligands and the receptor monomers leading to receptor dimerisation (Schlessinger et al., 2000). This allows auto-phosphorylation and subsequent phosphorylation of downstream signalling molecules. Violet indicates the kinase domains, purple FGF ligands and the tyrosine phosphorylation sites are shown as red circles.

Four main signalling pathways can be activated: Mitogen-activated protein kinase (MAPK)/extracellular-signal-regulated kinase (ERK), Phosphoinositide 3-kinase (PI3K)/AKT, phospholipase γ (PLC γ) and Janus kinase (JAK)/signal transducer and activator of transcription (STAT) (Beenken and Mohammadi, 2009; Eswarakumar et al., 2005; Furdui et al., 2006; Goetz and Mohammadi, 2013; Turner and Grose, 2010). These pathways are involved in cellular proliferation, differentiation and survival. The different FGFRs target the same proteins, but differ in the strength of their kinase activity (Raffioni et al., 1999). It is therefore unclear if the diversity in FGFs and respective FGFRs enrich the extent of cellular signalling or merely provide further extracellular binding sites for the different FGFs. A pivotal study of FGFR2 signalling indicated that differential ligand binding can activate downstream pathways that lead to distinct downstream cellular processes (Francavilla et al., 2013).

FGFR substrate 2 (FRS2) is a major FGFR kinase substrate and acts as an essential component for the assembly of multiprotein complexes, therefore mediating the initiation of multiple FGF-FGFR-induced pathways, such as PI3K and MAPK pathways. PLCγ and JAK/STAT pathways are mediated through mechanisms independent of the docking protein FRS2. It was identified as a 90 kDa protein that is anchored to the plasma membrane by a myristolated N-terminus and is constitutively associated with FGFR1 at the amino acids 407-433 of the intracellular juxtamembrane region (Kouhara et al., 1997; Mohammadi et al., 1996; Wang et al., 1996; Xu et al., 1998). FRS2 binds to FGFR1 via a phosphotyrosine binding domain (PTB), which occurs without ligand stimulation (Ong et al., 1997). Activation of FGFR leads to FRS2α phosphorylation at tyrosine residues in the C-terminal region, and therefore creates binding sites for proteins containing SH2 domains, such as growth factor receptor-bound protein 2 (GRB2) and Src homology region 2-containing protein tyrosine phosphatase 2 (SHP2) (Kouhara et al., 1997; Ong et al., 1997). The formation of this complex then enables signal activation and further initiation of the PI3K and MAPK pathways (Lax et al., 2002; Wong et al., 2002) **(Figure 1.3)**.

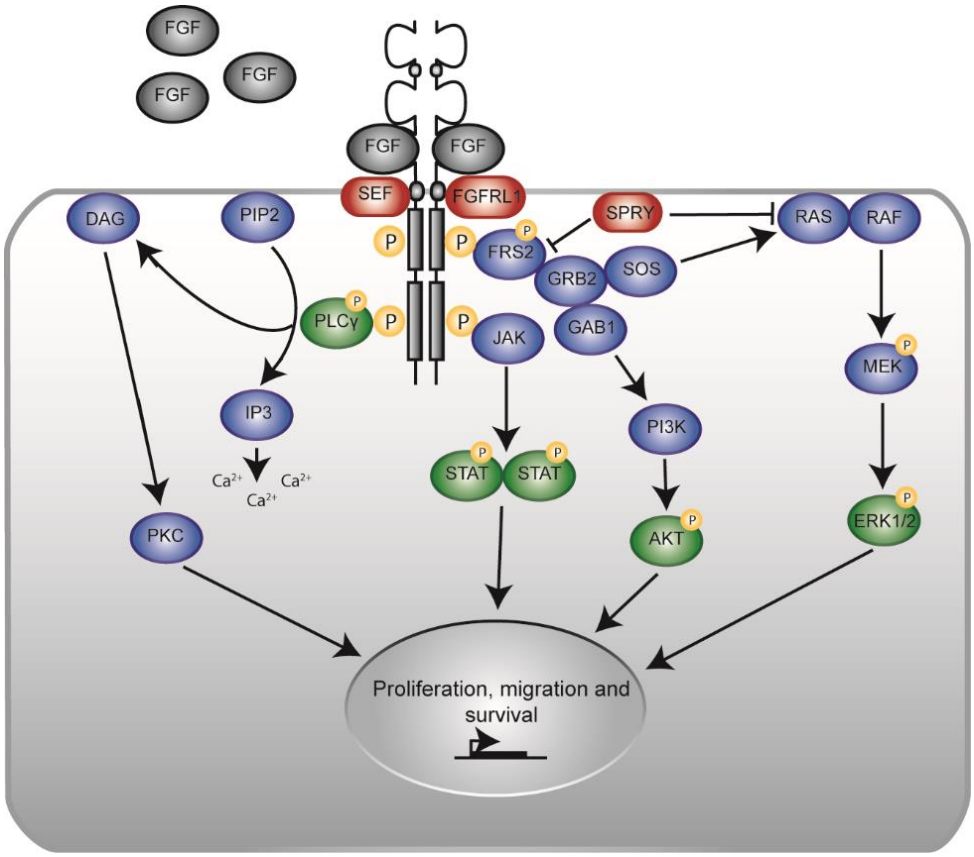

Figure 1.3. FGF induced downstream signalling of FGFR.
Schematic representation of the FGF signalling pathway, where FGF binds to an extracellular domain of FGFR resulting in receptor dimerisation and transphosphorylation of the tyrosine kinase domain. This leads to the activation of four signalling cascades: MAPK, PLCγ, PI3K and STAT. The MAPK or ERK pathway acts on cellular proliferation, differentiation, apoptosis and migration (Dhillon et al., 2007). It can influence the cell cycle, for example via activation of the transcription factor c-MYC or by upregulation of Cyclin D1. The PI3K/AKT signalling pathway regulates cell survival, proliferation and angiogenesis through nuclear and cytoplasmic domains (Fruman et al., 1998; Gotoh, 2008). In the STAT pathway, STAT dimers bind to γ-activated site (GAS) enhancers in the nucleus where they activate or repress gene transcription (Darnell, 1997). Upon activation, these pathways lead to cellular responses such as proliferation, migration and survival. Negative regulators are shown in red boxes (adapted from Carter et al. 2015).

1.3.2 MAPK/ ERK pathway

The next step in MAPK activation is the recruitment of the rat sarcoma (RAS) protein to the FGFR/FRS2/GRB2/son of sevenless (SOS) complex. GRB2 harbours an N-terminal SH3 domain that can bind constitutively to proline-rich regions in the RAS-guanine exchange factor SOS, which catalyses the exchange of guanosine diphosphate (GDP) for guanosine triphosphate (GTP) on the membrane bound small GTPase protein RAS, resulting in its activation. The recruited SOS activates the RAS GTPase which initiates a serine/threonine kinase cascade by recruitment and activation of rapidly accelerated fibrosarcoma (RAF). RAF kinase then phosphorylates and activates MAPK kinase (MEK, MEK1 and MEK2), which results in mitogenic activity and cell survival (Eswarakumar et al., 2005). Phosphorylated MAPK then activates transcription factors in the nucleus, for example cellular homologue of v-MYC (c-MYC), thereby influencing the cell cycle. It is also involved in the regulation of cell proliferation, survival and migration and was found to be associated with resistance towards targeted treatment (Bockorny et al., 2018; McCubrey et al., 2007; Yadav et al., 2012).

1.3.3 The PI3K/AKT signalling pathway

The PI3K/AKT signalling pathway plays a role in anti-apoptotic signalling but also cell growth and proliferation (Dailey et al., 2005; Gotoh, 2008). Downstream of PI3K, an anti-apoptotic protein kinase (AKT) gets activated. Growth-factor mediated activation of AKT involves a PH-domain dependant membrane translocation step where AKT is recruited to the plasma membrane with the help of phosphatidylinositol-3,4,5-trisphosphate (PIP_3) generated by PI3K. Once at the membrane, AKT is phosphorylated by PDK1 at Thr308 and other kinases, including mTORC2, at Ser473. Thr308 phosphorylation partially activates AKT, while phosphorylation of both, Thr308 and Ser473, sites results in full activation (Scheid and Woodgett, 2003; Hanada et al., 2004). Once PIP_3 levels decrease, AKT activity is attenuated through dephosphorlyation by serine/threonine phosphatases (Nicholson and Anderson, 2002).

GRB2 can also associate with GAB1 (GRB2-associated binder-1), which shows similarity to IRS-1 (insulin-receptor substrate-1) (Holgado-Madruga et al., 1996). Upon receptor activation, phosphorylated FRS2 forms a complex with SOS and GAB1 binds to FRS2-activated GRB2 via its C-terminal SH3 domain, becomes phosphorylated in turn and forms a multi-complex with downstream effector proteins, including the p85 regulatory subunit of PI3K, hence activating the PI3K/AKT signalling pathway (Turner and Grose, 2010).

PI3K is an important regulator of phosphoinositide lipids, which are a key component of the plasma membrane. Since their phosphorylation status is important in cellular signalling, it needs to be tightly regulated by kinases such as PI3K in response to FGFR activation (Balla, 2013). PI3K isoforms can be subdivided into three distinct classes: Class I, Class II and III, based on their structural characteristics and substrate specificity (Fruman et al., 1998). Class I is the best understood and is known to be activated upon receptor phosphorylation (Vanhaesebroeck et al., 2010).

The class I isoforms are heterodimers consisting of a catalytic subunit (p110) and the adaptor/regulatory subunit p85 and can be further subdivided into class IA and IB. Class IA are activated by receptors with protein kinase activity whereas subclass IB is activated by receptors coupled to G proteins. Class IA has three potential catalytic subunits p110α (*PI3CKA*), p110β (*PIK3CB*), p110δ (*PIK3CD*) and five adaptor subunit isoforms generated by alternative splicing of p85α to p55α and p50α (PIK3R1), and p85β (*PIK3R2*) and p55γ (*PIK3R3*). Subunit p110α and 110β isoforms are ubiquitously expressed and have been shown to be crucial for normal development (Bi et al., 1999). In class IB PI3Ks, the catalytic subunit p110γ (*PIK3CG*) can bind two regulatory subunits, p101 and p87 (Thorpe et al., 2015), and is mainly expressed in leukocytes (Chantry et al., 1997). Therefore, four distinct PI3K class I isoforms exist: PI3Kα, PI3Kβ, PI3Kδ, PI3Kγ.

The FRS2/GRB2/GAB1 complex recruits PI3K to the receptor with the p85 subunit, which causes a conformational change in the p110 subunit. The catalytically active PI3K can then phosphorylate the inositol ring of phosphoinositide lipids at the 3'-position, converting phosphatidylinositol (4,5) bisphosphate (PIP_2) to

phosphatidylinositol (3,4,5) trisphosphate (PIP_3). Subsequently PIP_3 recruits signalling molecules containing pleckstrin homology (PH) domains, including phosphoinositide-dependent kinase-1 (PDK1). This, in turn, phosphorylates and activates serine/threonine AKT (PKB) on threonine 308 (thr308) at the membrane (Alessi et al., 1997; Franke et al., 1995; Lietzke et al., 2000).

AKT is further implicated with the mammalian target of rapamycin (mTOR) pathway via tuberous sclerosis complex (TSC). mTOR protein complexes can be subdivided into mTOR complex 1 and 2 (mTORC1, 2), depending on their constituent proteins. mTORC2 phosphorylates AKT at serine 473 (ser473), resulting in complete activation - meaning a five-fold increase of activity compared to the activity of phosphorylated protein at thr308 alone (Facchinetti et al., 2008; Sarbassov et al., 2005). AKT functions further by promoting cell survival via regulation of anti-apoptotic targets, such as B-cell lymphoma 2 (BCL2), via mTORC1, through activation of ribosomal S6 kinase (S6K). The release of eukaryotic translation initiation factor 4E binding protein 1 (EIF4EBP1) then leads to transcriptional repression and allows for translation of pro-survival mediators (Wang et al., 2006). In addition, PI3K has been implicated in RAS activation, as PI3K was found to associate with GTP-bound RAS (Kodaki et al., 1994; Rodriguez-Viciana et al., 1994).

Class II and III subfamilies are less studied than Class I and their functional importance remains unclear. Class II PI3K (PI3KC2) have three members in vertebrates, two of the three class II isoforms PI3KC2α and β are widely distributed throughout mammalian tissue however less is known about the third γ isoform. It is thought that class II PI3Ks interact with proteins that are involved in adaptor functions. PI3KC2α and β could be associated with clathrin-coated vesicles as they contain an N-terminal clathrin-binding (CB) domain (Gaidarov et al., 2001; Posor et al., 2013). The PI3KC2β N-terminus can also bind the scaffold protein intersectin, that is involved in the synthesis of PIP_3 (Das et al., 2007). Less is known about PI3KC2γ and protein interactions have not been tested. Class II PI3Ks also contain a RAS-binding domain (RBD), although this mechanism is not well characterised. All three members of the PI3KC2 subfamily own a unique C-terminal extension that carries a

C2 domain and a PX domain that binds favourably to PIP_2 (Stahelin et al., 2006). The single class III PI3K, initially described as vacuolar protein sorting 34 (VPS34) and also known as *PIK3C3* is conserved in all eukaryotes (Schu et al., 1993). VPS34 can bind to adaptor protein VPS15, which is myristoylated at the N-terminus, and forms an intracellular membrane-bound heterodimer controlling VPS34 catalytic activity that can influence cellular outcomes such as autophagy and endosomal trafficking by engaging with other key membrane proteins such as RAB5 GTPase (Backer, 2008; Christoforidis et al., 1999; Vanhaesebroeck et al., 2010).

1.3.4 The PLCγ pathway

The PLCγ pathway is initiated by auto-phosphorylation of Tyr^{766} of FGFR1 and FGFR2 and subsequent association of PLCγ to the phosphorylated site via its SH2 domain, where it is itself phosphorylated and thus gains its catalytic activity (Burgess et al., 1990; Mohammadi et al., 1991; Spivak-Kroizman et al., 1994). PLCγ is a phosphodiesterase and is recruited to the membrane, where it cleaves PIP_2, resulting in formation of inositol triphosphate (IP_3) and diacylglycerol (DAG) (Carpenter and Ji, 1999; Klint and Claesson-Welsh, 1999). IP_3 causes the release of calcium ions from the endoplasmic reticulum (Streb et al., 1983), which together with DAG induces the activation of protein kinase C (PKC) (Rameh et al., 1998; Yun et al., 2010). In addition, STAT-dimers translocate to the nucleus, which bind to γ-activated site (GAS) enhancers to control gene transcription (Darnell, 1997). High PKC expression can then relieve inhibition of RAF and reactivate the MAPK pathway (Corbit et al., 2003). Ligand-dependent activation of PLCγ is the acknowledged canonical signalling pathway, however recent studies have shown that signalling can also be initiated in the absence of FGF ligand by PLCγ1 binding to the C terminus of FGFR2 in an SH3-dependent manner. As this usually occurs when cellular PLCγ1 concentration levels exceed GRB2 levels, it could present an explanation for low GRB2 expression levels, heightened PLCγ1 activity and metastatic phenotype in tumour cells (Fearon and Grose, 2014; Park et al., 2012; Sala et al., 2008).

1.3.5 The JAK/ STAT pathway

Upon FGFR dimerisation and auto-phosphorylation, JAKs are phosphorylated, leading to multimerisation by bringing two JAKS into close proximity resulting in trans-phosphorylation. An FGFR/JAK complex is formed that serves as a docking site for STATs, which are a family of transcription factors that are latent, residing in the cytoplasm until activated. The SH2 domain of STATs is in turn tyrosine phosphorylated and STAT dimers translocate to the nucleus, where they bind to GAS enhancers to activate or repress gene transcription (Darnell, 1997). In addition to influencing cell proliferation and differentiation (Ebong et al., 2004), the JAK-STAT pathway is also fundamental for cytokines and growth factors leading to haematopoiesis, lactation and development of the immune system and mammary glands (Ghoreschi et al., 2009; Liongue et al., 2012; O'Shea et al., 2002). A relatively recent study showed that FGFR4 silencing prevents STAT3 phosphorylation and subsequently the expression of anti-apoptotic protein c-FLIP (Turkington et al., 2014).

1.4 Regulation of FGF signalling

Given its crucial roles, the FGF signalling pathway needs to be tightly regulated. This is ensured through both positive and negative feedback loops. These regulatory proteins, which are co-expressed with FGFs, inhibit FGF signalling by creating a negative feedback loop, but are also themselves controlled by FGF signalling **(Figure 1.4)**. Key regulators are Sprouty (SPRY) proteins, which are MAPK phosphatases and encompass Spry1-Spry4 (Hacohen et al., 1998). Upon RTK stimulation, Spry1 and 2 but not 4 are phosphorylated, whereas for Spry3, no evidence for growth factor-induced phosphorylation has been described (Fong et al., 2003; Mason et al., 2004). SPRYs have been implicated in several developmental and physiological processes and depending on the kinase and pathways activated, different SPRYs selectively control growth factor effects and therefore induce varying signal transductions and responses (Hanafusa et al., 2002; Sasaki et al., 2003; Yusoff et al., 2002). SPRYs can inhibit receptor tyrosine kinase signalling by directly interacting with RAF and prevent its phosphorylation, leading to blockage of MAPK signalling, or it can compete for GRB2 binding, interfering with the FRS2α/GRB2 complex and thus counteract SOS-induced RAS activation (Sasaki et al., 2003; Thisse and Thisse, 2005).

Further regulatory proteins include Sprouty-related Enabled/vasodilator-stimulated phosphoprotein Homology 1 Domain-containing proteins (SPRED1 and 2), which also inhibit MAPK signalling (Wakioka et al., 2001). SPREDs form complexes between RAS and RAF and therefore counteract activation of MEK.

Other mediators that negatively control FGF signalling are MAPK phosphatase 3 (MKP3) and Similar Expression to FGF (SEF). MKP3 affects downstream MAPK signalling by dephosphorylating ERK1 and ERK2. SEF acts at various points of the signalling pathway such as in MEK signalling (Yang et al., 2003), inhibition of RAS activation resulting in PI3K pathway inhibition (Kovalenko et al., 2003) or directly by interacting with the receptor with its transmembrane form, causing inhibition of receptor signalling and phosphorylation of FRS2α and also inhibiting ERK phosphorylation (Kovalenko et al., 2003; Thisse and Thisse, 2005; Tsang et al., 2002; Xiong et al., 2003).

Another mechanism of negative regulation involves direct phosphorylation of MAPK pathway proteins such as SOS, which hinders its interaction with GRB2, resulting in less SOS at the membrane, thus lowering RAS activation (Buday et al., 1995). Also RAF can be phosphorylated, which reduces RAF kinase activity and hence diminishes MEK and MAPK phosphorylation (Ueki et al., 1994). Furthermore GAB1 can be directly phosphorylated by MAPK leading to a decrease in PI3K interacting with GAB1 and thus reduced AKT pathway activation (Gual et al., 2001). Ultimately, phosphatase and tensin homolog (PTEN) can counteract the PI3K pathway by converting PIP_3 back to PIP_2 (Makker et al., 2014).

Pleckstrin homology like domain A (PHDLA) family members, have also been implicated in negative regulation of the PI3K pathway (Kawase et al., 2009). Three known family members exist, PHLDA1, PHLDA2 and PHDLA3 which all contain a PH domain and thus are able to bind phosphoinositol lipids. While PHLDA2 is assumed to be involved in embryonic development, PHLDA1 and 3 were found to be expressed in adult tissue (Frank et al., 1999). PHLDA3 is the most characterised family member and defined as a possible tumour suppressor (Kawase et al., 2009). It has been shown to be a direct target of p53, creating a negative feedback loop between

AKT and PHLDA3 (Liao and Hung, 2010). It also negatively regulates AKT by competing with AKT for PIP_3 binding sites and thus inhibiting AKT phosphorylation leading to apoptosis (Kawase et al., 2009; Ohki et al., 2014). PHLDA1, like PHLDA3, has also been found to interact with PIP_3 and thus reduce AKT signalling and thereby play a role in apoptosis (Hossain et al., 2003; Murata et al., 2014; Neef et al., 2002; Toyoshima et al., 2004). Recent work in our group has investigated the role of PHLDA1 in drug resistance, where downregulation of PHLDA1 resulted in AKT signalling recovery, thus implying that PHLDA1 acts as a negative regulator of AKT (Fearon et al., 2018).

Other regulatory mechanisms are receptor internalisation after receptor activation, and subsequent receptor degradation and recycling, which are regulated by CBL-mediated ubiquitination (Thien and Langdon, 2001). In respect to the receptor, signalling can also be regulated by auto-inhibition (Plotnikov et al., 1999; Schlessinger et al., 2000; Stauber et al., 2000). FGFRs exist in an equilibrium of an 'open' and 'closed' conformation. Alternatively, spliced immunoglobulin domain I (IgI) and the acid box of the linker region between IgI and IgII minimise inadvertent FGF signalling by forming a 'closed' auto-inhibited state (Kalinina et al., 2012). The acid-box containing linker region directly suppresses HS-binding affinity of FGFR and thus inhibits receptor activation. It therefore only allows ligands with high receptor affinity to bind to the receptor by overcoming auto-inhibition. Loss of the linker region has been found to be involved in cancer (Kobrin et al., 1993; Mansson et al., 1989).

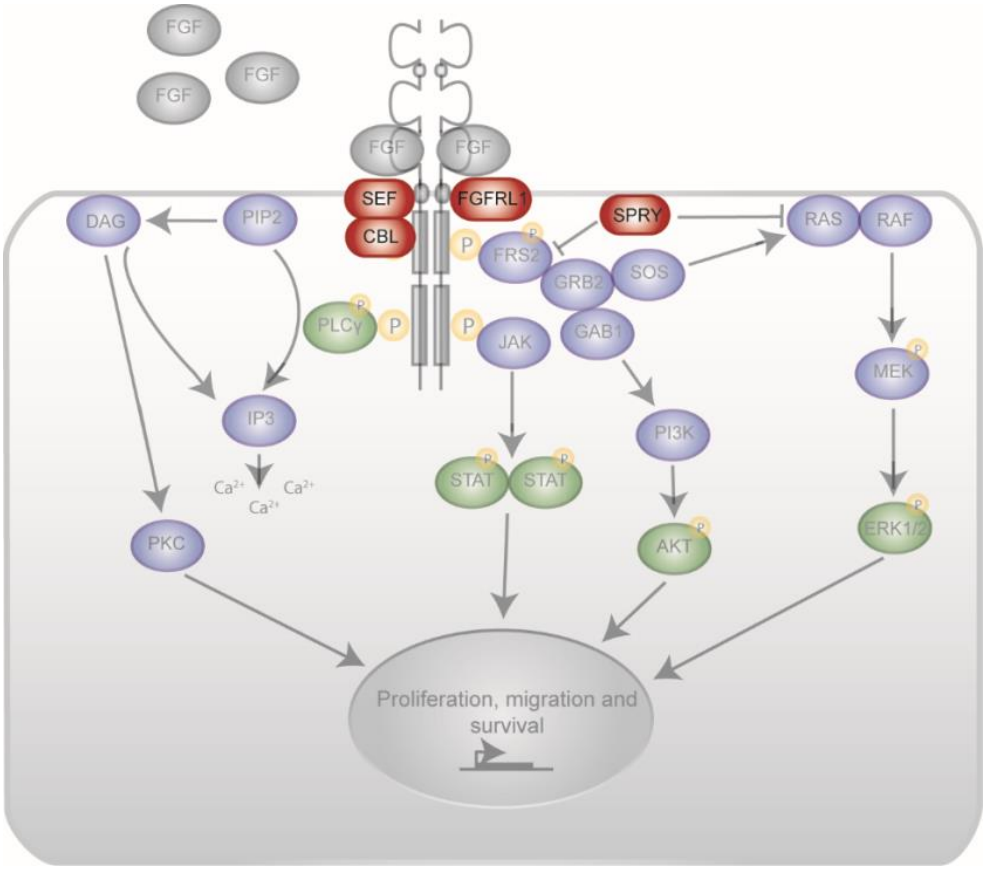

Figure 1.4. Negative regulation of FGFR signalling.
There are a number of mechanisms to negatively regulate FGFR signalling. These include recruitment of additional proteins (red boxes) (Hacohen et al., 1998; Wakioka et al., 2001; Wang et al., 2002; Yang et al., 2003), as well as downstream elements such as the MAPK pathway acting upstream to modify activity (Buday et al., 1995; Gual et al., 2001; Ueki et al., 1994).

1.5 Pathologies resulting from aberrant FGFRs

1.5.1 Developmental disorders

FGF signalling plays a crucial role in developmental pathways such as embryogenesis, development and organogenesis (De Moerlooze et al., 2000). Therefore aberrations in the FGF signalling pathway have been linked to human diseases such as congenital syndromes, skeletal dysplasias and deafness (Kan et al., 2002; Turner and Grose, 2010; Wilkie et al., 2002). These are mostly due to gain or loss of function mutations in either the ligands or the receptors and such germline mutations are known drivers for a range of developmental disorders (Beenken and Mohammadi, 2009).

In several craniosynostosis syndromes such as Pfeiffer syndrome, Jackson-Weiss syndrome, Muenke syndrome, and osteoglophonic dysplasia, gain-of-function missense mutations are found (Ibrahimi et al., 2004; Muenke et al., 1994; Roscioli et al., 2000; Rutland et al., 1995; White et al., 2005). Craniosynostosis syndromes are autosomal dominant diseases affecting cranial suture closure and skeletal and soft tissues. In such diseases, FGFR1 and FGFR2 mutations in the linker region between IgII and IgIII loops are found, which can alter the specificity of the receptor for ligands (Chen et al., 2003; Eswarakumar et al., 2004; Ibrahimi et al., 2001; Yu et al., 2000). For example, Pfeiffer syndrome type I is linked to *FGFR1* and *FGFR2* mutations, whereas type II and III with *FGFR2* mutations only. In Pfeiffer syndrome type I, 5% of patients harbour a gain-of-function P252R mutation of FGFR1, which occurs at the linker region between D2 and D3, causing receptor over activation (Robin et al., 1994). As Pfeiffer, Jackson-Weiss and Muenke syndrome phenotypes can be caused by different FGFRs, this could suggest potentially redundant functions of these receptors in skeletal development (Ibrahimi et al., 2004; Schell et al., 1995). Kallmann syndrome 2 (hypogonadotropic hypogonadism 2) with or without anosmia has been identified to be caused by loss of function missense mutations in *FGFR1*, resulting from a lack of production of certain hormones that direct sexual development (Dodé et al., 2003; Pitteloud et al., 2005).

Apert syndrome is driven by activating mutations S252W and P253R in FGFR2 and these have been modelled in mice (McDowell et al., 2006; Wang et al., 2005). These mutations are thought to increase ligand affinity for the receptor and cause uncontrolled receptor activation (Ibrahimi et al., 2001). It is suggested that they enhance the expression of FGFR2IIIb and its mesenchymal ligand FGF10, resulting in premature fusion of cranial plates, which is a key feature of this disease (Yokota et al., 2014). Apert mutations all remain ligand dependent. The S252W mutation induces a modification of the receptor that causes the receptor to remain on the cell surface for a prolonged time rather than undergoing rapid recycling, as would a normal receptor. This affects downstream signalling pathways resulting in increased ERK phosphorylation and hence drives cell proliferation and migration capabilities as well as premature differentiation (Ahmed et al., 2008).

1.5.2 Cancer

Cancer is one of the leading causes of death (Cancer Statistics, WHO | World Health Statistics 2018). In 2012, the worldwide cancer burden was 14.1 million new cases and 8.2 million cancer-related deaths worldwide. Cancers such as lung, breast, colorectal and stomach are the most commonly diagnosed cancers in Europe.

Hanahan and Weinberg presented six characteristics, so called hallmarks of cancer that healthy cells undergo to become cancerous cells. These include uncontrolled and sustained proliferation, evasion of cell cycle control, resistance to programmed cell death, replicative immortality, ability to induce angiogenesis and ability to invade the vasculature and other tissues to metastasise (Hanahan and Weinberg, 2000). In 2011, a revised list of cancer hallmarks was postulated, encompassing 10 characteristics with two additional enabling hallmarks (Hanahan and Weinberg, 2011) **(Figure 1.5)**. Additonal characteristics include development of genomic instability therefore generating random mutations and inflammatory state premalignant cells. Furthermore, cancer cells are identified to reprogram energy cell metabolism and actively evade from elimination by immune cells. Cancer cells acquire these characteristics by activation of oncogenes that are the drivers of these processes or

downregulate or inhibit tumour suppressors that would suppress these processes in normal cells.

Deregulated FGF signalling can increase cellular proliferation, confer resistance to cell death, increase motility and invasiveness, drive angiogenesis, enhance metastasis, and induce resistance to chemotherapy (Turner and Grose, 2010). Perturbations of the pathway can occur through a variety of mechanisms; over-expression of FGFs/FGFRs, mutations in FGFRs, translocations and loss of regulatory mechanisms **(Figure 1.6)**. The majority of such cell signalling aberrations are of an activating nature and thus enhance proliferation, migration and angiogenesis resulting in a more malignant phenotype (Turner and Grose, 2010).

Furthermore, negative feedback regulators play a critical role in keeping the FGF signalling pathway in control. Loss of feedback control has been related to prostate cancer, where a decrease of the signalling antagonists SPRY and Sprouty-related (SPRED) has been documented (Assinder et al., 2015).

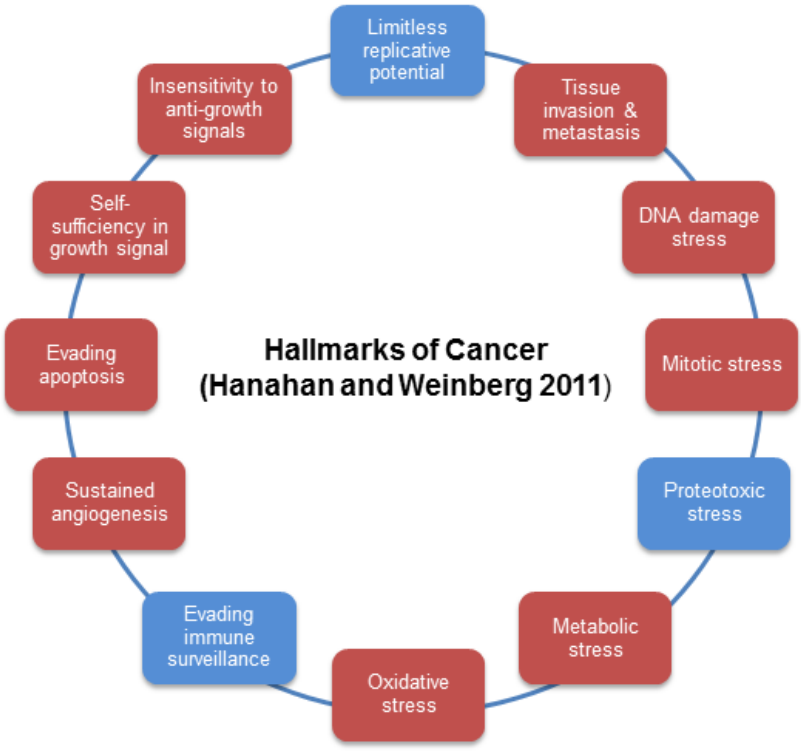

Figure 1.5. FGF signalling in the Hallmarks of Cancer.
Adapted from Hanahan and Weinberg (2011), with hallmarks affected by FGF signalling highlighted in red (Tanner and Grose, 2016).

1.5.2.1 Receptor amplification

FGFRs can be activated through amplification, which is a segmental copy number gain resulting in receptor overexpression and correlates with poor survival. Amplifications in *FGFR3* are less commonly encountered in different types of cancers (Nord et al., 2010). In contrast, *FGFR1* and *FGFR2* amplifications have been described in a number of different cancers (Katoh, 2010). In gastric cancer, roughly 10% harbour *FGFR2* amplifications, which are correlated with poor prognosis and diffuse cancer types. Receptor signalling can occur through a ligand-independent manner in gastric cancer cell lines with C-terminally truncated FGFR2 (Kunii et al., 2008; Takeda et al., 2007). Due to the C-terminal FGFR2 truncation, signalling attenuation mechanisms are inhibited as the receptor cannot be internalised, resulting in constitutive receptor activation (Cha et al., 2009). *FGFR1* and *FGFR2* amplifications have also been implicated in various cancers and associated with poor survival. Amplification of chromosomal region 8p11-12 was also commonly found in 10% of oestrogen receptor (ER)-positive breast cancers (Adnane et al., 1991; Courjal et al., 1997; Jacquemier et al., 1994; Reis-Filho et al., 2006).

Recent studies have also indicated amplifications of *FGFR1* in non-small cell lung carcinoma (NSCLC) cell lines, with 21-22% of squamous cell carcinoma harbouring *FGFR1* amplifications. Additionally, 3% of lung adenocarcinoma with *FGFR1* amplifications were shown to be dependent on FGFR1 activity for cell growth (Ahmad et al., 2012; Freier et al., 2007). Not all lung cancer cell lines with *FGFR1* amplifications showed sensitivity to FGFR inhibitors. This may be due to different phosphorylation status of FRS2. However, in the majority of cell lines tested, the FGFR inhibitor PD1703074 potently affected tumour growth and survival. *FGFR1* has also been found to be amplified in oral squamous carcinoma (Freier et al., 2007) and has been found at a low incidence rate in ovarian cancer (Gorringe et al., 2007), bladder cancer (Simon et al., 2001) and rhabdomyosarcoma (Missiaglia et al., 2009). *FGFR1* and *FGFR2* were also found to be amplified in 47% of hormone resistant prostate cancers and *FGFR3* was amplified in 3% bladder cancers. *FGFR4* was found to be amplified in 30% of adult adrenocortical tumours (Brito et al., 2012). In the majority of cancers, amplification of the receptor was associated with worse

prognosis and more malignant cancer type. Patients harbouring amplifications have been identified as suitable candidates for FGFR-targeted therapy compared to individuals with non-amplified tumours (André et al., 2013; Cheng and Alper, 2014; Soria et al., 2014). However, treatment of patients with EGFR-targeted monoclonal antibody, Cetuximab, yielded good results initially however resistance towards the drug was acquired (Zhang et al., 2014). Xenograft experiments determined the cause as concomitant *FGFR* amplification, and FGFR2-targeted therapy led to re-sensitisation to Cetuximab, highlighting the complexity of receptor tyrosine cell signalling.

1.5.2.2 Autocrine and paracrine stimulation/Isoform switching

Most of the common FGFR aberrations are ligand-independent and result in constitutive receptor activation. However, ligand-dependent signalling is also important in driving cancer. This can be through autocrine ligand production of cancer cells or paracrine production by stromal cells. This has been confirmed using mouse models where FGF was ectopically expressed in either epithelial or stromal cells, promoting carcinogenesis (Callahan and Smith, 2000; Memarzadeh et al., 2007). The first evidence for autocrine signalling arose from melanoma cancer studies where high FGFR1 and FGF2 mRNA levels were observed and, with the use of xenograft experiments, an FGFR1-FGF2 autocrine loop was identified as promoting melanoma formation (Lefèvre et al., 2009; Wang et al., 2017). Epithelial ovarian cancer shows heightened signalling via autocrine stimulation of FGFR2IIIb by its ligand FGF7 (Steele et al., 2001). An autocrine FGF2-FGFR1IIIc feedback loop has also been proposed in non-small lung cancer cell lines resistant towards EGFR-inhibitor Gefitinib (Marek et al., 2009).

Isoform switching is commonly observed in cancers and is associated with a more malignant cancer phenotype (Ishiwata et al., 2012; Kawase et al., 2009; Peng et al., 2014; Turner and Grose, 2010). In epithelial cells, the FGFR2IIIb isoform is commonly expressed, whereas in mesenchymal cells FGFR2IIIc is expressed. In breast cancer, epithelial expression of FGFR2IIIc resulted in a more invasive cancer phenotype

(Shirakihara et al., 2011), and in pancreatic cancer cells, overexpression of FGFR2IIIc is associated with enhanced tumour growth and aggressiveness (Ishiwata et al., 2012).

1.5.2.3 Fusion genes

Chromosomal translocations resulting in fusion of *FGFR1* with other genes have been reported frequently in myeloproliferative disorders such as EMS (eosinophilic myeloproliferative syndrome) and AML (acute myeloid leukaemia) (Cross and Reiter, 2008; Roumiantsev et al., 2004; Xiao et al., 1998). EMS is also called 8p11 myeloproliferative syndrome, as chromosomal band 8p11 is involved in chromosomal translocation process. Chromosomal translocation occurs through the rearrangement of two non-homologous parts and a gene fusion can be generated when the translocation joins two otherwise separated genes. This can result in an amino-terminal peptide fusing with the cytoplasmic kinase domain of FGFR1. Commonly, a fusion between 13p12 *ZNF198* encoding a zinc-finger protein normally localised to the nucleus occurs with FGFR1 (Popovici et al., 1998; Reiter et al., 1998). However, as it is missing the nuclear localisation signal the resultant cytoplasmic tyrosine kinase is constitutively active due to zinc-finger mediated homodimerisation. Oncogenic fusion genes that activate FGFR tyrosine kinase domains also occur in glioblastoma, bladder, lung, breast, cervical, thyroid, oral and prostate cancers (Carneiro et al., 2015; Costa et al., 2016; Majewski et al., 2013; Parker and Zhang, 2013; Singh et al., 2012; Williams et al., 2013; Wu et al., 2013).

With FGFR1, at least 11 fusion partners have been identified, including *ZNF198* and *BCR* (Jackson et al., 2010; Xiao et al., 1998). FGFR1 and FGFR3 fused to transforming acidic coiled-coil 1 (TACC1) and TACC3 have been identified frequently in glioblastoma (Parker et al., 2013; Singh et al., 2012). *FGFR1-TACC1* and *FGFR3-TACC3* gene fusions have also been identified in NSCLC, bladder cancer, multiple myeloma and long squamous cell carcinoma (Costa et al., 2016; Wu et al., 2013). These gene fusions can result in constitutively active FGFR kinase activity in the mitotic spindle. In multiple myeloma, *FGFR3-TACC3* fusion also results in 3' UTR deletions allowing the fusion gene to escape microRNA regulation (Parker et al., 2013).

In cholangiocarcinoma, translocations involving *FGFR2* leading to fusion genes with *AHCYL1*, *BICC1*, *MGEA5*, *AFF3* and *TACC3* have been encountered. Bicaudal C homolog 1 (BICC1), which is an RNA-binding molecule that regulates gene expression, was found to be fused to full-length FGFR2. The gene fusion again is suggested to induce enhanced receptor activity by facilitating oligomerisation. Prostate cancer gene fusions involving full-length FGFR2 have been identified with *FGFR2* under the control of solute carrier family 45, member 3 (SLC45A3), an androgen-regulated promoter, resulting in FGFR2 overexpression. It is assumed that targeting fusion proteins, where the kinase domain is included, could be a potential treatment strategy, as in the case of FGFR2-SLC45A3 it suggested to be both susceptible to anti-androgens and FGFR-targeted therapy (Arai et al., 2014; Wu et al., 2013).

1.5.2.4 Receptor mutation

Point mutations in FGFRs can enhance ligand binding or alter ligand specificity if the mutation is in the extracellular domain of the receptor. Mutations in the ligand-binding and transmembrane domain may induce dimerisation of the receptor. Commonly, mutations occur in the kinase domain, which also constitutively activate the receptor. Mutations in the intracellular domain can impair degradation of the receptor, which again results in constitutive signalling (Cho et al., 2004; Haugsten et al., 2010). However, also loss of function mutations have been associated with cancer (Gartside et al., 2009; Greulich and Pollock, 2011).

In a number of cancers, somatic mutations have been found that were identical to germ line mutations in FGFRs found in developmental syndromes (Kan et al., 2002; Pollock et al., 2007). FGFR2 missense mutations have been commonly described in endometrial and gastric cancer (Dutt et al., 2008; Jang et al., 2001; Pollock et al., 2007). In endometrial cancer (Byron and Pollock 2009), these mutations mirror mutations found in chondrodysplasias, such as S252W and N550K mutations in Apert and Pfeiffer syndromes, and result in receptor activation (Fearon and Grose, 2014; Pollock et al., 2007). They are highly sensitive to FGFR inhibition (Dutt et al., 2008) and, more recently, have been well studied in NSCLC (Tchaicha et al., 2014). Such *FGFR2*

mutations are assumed to drive tumourigenesis by changing the ligand affinity or inducing ligand-independent dimerisation (Tanizaki et al., 2015). In 57% of gastric cancer patients, at least one allele of the common G388R variant of FGFR4 was present and expression of this allele was linked with worse prognosis (Ye et al., 2010). Mutations in FGFR3 have been observed in 25% cervical and 35% bladder carcinoma, that are identical to activating mutations in thanatophoric dysplasia (Cappellen et al. 1999). In 7.5% of rhabdomyosarcomas, FGFR4 is mutated in the tyrosine kinase domain, and associates with advanced stage and poor survival (Taylor et al., 2009). Noteworthily, *FGFR3* and *HRAS* mutations are mutually exclusive in bladder cancer (Jebar et al., 2005), however that is not the case with *PIK3CA* mutations (López-Knowles et al., 2006; Platt et al., 2009). Similarly, in endometrial cancer *KRAS* and *FGFR2* mutations are mutually exclusive (Byron et al., 2008). This indicates redundancy in the ability of a single activation mechanism to fully induce MAPK signalling in these cancers, whereas PI3K signalling can be induced with multiple 'hits' (Byron et al., 2008; Jebar et al., 2005). The importance and functionality of such mutations in tumourigenesis, and the potential to target them therapeutically, has been validated in mouse models (Tchaicha et al., 2014).

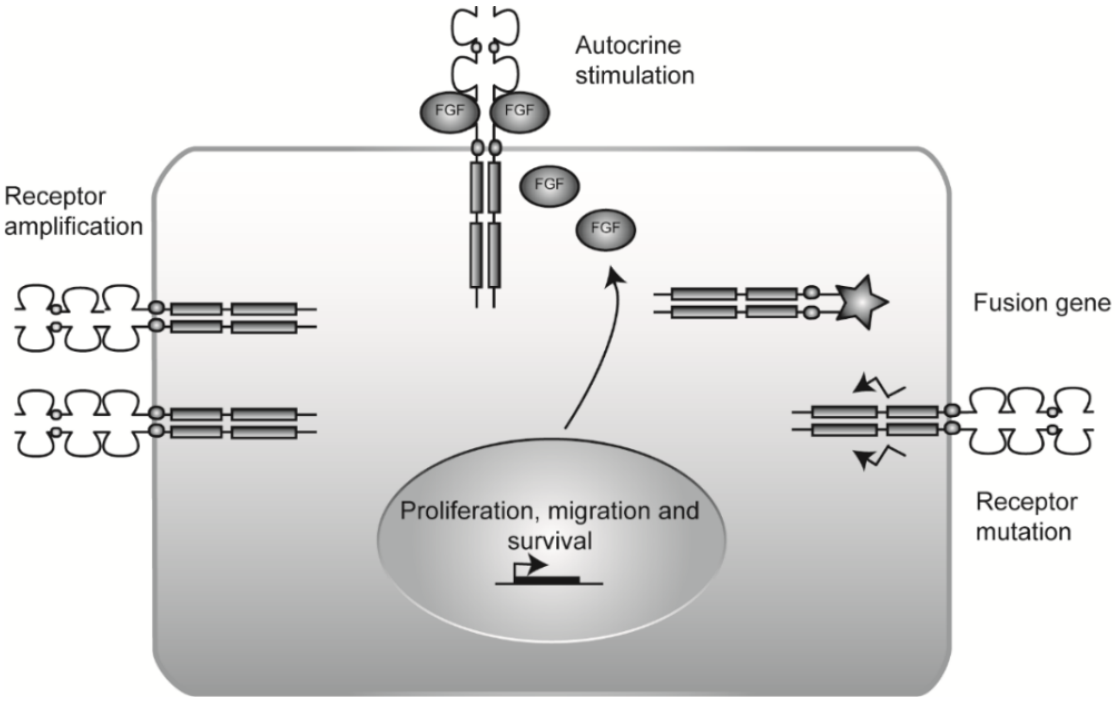

Figure 1.6. Mechanisms by which FGF signalling can be altered in cancer.
The FGF pathway can be corrupted by a number of means, most frequently due to activating mutations in receptors, which result in either promiscuous ligand binding or ligand-independent firing (Beenken and Mohammadi, 2009). Alternatively, inappropriate expression of ligand or mis-splicing of receptors can lead to autocrine signalling; receptor amplification can result in enhanced signalling, or fusion proteins resulting from chromosomal translocations can give constitutively active kinase activity (Turner and Grose, 2010). Not illustrated above, loss of negative regulators can also lead to dysregulation of signalling (Carter et al., 2015; Tanner and Grose, 2016).

Table 1.1. FGFR-related malignancies and related cancer types.
Table of all five FGFRs and their alterations, summarising the different alterations and, for each, the three cancer types in which they have been reported to occur most frequently.

Receptor	Related Cancer
FGFR1	
Amplification	**Lung (16.3%)** (Cancer Genome Atlas Research Network, 2012) **Breast (10.8%)** (Cancer Genome Atlas Network, 2012) **Bladder (8.7%)** (Cancer Genome Atlas Research Network, 2014a)
Mutation	**Stomach (4.2%)** (Cancer Genome Atlas Research Network, 2014b) **Melanoma (4.1%)** (Hodis et al., 2012) **Lung (3.4%)** (Peifer et al., 2012)
Deletion	**Prostate (8.2%)** (Grasso et al., 2012) **Lung (3.3%)** (Imielinski et al., 2012) **Bladder (3.1%)** (Iyer et al., 2013)
FGFR2	
Amplification	**Stomach (5.2%)** (Cancer Genome Atlas Research Network, 2014b) **Breast (1.9%)** (Cancer Genome Atlas Network, 2012) **Ovary (1.9%)** (Cancer Genome Atlas Research Network, 2011)
Mutation	**Endometrium (12.5%)** (Cancer Genome Atlas Research Network et al., 2013) **Cholangiocarcinoma (10%)** (Jiao et al., 2013) **Melanoma (4.4%)** (Krauthammer et al., 2012)
Deletion	**Prostate (1.6%)** (Grasso et al., 2012) **Lung (0.9%)** (Cancer Genome Atlas Research Network, 2014c) **Glioblastoma (0.4%)** (Brennan et al., 2013)
FGFR3	
Amplification	**Sarcoma (3.4%)** (Barretina et al., 2010) **Bladder (3.1%)** (Cancer Genome Atlas Research Network, 2014a) **Glioblastoma (2.5%)** (Brennan et al., 2013)
Mutation	**Bladder (19.3%)** (Kim et al., 2015) **Melanoma (3.3%)** (Krauthammer et al., 2012) **Multiple Myeloma (2.4%)** (Lohr et al., 2014)
Deletion	**Lung (1.7%)** (Cancer Genome Atlas Research Network, 2012) **Prostate (1.6%)** (Grasso et al., 2012) **Stomach (1.4%)** (Cancer Genome Atlas Research Network, 2014b)
FGFR4	
Amplification	**Kidney (6.5%)** (Cancer Genome Atlas Research Network, 2013) **Prostate (3.3%)** (Grasso et al., 2012) **Bladder (1.6%)** (Cancer Genome Atlas Research Network, 2014a)
Mutation	**Melanoma (5%)** (Hodis et al., 2012) **Lung (4.3%)** (Ding et al., 2008) **Colorectum (4.2%)** (Seshagiri et al., 2012)
Deletion	**Bladder (1.6%)** (Cancer Genome Atlas Research Network, 2014a) **Stomach (1.4%)** (Cancer Genome Atlas Research Network, 2014b) **Lung (0.6%)** (Cancer Genome Atlas Research Network, 2012)
FGFRL1	
Amplification	**Sarcoma (3.4%)** (Barretina et al., 2010) **Prostate (2.8%)** (Barbieri et al., 2012) **Bladder (2.4%)** (Cancer Genome Atlas Research Network, 2014a)
Mutation	**Bladder (9.1%)** (Guo et al., 2013) **Colorectum (5.6%)** (Seshagiri et al., 2012) **Lung (2.7%)** (Imielinski et al., 2012)
Deletion	**Prostate (1.8%)** (Baca et al., 2013) **Lung (1.7%)** (Cancer Genome Atlas Research Network, 2012) **Stomach (1.7%)** (Cancer Genome Atlas Research Network, 2014b)

1.6 FGFR-driven cancers

It is clear that FGFR signalling can drive many different cancers. In this project, the focus lies on FGFR-driven gastric, endometrial and lung cancer **(Figure 1.7)**. Lung and gastric cancer are two of the major cancer types and mark the number one and three cancer-associated deaths respectively (Siegel et al., 2015; Torre et al., 2015). Furthermore, endometrial cancer is the main gynaecological cancer type (Plagens-Rotman et al., 2016).

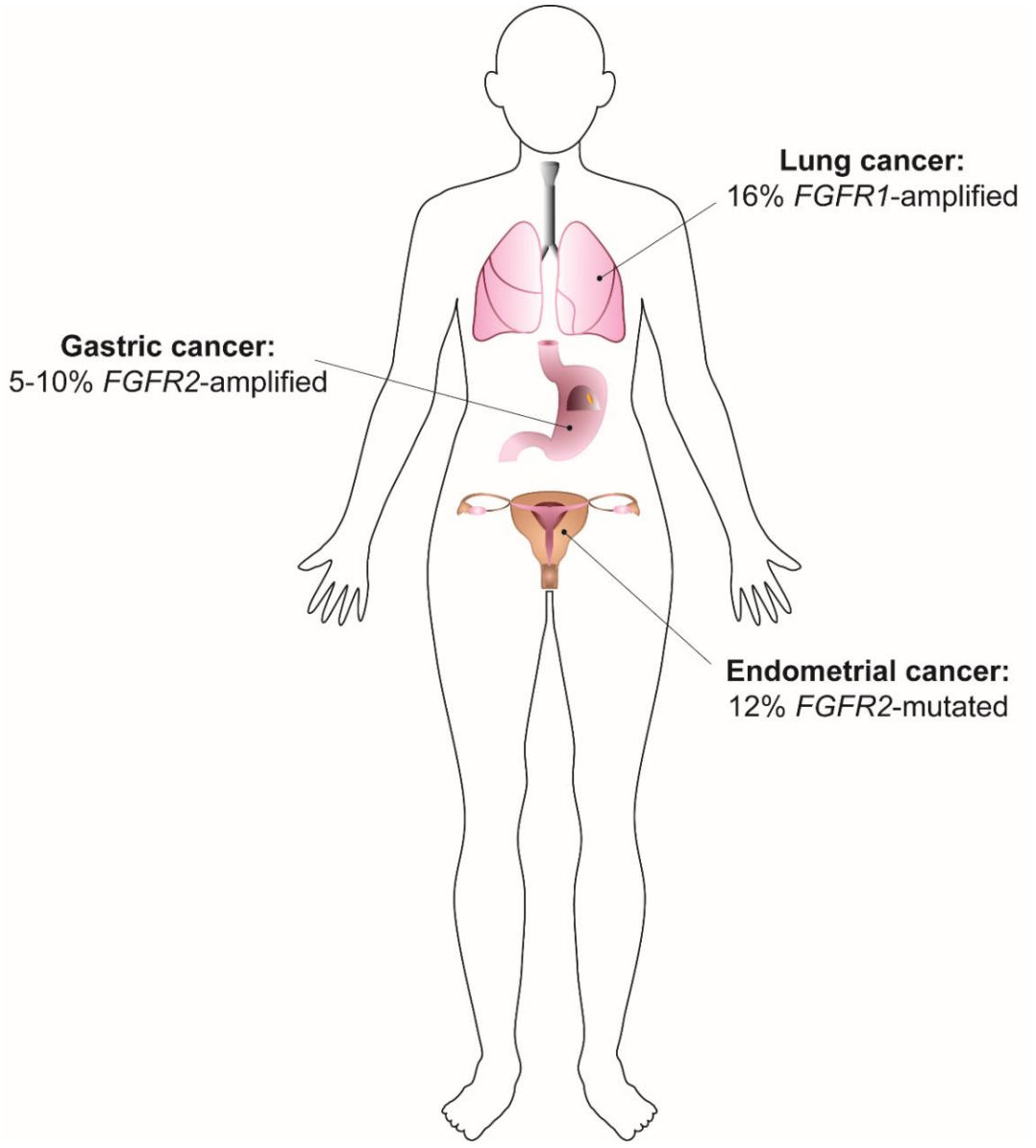

Figure 1.7. Incidence and localisation of lung, gastric and endometrial cancer with FGFR alterations. 16% of lung cancer patients harbour *FGFR1*-amplified cancers (Heist et al., 2012), whereas 5-10% are *FGFR2*-amplified in gastric cancers (Kunii et al., 2008) and 12% of endometrial cancers are *FGFR2*-mutated (Byron et al., 2008).

1.6.1 Gastric cancer

Stomach, or gastric cancer, is the third most common cause of cancer-associated deaths in the word (WHO | World Health Statistics 2018). In 2012, an estimated 951,600 stomach cancer cases and 723,100 deaths were reported (Ferlay et al., 2015). It presents a large obstacle to treat due to its difficult diagnosis and most patients only start treatment with advanced disease stage. This is due to the slow development of stomach cancer over many years, with pre-cancerous changes occurring in the inner lining (mucosa), which rarely causes any symptoms. Approximately 80-96% of stomach cancers are gastric adenocarcinomas, arising from the mucosa. Other cancers can also be lymphoma, gastrointestinal stromal tumour (GIST) or carcinoid tumours, however these are much more infrequent (Abeloff's Clinical Oncology - 4th Edition).

Gastric cancer associated risk factors are linked firstly to diet, such as food preservation, and low consumption of fresh fruits and vegetables (Karimi et al., 2014) and also *Helicobacter pylori* infection (90% of cases) (Anderson et al., 2010; Plummer et al., 2015). Early treatment and eradication of this bacterial infection could prevent the development of cancer. Gastric adenocarcinomas are extremely diverse in respect to phenotype and genetics and can be mainly distinguished into stages 0-IV based on the origin of the cancer and invasion of nearby blood vessels **(Figure 1.8)**. The stomach lining is rich in a network of blood vessels and therefore as the cancer becomes more advanced, cells can easily spread to lymph nodes or other organs such as liver, lungs and also bones. Although such cancers are highly treatable in early stages with surgery or chemotherapy, advanced stages (clinical stage IV) result in a median survival of only 9-10 months. Since the middle of the 20th century, incidence and mortality of gastric cancer have steadily declined in the West due to advances in food storage and preservation and also declining *Helicobacter pylori* infections through improved sanitation and antibiotics (Parkin, 2006). Additionally, it was observed that in countries with a large smoking population, a reduction in smoking has been associated with a reduction in gastric cancer (Bertuccio et al., 2009). Despite a decrease in overall gastric adenocarcinoma, gastric cancers of the cardia are on the rise in the Western hemisphere. This may be due to increasing obesity or also due to improved classification of gastric cancers (Camargo et al., 2011; Corley and Kubo, 2004; de

Martel et al., 2013; Devesa et al., 1998; Steevens et al., 2010). Hence, due to the heavy burden of gastric cancer and limited treatment options, advancements in treatment options are of fundamental importance.

A number of genetic changes have been observed in gastric cancers such as alterations in *p53*, *c-erbl-2*, *c-MET*, *adenomatous polyposis coil* (*APC*) and *deleted in colorectal cancer* (*DCC*) (Correa and Shiao, 1994; Stemmermann et al., 1994; Wright et al., 1992). Approximately 5-10% of stomach cancers harbour *FGFR2* amplifications (Kunii et al., 2008) and targeting those is a potential therapeutic approach. However, as with many cancers, resistance arises and in some cases this may be from epithelial to mesenchymal transition (EMT) following treatment with FGFR inhibitors (Grygielewicz et al., 2016).

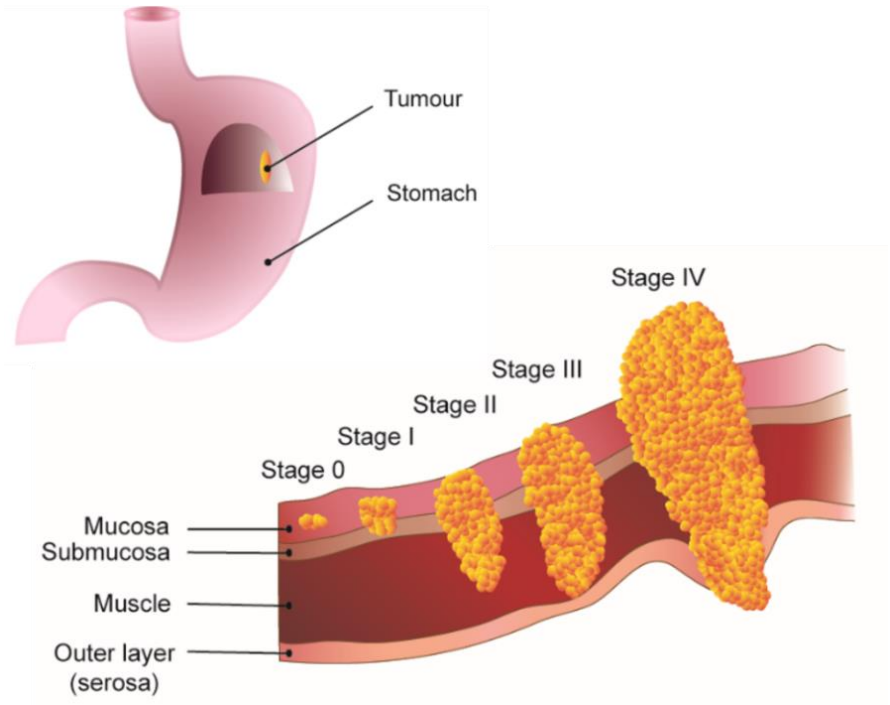

Figure 1.8. Schematic representation of gastric cancer and pathological stages.
Most gastric cancers origin in the inner lining of the mucosa in the stomach and more advanced gastric cancers can then evade the gastric lining via the bloodstream to lymph nodes and more distal organs. **Stage 0:** Carcinoma *in situ*, high grade dysplasia in the stomach lining contained within the mucosa. **Stage I:** Tumour cells have grown into surrounding layers such as the lamina propria, the muscularis mucosa and the submucosa. **Stage II:** The cancer has grown into the surrounding layers and nearby lymph nodes. **Stage III:** The cancerous cells grow into the muscularis propria or subserosa or serosa layer and nearby lymph nodes. **Stage IV:** The cancer cells grow into any layer and infiltrate blood vessels and lymph nodes, eventually forming secondary tumour sites at distant organs such as the liver, lungs, brain or peritoneum (Hu et al., 2012; Japanese Gastric Cancer Association, 1998).

1.6.2 Endometrial Cancer

In the developed world, endometrial cancer is the most common gynaecological disorder and fourth most common cancer in the female population (Byron et al., 2008; Pollock et al., 2007). In 2012, 320,000 new cases of endometrial cancer were diagnosed worldwide (Ferlay et al., 2015). Patients usually exhibit an early stage tumour restricted to the endometrium, which is the lining of the uterus, with little or no migration into adjacent tissue (Amant et al., 2005). Endometrial cancer is highly treatable with surgery, such as hysterectomy, and more than 80% of patients survive for at least 5 years after diagnosis. However, a hysterectomy can have dramatic consequences, such as oestrogen deprivation resulting in increased risk of cardiovascular syndromes (Atsma et al., 2006) and loss of fertility in patients who are pre-menopausal upon diagnosis (Lau et al., 2014; Wright et al., 2009).

Clinical innovation within endometrial cancer research has advanced compared to other cancer treatments, possibly because 75% of women are diagnosed with early disease stage (stage I or II) **(Figure 1.9)** and favourable outcomes with a 5-year survival of 75-90% (Creasman et al., 2001; Morice et al., 2016; Rose, 1996). However, in patients with later stages and higher grade tumours, the disease commonly relapses despite surgery, adjuvant radiotherapy, chemotherapy and clinical outcomes are extremely poor (Chaudhry and Asselin, 2009; del Carmen et al., 2012; Del Carmen et al., 2011; Ueda et al., 2008). Therefore, overall survival has not dramatically improved, and endometrial cancer remains one leading cause of cancer-associated deaths in women, and a greater understanding of the molecular mechanisms is essential.

There are primarily two divisions of endometrial cancer; endometrioid, which accounts for 80% and 20% non-endometrioid, which is further subdivided into serous and clear-cell carcinoma. Although non-endometrioid cancers are less common they are higher grade by definition. Long-lasting unopposed oestrogen exposure can lead to endometrial hyperplasia, which increases possibility of the emergence of atypical hyperplasia and eventually results in excessive proliferation of the endometrium (Amant et al., 2005).

There are various genetic alterations observed in endometrial cancer, such as microsatellite instability in 25-30% of cases (Catasús et al., 1998; Duggan et al., 1994) and PTEN modifications in 37-61% of cancers, which ultimately results in the dysregulation of the PI3K pathway (Yeramian et al., 2013). Furthermore, frequent mutations affect genes such as *PIK3CA* and *KRAS* (Byron et al., 2008; Yeramian et al., 2013).

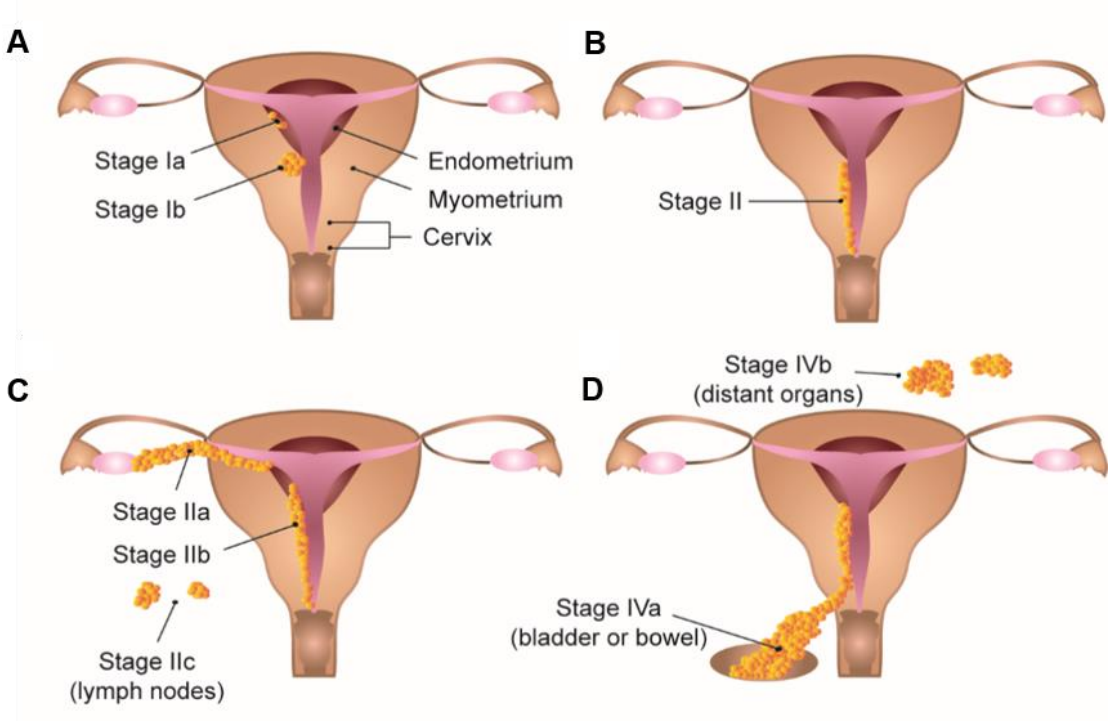

Figure 1.9. Schematic representation of endometrial cancer.
(A) Stage Ia endometrial tumours are limited to the endometrium while stage Ib tumours frequently infiltrate into the muscle wall. **(B)** Stage II tumours are characterised by invasion into the cervix. **(C)** In stage III cancer, tumour cells invade other parts of the pelvis and can be subdivided into tumours spreading to the ovaries (IIIa), into the vagina (IIIb) and those which infiltrate lymph nodes (IIIc). **(D)** The highest grade tumours are the ones that have metastasised to the bladder or bowel (IVa) or to more distant tissues (IVb). The surgical stage of tumours reflects the five year survival rate of approximately 85% for stage I, 75% for stage II, 45% for stage III and 25% for stage IV (Amant et al., 2005).

FGFR2 mutations have been found in approximately 12% of endometrial cancers (Byron et al., 2008). These point mutations act as oncogenic drivers, with S252W and N550K being the most common mutations. These mutations were shown to affect FGF binding affinity and lead to constitutive receptor activation, respectively (Pollock et al., 2007). Knockdown of FGFR2 in endometrial cell lines (MFE-296, AN3CA, MFE-280) expressing FGFR2 activating mutations, resulted in decreased cellular proliferation and survival, compared to FGFR2 wild-type cell lines (Dutt et al., 2008), suggesting a dependence of those endometrial cancers on *FGFR2* mutations. FGFR inhibitors can be used to block growth of such cancers, as observed with the TKI inhibitor PD173074 (Byron et al., 2008). Currently, other means to target FGFR-driven cancers are in clinical development, such as TKI inhibitors with varying specificity, monoclonal antibodies and ligand traps **(Figure 1.11, Table 1.2)**.

In recent studies within our lab, down-regulation of PHLDA1 was identified as a critical factor in the establishment of resistance to FGFR targeting. Upon FGFR2 inhibition, PI3K signalling is decreased and, as a compensatory mechanism, PHLDA1 expression is diminished. Since the normal role of PHLDA1 in the cell is to buffer AKT signalling by competing for PIP_3 binding, although PI3K signalling is decreased, AKT signalling can be kept constant, since there is reduced competition with PHLDA1 for free PIP_3 binding sites (Fearon et al., 2018). The identification and dissection of the mechanism of action is of utmost importance in providing greater insights into the establishment and circumvention of drug resistance and finding new targetable nodes.

1.6.3 Lung cancer

Lung cancer is abnormal growth of respiratory epithelial cells and is the major cause of cancer-related deaths worldwide, causing an estimated 1.8 million new cases and 1.59 million deaths in 2012, which accounts for 12.9% of all new cancer diagnoses (Ferlay et al., 2015). Even in developed countries, survival is low and lung cancer mortality rates are generally similar to incidence rates.

The incidence and mortality of lung cancer increases with age and 5-year survival rates for lung cancer are very low, with 7.8% for men and 9.3% for women. This is due to the fact that 70% of lung cancers are diagnosed at advanced stages when treatment is less successful (Siegel et al., 2012).

The major risk factor for lung cancer development is smoking and lung cancer developments have been heavily shaped by tobacco use (Doll et al., 2005; Doll and Hill, 1950; Jemal et al., 2008; Thun et al., 2012). More than 50 carcinogens have been identified in tobacco smoke, with polynuclear aromatic hydrocarbons (PAHs) and tobacco-specific N-nitrosamines (TNSAs) being the most important (Hoffmann and Hoffmann, 1997; Shields, 2002). Death rates have dramatically decreased by 45% since 1990 in men and 19% in women since 2002, due to a decline in smoking.

Other risk factors for lung cancer development are exposure to carcinogens such as radiation of radon (miners), asbestos exposure, or microscopic particles such as silica, wood dust and indoor and outdoor air pollution (Alberg et al., 2002; Spyratos et al., 2013; Turner et al., 2011; Vineis et al., 2004). Furthermore lifestyle, diet and genetics have been connected to the development of lung cancer (Alavanja et al., 1996; De Stefani et al., 1997; Ruano-Ravina et al., 2003, 2000; Swanson et al., 1997). Gender and race were also factors associated with a higher incidence in lung cancer, where women are more affected than men, and African Americans exhibit higher risks than European men (Gasperino, 2011; Gasperino and Rom, 2004; Harris et al., 1993; Jemal et al., 2009; Schabath et al., 2016). Socioeconomic status and geographic location may also have implications (Parkin et al., 2005).

According to the WHO classification, lung cancer is subdivided into small cell lung cancer (SCLC), which makes up nearly 18% of tumours and NSCLC such as squamous cell carcinoma (SCC), adenocarcinoma (ADC) and large cell carcinoma (LCC) accounting for 78-80% of lung cancers (Travis, 2011). Lung cancer can be divided into four stages (Stage I-IV) **(Figure 1.10)**.

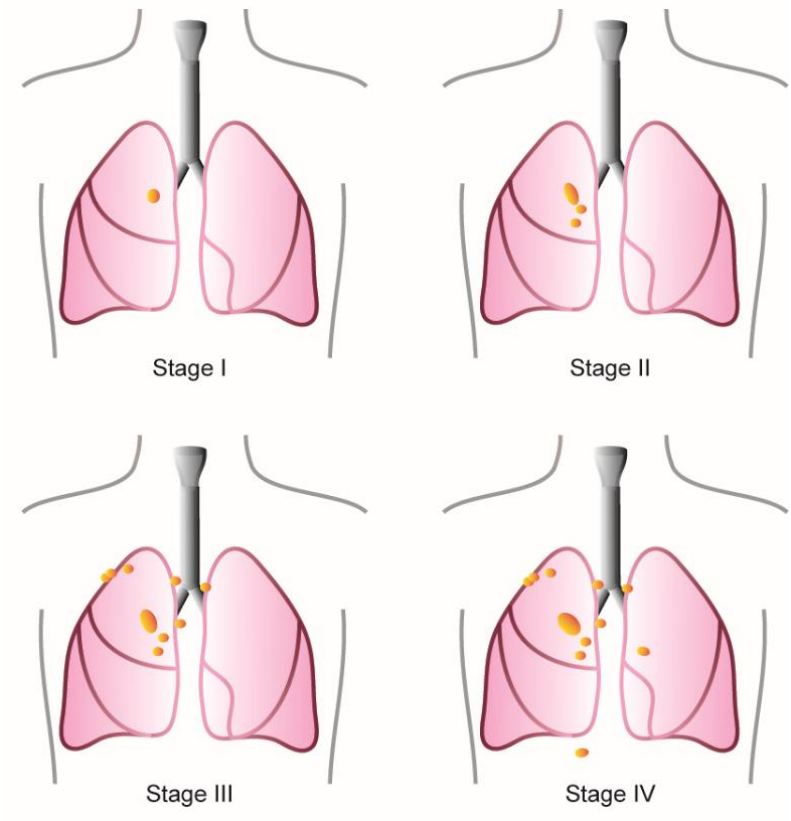

Figure 1.10. Schematic representation of lung cancer.
Lung cancer can be divided into four stages. **Stage I:** Cancer cells are present in the underlying lung tissues. **Stage II:** The cancer may have spread to nearby lymph nodes or into the chest wall. **Stage III:** The cancer cells are spreading from the lungs to the lymph nodes or to nearby structures and organs, such as the heart, trachea and oesophagus. **Stage IV:** There is metastasis throughout the body and may affect the liver, bones or brain. When NSCLC has spread outside of the lungs, successful treatment can be difficult. The 5-year survival rate for stage IV NSCLC is around 1% (Beadsmoore and Screaton, 2003).

In recent years with better classification methods, advances in the development of targeted therapy towards oncogenes and activated pathways in different lung cancer types was achieved (Larsen and Minna, 2011). Such oncogenic modifications are mutations in Epidermal Growth Factor Receptor (EGFR) or amplifications in *c-MET* resulting in resistance towards EGFR inhibition (Engelman et al., 2007; Kosaka et al., 2011). *KRAS* is commonly mutated in lung cancers and, as RAS is activated downstream of EGFR, it is likely that they are EGFR-inhibitor resistant (Petersen, 2011; Toyooka et al., 2011). *FGFR1* amplifications have been reported in up to 16% of lung cancers (Heist et al., 2012). It has also been observed that expression of FGFR1 and its ligand FGF2 was upregulated in NSCLC, providing an escape mechanism for cell survival of cancers that are resistant to Afatinib (Azuma et al., 2014).

1.7 Targeted therapeutics

FGF signalling represents an attractive therapeutic target in cancer, due to its function in cellular crosstalk, proliferation, anti-apoptosis, angiogenesis, EMT, invasion and drug resistance, and the frequency of FGFR alterations in a wide variety of cancers (Heinzle et al., 2011; Katoh and Katoh, 2009; Korc and Friesel, 2009; Nilsson et al., 2010; Ota et al., 2009). Many studies have proven pre-clinical efficacy of FGFR-targeted therapy in cancer cells, with reductions in proliferation or invasion in cancers (André et al., 2013; Byron et al., 2008; Chioni and Grose, 2012; Coleman et al., 2014; Grygielewicz et al., 2016; Nogova et al., 2017; Saka et al., 2017; Tabernero et al., 2015; Zhang et al., 2012). However, even specific FGFR inhibitors have off-target effects, which presents difficulties in successful treatment (Gudernova et al., 2016; Mohammadi et al., 1998). Due to the importance of FGFRs in numerous pathologies, a range of treatment options, including kinase inhibitors, ligand traps and antibodies have been and are currently in development **(Figure 1.11)**. The compounds, which are currently in the pipeline for FGFR-targeted treatment, are listed in **Table 1.2**.

1.7.1 Kinase inhibitors

The most clinically advanced FGFR therapeutics to date are multi-kinase inhibitors, which target the kinase domain of receptors, thereby preventing downstream signalling. There are a number of kinase inhibitors currently in clinical trials (Chen et al., 2005; Machida et al., 2005; Matsui et al., 2008; Sarker et al., 2008), each of which are small molecule inhibitors, which bind to the ATP-binding pocket of the kinase domains with differing affinities. Thus, there are broad range multi-kinase inhibitors but also more specific FGFR-directed inhibitors (Zhang et al., 2009). Broad range inhibitors are usually weak against FGFR-driven cancers, thus there is a shift on the focus to more specific FGFR-targeting inhibitors.

The Vascular Endothelial Growth Factor (VEGF) receptor and FGFR kinase share high structural similarity and several VEGFR kinase inhibitors also inhibit FGFR and *vice versa*. Inhibiting both VEGFR and FGFR has the advantage that two pro-angiogenic pathways or angiogenesis and proliferation are targeted simultaneously, however many tyrosine kinase inhibitors (TKI) that affect multiple targets are less

active towards FGFRs and the clinical outcome is unreliable. It can also have cumulative effects on the advent of side effects, limiting the deliverability of the drug to achieve doses necessary to inhibit FGFR. Ponatinib is a broad-reaching TKI that has shown a dismal toxicity profile and was withdrawn for the treatment of chronic myeloid leukaemia (CML) due to a high proportion of patients developing arterial and venous thromboses (Cortes et al., 2013; Gainor and Chabner, 2015). Thus, pharmaceutical companies aim to develop FGFR specific inhibitors, which has been complicated by hyperphosphatemia-mediated tissue calcification due to blockade of the release of FGF23 from bone and its signal in the kidney (Brown et al., 2005). Kinase inhibitors such as Dovitinib and Lucitanib, although also having off-target effects, have shown potent effects in clinical trials with patients who harbour *FGFR* amplifications, compared to those that do not (André et al., 2013; Soria et al., 2014). PD173074 is an FGFR inhibitor with weak affinity towards other tyrosine kinases, however due to poor pharmacokinetics this drug is only used as a tool compound to investigate FGFR-inhibitor mediated effects (Knights and Cook, 2010). Treatment with PD173074 resulted in cell death and cell cycle arrest in endometrial cancer cell lines (Byron et al., 2008) and is connected to the inhibition of both FGFR1 and FGFR2 transphosphorylation. PD173074 also impaired cell proliferation in a small cell lung cancer model, in cell lines and in xenograft tumours (Pardo et al., 2009).

Other kinase inhibitors, such as AZD4547 and BGJ398, currently in phase II clinical trials for solid tumours, are more promising compounds (Clinicaltrials.gov, 2018). These small molecules selectively inhibit FGFR1, 2 and 3, resulting in growth reduction and apoptosis, especially in cancers with known FGFR alterations. Nevertheless, as was observed with other kinase inhibitors, off-target effects such as activity towards VEGFR2 follow at high concentrations (Gavine et al., 2012; Guagnano et al., 2011).

1.7.2 Orthosteric receptor binding

While small molecule kinase inhibitors remain the most clinically advanced FGFR-targeted therapeutics, other methods such as antibody-based approaches were developed by targeting specific receptor isoforms. Antibodies are supposed to be more specific to particular FGFRs and therefore could potentially limit pan-FGFR inhibition toxicity. For example, GP369, an anti-FGFR2IIIb antibody, has been investigated both *in vitro* and *in vivo* and shown to suppress the IIIb isoform in FGFR2-amplified breast and gastric cancer cell lines (Nord et al., 2010) and has revealed promising results in animal models where the growth of xenograft tumours with *FGFR2* mutations was reduced in GP369-treated mice (Bai et al., 2010). Moreover, an FGFR3 antibody, MGFR1877S, was in phase I clinical trials for multiple myeloma and advanced solid tumours (Carter et al., 2015, Clinicaltrials.gov, 2018). Beyond cancer therapy, antibody-based approaches have been applied, for example with KRN23, which is an anti-FGF23 antibody currently in phase II trials for X-linked hypophosphatemia (Carpenter et al., 2014).

1.7.3 Allosteric receptor binding

More recently, allosteric receptor inhibitors have been described and the allosteric inhibitor SSR128129E has been found to decrease cancer progression and inflammation using a mouse model of pancreatic cancer and an arthritis model (Bono et al., 2013). Furthermore, it has not shown signs of vascular side effects in the mice. SSR128129E does not compete with FGFs for FGFR binding but inhibits FGF-induced signalling by allosteric blockade through the formation of an FGF:FGFR complex that cannot be internalised and hence limits signalling. The use of this drug could therefore present a potent alternative to the use of TKIs (Herbert et al., 2013, 2016).

1.7.4 Ligand traps

In another approach, FGF-ligand trap antibodies such as FP-1039 (GSK3052230), have been developed to inhibit ligand binding to the receptor (Harding et al., 2013). It consists of an extracellular portion of FGFR1c fused to the Fc domain of IgG1 and allows targeting of mitogenic FGF ligands, without affecting hormonal FGFs. This approach reduces toxicity while still being active towards tumours observed in lung and endometrial cancer models (Harding et al., 2013). This trap acts as an FGF 'sponge' by binding multiple FGFs, resulting in anti-proliferative and anti-angiogenic effects. It has demonstrated efficacy *in vitro* and *in vivo* in a phase I clinical trial in patients with advanced solid tumours (Tolcher et al., 2016). This mode of action may be beneficial for the treatment of pathological FGF-stimulated activation of FGFRs; however, it is not suitable to treat tumours with kinase aberrations which result in constitutive activation of receptor signalling.

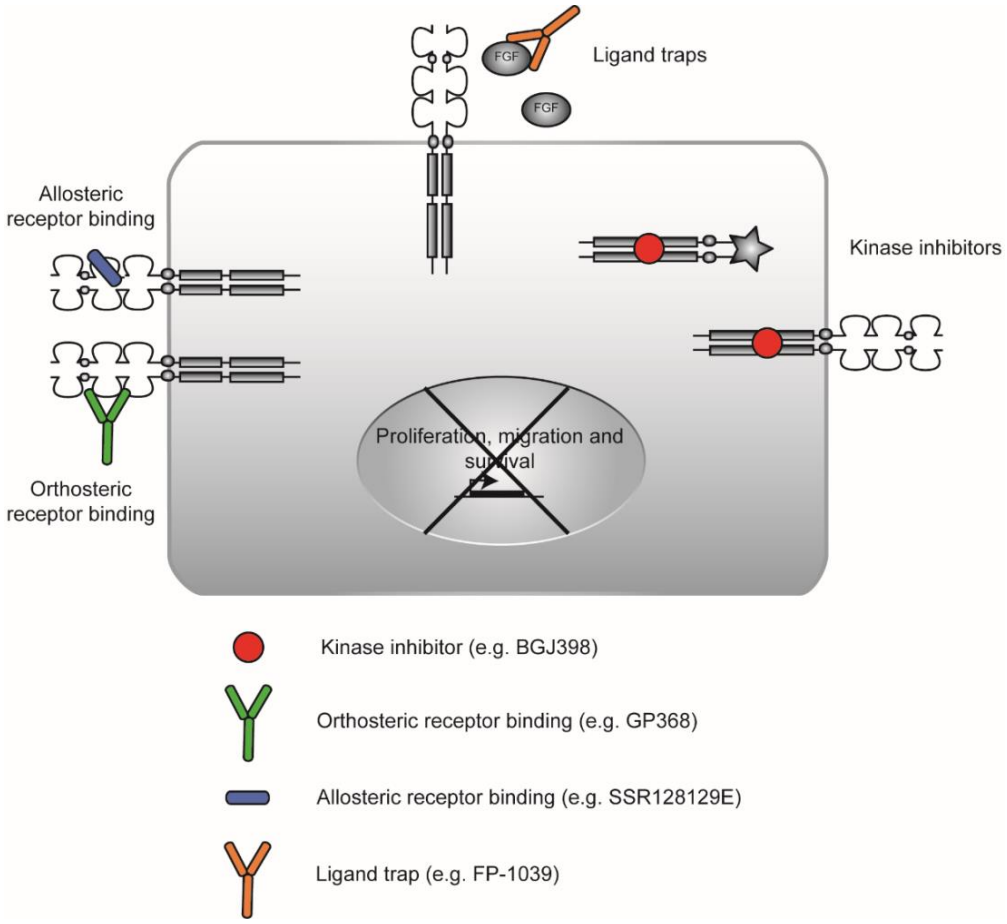

Figure 1.11. Therapeutic approaches for targeting FGFR signalling.
Illustration of the different therapeutic categories. Kinase inhibitors (red circles) represent the most numerous drugs. Other approaches include orthosteric antibody-based therapies to block receptor binding (green), ligand traps (orange) and allosteric inhibitors (blue) (Tanner and Grose, 2016).

Table 1.2. The FGFR-targeting compounds in the development pipeline.
Current status of therapeutics aiming at the FGF signalling pathway, describing the drug type, specificity, developmental status and target cancers. The colour code of the compounds refers to the class of therapy, as shown in **Figure 1.11**. Clinical status and indications are based on information from clinicaltrials.org, and information is correct as of July 2015 (Tanner and Grose, 2016).[1]

Compound	Manufacturer	Target	Status	Cancer type
Multi TKI inhibitors				
Ponatinib (AP24534)	Ariad Pharma	FGFR, PDFGR, VEGFR	Approved Phase II	CML, AML
Nintedanib (BIBF1120)	Boehringer Ingelheim	FGFR, PDGFR, VEGFR	Submitted Phase III	HCC
Lenvatinib (E7080)	Eisai	FGFR, PDGFR, VEGFR	Submitted Phase II/III	Thyroid, HCC, endometrial, melanoma, glioma, NSCLC
Orantinib (TSU-68)	Taiho Pharma	FGFR, PDGFR, VEGFR	Phase III	HCC
Lucitanib (E3810)	Clovis Oncology/ Servier	FGFR1, VEGFR	Phase I/II	ER+ Breast cancer, multiple solid tumours
Dovitinib (TKI258)	Novartis	FGFR, PDGFR, VEGFR, FLT3, c-KIT	Phase II	Multiple cancers including endometrial and breast
Brivanib (BMS-582664)	Bristol-Meyers Squibb	FGFR, VEGFR	Phase III	HCC
ENMD-2076	CASI Pharma	FGFR1-2, PDGFR, VEGFR, FLT3, c-KIT, Aurora Kinase	Phase I/II	Breast, ovarian
ARQ 087	ArQule	FGFR	Phase I	Multiple solid tumours
FGFR-specific TKI inhibitors				
AZD4547	Astra Zeneca	FGFR1-3	Phase II	Multiple solid tumours
BGJ398	Novartis	FGFR1-3	Phase II	Multiple solid tumours, melanoma
LY2874455	Eli Lilly	FGFR1-4	Phase I	Multiple solid tumours
Debio 1347	Debiopharm	FGFR1-3	Phase I	Solid tumours
TAS-120	Taiho Pharma	FGFR1-4	Phase I/II	Solid tumours, multiple myeloma
JNJ42756493	Astex pharma/ Janssen	FGFR1-4	Phase I	Solid cancers, lymphoma, urothelial
FGFR antibodies				
MGFR1877S	Genentech/ Roche	FGFR3	Phase I	Solid tumours, multiple myeloma
SSR128129E	MedKoo Biosciences	FGFR1	Preclinical	Only mouse tumour models
FGF traps				
FP-1039 (GSK3052230)	Five prime therapeutics/ GSK	FGF1, FGF2, FGF4	Phase I	Solid tumours

[1]Abbreviations: AML: acute myeloid leukaemia; CML: chronic myeloid leukaemia; ER+: oestrogen receptor positive; HCC: hepatocellular carcinoma; NSCLC: non-small cell lung cancer. Red: Kinase inhibitors, Green: Blocking antibodies; Blue: Allosteric inhibitor; Orange: Ligand traps.

Within my project, three different FGFR inhibitors, PD173074 (PD), AZD4547 (AZD), and NVP-BGJ398 (BGJ) have been used **(Figure 1.12)**, all of which display different kinase affinities. PD, which inhibits both VEGFR and FGFR, is classified as a broader kinase inhibitor compared to AZD, which is currently in phase II clinical trials for lung cancer (Gavine et al., 2012), gastric and oesophagogastric cancers with *FGFR2* amplifications (Smyth et al., 2013). It has been shown to target FGFR1-3, resulting in apoptosis and growth inhibition in FGFR-driven cancers. However it has been found to have off-target effects against VEGFR2, Insulin-like growth factor (IGF), PI3K and AKT, although these are lower than the effect on FGFR (Wheeler and Yarden, 2015).

BGJ is a selective FGFR1-3 inhibitor in phase II clinical trial and has been shown to have an effect in *FGFR1*-amplified squamous NSCLC, but also *FGFR3*-amplified bladder cancer, *FGFR2*-fused cholangiocarcinoma, and *FGFR1*-amplified breast cancer (Sequist et al., 2014).

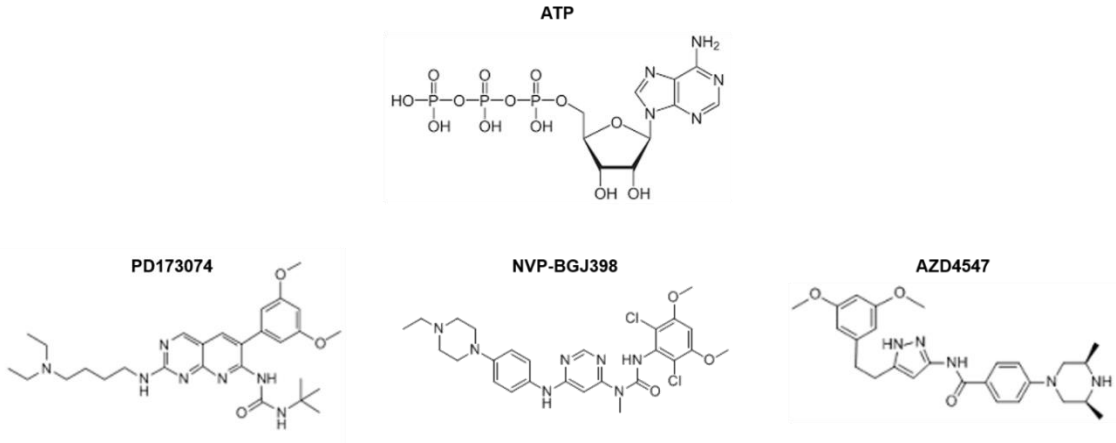

Figure 1.12. Structure of ATP and three FGFR inhibitors PD173074, NVP-BGJ398 and AZD4547.
The FGFR inhibitors shown are pyrazoloamide derivatives, which compete with ATP for binding to the ATP-binding pocket of the FGFR, causing inhibition of FGFR-induced signalling (Gavine et al., 2012; Mohammadi et al., 1998).

1.8 Resistance to targeted therapy in cancer

The targeting of specific oncogenic signalling pathways in tumours with specific molecular alterations has led to personalised medicine in cancer therapy, where drugs target those specific molecular alterations. However due to the heterogeneity of cancer cells and the unique genetic landscape, the response to cancer therapies differs greatly and resistance to both common cytotoxic chemotherapeutics and also targeted therapies has been observed (Holohan et al., 2013).

The development of drug resistance poses a major obstacle towards successful treatment of cancer patients and occurs with all commonly used cancer chemotherapeutics. This can be due to cancer cells already being innately resistant or due to them acquiring resistance during disease progression following treatment. There are a multitude of ways cancer cells can acquire resistance towards therapeutics. This is important for different types of cancers and many patients with advanced disease relapse due to resistance (Chaudhry and Asselin, 2009; Gnanamony and Gondi, 2017; Manzano et al., 2016; Marin et al., 2016; Shanker et al., 2010; Shi and Gao, 2016; Zhang and Fan, 2007). To overcome and inhibit the advent of drug resistance, a thorough understanding of the mechanisms of the process is required.

There are physiological factors involved in drug resistance, such as impaired drug delivery due to weak vascularisation of large tumours, where there is limited drug diffusion (Galmarini et al., 2000). Slow growing tumours have shown to be less sensitive towards chemotherapy as common chemotherapeutic agents are designed to target cells proliferating at a faster rate (Kondoh et al., 2010; Ramirez et al., 2016).

Heterogeneity is the natural formation of different variants through genetic, epigenetic and transcriptomic properties. Genomic instability can generate a great level of intercellular heterogeneity in cancers and, during progression, cancers can become even more heterogeneous (Gerlinger et al., 2012; Heppner, 1984). The tumour contains a collection of cells with distinct molecular signatures and thus different levels of sensitivity towards drugs (Dagogo-Jack and Shaw, 2018). Intrinsic factors may arise through primary genotypic variations, different cell cycle stages, stochastic

variations and hierarchical organisation according to the stem cell theory (Plaks et al., 2015). Extrinsic factors encompass pH, hypoxia and paracrine signalling interactions with other cancer or stromal cells (Fluegen et al., 2017; Gupta et al., 2011; Kreso et al., 2013; Nathanson et al., 2014).

Studies using *in vitro* resistance models and generating resistant cells, have allowed comparison with drug sensitive parental cell lines and have revealed several cellular mechanisms by which cancer cells can acquire resistance. Such mechanisms are reductions in drug accumulation, availability of the active drug in the cells, efficacy of the drug on cellular targets and pro-survival signals which aid cells to evade apoptosis (Giaccone and Pinedo, 1996; Longley and Johnston, 2005).

A common way of acquiring resistance is the upregulation of efflux proteins, so that drugs are pumped out of the cell before they can inhibit their target (Gottesman, 2002) **(Figure 1.13)**. The drug uptake process is not well understood; however, transporters were identified and implicated in drug trafficking. Accelerated drug efflux can be mediated by P-glycoprotein (P-gp), which belongs to the family of ATP-binding cassette (ABC) transporters. P-gp was first observed in cells resistant to broad spectrum drugs such as taxanes, vinca alkaloids, anthracyclines and methotrexate (Gottesman, 2002; Polgar and Bates, 2005). In acute myeloid leukaemia (AML), approximately 30% of patients express P-gp when they are diagnosed, however when patients relapse P-gp upregulation is detected in 50% of patients. Furthermore, P-gp expression is associated with a reduced rate of complete remission and a higher risk for the emergence of resistance (Gottesman, 2002; Leith et al., 1999). P-gp is also expressed in the gastrointestinal tract, where it minimises oral bioavailability of drugs (Kagan et al., 2010; Zhou, 2008).

Cancer cells can become insensitive to a drug due to cell cycle stage. Thus, a chemotherapeutic drug can impact the cell cycle, thereby lessening the effect of other chemotherapeutic agents. Cell damage induces cell death and is mediated by three fundamental events: necrosis, apoptosis and autophagy. Apoptosis plays an important role in animal development and tissue homeostasis (Galluzzi and Kroemer, 2008; Jacobson et al., 1997; Oberst et al., 2008). It has been typically divided into the intrinsic pathway mediated by mitochondria and the extrinsic pathway mediated by death receptors on the cell membrane. Apoptosis by these two pathways results in activation of the family of cysteine aspartyl-specific proteases (caspases) (Ashkenazi and Dixit, 1998; Hengartner, 2000; Pradelli et al., 2010). The internal pathway begins in mitochondria and involves BCL2 and AKT, anti-apoptotic proteins, and Bax, Bak and caspase-9, pro-apoptotic proteins. Most anti-cancer drugs have been shown to induce classical apoptosis and defects in proteins involved in apoptosis are associated with resistance to anti-cancer therapies. For example, overexpression of anti-apoptotic genes (e.g *Bcl-2*, *Bcl-Xl*), expression of soluble death receptors, and inactivation of pro-apoptotic genes through downregulation or mutation (Igney and Krammer, 2002). Furthermore, mutations in the tumour suppressor p53 can result in drug resistance by inhibiting activation of apoptosis, and treatment with DNA damaging alkylating agents has been associated with incidence of p53 mutations in patients and could explain resistance to second line chemotherapeutics (Sturm et al., 2003).

Changing drug metabolism plays an important role in drug resistance. It consists of phase I reactions such as oxidation, reduction and hydrolysis or phase II reactions, such as consumption and conversion. These reactions reduce the activation of pro-drugs and induce drug inactivation. Cancer cells can use this to their advantage by increasing detoxification with the help of cytochrome P450 (phase I) or glutathione transferases (phase II) and therefore become drug resistant (Longo-Sorbello and Bertino, 2001).

Importantly, when therapeutics are dependent on modifications, such as mutations or changes in expression levels of targets, this will eventually result in drug resistance. Intrinsic or acquired resistance can be caused by mutations in the kinase domain that alter the conformation of the receptor and therefore modify drug binding (Byron et al., 2013). Gatekeeper mutations are most frequently secondary mutations in connection with resistance to TKIs (Antonescu et al., 2005; Branford et al., 2002; Chell et al., 2013; Gounder and Maki, 2011; Heinrich et al., 2003, 2008; Mauro, 2006; Sleijfer et al., 2007; Van Glabbeke et al., 2005). ATP-competitive small molecule kinase inhibitors can no longer bind to the ATP-binding pocket by steric inhibition induced by the gatekeeper mutation. Normally TKIs form a hydrogen bond with the residue where the gatekeeper mutation occurs allowing the inhibitor to enter the hydrophobic pocket and inhibit receptor activation. However, in a gatekeeper mutation the residue is substituted with a larger hydrophobic residue and sterically obstructs the hydrophobic cleft and the inhibitor can no longer inhibit the receptor (Byron et al., 2013). It has been found that the V565I gatekeeper mutation in FGFR2 inhibits Dovitinib in a similar manner (Byron et al., 2013).

Resistance towards Gefitinib is often associated with a threonine-to-methionine substitution at amino acid position 790 (T790M) of EGFR (Politi et al., 2010). It was also frequently encountered in patients already intrinsically resistant towards Gefitinib (Girard et al., 2010; Inukai et al., 2006; Mok et al., 2009). The existing hypothesis postulates that in patients who respond initially to Gefitinib, a small proportion of tumour cells with the resistance mutation already exist and are enriched upon Gefitinib treatment (Inukai et al., 2006).

The emergence of resistance in Vemurafenib-treated patients is one of the clearest examples of mutation-induced drug resistance (Davies et al., 2002; Flaherty et al., 2010). Half of all melanoma patients harbour a mutation in the serine-threonine protein kinase BRAF, of which 90% carry the V600E mutation resulting in constitutive activation of the target protein, activating the downstream MAPK pathway. Vemurafenib is a small molecule inhibitor targeted at V600E mutant BRAF (Tsai et al., 2008). Initially, in clinical trials, excellent results were observed, with 80% of

patients showing complete or partial regression (Flaherty et al., 2010). Nevertheless, the duration of the response only lasted 2 to 18 months, after which resistance to the drug was acquired (Flaherty et al., 2010). Several mechanisms have been identified by mutation profiling, such as activating mutations in MEK1 (Wagle et al., 2011), increased expression of MAP3K8 (Johannessen et al., 2010), activation of CRAF (Montagut et al., 2008) and up-regulation of platelet derived growth factor receptor β (PDGFRβ) (Nazarian et al., 2010). All of these modifications eventually lead to activation of the MAPK pathway, consequently circumventing BRAF inhibition. Studies with mouse models suggest that cyclical treatment with the drug could delay emergence of resistance and thus possibly extend patient life. With the help of *in vivo* studies, mice were implanted with BRAF mutant tumour cells and sequentially treated with the drug for four weeks followed by drug removal for two weeks. The control mice that were continuously dosed developed tumours, however sequentially treated mice did not (Das Thakur et al., 2013). This again suggests tumour heterogeneity to be responsible for a selective advantage giving rise to drug resistance, and suggests that acquired drug resistance comes at a cost to cell fitness.

Other important gatekeeper mutations observed in drug-resistant cancers have been identified in BCR-ABL (Young et al., 2006), FLT3 (Smith et al., 2015), FGFR1 (Liang et al., 2017) and FGFR2 (Byron et al., 2013; Goyal et al., 2017). Mutations in FGFR gatekeeper residues, as seen in FGFR4, were linked to embryonal rhabdomyosarcoma and neuroendocrine breast carcinomas (Ang et al., 2015; Shukla et al., 2012). Many cancers with aberrations along the FGF signalling axis have shown sensitivity towards FGFR inhibitors (Desai and Adjei, 2016; Katoh, 2016), however a number of cancer cells display intrinsic resistance (Byron et al., 2013). The FGFR V561M mutation was described to cause resistance to PD and FIIN-1. Similarly, the gatekeeper mutation, V555M, in FGFR3 in KMS-11 myeloma cells is suggested to induce resistance upon treatment with FGFR inhibitor AZ12908010 but also crossreacts with other FGFR inhibitors (Zhou et al., 2010).

Studies in gastric cancer suggest that FGFR-inhibitor resistant cells undergo EMT and this could be overcome by potential combination therapies by blocking avian

erythroblastosis oncogene B (ErbB)/ human epidermal growth factor receptor 2 (HER2). Also, in FGFR3-dependent bladder cancer cells, EMT has been observed with a change in signalling from FGFR3 to ErbB2/3 (Wang et al., 2015).

Co-activation of anti-apoptotic pathways causing enhanced survival is often observed in cancer cells, with deregulation of the PI3K/AKT pathway, which plays an important role in proliferation and apoptosis (Goltsov et al., 2011). This pathway has been suggested as a therapeutic target in chemoresistance and administration of Doxorubicin in combination with PTEN overexpression induced apoptosis in endometrial cancer cells (Wan et al., 2007) .

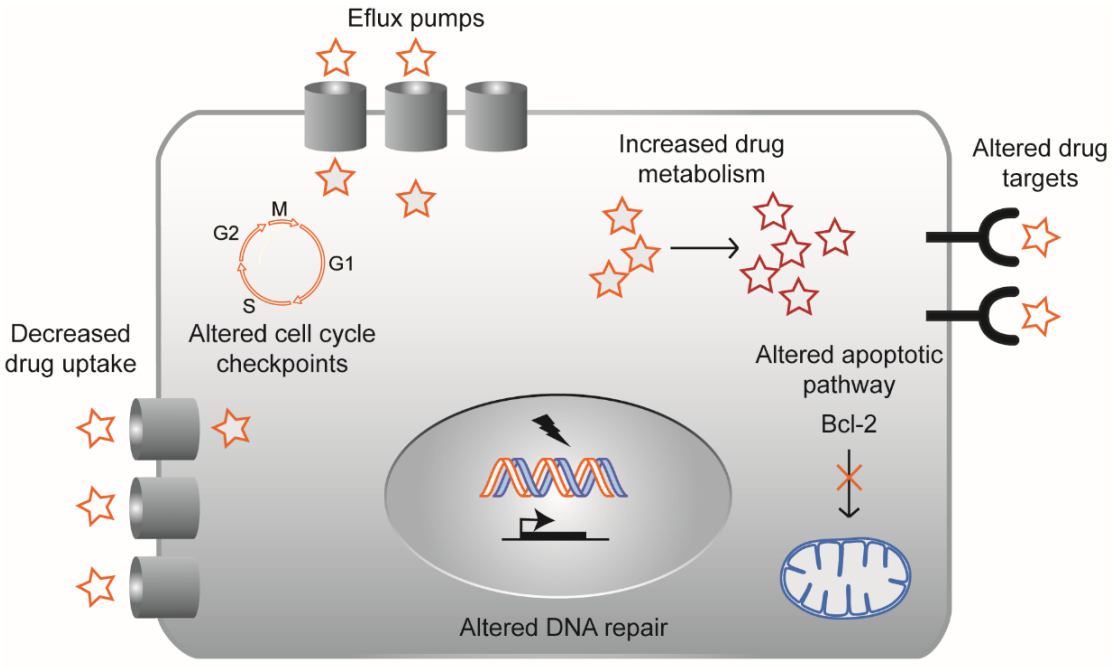

Figure 1.13. Drug resistance mechanisms in cancers.
Cancers can become resistant to therapeutics by activated efflux pumps, decreased drug uptake, altered cell cycle checkpoints, increased drug metabolism, altered apoptotic pathway and altered drug targets (Barouch-Bentov and Sauer, 2011; Housman et al., 2014; Kapse-Mistry et al., 2014).

Another common resistance mechanism is the activation of downstream signalling pathways such as gene aberrations in the MAPK pathway (Phipps et al., 2013). *RAS* mutations have been discovered in a multitude of pathologies and arise in 30% of all cancers (Eser et al., 2014; Fernández-Medarde and Santos, 2011; Nandan and Yang, 2011; Reifenberger et al., 2004). RAS proteins are small GTPases such as HRAS, NRAS and KRAS, which regulate a multitude of pathways including the MAPK and PI3K/AKT signalling pathways. KRAS G12D mutation is often found in lung and pancreatic ductal adenocarcinomas (PDAC) (Jackson et al., 2001; Zorde Khvalevsky et al., 2013). KRAS mutations have been associated with EGFR-inhibitor resistance in patients with lung adenocarcinoma (Pao et al., 2005) and also resistance to EGFR antibodies (Panitumumab and Cetuximab) in colorectal and squamous cell carcinomas of the head and neck (SCCHN) (Di Fiore et al., 2007; Lièvre et al., 2006; Mehra et al., 2011).

The PI3K/AKT pathway is an important pathway downstream of tyrosine kinase signalling and has been linked to resistance in a number of cancers. Also *PIK3CA* mutations are associated with resistance to EGFR inhibitors such as Erlotinib and Gefitinib and also poor survival in patients with NSCLC (Ludovini et al., 2011). There is evidence that suggests cross-talk between the MAPK and PI3K/AKT signalling pathways and their association with drug resistance to targeted therapeutics (Grant, 2008). Inhibition of the PI3K/AKT pathway using an mTOR inhibitor activates ERK, suggesting a feedback loop between mTORC1 and MAPK signalling (Rozengurt, 2014). Combination treatment targeting MEK/ERK and mTOR has shown to improve anti-tumour effects in a number of preclinical cancer models (Carracedo et al., 2008; Grant, 2008). Similarily, in FGFR3-driven cancers, activation of ErbB2/3 induced EMT combined with a switch from FGFR3 to ErbB dependency via increased ErbB-2/3 ligand production. Therefore, dual inhibition of the pathways involved, suggests beneficial effects to treat such cancers (Wang et al., 2015). Combination treatment of FGFR2 mutant gastric cancer with Mubritinib or AUY922 was also suggested in drug resistant cancer (Grygielewicz et al., 2016). Also in Imatinib-resistant GIST with elevated FGF2 ligand production through MAPK activation, combination treatment with c-KIT and FGFR3 inhibitors blocked tumour growth (Javidi-Sharifi et al., 2015).

Tumour heterogeneity is strongly influenced by the tumour microenvironment and *vice versa*. It is suggested that the tumour microenvironment can render cancer cells more adaptive (Casciari et al., 1992; Gatenby et al., 2007). There is growing evidence of the role the tumour microenvironment plays in cancer progression and physiology but also in the emergence of drug resistance (Correia and Bissell, 2012; Fang et al., 2008; Mumenthaler et al., 2015). The interaction between cancer cells, but also between cancer cells and stromal cells or ECM, and several other factors such as cytokines and growth factors, are all thought to have implications on the emergence of drug resistance. This is possibly induced by providing additional signals for tumour proliferation and survival (Dalton, 2003; Hazlehurst et al., 2003; Li and Dalton, 2006). The tumour microenvironment can protect cancer stem cells by acting as a therapeutic barrier and therefore shields them from being targeted efficiently, thus allowing the tumour to reoccur (Klemm and Joyce, 2015). The effect of stromal cells has also been found to play a role in drug resistance in oesophageal squamous cell carcinoma, where stromal cells could attenuate the effect of Lapatinib inhibiting the ErbB pathway by upregulating FGFR and c-MET signalling (Saito et al., 2015).

In order to study the influence of stromal cells on cancer cell signalling and impact on the formation of drug resistance, suitable cell biology models have to be established. These models should preferably be as representative as possible of the *in vivo* microenvironment but also comply with the principles for more ethical use of animals (in line with the 3Rs). Such 3D cell models, together with high throughput technologies such as RNA sequencing, will provide a greater insight into the processes employed by drug resistant cells and therefore offer opportunities to overcome resistance using rational drug combinations (Holohan et al., 2013). Finally, to overcome the obstacle of drug resistance in the therapy of cancer, we require a greater understanding of how resistance is acquired by understanding cell signalling as an interconnected network, capable of rewiring upon inhibition of the central signalling pathways.

1.9 Two-dimensional *versus* three-dimensional cell culture

Two-dimensional (2D) *in vitro* cell culture has been used for decades to study different cell types and to conduct various drug screening and testing. It has shown to be a reliable tool for drug discovery, for example in cancer research for identification of small molecules in colorectal cancer treatment or for the development of functional cell-based assays (Bialkowska and Yang, 2012; Sadikot et al., 2013). This monolayer system allows cells to be grown on a flat glass or polyester surface with medium on top, feeding the cell populations (Haycock, 2011). With the help of 2D cell culture, myriad biological breakthroughs have been achieved, providing a fast, reproducible, cost effective method whilst avoiding *in vivo* testing using animal models.

Despite 2D cell culture being a useful method to dissect certain molecular events, key characteristics in phenotype, function and even protein expression are often lost and therefore fail to recapitulate *in vivo* tissue responses (Bissell et al., 1982; Soares et al., 2012). 2D cultures do not accurately simulate the rich environment and complex processes observed *in vivo* such as cell signalling, chemistry or geometry (Ravi et al., 2015). Importantly, with the use of 2D cultures the complexity and heterogeneity of tumours cannot be accurately replicated and therefore leads to perturbed signalling in addition to morphological changes (Lee et al., 2007). Thus, scientific data from 2D experimentation can be misleading (Edmondson et al., 2014).

Cellular processes such as proliferation, differentiation, metabolism and motility, and also response to stimuli, are greatly influenced by the cellular microenvironment. These processes can be obstructed or absent in 2D systems (Chen et al., 1997; Itano et al., 2003; McBeath et al., 2004; Singhvi et al., 1994). It has been postulated that this is due to the flattening of the cells in 2D on the planar surface (von der Mark et al., 1977) and therefore loss of their differentiated phenotype (Petersen et al., 1992).

Animal models, such as genetically modified mice, provide a platform where the tumour microenvironment, vasculature and immune response can all be taken into account. However, there is a drive to reduce, replace and refine the use of animals in experiments, and furthermore such models are expensive, time consuming and not readily available for all biological questions. Thus, there is a demand for novel, physiomimetic models more representative of the *in vivo* environment. When cells are grown in three dimensions (3D), cells attachments occur freely around the entire cell surface, allowing development of their physiological form and function (Baker and Chen, 2012). **Table 1.3** presents an overview comparing 2D and 3D cultures.

There are a number of studies that underline the significance of 3D cell culture and reveal the apparent advantages of enabling a more physiological environment and recapitulation of the architecture of tissues compared to commonly used 2D monolayer systems (Ghajar and Bissell, 2010; Lee et al., 2007; Pampaloni et al., 2007; Rizki et al., 2008; Santiago-Walker et al., 2009). Geometry and composition to support cellular growth not only influences gene expression but also impacts on cell-cell communication. Genes that promote cell proliferation can be suppressed in 3D cell culture and therefore normalise the anarchic proliferation found in 2D cell culture (Edmondson et al., 2014; Maltman and Przyborski, 2010; Ravi et al., 2015).

Some cell lines grown in 3D cultures are less sensitive to anti-cancer agents than when grown in 2D, however the opposite effect has been observed in different cell lines and with other types of 3D culture techniques (Dhiman et al., 2005; Howes et al., 2007). Thus, investigating cancer in 3D cultures may reveal key insights in respect to drug activity *in vivo* that might not be observable in 2D alone. Additionally, mechanisms responsible for these differences could be discovered e.g. variations in signalling pathways or shift in target dependence in cells grown in 3D *versus* 2D culture methods.

Finally, it has to be taken into account that 3D cell culture is still a relatively new technique and underlying phenomena and implications cannot yet be fully grasped. Unfortunately, this method also has some disadvantages, which in time will be overcome by technical advances.

Table 1.3. Advantages and disadvantages of 2D *versus* 3D cell culture.

2D		3D	
Advantages	**Disadvantages**	**Advantages**	**Disadvantages**
• Cost effective • Well established • Easier to measure and analyse • Fast results	• Not representative • Lack of predictivity • No cell-cell interaction • Reduced signalling	• Physiomimetic • Interaction of cell types • More realistic • Reduction of animal models	• Throughput • Time consuming • Oxygen and nutrient flow • Cost-intensive

1.9.1 3D cell culture models

2D cell cultures lack the capability to accurately mimic the complexity and heterogeneity of tumours as observed *in vivo* and are not representative of the ECM environment found in multicellular organisms. With such simplified models, characteristics such as tissue specific architecture, homeostasis, mechanical and biochemical cues and cell-cell communication cannot be studied and this information is lost (Bissell et al., 2003; Cukierman et al., 2002, 2001; Nelson and Bissell, 2006). Growing cells in 3D would enable the study of cellular behaviour in a more physiological environment, where interactions between different cell types can be taken into account, especially the investigation of the tumour microenvironment in cancer cell signalling and tumour progression (Gligorijevic et al., 2014; Langley and Fidler, 2011; Onuigbo, 1975; Suh et al., 2014; Witz and Levy-Nissenbaum, 2006).

In the 1960s, the idea of organotypic models was developed by Wolff and Marin with the use of embryonic chick liver, where migration of cells was observed around liver explants that were cultivated and therefore tissue culture was induced under organ culture (Wolff, 1961; Wolff and Marin, 1960, 1957). In the early 1980s, Mina Bissell, a lead researcher at Lawrence Berkeley National Laboratory, first proposed 3D

culturing techniques and addressed the importance of tissue microenvironment in cancer research (Bissell et al., 1982). Furthermore, keratinocyte models, initially developed to study skin differentiation (Fusenig et al., 1983), have evolved from single monotypic cell models to multiple cell type models (Schmeichel and Bissell, 2003) and then further adapted in order to study tumour invasion in organotypic cultures using oral squamous cell carcinoma (Nyström et al., 2005).

3D cell culture models are predominantly important in investigating and visualising cancer cell invasion. In order to quantify cell invasion, Transwell® assays have been used where cells invade through a porous membrane towards a chemoattractant (Nyström et al., 2005). However, this system lacks stromal influence of mesenchymal cells and therefore paracrine signalling between two or more cell types is not incorporated (De Wever and Mareel, 2003; Liotta and Kohn, 2001; Mueller and Fusenig, 2002). Addition of stromal cells allows recapitulation of the physiologically-important aspects of cancer-stroma interactions and the investigation of the effect of stromal cells on proliferation and cellular behaviour of cancer cells.

This model has been further adapted and the organotypic culture model was created (Fusenig et al., 1983). More recently it has been adapted to the 3D culture properties of a range of different cancer types (Chioni and Grose, 2012; Coleman et al., 2014; Froeling et al., 2009; Mauchamp et al., 1998; Nyström et al., 2005; Sanderson et al., 1996; Vukicevic et al., 1990). Fibroblasts mixed with collagen and Matrigel™, as the ECM, form a stromal equivalent, upon which cancer cells are seeded. The optimal 3D cell culture would consist of either primary or immortalised stromal cells from the tissue of origin of the cancer under investigation. However, the successful use of these cells in such cultures is influenced by the amenability of the primary cells to tissue culture, as well as access to adequate amounts of primary tissue. To overcome such obstacles, immortalised primary mesenchymal cells from another tissue may be used as a substitute (Nyström et al., 2005).

Establishing 3D culture systems requires precise protocols, adequate cell lines, suitable 3D imaging options and quantitative analysis tools. With the invention of novel materials and better understanding of the *in vivo* microenvironment, the gained

information can be applied to choose suitable models to address a specific scientific question and therefore create more realistic model systems. This is not only limited to drug screening and cancer invasion studies but has also shown to be a valuable tool in the monitoring of hippocampal neurogenesis (Usui et al., 2017) and also in the development and engineering of cardiac tissue (Zimmermann et al., 2006). As all tissues types are unique, there are a great variety of techniques using different materials and manufacturing processes to choose from, depending on its properties and applications. Primarily, 3D cell culture techniques can be divided into scaffold-based and non-scaffold-based approaches **(Table 1.4)**. Further, cells can be embedded within a natural or synthetic matrix, cultured in sterile polystyrene inserts, as multicellular aggregates or without any matrix-based substrates.

1.9.1.1 Scaffold-based

Scaffolds can be useful in supporting cell growth. Due to the porosity of the material, scaffolds enable oxygen, nutrient and waste transport. Cells can proliferate and freely migrate within the scaffold structure as well as adhering to it (Breslin and O'Driscoll, 2013). However, when choosing scaffolds, the structure should, where possible, match the tissue of choice and therefore mimic its structure, scale and function. One caveat is that the larger and more complex the scaffold, the more laborious cell extraction from it may be, leading to artefacts in subsequent analysis. Regardless of the scientific question, the scaffold used must be suitable to ensure growth support and biocompatibility (Haycock, 2011). Scaffolds have shown promising results with *in vivo* tissue regeneration, as there is the possibility to recreate the natural structure and environment of living tissue (Tan et al., 2001).

Such scaffolds can be hydrogels, membranes and 3D matrices, and have been formed from materials that include metals, glasses, ceramics, polystyrene (PS) and polycaprolactone (PCL). Cells can be either seeded onto a 3D matrix or mixed within a liquid matrix material. Scaffolds can also be coated with biologically derived agents such as Matrigel™ or collagen which have been reported to enhance cell growth, attachment and mimic the ECM environment (Haycock, 2011; Bao et al., 2015). Hydrogel scaffolds are often used, as they exhibit a tissue-like stiffness and mimic the

ECM to a certain extent. The tissue-like structure of hydrogels can store nutrients and soluble factors secreted by communicating cells such as cytokines and growth factors which can freely move through the gel (Haycock, 2011). Furthermore, they contain high water properties and natural biomolecules (Huh et al., 2011) such as alginate, gelatin, hyaluronic acid, agarose, laminin, collagen or fibrin. However, the process to solidify the gel can be complex and therefore makes preparation and manipulation of the gels difficult. Synthetic and natural biopolymers can also be used for 3D cell culture ranging from inert to biodegradable materials (polyester, polyethylene glycol, polyamide, polyglycolic acid, polylactic acid) (Maltman and Przyborski, 2010).

1.9.1.2 Non-scaffold-based

Scaffold-free 3D cultures were first described in the 1970s by Robert Sutherland when he cultured spheroids using spinner flasks (Sutherland et al., 1970). Later experiments involved multicellular spheroids with Chinese hamster v79 lung cells, representing nodules as found in several animal and human carcinomas (Sutherland et al., 1971; Sutherland and Durand, 1984). Many different cell types have the natural tendency to form aggregates and therefore cells can re-establish contact and form a specific microenvironment that allows a phenotype similar to tissue. Spheroids are the most commonly used form of *ex vivo* 3D cell culture models. They are self-assembled spherical clusters of cells from single cell colonies such as cancer spheroids formed with NSCLC A549 (Zanoni et al., 2016) or Colo-699 lung cancer cells (Amann et al., 2014), or co-culture methods such as hanging drop, rotating culture or concave plate methods (Castañeda and Kinne, 2000; Hsiao et al., 2012; Pampaloni et al., 2007).

Non scaffold-based techniques such as forced-floating method or forced aggregation use low adhesion polymer-coated well-plates to form uniform spheroids (Baraniak and McDevitt, 2012; Breslin and O'Driscoll, 2013; Yamada and Cukierman, 2007). The well-plates are filled with a cell suspension and centrifuged, followed by spheroid generation (or formation). The hanging drop method was further adapted, which consists of a cell suspension aliquot in medium and incubated under the appropriate physiological conditions until spheroids are generated (Foty, 2011; Kelm et al., 2003; Ware et al., 2016). Plates are then inverted and the aliquots become droplets of cell

aggregates and therefore creating spheroids. Alternatively, the agitation based approach uses a bioreactor, where a cell suspension placed into a rotating bioreactor gradually transforms into aggregates through cell-cell collisions. Cells cannot adhere to the container wall due to the continuous stirring in the bioreactor. Eventually a broad range of non-uniform spheroids are formed (Breslin and O'Driscoll, 2013; Serra et al., 2012). Multicellular spheroids can be custom made with a range of different cell lines and can vary in final spheroid size depending on the cell types used (150-500μm in diameter).

The use of spheroids is especially useful in cancer research, as it enables quick evaluations of morphological alterations of transformed cells and ability to mimic heterogeneous cell populations incorporating regions of proliferation at the edges and also a quiescent core which eventually becomes necrotic (Mehta et al., 2012; Ryan et al., 2016; Ware et al., 2016). These alterations happen in both spheroids and tumours, due to the restricted inward and outward diffusion of nutrients and oxygen, causing hypoxia, accumulation of toxic molecules and changes in pH (Acker et al., 1987; Carlsson and Acker, 1988; Vinci et al., 2012).

Table 1.4. Overview of different 3D cell culture models.

	Method	Material	Advantages	Disadvantages
Scaffold-based	Polymeric Hard Scaffolds Alvetex®	Polystyrene (PS) and Polycaprolactone (PCL)	• Inert and stable • Ready to use and customisable • Cell-cell interaction • Cells are retrievable • Variety of size formats (6, 12, 24, 96-well) • Live imaging	• Additional processing steps • Laborious to image/harvest • High cell numbers • HTS not possible • No invasive studies • Media renewals
	Polymeric Hard Scaffolds Transwell® Inserts	Polycarbonate Polyethylene terephthalate (PET)	• Inert • Customisable • Live imaging	• Expensive • Media renewals • Difficult to retrieve cells • Variation through set up process
	Natural hydrogels	Matrigel™ Cultrex® Geltrex®	• pH and temperature sensitive • More physiological • Injectable	• Animal factors • Batch to batch variations • Degrades over time
	Synthetic hydrogels	PEG gels	• No animal factors • No batch to batch variation	• Bio-inert • Toxic substances • Difficult to sterilise
Non-scaffold-based	Hanging drop microplates	Microplates	• No scaffold needed • Low costs	• Uncontrolled spheroid size • Cell proliferation is low
	Spheroids	Cells native ECM Low attachment plates	• Easy to produce • Low costs • No additional materials needed	• Limited spheroid size • Lack of matrix interaction • Potentially unrealistic • Particle uptake
	Microfluidic 3D cell culture	Microfluidic system	• Minimal variations • Precise control of environment • Real time analysis • Very sophisticated model	• Skill intensive • Very expensive materials • Difficult to reproduce exact conditions

1.9.2 Limitations of 3D cell culture methods

A major limitation can be that a large number of cells are required for each experimental setup, which consequently has implications on the throughput of samples, undermining suitability for higher throughput screening (HTS). In addition, many 3D techniques are cumbersome and time-consuming, which is another limitation to perform large long-term experiments. A cost factor to consider is that large volumes of media and/or other cost-intensive reagents such as coating agents (collagen, fibronectin or Matrigel™) are required to grow 3D cell cultures. Furthermore, assays can last 2-4 weeks on average followed by either histological processing or microscopic evaluation, before the experimental outcome can be analysed. Due to these reasons there is a need to establish cheaper and faster models.

1.9.3 Organotypic culture models in cancer

The word 'organotypic' is used as a term to describe the process where tissue is harvested from an *in vivo* organism and placed *in vitro* in anticipation that it will continue its physiological functions and development as within the original organ. The cells or tissue are cultured *in vitro* with growth medium under physiological parameters. Organotypics have evolved dramatically and are not only used in oncology but also extensively in dermatology and neuroscience (Gähwiler, 1981a, 1981b, 1988; Hauw et al., 1972; Wolf, 1970). The most important aspect of an organotypic cancer model is the simulation of the physiological tumour-stromal microenvironment as observed *in vivo*. Organotypic models should simulate not only tumour progression, including cell invasion through basement membranes, but also the ECM architecture and spatial organisation and oncogenic signalling involved in the generation of drug resistance.

1.9.4 Tumour-stromal microenvironment

The tumour microenvironment, consisting of non-cancerous cells and the ECM is found to be one of the main factors influencing cancer growth. The cellular components comprise fibroblasts, neuroendocrine cells, endothelial, immune-inflammatory cells and blood and lymphatic vascular networks, which are required for normal tissue homeostasis (H. Li et al., 2007; J. Li et al., 2007). It has been implicated in the regulation of cell growth, metastatic potential and the outcome of therapy (Goubran et al., 2014; Quail and Joyce, 2013; Whiteside, 2008). The stromal cells are not malignant; however their role in supporting cancer cells is essential for the survival of the tumour and has therefore become an attractive therapeutic target. In a healthy state, the microenvironment can help protect against cancer development and invasion, however in a malignant state it may create more stubborn and aggressive malignancies (Mroue and Bissell, 2013). Paget's seed and soil hypothesis states that the seed (tumour cells) that metastasise through the blood vessels only develop and infiltrate the ECM where a suitable soil or optimal conditions for survival are found (Paget, 1989). The ECM is therefore essential for tissue organisation and cell survival (Hynes, 2009). To create one 3D model that takes all these parameters into account for all different cancer types and stages is a near impossible feat. Consequently, custom-made organotypic cancer models addressing a specific scientific question have to be designed.

1.9.5 Fibroblast biology in wound healing and cancer

Fibroblasts belong to the connective-tissue family, which additionally includes cartilage cells, bone cells, fat cells and smooth muscle cells; all of which are involved in the secretion of collagenous ECM and are responsible for the architectural framework of the body. The cells play an essential role in the support and repair functions of tissues and organs. Due to their adaptability of their differentiated state, they are important for responses to many different types of damages in all tissues and organs. Fibroblasts are the least specialised cells of the connective-tissue family and are elongated, spindle-shaped cells which can survive stress-like conditions that would be toxic for other cells (Kalluri, 2016). They secrete ECM rich in collagen type

I and type II (Li et al., 2007). Following wounding, nearby fibroblasts proliferate and migrate towards the wound vicinity, where they secrete collagen to repair the damaged tissue, but also act as regulators of inflammation and immunity. Myofibroblasts were identified in the wound healing process and contraction of the skin (Tarin and Croft, 1969; Tomasek et al., 2002) and are activated by transforming growth factor beta (TGF-β) signalling, expressing vimentin and alpha-smooth muscle actin (α-SMA) (Micallef et al., 2012; Rønnov-Jessen and Petersen, 1993).

Activated fibroblasts have been reported to support cancer cell growth, however they can function as positive and negative regulators. As fibroblasts release growth factors, cancer cells can derive advantageous growth, migration and also survival properties and therefore indirectly promote cancer progression, via subversion of pathways aimed at controlling tissue damage (Gaggioli et al., 2007). Fibroblasts associated with cancer are termed cancer-associated fibroblasts (CAFs) and conventional fibroblasts, normal-activated fibroblasts (NAFs) (Albrengues et al., 2015). NAFs may be able to suppress neoplastic development by reversing the growth-promoting effect of TGFβ and HGF secreted by CAFs (Kuperwasser et al., 2004). NAFs are thought to be involved in the suppression of tumour emergence by the deregulation of TGFβ signalling and therefore inducing prostatic intraepithelial neoplasia (Bhowmick et al., 2004). Conversely, normal fibroblasts were found to be transformed to CAF-like fibroblasts via secretion of TGF-β1 (Wen et al., 2015)

CAF-mediated drug resistance is a common phenomenon and CAFs are key players in promoting resistance to anti-cancer therapies. Mechanisms of resistance involving the stroma comprise the alteration of pathways involving cancer cell–ECM interactions, CAF–ECM adhesion and cytokine- or chemokine-induced signalling pathways (Meads et al., 2009; Paraiso and Smalley, 2013). The sensitivity of pancreatic carcinoma to chemo- or radio-therapy can be affected by CAFs secreting soluble factors, thus rendering tumour cells to become less sensitive to Gemcitabine treatment (Hwang et al., 2008). It has also been found that in neck squamous carcinoma, CAFs secrete MMP7 and therefore protect cancer cells from Cetuximab, and upregulate BCL-XL in PC3 cells and hence protect them from Sorafenib-induced

cell death (Kharaziha et al., 2012). CAFs are therefore a potential target in therapeutic resistance, underlining the importance of investigating their influence on cancer cells.

1.9.6 Alvetex® 3D organotypic model

Alvetex® scaffolds are highly porous polystyrene discs that provide a novel method of 3D cell culture. The scaffold is around 200μm thick and consists of a honeycomb of voids, each with a pore diameter of 36-40μm. Cells can therefore easily invade the substrate, with approximately 75 cells being accommodated in each void (Knight et al., 2011). No cell is further than 100μm away from the nutrient source, which ensures optimal exchange of nutrients, gases and waste products by passive diffusion similar to the typical *in vivo* environment, where cells are generally no more than 150-200μm away from a capillary (Jain et al., 2005; Sarveswaran et al., 2016). Since the scaffold is made up from polystyrene, it is completely inert and there is no risk of foreign unknown influences from protein or cytokines from animal-derived material. Additionally, Alvetex® can be used with conventional cell culture plastic, and requires no specialist equipment and is therefore not only suitable for routine use but also affordable. The scaffolds are highly stable even during long-term cell culture, meaning reduced experimental variability even over long-term studies.

Alvetex® is suitable for the majority of downstream analytical techniques. Alvetex® derived cell cultures can be processed just as normal tissue samples and can be used for histology according to standard procedures such as fixation, embedding, thin sectioning and counter-staining. These scaffolds are designed to stop cells changing their shape and cells maintain their natural 3D shape and structure, which can lead to the formation of 'mini slabs' of tissue like structures. Cells enter the scaffold where they retain their natural 3D architecture and do not flatten out like in conventional 2D cell culture. Introduction of the z-dimension allows cells within the Alvetex® scaffolds to retain their natural 3D form and thus help preserve the natural attributes of the cell and bring cells together in a more natural *in vivo*-like manner. This results in the formation of tissue-like structures and cell-to-cell interactions that are more representative of normal tissue function found *in vivo*. Different cells types can be grown in co-culture within the scaffolds, either as mixed populations or as distinct

layers of different cell types (Knight et al., 2011; I. Smith et al., 2015; Liu et al., 2017; Asano et al., 2018).

The architecture of Alvetex® **(Figure 1.14)** illustrates the voids which are interconnected by pores creating a scaffold with > 90% porosity. Once seeded onto Alvetex®, typically cells easily invade the scaffold and start to produce genuine, homogeneous 3D cellular structures that resemble micro-slabs of tissue (Knight et al., 2011). Cells therefore maintain their *in vivo* morphology and respectively behave and respond in a more physiological manner similar to that *in vivo* **(Table 1.5)**.

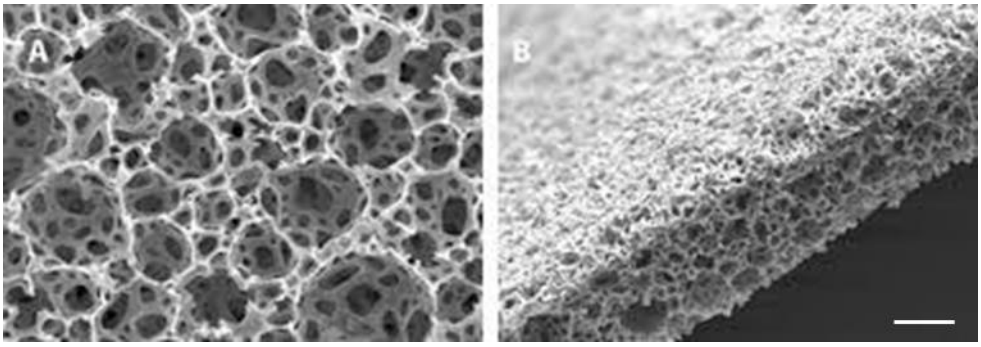

Figure 1.14. Scanning electron microscopy image of an Alvetex® scaffold.
High magnification **(A)** and transverse section **(B)** of the polystyrene membrane at a thickness of approximately 200µm. Alvetex® porosity of >90%. Source: Reprocell Ltd. The scale bar indicates 100µm.

Table 1.5. Features and benefits of usage of Alvetex® for cell culture work.

Feature	Benefits for 3D cell culture
Simple polystyrene	• Easy switch between 2D and 3D cell culture • Inert, no new experimental variables • Stable, does not degrade • Can be precoated with ECM proteins
Consistent scaffold structure	• Reproducible, consistent results, low batch to batch variability
Scaffold is only 200µm thick	• No cell is ever more than 100µm away from each other – mimics *in vivo* conditions • Cells can feed and excrete via passive diffusion
Very high porosity (>90%)	• Cells can easily and freely move in and around the scaffold
Void dimension is 36-40µm	• Up to 75 cells can occupy a single void

Alvetex® can be easily coated with ECM proteins such as collagen I, collagen IV, fibronectin, laminin or Matrigel™. Primary cells can be directly explanted into Alvetex®. The material comes as 200μm discs available as inserts or plates, such as the 12-well plate format or 24-well plate (useful when restricted cell penetration is required, cells are fed from the top of the scaffold only) and scaffold well inserts (6-well and 12-well inserts where cells are fed from above and below, easy to transfer cells into a fresh plate for long-term experiments and enables co-culture experiments). With inserts, there are also different media fill options such as feeding only from below, media in contact above and below but independent media compartments and media in contact above and below with connected compartments. The use of Alvetex® is compatible with downstream applications such as sectioning and counterstaining, immunohistochemistry, scanning and transmission electron microscopy, but also gene and protein expression analysis, isolation of cells for FACS and biochemical assays such as MTT and MTS assays. There is also Alvetex® Strata, which can be used to support the growth of human pluripotent stem cells on the surface of the membrane. This displays a new opportunity to readily access viable cells and enable continuous propagation and thus maintaining their 3D structural phenotype. The difference between Alvetex® and Alvetex® Strata is in the fine structure and architecture. In Alvetex® Strata the voids and pores are significantly smaller (13μm and 5μm diameter respectively). The concept of investigating propagating pluripotent stem cells on Alvetex® Strata was developed using human embryonal carcinoma cells, the malignant counterparts of embryonic stem cells (Przyborski et al., 2004). Cells changed their morphology in 3D and expressed high levels of stem cell markers Oct4 and SSEA-3 compared to 2D. Therefore growth in Strata promoted and maintained their stem cell phenotype.

There are already a number of studies and publications which have applied Alvetex® scaffolds within their research question. The scaffolds have been used with primary hepatocytes, where cytochrome p450 expression was found to be radically increased in 3D culture and cells showed greater sensitivity to cytotoxins (Schutte et al., 2011). Furthermore, co-culture experiments using adipose derived stem cells (ASCs) and

endothelial cells have been performed to generate pre-vascularised tissue-engineered constructs (Neofytou et al., 2011). Alvetex® scaffolds were used to investigate primary cells and long-term 3D culture and drug treatments histologically (Rajan et al., 2011). Gene expression studies using HepG2 cells with qPCR (Fox et al., 2010) and enhanced bone formation of osteoblast cells cultured in 3D using Alvetex® have been compared to 2D systems (Bokhari et al., 2007c). The growth of HepG2 liver cells in Alvetex® revealed an enhanced cell structure and function, producing more morphological features of mammalian liver tissue. Liver cultures were more heterogeneous and developed hepatic structures and showed improved viability and albumin secretion, reduced cell damage, enhanced resistance to methotrexate (MTX) induced cellular toxicity and increased metabolic activity (Bokhari et al., 2007a, 2007b). Alvetex® has also been used to study human stem cell derived neurons using environmental scanning electron microscopy. Furthermore cells can be visualised whilst in the scaffold membrane and cells can also be retrieved and RNA and protein can be extracted from the 3D cultures. Extracted protein was then used to perform immunoblotting to monitor expression of neural markers, enhanced neurite outgrowth and cellular differentiation (Hayman et al., 2005, 2004).

There are a range of drug resistance studies performed in conventional 2D cell culture (Goltsov et al., 2011; Zhang et al., 2009). However, as studies in 2D do not take into account the microenvironment and interactions between cells and their stroma, it would be of fundamental interest and value to investigate the formation of resistance in a 3D model system, where multiple cell types can be introduced into the scaffold and cells can move freely. In previous studies, it has been observed that increased cell-cell or cell-matrix interaction in 3D cultures can increase cell differentiation (do Amaral et al., 2011), alter cell signalling to ECM proteins (Page et al., 2013), change gene expression patterns (Luca et al., 2013) and alter expression of proteins linked to cell-matrix and cell-cell adhesions (Santini et al., 2000).

In this study, Alvetex® scaffolds were used to investigate how fibroblasts affect cancer cells in respect to the formation of resistance to FGFR inhibitors. In order to do so, FGFR-inhibitor resistant cancer cells were co-cultured with fibroblasts and grown in

Alvetex® scaffolds. Since the material is inert, substrates and factors such as collagen or Matrigel™ can be administered and modified in the model accordingly and be investigated using different methods such as live cell microscopy, immunostaining and biochemical assays.

Organotypic cell culture models such as Alvetex® do not replace animal studies to address a specific scientific question; however, in line with the three Rs (replace, reduce and refine) this system can deliver greater insights into the cellular and biochemical processes and therefore provide predictive information regarding cellular responses upon drug treatment.

1.10 Functional genomics and data analysis methods

1.10.1 Microarray and next generation sequencing (NGS)

The transcriptome encompasses the whole set of transcripts in a cell or tissue. This includes RNA molecules from protein coding (mRNA) to noncoding RNA, including rRNA, tRNA, lncRNA, miRNA. The key goal of transcriptomics is to catalogue all species of transcripts and identify the transcriptional architecture of genes in respect to their start sites, 5′ and 3′ ends, splicing patterns and other post-transcriptional modifications and to measure the varying expression levels of each transcript during development and under different conditions. The transcriptome reflects the genes that are being actively expressed at any given time in cells or tissue. Therefore deciphering the transcriptome is of central importance to understand molecular mechanisms and signalling pathways. Unraveling the transcriptome can also be a valuable way to trace phylogenetic relationships between individuals and discover biomarkers (Li et al., 2017).

Several different technologies have been used over the past years to measure gene expression. Recently, advances in genome sequencing have enabled high resolution gene expression analysis. Microarray technology, based on hybridisation, allows RNA samples to be interrogated by binding onto a chip containing single stranded DNA molecules, so called probes. RNA is extracted from cells or tissue, reverse transcribed and then labelled with a fluorescent dye. Sequences complementary to the probe will hybridise, allowing gene expression to be measured optically by the amount of fluorescence associated with each probe, using multiple samples in tandem (Allison et al., 2006; Tarca et al., 2006).

Platforms such as Illumina can simultaneously probe for over 47,000 gene transcripts. However, despite being a powerful and cheap option, it presents several limitations. One of the main flaws is background noise from non-specific binding of cDNA that are only partially complementary to the probe, thus resulting in unreliable expression measurements. Similarly, comparison between different transcripts in the same microarray can be imprecise and use of microarrays is restricted to the detection of differential gene expression of the same probe target between different samples

(Marioni et al., 2008). There is furthermore a dependence on the existing knowledge of the sequences of interest and probe sequences must be pre-specified.

RNA sequencing (RNA-Seq) is a more recent technology which provides greater resolution and also allows mRNA splice variant analysis (Qian et al., 2014). It is gradually replacing microarrays to measure gene expression levels, and exon arrays in alternative splicing analyses (Wang et al., 2008). Early RNA-Seq approaches applied Sanger sequencing technology, which was low throughput, costly and error-prone and generally not very quantitative. To overcome these limitations, tag-based methods were developed, such as serial analysis of gene expression (SAGE) (Harbers and Carninci, 2005; Velculescu et al., 1995), cap analysis of gene expression (CAGE) (Kodzius et al., 2006; Shiraki et al., 2003) and massively parallel signature sequencing (MPSS) (Brenner et al., 2000; Peiffer et al., 2008; Reinartz et al., 2002). Although these methods are high throughput and enable precise digital gene expression levels, they are still based on Sanger sequencing and short tags are not able to be mapped uniquely to the reference genome.

Only in recent times, with the emergence of next generation sequencing (NGS) technology, can we exploit the full potential of RNA-Seq. This method has already been used to map and quantify transcriptomes of *Saccharomyces cerevisiae*, *Schizosaccharomyces pombe*, *Arabidopsis thaliana*, mouse and human cells (Cloonan et al., 2008; Lister et al., 2008; Marioni et al., 2008; Morin et al., 2008; Mortazavi et al., 2008; Nagalakshmi et al., 2008; Wilhelm et al., 2008).

One of the main advantages of RNA-Seq is very low if any background signal, as it is possible to map DNA sequences distinctly to unique regions of the genome. There is no upper quantification limit, which relates with the number of sequences obtained. There is a large dynamic range of expression levels by which transcripts can be detected (Wang et al., 2009; Westbrook and Lucks, 2017). In contrast, microarrays lack the sensitivity for extreme conditions such as low or very high levels of expression and therefore have a smaller dynamic range. When compared to quantitative PCR (qPCR), RNA-Seq has shown to be highly accurate in quantifying expression levels (Nagalakshmi et al., 2008) and spike-in RNA controls of known concentration

(Mortazavi et al., 2008). RNA-Seq has also shown high levels of reproducibility for both technical and biological replicates (Cloonan et al., 2008). Another advantage is that RNA-Seq uses less input RNA as there are no cloning steps, and due to Helicos technology there is no amplification step involved.

The vast number of publications in high profile journals highlights the popularity of this new technique (Parkinson et al., 2009). It allows research groups to investigate aspects that were not accessible previously with microarrays, such as allele specific expression and identification of beforehand unknown transcribed regions (Montgomery et al., 2010; Trapnell et al., 2010). It is possible to not only look at gene expression but also alternative splicing (Pan et al., 2008), novel transcript expression (Guttman et al., 2010), allele specific expression (Degner et al., 2009), gene fusion events (Edgren et al., 2011) and genetic variation. As it is still a relatively novel technique, there is no common gold standard for analysis or standard pipelines yet and experimental and methodological biases exist (Hayden, 2012). Also, for the huge amount of data, specialised algorithms and more powerful servers are required to analyse the data properly (Pop and Salzberg, 2008).

The levels of different RNA species in a cell at any given time point are controlled by regulatory systems that feed back to each other and therefore allow cells to react to environmental changes and also maintain expression patterns specific to the particular cell type. These regulatory systems are (1) the regulation of the timing and rate of transcription initiation and elongation, (2) the regulation of the processing of transcripts, (3) the regulation of the rate of transcript degradation, (4) and the post-transcriptional modification of transcripts (Heyn et al., 2015).

1.10.2 RNA sequencing

The main steps in an NGS RNA-Seq workflow include; RNA fragmentation into random DNA or cDNA fragments, a so-called cDNA library followed by addition of adapters to the 5′ and 3′ ends of each fragment. The adapters contain functional elements that allow sequencing, including an amplification element and the primary sequencing site. Adapter-ligated fragments are then PCR amplified. Next, the cDNA library gets analysed by NGS, which results in short sequences which correspond to either one or both ends of the fragment. The library sequencing depth depends on the techniques with which the output data will be analysed. After that, short sequences from one end (single end sequencing) or both ends (paired end sequencing) are obtained with a length of typically 30-400bp. Single-read is associated with lower costs and a faster technique (1% of Sanger sequencing), where cDNA is only sequenced from one end. With paired-end methods, cDNA is sequenced from both sides and thus represents a more cost intensive and more laborious approach (Sengupta et al., 2011). Double stranded molecules are then denatured into single stranded molecules and loaded into a flow cell with surface-bound oligos complementary to the library adapters capturing the fragments. Bound fragments get amplified by bridge amplification to create clusters of identical molecules which serve as the templates for sequencing. Sequencing primers are added and clusters get reverse complemented at the same time. During each sequencing step, one fluorescently labelled nucleotide is added to each growing complementary strand. The dye of the nucleotides is different for each nucleotide type and a laser is then used to identify the location and identity of the nucleotide which was incorporated into the cluster. The fluorescent dye is removed together with the terminal group and the same process is repeated until the desired number of times, usually 30 to 200 times. At the end, a sequence of images with spots representing a cluster and the specific colour represents the base type **(Figure 1.15)**. Nucleotide sequences are usually in FASTQ file format. Once the newly identified sequences are obtained, gene expression levels can be analysed by aligning to a reference genome. After alignment, a number of analysis options are available such as single nucleotide polymorphism

(SNP), insertion-deletion (indel), identification, read counting for robust multi-array average (RMA) methods, phylogenetic or metagenomics analysis and more.

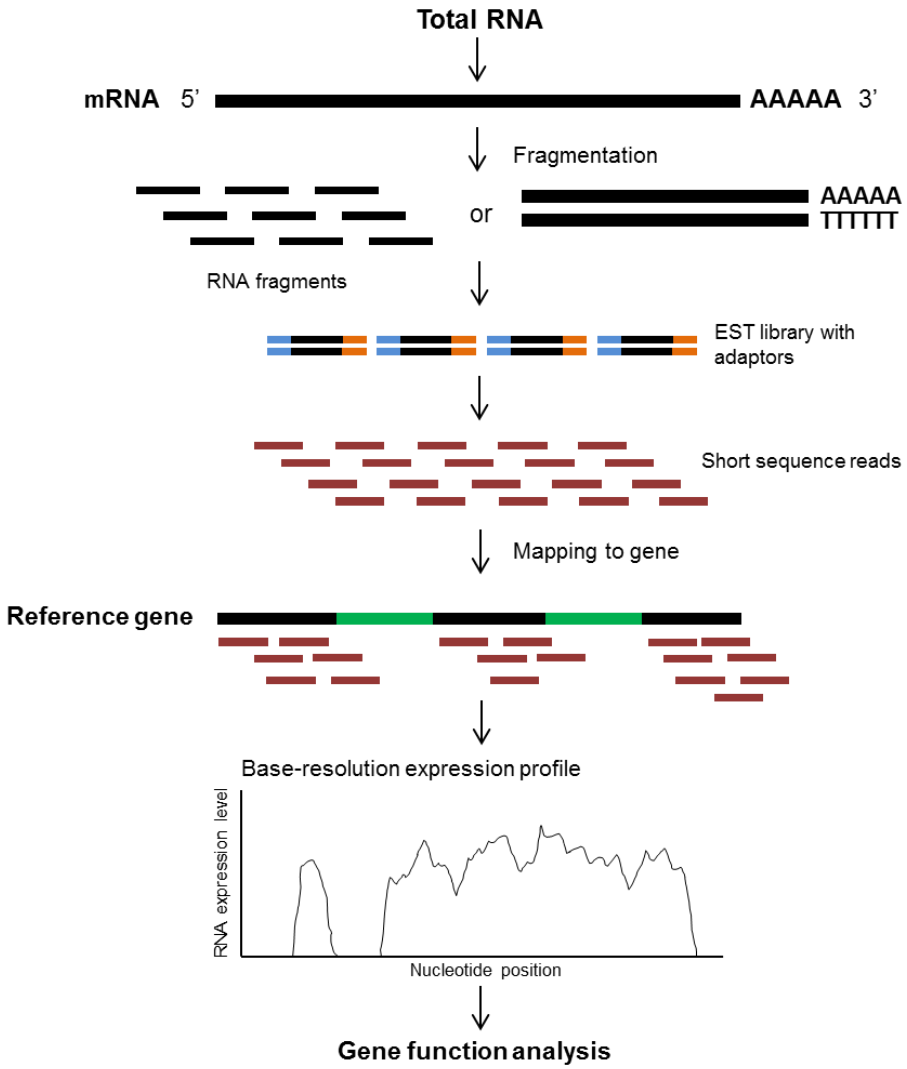

Figure 1.15. Schematic overview of RNA sequencing.
RNAs are first transformed into a library of cDNA fragments through either RNA fragmentation or DNA fragmentation. Sequencing adaptors (blue and orange) are then added to each cDNA fragment and a short sequence is obtained from each cDNA using high-throughput sequencing technology. The resulting sequence reads are aligned with the reference genome or transcriptome. This is then used to generate a base-resolution expression profile for each gene (Wang et al., 2009).

RNA-Seq is a valuable tool to understand transcriptomic dynamics during development and normal physiological changes and analysis and comparison of diseased and normal tissues, such as comparing cancerous cells to normal cells. In this project RNA-Seq will be used to study drug resistance mechanisms of cancer cells by comparing gene expression profiles of drug resistant cancer cell populations to their parental lines.

1.11 Aims and Objectives

FGFR2 is amplified in 5-10% of gastric cancer and 12% of endometrial cancer and *FGFR1* is amplified in 16% lung cancers. FGFR signalling in *FGFR1* and *2*-amplified cancer types has shown to be a suitable target for therapy (Byron et al., 2008; Dutt et al., 2008; Konecny et al., 2013; Desai and Adjei, 2016; Yashiro and Matsuoka, 2016). However, as resistance is a common side effect towards chemotherapy and hormone therapy and also resistance towards other small molecule inhibitors has been documented (Goltsov et al., 2012, 2011; Lito et al., 2013; Wagle et al., 2011; Zhang et al., 2009), efficacy of prolonged FGFR-targeted therapy is an important area of study. As discussed previously, cell signalling and morphology can be altered in 2D culture, and therefore 3D cell culture systems enable an *in vitro* system to be more physiologically relevant. Different cell types can be grown together to recreate a microenvironment that has shown to be essential for cancer signalling. Addition of a third dimension provides spatial organisation in which cellular cues and responses are similar to those *in vivo* (Haycock, 2011; Huh et al., 2011; J. Lee et al., 2008; McBeath et al., 2004; Ryan et al., 2016). These responses and gene expression changes can then be measured using RNA-Seq (Wang et al., 2009).

The aims of this study are:

1. Establish and optimise a 3D model using Alvetex® 3D cell culture technique and perform co-culture experiments with fibroblasts and cancer cells.
2. Generate drug resistant cells in 2D and 3D and investigate resistance of FGFR-driven cancers using FGFR inhibitors.
3. Use RNA-Seq, differential gene expression analysis and pathway analysis to measure gene expression differences between resistant populations in 3D with and without the influence of stromal cells, thereby dissecting differences in resistance mechanisms with and without stromal support.
4. Determine the mechanisms of drug resistance in *FGFR2*-amplified cancer cell lines using a combination of RNA-Seq analysis, biochemical techniques and *in silico* analysis, and use this knowledge to target resistant cell lines by synthetic lethality, target modulation or informed small molecule approaches.

Chapter II

Materials and Methods

2.1 Materials

2.1.1 Cell lines

The following cell lines have been used **(Table 2.1-Table 2.4).**

Table 2.1. Endometrial cancer cell lines.

Cell line	Origin	Differentiation state	FGFR status	Mutated genes	Source	Cat. No.
MFE-296	Endometrial cancer	Intermediately differentiated	FGFR2 mut.	PTEN PIK3CA PIK3R1	HPA	98031101
AN3CA	Endometrial cancer	Well differentiated	FGFR2 mut.	PTEN PIK3CA PIK3R1	ATCC	HTB-111

Table 2.2. Gastric cancer cell lines.

Cell line	Origin	Tumour source	FGFR status	Mutated genes	Source	Cat. No.
KATOIII	Gastric cancer	Metastasis	FGFR2 amp.	TP53	ATCC	HTB-103
NCI-N87	Gastric cancer	Metastasis	wt	SMAD4 TP53	ATCC	CRL-5822
SNU-16	Gastric cancer	Metastasis	FGFR2 amp.	CDKN2A TP53	ATCC	CRL-5974
SNU-5	Gastric cancer	Metastasis	wt	CDH1 CDKN2A TP53	ATCC	CRL-5973
AGS	Gastric cancer	Primary	wt	CDH1 CTNNB1 KRAS PIK3CA	ATCC	CRL-1739
SNU-1	Gastric cancer	Primary	wt	KRAS MLH1	ATCC	CRL-5971

Table 2.3. Lung cancer cell lines.

Cell line	Origin	Tumour source	FGFR2 status	Mutated genes	Source	Cat. No.
A549	Lung cancer	Primary	wt	KRAS	ATCC	CCL-185
H1299	Lung cancer	Primary	wt	NRAS	ATCC	CRL-5803
H520	Lung cancer	Metastasis	FGFR1 amp.	KRAS	ATCC	HTB-182

Table 2.4. Stromal cell lines.

Cell line	Origin	Tissue source	Source	Cat. No.
HFF2	Foreskin	Primary[2]	ATCC	SCRC-1042
MRC-5	Lung	Primary[3]	ATCC	CCL-171

[2] Normal human foreskin pooled from four individuals.
[3] Fibroblasts derived from lung tissue of a 14 week old aborted Caucasian male fetus.

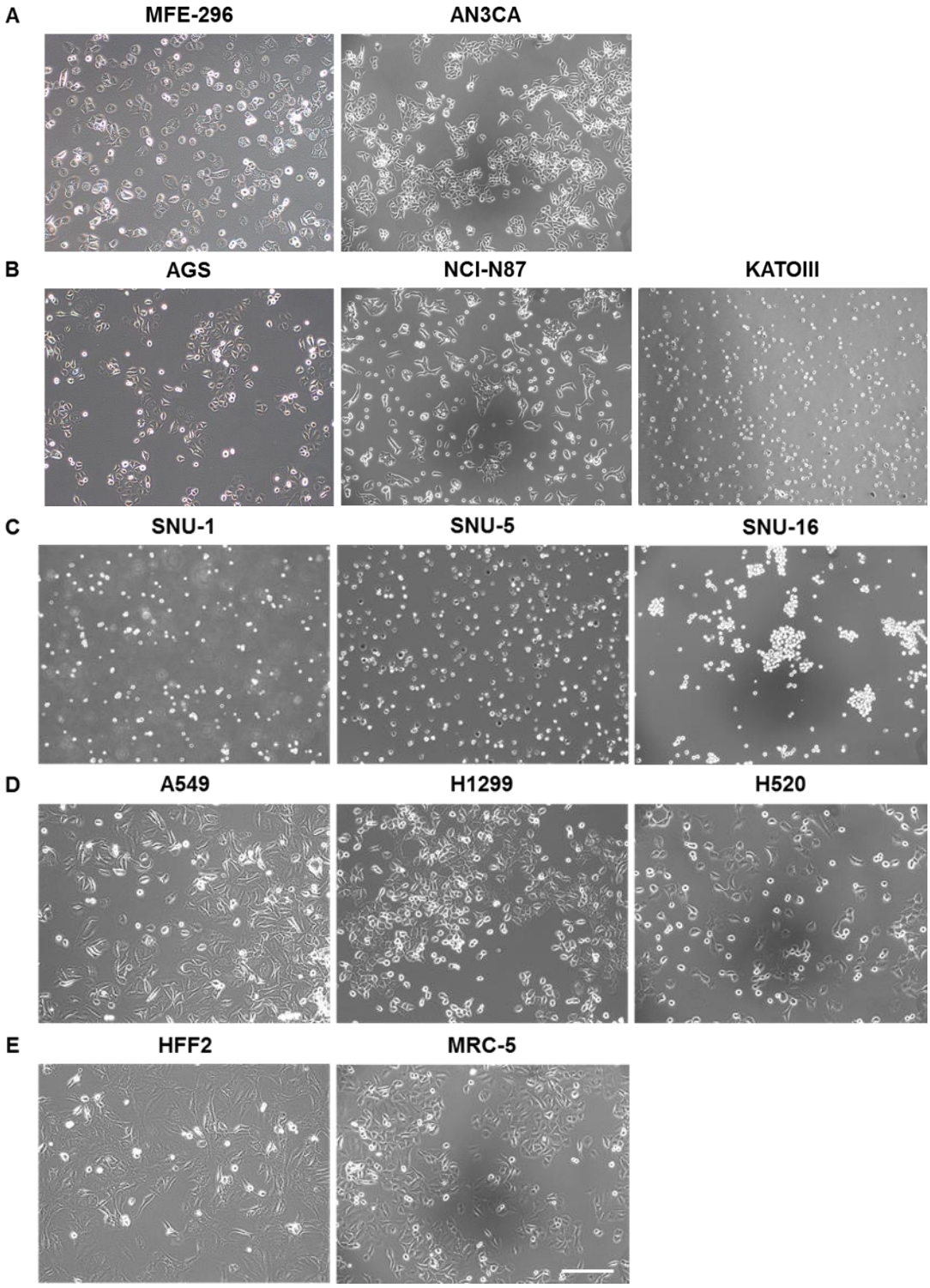

Figure 2.1. Morphology of endometrial, gastric, lung cancer and fibroblast cell lines.
(A) Endometrial cancer cell lines (AN3CA, MFE-296).
(B) Adherent gastric cancer cell lines (AGS, NCI-N87, KATOIII).
(C) Suspension gastric cancer cell lines (SNU-1, SNU-5 and SNU-16).
(D) Lung cancer cell lines (A549, H1299 and H520).
(E) Human foreskin fibroblasts (HFF2) and lung fibroblasts (MRC-5).
The scale bar indicates 25μm.

2.1.2 Chemicals and compounds

Table 2.5. Chemicals and the manufacturers.

Reagent	Source	Cat. No.
2-Mercaptoethanol	Sigma-Aldrich	M3148
10% Ammonium persulphate	Sigma-Aldrich	A3678
30% Polyacrylamide solution	Fisher Scientific	NC2010
Absolute Ethanol ≥99.8%	Sigma-Aldrich	15727
Acetic acid glacial	Fisher Scientific	10304980
Agar	Sigma-Aldrich	A7002
Agarose (UltraPure™)	Invitrogen	16500500
Bovine Serum Albumin (BSA)	Sigma-Aldrich	A8022
Collagen	Corning	354236
Citric acid monohydrate	Sigma-Aldrich	C7129
1,4-Diazabicyclo[2.2.2]octane (DABCO)	Sigma-Aldrich	D2522
DAKO Pen	DAKO	S2002
Diethylpyrocarbonate (DEPC)	Sigma-Aldrich	D5758
Dimethyl sulphoxide (DMSO)	Fisher Scientific	10080110
Doxycycline	Fisher Scientific	BP26531
DPX mountant	Sigma-Aldrich	06522
Dulbecco's Modified Eagle's Medium (DMEM)	Sigma-Aldrich	D8437
Epidermal growth factor (EGF)	Sigma-Aldrich	E9644
Ethidium bromide (EtBr)	Sigma-Aldrich	E1510
Ethylenediaminetetraacetic acid (EDTA)	Sigma-Aldrich	59418C
Foetal bovine serum (FBS)	Gibco	10500-604
Formalin (10% v/v neutral buffered)	Cellstor	BAF-0010-25A
Glucose (D+)	Fisher Scientific	10141520
Glycerol	AppliChem	A1123
Glycine	Fisher Scientific	BP381-1
Heparin sodium salt	Sigma-Aldrich	H4784
Isopropanol	Acros	389710025
LB broth	Sigma-Aldrich	L3147
Matrigel™	Corning	354234

Methanol	Sigma-Aldrich	322415
Mowiol	Hoechst	50661910
MTT	Sigma-Aldrich	M5655
MTS	Promega	G3581
Nonidet-P40™ (NP40)	Invitrogen	FNN0021
Opti-MEM™	Fisher Scientific	31985070
Paraformaldehyde (PFA)	Fisher Scientific	10630813
Penicillin/ Streptomycin	Sigma-Aldrich	P4333
Potassium chloride (KCl)	Fisher Scientific	10375810
Roswell Park Memorial Institute (RPMI-1640) Medium	Sigma-Aldrich	R8758
Skim milk	Sigma-Aldrich	70166
Sodium azide	Sigma-Aldrich	S2002
Sodium chloride (NaCl)	Fisher Scientific	BP3581
Sodium citrate anhydrous ($C_6H_7NaO_7$)	Fisher Scientific	BP327
Sodium dodecylsulphate (SDS)	Fisher Scientific	BP1311-1
Sodium bicarbonate ($NaHCO_3$)	Sigma-Aldrich	S5761
Sodium phosphate dibasic (Na_2HPO_4)	Sigma-Aldrich	S3264
TEMED	National Diagnostics	EC503
Tween-20	AppliChem	A1284
Xylene	Sigma-Aldrich	214736

2.1.3 Buffers, solutions and media

Table 2.6. Buffers and their composition.

Name	Composition
4% PFA in PBS	20g Paraformaldehyde PBS to a final volume of 500mL
Acetic ethanol	5mL Glacial acetic acid 20mL MilliQ-H_2O 100% Ethanol to a final volume of 500mL
Binding buffer (1X)	10mM Hepes (pH7.4) 140mM NaCl 2.5mM CaCl2
Blocking solution (Immunohistochemistry/ Immunofluorescence)	6g BSA 50µL NP40 PBS to a final volume of 50mL
10mM Citrate buffer (pH6.0)	0.256g Citric acid monohydrate 2.75g Sodium citrate ddH_2O to a final volume of 1L
Dulbecco's Modified Eagle Medium (DMEM)	500mL DMEM 5mL Penicillin/Streptomycin (10.000 units penicillin, 10mg streptomycin/mL) 50mL FBS (final concentration of 10%)
DEPC-treated water	1mL DEPC 1L ddH_2O
Lysis buffer	50mL 1M Tris-HCl (pH8.0) 25mL 2M KCl 5mL 0.5M EDTA (pH8.0) 4.5mL NP40 4.5mL Tween 20 ddH_2O to a final volume of 1L
Minimum Essential Medium (MEM)	500mL MEM 5mL Penicillin/Streptomycin (10.000 units penicillin, 10mg streptomycin/mL) 50mL FBS (final concentration of 10%)
Mounting solution	200µL DABCO 1.8mL Mowiol

Mowiol	6g Glycerin 2.4g Mowiol 6mL DEPC-treated water 12mL 0.2MTris-HCl (pH8.5)
Phosphate buffered saline (PBS) buffer (pH7.4)	137mM NaCl 2.7mM KCl 10mM Na_2HPO_4 2mM KH_2PO_4
PBS-Tween (PBST) buffer	137mM NaCl 2.7mM KCl 10mM Na_2HPO_4 2mM KH_2PO_4 0.1% Tween-20
Roswell Park Memorial Institute (RPMI) Medium-1640	500mL RPMI-1640 5mL Penicillin/Streptomycin 50mL FBS (final concentration of 10%)
Resolving gel buffer (pH8.8)	1.5M Tris Base-HCl 0.4% SDS ddH_2O to a final volume of 1L
SDS-PAGE Running Buffer (pH8.3)	5mM Tris 192mM glycine 0.1% SDS
SDS sample buffer (5X)	0.25% Bromophenol blue 0.5M DTT 50% Glycerol 10% SDS 0.25M Tris-Cl (pH6.8)
Stacking gel buffer (pH6.8)	0.5M Tris Base-HCl 0.4% SDS ddH_2O to a final volume of 1L
TAE buffer (1X)	40mM Tris (pH 7.6) 20mM acetic acid 1mM EDTA
TBE buffer (1X)	89mM Tris (pH 7.6) 89mM boric acid 2mM EDTA

TBS	10mM Tris-HCL (pH 8.0) 150mM NaCl
TBS-Tween (TBST) buffer	10mM Tris-HCL (pH 8.0) 150mM NaCl 0.1% Tween-20
Transfer buffer	25mM Tris-HCl (pH 7.6) 192mM glycine 20% methanol
Tris-Borate-EDTA (TBE) buffer	90mM Tris-HCl (pH 8.0) 80mM Boric acid 3mM EDTA

2.1.4 Dyes, kits and enzymes

Table 2.7. Dyes, kits, inhibitors and enzymes.

Name	Source	Cat. No.
Acarbose	Sigma-Aldrich	A8980
Ampicillin	Sigma-Aldrich	A9518
Annexin V Alexa Fluor 647 conjugate	Thermo Fisher Scientific	A23204
AZD4547	AstraZeneca	N/A
BGJ398	Novartis Pharma	N/A
DAB	Vector Laboratories	SK-4100
DAPI	Life Technologies	P36931
DNA polymerase	Qiagen	203203
FuGene® HD	Promega	E2311
GeneRuler 100bp (100bp – 1000bp)	Thermo Fisher Scientific	SM0241
GeneRuler 1kb (250bp – 10000bp)	Thermo Fisher Scientific	SM0311
INTERFERin®	Polyplus	409-10
Mayer's Haematoxylin	Sigma-Aldrich	MHS16
PD173074	Sigma-Aldrich	P2499
Phosphatase inhibitor	Calbiochem	524625
Picosirius Red	Polysciences Inc.	24901
Ponceau (0.1% (w/v) in 5% acetic acid)	Sigma-Aldrich	P7170
Propidium iodide	Sigma-Aldrich	P4864

Protease inhibitor	Calbiochem	539131
Protein assay reagent A	Bio-Rad Laboratories	500-0113
Protein assay reagent B	Bio-Rad Laboratories	500-0114
Protein assay reagent S	Bio-Rad Laboratories	500-0115
Puromycin	Santa Cruz Biotechnology	sc-205821
RIPA buffer	Millipore	20-188
RNase-free DNase	Qiagen	79254
Rneasy® Mini Kit	Qiagen	74104
SuperScript II Reverse transcriptase	Thermo Fisher Scientific	18080093
Sybr Green I Master Mix	Qiagen	204145
TDZD-8	Cayman Chemical Company	16287
Trypsin	Gibco, Paisley, Scotland	59418C
Vector ABC	Vector Laboratories	PK-6100
Weigert's Haematoxylin	Sigma-Aldrich	HT1079
ZymoPURE™ Plasmid Maxiprep Kit	Zymo Research	D4202

2.1.5 Antibodies

Table 2.8. Antibodies for IF and WB.

Primary antibody	Host	Dilution	Source	Cat. No.
anti-alpha-SMA	mouse	1:100	Sigma-Aldrich	A5228
anti-E-cadherin	mouse	1:100	BD Bioscience	610182
anti-EpCAM	rabbit	1:100	Invitrogen	MA5-12436
anti-FGFR1	rabbit	1:1000	Cell Signaling Technology	9740S
anti-FGFR2	rabbit	1:1000	Santa Cruz Biotechnology	sc-122
anti-GAPDH	mouse	1:1000	Millipore	MAB374
anti-HSC70	mouse	1:1000	Santa Cruz Biotechnology	sc-7298
anti-IgG	goat	1:200	Abcam	ab6740-1
Anti-MDR1	rabbit	1:1000	Abcam	ab170904
anti-Pan-cytokeratin	mouse	1:200	DAKO	70622

anti-PHLDA1	rabbit	1:1000	Abcam	ab133654
anti-phospho-AKT 473	rabbit Ser473	1:1000	Cell Signaling Technology	9271S
anti-phospho-AKT 308	rabbit Thr308	1:1000	Cell Signaling Technology	4056S
anti-phospho-ERK	rabbit Thr202/Tyr204	1:1000	Cell Signaling Technology	9101S
anti-REG1A	rabbit	1:1000	Abcam	ab47099
anti-total AKT	rabbit	1:1000	Cell Signaling Technology	9272S
anti-total ERK	rabbit	1:1000	Millipore	06-182
anti-Vimentin	mouse	1:200	DAKO	M0725

Secondary antibody	**Host**	**Dilution**	**Source**	**Cat. No.**
anti-mouse AF488	donkey	1:200	Life Technologies	A21202
anti-mouse AF546	donkey	1:200	Life Technologies	A10036
anti-rabbit AF488	goat	1:200	Life Technologies	A11034
anti-rabbit AF555	donkey	1:200	Life Technologies	A31572
anti-rabbit IgG-biotin	goat	1:200	DAKO	E0432
anti-mouse-HRP	goat	1:1000	Invitrogen	A28177
anti-rabbit-HRP	goat	1:1000	Invitrogen	32460
anti-rat-HRP	goat	1:100	Sigma-Aldrich	A9037

2.1.6 Equipment

Table 2.9. Equipment.

Name	Source
ALC International	PK121
BD FACS Aria™ II	BD Bioscience, USA
BD Fortessa	BD Bioscience, USA
Gel Docx XR	Bio-Rad Laboratories Inc.
IncuCyte™ ZOOM®	Essen Bioscience
Leica EG1150 H+C instrument	Leica Microsystems
Microm STP 120 Spin tissue processor	Microm/ Thermo Fisher Scientific
Microm HM335 microtome	Microm, Walldorf, Germany
NanoDrop One	Thermo Fisher Scientific
Pannoramic scanner	3D Histech Ltd.
Phase-contrast light microscope	Olympus, IMT-2, Japan
peqSTAR thermocycler	VWR
Ultra-Turrax homogenizer	Janke & Kunkel, Staufen, Germany
Zeiss Axiophot 2 light microscope with Axiocam Hrc camera	Carl Zeiss AG, Oberkochen, Germany
Zeiss LSM 710	Carl Zeiss AG, Oberkochen, Germany
Amersham Imager 600	GE Healthcare Life Sciences
StepOnePlus Real Time System	Applied Biosystems, Paisley, UK

2.1.7 Software

Table 2.10. Software.

Software	Source
ApE (A plasmid Editor), v2.047	M. Wayne Davis
Axiovision 4.2 or 4.6 software	Carl Zeiss, Oberkochen, Germany
BaseSpace	Illumina, San Diego, USA
BD FACSDIVA™	BD Bioscience, USA
CLC Genomics Workbench 6/7	CLC bio, a Qiagen Company, Aarhus, Denmark
Cytoscape	Institute of Systems Biology in Seattle, USA
FastQC	Brabraham Institute
FlowJo	FlowJo LLC, Ashland, Oregon, USA
Graph Pad Prism v5.03	Graph Pad Software Inc., La Jolla, USA
GSEA	Broadinstitute
Illustrator	Adobe Systems Inc., San José, California, USA
ImageJ 1.429	Wayne Rasband, NIH
Imaris	Bitplane
IncuCyte™ ZOOM® (v20151.2.5599)	Essen Bioscience
Ingenuity pathway analysis (IPA)	Qiagen Bioinformatics, Hilden, Germany
Pannoramic viewer	3D Histech Ltd.
Photoshop CS5/6	Adobe Systems Inc., San José, California, USA
R Studio	R Core Team
Roche Light Cycler 480 v1.5.0	Roche
StepOne Plus v2.2	Applied Biosystems, Carlsbad, California, USA
String	Academic consortium
Zen 2009	Carl Zeiss, Oberkochen, Germany

2.1.8 PCR reagents

Table 2.11. PCR reagents and the manufacturer.

Name	Source
dATP, dCTP, dGTP, dTTP (dNTPs)	Invitrogen/ Life Technologies
10X PCR buffer	
50mM $MgCl_2$	

2.1.9 Plasmids

Table 2.12. Plasmids.

Name	Source	Cat. No.
pMD2.G	Addgene	12259
pCMVR8.74	Addgene	22036
pLV-H2B-GFP	Addgene	11680
pLV-H2B-RFP	Addgene	26001
pcDNA3.1	Invitrogen	V790-20
pcDNA3.1 PIWIL1	Grützner, University of Adelaide	N/A
pmaxGFP	Lonza	VSC-1001
PL-SIN-PGK-EiP EGFP	Addgene	21312
PHLDA1 GFP	Addgene	32699
PHLDA1 siRNA	Dharmacon	M-01238901
pLV-Azurite	Addgene	36086
PHLDA1 shRNA	Sigma Mission	TRCN0000150307

2.1.10 Oligonucleotides

All Oligonucleotides used in this work were from Eurogenetec.Short hairpin sequences were purchased from Sigma MISSION®.

Table 2.13. PCR primers for generation of knockdown and overexpression.

Primers	Forward (5´-3´)	Reverse (5´-3´)
PIWIL1 attB	GGGGACAAGTTTGTACAAAAAAGCAGGCTTCATGACTG GGAGAGCCCGAGC	GGGGACCACTTTGTACAAGAAAGCTGGGTCTTAGAGG TAGTAAAGGCGG
REG1A shRNA 1	CCGGCCTGACCTCAAGCACAGGATTCTCGAGAATCCTGT GCTTGAGGTCAGGTTTTTG	AATTCAAAAACCTGACCTCAAGCACAGGATTCTCGAG AATCCTGTGCTTGAGGTCAGG
REG1A shRNA 2	CCGGAGTGGCACTGATGACTTCAATCTCGAGATTGAAGT CATCAGTGCCACTTTTTTG	AATTCAAAAAAGTGGCACTGATGACTTCAATCTCGAG ATTGAAGTCATCAGTGCCACT
REG1A shRNA 3	CCGGCGCTCCTACTGCTACTACTTTCTCGAGAAAGTAGT AGCAGTAGGAGCGTTTTTG	AATTCAAAAACGCTCCTACTGCTACTACTTTCTCGAGA AAGTAGTAGCAGTAGGAGCG

Table 2.14. Short hairpin sequences for generation of knockdowns.

Primers	Sequence
shRNA control	CCTAAGGTTAAGTCGCCCTCGCTCGAGCGAGGGCGACTTAACCTTAGG
PHLDA1 shRNA 1	CCGGCCTAATCCGTAGTAATTCCTACTCGAGTAGGAATTACTACGGATTAGGTTTTTG (TRCN0000150307)
PHLDA1 shRNA 2	CCGGCCTAATCCGTAGTAATTCCTACTCGAGTAGGAATTACTACGGATTAGGTTTTTG (TRCN0000150983)
PHLDA1 shRNA 3	CCGGCGAGCACATTTCTATTGTCTTCTCGAGAAGACAATAGAAATGTGCTCGTT (TRCN0000152275)

To generate a doxycycline inducible PHLDA1 expression construct, the full coding sequence of human PHLDA1 (NM_007350.3) was cloned into pDONR™221 (Invitrogen) and then transferred to pINDUCER21 (ORF-EG) (Addgene #46948) using Gateway™ technology (Invitrogen). Lentiviral production and transduction was performed as described in section 2.2.16, 2.2.17.

Table 2.15. Mycoplasma testing primers.

Primers	**Forward (5´-3´)**
GPO1 F	ACT CCT ACG GGA GGC AGC AGT A
GPO2 F	CTT AAA GGA ATT GAC GGG AAC CCG
MGSO R	TGC ACC ATC TGT CAC TCT GTT AAC CTC

Table 2.16. FGFR primers.

Primers	Forward (5´-3´)	Reverse (5´-3´)
FGFR1IIIa	AAA GCA CAT CGA GGT GAA CG	TTC ATG GAT GCA CTG GAG TC
FGFR1IIIb	TTA ATA GCT CGG ATG CGG AG	ACG CAG ACT GGT TAG CTT CA
FGFR1IIIc	TGC TGG AGT TAA TAC CAC CG	CCA GAA CGG TCA ACC ATG CA
FGFR2IIIa	AAG GTT TAC AGC GAT GCC CA	CTG CTG AAG TCT GGC TTC TT
FGFR2IIIb	AAG GTT TAC AGC GAT GCC CA	AGA GCC AGC ACT TCT GCA TT
FGFR2IIIc	GTG TTA ACA CCA CGG ACA AA	TGG CAG AAC TGT CAA CAA TG
FGFR3IIIb	GAG TTC CAC TGC AAG GTG TA	AAA TTG GTG GCT CGA CAG AG
FGFR3IIIc	AGA ACC TCT AGC TCC TTG TC	AGA ACC TCT AGC TCC TTG TC
FGFR4	TAT CTG GAG TCC CGG AAG TG	GTG TGT GTA CAC CCG GTC AA

Table 2.17. Primers used for qRT-PCR analysis.

Primers	Forward (5´-3´)	Reverse (5´-3´)
B2M	AGT TAA GTG GGA TCG AGA C	GCA AGC AAG CAG AAT TTG G
GAPDH	CCA TGG AGA AGG CTG GGG	CAA AGT TGT CAT GGA TGA CC
GLUT1	AAC TCT TCA GCC AGG GTC CAC	CAC AGT GAA GAT GAT GAA GAC
HPRT1	GAC CAG TCA ACA GGG GAC AT	CCT GAC CAA GGA AAG CAA AG
PHLDA1	CAG AGG GCA AGG AGA TCG AC	GTG GAT TTG ACC GCC AGG AT
PIWIL1	CAA GTA ATC GGA AGG ACA AA	CTA CCA ATG GAT TTT AGA CAA
REG1A	ACA GAG TTG CCC CAG GCC CGG	AGA ACT TGT CTT CAC AAG GCA
SI	CAT CCT ACC ATG TCA AGA GCC AG	GCT TGT TAA GGT GGT CTG GTT TAA ATT

2.2 Methods

2.2.1 2D Cell culture methods

2.2.1.1 Basic cell culture applications

To study gastric cancer, a panel of 6 cell lines was obtained from American Type Culture Collection (ATCC). Endometrial MFE-296 and AN3CA cells were obtained in house and lung cancer cell lines H1299 and H520 were kindly provided by Prof. John Marshall. Cells were cultured in suspension, as semi-adherent or adherent cells in a monolayer **(Table 2.18**) in culture flasks of various sizes (Corning, 25cm^2 (430639), 75cm^2 (430641U) and 175cm^2 (431080)) in a humidified atmosphere of 37°C and 5% CO_2.

2.2.1.2 Passaging cells

When cells reached approximately 80-90% confluence for adherent cultures and cells started clumping for suspension cells, medium was removed and trypsin/ethylenediaminetetraacetic acid (EDTA) (GE Healthcare) was added for 5-10 minutes and incubated to detach cells from the flask surface. Once cells were detached, trypsin was inactivated with the relevant medium **(Table 2.18)**. Cell suspensions were centrifuged at 250 relative centrifugal force (rcf/ x g, ALC International, PK121) for three minutes at room temperature (RT). Following centrifugation, supernatant was removed and the cell pellet was re-suspended in standard medium. If counting of cells was required, 10µL of the cell suspension was mixed with Trypan Blue and from the mixture 10µL was immediately added to a FastRead counting haemocytometer (Immune Systems, BVS100) and cells were counted manually under a light microscope (Olympus, IMT-2, Japan). Cells were sub-cultured at a 1:2 to 1:20 ratio, depending on their growth rates.

Table 2.18. Summary of cell lines.
All cell lines and respective cell culture medium used, together with their growth state. MEM = Modified Eagle's Medium, DMEM = Dulbecco's Modified Eagle's Medium, FBS = foetal bovine serum, L-Glut = L-Glutamine, NEAA = Non-essential amino acids, RPMI = Roswell Park Memorial Institute, Ham's F12 = F12 nutrient medium.

Cell line	Cell culture medium	Growth state
Endometrial cancer		
MFE-296	MEM, 10% FBS	adherent
AN3CA	DMEM, 10% FBS, 2mM L-Glut	adherent
Ishikawa	MEM, 5% FBS, 2mM L-Glut, 0.1% NEAA	adherent
Gastric cancer		
KATOIII	RPMI-1640, 20% FBS, 2mM L-Glut	semi-adherent
SNU-1	RPMI-1640, 10% FBS	suspension
SNU-16	RPMI-1640, 10% FBS	suspension
SNU-5	RPMI-1640, 20% FBS	suspension
AGS	Ham's F12, 10% FBS, 2mM L-Glut	adherent
NCI-N87	RPMI-1640, 10% FBS	adherent
Lung cancer		
H520	RPMI-1640, 10% FBS	adherent
A549	DMEM, 10% FBS	adherent
H1299	RPMI-1640, 10% FBS	adherent
Fibroblasts		
HFF2	DMEM, 10% FBS	adherent
MRC5	MEM, 10% FBS	adherent
Packaging cells		
HEK293T	DMEM, 10% FBS	adherent

2.2.1.3 Cryopreservation and thawing of cells

Stocks of each cell line were kept in liquid nitrogen for long-term storage. To freeze cells, cell pellets were taken up in respective freezing medium, consisting of complete growth medium and 5% DMSO for all gastric cancer cell lines or 90% FBS and 10% DMSO for other cell types, and pipetted into cryovials (Corning, 430489) and slowly frozen down at -80°C overnight and later transferred to liquid nitrogen (-196°C).

To recover cells from liquid nitrogen stocks, cell suspensions were thawed rapidly at 37°C in a water bath and transferred to a 15mL Falcon™ tube (Corning, CLS430791) with complete growth medium. The cell suspension was centrifuged at 250 x g for

three minutes to expel residual DMSO. The supernatant was discarded and the cell pellet was taken up in pre-warmed fresh complete growth medium **(Table 2.18)** and plated into the appropriate cell culture flasks. Cells were regularly tested for Mycoplasma with the primers shown in **Table 2.15**.

2.2.1.4 PCR cell line mutation

To ensure each cell line contained the mutations detailed in the literature, PCR-based cell line sequencing was performed. Primers were designed using Primer3Plus (Primer3Plus, 2015) to amplify an approximately 200 base pairs (bp) region around the mutation site. PCR using HotStarTaq Plus DNA Polymerase (QIAGEN) was then performed according to the manufacturer's instructions and using the PCR conditions detailed in **Table 2.19**.

The PCR product was subsequently run on a 1.5% agarose gel, containing Gel Red (Biotium), and visualised under Ultra Violet (UV) light to ensure a single, strong band was produced from the PCR.

2.2.2 PCR for FGF receptor expression

To verify the FGFR expression status of the cell lines used, primers for each FGFR were used with the PCR cycle settings per **Table 2.19**. PCR products were then run on an agarose gel containing Gel Red and visualised under UV light. All experiments were performed in triplicate.

Table 2.19. PCR cycle for the amplification of FGFR sequences.

Step	Temperature (°C)	Time (min)	Cycles
Initial denaturation	94	5	1
Denaturation	94	0.5	35
Annealing	58	0.5	
Extension	72	0.5	
Final extension	72	7	1
Hold	16	Indefinitely	

2.2.3 Serum starvation

Cells were seeded in 6-well plates in culture medium and incubated at 37°C, 5% CO_2. After 16 hours for adherent cells, medium was removed and cells were serum starved in FBS-free medium for 1, 2, 4, 8, 16 or 24 hours. For suspension cells, cells were serum starved immediately after counting. Control cells were treated with complete growth medium **(Table 2.18)** for 24 hours, after which all cells were lysed and protein was isolated as described in section 2.2.29. All experiments were performed in triplicate.

2.2.4 Stimulation assay

Respective cells were seeded in 6-well plates in culture medium and incubated at 37°C, 5% CO_2. After 16 hours, medium was removed and cells were serum starved in FBS-free medium for 4-6 hours. Again, suspension cells were serum starved immediately after counting. Media were then exchanged to FBS-free medium containing PD (Sigma-Aldrich, P2499) at a final concentration of 2μM, 1μM AZD (AstraZeneca, UK), 1.5μM BGJ (courtesy of Valerie Schuele, Novartis Pharma AG) or the equivalent volume of DMSO for control wells, for 1 hour. After 15 and 60 minutes 300ng/mL heparin (Sigma-Aldrich) was added to each well and 100ng/mL FGF2 or FGF10 (PeproTech) were used to stimulate cells. After 1 hour, cells were lysed and protein was isolated as described in section 2.2.29. All experiments were performed in triplicate

2.2.5 Cell counting

In order to count cells, cells were washed in PBS, pelleted and re-suspended in 1mL complete growth medium **(Table 2.18)**. From the cell suspension 10μL were mixed with 10μL Trypan Blue in an Eppendorf and 10μL were pipetted into a haemocytometer (FastRead) and viewed using a light microscope. Viable cells from three 4x4 squares were counted (Top left, bottom right and middle left) and averaged and adjusted for Trypan Blue addition (x2). The same procedure was used for all cell counting experiments for consistency.

2.2.6 Cell viability assay in 2D

FGFR inhibitors PD, AZD and BGJ were dissolved to a stock concentration of 10mM in DMSO and stored at -20°C, or 4°C for PD. Stock dilutions were then further diluted in complete growth medium **(Table 2.18)** when necessary.

Gastric, endometrial and lung cancer cells were seeded into 96-well plates and incubated at 37°C, 5% CO_2. The next day, cells were treated with a range of drug concentrations in technical triplicate and, as a control, cells were treated with DMSO at the same concentration as in the drug-treated wells. As a positive control for cell killing, and background signal, 0.01% Staurosporine was added to three wells. The 96-well plates were then incubated for 72 hours at 37°C.

To check viability of treated cells, a (4,5-dimethylthylthiazol-2-yl)-2,5-diphenyl tetrazolium bromide (MTT) assay was performed. Medium was removed after 72 hours incubation with the inhibitor, followed by addition of fresh medium containing 0.5 mg/mL MTT (Invitrogen). After 3 hours incubation, medium was replaced with DMSO to dissolve the formazan crystals. The absorbance was measured at 550nm using a spectrophotometer plate reader (Tecan Infinite F50). For some cell lines, such as the suspension cells and more recent cell viability assays, a 3-(4,5-dimethylthiazol-2-yl)-5-(3-carboxymethoxyphenyl)-2-(4-sulfophenyl) -2H-tetrazolium) (MTS) assay was used, whereby 10μL of the MTS reagent (Promega G3581) was directly added to the wells and absorbance was measured with the spectrophotometer after 1-4 hours, depending on the cell line used. The measured values were then normalised to DMSO controls after subtracting the background absorbance from the Staurosporine-treated wells and displayed graphically using Prism 5 (Graph Pad, USA). Half maximal inhibitory concentrations (IC_{50}) of inhibitors tested were calculated with Prism using the sigmoid dose–response function. All experiments were performed in biological triplicate.

2.2.7 Cell viability using IncuCyte™ ZOOM®

H520 cells were either seeded alone or 2:1 ratio in conjunction with MRC-5 H2B-GFP cells into 96-well plates at a density of 1.5 x 10^3 cells per well. The following day cells were treated with BGJ ranging from 0.03nM to 50μM and incubated for 72 hours. The plates were then simultaneously placed inside an IncuCyte™ ZOOM® imaging system (Essen BioScience), which consists of a microscope gantry that resides within a cell incubator and can obtain real time live cell imaging. Channel selection phase and fluorescence capturing was selected to distinguish fibroblast cells from cancer cells. Four images per well were captured every 30 minutes for two hours and cell viability, cell growth area and fluorescence intensity were measured over time.

2.2.8 Cell cycle analysis

In order to quantify DNA content, cells were harvested and washed in PBS. Cells were then fixed in ice-cold 70% ethanol which was added dropwise to the pellet whilst vortexing, thus avoiding the formation of clumps. Cells were fixed for 30 minutes at 4°C and pelleted. Cells were washed twice in PBS and subsequently centrifuged at 250 x g for 5 minutes to avoid cell loss when discarding the supernatant especially after spinning out ethanol. Next, cells were treated with 50μL of a 100μg/mL stock of RNase ensuring only DNA will be stained. DNA was either stained using Propidium Iodide (PI, Sigma-Aldrich, P4864) or 4',6-diamidino-2-phenylindole **(**DAPI, Life Technologies™, P36931) at a concentration of 50μg/mL from a 50X stock solution (2.5mg/mL). Stained cells were then analysed using BD LSR Fortessa and FlowJo, v10.7 (BD Biosciences).

2.2.9 Annexin V cell apoptosis assay

Cells were seeded at a density of 2.5 x 10^5 per well in 6-well plate and either treated on the same day (suspension cells) or the following day (adherent cells) with the respective reagents or DMSO (vehicle control) for 72 hours. Cells were then removed, washed with PBS and re-suspended in binding buffer (10mM HEPES, 140mM NaCl, 2.5mM $CaCl_2$) at a concentration of 10^6 cells/mL. Of the suspension, 100μL (10^5 cells in 100μL) were transferred to a 5mL round-bottom polypropylene tube. Annexin V-Alexa Fluor647 (2.5μL) and PI (2.5μL) were added to the cells, gently vortexed and

incubated for 15 minutes at RT in the dark. For each experiment control samples were prepared and left untreated, or only treated with either PI or Annexin V. Cells were analysed by BD LSR Fortessa and FlowJo, v10.7 (BD Biosciences).

2.2.10 Generation of FGFR inhibitor-resistant cell lines

Cells were seeded in their respective culture medium, as detailed previously, in 35mm dishes. After 24 hours, the appropriate concentration of inhibitor or DMSO control was added. Medium was changed every 2-3 days. After 7 or 14 days, adherent cells were detached from the dish using trypsin/EDTA or just removed and spun in the case of suspension cells and counted manually under a light microscope using a FastRead haemocytometer. All experiments were performed in triplicate. To generate the drug-resistant SNU-16^{BGJR} cell line, cells were exposed to increasing drug dosages over a time course of one month, were the drug dosage was doubled at every second passage starting with 100nM, reaching a final dosage of 1.5μM BGJ for SNU-16.

The same approach was used to generate BGJ-resistant H520 cells (H520^{BGJR}) reaching a final dosage of 1μM. The resistant cells were cultured until they again had growth kinetics in presence of drug similar to that of untreated parental cells.

For experiments with drug-resistant cells, the cells were kept in inhibitor and then medium was exchanged to inhibitor-free medium for 1h prior to cell seeding and treatment.

2.2.11 Immunofluorescence staining of cells on coverslips

Cells on coverslips were washed, fixed in 4% PFA and permeabilised with 0.1% Triton X-100/2% BSA, followed by blocking in 2% BSA/PBS for 1 hour. Coverslips were incubated with anti-E-Cadherin (BD Bioscience, 610182) primary antibody diluted 1:100 in 2% BSA/PBS for 1 hour at RT. After washing the coverslips in 2% BSA/PBS, a fluorescent anti-mouse secondary antibody at a dilution of 1:200 in 5% BSA/PBS was incubated for 1 hour at RT (followed by mounting using mounting medium supplemented with 1μg/mL DAPI).

2.2.12 Short interfering RNA (siRNA) knockdown

Cells were seeded in 6-well plates in complete medium. The following day, at approximately 40% confluence, the medium was replaced with 1mL of complete medium **(Table 2.18)**. Cells were transfected with a pool of four siRNA oligonucleotides targeting the gene of interest at a final concentration of 10nM. Control cells were transfected with a pool of non-targeting siGenome siRNA at the same concentration. Transfection of the siRNA was facilitated using INTERFERin® (Polyplus) at 4µL/100µL. INTERFERin® and siRNA complexes were prepared in Opti-MEM™ (Gibco by Life Technologies™), vortexed and incubated at RT for 20 minutes before 100µL of the mixture was added to cells in culture medium. Cells were incubated for 48 hours or 120 hours before cell lysis or drug treatment and confirmation of knockdown was performed by Western blot (section 2.2.29).

2.2.13 Plasmid preparation and bacterial transformation

Competent Stbl3 *E.coli* (Invitrogen) were thawed on ice and 1µg of plasmid DNA was added. After 30 minutes of incubation, bacteria were heat shocked at 42°C for 30 seconds. SOC medium (Invitrogen) was added to the vial on ice before incubation at 37°C for 1 hour with agitation. After incubation, 150µL of the cell suspension was pipetted onto an agar (Fisher Scientific) plate containing 100µg/mL ampicillin (Sigma-Aldrich, Poole, UK) and incubated overnight at 37°C. Bacterial colonies were picked and cultured in 5mL LB broth (Fisher Scientific) containing 100µg/mL ampicillin for 8 hours. Plasmids were isolated using a Qiagen mini prep kit (Qiagen, Manchester, UK) according to manufacturer's instructions.

2.2.14 Transfection of genes in cells using Lipofectamine®

Cells were seeded in a T75 culture flask at 40% confluence in standard medium. The following day, medium was removed and cells were washed with PBS. Opti-MEM™ was warmed to 37°C and 5mL added to each flask. For transfection control wells, 1µg/µL pmaxGFP (pGFP) (Lonza) was added to 1.25mL Opti-MEM™ in a Falcon™ tube. A second Eppendorf tube containing 25µL Lipofectamine® 2000 (Invitrogen) with 1.25mL Opti-MEM™ was prepared and both solutions were incubated at RT for 5 minutes. The contents of both tubes were then mixed and incubated at RT for 20

minutes. The total volume was then added to control flasks and incubated at 37°C for 4 hours. Medium was then removed and replaced with standard culture medium and cells incubated at 37°C for 48 hours. For pPHLDA1 transfection, 1µg/µL of plasmid was added to 1.25mL Opti-MEM™ and mixed with the Lipofectamine® 2000 preparation as above and added to the cells. After 16 hours, flasks were inspected under UV light for GFP expression. Cells were lysed and PHLDA1 levels analysed via Western blot, as outlined in section 2.2.29.

2.2.15 Transfection of genes using jetPRIME®

In a 6-well plate 1.5 x 10^5 cells were seeded in 2mL of culture medium. In the case of adherent cells, overnight incubation was required. However, suspension cells were treated immediately after seeding. Transfection was performed in the presence of serum by diluting 2µg DNA in 200µL jetPRIME® buffer, followed by vortexing for 10 seconds. 4µL jetPRIME® reagent was added, vortexed 10 seconds and incubated for 10 minutes at RT. The transfection mix was then added to the cells in serum containing medium and incubated at 37°C, 5% CO_2. The next day, medium was exchanged and cells were incubated for 24 to 48 hours prior to analysis by cell counting, PCR or Western blot.

2.2.16 Lentiviral particle production

To achieve stable expression of a desired gene in a cell line that shows difficulties with being transfected, due to toxicity issues or for experiments that require longer gene expression or knockdown of the gene, lentiviral expression systems have been used. Lentiviral particles containing fluorescence markers were used to differentiate between cells. The system is based on the human immunodeficiency virus, and uses four plasmids; pREV, pGAG/Pol, pVSVG, and a final plasmid for the vector to be inserted into the host cell. pREV and pGAG/Pol encode for viral proteins required for efficient viral packaging. pVSVG encodes a viral protein required for effective infection of the viral particles into the host cells (Dull et al., 1998). These plasmids are combined and transfected into HEK293T cells, that in turn generate and release viral particles into the cell culture medium. The supernatant of the medium can then be used to infect target cells **(Figure 2.2)**. To generate a Lentivirus expressing Azurite,

EGFP, H2B-RFP or GFP **(Figure 2.3)**, HEK293T cells were grown to approximately 50-70% confluence. Four hours before transfection, medium was changed to fresh DMEM supplemented with 10% FBS. 5µg lentiviral plasmid, 1.75µg of the envelope vector pMD2G and 3.2µg of pCMV-dR8.74 were mixed in 470µL Opti-MEM™ followed by subsequent addition of 30µL FuGene (Promega). The mixture was added dropwise onto the cells and incubated for 30 minutes at 37°C, 5% CO2. The next day, the medium was exchanged to normal growth medium and the following day the viral supernatant was collected and pelleted. Viral supernatant was then stored at -80°C until further use.

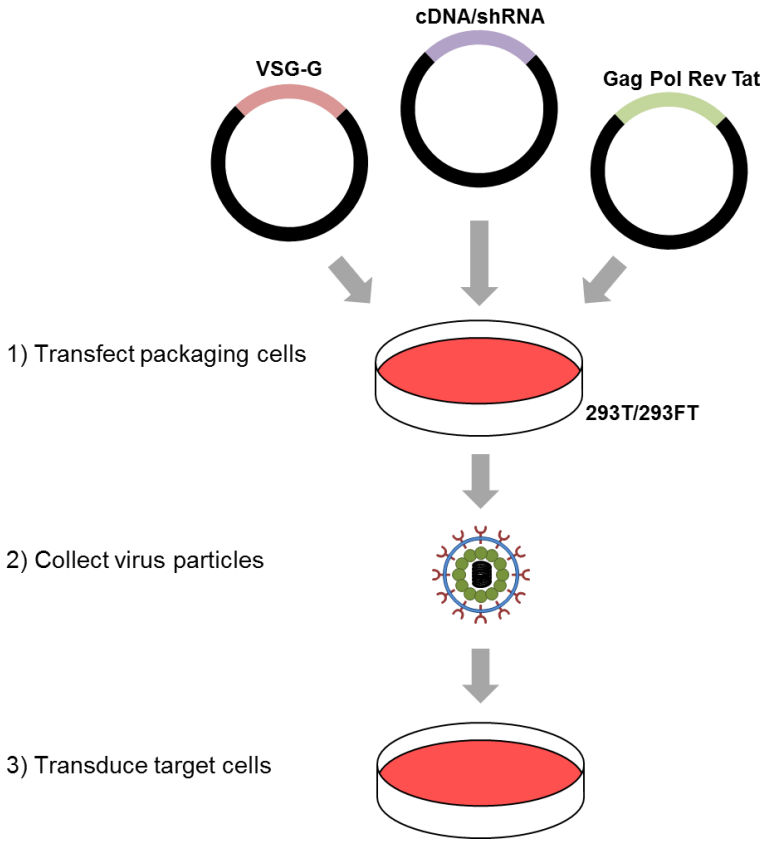

Figure 2.2. Schematic overview of lentiviral transfection.
HEK293 cells serve as packaging cells and are transfected with an envelope plasmid (red), a plasmid containing the gene of interest (purple, in this case the fluorescent marker) and packaging plasmid (green). The medium containing the virus is collected and target cells are transduced.

Figure 2.3. Histone H2B-RFP and H2B-GFP vectors, Azurite and EGFP vector map.

2.2.17 Infection of cells with lentiviral supernatant

To generate cancer cell lines expressing EGFP or Azurite, 1mL viral supernatant was added to 2mL of medium containing cells in a 6-well plate and incubated for 24 hours at 37°C, 8% CO_2. The following day, 1µg/mL Puromycin (Thermo Fisher Scientific) was added to the culture medium and cells were incubated at 37°C, 5% CO_2. The success of the stable transfection and integration of the fluorescent plasmid was then tested by fluorescence microscopy and FACS, performed by the Flow Cytometry Facility at Barts Cancer Institute.

2.2.18 Fluorescence activated cell sorting (FACS) of live cells

To assess EGFP expression or Azurite expression, adherent cells were washed, trypsinised and pelleted by centrifugation for 2 minutes at 250 x g. Suspension cells were pelleted immediately and cells were re-suspended in 500µL culture medium and transferred to round bottom polystyrene FACS tubes (Corning, #352235).

Cells were sorted using BD FACS Aria™ II (BD Bioscience, USA). Cells were gated based on forward scatter (FSC) and side scatter (SCC) to exclude debris and a second gate was set to exclude doublets on a dot plot of pulse area (FSC-A) *versus* height (FSC-H). H2B-RFP positive cells were detected with the yellow laser at 610nm bandpass filter and H2B-GFP positive cells were detected with the blue laser at 525nm bandpass filter.

2.2.19 Organotypic cell culture using Alvetex® scaffolds

Alvetex® scaffolds (Reprocell Ltd.) were used as a novel technique of 3D cell culture. The scaffold consists of a polystyrene membrane of 200µm with pore sizes of about 40µm. In this project mainly 12-well scaffold inserts were used **(Figure 2.4)**. Prior to cell seeding, the Alvetex® scaffold was first immersed in 70% EtOH followed by two PBS washes and a final culture medium wash. Cells were then seeded dropwise in the middle of the scaffold membrane and fed with medium from below **(Figure 2.5)**. For co-culture experiments, cells were transfected with lentiviral supernatant as described in 2.2.17 and in 2:1 ratio of cancer cells to fibroblasts **(Figure 2.6)**. Cells were grown up to 21 days and imaged live using a confocal laser scanning microscope (CLSM 710, Carl Zeiss). Additionally, the scaffolds were also fixed and embedded in paraffin for immunofluorescence or immunohistochemistry. Different formats of Alvetex® were used, 24 well-plates with free floating scaffolds, 12 well insert scaffolds and 96-well plates. Scaffolds were either coated with rat tail collagen I (BD Biosciences, 354236; 0.8mg/mL), Matrigel™ (BD Biosciences, 354234; 0.8mg/mL) or left uncoated. Collagen and Matrigel™-coated scaffolds were incubated at RT for 1-2 hours. Excess fluid was aspirated and cells were seeded immediately onto the scaffolds. The scaffolds containing the cells suspensions were incubated for a minimum of 30 minutes at RT to enhance attachment of cells prior to incubation at 37°C, 5% CO_2.

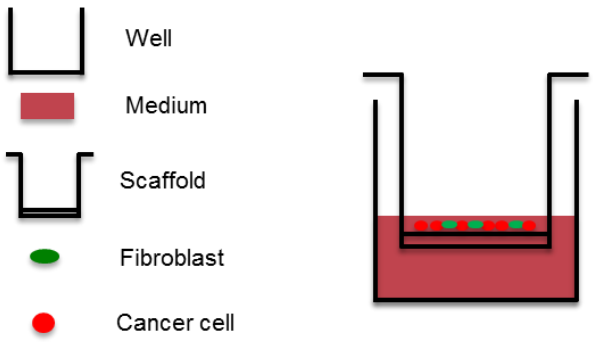

Figure 2.4. Schematic representation of the 3D cell culture model Alvetex®.
The Alvetex® 3D model consist of a polysterene membrane in an insert where cancer cells mixed with fibroblasts can be seeded onto. The insert are placed in a 6-well plate. Cultures are fed from underneath. This model can be used to assess the effects of pharmacological agents by inclusion of such drugs in the medium (Chioni and Grose, 2012, Coleman et al., 2014, Froeling et al., 2009). In this model, cells are fed every 2-3 days for the duration of the experiment, after which they are formalin fixed, sectioned and stained for a range of cellular markers.

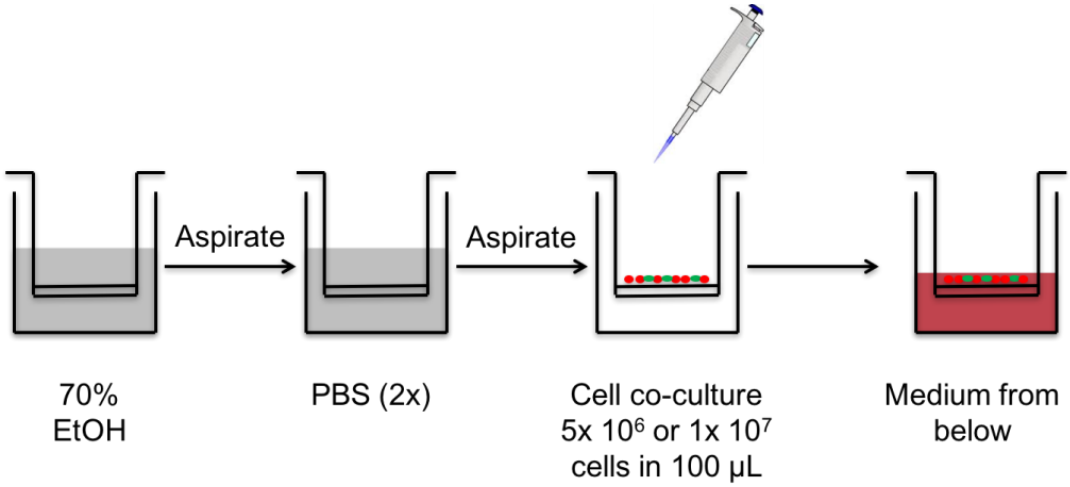

Figure 2.5. Alvetex® workflow for 12-well insert scaffolds.
Scaffolds were submerged in 70% EtOH followed by two PBS washes. Cells were then seeded on top of the scaffold and incubated at RT for 30 min. Medium was then fed from below to create a chemotactic gradient.

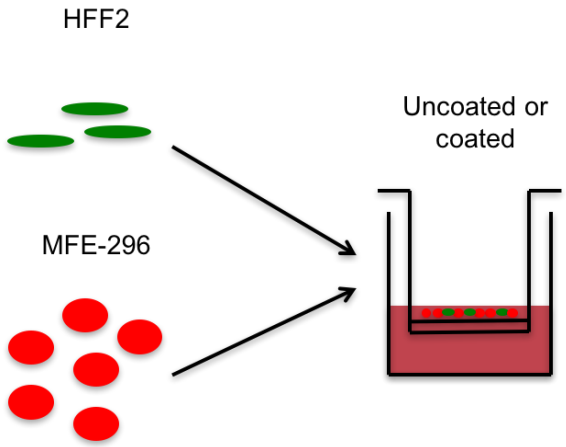

Figure 2.6. Alvetex® cell seeding.
Cells were seeded 2:1 cancer cells to fibroblasts onto uncoated, collagen or Matrigel™-coated Alvetex® scaffolds.

2.2.20 3D Cell viability assays

96-well Alvetex® plates consist of a black plate with a clear plastic base, with an Alvetex® scaffold at the bottom of each well. The Alvetex® scaffold has been heat welded to the base of the wells in a process which does not alter its physical structure. Cells growing in Alvetex® scaffolds are exposed to culture medium from above only and predominantly reside in the top portion of the scaffold. As with 2D culture, coating reagents to enhance cell attachment can be considered (e.g. ECM proteins).

As with the Alvetex® insert, prior to use, sample wells were rehydrated with 70% ethanol (~100µL). Ethanol was removed by aspiration and wells were washed once with 200µL PBS and then immediately with 200µL appropriate cell culture medium to avoid drying of the scaffold. Next, 200µL of medium containing 5 x 10^3 to 10^5 cells were seeded into the wells and incubated for 1 hour at RT before treatment to increase attachment and uniformity. The MTT or MTS assay was performed as described in section 2.2.6 with the exception, that before measuring absorbance, 100µL of medium in the wells was transferred to a clear 96-well plate and measured at 550nm with a spectrophotometer. All experiments were performed in technical triplicate.

2.2.21 3D drug resistance

In order to generate drug resistant cancer cells in 3D, 10^6 cells were seeded into 12-well insert Alvetex® scaffolds according to section 2.2.19. In terms of cell culture conditions, SNU-16 H2B-RFP cells were seeded alone or in co-culture with HFF2-EGFP cells (2:1). The following day medium was removed and medium containing 100nM BGJ or an appropriate concentration of the vehicle control was fed from below **(Figure 2.7)**. Medium was changed every second day and the concentration of the FGFR inhibitor was doubled at every second medium change. Control samples of the conditions were live imaged once a week using a confocal microscope. Monoculture and co-culture control wells were harvested after 2 weeks, BGJ-treated co-culture samples were harvested (section 2.2.26.1) after 4 weeks together and monoculture BGJ-treated cells were harvested after 8 weeks when resistant cell populations were observed.

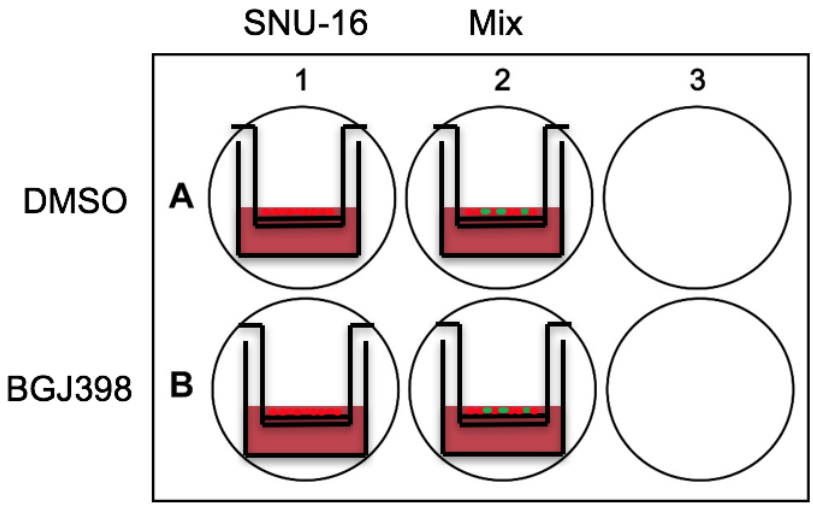

Figure 2.7. Generation of resistant cells in 3D experimental layout.
SNU16 H2B-RFP and HFF2-EGFP fluorescently tagged cells were seeded 2:1 or SNU-16 H2B-RFP cells alone into Alvetex® 12 well-insert scaffolds and treated either with the vehicle control DMSO or BGJ until resistant cell populations were observed.

2.2.22 Live image acquisition

Alvetex® scaffolds were removed from the 6-well plate using tweezers and placed onto a 35mm glass coverslip-bottomed dish (Greiner bio-one, 627 861). The confocal microscope was equipped with a heated chamber set to 37°C, 5% CO_2 to simulate the incubator conditions. The dish with the Alvetex® scaffold was then positioned into a heated 35mm dish-holder on an automated x-y scanning stage in the chamber. *In situ* overlapping sections of H2B-RFP positive cells in the z-axis were detected using a 568nm excitation line and 602nm emission and H2B-GFP or EGFP and H2B-GFP-positive cells were detected using a 488nm excitation line and 517nm emission. Along the z-axis, series of images of 700µm square (x-y plane) were acquired at constant 4µm intervals with a 1µm overlap to approximately 200µm depths through the scaffold, using a long working distance 20x air objective (Carl Zeiss, Objective LD Plan-Neofluar 20x/0.4 Corr M27). Per sample, three images were acquired to calculate statistical significance.

2.2.23 Image rendering using Imaris

The raw laser scanning microscope (.lsm) Z-stack data files acquired using the LSM 710 were imported to the image analysis software Imaris (Bitplane AG, Switzerland). With the base software, 3D images of the Z-stacks were rendered and background noise was removed, generating smooth surfaces, a higher resolution and sharper 3D images. Within a 700µm x 700µm x 200µm image, cellular volumes of H2B-RFP positive and EGFP or H2B-GFP positive cells were measured, which were represented in comma-separated value (.csv) files (in addition further parameters such as area, intensity, position, sphericity, and volume were also generated), allowing high content data analysis.

2.2.24 Cell retrieval from Alvetex® for RNA and protein extraction

As opposed to other common organotypic methods, cells in Alvetex® scaffolds can be retrieved from the scaffolds for RNA extraction or protein extraction. Scaffolds were removed from the wells and, with a sterile scalpel or sterile dissecting scissors, cut into small pieces to increase the surface of the detaching agent. The pieces were transferred to a sterile 15mL Falcon™ containing 5mL of 0.25% Trypsin-EDTA and incubated at 37°C, 5 % CO_2 and secured with autoclave tape on a shaking platform set to 100rpm for 10 minutes, thus ensuring the maximize the range of agitation. To increase detachment the tube was shaken by hand for 10 seconds followed by transferring the resulting cell suspension to a 50mL centrifuge tube and 5mL FBS-containing medium was added to neutralise the trypsin solution. Detached cells were kept at 37°C, 5% CO_2. Trypsinisation of the quarters was repeated with another 5mL 0.25% Trypsin-EDTA and transferred into the same 50mL tube. Cells were pelleted at 250 x g for 5 minutes and re-suspended in appropriate volume of medium for the downstream process.

2.2.25 Histology methods

2.2.25.1 Fixation, harvesting and processing organotypic samples

Alvetex® scaffolds were removed from the 6-well plate and fixed in 10% v/v neutral buffered formalin (Cellstor, BAF-0010-25A) for 12 hours at 4°C followed by washing with PBS twice. The membrane was removed from the scaffold using a scalpel, placed into histology embedding cassettes held in between two sponges and transferred to 70% v/v ethanol for at least three hours until embedded in paraffin. Samples were dehydrated, then processed through xylene and in 60°C paraffin, using a Leica ASP300 processor. Samples were embedded in paraffin using a Leica EG1160 H+C instrument and stored at 4°C. 4µm paraffin sections were cut using the Microm RM2255 microtome and placed on Superfrost™ slides, which were then incubated at 37°C overnight to dry the samples. The sections were then stored at RT or Haematoxylin-Eosin (H&E) stained using the Leica autostainer XL CV5030. Sample embedding and H&E staining was performed by the Histopathology Department, Barts Cancer Institute.

2.2.25.2 Deparaffinisation of paraffin-embedded tissue sections

Histological analysis of paraffin embedded samples required the sections to be completely free from paraffin and then rehydrated via increasing concentration gradients of ethanol. The sections were then stored in PBS until further use.

Table 2.20. Deparaffinisation and rehydration of paraffin-embedded samples.

Procedure	Duration
Xylene	2 x 10 min
100% EtOH	10 min
100% EtOH	2 min
90% EtOH	2 min
80% EtOH	2 min
50% EtOH	2 min
Distilled water	1 min

2.2.25.3 Immunofluorescence staining of paraffin-embedded scaffolds

Slides of 4µm thick paraffin sections of Alvetex® scaffolds were dewaxed in xylene and rehydrated through a series of graded ethanol and transferred to PBS. To retrieve antigens, slides were placed in 10mM sodium citrate buffer (pH 6.0) and boiled in the microwave for 11 to 20 minutes on maximum power. The slides were subsequently cooled using cold water for three minutes and then washed three times for 5 minutes with PBST, rinsed twice in PBS and then sections were encircled using a DakoPen. Samples were permeabilised with 0.2% Triton/PBS for 5 minutes at RT. Unspecific binding sites were blocked by incubating the slides in PBSABC buffer (containing 2% BSA, 10% FBS) for 1 hour at RT, followed by incubation in primary antibody at a dilution of 1:100 in PBSABC buffer overnight at 4°C in a humidified box. The following day, slides were washed three times with PBS and incubated with a fluorescence-conjugated secondary antibody at a dilution of 1:200 in PBSABC buffer for 1 hour at RT. The slides were washed again three times in PBST for 5 minutes and incubated with DAPI in PBS for 10 minutes. The slides were washed in PBS, dipped in distilled water and mounted with Mowiol before being stored at 4°C.

2.2.25.4 Microscope image acquisition

Confocal images were acquired at RT using a confocal microscope (LSM710; Carl Zeiss). Images were taken using a 20x air objective (Carl Zeiss, Objective LD Plan-Neofluar 20x/0.4 Corr M27). The acquisition software used was ZEN 2009 (Carl Zeiss). Thresholds were set per slice and remained constant for all images analysed.

Bright-field images were acquired at RT using a light microscope (Axiophot; Carl Zeiss) fitted with a camera (AxioCam HRz; Carl Zeiss). The objective used was a Plan Neofluar with 10x magnification and 0.3 aperture. The acquisition software used was AxioVision Release 4.8 (Carl Zeiss). The Pannoramic 250 high throughput scanner (3D Histech Ltd.) was used for whole and enlarged image acquisitions of the Alvetex® slides stained with H&E and IHC stainings.

2.2.25.5 Statistical data analysis

In all experiments, quantitative statistics were calculated with Prism 5, unless otherwise stated. Descriptive statistics are presented as a means ± standard errors. Comparisons between two sample groups used Student's T-tests, whereas comparison of more than two sample groups used one-way analysis of variance (ANOVA).

2.2.26 RNA methods

2.2.26.1 RNA isolation and purification from cells

Cells were seeded in 6-well plates and harvested at 80% confluency for RNA isolation using an RNeasy® Mini kit (QIAGEN, Manchester, UK). Cells were washed twice with PBS followed by the addition of 350µL RLT buffer per well. Cells were scraped, collected and placed into an Eppendorf and 250µL 100% EtOH was added and mixed thoroughly. RNA was then purified according to the manufacturer's instructions. To elute RNA, 20µL RNAse-free water was added and centrifuged as previously described. This step was repeated with 10µL RNAse-free water, yielding a total volume of 30µL. The concentration of the purified RNA was measured using a Nanodrop 1000 spectrophotometer and then stored at -80°C until further use.

2.2.26.2 cDNA synthesis

To synthesise cDNA, 1µL 50µM random hexamer primers (Thermo Fisher Scientific), 1µg of purified total RNA and 1µL dNTPs (10mM each) were diluted in RNAse-free water to a volume of 12µL. The mix was heated to 65°C for 5 minutes and then placed immediately into ice. To this mixture 4µL 0.1M Dithiothreitol (DTT) and 1µL 5X first strand buffer were added, mixed and incubated at RT for 2 minutes. Then 1µL (200 units) SuperScript™ II RT (Invitrogen) was added, mixed and reverse transcription was then achieved using a Flexigene thermal cycler (Techne, Stone, UK) according the settings of 25°C for 10 minutes, 42°C for 50 minutes, 70°C for 15 minutes. The resulting cDNA was then stored at -20°C.

2.2.26.3 Quantitative real time PCR (q-RT PCR)

For q-RT PCR, a master mix was prepared consisting of 1µL of cDNA mixed with RNAse-free water to a volume of 5µL per well. As for the respective primers (10mM forward and reverse primer in ddH_2O) (Custom Oligo, Invitrogen), 0.15µL were mixed with 4.85µL SYBR ROX (Qiagen) and pipetted into the cDNA. As a control, the same master mix was also prepared but instead probed with primers for the housekeeping genes *Glyceraldehyde 3-phosphate dehydrogenase* (*GAPDH*) or *Hypoxanthine-guanine phosphoribosyltransferase* (*HPRT*) (Custom Oligo, Invitrogen). Three replicates were performed per condition and gene. q-RT PCR was performed

in the StepOnePlus Real Time System (Applied Biosystems, Paisley, UK) as described in **Table 2.21**. The q-RT PCR reaction was evaluated by analysing the melt curves to assess qRT PCR amplicon length using the StepOne software v2.2.

Table 2.21. qRT-PCR steps in the StepOnePlus Real Time System.

	Cycles	Target (°C)	Duration
Preincubation	1	95	15 min
Amplification	40	95	30 s
		60	30 s
		72	30 s
Melting curves	40	56	60 s
		95	15 s
Cooling	1	4	30 s

The relative expression levels were calculated using the $2^{-\Delta\Delta CT}$ method (Livak and Schmittgen 2001). The mean values of each condition were related to the expression levels of the reference housekeeping genes *GAPDH* and *HPRT* for normalisation. Statistical analysis was then performed using Prism 5. In order to compare two groups of data, a Mann-Whitney test was used. Error bars indicate the mean standard deviation and asterisks show significance between compared groups.

2.2.27 RNA sequencing

Cells were grown in Alvetex® until resistant populations were found by live cell imaging, or until control wells were fully confluent. Cells were retrieved from scaffolds as described in section 2.2.24 and total RNA was extracted using the RNeasy® Plus RNA extraction kit (QIAGEN), according to the manufacturer's instructions. Additionally, working utensils were UV and RNAseZap-treated. Cell pellets were resuspended in RLT buffer supplemented with 1% ß-mercaptoethanol, which irreversibly denatures RNAses by reducing disulphide bonds and destroying the native conformation for the enzyme functionality together with guanidinium isothiocyanate (GITC) contained in the lysis buffer any RNAse present will be inactivated. In addition, a DNAse digestion step of the purified RNA with RNAse-free DNAse was included. RNA concentration and purity was checked with a

Nanodrop spectrophotometer. Total RNA was then run on agarose gels (0.2μg/mL) containing ethidium bromide and visualised in a UV chamber. To further check the quality of RNA, the RNA Integrity Number (RIN) of 100ng RNA was measured on a pico chip using the Agilent Bioanalyzer 2100, which is a microfluidics-based platform that separates and quantifies RNA molecules according to their sizes. Results were analysed using the 2100 Expert software (Syngene, Cambridge, UK). The resulting RIN number reflects the degree of degradation of the sample and a value above 7 is expected. From total RNA, mRNA was isolated, fragmented and primed with the help of AMPure XP beads. Then the first-strand cDNA was synthesised followed by second strand synthesis. The double-stranded cDNA was purified using 1.8X Agencourt AMPure XP beads followed by performing the end prep of the cDNA library. Next, adaptor ligation was performed and the ligation reaction was purified again using AMPure XP beads. The ligated DNA was then PCR enriched and purified again using the AMPure XP beads. The library quality was then evaluated on a Bioanalyser (Agilent High Sensitivity Chip). For the final amplification 12 cycles were used. Each sample was run in duplicate. The raw sequencing data were delivered in FASTQ format.

RNA sequencing was performed using the Illumina platform at Barts Genome Centre. The resulting data were analysed using Genome Studio, R, Microsoft Excel and Prism 5 software.

2.2.28 Pathway analysis

From the differential gene expression analysis data, different tools were used to analyse the up and downregulated pathways.

2.2.28.1 Database for Annotation, Visualisation and Integrated Discovery (DAVID)

The DAVID database v6.8 (beta) (http://david.niaid.nih.gov) is a free online bioinformatics resource developed by the Laboratory of Immunopathogenesis (LIB) and was used for an initial comparison of regulated genes. The database encompasses a full knowledgebase and provides a comprehensive set of functional annotation tools for investigators to understand biological meaning behind large list of genes. A list of the regulated genes is fed into the database and according to the Ensembl code annotated to a specific gene. This then allows identification of enriched biological themes in gene ontology (GO) terms and cluster genes into functional-related gene groups. Furthermore, it lists gene-disease associations, protein interactions and enables investigation of protein functional domains and motifs. Genes were then visualised on KEGG pathway maps. With DAVID however only gene IDs were used and fold changes were not taken into account.

2.2.28.2 Gene Set Enrichment Analysis (GSEA)

Gene set enrichment analysis can be used to study gene sets that have been grouped together due to their implications in the same biological pathway or location on a chromosome. Software enrichment scores (ES) were calculated, which represents the amount to which the genes in the set are over-represented at either the top or bottom of the list according to Kolmogorov-Smirnov statistics. Statistical significance of ES by phenotypic-based permutation test produced a null distribution for the ES. It was adjusted for multiple hypothesis testing for a large number of gene sets that were analysed one at a time. The enrichment scores for each set were normalised and false discovery rate was calculated.

Files with pre-ranked (.rnk file) and .chip file names of genes were uploaded and analysed using the 'GSEAPreranked' tool. As a gene set database,

c2.cp.kegg.v5.1.symbols.gmt was used. Perturabtions were set to 1000 and 'Ranked list' to rnk file and 'Chip platform' was used. The name of the analysis was set and as an enrichment statistics 'classical' was used. DEall files were used and p2 weighted with DEall genes or classical with DEall genes was set. Gene sets were set to 200 (http://software.broadinstitute.org/gsea/downloads.jsp. Subramanian 2015).

2.2.28.3 Ingenuity pathway analysis

IPA is an associative tool that is used to predict the effect on the organism and the mechanism of this effect from the data provided by the user. It allows drawing inferences between genes that can be tested to check their legitimacy. From the tool bar, the dataset was uploaded and saved as a .txt file. As a file format the flexible format was used. Contains column header was selected as yes. As an identifier, flexible was chosen. For analysis ID, observation 1 Log ration observation 2 p value was chosen and saved. In the next section analyse/filter dataset core analysis and run analysis was started. To analyse the outcome first canonical pathways were investigated, which displays the molecules of interest within well-established signalling or metabolic pathways. Next, upstream regulators were analysed to see which upstream molecules were predicted to have been activated or inhibited to have led to the expression patterns found in the dataset. Furthermore, downstream effects can be evaluated to explore the diseases and biological processes in the dataset. Regulator effects help to create hypotheses for how upstream regulators might drive downstream biology.

2.2.29 Western blotting

2.2.29.1 Isolation of proteins

Cells were washed twice with PBS followed by lysis in a suitable volume of Radioimmunoprecipitation assay (RIPA) buffer (Millipore, 20-188), supplemented with 1:100 protease (Millipore, 539131) and phosphatase inhibitors (Millipore, 524625). The cells were left on ice for 5 minutes before scraping with a rubber policeman and subsequently placed into Eppendorf tubes. After briefly vortexing the samples, cell debris were centrifuged at 15,000 x g for 15 minutes at 4°C. The supernatant containing the proteins was then transferred into fresh Eppendorf tubes and stored at -20°C or directly assayed for protein concentration.

2.2.29.2 Measuring protein concentration

Protein concentration of samples was determined with a BioRad DC protein assay (BIORAD, Reagent A, 500-0113; Reagent B, 500-0114; Reagent S, 500-0115) according to the manufacturer's protocol. Values were measured using a spectrophotometer at 650nm. Following protein concentration measurement and calculation of the standard curve consisting of different BSA concentrations in PBS, Laemmli sample buffer (5X) was added and samples were boiled at 100°C for 5 minutes. Samples were then stored at -20°C until further use.

2.2.29.3 Western blot analysis

Equal concentrations of denatured protein (15-40μg) were loaded onto 10% SDS-PAGE gels. After protein separation by electrophoresis, proteins were transferred to a nitrocellulose membrane (GE Healthcare Life Sciences, Whatman, 10 401 196). Ponceau S (Sigma-Aldrich®, P7170) was used to confirm adequate transfer. Membranes were then incubated in 5% milk in PBS at RT for 30 minutes, washed in PBS and incubated with primary antibody in 5% BSA/PBS overnight at 4°C. Membranes were subsequently washed with 0.1% Tween20-TBS (TBST) (Applichem, A13890500) and incubated with HRP-conjugated secondary antibody in 5% milk for 1 hour at RT. Specific protein bands were visualised using Amersham ECL Western Blotting Detection Kit (GE Healthcare, RPN2106) and photographic film (Super RX,

47410 19230). More recently, blots were imaged digitally (Amersham Imager 600), according to the manufacturer's instructions.

Table 2.22. Formulation of polyacrylamide gels for SDS-PAGE gels.

	Resolving Gel						**Stacking Gel**	
	5%	**7.5%**	**10%**	**12%**	**14%**	**15%**		
dH_2O	11.5mL	9.8mL	8.2mL	6.8mL	5.5mL	4.8mL		6.9mL
Resolving Gel Buffer (pH 8.8)	5mL	5mL	5mL	5mL	5mL	5mL	**Stacking Gel Buffer (pH 6.8)**	3mL
Bis-Acryl (30%)	3.3mL	5mL	6.7mL	8mL	9.3mL	10mL		2mL
10% APS	150µL	150µL	150µL	150µL	150µL	150µL		150µL
TEMED	15µL	15µL	15µL	15µL	15µL	15µL		15µL

When the membranes were probed with antibodies where cross-reaction was possible, membranes were stripped using Re-blot Plus Mild (Millipore, 2502) for 10 minutes, washed with PBS, blocked with 5% milk in PBS for 15 minutes and washed again in PBS. Membranes were then re-probed with primary antibody as described above.

Chapter III: Results Part I

FGFR-driven cancers, FGFR inhibitors and 3D Alvetex® model development

3.1 Introduction

Previous research has revealed that therapies targeting specific aberrations that drive carcinogenesis have led to promising responses in patients in the clinics. As FGFs and their receptors are potent cell proliferation and survival inducers, FGF signalling is often hijacked in cancer and many different types of cancers have acquired aberrations in FGFs but more importantly also in FGFRs. 7.1% of all tumour types have genetic alterations along the FGF-FGFR axis and specific FGFR alterations have been associated with certain types of tumours and therefore revealing FGFR aberrations as a suitable biomarker. Preclinical studies have further shown that FGFR2 is a promising therapeutic target in cancer and several FGFR inhibitors are in clinical trials for cancer treatment (Dienstmann et al., 2014).

In 2012, 320,000 new endometrial cancer cases have been diagnosed worldwide and even though approximately 12% of endometrial cancers harbour FGFR2 mutations, little is known about their importance in driving tumourigenesis of this cancer type (Byron et al., 2008). Multiple endometrial cancer cell lines with FGFR2 mutations are highly sensitive to FGFR inhibitors including PD (Dutt et al., 2008, Byron et al., 2008), Ponatinib (Gozgit et al., 2013, Kim et al., 2015), AZD (Kwak et al., 2015), BGJ and Dovitinib (Konecny et al., 2013).

In gastric cancer, 5-10% harbour *FGFR2* amplifications and/or mutations (Carter et al., 2017; Chon et al., 2017; Jung et al., 2012). It is considered the third leading cause of death from malignant disease worldwide with 989,000 new cases of gastric cancer and 738,000 deaths worldwide (Ferlay et al., 2010). Furthermore, the 5-year survival rate is only 30-35% and the presence of *FGFR2* amplifications in patients is associated with poorer overall survival, poor prognosis and more wide spread disease (Jung et al., 2012; Shoji et al., 2015). Gastric cancer cell lines with *FGFR2* amplifications show evidence of ligand-independent signalling and are highly sensitive to FGFR inhibitors (Takeda et al., 2007). It has further been shown that TKIs such as AZD show activity in several colorectal and gastric cancer cell lines (Xie et al., 2013) and those patients harbouring cancers with *FGFR2* amplifications could benefit from FGFR-targeted drug therapy.

Lung cancer FGFR aberrations are of particular importance and *FGFR1* is amplified in as many as 16-19% of squamous non-small cell lung cancers (SqCLC) (Preusser et al., 2014). Lung cancer is the most common cancer in the world and in 2012 1.6 million lung cancer associated deaths were estimated (Didkowska et al., 2016). In preclinical studies, it was shown that a subset of *FGFR1*-amplified small cell lung cancer is highly sensitive to FGFR-inhibitor treatment with PD and studies involving xenograft models transplanted with transformed cells derived from *FGFR1*-amplified NSCLC cancer patients have shown that AZD halts tumour growth and promotes regression (Pardo et al., 2009; Zhang et al., 2012).

Given the abundance of FGFR-specific therapies that are currently in clinical trials for several cancer types, coupled with the high occurrence of FGFR aberrations in endometrial, gastric and lung cancer worldwide, it is of utmost importance to investigate the effects of these alterations and of targeted drug therapy. Especially long-term drug treatment has to be investigated as chemoresistance is a major issue in targeted therapies as was observed previously in several cancers (Flaherty et al., 2010; Holohan et al., 2013; Wagle et al., 2011).

Previous work in the group focussed on the role of FGFR2 mutations in endometrial cancer and its role in drug resistance to delineate cellular mechanisms on how drug-resistant endometrial cancer cells emerge. From this work, a promising protein was identified that is involved in drug resistance and its targeting could circumvent drug resistance in these cancers (Fearon et al., 2018). However, cancers from different tissues can show different reliance on downstream signalling pathways and therefore it is essential to investigate FGFR inhibitor treatment of cancer from different tissue origin. Furthermore, alternative FGFR aberrations such as receptor amplifications could result in a different outcome compared to cancers harbouring FGFR mutations.

This study mainly focusses on gastric cancers harbouring *FGFR2* amplifications and to study FGFR inhibitor treatment, we used Infigratinib (BGJ), an orally bioavailable pan-FGFR inhibitor with potent anti-angiogenic and anti-proliferative properties in FGFR-mutant or *FGFR*-amplified cancers (Guagnano et al., 2011). In a global phase I clinical trial of BGJ in patients with advanced solid tumours with *FGFR* gene

alterations (Nogova et al., 2017), out of a cohort of 132 patients with *FGFR1*-amplified squamous cell NSCLC and *FGFR3*-mutant bladder/urothelial cancer treated with BGJ ≥ 100 mg/d, 7 patients achieved partial response. BGJ is currently being evaluated in phase II trials as a single agent in several FGFR-dependent malignancies (NCT02160041, NCT02150967). As small molecule inhibitors are the most advanced compounds in clinical trials, it is essential and of particular interest to investigate the effects of such drugs on cancers harbouring FGFR aberrations.

In this chapter, gastric cancer cells were characterised in respect to cell proliferation, cell death and cell signalling by treating them with FGFR inhibitors and also compared to endometrial and lung cancer cell lines harbouring FGFR aberrations to delineate similarities in treatment outcomes. Additionally, a novel 3D model was developed and optimised, due to the every growing need for more physiological experimental setups. Furthermore, in a 3D model multiple cell types can be grown together therefore creating a tumour microenvironment that has been found to greatly influence tumourigenesis (Wang et al., 2017).

3.2 Cancer cell line characterisation

The main focus of this work lies on gastric cancer cell lines harbouring *FGFR*-amplifications and therefore a gastric cancer panel from ATCC (TCP-1008™) was purchased. From the six gastric cancer cell lines, two harboured *FGFR2* amplifications and the rest were wild-type for FGFR2. SNU-16 and KATOIII are *FGFR2*-amplified and both have a TP53 mutation and SNU-16 additionally has a *CDKN2A* mutation (for mutation profiles of all gastric cancer cell lines see **Table 2.1-Table 2.4** in the methods section). Initial experiments and optimisations were undertaken with MFE-296 and AN3CA cell lines and compared to cells of the gastric cancer panel and furthermore lung cancer cell lines, H520 and H1299 that were kindly provided by Prof. Marshall and Prof. Sharp (BCI).

After extensive literature search, SNU-16 cells were chosen for the main study as they exhibited particularily high levels of *FGFR2* amplifications, while SNU-1 were chosen as their wild-type counterpart, which are like SNU-16 also suspension cells (Kunii et al., 2008; Xie et al., 2013). To establish the role of FGFR mutations, MFE-296 and AN3CA that harbour the N550K *FGFR2* mutation (COSMIC), were chosen, which results in constitutive activation of kinase activity (Byron et al., 2008). **Table 3.1** summarises the cell lines, which have been used.

Table 3.1. Cancer cell lines that were predominately used in the project.

Name	Cancer type	Receptor alteration	Mutations
SNU-16	gastric	*FGFR2* amplification	p53, CDKN2A
SNU-1	gastric	*FGFR2* wt	KRAS, MLH1
AGS	gastric	*FGFR2* wt	CDH1, CTNNB1, KRAS PIK3CA
MFE-296	endometrial	FGFR2 mutation (N550K)	PI3Ka, PTEN
AN3CA	endometrial	FGFR2 mutation (N550K, K310R)	PTEN
H520	lung	*FGFR1* amplification	p53
H1299	lung	*FGFR1* wt	p53

3.3 Cell survival of endometrial, gastric and lung cancer cells treated with RTK inhibitors

As FGFR inhibitors are being investigated in clinical trials for different types of cancers (Clinicaltrials.gov, 2018), the effects of FGFR inhibition in endometrial, gastric and lung cancers were assessed. Three different FGFR kinase inhibitors were used: PD, which is a common small molecule tool compound (Knights and Cook, 2010), AZD and BGJ (see section 1.7), which are currently in trials for *FGFR1* and *2*-amplified solid tumours and are potent, selective and orally bioavailable inhibitors of FGFR tyrosine kinases 1-4 (Clinicaltrials.gov, 2018). To assess their potential to block RTK signalling in cancer cells, survival assays were performed. Cells were treated with a range of different concentrations of AZD and BGJ and cell survival was analysed 72 hours post drug treatment. Cells were analysed using either MTT for adherent or MTS for suspension cells. Gastric SNU-1 cells from the gastric cancer panel, which are *FGFR2*-wildtype, were not sensitive to lower concentrations of BGJ as shown by a shift to the right, while *FGFR2*-amplified gastric SNU-16 cancer cells were highly sensitive to FGFR2 inhibition **(Figure 3.1)**, which is also reflected in the difference of IC_{50} values comparing *FGFR2*-amplified and wildtype cell survival. SNU-16 cells also showed similar survival curves upon treatment with AZD, which resulted again in sensitivity and reduction of cell numbers with increasing drug concentration **(Appendix Figure 8.1)**. AGS cells, which also express wild-type *FGFR2*, served as an adherent control cell line. The AGS cell line, similarly to SNU-1 cells, was less sensitive to low FGFR inhibitor concentrations and was eventually killed after using the maximum dose of 1μM of BGJ **(Figure 3.2)**.

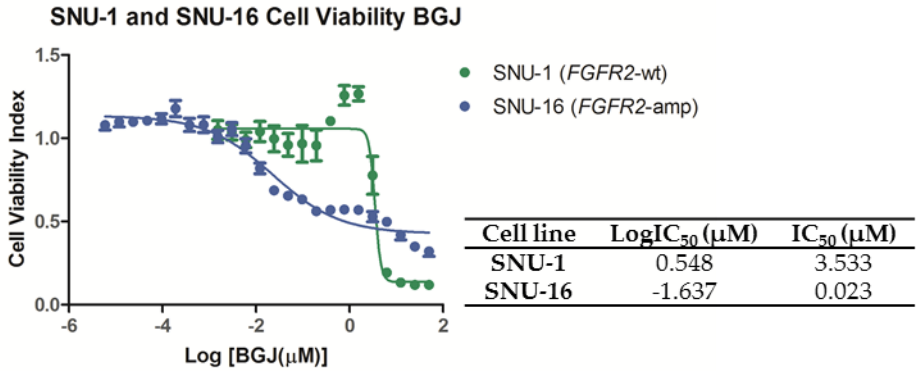

Cell line	LogIC$_{50}$ (μM)	IC$_{50}$ (μM)
SNU-1	0.548	3.533
SNU-16	-1.637	0.023

Figure 3.1. SNU-16 cells are sensitive towards BGJ.
SNU-1 and SNU-16 gastric cancer cells were plated in triplicate into 96-well plates and exposed to BGJ concentrations ranging from 1.5nM to 50μM for SNU-1 cells and ranging from 0.006nM to 50μM for SNU-16 cells. Cell viability was measured after 72h incubation. Control cells were treated with DMSO and as a background control 1% Staurosporine was added to wells containing cells. The cell viability index was then measured subtracting the background signal and adjusting to the controls. An average of three biological MTS experiments in technical triplicate is shown with error bars indicating standard error of the mean (SEM). The green curve represents SNU-1 cells and the blue curve represents SNU-16 cells. LogIC$_{50}$ and IC$_{50}$ values were calculated in GraphPad Prism 5.

For other gastric cell lines, the optimal treatment dose for AZD and BGJ, was also determined **(Appendix Figure 8.2)**. Lung cancer cell line A549, which is *FGFR1* wildtype and *FGFR1*-amplified H520 cells were also exposed to BGJ and AZD to show that drugs are not universally toxic **(Appendix Figure 8.3)**.

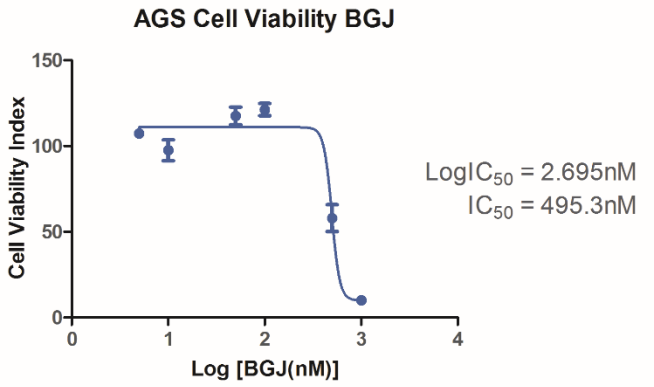

Figure 3.2. *FGFR2* wildtype gastric cancer cells are less sensitive to FGFR inhibition.
AGS cells were treated with drug concentrations ranging from 0.5 to 1000nM of PD, AZD or BGJ. Cell viability was measured after 72h incubation. Control cells were treated with DMSO and as a background control 1% Staurosporine was added to wells containing cells. The cell viability index was then measured subtracting the background signal and adjusting to the controls. An average of three biological MTS experiments in technical triplicate is shown with error bars indicating SEM. LogIC$_{50}$ and IC$_{50}$ values were calculated in GraphPad Prism 5.

3.4 *FGFR2* gene amplification confers sensitivity in gastric cancer to selective FGFR inhibition in 2D

To compare and assess sensitivity towards FGFR inhibition of SNU-16 and SNU-1 cell lines, cells were grown in presence of FGFR inhibitor BGJ, followed by cell counting **(Figure 3.3A)**. SNU-16 cells generally grew at a lesser pace than SNU-1 cells and cell numbers were significantly reduced upon FGFR inhibition. In SNU-1 cells on the other hand, cell numbers remained unchanged between vehicle and drug-treated conditions. The reduction in cell numbers in SNU-16 cells, was also shown to be a dose-dependent effect, as an increase in inhibitor concentration resulted in a significantly increased reduction in cell counts compared to vehicle-treated cells **(Figure 3.3B)**.

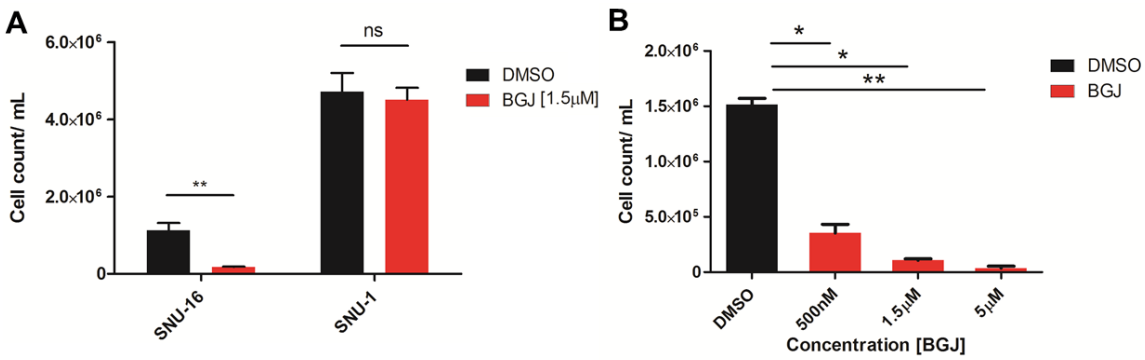

Figure 3.3. FGFR inhibition in *FGFR2*-amplified gastric cancer cells results in a dose-dependent reduction in cell numbers.
FGFR2-amplified SNU-16 and wildtype SNU-1 cells were seeded into 6-well plates and treated with 1.5μM BGJ for 72h **(A)**. In another experiment, SNU-16 cells were exposed to 500nM, 1.5μM or 5μM BGJ or vehicle and incubated for 72h **(B)**. The medium containing the cells was collected and resuspended in 1mL complete growth medium and SNU-16 cell numbers were assessed using Trypan blue and cell counting with a haemocytometer using a light microscope. Experiments were performed in biological triplicate with error bars indicating SEM. Statistical analysis was performed using Student's T-test, *p<0.05, **p<0.01.

To assess the potential of ATP-competitive inhibitors to block RTK signalling in cancer cells, they were treated with FGFR inhibitors PD, AZD and BGJ. Previous data have shown endometrial cancer cells to be sensitive to FGFR inhibition in 2D culture using PD (Byron et al., 2008). To confirm this in the cell lines used in my project, cells were treated with 1μM PD, AZD or BGJ, or DMSO at the same concentration as a vehicle control. Cell signalling was then analysed using Western blot after three days

incubation of the cells with the different drugs. Again, blots were probed for signalling antibodies of the ERK and AKT pathway and the housekeeping protein HSC70 was used as a loading control **(Figure 3.4, Figure 3.5)**. SNU-16 cell protein lysates were analysed, showing a significant decrease in phosphorylation of signalling proteins AKT and ERK in drug-treated cells **(Figure 3.4A)**. Levels of p-AKT were more reduced with FGFR inhibitor treatment compared to p-ERK protein expression levels. Total AKT and ERK signalling remained unchanged upon FGFR inhibition. To compare signalling of *FGFR2*-amplified gastric cancer cells to *FGFR2* wildtype gastric cancer cells, the same was also done for SNU-1 and AGS cell lines. Again, cells were treated with the three FGFR inhibitors and with vehicle at the same concentration in control wells. AGS and SNU-1 cancer cells were not affected by the drug in the same manner as SNU-16 cells. AKT phosphorylation in SNU-1 and AGS cells could have been inhibited at different, potentially shorter, time points compared to SNU-16 cells. Therefore no distinct change in AKT phosphorylation levels was observable in drug-treated cells as compared to vehicle-treated cells on the protein level at the chosen timepoint. SNU-16 cells were also subjected to increasing dosages of BGJ and Western blot analysis was performed **(Figure 3.4B)**. With increasing BGJ concentration, p-ERK was gradually decreased and with 5μM BGJ, t-AKT showed a slight reduction in protein expression levels compared to the vehicle control.

To investigate if amplifications of the kinase domain also affect sensitivity in respect to FGFR1, cell signalling of lung cancer cell lines harbouring *FGFR1* amplifications was measured and it was confirmed that H520 cells are highly *FGFR1*-amplified compared to other lung cancer cells **(Appendix Figure 8.4)**. Signalling upon drug treatments with PD, AZD and BGJ was then compared to lung cancer cell lines that are wildtype for *FGFR1* and also to lung fibroblasts **(Figure 3.5)**. AKT and ERK phosphorylation was significantly reduced in *FGFR1*-amplified H520 cells, whereas it remained unchanged in H1229 *FGFR1* wildtype lung cancer cells. MRC-5 lung fibroblasts did not express p-AKT and exhibited unchanged p-ERK signalling.

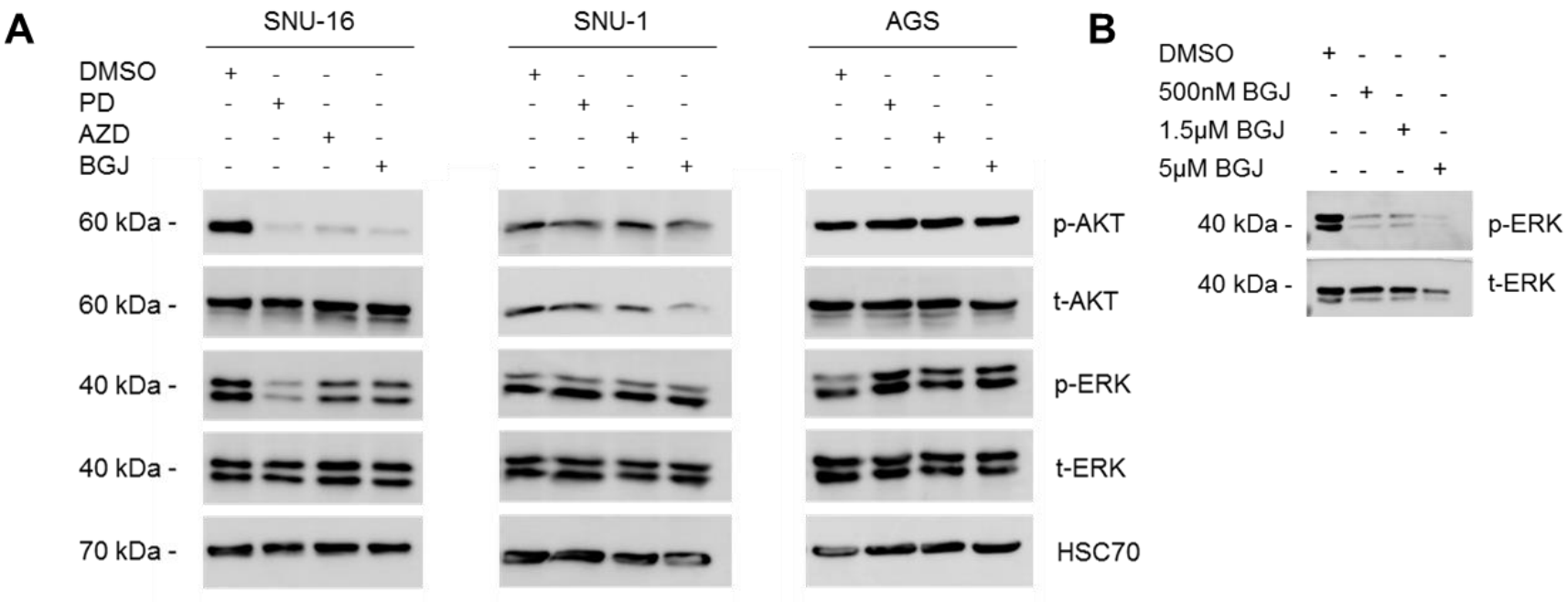

Figure 3.4. AKT and ERK signalling in *FGFR2*-amplified gastric cancer cells are reduced with FGFR inhibitor treatment compared to *FGFR2* wildtype cells and p-ERK signalling is reduced in a dose-dependent manner.
SNU-16, SNU-1 and AGS cancer cells were seeded into 6-well plates and treated with 1μM PD, AZD or BGJ for 72h, followed by measuring AKT and ERK signalling to assess the effects of the drugs on FGF signalling **(A)**. SNU-16 harbour *FGFR2* amplifications and show a significant decrease in p-AKT (Ser743) and p-ERK signalling in drug-treated samples. AGS and SNU-1 cancer cells are *FGFR2*-wild-type and showed less sensitivity towards the different drugs used. The blots are representative of three individual experiments. Increasing the inhibitor concentration (500nM, 1.5 and 5μM BGJ) in SNU-16 cells resulted in a dose-dependent reduction in p-ERK expression levels **(B)**. The blots are representative of three individual experiments **(Appendix Figure 8.5)**.

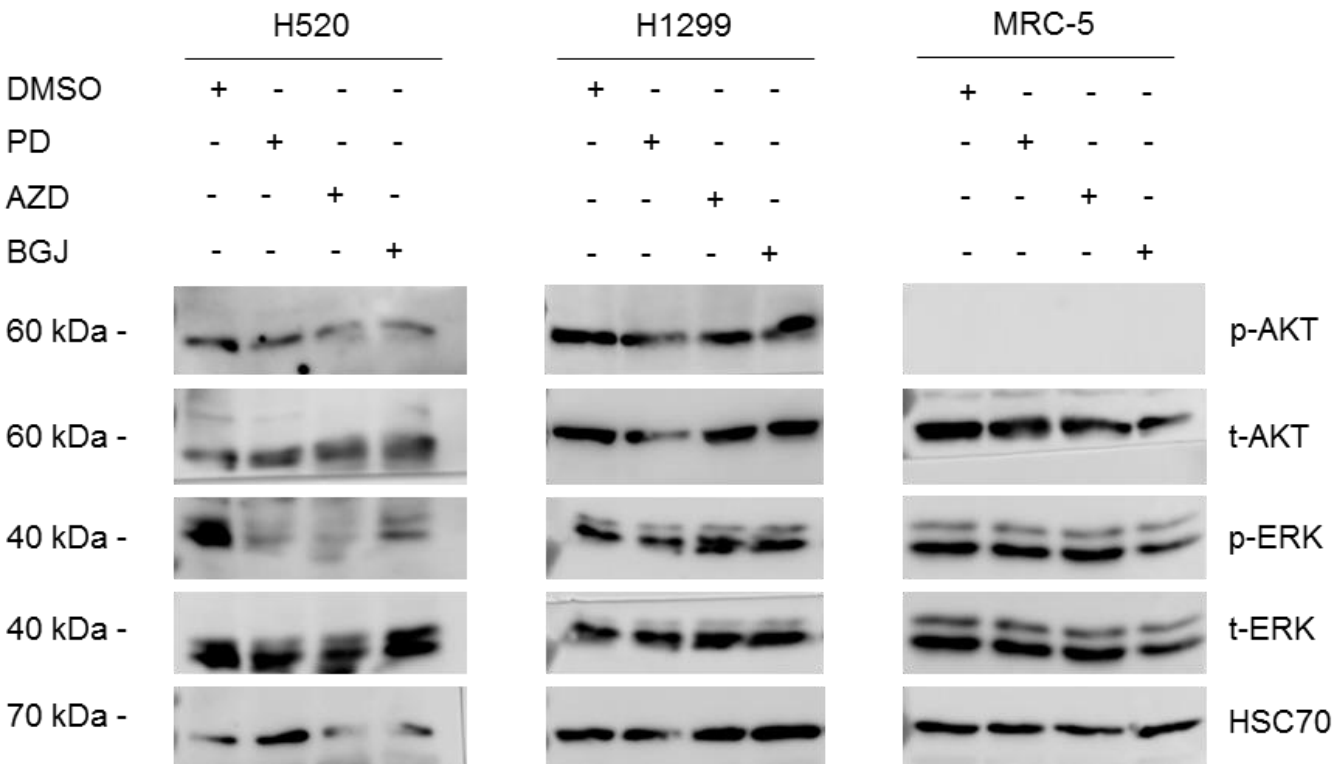

Figure 3.5. *FGFR1*-amplifed lung cancer cell lines exhibit reduced phosphorylation of AKT and ERK signalling compared to *FGFR1* wildtype lung cancer cells.
H520, H1299 lung cancer cells and MRC-5 lung fibroblast cells were treated with 1μM PD, AZD or BGJ for 3 days and AKT and ERK signalling was assessed to see if there is an effect of the drug on FGF signalling. H520 cells harbour *FGFR1* amplifications and show a significant decrease in p-ERK signalling in drug-treated samples. p-AKT only seems slightly reduced. H1299 cancer cells are *FGFR1*-wildtype and showed no sensitivity towards the different drugs used. The same was true for MRC5 cells, however, no p-AKT could be detected. HSC70 served as loading control. The experiment was performed three times with the same result **(Appendix Figure 8.6-Appendix Figure 8.8)**.

3.5 Fibroblast growth factor stimulation promotes AKT and ERK signalling in *FGFR1*/2-amplified and *FGFR2*-mutated cells

To assess the effect of cancer cell stimulation and inhibition, MFE-296, SNU-16 and H520 cells were serum starved and treated with 100ng/mL FGF2 or FGF10 for 15 and 60 minutes. MFE-296 cells were only treated with FGF2 but with all three FGFR inhibitors PD, AZD or BGJ or vehicle control. In the case of SNU-16 and H520 cells, only BGJ was used but both FGF2 and FGF10. FGF2 was chosen for MFE-296 cells as it activates the IIIC variants of FGFR1 and FGFR2 efficiently, which are expressed by MFE-296 cancer cells.

FGF2 stimulation in MFE-296 cells activated the MAPK pathway, as shown by increased ERK phosphorylation on threonine and tyrosine residues 202 and 204 (thr202 and tyr204). Upon treatment of the cells with FGFR inhibitors, p-ERK signalling was inhibited **(Figure 3.6)**. The effect varied between inhibitors used and was completely abolished in BGJ-treated MFE-296 cells whereas with PD and AZD, still slight levels were expressed at 15 minutes.

FGF2 stimulation also increased AKT signalling in MFE-296 cells and with all three FGFR inhibitors phosphorylation of AKT was decreased. Upon inhibition, p-AKT levels were decreased but returned back to normal at the 60 minutes FGF2 stimulation time point. Overall comparable data were observed in MFE-296 cells with the different FGFR inhibitors.

FGF stimulation of *FGFR2*-amplified SNU-16 gastric cancer and *FGFR1*-amplified H520 lung cancer cells and subsequent inhibitor treatment resulted in decreased p-ERK signalling. In SNU-16 cells both FGF2 and FGF10 stimulation increased ERK phosphorylation **(Figure 3.7)**. In H520 cells, FGF2 stimulation lead to increased p-ERK levels at 15 and 60 min and was efficiently blocked upon FGFR inhibitor treatment with BGJ. Similar results were achieved with FGF10, however less intense than with FGF2 **(Figure 3.8)**.

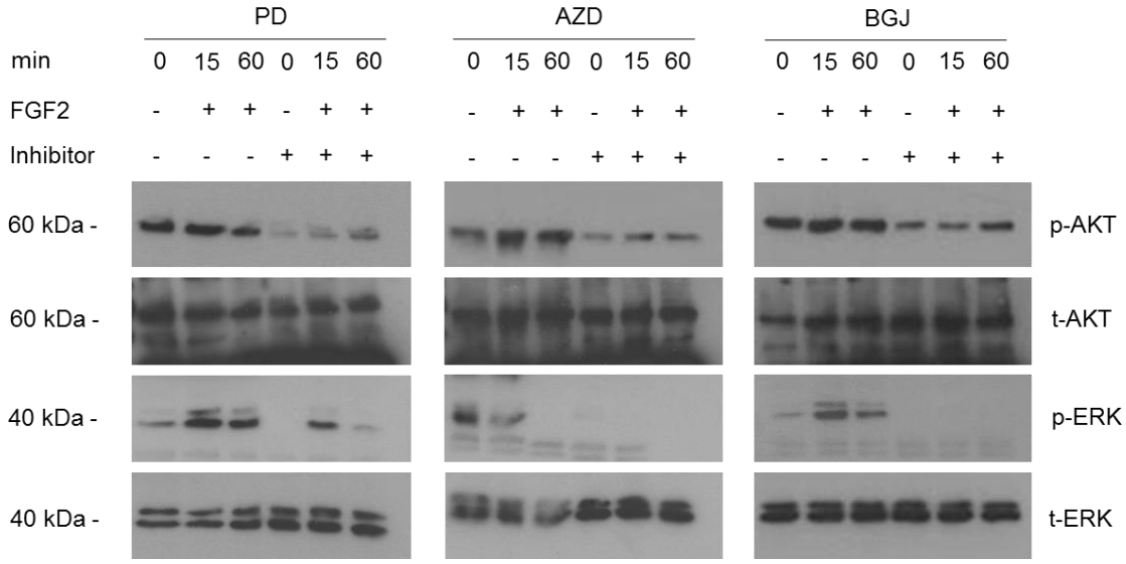

Figure 3.6. Effect of FGF2 stimulation and FGFR2 inhibition on cell signalling in MFE-296 cells.
MFE-296 cells were grown in 6-well plates and were serum-starved for 6 hours and stimulated with 100ng/mL FGF2 in the presence of 300ng/mL heparin in serum-free medium for 15 and 60 minutes. Where indicated cells were treated with 1μM PD, AZD or BGJ for 1 hour. Cells were then harvested and protein lysates were analysed on a 10% PAGE gel and immunoblotted with antibodies directed against p-ERK, t-ERK, p-AKT and t-AKT. Stimulation of MFE-296 cells activated the MAPK pathway, which was inhibited by 1μM PD, AZD or BGJ. FGF2 stimulation also increased p-AKT signalling which was again inhibited by the FGFR inhibitors. 20μg protein was loaded in each lane.

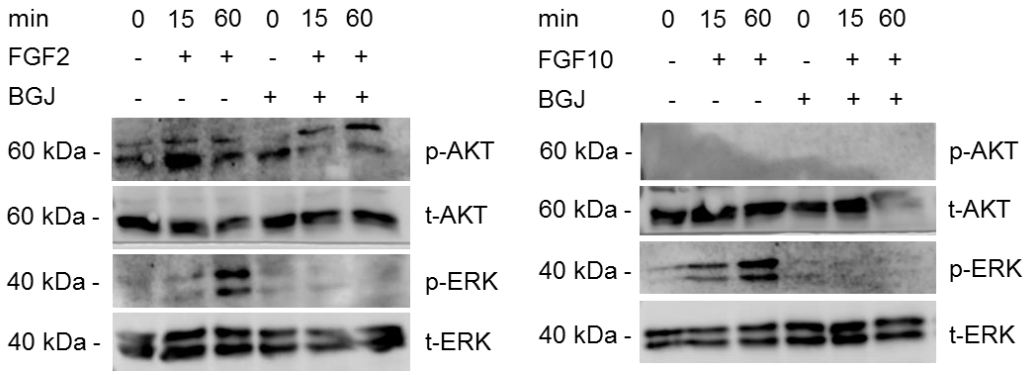

Figure 3.7. Effect of FGF2 and FGF10 stimulation and FGFR2 inhibition on cell signalling in SNU-16 cells.
SNU-16 cells were grown in 6-well plates and were serum-starved for four hours and stimulated with 100ng/mL FGF2 or FGF10 in the presence of 300ng/mL heparin in serum-free medium for 15 and 60 minutes. Where indicated cells were treated with 1μM BGJ for 1 hour. Cells were then harvested and protein lysates were analysed on a 10% PAGE gel and immunoblotted with antibodies directed against p-ERK, t-ERK, p-AKT and t-AKT. Stimulation of SNU-16 cells with both FGF2 and FGF10 activated the MAPK pathway, which was inhibited by 1μM BGJ. FGF2 stimulation also increased p-AKT signalling which was again inhibited by the FGFR inhibitors. 20μg protein was loaded in each lane.

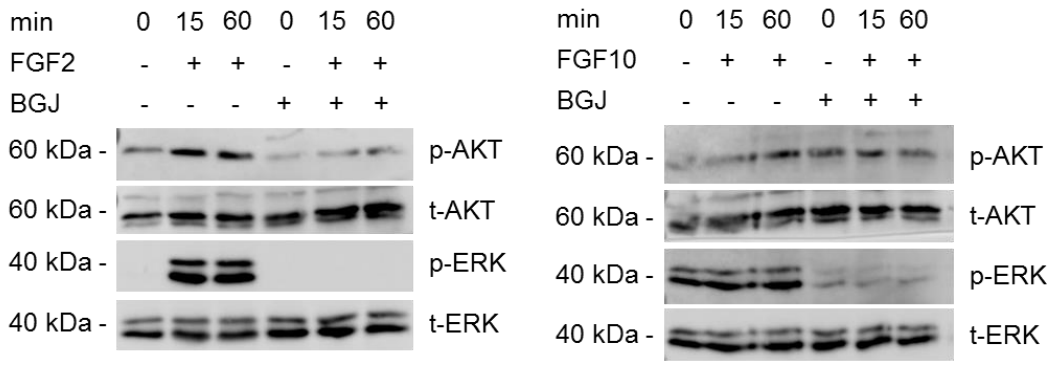

Figure 3.8. Effect of FGF2 and FGF10 stimulation and FGFR2 inhibition on cell signalling in H520 cells.
H520 cells were grown in 6-well plates and were serum-starved for four hours and stimulated with 100ng/mL FGF2 or FGF10 in the presence of 300ng/mL heparin in serum-free medium for 15 and 60 minutes. Where indicated cells were treated with 1μM BGJ for 1 hour. Cells were then harvested and protein lysates were analysed on a 10% PAGE gel and immunoblotted with antibodies directed against p-ERK, t-ERK, p-AKT and t-AKT. Stimulation of H520 cells with both FGF2 and FGF10 activated the MAPK pathway, which was inhibited by 1μM BGJ. FGF2 stimulation also increased p-AKT signalling which was again inhibited by the FGFR inhibitors. 20μg protein was loaded in each lane.

3.6 Alvetex® organotypic 3D cell culture model development

Thus far, investigations have focussed on cancer cells alone in 2D culture. However, my aim was to determine the effect of stromal support on drug resistance in 3D. In order to investigate the effect of FGFR2 inhibition in a more physiologically relevant form, a 3D organotypic model was developed. It is based on a 3D scaffold method, Alvetex®, which consists only of a polystyrene scaffold membrane. First of all, different seeding concentrations were tested with 2.5 x 10^5, 5.0 x 10^5 and 1.0 x 10^6 cells per scaffold **(Figure 3.9)**. Using the highest cell density did not overfill the scaffold and therefore going forward this cell seeding density was used for all experiments.

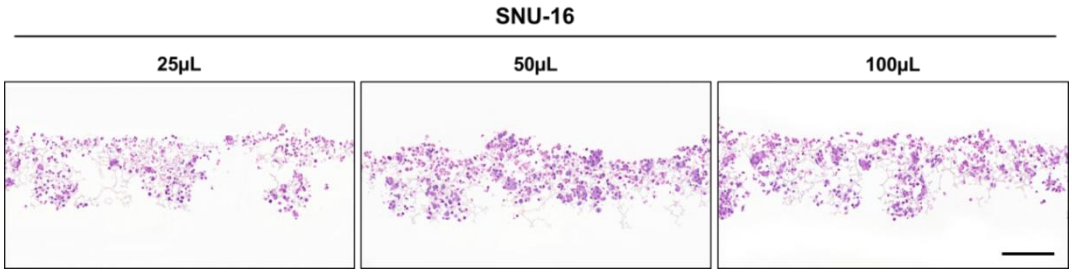

Figure 3.9. Cell seeding concentrations.
SNU-16 cells were resuspended at a concentration of 1 x 10^7 cells/mL and 25 (2.5 x 10^5), 50 (5.0 x 10^5) or 100μL (1.0 x 10^6) of the cell suspension were seeded into Alvetex® scaffolds. After one week incubation, the scaffolds were fixed, paraffin-embedded and H&E stained. The images are representatives of three individual experiments. The scale bar indicates 100μm.

The 3D model was also developed to investigate the tumour environment and investigate the effect of fibroblast signalling upon cells, as the tumour microenvironment is recognised to play an essential role in cancer malignancy (Wang et al., 2017). To investigate stromal support, human foreskin fibroblasts (HFF2) were used. Ideally, HFF2 cells should not be sensitive towards the drug and therefore cell viability of HFF2 cells was assessed and showed no sensitivity towards BGJ **(Figure 3.10)** or AZD **(Appendix Figure 8.9)**.

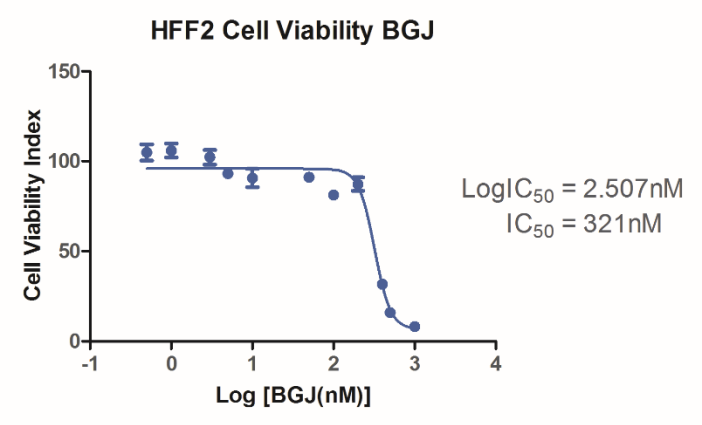

Figure 3.10. Human foreskin fibroblasts are less sensitive towards BGJ.
HFF2 cells were plated in triplicate into 96-well plates and exposed to BGJ concentrations ranging from 0.5 to 1000nM. Cell viability was measured after 72h incubation. Control cells were treated with DMSO and as a background control 1% Staurosporine was added to wells containing cells. The cell viability index was then measured subtracting the background signal and adjusting to the controls. An average of three biological MTS experiments in technical triplicate is shown. $LogIC_{50}$ and IC_{50} values were calculated in GraphPad Prism 5.

The effect of drug inhibition on HFF2 cells was also assessed on the protein level, and expression levels of AKT and ERK signalling were unaffected in HFF2 cells upon drug treatment with AZD **(Appendix Figure 8.10)**. Fluorescently transfected HFF2 cells behaved in the same manner as untransfected cells in respect to sensitivity towards FGFR inhibition.

3.7 Visualisation of cancer cells and fibroblasts in Alvetex® scaffolds

To visualise and distinguish co-culture cells in the scaffolds, cells were fluorescently tagged (according to section 2.2.17). MFE-296 cells were initially transfected with viral supernatant with an Azurite construct (viral supernatant was provided by Dr. E. Carter) and HFF2 cells with EGFP, which was available in the laboratory. Transfection of MFE-296 cells with a lentiviral plasmid expressing the Azurite blue resulted in MFE-296-Azurite cells **(Figure 3.11A)**. The same was also performed for HFF2 cells with a construct expressing EGFP, giving rise to HFF2-EGFP cells **(Figure 3.11B).** Cells were grown for 8 passages and then sorted using flow cytometry to assess efficiency of the transduction and selected for MFE-296 Azurite and HFF2-EGFP positive cells.

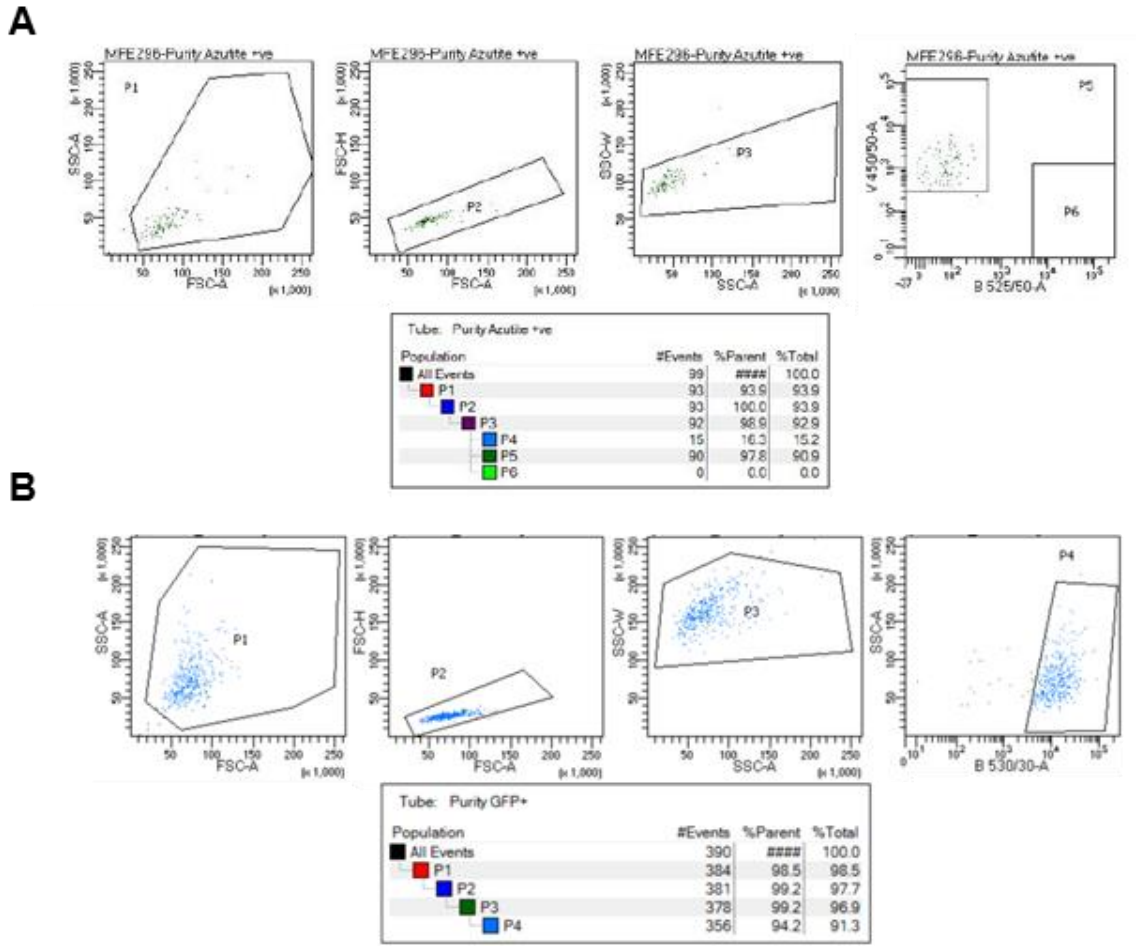

Figure 3.11. Cell sorting of MFE-296-Azurite and HFF2-EGFP cells.
Azurite and EGFP-transduced MFE-296 and HFF2 cells were grown for 8 passages followed by cell sorting using FACS. P1 displays the selection of live cells and P2 and P3 were used to discriminate cell doublets. P4 the selects for EGFP-positive cells using channel B530/30-A to detect EGFP signal. P5 selects for Azurite-positive MFE-296 cells using channel B525/50-A.

EGFP transfection efficiency in HFF2 cells was high, with over 98% of cells being EGFP positive **(Figure 3.12,).**

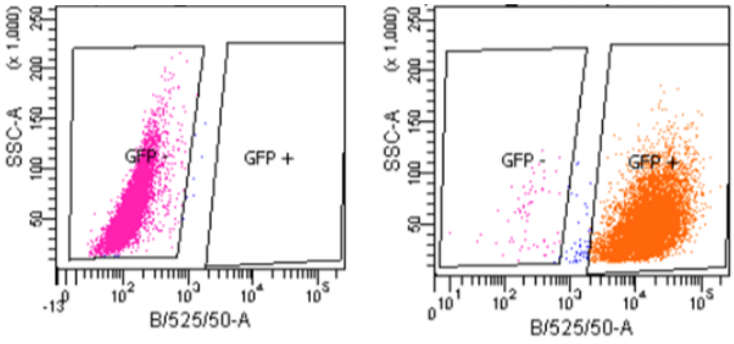

Figure 3.12. EGFP expression level of untransfected HFF2 fibroblasts and EGFP plasmid transfected HFF2 cells.
HFF2 cells were transfected with a lentiviral plasmid expressing EGFP and grown for 8 passages followed by FACS cell sorting.

As a preliminary experiment, HFF2 cells were grown for 7 days, either mixed with cancer cells, or only HFF2-EGFP alone on coverslips, and visualised by fluorescence microscopy **(Figure 3.13)**. EGFP labels the cytoplasm, allowing to visualise the morphology of cells. MFE-296 cells stained positive for E-cadherin.

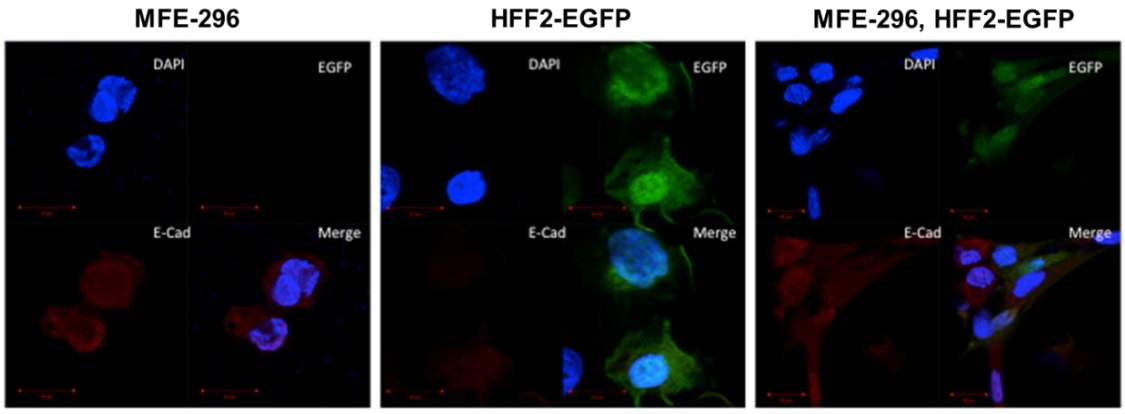

Figure 3.13. Co-culture Immunofluorescence of HFF2-EGFP cells and resistant MFE-296 and parental cells.
MFE-296 and HFF2-EGFP cells were either seeded alone or in co-culture on coverslips. The following day coverslips were PFA-fixed and imaged with a fluorescence confocal microscope. MFE-296 cells stain for E-Cadherin while EGFP-transduced cells were visualised using the GFP channel. The cell nuclei were stained using DAPI.

The role of the tumour stroma has shown to have an effect on the formation of resistance in different cancers (Donner, 2012; Olson and Joyce, 2013; Wang et al., 2009). Therefore, studying the interaction between fibroblasts and cancer cells could give a greater insight into mechanisms underpinning resistance. 3D organotypic models provide a more physiomimetic system to study this. In my project, I have used Alvetex® scaffolds, where endometrial MFE-296 and gastric SNU-16 cancer cells were seeded together with HFF2. MFE-296 cancer cells and HFF2 fibroblasts were labelled previously with fluorescent markers using lentiviral constructs, creating MFE-296-Azurite and HFF2-EGFP. The cells were then seeded in a 2 (cancer): 1 (fibroblast) ratio into scaffolds and incubated for 30 min at RT. The scaffolds were then fed from below with complete growth medium to create a chemotactic gradient stimulating the cells to migrate towards the medium. Cells were grown in scaffolds for 7-14 days, with medium changes every two days. After seven days, the scaffolds were imaged via confocal laser scanning microscopy (Zeiss LSM 710) to produce high resolution detailed images. Scaffolds were placed into a 30mm dish in a humidified and heated (37°C) chamber. Since the cells were transduced with fluorescent markers, lasers were adjusted to 488nm emission for fibroblasts (green) and 450nm emission for cancer cells (blue). Z-stacks were acquired at 4µm intervals with a 1µm overlap to circa 200µm depth using a long working distance 20x objective (LWD 20x).

Cell survival of gastric, endometrial and lung cancer cells was also compared to cells grown with or without stromal cells or cells grown in 2D *versus* 3D in 96-well Alvetex® plates **(Appendix Figure 8.11)**. Cells grown together with fibroblasts and cells grown in 3D were both less sensitive to FGFR inhibition using BGJ, highlighting the importance to study cancer in presence of fibroblasts and also in 3D. Growth of lung cancer cells upon FGFR inhibition with and without stromal support was also analysed with IncuCyte™ ZOOM®, allowing to measure cell confluence and average area. Again, cells grown with lung fibroblasts resulted in higher cell confluence and average area and therefore decreased sensitivity to FGFR inhibition **(Appendix Figure 8.12)**.

3.8 Optimising coating methods and scaffold formats

3.8.1 Scaffold coating

Since Alvetex® scaffolds consist of polystyrene scaffold webs, it could be coated with collagen and Matrigel™. However, compared to collagen and Matrigel™-coated scaffolds, the uncoated scaffolds showed the best attachment and proliferation of MFE-296-Azurite and HFF2-EGFP cells **(Figure 3.14).** The fluorescence image displays live cell image acquisition through the scaffold with both HFF2-EGFP and MFE-296-Azurite cells, with highest cell numbers in uncoated scaffolds compared to collagen and Matrigel™-coated scaffolds in 24-well plates.

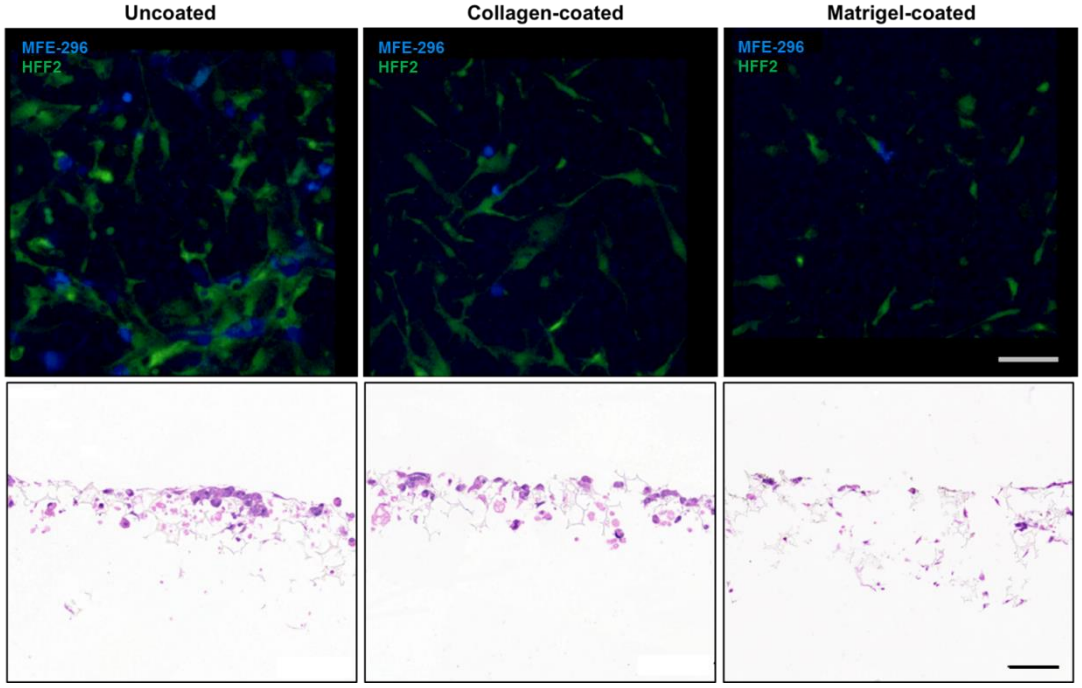

Figure 3.14. Different coating methods of 24 well-plate Alvetex® scaffolds.
(A) Confocal microscopy of 24 well-plate Alvetex® scaffolds either coated with collagen or Matrigel™ or left uncoated with MFE-296 and HFF2 cells. Comparison of coatings such as with collagen and Matrigel™ of the 24 well plate Alvetex® scaffolds. **(B)** H&E staining of 24 well-plate Alvetex® scaffolds either coated with collagen or Matrigel™ or left uncoated. Comparison of coatings such as with collagen and Matrigel™ of the 24 well plate Alvetex® scaffolds. Scale bars indicate 100μm.

After 7-14 days, Alvetex® scaffolds were fixed with 10% formalin, embedded in paraffin and subsequently stained for H&E **(Figure 3.14)**. In the H&E staining, it is clear that the uncoated scaffold remained more intact as compared to the collagen and Matrigel™-coated scaffolds, and there were more cells present in uncoated scaffolds.

3.8.2 Scaffold formats

There are different Alvetex® formats available, not only in size of the scaffolds but also the pore size of the polystyrene material. In the Alvetex® scaffolds, the pore size is 42µm and in Alvetex® Strata the pore size is 15µm. Therefore, it is more difficult for the cells to distribute in the Strata scaffold. As the scaffold was more rigid because of the denser pores, the scaffold did not disrupt when embedded scaffolds were sectioned. It was not possible to see cells using live cell imaging using confocal microscopy (Zeiss LSM 710), therefore scaffolds were embedded in paraffin and sections were stained for H&E. Although SNU-16 cells were used, which are generally smaller cells, only very few cells invaded the scaffold. For these reasons, this format was not further used in this project. **(Appendix Figure 8.13)**.

To check if there is a difference between growing cells in a 24-well plate Alvetex® or in 12-well inserts, scaffold coating and cell growth was analysed in 12-well inserts. 12-well inserts were coated with Matrigel™ or left uncoated. Again, uncoated scaffolds displayed a better cell attachment and cells grew better than in Matrigel™-coated scaffolds **(Figure 3.15)**. Compared to 24-well plates, more cells were observed in 12-well inserts as medium can be fed from below only if desired.

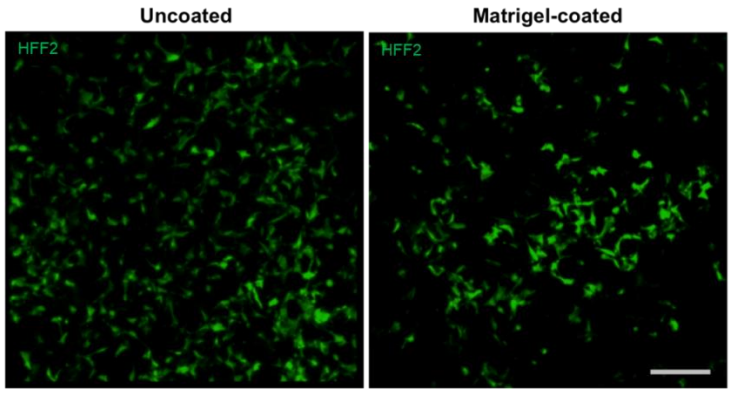

Figure 3.15. HFF2 cells exhibit increased attachment to uncoated scaffolds than Matrigel™-coated scaffolds.
EGFP-positive HFF2 cells were seeded into 12-well Alvetex® inserts left uncoated or coated with Matrigel™. After one week incubation, cells were imaged live with a fluorescence microscope. The scale bar indicates 100µm.

Similarly, in collagen-coated scaffolds using 12-well inserts, fewer cells grew compared to uncoated scaffold inserts **(Figure 3.16)**. Therefore, for all future experiments 12-well inserts were used, as using this format delivered the best cell attachment and growth results.

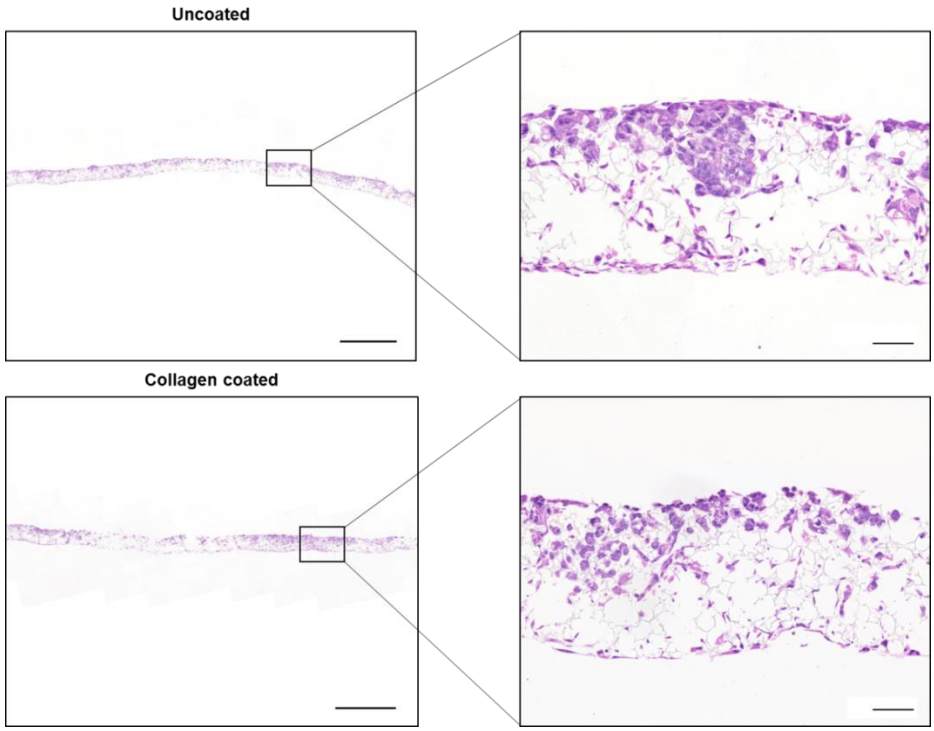

Figure 3.16. Growing cells in uncoated Alvetex® scaffolds delivers the best results.
Comparison of H&E staining of an uncoated 12-well insert Alvetex® scaffold and H&E staining of a collagen-coated 12-well insert Alvetex® scaffold containing MFE-296 cells. Scaffolds were coated or left uncoated and incubated for 1h followed by cell seeding. The cells in the scaffolds were incubated for one week followed by fixation, paraffin-embedding and H&E staining. The whole scaffold scale bar indicates 2000µm and magnification scale bar indicates 100µm.

3.8.3 Drug treatment of co-cultures in Alvetex® scaffolds

To test the effect of FGFR inhibitors on co-culture cells in 3D, fluorescently labelled MFE-296-Azurite and HFF2-EGFP fibroblasts were seeded at a 2:1 ratio into 12-well insert scaffolds. Per well, 10^7 cells in 100µL were seeded, incubated for 30 min at room temperature and fed from below with complete growth medium and incubated at 37°C. The next day, cells were treated with two different dosages of the drug and investigated using fluorescent confocal microscopy 7 days after drug treatment. Simultaneously, scaffolds were also stained for H&E **(Figure 3.17)**. From the fluorescence images and also H&E staining, where also the whole scaffold could be

imaged, it could be shown that MFE-296 cells co-cultured with HFF2 cells were indeed sensitive towards AZD and more cells could be killed with a higher drug concentration or cells stopped growing and therefore resulted in lower cell numbers compared to vehicle-treated cells in 3D. In this experiment it could also be observed that the fuller the scaffold the more intact it remained as, due to the low cell number in the drug-treated sample, the scaffold was disrupted upon fixation and sectioning.

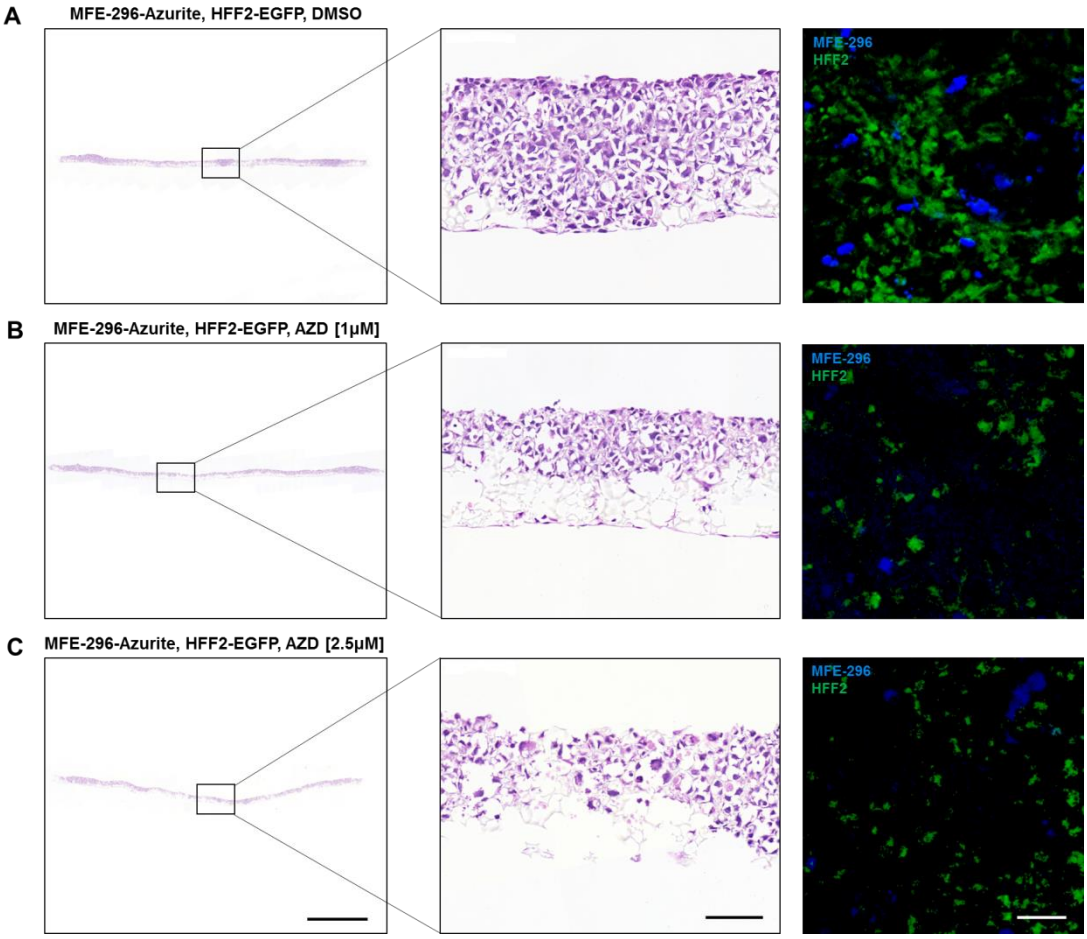

Figure 3.17. AZD treatment of *FGFR2*-mutated endometrial cells kills cells with increasing dosage. Endometrial MFE-296 cells were seeded 2:1 with fibroblasts into 12-well insert Alvetex® scaffolds and grown for one week and imaged with confocal fluorescence microscopy, followed by fixation, paraffin-embedding and H&E staining and imaging with the Pannoramic scanner. Cells were treated with 1µM **(B)** or 2.5µM AZD **(C)** or as a control cells were treated with DMSO **(A)**. Blue cells indicate MFE-296-Azurite cells and green HFF2-EGFP cells. Whole scaffold scale bar (left panel) indicates 2000µm and magnification and fluorescence scale bars indicate 100µm.

The same was also performed for the FGFR inhibitor BGJ, to check if there was a similar effect by treating MFE-296-Azurite and HFF2-EGFP fibroblasts with another FGFR inhibitor. With this drug a higher concentration was used and with the highest

drug concentration, cells were almost entirely killed compared to the vehicle control **(Figure 3.18)**.

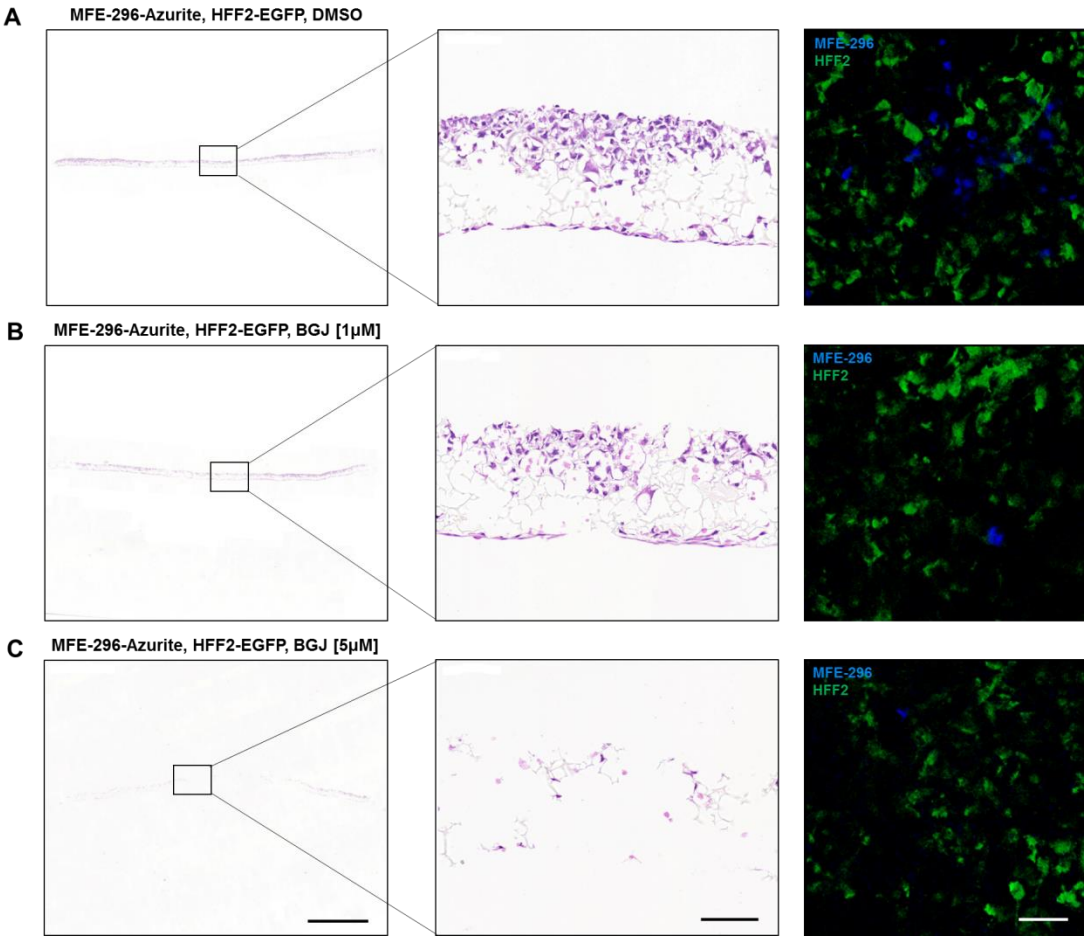

Figure 3.18. BGJ treatment of *FGFR2*-mutated endometrial cells kills cells with increasing dosage. Endometrial MFE-296 cells were seeded 2:1 with fibroblasts into 12-well insert Alvetex® scaffolds and grown for one week and imaged with confocal fluorescence microscopy, followed by fixation, paraffin-embedding and H&E staining and imaging with the Pannoramic scanner. Cells were treated with 1µM **(B)** or 5µM BGJ **(C)** or as a control cells were treated with DMSO **(A)**. Blue cells indicate MFE-296-Azurite cells and green HFF2-EGFP cells. Whole scaffold scale bar (left panel) indicates 2000µm and magnification and fluorescence scale bars indicate 100µm.

Similarly, SNU-16 suspension cells were seeded into 12-well Alvetex® scaffolds and treated with BGJ. Again, cells treated with BGJ were highly sensitive to the drug and cell numbers were dramatically reduced **(Figure 3.19)**. Also, this shows that suspension cells can be grown in Alvetex® scaffolds. To see how BGJ drug treatment affected SNU-16 in co-culture with stromal cells, cells were again treated with BGJ, leading to a significant decrease in cell number. HFF2 cells gathered at the bottom of the scaffolds whereas SNU-16 remained mostly near the top **(Figure 3.20)**.

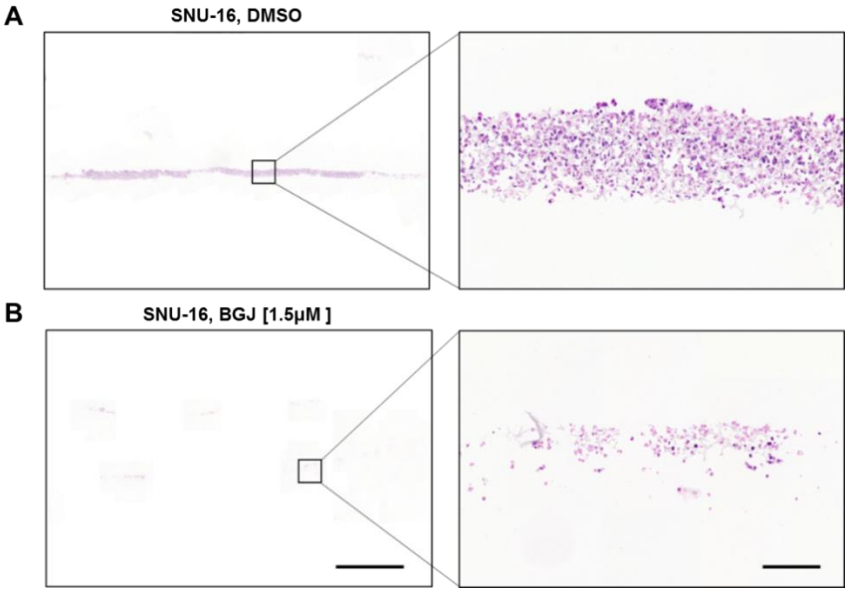

Figure 3.19. SNU-16 cells grown in Alvetex® are highly sensitive to BGJ inhibition.
FGFR2-amplified SNU-16 cells were seeded into 12-well Alvetex® inserts, treated with vehicle or 1.5μM BGJ and grown for one week with medium exchanges every second day, followed by fixation, paraffin-embedding and H&E staining. The whole scaffold scale bar indicates 2000μm and magnification scale bar indicates 100μm.

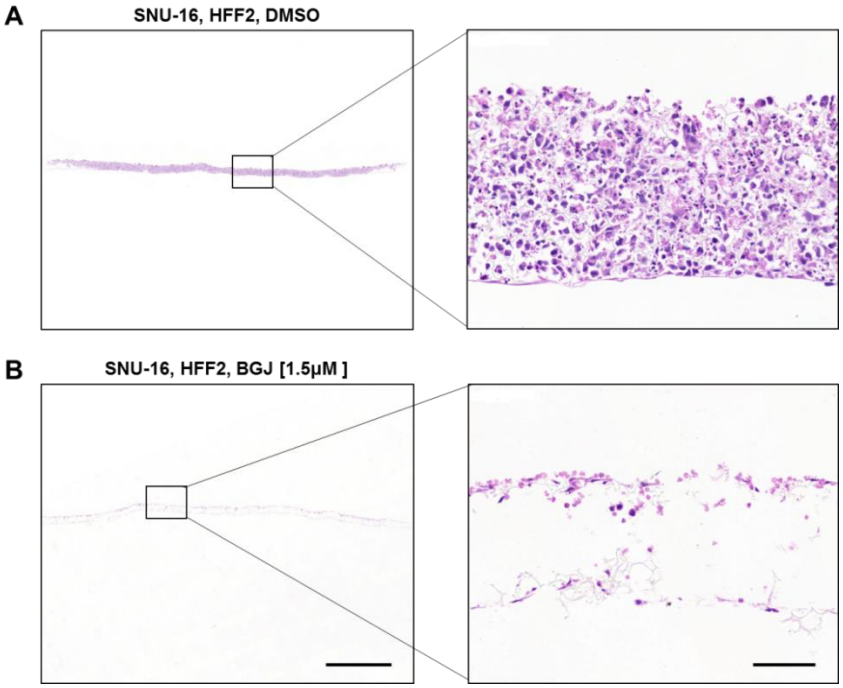

Figure 3.20. *FGFR2*-amplified cancer cells with stromal cells are sensitive to FGFR inhibition.
FGFR2-amplified SNU-16 cells together with HFF2 cells were seeded 2:1 into 12-well Alvetex® inserts, treated with vehicle or 1.5μM BGJ and grown for one week with medium exchanges every second day, followed by fixation, paraffin, embedding and H&E staining. Whole scaffold scale bar indicates 2000μm and magnification scale bar indicates 100μm. The experiment was performed twice **(Appendix Figure 8.14)**.

FGFR2 wildtype SNU-1 suspension cells were also exposed to BGJ in Alvetex® 12-well inserts and did not show sensitivity to the drug in 3D **(Figure 3.21)** and also in co-culture with stromal cells **(Figure 3.22)**.

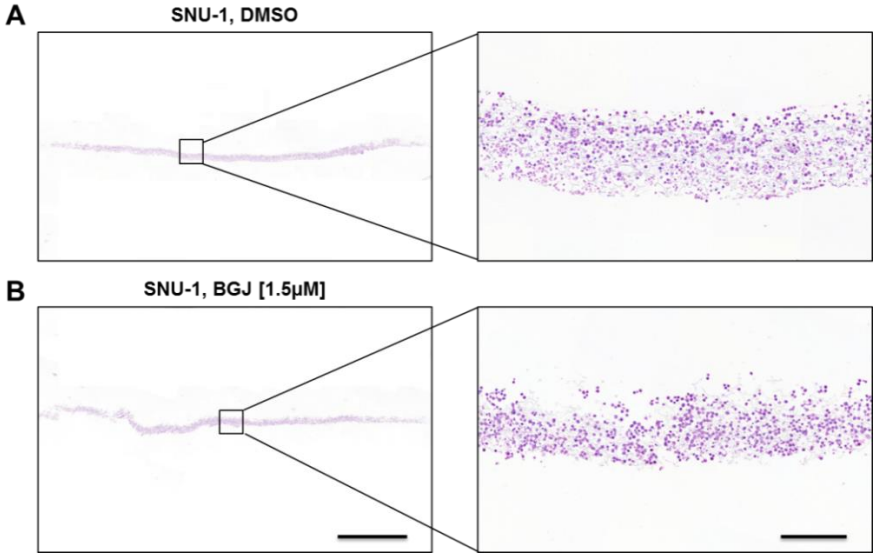

Figure 3.21. *FGFR2* wildtype gastric cells are not killed through FGFR inhibition.
FGFR2-wt SNU-1 cells were seeded into 12-well Alvetex® inserts, treated with vehicle **(A)** or 1.5µM BGJ **(B)** and grown for one week with medium exchanges every second day, followed by fixation, paraffin, embedding and H&E staining. Whole scaffold scale bar indicates 2000µm and magnification scale bar indicates 100µm.

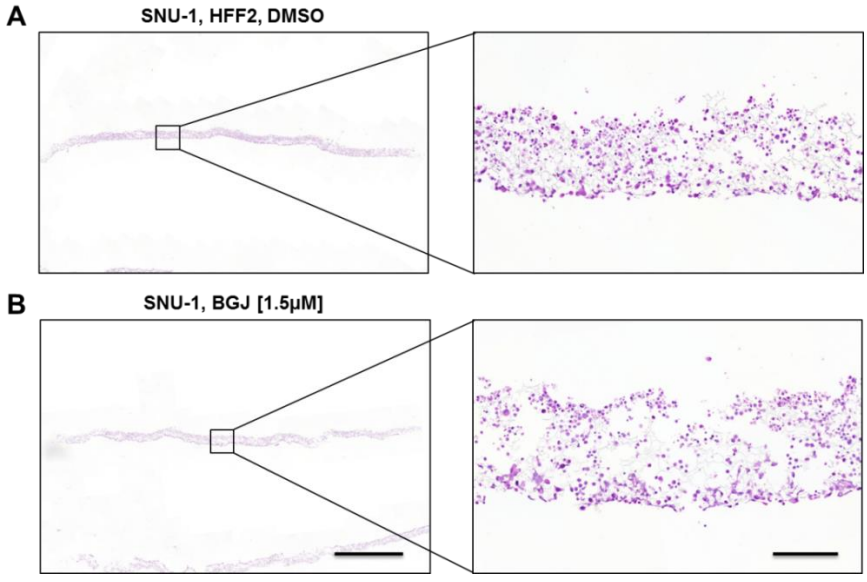

Figure 3.22. *FGFR2* wildtype gastric cells co-cultured with stromal cells are drug-insensitive.
FGFR2-wt SNU-1 cells together with HFF2 cells were seeded 2:1 into 12-well Alvetex® inserts, treated with vehicle **(A)** or 1.5µM BGJ **(B)** and grown for one week with medium exchanges every second day, followed by fixation, paraffin, embedding and H&E staining. Whole scaffold scale bar indicates 2000µm and magnification scale bar indicates 100µm.

Drug sensitivity of fibroblasts was also investigated. HFF2 cells seeded into Alvetex® scaffolds and treated with BGJ did not show sensitivity towards the drug **(Figure 3.23)** and are therefore ideal to use for the co-culture model, where fibroblasts cells should not be killed by FGFR inhibition.

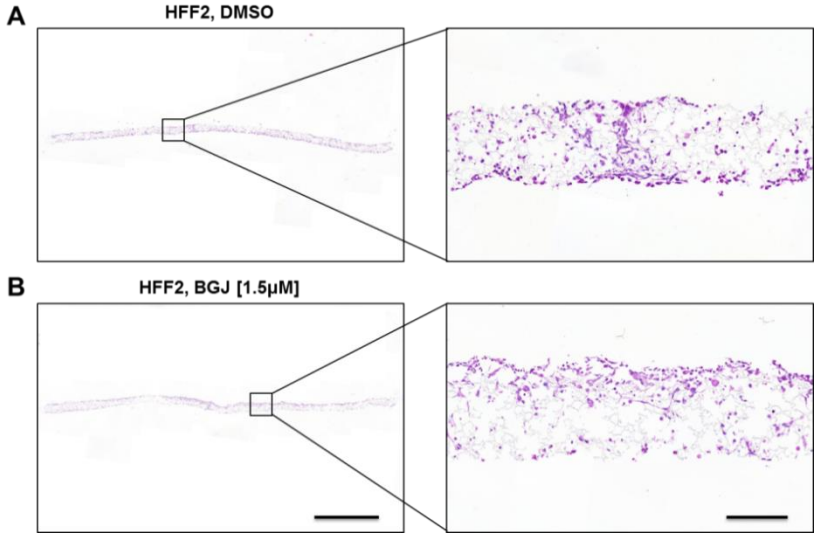

Figure 3.23. Fibroblast cells are not sensitive towards FGFR inhibitors.
HFF2 cells were seeded into 12-well Alvetex® inserts, treated with vehicle or 1.5µM BGJ and grown for one week with medium exchanges every second day, followed by fixation, paraffin, embedding and H&E staining. Scale bar in the whole scaffold image indicates 2000µm and in the magnified image 100µm. The experiment was performed twice **(Appendix Figure 8.15)**.

Also, cells with *FGFR1* amplifications, such as H520 lung cancer cells, showed to be highly sensitive towards BGJ drug inhibition **(Figure 3.24)**.

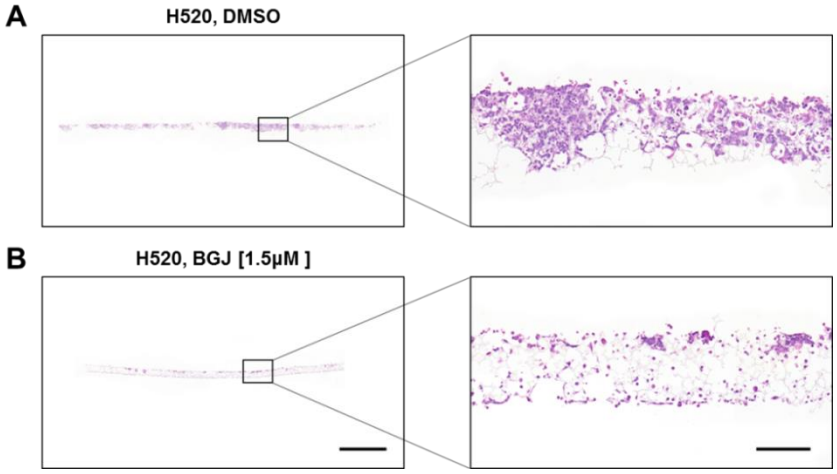

Figure 3.24. *FGFR1*-amplified lung cancer cells are sensitive to FGFR inhibition.
FGFR1-amplified H520 were seeded into 12-well Alvetex® inserts, treated with vehicle or 1.5µM BGJ and grown for one week with medium exchanges every second day, followed by fixation, paraffin, embedding and H&E staining. Whole scaffold scale bar indicates 2000µm and magnification scale bar indicates 100µm.

3.9 Visualisation and analysis of data in 3D using Imaris

To measure cell growth in 3D, Z-stacks were acquired at intervals of 4µm so that the whole scaffold thickness could be imaged via confocal microscopy. The individual Z-stacks can then be merged together using Imaris software, which compiles each Z-stack section to create a 3D image, thus allowing the interpretation of 3D microscopy datasets with segmentation options. Imaris rendered Z-stacks of MFE-296-Azurite and HFF2-EGFP cells grown cells in 3D in Alvetex® allowing the visualisation of cell interactions and cell morphology. Since MFE-296 do not tend to clump together, individual cells could be identified with Imaris **(Figure 3.25)**.

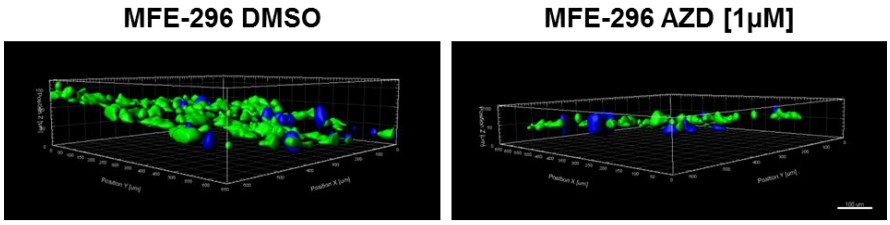

Figure 3.25. MFE-296 cells treated with AZD in Alvetex® scaffolds rendered in Imaris.
MFE-296-Azurite and HFF2-EGFP cells were grown in co-culture 2:1 in Alvetex® scaffolds and treated with 1µM AZD followed by fluorescence confocal microscopy after 72h. Z-stacks were then rendered into a 3D image with Imaris. The scale bar indicates 100µm.

SNU-16 cells however, were clumping together and single cells could not be clearly identified using Imaris despite adjusting settings in Imaris to segregate cells **(Figure 3.26)**. Therefore, to be able to compare cell growth more precisely between conditions, cell volume was compared for SNU-16 cells.

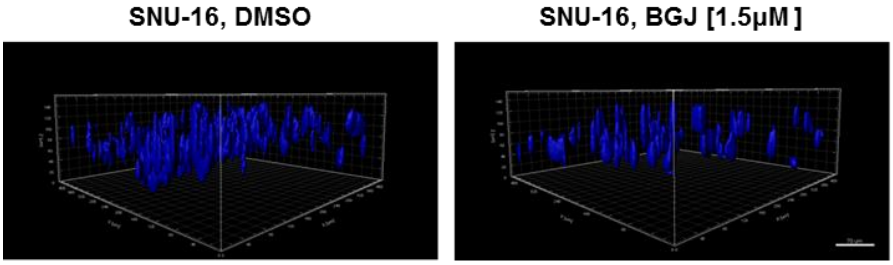

Figure 3.26. SNU-16 cells treated with BGJ in Alvetex® scaffolds and rendered with Imaris.
Untagged SNU-16 cells were seeded into Alvetex® scaffolds and treated with vehicle of 1.5µM BGJ and grown for 72h. DAPI was added to the medium to stain the cell nuclei of SNU-16 cells and Z-stacks were acquired with fluorescence confocal microscopy. Z-stacks were then rendered in Imaris. The scale bar indicates 100µm.

To visualise SNU-16 cells, initially cells were also transfected with Azurite, however the signal was very low and cells could not be properly identified in scaffolds with fluorescence live cell imaging. Instead of using Azurite, an H2B-RFP construct was used that only stains the nucleus of the cells and did not affect the morphology of cells **(Appendix Figure 8.16)**. Cells were then sorted for H2B-RFP expression, as done previously for Azurite and EGFP-positive cells **(Appendix Figure 8.17)**. Fluorescent cells were also generated for H520 lung cancer and MRC-5 lung fibroblasts **(Appendix Figure 8.18)**. Combining visualisation of cells with a fluorescent marker and Imaris, cell concentration was assessed. For SNU-16 cells, the highest cell concentration was used to generate drug resistant cells in 3D **(Figure 3.27)**.

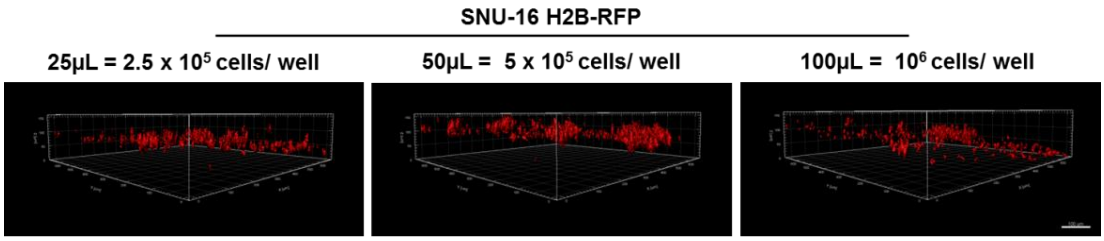

Figure 3.27. Cell seeding densities for SNU-16 cells in Alvetex® 12-well inserts.
H2B-RFP-positive SNU-16 cells were seeded into Alvetex® scaffolds at different concentrations and grown for one week followed by Z-stack acquisition with fluorescence confocal microscopy and rendering with Imaris. The scale bar indicates 100µm.

Since MFE-296 and SNU-16 cells exhibit different proliferation rates, the optimal cell seeding ratio was also assessed in Alvetex® scaffolds for SNU-16 cells. Since SNU-16 cells appear to grow slower than HFF2 cells, again a ratio of 2:1 was ideal for SNU-16 and HFF2 cells to assess drug resistance in co-culture cells in 3D **(Figure 3.28)**.

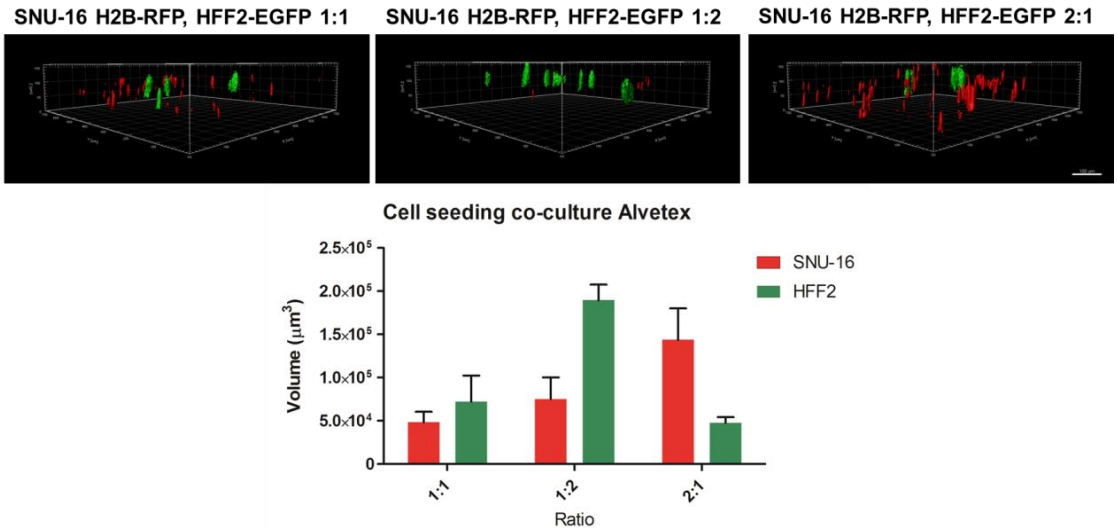

Figure 3.28. Co-culture of SNU-16 H2B-RFP and HFF2-EGFP cells.
SNU-16-H2B-RFP and HFF2-EGFP cells were seeded 1:1, 1:2 or 2:1 in Alvetex® scaffolds and grown for one week. Z-stacks were acquired and rendered in Imaris. Simultaneously, scaffolds were fixed, paraffin-embedded and H&E stained (H&E stainings and additional replicates in **Appendix Figure 8.19**).

3.9.1 Cell retrieval from Alvetex® scaffolds

To extract RNA from cells grown in 3D, cells had to be retrieved from the Alvetex® scaffolds. Co-cultures of MFE-296-Azurite and HFF2-EGFP were grown in uncoated scaffolds for 14 days. Scaffolds were washed twice in PBS and cut into smaller pieces and incubated in trypsin/EDTA in a shaker for 15 min at 37 °C at 100rpm. Then medium was added to trypsin/EDTA and collected in another 15mL Falcon tube. This step was repeated twice with fresh trypsin/EDTA and cells were then together with the previous suspension pelleted, resuspended in 300µL complete growth medium and taken to flow cytometry for cell sorting (ARIA II).

As a control, MFE-296 and HFF2 cells without fluorescent markers were grown in parallel in Alvetex® scaffolds for 14 days on uncoated scaffolds. Cells were harvested as described above and no cells positive for Azurite (P4) or EGFP (P6) could be measured **(Figure 3.29)**.

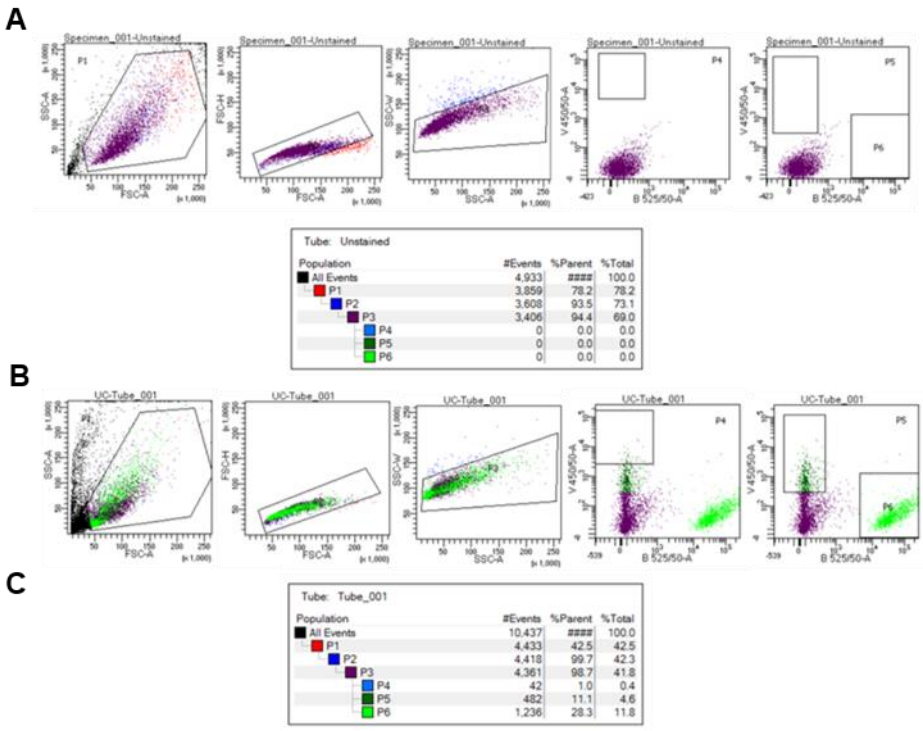

Figure 3.29. FACS after cell retrieval from Alvetex® scaffolds.
(A) FACS of MFE-296 cells and HFF2 fibroblasts without a fluorescent marker retrieved from uncoated Alvetex® scaffolds. **(B)** FACS of MFE-296 cells and HFF2 fibroblasts with fluorescent markers retrieved from uncoated Alvetex® scaffolds. In the first panels of the FACS data the gating was adjusted to select for healthy cells excluding dead cells and debris (P1). In the second and third panels gates were created to exclude duplicates. In the fourth and fifth panels Azurite and EGFP positive cells were gated (P4 and P5). **(C)** Overview of the events of the ungated and gated FACS measurements.

With this method, it was shown that it was possible to retrieve cells from the scaffolds, and this will be applied for future experiments. SNU-16-H2B-RFP and HFF2-EGFP cells were then grown in Alvetex® 12-well inserts, treated with BGJ and rendered with Imaris as a trial experiment **(Figure 3.30)**.

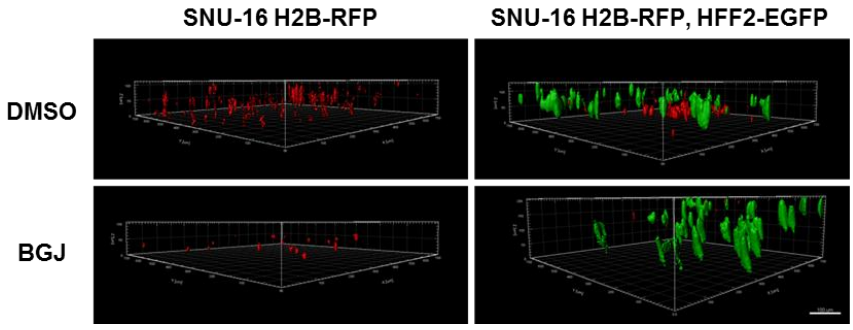

Figure 3.30. SNU-16-H2B-RFP cells alone and together with HFF2 cells in Alvetex®.
SNU-16 cells were either seeded alone or together with HFF2 cells into Alvetex® scaffolds. After 24h the medium was exchanged to medium containing 1.5µM BGJ and depending on the density of the cells, exchanged every 1-2 days. Scaffolds were imaged after one week. Z-stacks were acquired, rendered with Imaris.

3.10 Discussion

3.10.1 FGFR aberrations are predictors for drug sensitivity

The primary aim of this study was to investigate the effect of *FGFR2* amplifications in gastric cancer cells on drug sensitivity to FGFR inhibitors in a 3D setting, with the help of stromal cells. Initial investigations provided new insights into the significance of *FGFR* amplifications in gastric and lung cancer and FGFR2 mutations in endometrial cancer. Three different FGFR kinase inhibitors PD, AZD and BGJ were tested, with similar effects on the cancer cells studied. *FGFR*-amplified and mutated cells were sensitive to drug and cell death was induced. FGFR wildtype cell lines were less sensitive to FGFR inhibition and this has been shown by the difference in IC_{50} values between *FGFR2*-amplified and *FGFR2* wildtype gastric cancer cells, with a higher IC_{50} value in *FGFR2* wildtype cells. This was also confirmed from findings from tumour tissue of gastric cancer patients where *FGFR2* was genetically amplified. Furthermore, this is consistent with data where an array of gastric cancer cell lines with *FGFR*2 amplifications were tested in response to AZD (Xie et al., 2013). *FGFR2*-mutated endometrial MFE-296 cancer cells were previously used in the group and showed sensitivity to FGFR inhibition due to a mutation in the kinase domain of the receptor. Also *FGFR1*-amplified H520 lung cancer cells were tested and showed sensitivity to FGFR inhibitors. *FGFR* wildtype cells were eventually killed due to off target effects of increasing drug concentrations.

Previous studies have used PD treatment to investigate the effect of FGFR inhibition on gastric cancer cells and, where protein expression levels were investigated, the findings were consistent with data that showed that SNU-16 cells were more sensitive to FGFR inhibition than SNU-1 or AGS cells (Kunii et al., 2008).

Upon stimulation of *FGFR*-amplified cell lines with FGF2 and FGF10, cell signalling was elevated. Both SNU-16 and H520 cells showed to be activated more by FGF2 than FGF10 as FGF2 signals through all FGFRs while FGF10 is more specific to FGFR2b (Jaskoll et al., 2005; Ornitz and Itoh, 2015).

3.10.2 3D Alvetex® model optimisation

The use of 3D organotypic cultures is increasing and has been used to investigate cell-cell interactions and phenotypic effects upon drug treatments, as they are more closely mimicking the *in vivo* properties of tumours (Chioni and Grose, 2012; Coleman et al., 2014; Froeling et al., 2009; Gaggioli et al., 2007). An ideal 3D organotypic model should display a tissue-specific physiological microenvironment that enables cells to proliferate, form aggregations and differentiate. Such a model should allow cell-cell and cell-ECM interactions and address tissue-specific stiffness, oxygen and nutrients diffusion and metabolic waste (Griffith and Swartz, 2006). To this day, there are no 3D models that include all necessary parameters in providing a scaffold to support cell growth for long term applications without any interference. Therefore 3D models have to be chosen for specific applications. More traditional cell culture models include spinner flasks (Sutherland et al., 1971) or gyratory rotation devices (Breslin and O'Driscoll, 2013), which allow the generation of 3D spheres, however this is not compatible for HTS applications. Scaffold-based 3D models mimic cell-cell and cell-ECM interactions the closest and therefore for this project a relatively recent scaffold model, Alvetex®, was established to study drug resistance. The 3D model should allow an increased surface area for cells to interact with each other and investigate the effect of stromal cells on cancer signalling. The advantages of this model over conventional 3D models is the ability to assess drug treatment over prolonged time periods, making it suitable to generate resistant cells in 3D where other models tend to either spontaneously disintegrate in the case of spheroids, or shrink in the case of gel based 3D models (Khaitan et al., 2009; Nath and Devi, 2016).

Another advantage is the ability to grow cells without influence from animal proteins that could render the model less physiomimetic. The scaffolds could be coated with surfactants if desired. However, the reconstituted ECM from Matrigel™ was derived from a mouse sarcoma line and, although it has shown to increase engraftment and attachment of cells, it has also been shown to activate signalling pathways and stimulate cells to transform into a more primitive state. Therefore it may be unsuitable to use to study cell signalling in human cancers (Henson et al., 2007). Fortunately, cell

attachment of MFE-296 cells to scaffolds was observed to be the highest in uncoated scaffolds. Rather than helping cells attach to the scaffold, it seemed as if the surfactant was blocking the pores therefore hindering cell invasion into the scaffold. The surfactant concentration could have been diluted, however as attachment in uncoated scaffolds was already high and leaving scaffolds uncoated was desired, all experiments were conducted with uncoated scaffolds.

Adherent MFE-296 and HFF2 cells attached readily to the scaffold as these cells regained their morphology in the 3D structure and are rather large cells. However, SNU-16 cells were suspension cells and also smaller. Therefore due to cell loss, a larger number of cells had to be seeded compared to other cell types. There are different formats available, such as 6-well and 12-well inserts and 12, 24-well and 96-well plates. The well-plate formats would be simpler in utilisation and useful for HTS applications, as scaffold membranes reside in the plate and are not required to be transferred, and medium is added from the top. However, due to the fact that the scaffolds sit at the bottom of the well-plate no chemical gradient can be established as can be done with scaffold inserts, where medium can be either only fed from the top or below only or both. This was especially important for SNU-16 cells as it was observed that the highest cell attachment was achieved using 12-well inserts and feeding medium only from below, therefore enabling the cells to migrate into the scaffold. Furthermore, better results were observed with SNU-16 cells when the cell suspension volume was kept low and incubating scaffolds with the cells at room temperature for 30min to 1h prior to submerging the scaffolds in medium, which further aided attachment of suspension cells.

Stromal cells are recognised to play an important role in malignancy of cancer cells, creating a niche for tumour cells protected from the influences of drug inhibition (Olson and Joyce, 2013; Wang et al., 2017; Whiteside, 2008). To investigate the effect of stromal cells on *FGFR2*-amplified gastric cancer cells in 3D, the effect of drug inhibition was also assessed in fibroblasts. Both HFF2 and MRC-5 lung fibroblasts were not sensitive to drug inhibition and, interestingly, initial experiments showed that when cancer cells were treated with FGFR inhibitors in presence of fibroblasts,

cell viability was increased, with higher IC_{50} values compared to cancer cells alone. Even more so, growing co-culture cells in 3D compared to 2D using MFE-296 and HFF2 cells in a cell viability assay resulted in higher IC_{50} values in 3D 96-well plates, highlighting the importance to study cancer drug response in 3D in the presence of fibroblasts. Cancer cells normally grow at a lower pace than fibroblasts and therefore, for co-culture experiments, the optimal ratio of cancer cells and fibroblast had to be determined, revealing the best results with double the cancer cells compared to fibroblasts. Fibroblasts could have been also treated with mitotic inhibitors such as Mitomycin C that would stop proliferation of fibroblasts (Ponchio et al., 2000). Cells also regained their natural cell shape in Alvetex® scaffolds, which was especially observed with fibroblasts as they regained their spindle-like morphology. Interestingly fibroblasts, when seeded together with cancer cells, migrated through the scaffold and resided more in the bottom half of the scaffold, whereas cancer cells remained in the top half of the scaffold, which could be due to the migratory properties of fibroblast cells (Kole et al., 2005).

The effects of drug treatment in 3D were consistent with previous data acquired in 2D, and FGFR inhibitor treatment of cells in 3D resulted in cell death. Insensitivity to the drug was recapitulated with SNU-1 cells in the 3D model, which suggests that the growth inhibition in SNU-16 and H520 cells upon FGFR inhibition resulted through blockade of aberrant FGFR signalling rather than off-target effects of the drug.

3.10.3 Visualisation, analysis and cell retrieval of cells for 3D experiments

Most groups use histology to assess growth of cancer cells in 3D at a predetermined time point (Fang et al., 2016; Xu et al., 2016). In this project however, it was attempted to monitor the emergence of drug resistant populations in 3D. To achieve this, cancer cells and fibroblasts were transduced with fluorescent markers and, since the scaffold is thin and made of transparent polystyrene, it was possible to image through the whole scaffold. However, attempts to image through the medium in the well-plate were unsatisfactory and therefore inserts were transferred to a glass-bottom dish prior to imaging. Rendered Z-stacks allowed quantification of cells and showed changes in cell morphology. Over time, less MFE-296 cells expressed Azurite, whereas the proportion of HFF2 expressing EGFP was high, similar to post cell sorting. Thus, I suspected that the cells lose the fluorescent marker over time. SNU-16 cells did not express Azurite efficiently and therefore a nuclear marker was used for SNU-16 cells instead of a cytoplasmic marker.

As the scaffold consists of inert polystyrene, the cells could be trypsinised and retrieved from the scaffold. This was improved by cutting the scaffold into small pieces and increasing trypsin volume and trypsinisation repeats on a shaker, allowing gentler cell retrieval for further analysis.

With the optimisation of the 3D model and the generation of fluorescent cancer and stromal cells, the tools were established to investigate the formation of drug-resistant cancer cells in 3D with and without stromal support.

Chapter IV: Results Part II

Generation of resistant cells in 2D and 3D cultures and RNA sequencing

4.1 Introduction

Knowledge about molecular modifications that drive cancer progression and their effect on the response to therapies has encouraged the development of novel target treatments. The fibroblast growth factor-receptor interaction (FGF-FGFR) is a common target for different types of cancer (Ornitz and Itoh, 2015). Furthermore, specific alterations of FGFR are more prevalent in certain types of cancer and therefore could represent potential biomarkers.

In the previous chapter, such cancers were characterised and it was shown that cancers with FGFR alterations are sensitive towards FGFR inhibition, both in 2D and 3D. Small molecule inhibition is the most widely used means of therapy and FGFR signalling has been postulated as a viable therapeutic target, especially in FGFR altered cancers (Byron et al., 2008; Konecny et al., 2013; Schmidt et al., 2015). However, resistance to both chemo- and hormone therapy is common in recurrent endometrial, gastric and lung cancer, and acquired or intrinsic resistance to small molecule inhibitors have been described in other carcinomas (Goltsov et al., 2012; Lito et al., 2013; Wagle et al., 2011; Zhang et al., 2009). The outcome and efficacy of long-term FGFR-targeted therapy however, is an important aspect to study.

Intrinsic or acquired drug resistance to kinase inhibitors is one of the major difficulties in successful cancer therapy, which is not only the case for conventional chemotherapy but also targeted drug therapies (Holohan et al., 2013). The survival of cancer patients largely relies on early cancer detection and effective treatment. We require a greater understanding of how resistance is acquired and need to view cell signalling as an interconnected network, capable of rewiring upon inhibition of dominant signalling pathways. Drug resistance is a multifaceted problem and can occur in different stages e.g.; (1) reduced drug accumulation in cells due to decreased uptake or efflux through pumps; (2) decreased activity of the drug; (3) diminished efficacy due to increased target or; (4) increased ability of cancer cell to repair the damage caused by the drug. Other mechanisms are evasion of apoptosis or deregulation of apoptotic pathways and upregulation of proliferation and survival signalling pathways. Furthermore, the tumour microenvironment and in particular

the involvement of stromal cells, has been suggested to be linked to the emergence of resistance in supporting cancer cell growth through the release of growth factors and proteases to move through the ECM and therefore act as tumour-promoting cells (Bissell et al., 2005; Sung et al., 2007; Whiteside, 2008).

This results chapter focusses on drug resistance in FGFR-driven cells and the generation of drug resistance both in 2D conventional cell biology, and in 3D. In the 3D model, additionally, the effect of stromal support in drug resistance will be investigated and compared to cancer cells alone. During the development of drug resistance, cancer cells rewire their signalling networks and gene expression and signalling pathways in drug-resistant cancer cells and normal cancer cells, with and without stromal support, will be compared using RNA-Seq.

4.2 Drug resistance in 2D

In order to generate FGFR-inhibitor resistant gastric cancer cell lines, SNU-16 cells were treated with FGFR inhibitor BGJ. As shown previously in section 3.3, SNU-16 cells are highly sensitive towards FGFR inhibitors. To generate BGJ-resistant SNU-16 cells, cells were exposed to increasing doses of BGJ over a time-course of two months leading to a final dosage of 1.5μM BGJ. Every second medium exchange the dosage of the drug was doubled and cells were left to grow. Once resistant cells, with similar growth rates as uninhibited cancer cells, were generated, cells were then maintained with complete growth medium supplemented with 1.5μM BGJ.

As opposed to publications from other groups (Grygielewicz et al., 2016), the morphology of the cells did not appear to change **(Appendix Figure 8.20)**. However, the cells seemed to proliferate much faster and medium had to be exchanged much more frequently compared to the parental cells as indicated by a colour change of the medium from red to orange through a metabolic effect and through cell counting of parental and drug-resistant SNU-16 cells.

To investigate whether the cells were resistant towards the FGFR inhibitor, parental SNU-16 and BGJ-resistant SNU-16 (SNU-16^{BGJR}) were exposed to a wide range of concentrations of the BGJ inhibitor over 72 hours and cell viability was measured via

MTS assay **(Figure 4.1)**. As a vehicle control, DMSO was used and drug concentrations were adjusted so that all samples contained the same amount of DMSO. Staurosporine was used as a positive control as it is a potent, non-selective inhibitor of protein kinases to induce cell death.

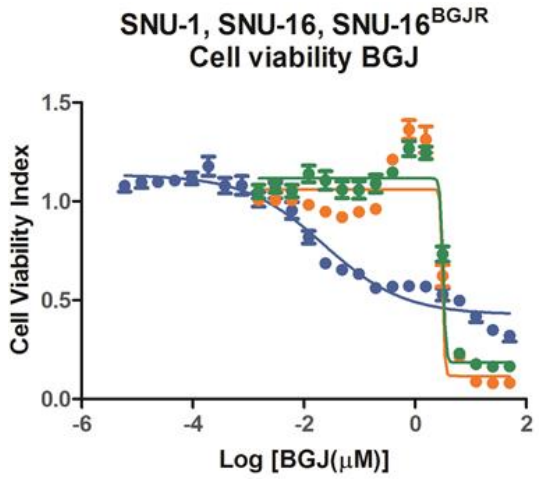

Cell line	$LogIC_{50}$ (μM)	IC_{50} (μM)
SNU-1	0.504	3.189
SNU-16	-1.637	0.023
SNU-16^{BGJR}	0.498	3.145

Figure 4.1. Cell viability index curve of SNU-1, SNU-16 and SNU-16^{BGJR} in 2D.
Parental and BGJ-resistant SNU-16 gastric cancer cells were plated in triplicate into 96-well plates and exposed to BGJ concentrations ranging from 1.5nM to 50μM for SNU-1 and SNU-16^{BGJR} cells and ranging from 0.006nM to 50μM for SNU-16 cells. Cell viability was measured after 72h incubation. Control cells were treated with DMSO and as a background control 1% Staurosporine was added to wells containing cells. The cell viability index was then measured subtracting the background signal and adjusting to the controls. An average of three biological MTS experiments in technical triplicate is shown with curves indicating the average of the mean with the corresponding error bars showing SEM. $LogIC_{50}$ and IC_{50} values were calculated in GraphPad Prism 5.

In the resistant cell line, a clear shift to the right and therefore higher BGJ concentration tolerance was observed with the curve being a plateau compared to the parental cell line curve. This confirms that resistant cells are less sensitive toward the drug. Additionally, the effect of other FGFR inhibitors such as AZD and PD were tested on SNU-16^{BGJR} cells indicating a cross resistance to other FGFR inhibitors **(Appendix Figure 8.21)**.

To further confirm drug resistance, drug sensitivity was compared to SNU-16 parental cells and also SNU-1 cells, which harbour no *FGFR2* amplifications or mutations. Cells were grown in 6-well plates and either treated with DMSO control or BGJ and grown for 72 hours. Cells were then harvested and resuspended in complete growth medium before being counted using Trypan blue with a haemocytometer and a light microscope. BGJ drug-sensitive 'parental' SNU-16 cells exhibited reduced growth in the presence of BGJ **(Figure 4.2),** whereas SNU-16^{BGJR} and SNU-1 showed no sensitivity towards BGJ and exhibited similar growth as compared to controls.

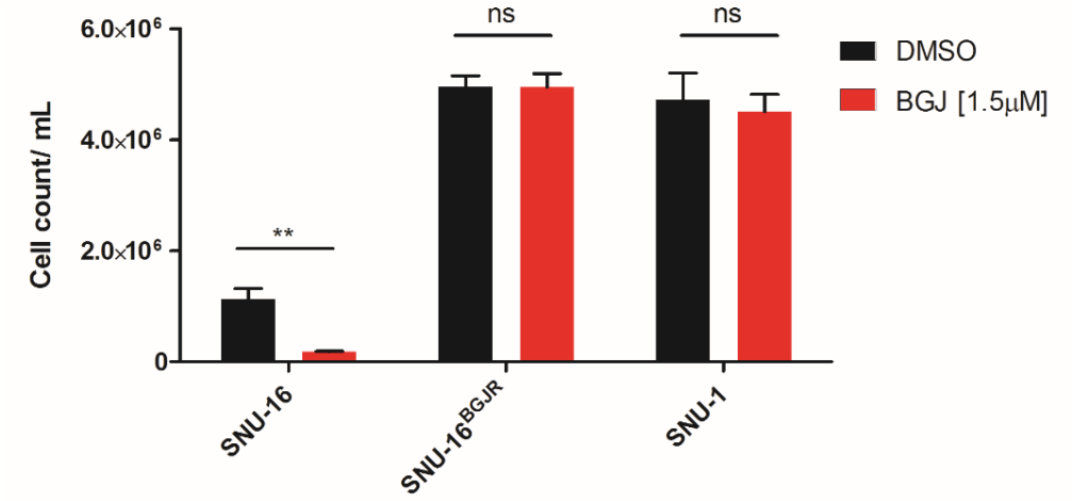

Figure 4.2. SNU-16 cells are highly sensitive towards BGJ.
FGFR2-amplified SNU-16 and BGJ-resistant SNU-16 (SNU-16^{BGJR}) and *FGFR2* wildtype SNU-1 cells were plated in triplicate into 6-well plates and treated with 1.5μM BGJ for 72h. Cells were harvested and resuspended in 1mL complete growth medium and counted using Trypan blue with a haemocytometer. DMSO control treated cell numbers are represented by black filled columns and drug-treated samples with red columns. The graphs show the average of the mean with the corresponding error bars showing SEM. The experiment was performed in biological triplicate. Student's T-test, **p<0.01.

Another method to observe drug sensitivity was to measure cell signalling upon drug treatment of SNU-16^{BGJR} cells. As performed previously, for SNU-16 cells, the resistant counterpart was subjected to 1μM PD, 1μM AZD or 1.5μM BGJ and Western blot analysis was performed. As opposed to SNU-16 cells, resistant cells did not show lower p-ERK levels and no p-AKT signalling was measurable in drug resistant SNU-16 cells **(Figure 4.3)**.

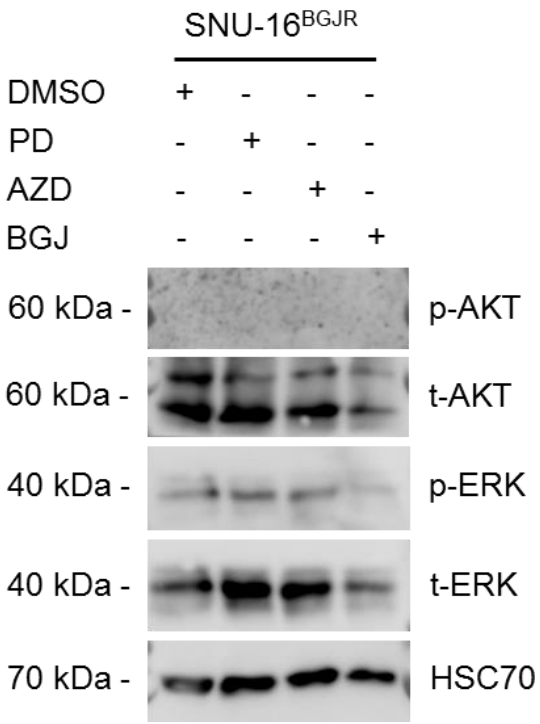

Figure 4.3. SNU-16^{BGJR} cells treated with FGFR inhibitors are not sensitive towards FGFR inhibition. Cells were plated into 6-well plates and treated with vehicle (DMSO) or 1μM PD, 1μM AZD or 1.5μM BGJ for 72h. 20μg lysate was loaded per lane and specific proteins detected using antibodies against p-AKT, p-ERK, t-AKT, t-ERK. HSC70 served as a loading control. The blots shown are representatives of two independent experiments.

To determine the effect of drug resistance in the resistant cells, cells were plated into 6-well plates and medium was exchanged with complete growth medium without BGJ. Cells were harvested over a time range of 24 hours with time-points after 1h, 2h, 4h, 8h, 16h and 24h. Control wells were kept with medium containing BGJ. p-AKT initially increased after 1h but then gradually decreased towards the 24 hour time-point. However, p-ERK reappeared, following initial downregulation, being back to baseline levels after 24 hours **(Figure 4.4).**

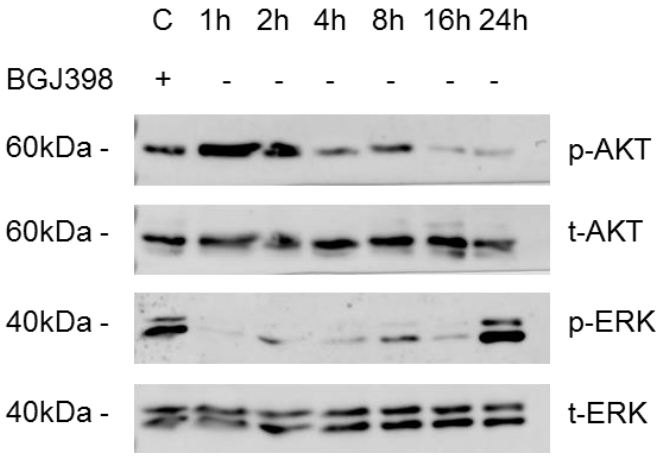

Figure 4.4. Removing BGJ from SNU-16^{BGJR} cells suggests cross-talk between p-ERK and p-AKT signalling.
BGJ resistant SNU-16 cells were plated into 6-well plates and incubated overnight in medium containing BGJ (1.5μM). The next day, the medium was exchanged to complete growth medium without BGJ and cells were harvested after 1h, 2h, 4h, 8h, 16h and 24h. As a control, cells were kept in complete growth medium containing 1.5μM BGJ. 20μg protein was used for Western blot analysis and probed for p-AKT and p-ERK and as controls, t-AKT and t-ERK. The blots shown are a representative of two independent experiments **(Appendix Figure 8.22)**.

4.3 Drug resistance in 3D culture

The standard method to study drug resistance in cancers is to study biochemical, physiological and morphological cues in 2D monolayer cultures. There are only a few *in vivo* alternatives to study the effects and there is a need for a more physiological model representing signalling within cancer cells.

There have been a vast number of advancements in 3D cell culture to mimic the *in vivo* microenvironment and signalling processes, not only between cancer cells but also other cell types playing a role in cancer progression such as stromal cells (De Wever and Mareel, 2003; Hanchen et al., 2007). Many cells in the stroma contain tumour-suppressing abilities and are responsible for the integrity of epithelial cells (De Wever and Mareel, 2003). However, these properties can change during malignancy and eventually lead to tumour growth and migration through the expression of ECM molecules and growth factors such as TGF-β, VEGF and FGFs (Hughes, 2008). The diversity of cells and amount of ECM proteins in the tumour microenvironment plays a major role in the emergence of drug resistance, as it can create a barrier that the drugs must cross in order to reach cancer cells and promote metastasis (Affo et al., 2017; Kopanska et al., 2016; Romero-López et al., 2017; Shin and Mooney, 2016). Furthermore, fibroblasts have been found to be involved in the activation of signalling pathways, such as the Wnt/β-catenin signalling pathway, in many types of cancers including ovarian cancer, NSCLC and glioblastoma (Aprelikova et al., 2013; Johnson et al., 2013; Kaur et al., 2016). It is therefore of fundamental importance to additionally investigate the influence of stromal cells on drug resistance in cancer cells using a suitable cell culture model.

Due to these reasons, and to study drug resistance mechanisms in cancers such as *FGFR2*-driven gastric cancer cells, I developed a novel 3D cell culture model and optimised it to address specific scientific questions (See Chapter III). This approach is ideal for long-term experiments such as to investigate the emergence of drug resistance in 3D in cancer cells over time.

4.3.1 Drug-resistant SNU-16 cells in Alvetex® scaffolds

BGJ-resistant SNU-16 cells that were generated in 2D were seeded into Alvetex® scaffolds to investigate growth properties of the resistant cells. As was observed with SNU-16 cells, the SNU-16^{BGJR} cells attached to the scaffold grew within it and formed cell aggregates. After growing the cells for 1 week, the scaffolds were PFA-fixed and paraffin-embedded, followed by H&E staining **(Figure 4.5)**.

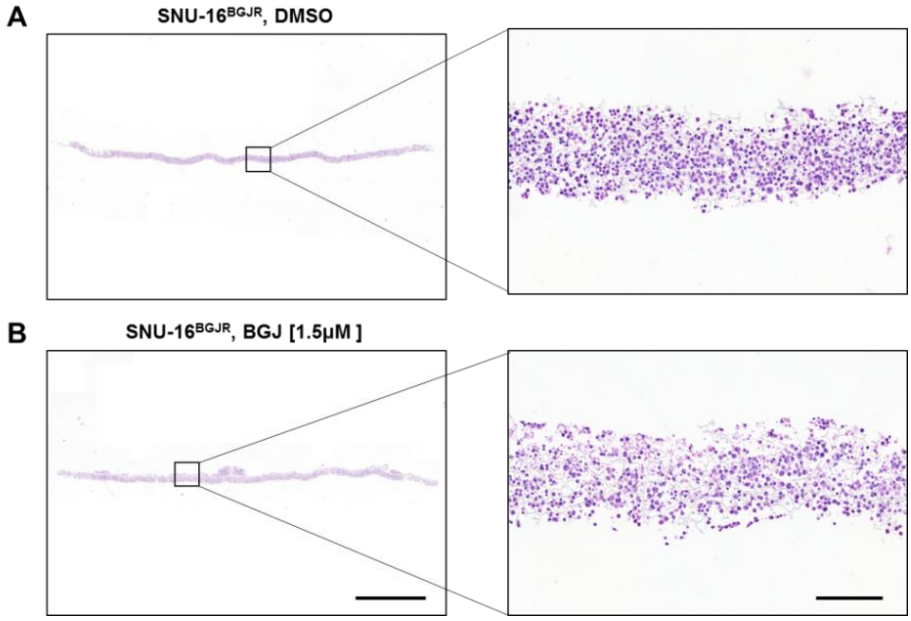

Figure 4.5. BGJ-resistant SNU-16 cells were insensitive to BGJ treatment in Alvetex®.
SNU-16^{BGJR} cells were seeded into 12-well insert Alvetex® scaffolds and incubated overnight. The cells were grown in the scaffolds for 1 week. Medium containing 1.5μM BGJ was fed from below and exchanged every 2 days. The experiment was performed in triplicate **(Appendix Figure 8.23, Appendix Figure 8.24)**. Scale bar indicates 1000μm in the left panel and 100μm in the enlarged panel.

Next, SNU-16^{BGJR} cells were mixed in a 2:1 ratio with HFF2 cells, as determined in Chapter III, and seeded into scaffolds. After 7 days culture, they were PFA-fixed, paraffin-embedded and stained with H&E for analysis. As primary gastric stromal cells are difficult to obtain, HFF2 cells were used, representing the stromal component. The co-cultured cells grew uniformly in the scaffold, and as with the SNU-16^{BGJR} cells alone, did not exhibit sensitivity towards the inhibitor. Growth within the scaffold was also compared between resistant cells alone and in conjunction with fibroblasts **(Figure 4.6)**. BGJ-sensitive SNU-16 cells were compared

to SNU-16^{BGJR} cells and SNU-1 cells, which are not sensitive towards the inhibitor as they do not harbour *FGFR* amplifications **(Figure 4.7).** SNU-16 cells were sensitive as seen by decreased cell growth and SNU-1 and SNU-16^{BGJR} cells showed no sensitivity, and within 1 week proliferated until the scaffolds were fully occupied by cells.

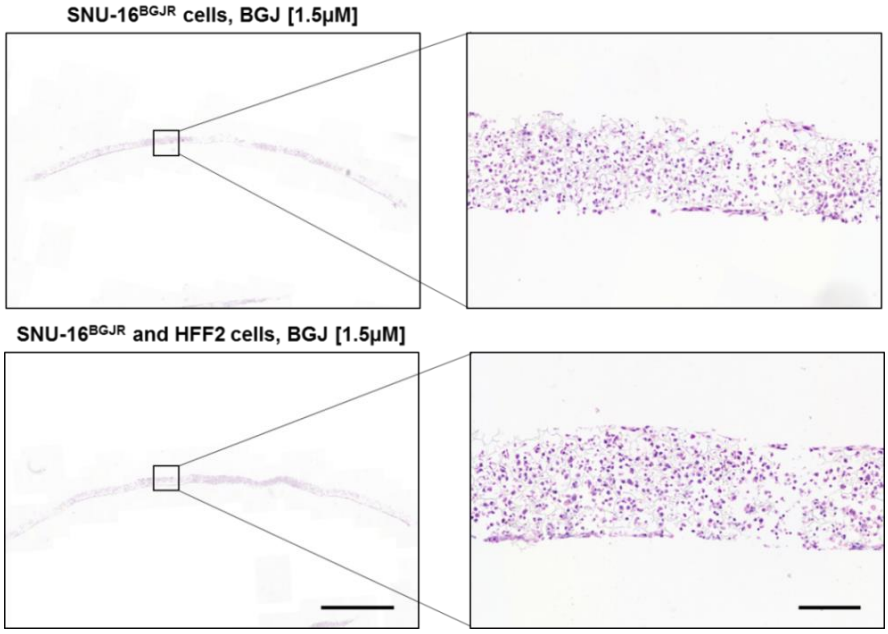

Figure 4.6. SNU-16^{BGJR} grown alone and with HFF2 cells in Alvetex® displayed no sensitivity to FGFR inhibition.
SNU-16^{BGJR} cells were grown alone or mixed with HFF2 cells 2:1 and were seeded into 12-well insert Alvetex® scaffolds and incubated overnight. The cells were grown in the scaffolds for 1 week. Medium containing 1.5µM BGJ was fed from below and exchanged every 2 days. The experiment was performed twice **(Appendix Figure 8.25)**. Scale bar indicates 1000µm in the left panel and 100µm in the enlarged panel.

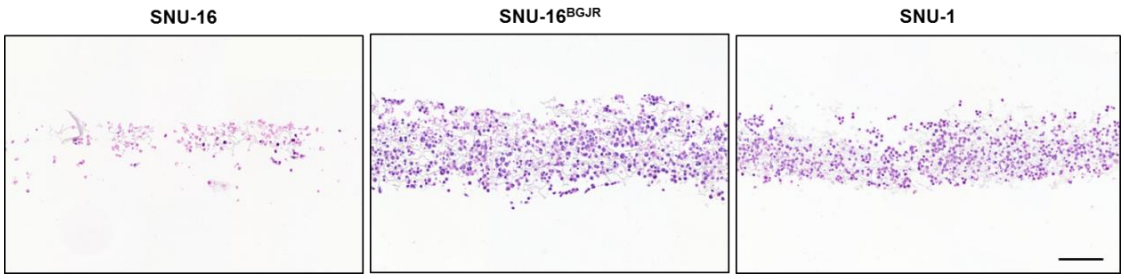

Figure 4.7. *FGFR2*-amplified gastric cancer suspension cells are killed by FGFR inhibition compared to drug-resistant and *FGFR2* wildtype gastric cancer cells.
Cells were seeded into 12-well insert Alvetex® scaffolds and incubated overnight. Medium containing 1.5µM BGJ was fed from below and exchanged every 2 days. Scaffolds were grown for 1 week followed by PFA-fixation, paraffin-embedding and H&E staining. The experiment was performed in triplicate. Scale bar indicates 100µm.

4.3.2 Generation of drug-resistant gastric cancer cells in 3D using Alvetex®

As previously described, the 12-well insert format of Alvetex® and feeding medium solely from below produced the best results in respect to cell attachment and growth. Therefore, to generate and monitor BGJ drug resistant cells in 3D, 12-well inserts were used and medium was only fed from below to avoid cell loss. To investigate the effect of fibroblast signalling on cancer cells, and its involvement in drug resistance, another condition where SNU-16 cells were mixed with HFF2 cells in a 2:1 ratio, as previously determined, was incorporated in the experimental setup. SNU-16 H2B-RFP (red) cells and SNU-16 H2B-RFP admixed with HFF2-EGFP (green) were seeded into 12-well insert scaffolds. After 24h the medium was exchanged to medium containing BGJ and subsequently exchanged every 1-2 days. Cells were exposed to increasing dosages of BGJ. During every other medium exchange the drug concentration was doubled, until reaching 500nM final concentration of BGJ and until resistant populations were observed using confocal microscopy **(Figure 4.8)**. Z-stack *in situ* 3D images were acquired using live cell imaging confocal microscopy once a week and, after 4 weeks, DMSO-treated SNU-16 cells and DMSO and BGJ-treated co-culture cells were harvested. BGJ-treated SNU-16 cells without stromal support were harvested after 8 weeks, when similar cell volume populations to DMSO-treated were observed **(Figure 4.9)**. BGJ-treated SNU-16 cells were initially highly sensitive even to lower BGJ concentrations. However, over prolonged exposure, cells grew exponentially and caught up with vehicle-treated SNU-16 cells. Interestingly, co-culture cells formed drug resistant populations much faster than cancer cells alone. In vehicle-treated co-culture, SNU-16 cells initially grew as expected however cell numbers decreased, which could be due to cell overgrowth and cells not receving enough nutrients although towards later stages, medium was exchanged daily. Also, fewer HFF2-EGFP cells were found in DMSO-treated co-cultures compared to BGJ-treated cells. Prolonged BGJ treatment of co-culture cells seemed to accelerate HFF2 cell growth. Additionally, a better cell attachment to the scaffold was observed in co-cultured cells **(Figure 4.10)**. Z-stacks were rendered using Imaris and from the information that can be acquired with Imaris analysis, differences in cell volume was measured and compared.

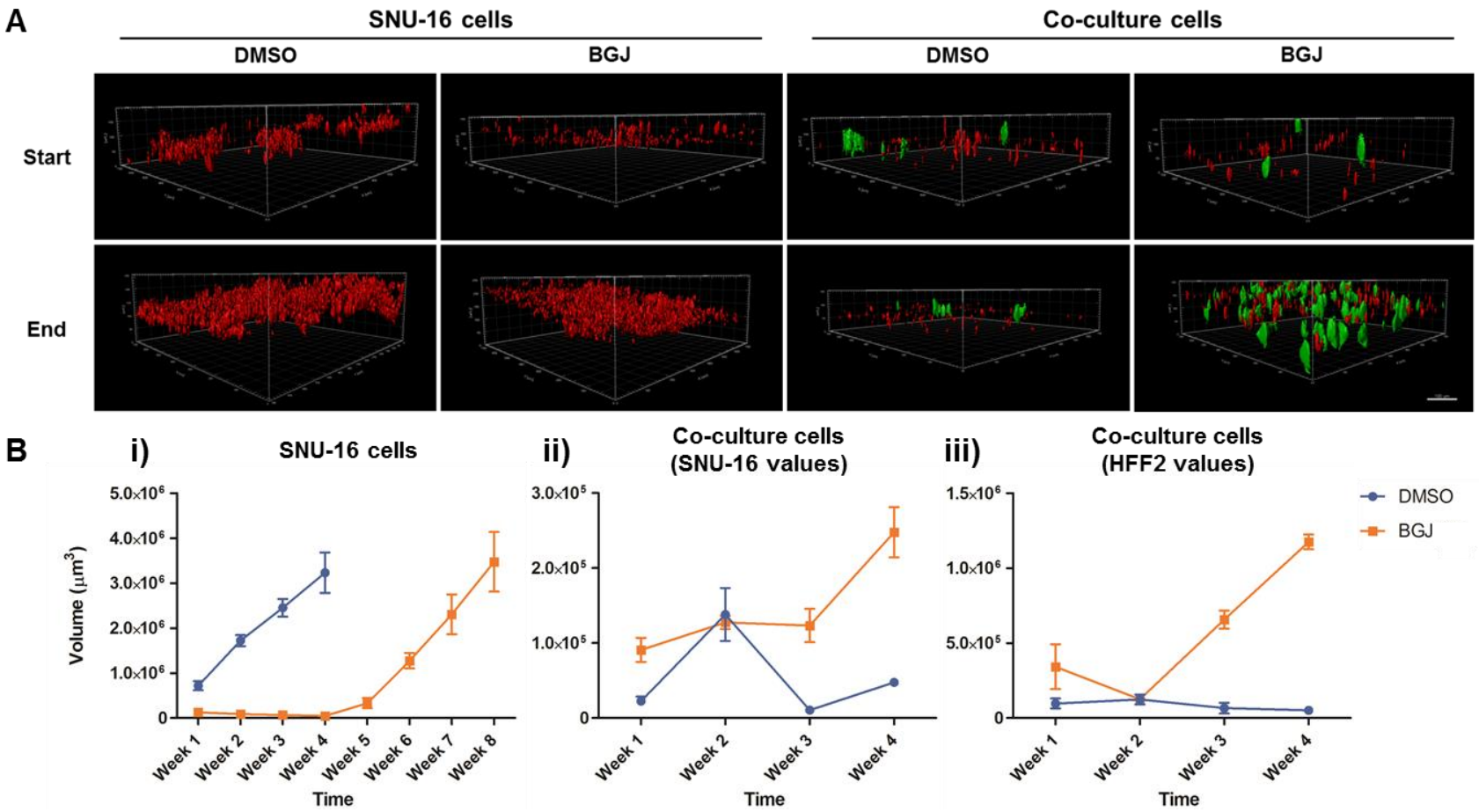

Figure 4.8. Gastric cancer cells with and without stromal support were rendered resistant in 3D using Alvetex® scaffolds.
(A) Imaris rendered live cell images of SNU-16 cells alone and SNU-16 cells co-cultured with HFF2 cells. Cells were grown in Alvetex® scaffolds and treated with increasing dosages of BGJ until resistant populations of the fluorescently-labelled cells were observed via confocal microscopy. Images were taken once weekly **(Appendix Figure 8.26-Appendix Figure 8.31)**; here only start and end time point images are shown. Red cells (H2B-RFP) indicate SNU-16 cells and green cells (EGFP) indicate HFF2 cells. The experiment was performed in biological and technical triplicate. Scale bar indicates 100μm. **(B)** Change in cell volume of DMSO-treated (blue) and BGJ-treated (orange) SNU-16 3D cultures. **(i)** Cell volumes of DMSO treated and BGJ-treated SNU-16 cells grown in Alvetex® alone for four and 8 weeks respectively. **(ii)** Cell volumes of DMSO and BGJ-treated SNU-16 cells grown in co-culture in Alvetex® over a time period of four weeks. **(iii)** Cell volumes of HFF2 cells grown in co-culture and treated with DMSO or BGJ over four weeks in Alvetex®.

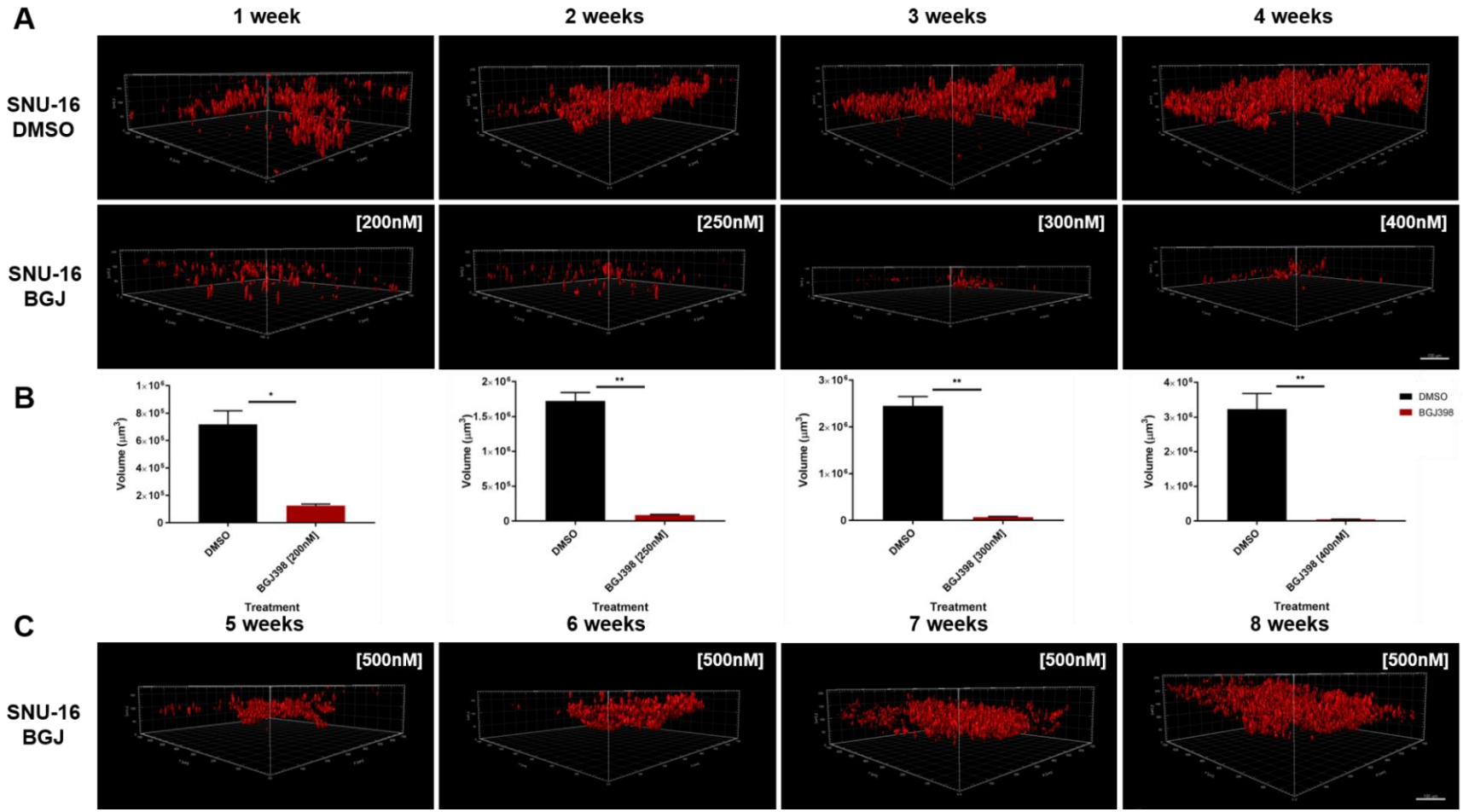

Figure 4.9. Drug-resistant gastric cancer cells were generated after 8 weeks in 3D using Alvetex® for cancer cells alone and after four weeks for cancer cells with stromal support.

Comparison of SNU-16 cells treated with vehicle or BGJ with different dosages over a time span of 4 weeks. **(B)** Analysis of SNU-16 treated with vehicle or BGJ over four weeks. Student's T-test, *p<0.05, **p<0.01. **(C)** Imaris images of SNU-16 treated with BGJ of week 5, 6, 7 and 8. The experiment was performed in biological and technical triplicate. Per condition three images were taken using a confocal microscope. Scale bar indicates 100µm.

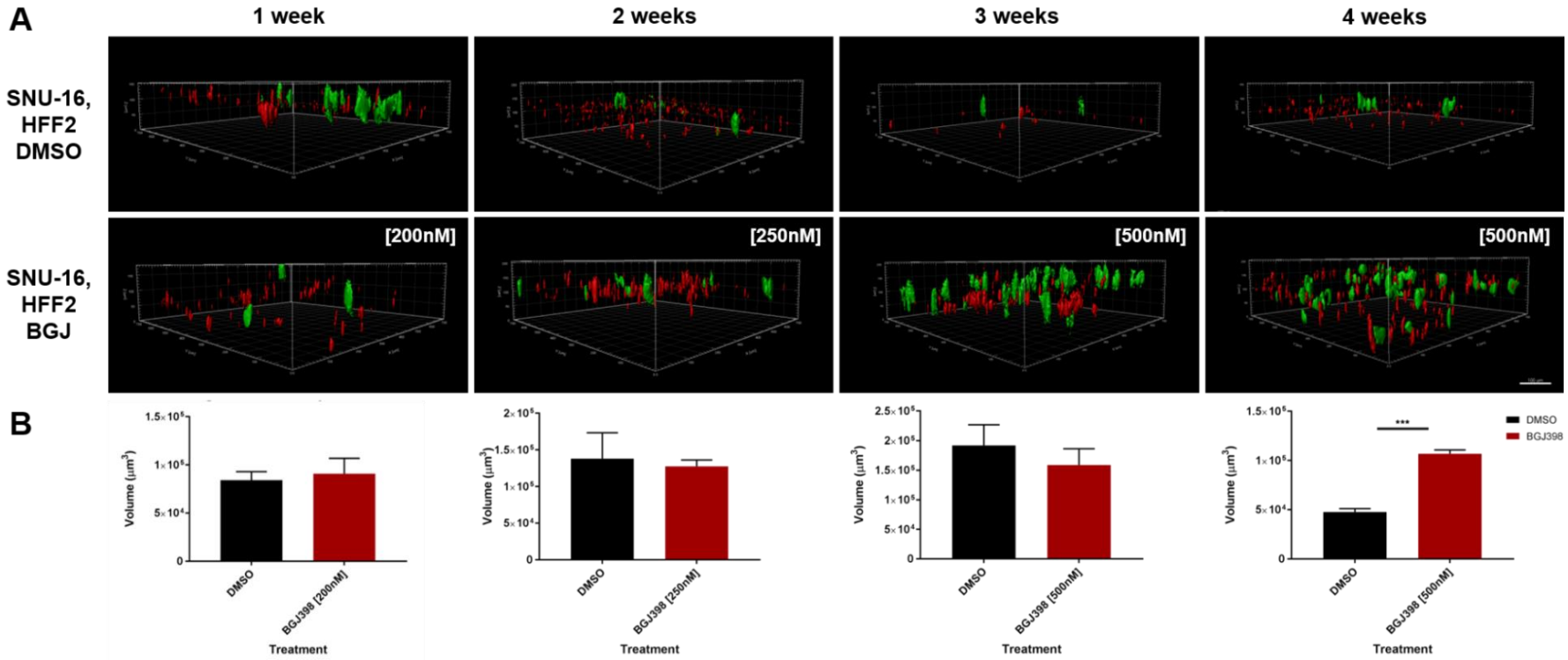

Figure 4.10. Drug-resistant gastric cancer cells with stromal support were generated after four weeks in 3D using Alvetex®.
(A) Comparison of co-culture cells treated with vehicle or BGJ with different dosages over a time span of four weeks. **(B)** Histogram analysis of the change of the volume of co-culture cells treated with vehicle or BGJ over a time span of four weeks. Student's T-test, ***p<0.005. The experiment was performed in biological and technical triplicate. Per condition three images were taken using a confocal microscope. Scale bar indicates 100µm.

In parallel, replicates of the experiment were fixed, paraffin-embedded and sectioned, followed by H&E staining **(Figure 4.11)**. H&E staining of the fixed scaffolds from each condition showed the effect of BGJ on cell numbers of SNU-16 cancer cells alone and SNU-16 cancer cells in combination with HFF2 cells. RNA was harvested from the scaffolds according to the description in section 2.2.26.1 for RNA sequencing.

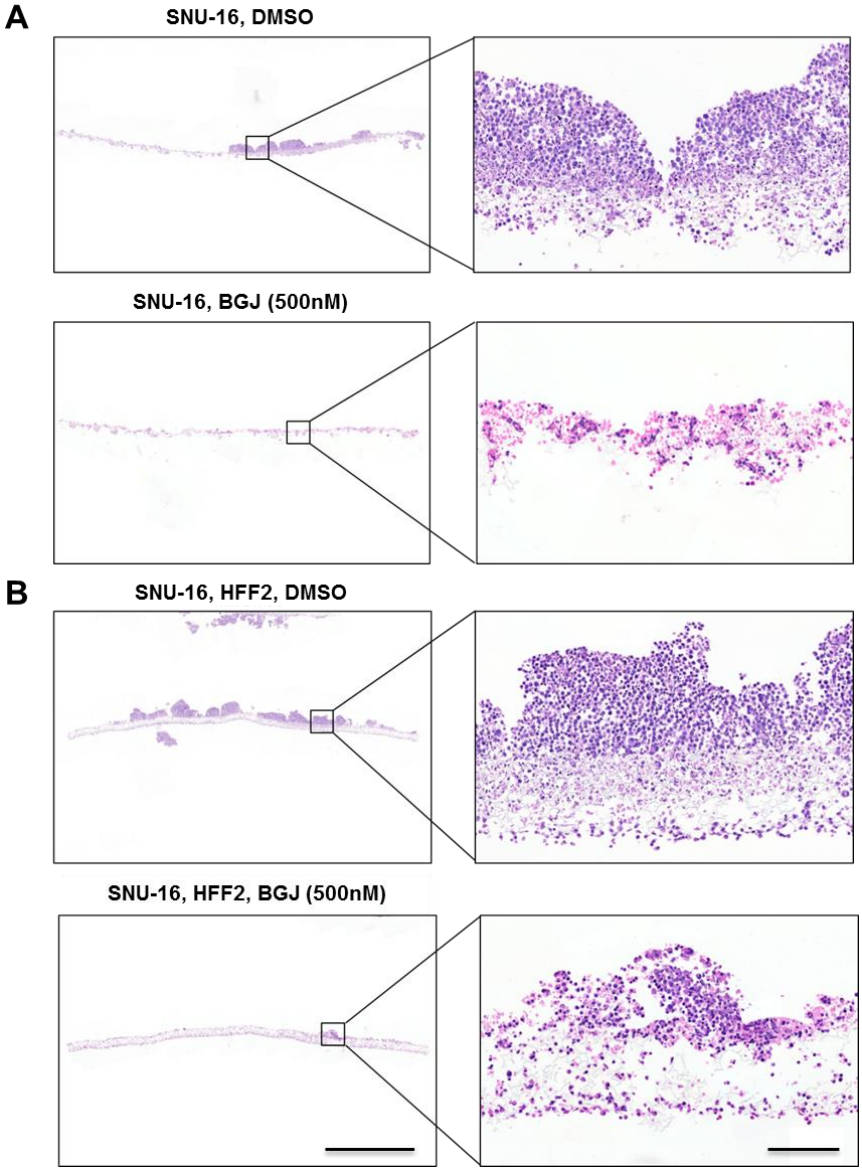

Figure 4.11. H&E images of parental SNU-16 cells and co-culture cells grown in Alvetex®.
(A) H&E staining of SNU-16 cells in Alvetex® treated with DMSO or BGJ. Once cell density was reached (four weeks for DMSO-treated and 8 weeks for BGJ-treated cells), scaffolds were fixed in formalin, processed to paraffin and stained with H&E. **(B)** H&E staining of SNU-16 cells co-cultured with HFF2 cells in Alvetex®**.** Once cell density was reached (four weeks for both DMSO-treated and BGJ-treated cells), scaffolds were fixed in formalin, processed to paraffin and stained with H&E. The right panel shows the magnification of the scaffold. The scale bar in the left panel represents 1000µm. The scale bar in the right panel indicates 100µm.

4.4 Cluster profiles of gastric cancer cells are formed in respect to treatment and cell conditions

Thousands of genetic variants have been associated with cancer and disease-associated SNPs affect gene expression levels (Ciriello et al., 2013; Stranger et al., 2007). Changes in gene expression might be important in mechanisms for genetic variants to have an effect on the resulting phenotype. As RNA sequencing produces short cDNA sequences, rather than hybridisation intensities as with microarrays, it can also elucidate aspects of gene structures, including position of introns, exons, transcription start sites, and polyadenylation sites. Using RNA-Seq, it is possible to determine not only whether a treatment or condition affects overall RNA abundance but also whether it affects splicing patterns, transcription start site use, and many other aspects of RNA transcription and post-transcriptional processing. The RNA-Seq technique was first reported in 2008 (Lister et al., 2008; Mortazavi et al., 2008; Nagalakshmi et al., 2008). Of these, the best cited is Mortazavi et al. from the laboratory of Barbara Wold at Caltech. This article introduced the concept of Reads Per Kilobase of transcript per Million mapped reads (RPKM) as a measure of gene expression.

In order to compare FGFR inhibitor resistance in 3D, 12 samples were used for RNA-Seq; vehicle-treated SNU-16 cells, BGJ-resistant SNU-16 cells and the same for conditions with HFF2 cells in combination each in biological triplicate. After harvesting and purification of RNA from the scaffolds, the RNA integrity number (RIN) value was measured, where a value over 8 was achieved for all samples and therefore suitable to perform RNA-Seq. RNA-Seq was performed by the Barts and The London Genome Centre using the Illumina platform with NextSeq™ 500 High Output Run (150 cycles) with a read length of 75 base pairs (bp) and required 20M reads per sample with paired end sequencing, which increases the mapping efficiency. As an input, 100ng RNA was used and paired fastq files were generated using the CASAVA software (Illumina), followed by quality control. RNA-Seq reads in the FASTA output were mapped to the human genome (hg38) HTSeq and 60-70% of reads aligned uniquely to the hg38 feature **(Appendix Table 8.1)**. Differential expression analysis was then performed using Limma. The p values were further

adjusted using the Benjamini and Hochberg procedure (Glueck et al., 2008), which was performed with R studio using Bioconductor, with the bioinformatics department performing the initial analysis. In order to identify significantly regulated genes, a fold change criteria of |LogFC|>2 with an adjusted p-value <0.05 was applied.

Table 4.1. Conditions used for differential gene expression analysis.

Name	Description
SNU-16d	DMSO-treated SNU-16 cells
SNU-16b	BGJ-treated SNU-16 cells
FIBROd	DMSO-treated co-culture cells
FIBROb	BGJ-treated co-culture cells

The aim was then to compare differentially expressed genes in SNU-16b, resistant to BGJ (SNU-16^{BGJR}) with SNU-16d (SNU16 parental cell line) treated with DMSO and FIBROb, co-culture cells consisting of SNU-16 cells and HFF2 cells resistant to BGJ (Co-culture^{BGJR}) *versus* FIBROd, which are co-culture cells treated with vehicle.

After transcriptome analysis was performed as an initial sanity check, principal component analysis (PCA) was performed to evaluate variation and reveal strong patterns between datasets but also to check if sample classes cluster separately. It was developed for large data to tease out differences and relationships between samples and it extracts the fundamental structure of data without the need to build a model to represent it. Reduction of the number of variables into a smaller set of variables (principal components) eases interpretation of original data and allows detection of relationships. Therefore, PCA is essentially summarising variance (Black and Watanabe, 2011; David and Jacobs, 2014; Ma and Dai, 2011; Zhang and Castelló, 2017).

The PCA plot for the datasets described above encompasses all 12 samples **(Figure 4.12)**. All triplicates cluster closely, indicating the replicates have a highly similar signature. Since co-culture cells also contain HFF2 cells, PC1 is lower and the triplicates go in the same direction. The same is true for SNU-16 cells alone which have a higher PC1 value. Also in respect to treatment the replicates cluster closer to each other and BGJ-treated replicates have a lower PC2 value. Therefore, the replicates cluster according to their cell components and treatment. These results indicate that DMSO-treated SNU-16 cells and SNU-16 cells exposed to HFF2 cells are transcriptionally different from SNU-16 cells and SNU-16 cells exposed to HFF2 treated with BGJ. Importantly, adding a stromal component also separates transcription profiles both in DMSO and BGJ-treated cells.

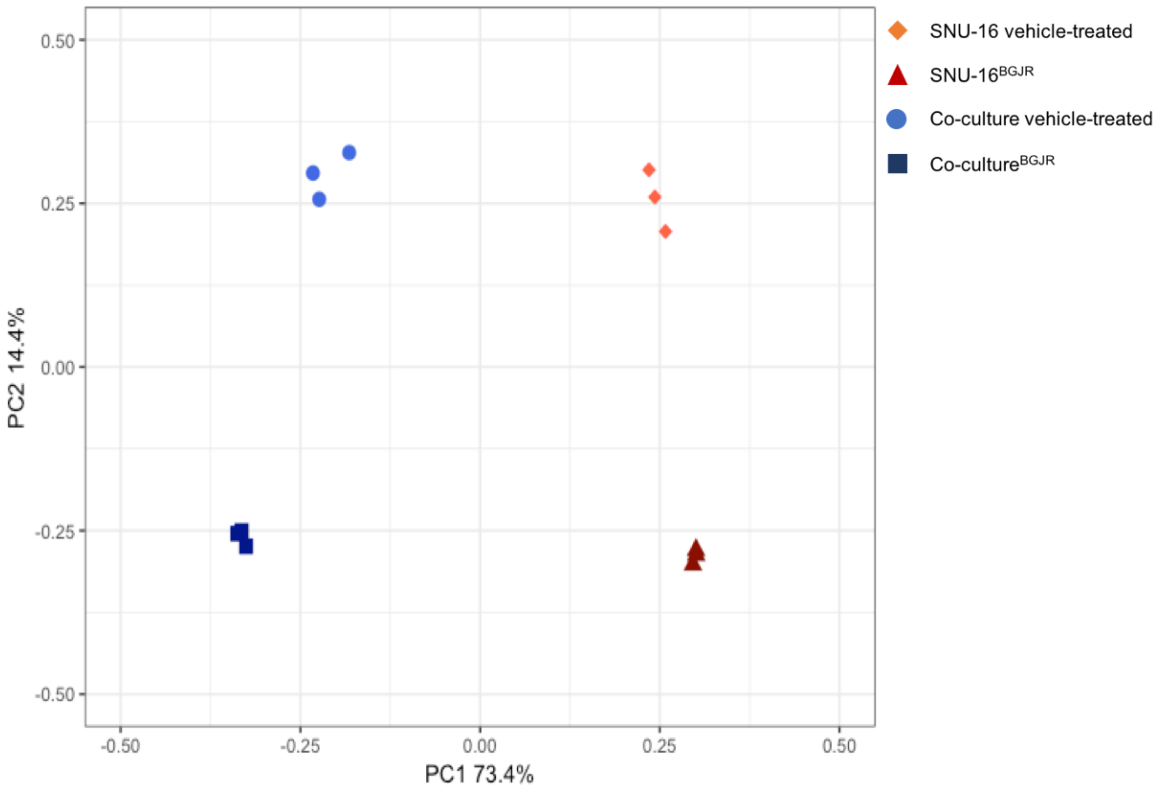

Figure 4.12. Gene expression profiles of SNU-16 and co-culture cells grown in Alvetex® cluster closely according to treatment and cell type.
Principal component analysis plot of SNU-16 cells (diamond) and SNU-16 cells with HFF2 (circle) treated with vehicle (DMSO) and BGJ-resistant SNU-16 cells alone (triangle) and co-cultured with HFF2 (square) in 3D Alvetex® model, showing the variation in the RNA sequencing data. Each shape of the same colour represents a biological triplicate and shows the degree of variance per conditions and replicate. Triplicates cluster together and different conditions cluster separately.

To help with further interpretation, a dendrogram was built showing the relationships between the different samples **(Figure 4.13)**. This plot shows a clustering dendrogram where samples that are most similar occupy closer positions in the tree (measured by height), while samples that are less similar are separated by larger numbers of branch points.

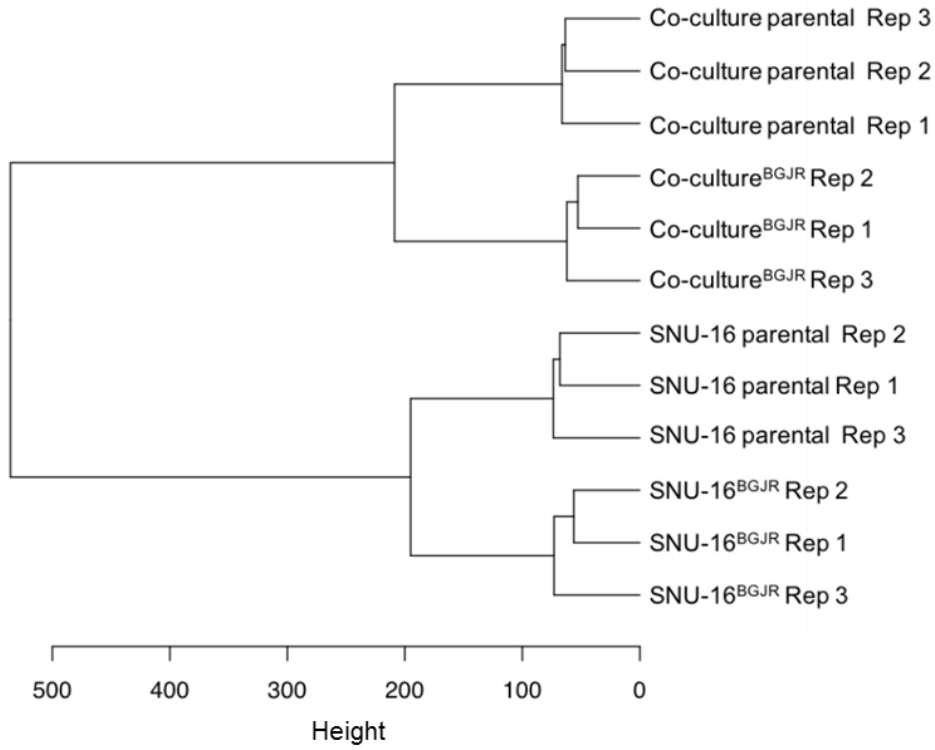

Figure 4.13. Gene expressions of cells cluster more closely according to their cell type than treatment.
The figure shows a cluster dendrogram showing the number of branches separating samples indicating the similarities between conditions. Treatment samples are named BGJR, control samples are named parental. It resulted in the clustering of two discrete clusters representing the distinct transcriptome signatures of the two cell type conditions. Within the two clusters, another two distinct clusters according to the treatments were generated.

A dendrogram merges the closest pair of classes and then further merges the next closest pair followed by the succeeding pair until all classes are merged. The distances between all pairs of classes are then updated after every merger and the distances at which the signatures of classes are merged are then used to construct a dendrogram. The distances at which each pair of classes is merged can then be interpolated using the scale bars of the dendrogram graph.

There are a vast number of tools available to analyse RNA-Seq data. Networks of genes can be generated and up and downstream effects investigated, together with diseases associated with the gene signatures in the datasets. Importantly, pathway analysis can give an idea which pathways are significantly up and downregulated and therefore represent a key pathway for the cancer cell.

Networks of the significantly regulated genes were generated using STRING and Cytoscape (with the ClueGo plugin) to generate gene interaction networks. Next, pathway analysis tools including Ingenuity pathway analysis (IPA), DAVID, KEGG pathways and GSEA were used and different approaches were applied to identify targetable regulated pathways and genes.

4.4.1 Expression analysis of SNU-16 cells alone

In total, 1588 genes were analysed. Of these, 603 genes were significantly regulated, from which 235 genes were upregulated in DMSO-treated SNU-16 cells and 368 genes were upregulated in SNU-16^{BGJR}.

First of all, gene interaction networks were generated using STRING **(Appendix Figure 8.32, Appendix Figure 8.33)** and cytoscape. Cytoscape is an open source software platform to help visualise complex molecular interaction networks with the incorporation of expression profiles and other data. To generate the interaction networks of all regulated genes in a dataset, the ClueGo plugin was used. The ClueGo plug-in visualises the non-redundant biological terms for large clusters of genes into a functionally grouped network **(Figure 4.14)**. With this the interconnected nature of this dataset was shown as a static image. However, the tool is interactive and was used to identify overlapping pathways and gene interactions that can be analysed using the software.

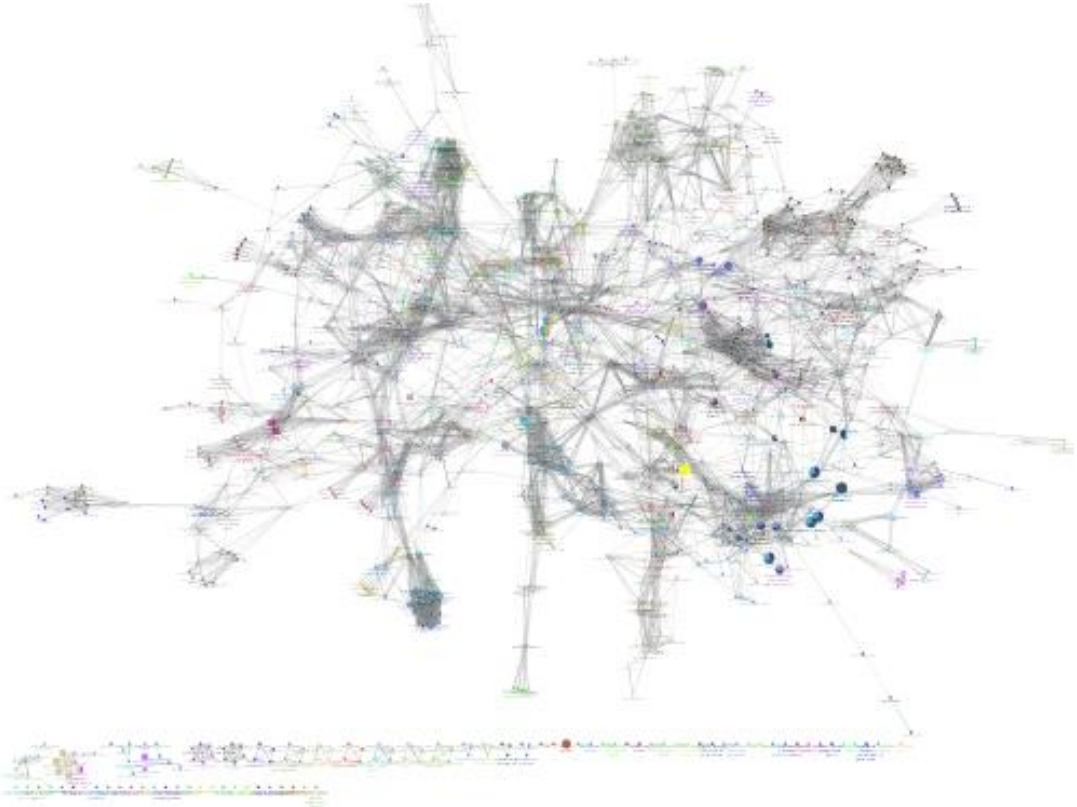

Figure 4.14. Regulated genes of gastric cancer cells form a network interaction diagram.
Interaction networks of gene expressions of gastric cancer cells made resistant to BGJ in Alvetex® were built using only genes that were significantly regulated (>2, <-2). Genes that did not form interaction networks with other significantly regulated genes were excluded.

The volcano scatter plot enables quick visual identification of those data points that display large magnitude changes that are also statistically significant **(Figure 4.15).**

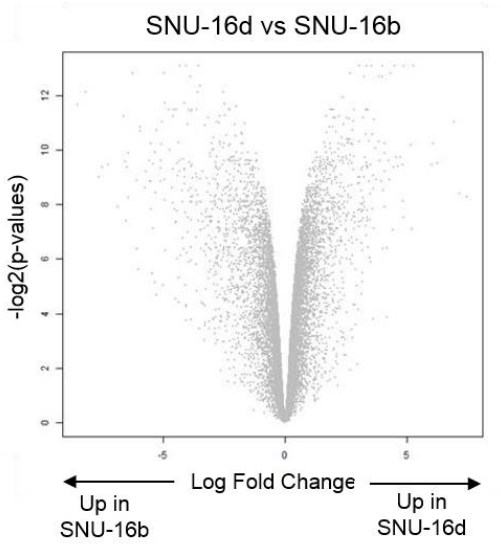

Figure 4.15. Volcano plot of SNU-16 vs SNU-16^{BGJR} cells.
The volcano scatter plot indicates significance *versus* fold-change on the y and x-axes.

The effect of the clustering is further supported by the depiction of gene expression patterns in a heat map of significantly regulated genes, which is a 2D representation of data, where values are represented by colours indicating genes that drive the observed clustering pattern **(Figure 4.16)**. Gene expression changes between biological replicates were similar, however distinct patterns were observed between drug-treated and vehicle-treated SNU-16 cells in 3D.

From the significantly regulated genes, the top 20 targets that were found to be up- and downregulated in SNU-16 cells, treated with DMSO over 8 weeks, were investigated in more detail **(Figure 4.17)**. An overview of the full names and functions of the top 5 candidates that are up and downregulated in BGJ-treated SNU-16 cells are listed in the Appendix **(Appendix Table 8.2, Appendix Table 8.3)**. Numerous significantly upregulated genes belong to sugar metabolism pathways with *sucrase-isomaltase (SI)* being upregulated the most, by over 8-fold. Other upregulated genes are commonly involved in cytotoxic metabolism. In the downregulated genes, *Piwi-like protein 1 (PIWIL1)* was downregulated by over 7-fold.

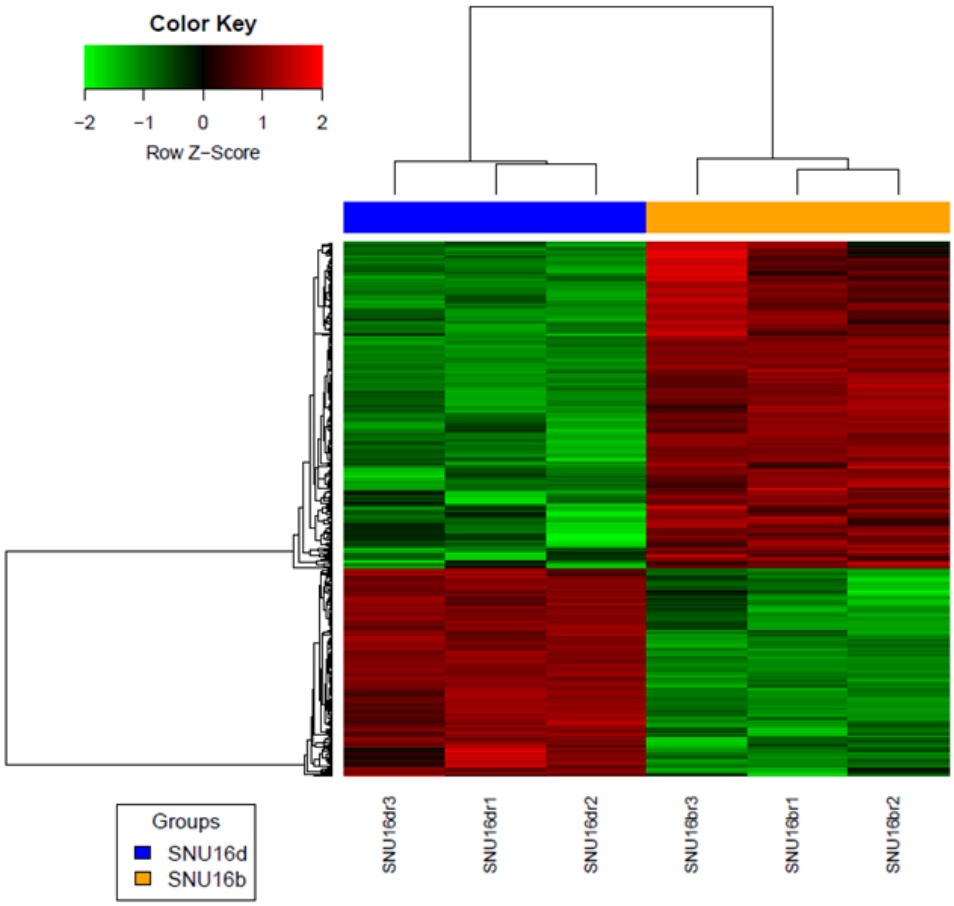

Figure 4.16. Heat map of SNU-16 cells *versus* SNU-16^{BGJR} cells in 3D.
The heat map shows all the significantly regulated genes between DMSO-treated (SNU-16d, blue) and BGJ-treated (SNU-16b, yellow) SNU-16 cells, explaining the variation seen in the PCA plot. Red genes indicate upregulation, while green indicates downregulation of genes. Each condition was sequenced in biological triplicate.

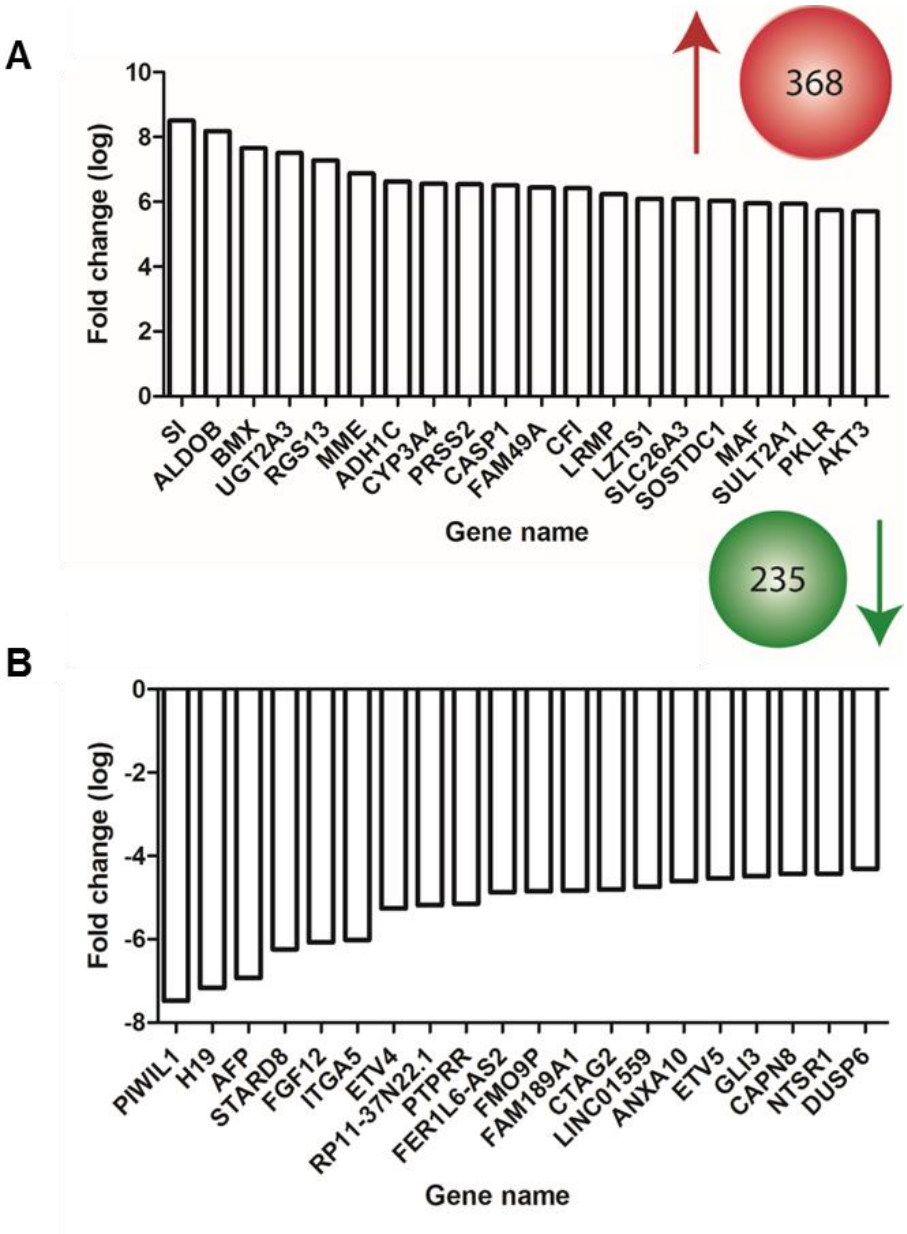

Figure 4.17. Top 20 up and downregulated genes in SNU-16^{BGJR} compared to parental SNU-16 cells. RNA was extracted from parental SNU-16 cells and SNU-16^{BGJR} grown in Alvetex® scaffolds. RNA sequencing showed in total 603 genes that were significantly altered. **(A)** 368 genes were significantly upregulated in SNU-16^{BGJR} cells compared to parental SNU-16 cell line (top panel). The 20 transcripts with the highest fold change relative to the parental cells are shown. **(B)** 235 genes were significantly downregulated compared to parental SNU-16 cell line (bottom panel). The 20 transcripts with the highest negative fold change relative to the parental cells are shown. Three technical and three biological replicates of each condition were run on the Illumina platform, followed by differential gene expression analysis by calculating the fold change between the resistant populations compared to the parental cells.

4.1.1 Expression analysis of co-culture cells

The same approach was also used with SNU-16 cells exposed to the influence of fibroblasts, and gene interaction networks were generated. In total, 1385 genes were analysed in co-culture cells. Among the 662 genes that were significantly regulated, 359 genes were upregulated in DMSO-treated co-culture cells (FIBROd) and 303 genes were upregulated in BGJ-treated co-culture cells (FIBRObj). The interaction network shows the connections and interactions of all significant genes in this dataset, excluding genes that did not form any interactions **(Figure 4.18)**. The volcano plot indicates scattering of genes, which is much narrower compared to the cancer cells alone **(Figure 4.19)**.

Figure 4.18. Regulated genes of gastric cancer cells co-cultured with stromal cells form a network interaction diagram.
Interaction networks of gene expressions of co-culture cells made resistant to BGJ in Alvetex® were built using only genes that were significantly regulated (>2, <-2). Genes that did not form interaction networks with other significantly regulated genes were excluded.

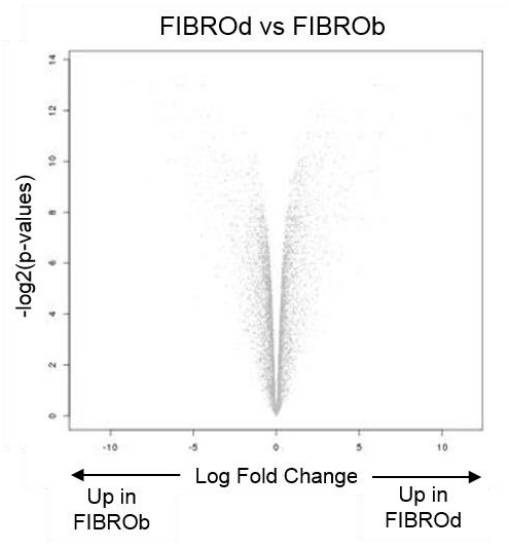

Figure 4.19. Volcano plot of co-culture cells.
The volcano scatter plot indicates significance *versus* fold-change on the y and x axes.

Again, the effect of the clustering is further supported by the depiction of gene expression patterns in a heat map of co-culture cells of significantly regulated genes **(Figure 4.20)**. Similarly, as in the cancer cells alone, expression profiles of biological replicates move in the same direction and also treatments cluster together and exhibit similar expression profiles. As for SNU-16 cells before, from the significantly regulated genes, the top 20 up- and downregulated genes were plotted in a graph with *regenerating islet-derived 1* (*REG1A*) and *REG1B* being the most upregulated genes by 12-fold and 10-fold respectively and *Alpha-fetoprotein* (*AFP*) was downregulated the most by 12-fold **(Figure 4.21)**. In the appendix, descriptions of the top 5 up- and downregulated genes and functions can be found in more detail **(Appendix Table 8.4, Appendix Table 8.5)**.

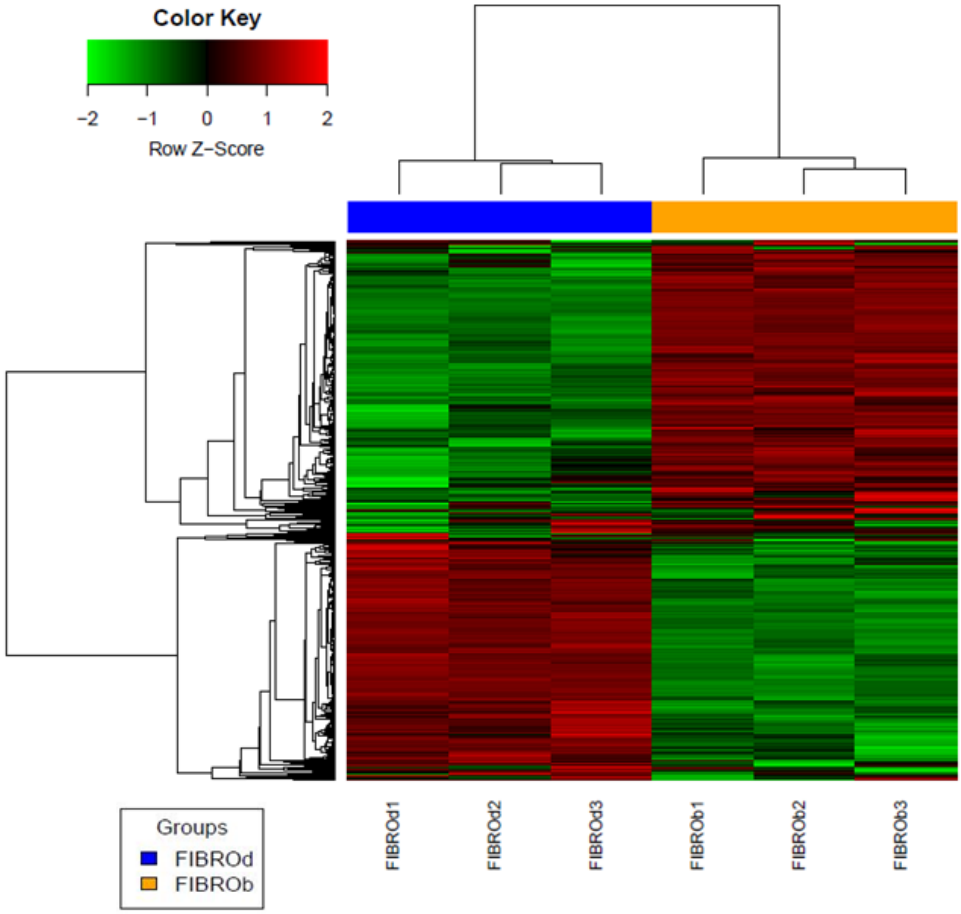

Figure 4.20. Heat map co-culture cells.
The heat map shows all the significantly regulated genes between DMSO-treated (FIBROd, blue) and BGJ-treated (FIBROb, yellow) co-culture cells, explaining the variation seen in the PCA plot. Red genes indicate upregulation, while green indicates downregulation of genes. Each condition was sequenced in biological triplicate.

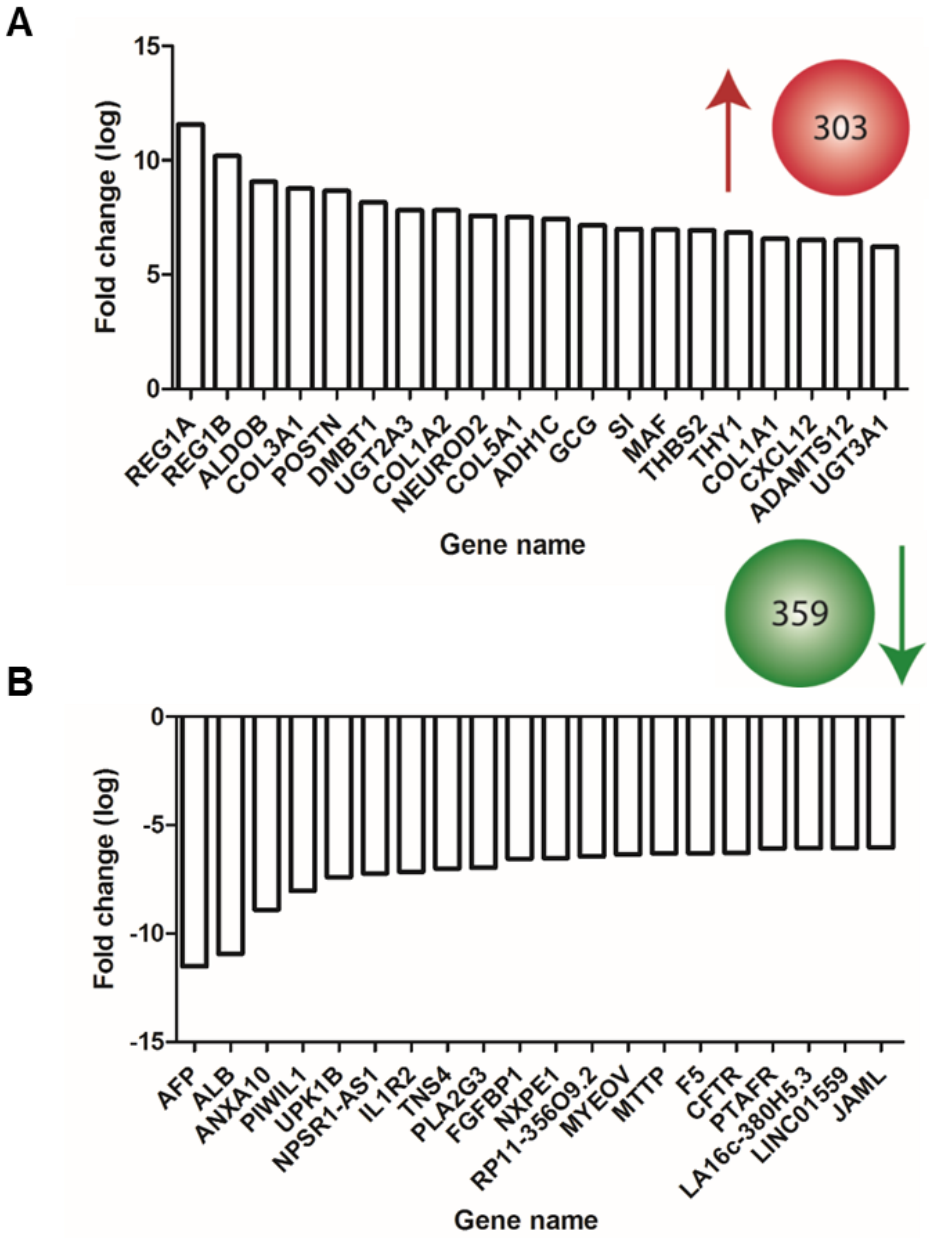

Figure 4.21. Top 20 up and downregulated genes in co-culture cells.
RNA was extracted from parental co-culture (SNU-16 and HFF2) cells and co-culture^{BGJR} grown in Alvetex® scaffolds. RNA sequencing showed in total, 662 genes that were significantly altered. **(A)** 303 genes were significantly upregulated in co-culture^{BGJR} cells compared to parental co-culture cells (top panel). The 20 transcripts with the highest fold change relative to the parental cells are shown. **(B)** 359 genes were significantly downregulated compared to parental co-culture cells. The 20 transcripts with the highest negative fold change relative to the parental cells are shown. Three technical and three biological replicates of each condition were run on the Illumina platform, followed by differential gene expression analysis by calculating the fold change between the resistant populations compared to the parental cells.

To compare up and downregulated genes between monoculture and co-culture conditions, Venn diagrams were generated, comparing common genes between SNU-16 cells and SNU-16 cells with HFF2 cells in the upregulated **(A)** and downregulated datasets **(B)**. 100 genes were found to be upregulated in both SNU-16 cells alone and co-culture cells, whereas 80 genes were downregulated in the two datasets **(Figure 4.22)**.

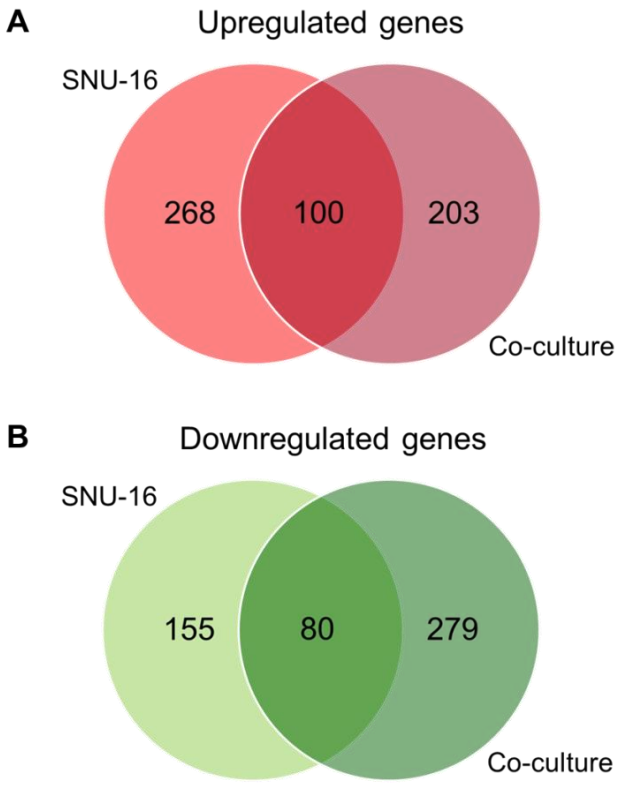

Figure 4.22. Monoculture and co-culture conditions show similarities in gene regulation.
Significantly regulated genes of SNU-16 and co-culture cells were compared to each other and Venn diagrams of shared and distinct genes were generated. **(A)** Common upregulated genes comparing SNU-16 and co-culture cells. **(B)** Common downregulated genes comparing SNU-16 and co-culture cells.

In addition to comparing co-culture cells and monoculture to their vehicle controls, conditions were also compared to each other so that, when comparing DMSO treated SNU-16 cells to DMSO-treated co-culture cells 2480 were regulated in total, 1591 genes were upregulated in DMSO-treated SNU-16 cells and 1385 genes were upregulated in DMSO-treated co-culture cells. In FGFR inhibitor treated cells, 3413 genes were regulated, among which 2028 genes were upregulated in SNU-16^{BGJR} cells.

Additonally, heat maps of up and downregulated genes of comparisons between DMSO-treated SNU-16 and co-culture and also BGJ-treated SNU-16 and co-culture cells were generated **(Appendix Figure 8.34, Appendix Figure 8.35).** Furthermore, all four datasets were compared to each other, identifying common genes that were shared between all datasets generated from differential gene expression analysis **(Appendix Figure 8.36).**

4.5 Drug-resistance in gastric cancer is potentially driven by metabolic processes

Gene products do not work alone, but rather in an intricate network of interactions, making it essential to study gene networks. When analysing RNA-Seq data, a fundamental aspect of the analysis is to investigate groups of genes that are functionally meaningful. A response is shown by the enrichment of association of genes within the gene set to experimental condition or sample.

First of all, the node is identified, which represents a list of genes and therefore a one-dimensional representation of the data. A pathway is then a linked list of interconnected nodes and as such a two-dimensional representation of the data. As a next step a network can be built which then represents interconnected pathways and gives information about cellular function and regulatory processes and therefore reveals a multi-dimensional representation. This is useful to determine if the differentially expressed genes are associated with a certain biological process or molecular function.

Network analysis shows key components of different pathways and how they interact with one another. This can be useful for identifying regulatory events that influence multiple biological processes and pathways (Curtis et al., 2005; Werner, 2008). Therefore, pathway analysis forms the bridge to the future and will help to fully understand the molecular basis of diseases such as cancer and the emergence of drug resistance. To date, there is limited software available to analyse RNA-Seq data. However, there are a vast number of methods to analyse microarray data which can be well applied to analyse RNA-Seq data.

Initially, datasets were analysed using the DAVID tool, which condenses a list of genes or associated biological terms into organised classes of related genes or biology, called biological modules. This organization is accomplished by mining the complex biological co-occurrences found in multiple sources of functional annotation. It is a powerful method to group functionally related genes and terms into a manageable number of biological modules for efficient interpretation of gene lists in a network context (Dennis et al., 2003; Huang et al., 2009a, 2009b).

DAVID bioinformatics resources consist of an integrated biological knowledge base and analytics tools aimed at systematically extracting biological meaning from large gene/protein lists. The procedure first requires uploading a gene list containing any number of common gene identifiers followed by analysis using one or more text and pathway-mining tools such as gene functional classification, functional annotation chart or clustering and functional annotation table. With this, it is possible to gain an in-depth understanding of the biological themes in lists of genes that are enriched in genome-scale studies.

Table 4.2 Significantly regulated pathways using KEGG in DAVID.
Only significantly regulated genes (threshold=2, -2) were included of SNU-16 **(A)** and co-culture **(B)** cells. Significant pathways are indicated by p<0.05. Pathways of particular interest are highlighted in red.

A

Pathway name	Genes	p-value
Retinol pathway	11 (1.9%)	<0.001
Drug metabolism	11 (1.9%)	<0.001
Protein digestion and absorption	11 (1.9%)	0.001
Metabolism of xenobiotics (cytochrome P450)	10 (1.8%)	0.001
Alpha-Linolenic acid metabolism	6 (1.1%)	0.002
Hematopoietic cell lineage	10 (1.8%)	0.002
Linoleic acid metabolism	6 (1.1%)	0.003
Cell adhesion molecules	13 (2.3%)	0.004
Drug metabolism – other enzymes	7 (1.2%)	0.005
Chemical carcinogenesis	9 (1.6%)	0.007

B

Pathway name	Genes	p-value
Retinol pathway	12 (2.0%)	<0.001
Chemical carcinogenesis	11 (1.9%)	0.011
Metabolism of xenobiotics (cytochrome P450)	10 (1.7%)	0.021
ECM-receptor interaction	10 (1.7%)	0.096
Drug metabolism (cytochrome P450)	8 (1.4%)	0.004
Protein digestion and absorption	9 (1.5%)	0.004
Staphylococcus aureus infection	7 (1.2%)	0.005
Steroid hormone biosynthesis	7 (1.2%)	0.007
Arachidonic acid metabolism	7 (1.2%)	0.009
Pathways in cancer	21 (3.6%)	0.11

Retinol pathway

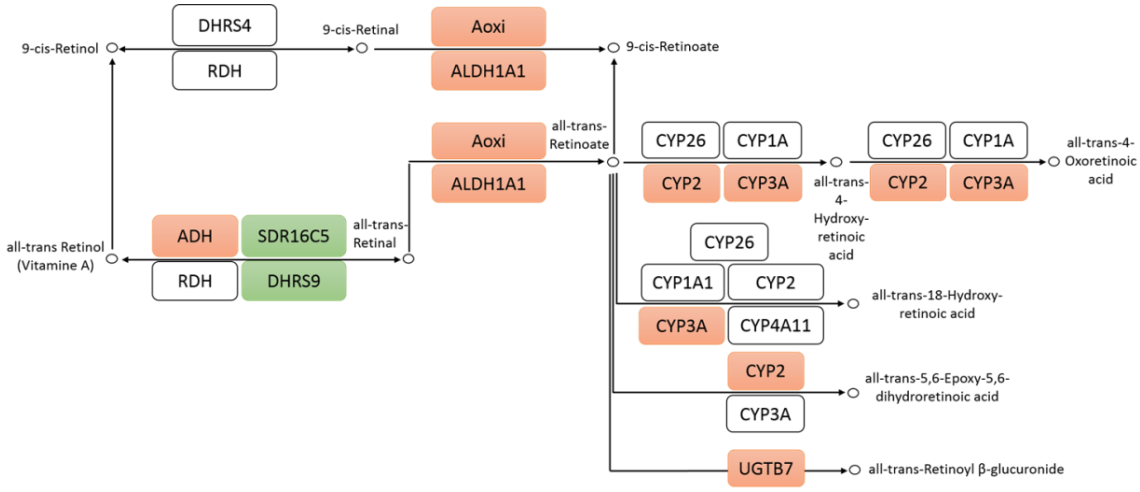

Figure 4.23. The retinol pathway is significantly upregulated in drug-resistant gastric cancer cells. Upregulated genes are highlighted in red and downregulated genes are indicated in green.

4.5.1 BGJ-resistant SNU-16 cells undergo metabolic changes and switch energy metabolism

Expression profiles were analysed using GSEA to detect altered pathways and results were cross-referenced with genes in the KEGG database to determine the signalling pathways responsible for the differential clustering observed in PCA. Using the normalised enrichment scores (NES), significantly regulated pathways were grouped into functional classes. In total, 14 pathways were upregulated (FDR<0.05) in SNU-16^{BGJR} cells, with 57% of the significantly upregulated pathways belonging to the metabolic category, 22% categorising to genetic information processing and each 7% into organismal systems, environmental information processing and human diseases **(Figure 4.24A)**. In contrast, among the downregulated pathways, 12 pathways were significantly downregulated of which 33% categorise to human diseases, 25% to metabolic pathways, 17% to both genetic and environmental information processing and 8% to cellular processes **(Figure 4.24B)**.

The most upregulated pathways in the metabolic processes were drug (NES=3.042, FDR<0.001) and xenobiotic (NES=2.786, FDR<0.001) metabolism by cytochrome P450. Furthermore, amongst the metabolic pathways, retinol (NES=2.425, FDR<0.006), steroid hormone (NES=2.122, FDR<0.028), starch and sucrose (NES=2.092,

FDR<0.029), drug metabolism by other enzymes (NES=2.060, FDR<0.033), glutathione (NES=2.053, FDR<0.032) and fatty acid metabolism (NES=1.977, FDR<0.045) were upregulated significantly. 22% of upregulated pathways fall into the category of information processing, with the ribosome pathway as the most upregulated (NES=2.954, FDR<0.001), followed by graft *versus* host disease (NES=2.324, FDR<0.011) and maturity onset diabetes of the young (NES=2.263, FDR<0.015). Other pathways that were upregulated included the Renin angiotensin system (NES=2.577, FDR<0.001) of the organismal systems, which has been implicated in the development or invasion of several kinds of cancer tissue (Wegman-Ostrosky et al., 2015). In environmental information processes, cell adhesion molecules (CAMs) (NES=2.193, FDR<0.019), and autoimmune thyroid disease in human diseases (NES=2.100, FDR<0.030) were significantly upregulated **(Table 4.3A)**.

Among the human diseases in the downregulated pathways, the arrhythmogenic right ventricular cardiomyopathy (ARVC) pathway was downregulated the most (NES=-2.614, FDR<0.006), followed by hypertrophic cardiomyopathy (NES=-2.459, FDR<0.004), dilated cardiomyopathy (NES=-2.301, FDR<0.009) and Huntington's disease (NES=-2.037, FDR<0.033). In the metabolic pathways, steroid biosynthesis (NES=-2.369, FDR<0.009), biosynthesis of unsaturated fatty acids (NES=-2.368, FDR<0.007) and oxidative phosphorylation (NES=-2.331, FDR<0.009) were downregulated significantly. Oxidative phosphorylation is involved in the generation of energy in the form of adenosine triphosphate (ATP), which takes place in the mitochondria. This pathway is used by all aerobic organisms and is highly efficient, however mitochondria consume cellular oxygen, releasing reactive oxygen species as a by-product (Solaini and Harris, 2005), which have been implicated in cancers by inducing oxidative damage. ROS are needed by cancer cells to grow due to their accelerated growth, however this can also induce death in cancer cells (Denko, 2008; Nogueira et al., 2008) and therefore cancer cells have been found to switch to other energy sources such as glycolysis. Cancer cells take up glucose for aerobic glycolysis, which is an inefficient method for energy production and is referred to as the Warburg effect (Warburg, 1956). However, cancer cells use the catabolism of glucose to produce pyruvate or lactate in the cytoplasm and use this as fuel. Cancer

cells can therefore adapt to environmental changes and have a selective advantage under unfavourable conditions (Chen et al., 2008; Marusyk and Polyak, 2010). In genetic information processing, the proteasome pathway (NES=-1.984, FDR<0.039) was further downregulated and in environmental information processing, cytokine-cytokine receptor interaction (NES=-2.087, FDR<0.031) and the calcium signalling pathway (NES=-1.934, FDR<0.050) were significantly decreased **(Table 4.3B)**.

Based on extensive literature research and the outcomes of the GSEA analysis, the top up and downregulated pathways were investigated more closely and enrichment profiles were generated and upregulated genes responsible for the enrichment of these pathways were crosschecked with the genes in the dataset **(Figure 4.25, Figure 4.26)**.

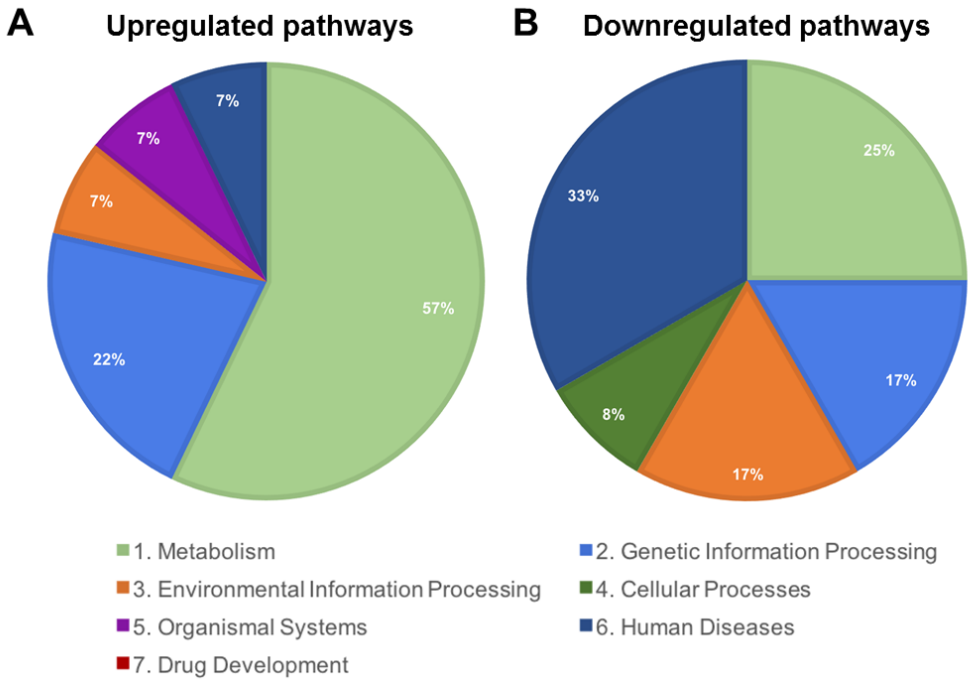

Figure 4.24. Categorisation of enriched pathways according to KEGG in SNU-16^{BGJR} cells compared to parental cells.
Pie charts indicate the percentages of all upregulated **(A)** and downregulated **(B)** pathways of SNU-16 cells^{BGJR} cells compared to parental SNU-16 cells in 3D. Expression profiles were analysed using NES from GSEA linked to the KEGG pathway database. NES: normalised enrichment score.

Table 4.3. Significantly regulated pathways according to KEGG.
GSEA identified multiple enriched pathways based on the KEGG gene set. **(A)** Significantly most upregulated and **(B)** downregulated pathways. FDR-value<0.05. Pathways of particular interest are highlighted in red.

A

Upregulated pathways	NES	*FDR* value
Cytochrome P450 (drug)	3.042	<0.001
Ribosome	2.954	<0.001
Cytochrome P450 (xenobiotics)	2.786	<0.001
Renin angiotensin system	2.577	0.001
Retinol metabolism	2.425	0.006
Graft versus Host disease	2.324	0.011
Maturity onset Diabetes of the young	2.262	0.013
Cell adhesion molecules (CAMS)	2.193	0.019
Steroid hormone biosynthesis	2.122	0.028
Autoimmune thyroid disease	2.100	0.030
Starch and sucrose metabolism	2.092	0.029
Drug metabolism other enzymes	2.060	0.033
Glutathione metabolism	2.053	0.032
Fatty acid metabolism	1.977	0.045

B

Downregulated pathways	NES	*FDR* value
Arrhythmogenic right ventricular cardiomyopathy (ARVC)	-2.614	0.006
Spliceosome	-2.614	0.003
Hypertrophic cardiomyopathy (HCM)	-2.459	0.004
Steroid biosynthesis	-2.369	0.009
Biosynthesis of unsaturated fatty acids	-2.368	0.007
Oxidative phosphorylation	-2.332	0.009
Dilated Cardiomyopathy	-2.301	0.009
Cytokine receptor interaction	-2.087	0.031
Focal adhesion	-2.044	0.035
Huntington's Disease	-2.037	0.033
Proteasome	-1.984	0.039
Calcium signalling pathway	-1.934	0.050

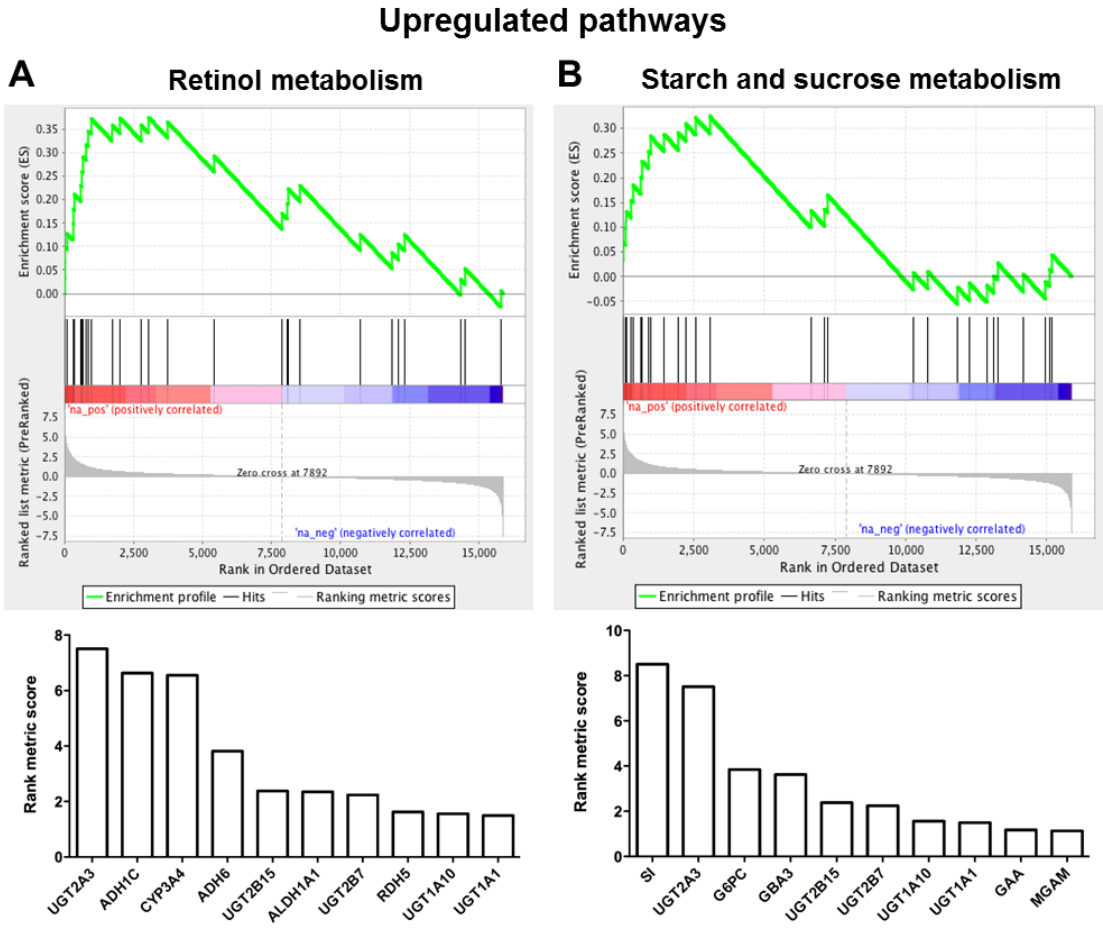

Figure 4.25. GSEA expression profiles of significantly upregulated pathways in SNU-16^{BGJR} cells.
Enrichment plots of upregulated pathways from the comparison between SNU-16 and SNU-16^{BGJR} cells using KEGG. SNU-16^{BGJR} cells were positively enriched for the retinol pathway **(A)** and starch and sucrose metabolism **(B).** Vertical lines indicate the positions of the genes along the comparison for each gene set. Cut-off *FDR* value<0.05. Genes involved in enrichment of retinol pathway and starch and sucrose pathway are shown below the graphs with respective fold changes **(Table 4.4)**.

Table 4.4. Significant genes driving upregulated pathways in SNU-16^{BGJR} cells.

A

Description	Log FC
UDP glucuronosyltransferase 2 family, polypeptide A3 (UGT2A3)	7.508
Alcohol dehydrogenase 1C (class I), gamma polypeptide (ADH1C)	6.631
Cytochrome P450 family 3 subfamily A member 4 (CYP3A4)	6.555
UDP glucuronosyltransferase 2 family, polypeptide B15 (UGT2B15)	2.379
Aldehyde dehydrogenase 1 family member A1 (ALDH1A1)	2.351
UDP glucuronosyltransferase 2 family, polypeptide B7 (UGT2B7)	2.238

B

Description	Log FC
Sucrase-isomaltase (SI)	8.506
UDP glucuronosyltransferase 2 family, polypeptide A3 (UGT2A3)	7.508
Glucose-6-phosphatase (G6PC)	3.843
Glucosidase, beta, acid 3 (GBA3)	3.621
UDP glucuronosyltransferase 2 family, polypeptide B15 (UGT2B15)	2.378
UDP glucuronosyltransferase 2 family, polypeptide B7 (UGT2B7)	2.238

As glucose and sucrose metabolism seems to play an important role in drug resistance, the starch and sucrose metabolism raised interest, which has been among the significantly regulated pathways in the dataset. When crosschecking back to the individual gene expression levels, *SI* and *UGT2A3* were the top two genes involved in the pathway.

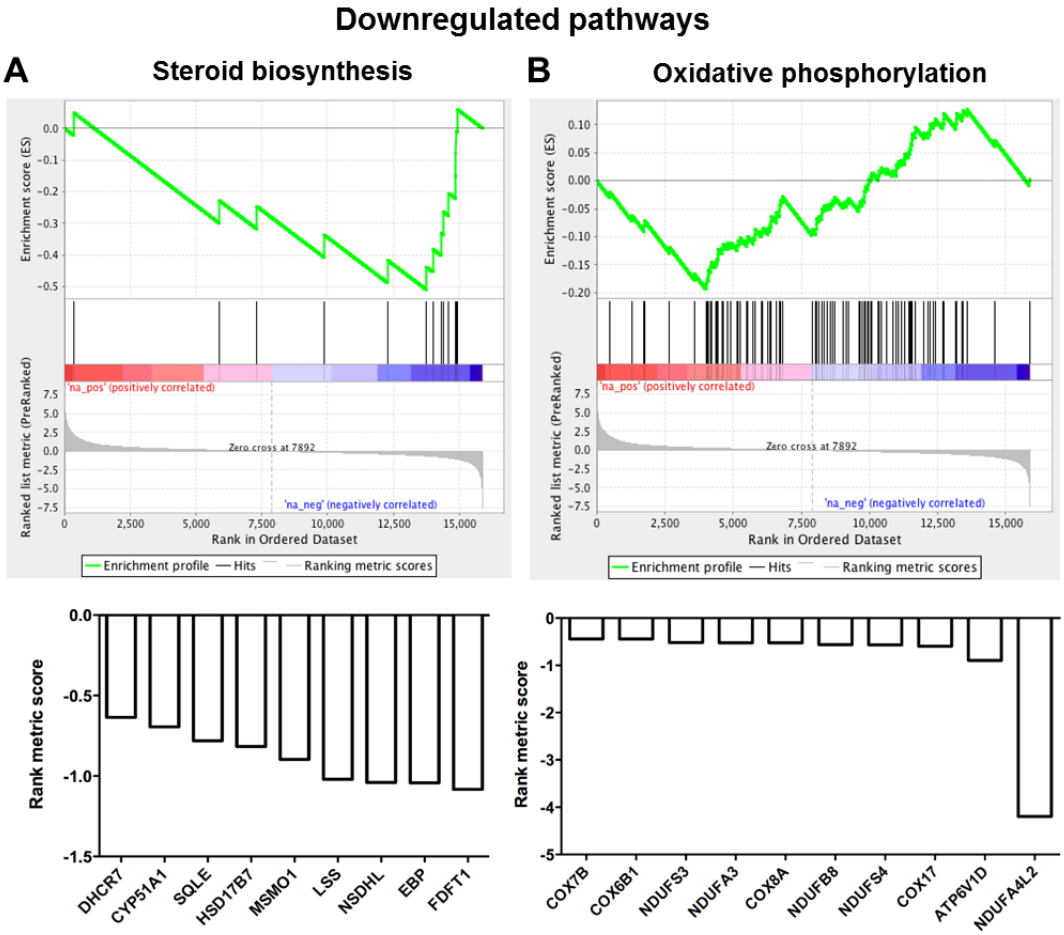

Figure 4.26. GSEA expression profiles of significantly downregulated pathways in SNU-16^{BGJR} cells. Enrichment plots of downregulated pathways from the comparison between SNU-16 and SNU-16^{BGJR} cells using KEGG. SNU-16^{BGJR} cells were negatively enriched for the steroid biosynthesis **(A)** and oxidative phosphorylation **(B).** Vertical lines indicate the positions of the genes along the comparison for each gene set. Cut-off *FDR* value<0.05. Genes involved in enrichment of retinol pathway and starch and sucrose pathway are shown below the graphs.

In the oxidative phosphorylation pathway, the only significantly downregulated genes was *NADH dehydrogenase (ubiquinone) 1 alpha sub-complex, 4-like 2 (NDUFA4L2)* with a fold change of -4.192.

4.5.2 BGJ-resistant co-culture cells produce increased levels of ECM proteins

As for SNU-16 cells, regulated pathways comparing DMSO-treated and BGJ-treated co-culture cells were grouped into functional classes using the KEGG database. In co-culture cells the majority of the upregulated pathways categorise into human diseases with 44%, followed by 19% organismal systems, 15% environmental processes, each 11% metabolic and cellular processes **(Figure 4.27A)**. Among the downregulated genes 67% categorise into metabolic pathways, 18% in genetic information processing and 11% and 4% in human diseases and organismal systems respectively **(Figure 4.27B)**.

Among the upregulated pathways the ECM receptor interaction pathway (NES=3.644, FDR<0.001) was upregulated the most **(Table 4.5A, Figure 4.28A)**, which represents the interaction with the stromal component. As observed before with cancer cells alone, CAMs were upregulated significantly (NES=1.922, FDR<0.033). In contrast to cancer cells alone, among the downregulated pathways, the ribosome pathway was downregulated the most (NES=-4.031, FDR<0.001) **(Table 4.5B)**. However, similarly to SNU-16 cells alone, oxidative phosphorylation (NES=-3.424, FDR<0.001) and steroid biosynthesis (NES=-2.407, FDR<0.003) were downregulated. The ribosomal pathway was downregulated by the downregulation of ribosomal proteins (RPs) **(Figure 4.28B)**. Many RPs also fill several roles that are independent of protein biosynthesis, called extra-ribosomal functions (Vaarala et al., 1998). For example RPS29, which was one of the genes contributing to the enrichment of the ribosome pathway in the BGJ-resistant co-culture cells, has been found to be implicated with tumour suppressor activity (Coppock et al., 2000). In the case of oxidative phosphorylation, again as with cancer cells alone, a switch to other energy metabolisms such as glycolytic energy production could have occurred.

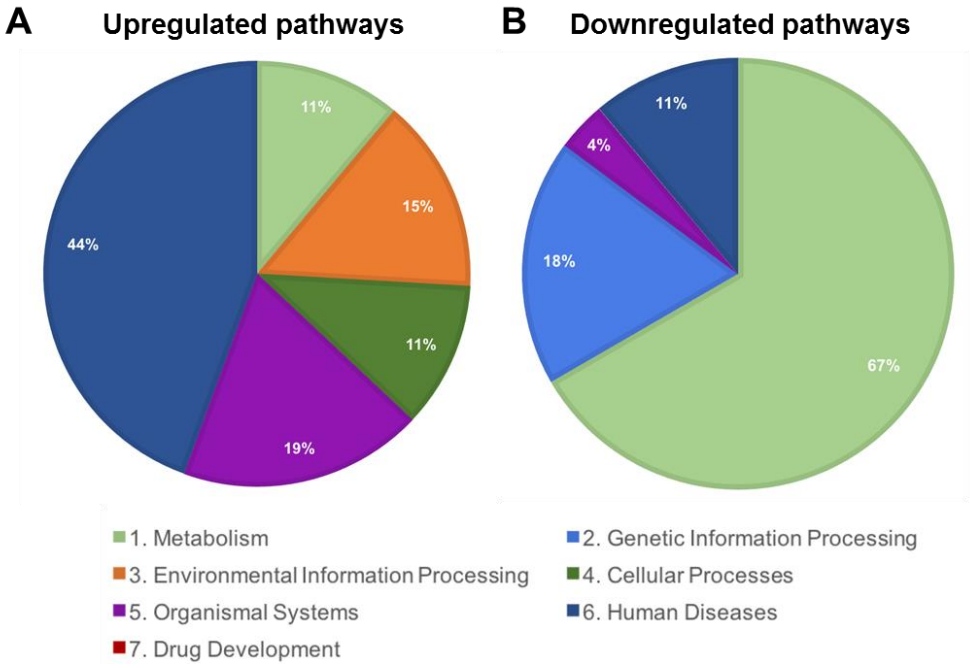

Figure 4.27. Categorisation of enriched pathways according to KEGG in co-culture^{BGJR} cells compared to parental cells.
Pie charts indicate the percentages of all upregulated **(A)** and downregulated **(B)** pathways of co-culture^{BGJR} cells compared to parental co-culture cells in 3D. Expression profiles were analysed using GSEA linked to the KEGG pathway database.

Table 4.5. Significant regulated pathways according to KEGG in co-culture cells.
Upregulated **(A)** and downregulated **(B)** pathways according to NES. Biologically interesting pathways based on literature search are highlighted in red.

A

Upregulated pathways	NES	*FDR* value
ECM receptor interaction	3.644	<0.001
Focal adhesion	3.075	<0.001
Lysosome	2.683	0.001
Neuroactive ligand receptor interaction	2.643	0.001
Arrhythmogenic right ventricular cardio myopathy (ARVC)	2.498	0.003
Glycosaminoglycan degradation	2.391	0.004
Regulation of actin cytoskeleton	2.376	0.004
Basal cell carcinoma	2.322	0.007
Intestinal immune network for IGA production	2.256	0.009
Toll like receptor signalling pathway	2.210	0.011
Glycosaminoglycan biosynthesis chondroitin sulphate	2.190	0.011
RIG I like receptor signalling pathway	2.185	0.011
Systemic lupus erythematosus	2.134	0.014
Viral myocarditis	2.068	0.020
Hypertrophic cardiomyopathy (HCM)	2.029	0.024
Graft versus host disease	2.009	0.025
Glycosphinogolipid biosynthesis ganglio series	1.982	0.027
Dilated cardiomyopathy	1.960	0.029
Asthma	1.948	0.030
Complement and coagulation cascades	1.945	0.029
Cell adhesion molecules (CAMs)	1.922	0.033
Allograft rejection	1.918	0.032
Colorectal cancer	1.918	0.031
Type I diabetes mellitus	1.865	0.040
Pathways in cancer	1.845	0.043
Hematopoietic cell lineage	1.838	0.043
Hedgehog signalling pathway	1.828	0.043

B

Downregulated pathways	NES	*FDR* value
Ribosome	-4.031	<0.001
Huntington's disease	-3.459	<0.001
Oxidative phosphorylation	-3.424	<0.001
Parkinson's disease	-3.414	<0.001
Citrate cycle, TCA cycle	-3.129	<0.001
RNA degradation	-3.059	<0.001
Alzheimer's disease	-3.047	<0.001
Glycerolipid Metabolism	-2.591	0.001
Valine, Leucine and Isoleucine degradation	-2.442	0.003
Arginine and proline metabolism	-2.411	0.003
Steroid biosynthesis	-2.407	0.003
Terpenoid backbone biosynthesis	-2.296	0.005
Spliceosome	-2.289	0.005
Metabolism of xenobiotics by cytochrome P450	-2.232	0.008
Arachidonic acid metabolism	-2.173	0.011
Butanoate metabolism	-2.164	0.010
Base excision repair	-2.153	0.010
Drug metabolism cytochrome P450	-2.069	0.017
Amino sugar and nucleotide sugar metabolism	-1.980	0.030
Pyrimidine metabolism	-1.980	0.028
Retinol metabolism	-1.964	0.030
Purine metabolism	-1.929	0.034
Phenylalanine metabolism	-1.923	0.034
Steroid hormone biosynthesis	-1.914	0.035
Aminoacyl TRNA biosynthesis	-1.900	0.037
Cardiac muscle contraction	-1.884	0.039
Mismatch repair	-1.864	0.042

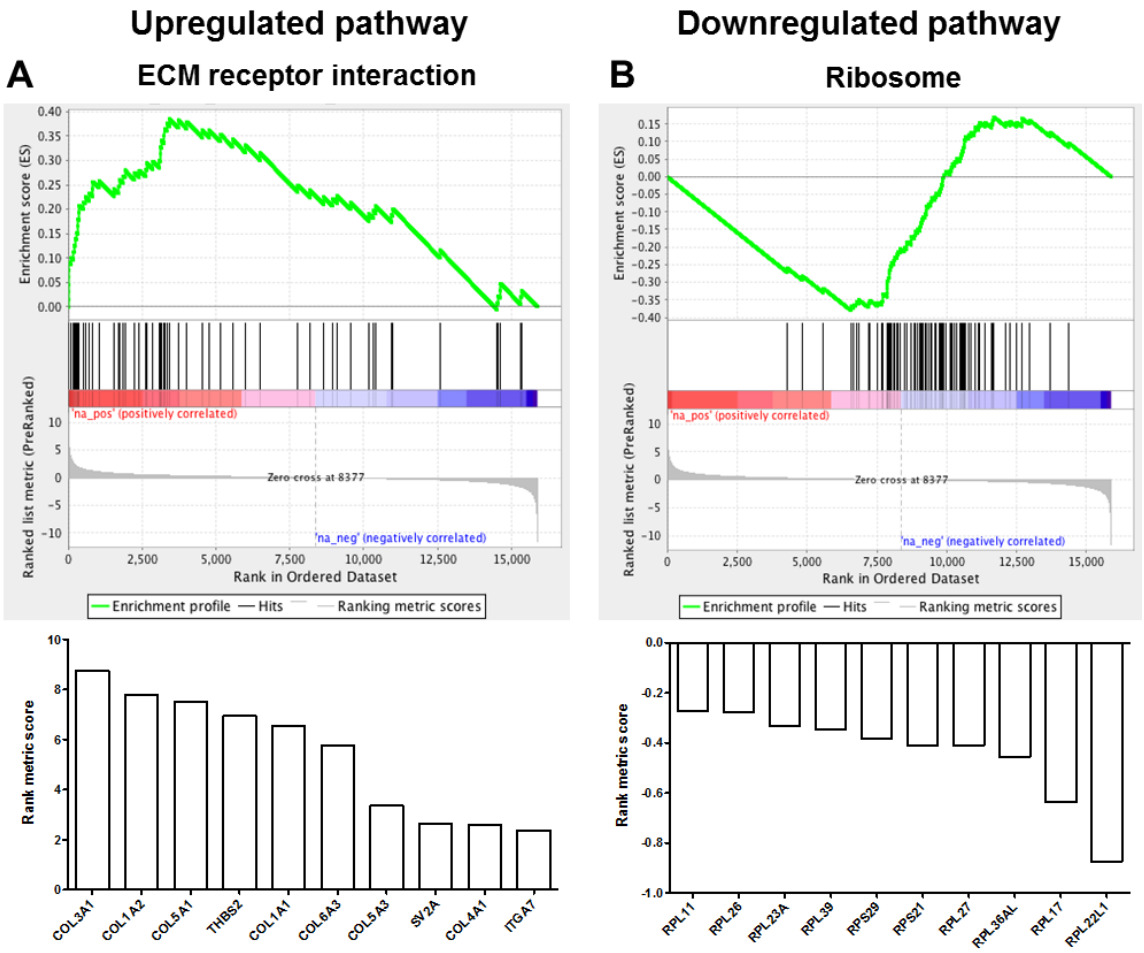

Figure 4.28. Up and downregulated pathways in co-culture cells.
Enrichment plots of downregulated pathways from the comparison between vehicle-treated and BGJ-treated co-culture cells using KEGG. Co-culture^{BGJR} cells were positively enriched for the ECM interaction pathway **(A)** and negatively enriched for the ribosome pathway **(B)**. Vertical lines indicate the positions of the genes along the comparison for each gene set. Cut-off *FDR* value<0.05. Genes involved in enrichment of the ECM interaction pathway are shown below the graphs **(Table 4.6)**. No significant genes were encountered in the ribosome pathway.

Table 4.6. ECM pathway upregulated genes in RNA sequencing data.

Description	Log FC
Collagen, type III, alpha 1 (COL3A1)	8.760
Collagen, type I, alpha 2 (COL1A2)	7.800
Collagen, type V, alpha 1 (COL5A1)	7.502
Thrombospondin 2 (THBS2)	6.937
Collagen, type I, alpha 1 (COL1A1)	6.567
Collagen, type VI, alpha 3 (COL6A3)	5.750
Collagen, type V, alpha 3 (COL5A3)	3.366
Synaptic vesicle glycoprotein 2A (SV2A)	2.649
Collagen, type IV, alpha 1 (OL4A1)	2.577
Integrin subunit alpha 7 (ITGA7)	2.385

Pathways of cancer cells alone and co-culture cells were compared and overlapping pathways were investigated. In the upregulated pathways, drug-resistant SNU-16 and co-culture cells shared 57 pathways and 46 in the downregulated pathways. In the common pathways sucrose and starch was upregulated indicating that sugar plays an important role in energy metabolism in both conditions. Among the downregulated pathways as described above, oxidative phosphorylation is downregulated in both conditions.

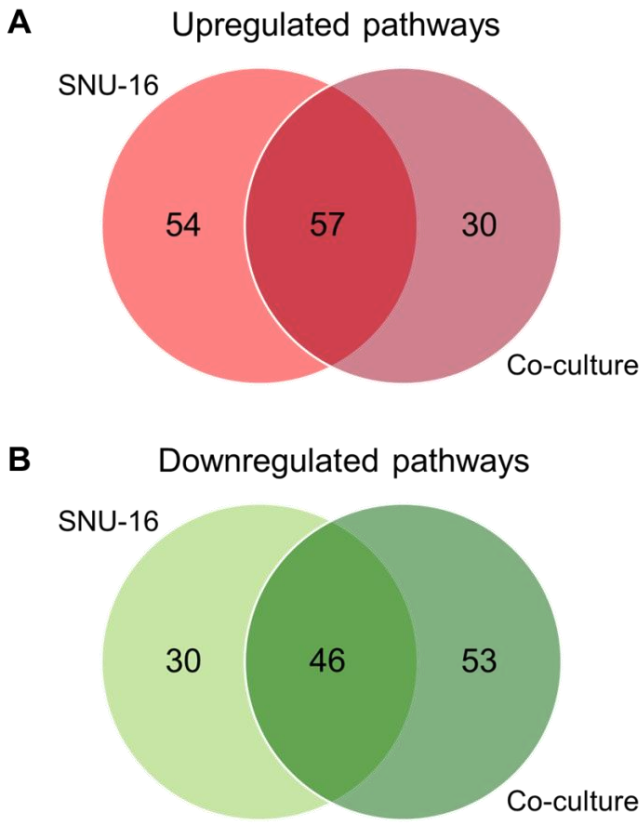

Figure 4.29. Upregulated and downregulated pathways of gastric cancer alone and in co-culture reveal a singifcant overlap.
Venn diagrams of common upregulated genes comparing SNU-16 and co-culture cells **(A)** and common downregulated genes comparing SNU-16 and Co-culture cells **(B)**.

Further analysis using ingenuity pathway analysis (IPA), allowed more specific analysis of interactions and regulation of the genes, spatial organisation **(Appendix Figure 8.37)**, pathways alterations and also comparisons of analysed datasets.

Pathways were also analysed with SPIA **(Appendix Figure 8.38)**, which is a Bioconductor package in R, however the main focus will be on IPA.

Initially, the FGF signalling pathway sparked interest, which revealed that pathways downstream of FGFR were upregulated in SNU-16^{BGJR} cells **(Figure 4.30)**. What particularly drives the pathway according to the IPA database is AKT signalling, resulting in cell survival and cAMP response element-binding protein (CREB) upregulation, which are transcription factors increasing transcription of genes that ultimately lead to cell differentiation, growth, morphogenesis and angiogenesis (Gubbay et al., 2006; Li et al., 2011). This could be induced by other RTKs such as MET activation through hepatocyte growth factor (HGF), which was upregulated in the SNU-16^{BGJR} dataset.

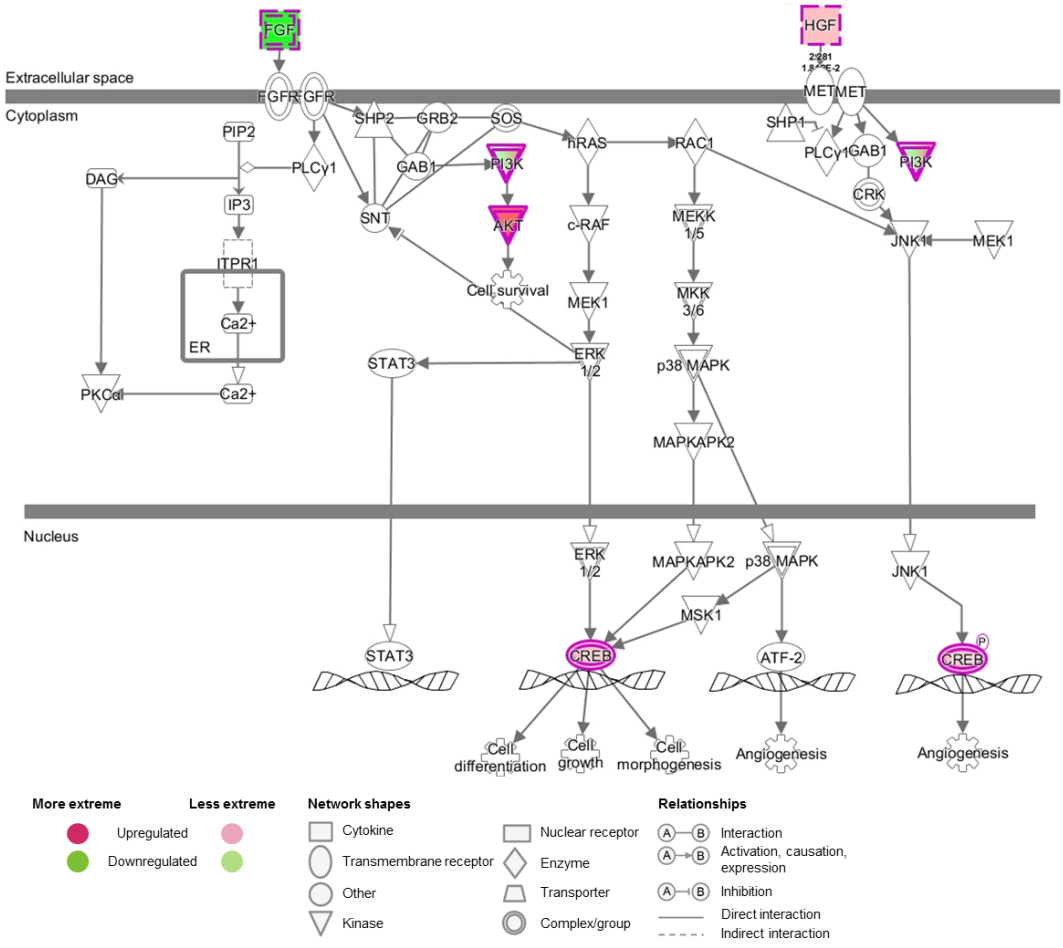

Figure 4.30. FGF signalling pathway in SNU-16^{BGJR} cells.
FGF signalling is downregulated in drug-resistant SNU-16 cells, whereas HGF is upregulated, which leads to activation of pathways downstream of FGF signalling and specifically upregulation of AKT and upregulation of CREB, ultimately activating transcription of genes involved in cell differentiation, growth, morphogenesis and angiogenesis.

CREB can be activated through phosphorylation of kinases, such as AKT, p90Rsk, protein kinase A, and calcium/calmodulin-dependent kinases (Sun et al., 1994). It is involved in the regulation of genes including *cyclins*, *Bcl-2* and *Egr-1*, which through aberrant expression induce oncogenesis. In a number of human cancers including acute myeloid leukaemia (AML) and non–small cell lung cancer, CREB was upregulated resulting in constitutive phosphorylation and malignant transformation of cells (Seo et al., 2008; Shankar et al., 2005).

The retinol pathway was particularly interesting in cancer cells alone as it was significantly upregulated in DAVID and GSEA using KEGG and was investigated using IPA **(Figure 4.31)**. In SNU-16^{BGJR} cells, cellular triacylglycerol lipase, retinol-binding protein, carboxylesterase and retinal dehydrogenase were upregulated, which are involved in retinol regulation and *all-trans* retinol and retinoate production. The main factor driving the pathway, however is the cellular retinol-binding protein (CRBP). It is an intracellular cytosolic protein, which transport and mediate metabolism and function of retinol, retinal and retinoic acid and belong to the fatty acid binding-protein gene family (Glatz and van der Vusse, 1996). CRBP are potentially involved in the transformation of retinol to retinoic acid by oxidation in target tissues and therefore regulation of retinoic acid in cells (Ghyselinck et al., 1999; Napoli, 1999). Two CRBPs are known, CRBP-1 and 2, with CRBP-1 playing and vital role in the uptake of retinol followed by esterification and therefore enhancing bioavailability and transcriptional activity. Furthermore, CRBP-1 has been associated with embryonic development, growth, vision and survival of vertebrates (Dirami et al., 2004; Doldo et al., 2015). Further, a correlation between loss of CRBP-1 and breast cancer development was found, and CRBP was identified as a suppressor of anchorage-independent growth (Kuppumbatti et al., 2001). Additionally to loss of CRBP-1 in breast cancer, CRBP-1 downregulation has been encountered in endometrial, ovarian and prostate cancer and was associated with increased malignancy (Jerónimo et al., 2004; Kuppumbatti et al., 2000; Orlandi et al., 2006; Roberts et al., 2002). Whereas in in lung adenocarcinoma and laryngeal cancer, CRBP-1 was upregulated and was associated with poor prognosis (Chen et al., 2018; Doldo

et al., 2015; Peralta et al., 2010). Similarly, upregulation of CRBP in drug-resistant gastric cancer cells could signify a more aggressive cancer type.

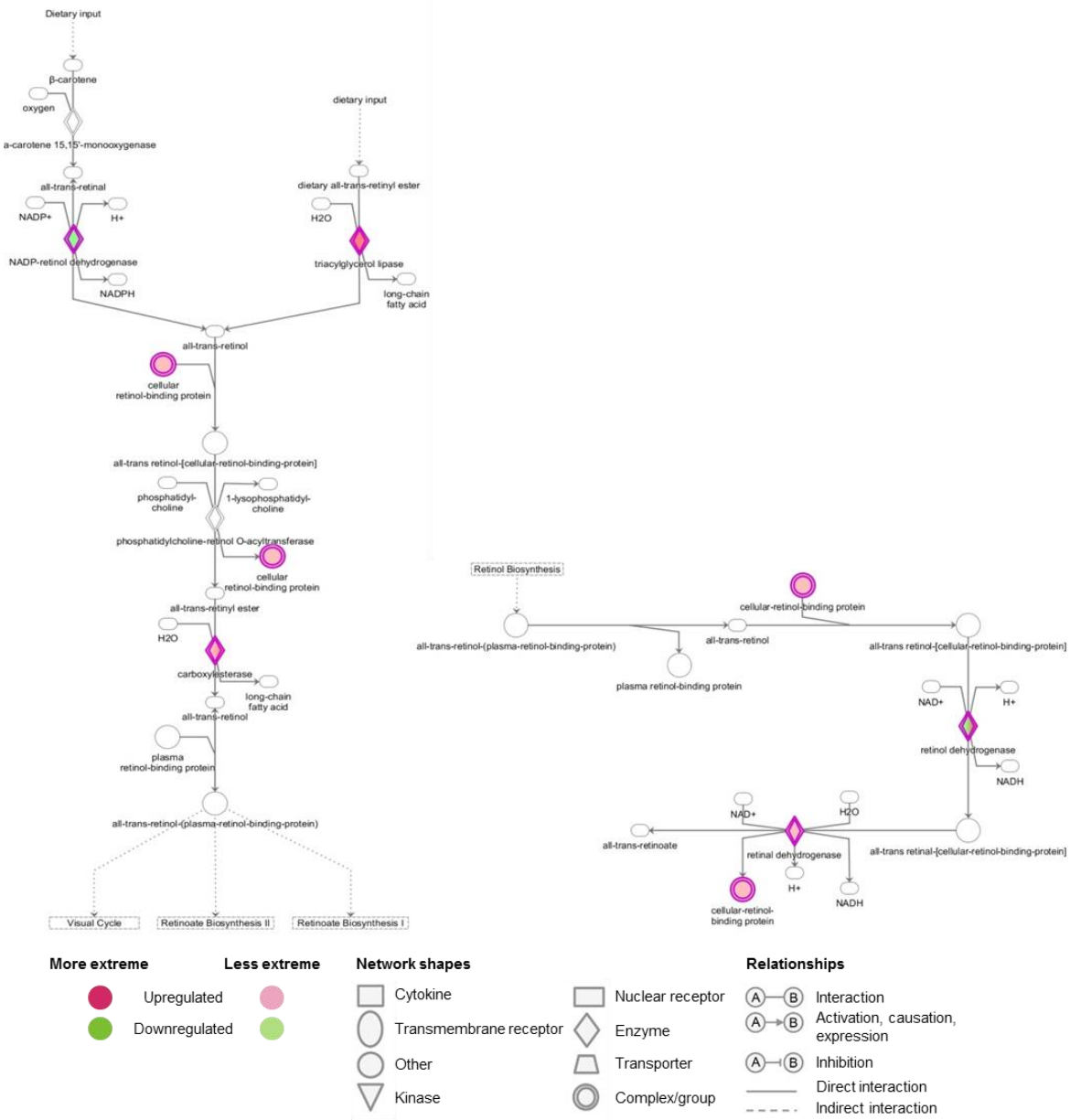

Figure 4.31. Retinol and retinoate biosynthesis.
The retinol pathway was upregulated in drug-resistant SNU-16 cells through the upregulation of CRBP and tricylglycerol lipase, carboxylesterase and retinol dehydrogenase.

From previous analysis, the sucrose metabolism has been found to be enriched in drug-resistant SNU-16 cells and was also found upregulated using IPA **(Figure 4.32)**. SI and ALDOB, which are significantly upregulated in this pathway, are both involved in sugar degradation.

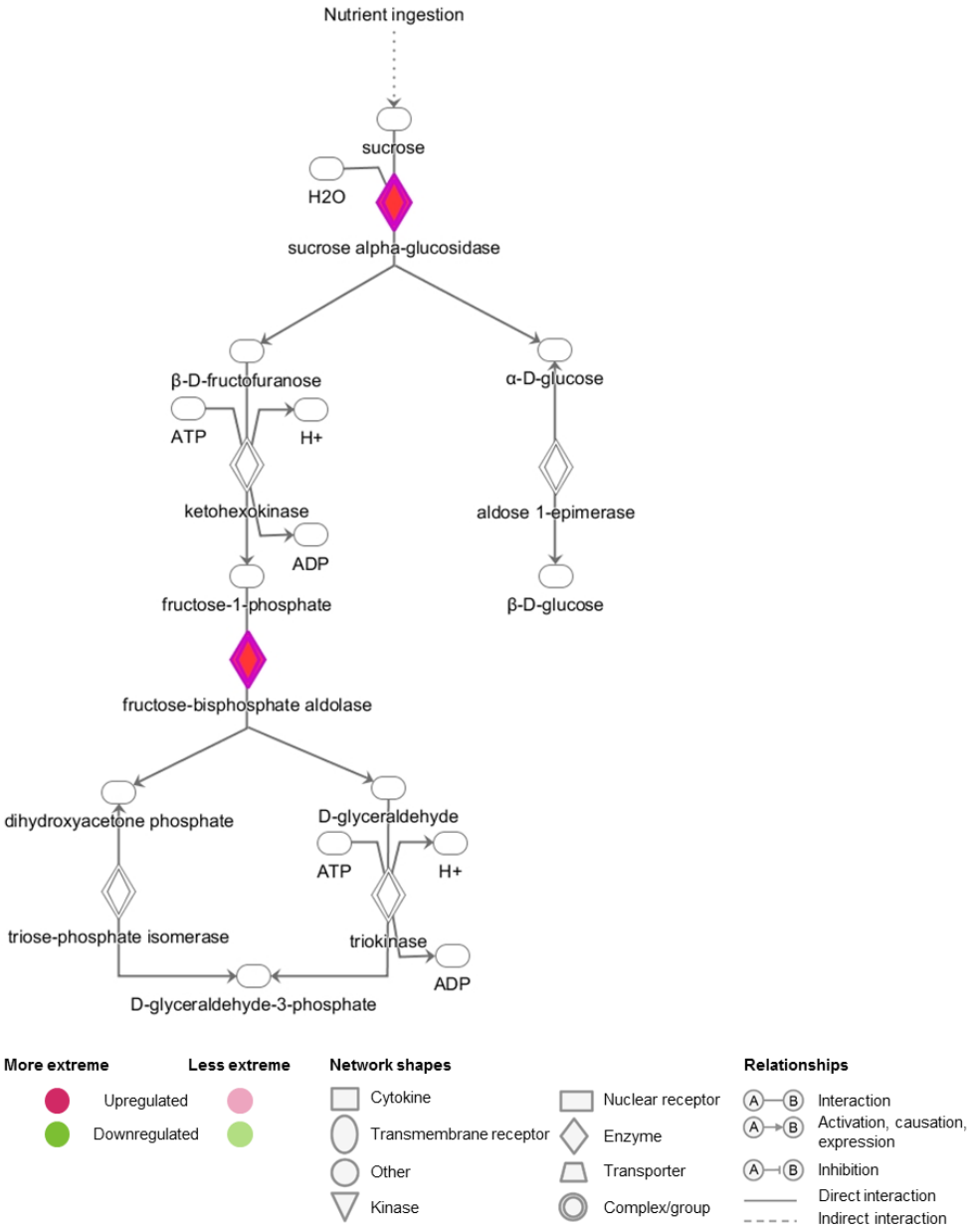

Figure 4.32. Sucrose degradation in SNU-16^{BGJR} cells compared to parental SNU-16 cells.
Sucrose alpha-glucosidase (SI) and fructose-bisphosphate aldolase (ALDOB) are both significantly upregulated in the sucrose degradation pathway, which ultimately results in increased glucose and ATP production.

Comparing significantly upregulated pathways in IPA, the serotonin degradation pathway seemed to play a role in drug resistance both in SNU-16 and also co-culture cells **(Appendix Figure 8.39)**. Serotonin has been found to stimulate tumour growth in aggressive cancers and elicits mitogenic activity both in normal and cancer cells (Sarrouilhe et al., 2015). This could indicate that SNU-16 cells upregulate serotonin production to accelerate growth and angiogenesis in the cells.

With IPA, also interaction networks with genes of interest that were significantly up- and downregulated can be generated. From these networks, direct influences on the genes of interest were found and direct interactions investigated **(Appendix Figure 8.40-Appendix Figure 8.42)**. For example, from the REG1A interaction map **(Appendix Figure 8.42)**, a direct interaction between REG1A and BCL2L1, can be found. BCL2L1, which belongs to a protein family, sharing Bcl-2 homology domains, encodes a pro-survival signal and therefore upregulation of REG1A in co-culture cells could indicate enhanced resistance to apoptosis.

In drug-resistant co-culture cells, together with the sucrose degradation metabolism also the glycolysis I pathway has been found to be upregulated **(Figure 4.33)**. This is an oxygen-independent metabolic pathway, which could support downregulation of oxidative phosphorylation in drug-treated cells. It mainly utilises fructose to generate energy, which is cleaved by sucrose-isomaltase in the sucrose metabolism. Most of the energy of cancer cells is derived from glycolysis, which means glucose is converted to lactase although oxygen is available. This method, which is termed Warburg effect generates less energy than oxidative phosphorylation (Warburg, 1956), however cancer cells potentially benefit from this pathway as it provides them with precursors for biosynthetic pathways such as amino acids, NADPH and ribose sugars needed for DNA and RNA synthesis. Factors that mainly drove the pathway in drug-resistant SNU-16 cells were ALDOB, as before resulting in increased glucose generation, and hepatocyte nuclear factor 1 homeobox B (HNF1β), which was involved in transformation of intracellular metabolism to enhance aerobic glycolysis and therefore also contributing to the Warburg effect. In ovarian carcinoma cells, HNF1β expression resulted in a reduction of intracellular ROS and thus resistance to

ROS ,which may be a consequence of the Warburg effect and therefore helps cells survive in hypoxic conditons under oxidative stress (Amano et al., 2015). Neurogenic differentiation 1 (NeuroD1) regulated the expression of insulin genes and mutations in this gene can lead to maturity-onset diabetes of the young 6 (MODY6) (Horikawa et al., 2018). NeuroD1 upregulated β cell development in drug-resistant cells and as β cells are involved in insulin storage and release increased levels of insulin could be produced in drug-resistant cells. There have been links between gastric cancer and diabetes and there could be shared risk factors such as, hyperglycemia, *H. pylori* infection, high salt intake, medications and comorbidities (Malecki et al., 1999; Tseng and Tseng, 2014). Insulin showed to affect proliferation of gastric cancer cells, inducing chemoresistance of gastric cancer cells to 5-fluorouracil, which is possibly involving upregulation of P-glycoprotein (Wei et al., 2015).

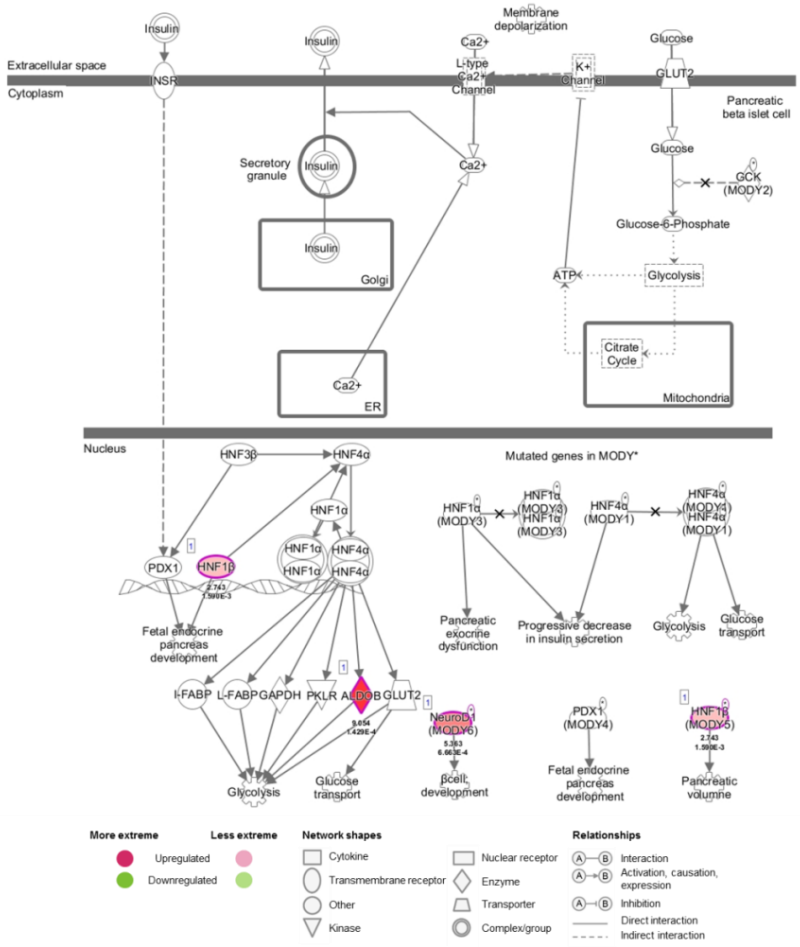

Figure 4.33. Glycolysis I pathway upregulation in co-culture cells.
Hepatocyte nuclear factor 1 homeobox B (HNF1β) activates or inhibits transcription of target genes and was upregulated in SNU-16^{BGJR} cells affecting foetal endocrine pancreas development and volume. Also ALDOB, which results in increased glucose production, was upregulated. Furthermore, Neurogenic differentiation 1 (NeuroD1) was upregulated, which in turn upregulates β cell development.

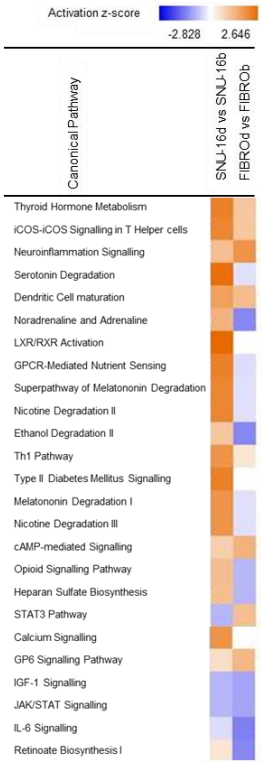

Figure 4.34. Comparison of pathways in cancer cells alone and with stromal cells.
Red boxes indicate upregulated pathways with increasing intensity, while blue indicates downregulated pathways.

Expression of pathways in both datasets including SNU-16 cells *versus* co-culture cells can be visualised **(Figure 4.34)**, with thyroid hormone metabolism being most upregulated in both datasets. Thyroid hormones play important roles in regulating normal metabolism, development, and growth, however they can also stimulate cancer cell proliferation (Lin et al., 2016) and therefore play a role in cancer growth in SNU-16 and co-culture cells.

Taken together, these data have shown that *FGFR2*-amplified gastric cancer cells could be rendered resistant to FGFR inhibition in 2D, but also in 3D with and without stromal support. Alvetex® scaffolds have been proven to be a suitable model to study drug resistance over longer time periods. Differential gene expression analysis from RNA-Seq data with different tools and databases have revealed interesting genes and pathways including pathways involved in cytoprotective mechanisms but also energy metabolism and, in the case of co-cultured cells, also ECM structure, which could be further analysed using different approaches such as substrate modifications, drug treatments in addition to overexpression and knockdown of genes.

4.6 Discussion

4.6.1 Drug resistance in 2D

Due to the high level of *FGFR2* amplifications of SNU-16 cells, drug resistance was studied with these cells. Over prolonged exposure to FGFR inhibition, SNU-16 cells acquired resistance. This was confirmed by regaining proliferation rates similar to untreated cells and exhibiting similar cell viability and growth properties to FGFR2 wildtype SNU-1 cells. This was further confirmed through protein expression levels of drug-resistant cells similar to *FGFR2* wildtype cancer cells. Often with drug-resistant SNU-16 cells, no p-AKT signalling was detected, which could be due to several reasons, such as high-speed centrifugation, where proteins of larger sizes can be captured in the pellet, antibody quality or the cells simply not expressing it anymore (due to the age of the cells). No morphological changes were encountered and cells were still in suspension rather than undergoing EMT as described (Grygielewicz et al., 2016). This could be due to different incubation conditions or other environmental properties or differences in media composition. However, resistant SNU-16^{BGJR} cells proliferated at a faster rate compared to the parental cell line as observed in several experiments when the same cell number was seeded and compared. SNU-16^{BGJR}, conversely to the parental cell line, exhibited similar protein expression levels as SNU-1 cells and showed no sensitivity to FGFR inhibitor treatment. Resistant cell lines were also generated with the H520 lung cancer cell line, giving rise to H520^{BGJR} cells **(Appendix Figure 8.43).** H520 cells initially grew evenly and dispersedly, however upon drug resistance observations showed the formation of clumps and cell aggregates. With the generation of drug-resistant lung cancer cells, cell signalling and drug sensitivity could be further assessed in the future.

4.6.2 Drug resistance in 3D and RNA sequencing

A healthy tissue stroma acts as a barrier against tumourigenesis but, in the presence of tumour cells, crucial changes are initiated that transform the environment into one that supports tumourigenesis (Junttila and de Sauvage, 2013). The stroma constitutes a large proportion of solid tumours and in some carcinomas, makes up more than 80% of the overall tumour mass. Stromal cells constitute to a heterogeneous population of different cell types; the tumour stroma is composed of neoplastic cells, but also non-malignant cells, such as normal stromal cells, infiltrating immune cells, cytokines and chemokines, and specialised fibroblasts, such as CAFs, all embedded in a network of extracellular matrix proteins (collagen, laminin, elastin and fibronectin) (Rupp et al., 2015). In colorectal cancer for example, the stroma is in direct contact with the adenoma and once it becomes activated, an altered phenotype is displayed that produces growth-promoting factors, as well as enhancing tumour cell proliferation and migration, thus speeding up tumourigenesis and depicting important drivers of tumourigenesis (Mo et al., 2016).

Fibroblasts, a major cell type also in the colonic stroma, are responsible for tissue-remodelling and homeostasis by providing a structural scaffold and regulating growth factors (Chen et al., 2014). Myofibroblasts, found surrounding the colonic crypt, are mainly involved in the synthesis of various collagens and other extracellular matrix proteins, thus producing the scaffold (Kalluri, 2016). In tumour tissues, activated fibroblasts can be identified by their expression of α-SMA. Stromal cells possibly co-evolve with cancer cells to become CAFs, which have been implicated to promote tumour development and progression (Gaggioli et al., 2007), as they have the ability to nourish cancer cells with an abundance of growth factors. CAFS have genetic and epigenetic changes which lead to alterations in expression and metabolic mechanisms (Kiaris et al., 2004). Thus, cancer cells are capable of reprogramming normal fibroblasts into CAFs with pro-tumourigenic activity and enhanced cell proliferation, a process that is mediated by cancer cell-derived factors (Mukaida and Sasaki, 2016). Little is known regarding the epithelial-stromal

interactions during the very early stages of development of resistance and therefore it is of utmost importance to study the influence of stromal cells on cancer cells.

The 3D Alvetex® structure is highly versatile and has proven useful to study resistance experiments and for co-culture cells, as SNU-16 cells could be grown together with HFF2 cells in the structure over longer time periods up to 8 weeks where other 3D models often fail (Mewes et al., 2012). To study stromal interaction, HFF2 cells were used in co-culture with SNU-16 cells due to the difficulties involved with obtaining tissue specific primary gastric fibroblasts. To generate resistant cells in 3D, the drug dose to generate resistant cells in 2D had to be lowered as cells in 3D were more sensitive to the drug as shown by reduced cell numbers compared to vehicle-treated cells. Potentially, this experiment could be repeated and the cultures could be kept longer so that the same drug concentration as in 2D could be reached.

Interestingly, SNU-16 cells with stromal support were observed to become resistant faster than cancer cells alone, which almost took double the amount of time (4 *versus* 8 weeks). When comparing DMSO-treated to BGJ-treated co-culture cells, a larger number of fibroblasts were retained within the scaffolds in the BGJ-treated condition. In the DMSO-treated condition, fibroblasts migrated through the scaffold and attached to the bottom of the 6-well plate. It is possible that the drug-induced stress helps the HFF2 cells to attach to the scaffold or stops the fibroblasts from migrating through. Additionally, the influence of the drug could alter their morphology and slow or stop them from migrating through the scaffold. It is known that fibroblasts express various matrix metalloproteinases (MMPs), which are responsible for remodelling of the ECM. These are necessary for many physiological events such as wound repair however are often also dysregulated in a variety of diseases including cancers. MMPs can influence the tumour environment through the induction of angiogenesis, tumour growth, and metastasis (Bhowmick et al., 2004; Kalluri, 2016). The use of MMP small molecule inhibitors such as Marimastat induced morphological changes in fibroblasts in a breast cancer study (Sparano et al., 2004; Zucker et al., 2006). Another study has also discussed cytoskeletal transformations in fibroblasts upon various drug treatments using elasticity measurements with an

atomic force microscope (AFM) (Rotsch and Radmacher, 2000). Stress fibers are cytoskeletal structures, which are composed of cross-linked actin filament bundles in fibroblasts which are the contractile structure in these cells and these undergo continuous assembly and disassembly, which allows cells to maintain cellular tension and adapt to various forces (Hirata et al., 2007; Kaunas et al., 2005). Drug treatments could therefore affect stress fibers in fibroblasts that impact elasticity of cells.

External factors may have led to fluctuations and variations between samples and data collection time points. This could be due to the fact that live cell 3D culture samples had to be transported from the ground floor laboratory to the microscopy suite on the third floor in a Styrofoam box. During transportation cells could have dislodged from the scaffold. Additionally, acquisition of one Z-stack sample took approximately 15 minutes, although the scaffolds were kept in a temperature controlled and humidified gas chamber during imaging, fluctuations in temperature and CO_2 concentration could have affected cell growth and attachment. Medium exchanges were performed very carefully and medium was only fed from below, to avoid cells from being forcefully removed, however it could still be that some cells were flushed out. Also during optimisation, it has been observed that fibroblasts migrate through the scaffold, especially in the vehicle-treated conditions, and attached to the well-plate bottom. Therefore to avoid toxic waste accumulation from cells and to ensure sufficient nutrient supply, in addition to exchanging the medium regularly, scaffolds were transferred to fresh well-plates once a week post-imaging.

The scaffolds were imaged over time to observe changes in cell growth, the effect of drug treatment and the formation of resistant cells. Scaffolds had to be removed from the 6-well plate and transferred to a sterile glass-bottom dish. In some of the Imaris images, cell layers appeared to be tilted, this may be due to the ability of some cells to invade deeper into the scaffold and also simply that the scaffold was not perfectly straight. This may be due to a drop of liquid or not sitting perfectly flat in the glass bottomed dish. As SNU-16 cells prefer to form clumps of cells in aggregates, it is difficult to distinguish single cells from each other even when adjusting the parameters in Imaris. Therefore, rather than comparing cell numbers, cell volumes

were calculated and compared between conditions. Vehicle-treated SNU-16 cells rapidly proliferated in the scaffold and were harvested after four weeks, whereas the BGJ-treated cells grew very slowly and only after a time span of four weeks started recover and form resistant populations until harvesting at 8 weeks. Once drug-resistant populations were formed, as observed by 3D live cell imaging, cells were extracted from the scaffold. Although this process was performed carefully and rapidly, the dissociation and lysis could have effects on the cellular signalling of these cells (Day et al., 2016; Fulda et al., 2010). RNA concentration and purity checks were performed with a Nanodrop spectrophotometer and all samples possessed a high enough RNA concentration and purity with A260/A230 between 2.07-2.16. However, to perform successful RNA sequencing the integrity of RNA (RIN) (Gallego Romero et al., 2014) is crucial to generate RNA-Seq libraries and should have a RIN value of at least 6.5., which all of the samples exceeded. Triplicates of DMSO and BGJ-treated SNU-16 cells alone and co-culture grown in 3D were run for RNA sequencing. However, ideally an additional condition, where mixed co-culture cell populations could have been separated using FACS, would have been useful to investigate the influence of HFF2 cells on the cancer cells in a more isolated manner. Due to the cost limitations of this method, only the essential samples were run for RNA sequencing.

4.6.3 Differential gene expression analysis

Commonly, for interpretation of gene expression datasets, gene set enrichment analysis based on functional annotation of the differently expressed genes is performed to associate genes with a certain biological process or molecular function. With GSEA, regulated pathways could be clustered into functional classes. In BGJ-resistant SNU-16 cells the majority of pathways have been found to harbour a metabolic or xenobiotic function, which could be due to increased proliferation of cancer cells and also to metabolise the drug. *MET* overexpression has been associated with several epithelial and mesenchymal cancers and represents a prognostic factor associated with malignancy and has been found in a large number of gastric cancer patients (Zhang et al., 2016). MET overexpression for example, has been implicated with resistance to EGFR inhibitors in lung cancer (Hammerman et al., 2009) and high HGF expression levels were found to induce resistance to c-MET RTK inhibitors in gastric cancer (Ahn et al., 2017).

In respect to downregulated pathways, one pathway particularly stood out both in cancer cells alone and in co-culture cells, such as oxidative phosphorylation. Cancer cells adapt their metabolism to ensure enough molecules to promote tumour growth and hence also modify their environment. Cancer cells often have a higher glucose consumption than normal cells and often require other means of ATP generation and therefore activate glycolysis (Shanmugam et al., 2009). A downregulation in oxidative phosphorylation could therefore indicate that such a switch has occurred and although oxidative phosphorylation is more efficient in ATP formation, the release of ROS could damage cancer cells. This could tie in well with drug-resistant cancer cells increasing glucose generation through increased sucrose and starch pathway activity and consequently switching to glycolysis from oxidative phosphorylation.

The ECM is the most abundant component in tumour microenvironment and can regulate tumour cell behaviours and tissue tension homeostasis (Paszek et al., 2005). The upregulation of the ECM in drug-resistant co-culture cells, might possibly be due to co-culture cells forming their own matrix with increased ECM proteins to create a stiffer ECM architecture and therefore obstructing the drug reaching their target or

slowing this process down and therefore cancer cells can acquire resistance towards the drug (Nguyen et al., 2014; Schrader et al., 2011; Shin and Mooney, 2016). Cancer cells have also been found to use the remodelled stiff matrix as invasion highways, as seen with glioma cells exploiting a matrix rich in blood vessels and rigid myelin sheath bundles (Giese et al., 1996). Collagen serves as a major scaffold of the tumour microenvironment and its remodelling can promote tumour infiltration, angiogenesis, invasion and migration (Page-McCaw et al., 2007). Collagen was seen as a passive barrier to resist tumour cells; it is now understood that collagen plays an active role in promoting tumour progression (Fang et al., 2014). A change in collagen levels in the tumour microenvironment releases biomechanical signals, which signal to both tumour and stromal cells, triggering a cascade of biological events and increased or decreased deposition of collagen can be associated with augmented malignancy (Arnold et al., 2010; Levental et al., 2009). Interestingly, many collagen-encoding genes and other matrix building blocks were found to be upregulated in inhibitor-resistant co-culture cells, which could indicate that drug-resistant co-culture cells upregulated the ECM pathway producing more ECM molecules and therefore possibly creating a stiffer ECM architecture, thus blocking drug activity on the cells. When cross-checking with the genes that are responsible for the enrichment of the pathway, many of the *COL* genes are significantly upregulated, which is a further indication for a potential role of collagens in drug resistance, as overexpression could protect cancer cells against chemotherapeutic agents by lengthening the time needed for the penetration of the collagen network, which can result in drug resistance (Januchowski et al., 2016; Netti et al., 2000). This could therefore influence the malignancy of cancer cells and make them resistant to the drug by ECM remodelling. Therefore, not only cancer cells have to be taken into account when treating cancer also targeting stromal cells could be a viable method (Gaggioli et al., 2007).

In drug-resistant SNU-16 cells, the ribosome pathway, which is essential for protein synthesis, was significantly upregulated, indicating altered mRNA translation, which is important in cancer initiation (Chu et al., 2016). The pathway could be potentially upregulated to support accelerated proliferation and growth of drug-resistant cells. In drug-resistant co-culture cells however, the ribosome pathway was significantly

downregulated. While it was proven that ribosome biogenesis is required for active proliferation, it is not the only function of RPs and they have also been implicated in cellular transformation and the perturbation of RPs may reduce the levels of survival/protective factors and therefore could favour cancer development and progression (Steller, 1995).

4.6.3.1 The retinol pathway is a double-edged sword in SNU-16 and co-culture cells

Using both DAVID and GSEA, the retinol pathway raised particular interest, as it was significantly regulated both in SNU-16 cells alone and in co-culture cells. Retinol, or vitamin A, has received great medical interest in the past and has been used for thousands of years for treatment. It cannot be synthesised and is ingested through diet in the form of retinol, retinyl ester, or β-carotene. It is stored as retinyl esters in hepatic tissue in stellate cells and gets reversibly oxidised to retinal through retinol dehydrogenases (O'Byrne and Blaner, 2013). Retinal dehydrogenases further oxidise retinal irreversibly to *all-trans* retinoic acid (*all-trans* RA) and is then further oxidised by mainly CYP26. Retinoic acid is the active metabolite and was found to regulate various biological processes such as development, differentiation, proliferation, and apoptosis (Lai et al., 2003; Noy, 2010; Ross et al., 2000; Wang and Kirsch, 2002). Retinol has six biologically active isoforms and different isomers activate different receptors, thus leading to different biological effects. There are two distinct classes of receptors for retinoids: retinoic acid receptors (RAR) and rexinoid receptors (RXR), which belong to the peroxisome proliferator-activated receptor (PPAR) family. RARs are also known to interact with the oestrogen signalling pathway (Ross-Innes et al., 2010). Rexinoids are retinoids that specifically bind to RXR and have been used effectively in cancer therapy (Bushue and Wan, 2010). Retinoids are comprised of three units: a bulky hydrophobic region, a linker unit, and a polar terminus, which is usually a carboxylic acid (Das et al., 2014). There are different types of retinoid-binding proteins, which are isomer specific and located in either intracellular or extracellular compartments (Noy, 2000). They stabilise retinoids and make them soluble, but also have a role in transportation and metabolism of retinoids. Therefore, retinoids together with binding proteins and nuclear receptors elicit cellular actions. Vitamin

A, which circulates in the blood, is bound to serum by retinol binding protein (RBP) and then once in the cell together with *all-trans* retinal is associated with different isoforms of cellular retinol-binding proteins (CRBP), while *all-trans* retinoic acid binds to cellular retinoic acid-binding protein isoforms (CRABP). Therefore, the retinol binding protein and receptor work together, to exert the specific effects of RAs. RAs can also bind both PPARβ and δ, which are the receptors for fatty acids (Berry and Noy, 2009; Schug et al., 2007; Shaw et al., 2003).

Secretion of RBP is regulated by the availability of retinol and the intracellular concentrations of retinoids are controlled by a number of metabolic enzymes, which react in response to external signals (Wolf, 2007). However, RBP secretion is inhibited by Vitamin A deficiency, resulting in protein accumulation in the endoplasmic reticulum of hepatic parenchymal cells. In the presence of retinol, RBP binds retinol and moves along the Golgi apparatus and is then secreted into blood. Retinol dehydrogenases (ADHs) oxidize retinol to *all-trans* retinal, which is further metabolised to RA by retinaldehyde dehydrogenases (ALDHs). In particular, RDH10 which metabolises retinol to retinaldehyde is an essential enzyme in this metabolic pathway. The synthesis and metabolism of the bioactive metabolites of retinol are sometimes impaired in cancer cells in contrast to normal cells. A number of studies indicate that retinoids halt cell cycle progression in cancer via signalling pathways, either directly or indirectly through altering cyclins, cyclin-dependent kinases (CDKs) and cell-cycle inhibitors (Mongan and Gudas, 2007). Thus, RA can cause a block in the G1 phase of the cell cycle inducing an increase in the proportion of cells in the G0/G1 phase and a decrease in cells in S phase. Among the RARs, RARβ2 can be activated by RA resulting in its inhibitory effect on cell proliferation (Altucci et al., 2007; Faria et al., 1999; Seewaldt et al., 1995). Cyclin D1, one of the regulators of cell-cycle progression is often overexpressed in a number of cancers such as head and neck, lung, stomach, and breast (Kim and Diehl, 2009). Furthermore, treatment with retinoids has been associated with an increase in ubiquitination and proteolysis of cyclin D1 in human bronchial cells (Ma et al., 2005) and in a decrease in cyclin D1 messenger RNA (mRNA) and protein levels in HepG2 human hepatoma cells (Suzui et al., 2002), which results in decreased CDK activity hindering cells to transition from

S phase to G1 phase (Malumbres and Barbacid, 2009). Retinoids can also induce apoptosis in cancers and post-maturation apoptosis in acute promyelocytic leukaemia (APL) by inducing tumour-selective death ligand (TRAIL) (Altucci et al., 2007). Consequently, since retinoids can both promote cell-cycle arrest but also induce apoptosis, they could be useful drugs for the treatment of cancers. However, many cancers become resistant to retinoids. Upon retinol deprivation a different type of programmed cell death occurs independent of receptor activation, which is accompanied by an increase in reactive oxygen species, reductions in ATP and NAD^+, and PARP-1 activation (Chiu et al., 2008). Inhibition of PARP-1 prevents this form of programmed cell death, indicating that retinol levels are needed to prevent depletion of NAD^+ and cell death. Therefore, retinoids have gained great attention as a chemotherapeutic due to their influences on differentiation, anti-proliferative, pro-apoptotic, and effects as an anti-oxidant. The most abundant retinoid is *all-trans* retinoic acid (ATRA), which is in clinical trials for lymphoma, leukaemia, melanoma, lung cancer, cervical cancer, kidney cancer, neuroblastoma, and glioblastoma (Bushue and Wan, 2010). In 1995, the FDA approved ATRA for treating promyelocytic leukaemia (APL) and promotes the degradation of mutant promyelocytic leukaemia protein (PML)-RARα and release of co-repressors (Grignani et al., 1998; Yoshida et al., 1996). In addition to cell cycle arrest, ATRA also induce post-maturation apoptosis through the activation of TRAIL (Jiménez-Lara et al., 2004). Similarly to other therapeutics, resistance towards retinoids arises and displays a major obstacle in successful treatment. Deregulation of retinoid signalling is quite common in carcinogenesis, for example epigenetic silencing of RARβ or translocation of RARα to generate oncogenic fusion proteins (Freemantle et al., 2003).

Due to the importance of retinol metabolism in cell-cycle and apoptosis and the fact that it was significantly upregulated in SNU-16^{BGJR} cells, it raised tremendous interest. In the retinol pathway, a shift to the right can be observed **(Figure 4.24)**, potentially driving the formation of 4-oxo-retinoic acid, which is a biologically active geometric isomer of RA and enhances gap junctional communication in cells (Hanusch et al., 1995; Pijnappel et al., 1993). Metabolic transformation of ATRA to 4-hydroxylated RA appears to be primarily catalysed by cytochrome P450 (CYP26) in human skin cells,

which was also upregulated in the dataset. Stromal CYP26 can metabolise pharmacological concentrations of ATRA and neutralise the drug's activity to induce differentiation (Su et al., 2015). Additionally, ATRA was found to induce stromal CYP26, which creates a protective environment and, with the use of CYP26 inhibitors, microenvironment-induced ATRA-resistance could be overcome (Norsworthy et al., 2015; Su et al., 2015). Furthermore, the generation of retinoyl-glucuronide was enhanced and when investigating the retinol pathway with GSEA and crosschecking what might drive the pathway, UDP glucuronosyltransferase (UGT2A3), which is a microsomal enzyme, was significantly upregulated. Such enzymes are responsible for the glucuronidation of exogenous and endogenous compounds, such as drugs, and high expression levels have been implicated in tissues involved in drug clearance, which is mostly the liver followed by the gastrointestinal tract and the kidneys. Drug-resistant SNU-16 cells could therefore use UGT enzymes for drug elimination. Other genes that lead to enrichment of the pathway were *Cyp* genes and *ADH1C*, which metabolise a wide selection of substrates including ethanol and retinol.

Previous studies have shown retinoyl-glucuronide to be present in several tissues in vitamin A deficient rats given retinoic acid and has been found to be involved in detoxification (Silva and DeLuca, 1982). However, another possibility would involve CRBP-1, which is controlling the availability of retinol in cells and was associated with inhibition of early steps in transformation. Downregulation of CRBP-1 was observed in several cancers (Kuppumbatti et al., 2000; Orlandi et al., 2006), including gastrointestinal cancers (Esteller et al., 2002) resulting in loss of cellular differentiation and tumour progression. When comparing to IPA data however, it becomes clear that CRBP genes are upregulated and contribute to the upregulation of the pathway in SNU-16^{BGJR} cells, which could indicate, that together with retinoids, activation of other pathways occur, resulting in a more malignant phenotype of SNU-16 cells. Recently, CRBP-1 has been associated with wound healing and arterial tissue remodelling processes, which cancer cells potentially can use to their advantage (Cvetković et al., 2003; Neuville et al., 1997).

In co-culture cells however, the retinol pathway is downregulated. According to IPA, this is driven by downregulation of NADP-retinol dehydrogenase and triacylglycerol lipase, which enable the oxidation of retinol to retinol and from retinyl ester to retinol. This could indicate that less retinol is generated and retinal is favoured. It could therefore be that co-culture cells decrease ATRA production in cells to avoid cell proliferation arrest and induction of apoptosis in cells. Therefore, the implication of retinol in SNU-16 cells is an interesting pathway to study and understand the double edged activity of the metabolic pathway.

4.6.4 Significantly regulated genes of interest

4.6.4.1 Sucrase-Isomaltase upregulation and the role of glucose

Interestingly, when comparing cancer cells alone, many upregulated genes in SNU-16^{BGJR} cells were involved in sugar metabolism and cytoprotective mechanisms. *Sucrase-Isomaltase* (SI), which was the top hit among the upregulated genes in drug-resistant gastric SNU-16 cells and was also upregulated in co-culture cells, is a disaccharide glycoprotein hydrolase, which is normally restricted to the brush border membrane of the enterocytes of the small intestine (Zweibaum et al., 1983). Its purpose is the digestion of carbohydrates, such as starch, sucrose and isomaltase to ultimately produce energy in the form of ATP (Berg et al., 2002). It was found to be significantly enhanced during neoplastic transformation of the colonic epithelium, and 55% of primary colorectal cancers expressed SI and resulted in a 1.83-fold increased risk of death from colorectal carcinoma (Jessup et al., 1995). Due to its high expression in colon cancers and also Barrett's mucosa, it could serve as a biomarker of early neoplastic dysplasia (Zweibaum et al., 1983; Iannettoni et al., 1996). Increased sucrase expression was also found with enhanced invasion by human gastric carcinomas with progression (Nakamura et al., 1998). These publications could indicate that higher SI levels in BGJ-resistant SNU-16 cells could give them an advantage over parental SNU-16 gastric cancer cells by generating more ATP and therefore more energy as tumours require ATP and NADH, not only for metastasis and proliferation, but also for survival (Oronsky et al., 2014). ATP is also elevated in the tumour microenvironment and affects Ca^{2+} signalling and has effects on anti-

apoptotic (Bcl-2) and pro-apoptotic (Bax) proteins, promoting cancer transformation and progression (Song et al., 2016).

4.6.4.2 Upregulation of ALDOB as an alternative way for ATP generation

Aldolase B (ALDOB) was the second most upregulated gene in SNU-16^{BGJR} cells compared to parental cells and was also upregulated in drug-resistant co-culture cells. ALDOB plays an essential role in glycolysis and gluconeogenesis (Vella, 1995). ALDOB is one of three isoenzymes of human aldolases, normally expressed in liver, kidney and intestine (Tolan et al., 1987). It catalyses the reversible cleavage of fructose 1,6-bisphosphate (FBP) into glyceraldehyde 3-phosphate (G3P) and dihydroxyacetone phosphate (DHAP) as well as the reversible cleavage of fructose 1-phosphate (F-1-P) into glyceraldehyde and DHAP. It is therefore involved in the breakdown of glucose and is particularly important in the metabolism of fructose. When fructose is absorbed it is phosphorylated by fructokinase into F-1-P, which is broken down into glyceraldehyde and DHAP and further phosphorylated by triose kinase to form G3P. These products can then be used in the glycolytic-gluconeogenic pathway and can be turned into either glucose or pyruvate (Ye et al., 2018). Aberrant expression of ALDOB has been studied in hepatocellular carcinoma and gastric cancer (Asaka et al., 1988; Peng et al., 2008; Song et al., 2004; Tao et al., 2015). High expression of ALDOB is associated with poor prognosis for rectal cancer patients receiving neoadjuvant concurrent chemoradiotherapy (CCRT) and is associated with poor tumour advancement, lymphovascular and perineural invasion before and after CCRT but also poor response to CCRT, and therefore is an interesting target for patients with rectal cancer (Tian et al., 2017). It is also associated with hepatocellular carcinoma (HCC), which often exhibits an aberrant expression of glycolytic enzymes, such as type II hexokinase (HKII) and ALDOB and cancer cells with a high glycolytic rate have shown to have an advantage in tumour growth (Peng et al., 2008).

Most malignant cells generate ATP mainly via glycolysis and lactic acid fermentation but not via the tricarboxylic acid (TCA) cycle (Warburg, 1956). This phenomenon is termed 'the Warburg effect', and has proven to be useful to detect malignancy (Devic, 2016). Therefore, by upregulating SI and ALDOB, BGJ-resistant cancer cells could

have a growth and survival advantage by upregulating glucose metabolism and therefore alternative ATP generation in contrast to oxidative phosphorylation, which was found to be downregulated in both datasets.

4.6.4.3 PIWIL1 induces self-renewal capacity in cancer stem cells

Cancer is driven by genetic abnormalities as described previously, however it can also additionally be induced by aberrant epigenetic alterations. Such changes are for example alterations in DNA methylation, histone modifications and small noncoding RNA deregulation (Kanwal and Gupta, 2012). There are three major classes of small regulatory RNAs; microRNAs, small interfering RNAs (siRNAs) and PIWI-interacting RNA (piRNA). Being only identified in 2006, piRNAs are a relatively recent discovery and were found to interact with P-element-induced wimpy testis (PIWI) proteins, which are a subclass of the conserved Argonaute family of proteins and play a role in germline cells (Girard et al., 2006; Grivna et al., 2006; Watanabe et al., 2006). Argonaute proteins contain PIWI-Argonaute-Zwille (PAZ) and PIWI motifs that are involved in stem cell self-renewal, RNA silencing and translational regulation in various organisms and are suggested to play a role as an intrinsic regulator of the self-renewal capacity of germline and haematopoietic stem cells. PIWI proteins bind piRNAs, which are thereby amplified in a Dicer-independent manner resembling a ping pong cycle (Brennecke et al., 2007; Vagin et al., 2006). This then leads to transposon repression through base-pairing and degradation (Gunawardane et al., 2007). Reactivation of PIWI expression, primarily PIWI-like protein 1 (PIWIL1) and 2 (PIWIL2), through aberrant DNA methylation resulting in genomic silencing has been documented in numerous types of tumours (Qiao et al., 2002; Tan et al., 2015; Litwin et al., 2018). Small non-coding RNA (ncRNA) deregulation has been investigated in several types of cancer in recent years (Kanwal and Gupta, 2012) and these aberrations have been found to be connected to the hallmarks of cancer including deregulated cell proliferation, altered apoptosis, genomic instability, invasion, and metastasis (Tan et al., 2015), which drive the transformation of wild-type cells into malignant cells with metastatic potential and infinite proliferation capacities (Kanwal and Gupta, 2012; Kristensen et al., 2009). PIWIL expression varies based on the tissue of origin, such as in urological tumours (RCC and bladder cancer),

the expression of *PIWIL* genes is more likely to be downregulated and loss of expression is associated with a more aggressive phenotype and reduced survival (Iliev et al., 2016). Several mechanisms of how PIWIL1 promotes tumour progression have been suggested, such as cell cycle arrest at the G2/M stage in gastric cancer cells (Liu et al., 2006), CDK1 silencing through methylation in osteosarcoma (Siddiqi et al., 2012) and PIWIL1 as a target of RAS-associated domain family protein 1 C (RASSF1C) in lung cancer (Reeves et al., 2014). RASSF1C possibly phosphorylates ERK members and hence activates MEK-ERKl/2 signalling, which results in infinite self-renewal of tumour stem cells. It has been suggested that the PIWI-piRNA complex contributes to cancer development and progression by promoting a stem-like state of cancer cells, or cancer stem cells (CSCs) (Ng et al., 2016; Siddiqi et al., 2012; Siddiqi and Matushansky, 2012) and plays a driving role in degradation or inhibition of tumour suppressor genes or oncogenes (Moyano and Stefani, 2015). Thus PIWI-piRNA complexes contribute to carcinogenesis by aberrantly methylating DNA, which results in genomic silencing and induction of a stem-like state of cancer cells (Moyano and Stefani, 2015; Ng et al., 2016; Siddiqi et al., 2012; Siddiqi and Matushansky, 2012).

PIWIL1 is therefore an interesting target and was the most downregulated candidate in the mono cell BGJ-resistant SNU-16 dataset, and was also found to be downregulated in co-culture cells. It could therefore be that PIWIL1, together with piRNA, supports SNU-16 cancer cells by induction of self-renewal capacity in these cells or in the activation or repression of oncogenes and tumour suppressor genes respectively. This however has to be further elucidated with experiments addressing these questions, potentially by overexpressing PIWIL1 in cells, where PIWIL1 is downregulated, by plasmid transfection. Also, PIWIL1 could be knocked down with shRNAs in parental cells to observe if this would render cells less sensitive to FGFR inhibition.

4.6.4.4 REG genes induce glucose repression to survive

Top candidates in co-cultured cells were members of the regenerating family also known as islet cells regeneration factor (ICRF) or islet of Langerhans regenerating protein (REG), with *REG1A* and *REG1B*, the most upregulated genes. They belong to the calcium-dependent lectin (C-type lectin) gene superfamily (Hartupee et al., 2001) and encode five small proteins, secreted by the exocrine pancreas, including REG1A and B. These proteins are primarily involved in liver, pancreatic, gastric and intestinal cell proliferation or differentiation (Miyaoka et al., 2004; Unno et al., 1992). They were first regarded as endogenous growth factors isolated from pancreatic islet β cells (Terazono et al., 1988; Watanabe et al., 1990) and are acute phase reactants, lectins, anti-apoptotic factors, or growth factors for pancreatic islet cells, neural cells, and epithelial cells in the digestive system (Broekaert et al., 2002; Dusetti et al., 1994). REG genes were found to be sensitive to tissue injury and served as a prognostic indicator of tumour survival. They could serve as early biomarkers of carcinogenesis and have been found in gastric cancer previously (Watanabe et al., 1990; Zenilman et al., 1997). High REG1A mRNA expression was also associated with a susceptibility to Dacarbazine and Cisplatin in melanoma (Sato et al., 2013). Thus, it could therefore be an interesting novel therapeutic target.

Additionally, there has been extensive evidence for the involvement of aberrant REG1A expression in cancer development in oesophagus, stomach, colon, pancreas, liver, lung, breast, and bladder cancer (Astrosini et al., 2008; Cavard et al., 2006; Geng et al., 2009; Hayashi et al., 2008; Kimura et al., 1992; Lee et al., 2008; Minamiya et al., 2008; Motoyama et al., 2006; Sasaki et al., 2008; Sekikawa et al., 2008; Yoshino et al., 2005). Promoter methylation could be one of the regulatory mechanisms for REG1A expression in melanomas and could therefore be an interesting biomarker (Sato et al., 2013). Furthermore, in ErbB2-positive breast cancer patients, REG1A expression was higher than those with ErbB2-negative disease and the 10-year survival rate amongst patients with lower levels of REG1A was significantly higher than those with increased levels (Sasaki et al., 2008). REG1A has also been implicated as a regulatory subunit in glucose repression and associates with serine/threonine-protein

phosphatase PP1-2 (GLC7) to regulate the glucose repression regulatory pathway (Tu and Carlson, 1995). In co-culture cells, upregulation of REG1A and B could therefore be an indication for the cells trying to lower gluconeogenesis to avoid hyperglycemia, which is associated with high ROS levels. By upregulation of *REG* genes, cancer cells potentially protect themselves from ROS-induced damage or cell death. It is therefore interesting to investigate altered REG1A expression in co-culture cells to see if altering expression of REGs could induce apoptosis or necrosis and resensitise cancer cells.

4.6.5 Conclusion

Pathway analysis depends on existing databases and the data used are not always completely annotated, with many gene interactions therefore relatively speculative. Additionally, most canonical pathways are built from knowledge acquired from a small number of experiments with narrow cell models. Therefore, interpretation of such data from different tissue has to be done with caution. Still it is of importance to find targetable pathways to treat cancer drug resistance and gene expression analysis and pathway analysis is an appropriate method to search for essential pathways and targetable nodes.

In the next Results chapter, the most promising targets from the RNA sequencing results have been validated using different approaches such as drug combinations, shRNA knockdown and overexpression and alteration of medium components.

Chapter V: Results Chapter Part III

Target validation

5.1 Introduction

In the previous chapter, it has been demonstrated that using Alvetex® is an ideal model to generate BGJ-resistant SNU-16 cells in 3D to study drug resistance. Alvetex® scaffolds have been applied to a vast number of scientific purposes, however no resistance studies have been performed to date (Gomez-Roman et al., 2017; Knight et al., 2011; Ugbode et al., 2016). There are a number of publications supporting the importance of the tumour microenvironment, and particularly the influence of stromal cells, on drug resistance (Donner, 2012; Paraiso and Smalley, 2013; Sebens and Schafer, 2012; Zhang and Huang, 2011). Using RNA-Seq to compare drug resistance in the presence or absence of fibroblasts, a number of highly interesting genes and associated pathways have been revealed (Chapter IV). Interestingly, in the cancer cell monoculture condition, many genes were significantly regulated that were specific to the gastric or intestinal milieu. Also, interestingly, but perhaps predictable, was that many genes are involved in cytoprotective or xenobiotic mechanisms. The most interesting aspect however was the upregulation of genes involved in metabolic processes such as glucose metabolism (*SI, ALDOB, UGT2A)* with *SI* and *ALDOB* being the top hits **(Figure 5.1)**. In the co-culture studies, many regulated genes were involved in collagen synthesis or members of the regenerating family. Myriad analysis tools are available, using different algorithms and databases. In respect to pathway analysis, of particular interest was the retinol pathway, as it was altered both in cancer cells alone and co-culture cells. Furthermore, the sucrose and starch pathway was strongly upregulated, which is mainly driven by SI and ALDOB, which are enzymes involved in sucrose and fructose degeneration and glucose production. This aligns well with a downregulation in oxidative phosphorylation, indicating a switch to glycolytic metabolism. *PIWIL1* was downregulated the most in drug-resistant SNU-16 cells and was also among the top downregulated genes in co-culture cells and could therefore be an essential gene involved in drug resistance. REG1A was upregulated the most in drug-resistant co-culture cells and is specific to co-culture cells and could explain the difference with stromal support.

Different approaches have been used to analyse and compare the different datasets to identify targetable nodes involved in drug resistance in FGFR-driven cancers in 3D, which will be discussed in this chapter.

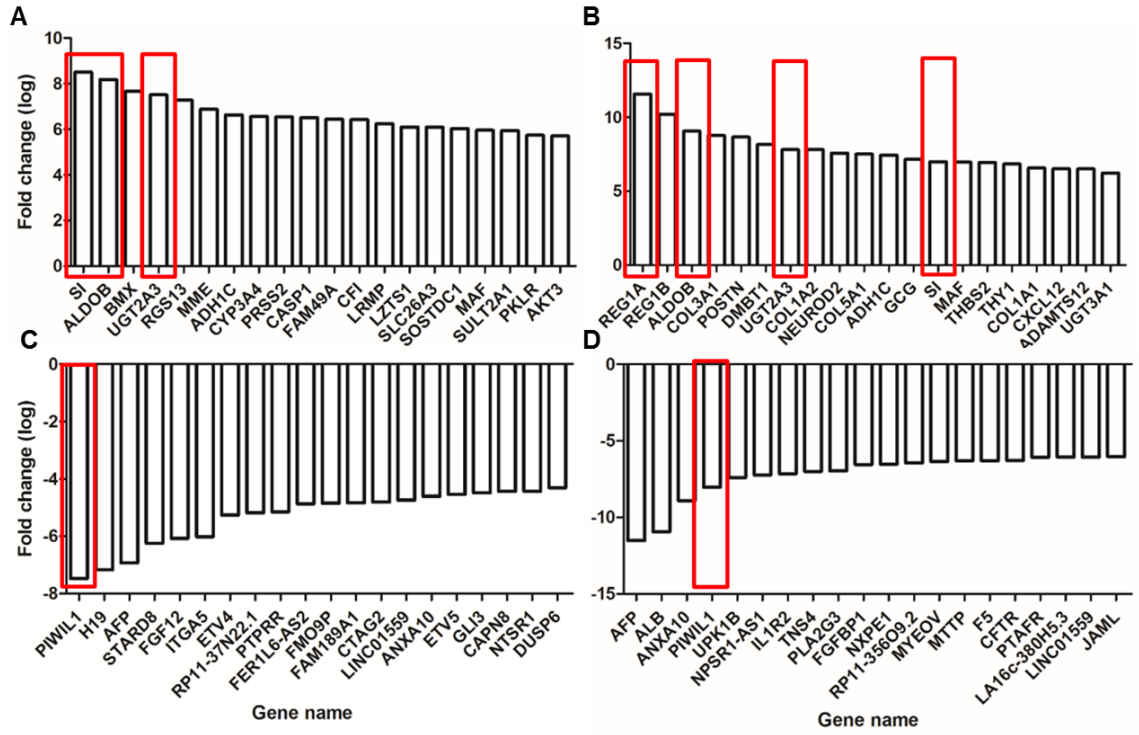

Figure 5.1. Genes of interest in drug-resistant SNU-16 and co-culture cells used for target validation. Upregulated genes in BGJ-resistant SNU-16 cells alone **(A)** and BGJ-resistant co-culture cells **(B)** that were interesting targets included SI, ALDOB and UGT2A3 which were found in both cancer cells alone and co-culture cells. Drug-resistant co-culture cells furthermore highly expressed REG1A, which was validated as well. PIWIL1 was both significantly downregulated in drug-resistant cancer cells alone **(C)** and co-culture cells **(D).**

5.2 Retinol pathway

The retinol pathway was identified as being significantly regulated using DAVID and GSEA, and was upregulated in SNU-16^{BGJR} cells **(Figure 4.23, Figure 4.31)**. To investigate the importance of the retinol pathway on the emergence of drug resistance in SNU-16 cells, cells were treated with *all-trans* retinoic acid (ATRA). We hypothesised that addition of ATRA to resistant cells would resensitise the drug resistant cancer cells given the effects on differentiation. Retinoic acid treatment has been connected to reduced motility of pancreatic stellate cells, resulting in reduced proliferation and increased apoptosis in pancreatic cancer cells (Froeling et al., 2011).

The effect of ATRA was analysed using cell cycle analysis with FACS, in MFE-296 cells **(Figure 5.2, Appendix Figure 8.44)**, SNU-16 parental cells **(Appendix Figure 8.45, Appendix Figure 8.46)** and BGJ-resistant SNU-16 cells **(Figure 5.3)**. Distinct subpopulations could be identified in MFE-296 cells and treatment of MFE-296 cells with BGJ led to an increase in cells in G1 phase and also increased sub G1 fraction, indicating cell cycle arrest and increased cell death. This was supported by a reduced number of cells in S and G2 phase, indicating fewer proliferating cells. However, ATRA treatment did not have a dramatic effect in MFE-296 cells, except a potential tendency to increase the fraction of cells in G2. In contrast, SNU-16 cells were highly sensitive to BGJ treatment, and also did not form homogenous populations as was observed with MFE-296 cells, hence posing a difficulty in data analysis. However, in respect to the G1 subpopulation, it could be concluded, that upon BGJ treatment, the G1 subpopulation slightly increases whereas the G2 subpopulation shows a tendency to decrease **(Appendix Figure 8.45)**. In response to ATRA, there was a tendency for a decrease in the G1 subpopulation **(Appendix Figure 8.46)**. Treatment of BGJ-resistant SNU-16 cells with ATRA did not show a clear indication on the effect of ATRA on cell cycle behaviour, with merely a tendency of a reduction of cells in S phase **(Figure 5.3)**.

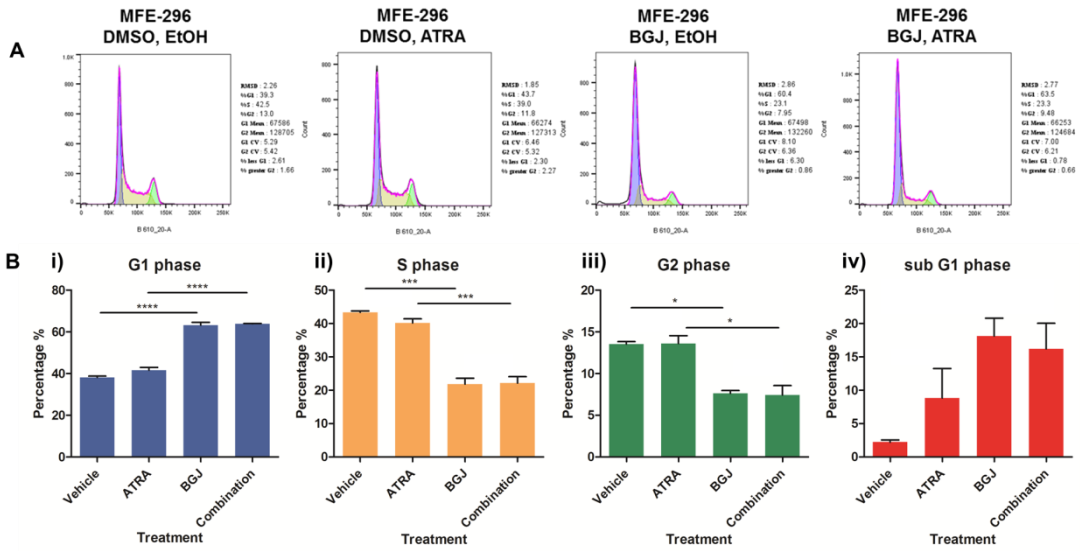

Figure 5.2. ATRA treatment in MFE-296 cells results in a shift to G1 and reduction in G2 and S phase. Endometrial MFE-296 cancer cells were plated into 6-well plates and treated with 1µM ATRA and 1.5µM BGJ and corresponding vehicle controls. After 72h cells were fixed in 70% Ethanol, followed by propidium iodide (PI) staining and cell cycle analysis using flow cytometry. Typical cell cycle profiles are shown for one of three individual biological replicates **(Appendix Figure 8.44)**. The histogram shows the values indicating the average proportion of cells in the different phases (G1=blue, S=yellow, G2=green, sub G1=red). The error bars indicate SEM. Statistical analysis was performed using one-way ANOVA analysis, p<0.05=*, p<0.01=**, p<0.005=***.

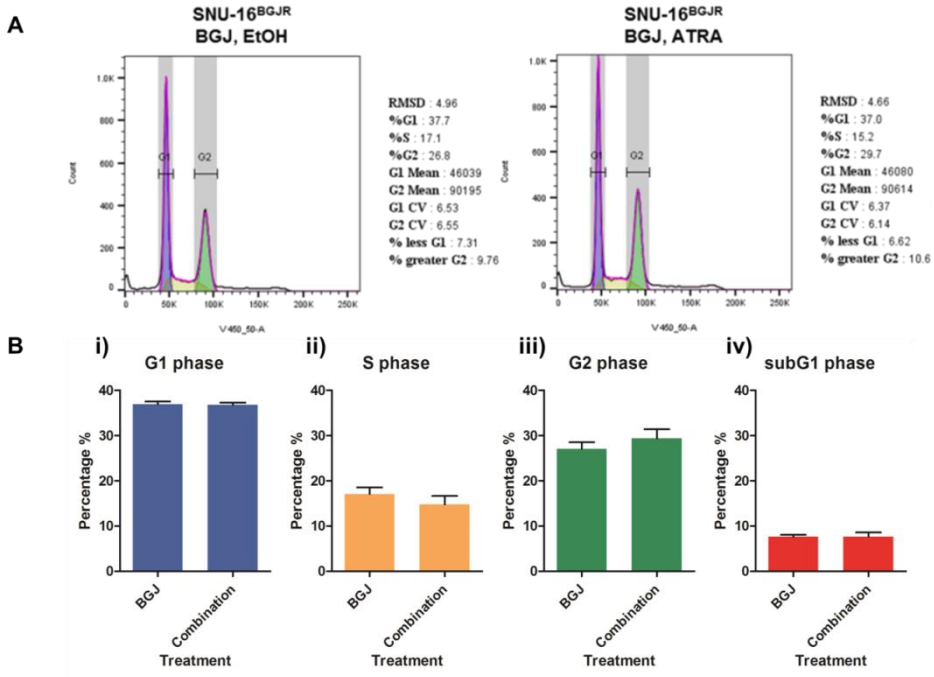

Figure 5.3. ATRA treatment of SNU-16^{BGJR} potentially reduces proliferation.
BGJ-resistant SNU-16 cancer cells were plated into 6-well plates and treated with 1µM ATRA and 1.5µM BGJ and corresponding vehicle controls. After 72h cells were fixed in 70% Ethanol, followed by DAPI staining and cell cycle analysis using flow cytometry. Typical cell cycle profiles are shown for one of three individual biological replicates **(Appendix Figure 8.47)**. The histogram shows the values indicating the average proportion of cells in the different phases (G1=blue, S=yellow, G2=green, sub G1=red). The error bars indicate SEM. Statistical analysis was performed using one-way ANOVA, p<0.05=*, p<0.01=**, p<0.005=***.

Another means to investigate the effect of compounds such as ATRA on cell behaviour is to measure the percentage apoptotic cells with Annexin V. This was done for SNU-16 and BGJ-resistant SNU-16 cells upon FGFR inhibition, where increased apoptotic and necrotic cells could be measured with BGJ treatment **(Appendix Figure 8.48)**. As retinoic acid is involved in the regulation of apoptosis, I was interested to investigate the effect of growing cells in the presence of ATRA and BGJ and measure apoptosis and necrosis in cells. MFE-296 cells in presence of ATRA, displayed less necrosis and cells showed less sensitivity to combination treatment, as indicated by increased live cell counts and decreased numbers of necrotic cells **(Figure 5.4)**.

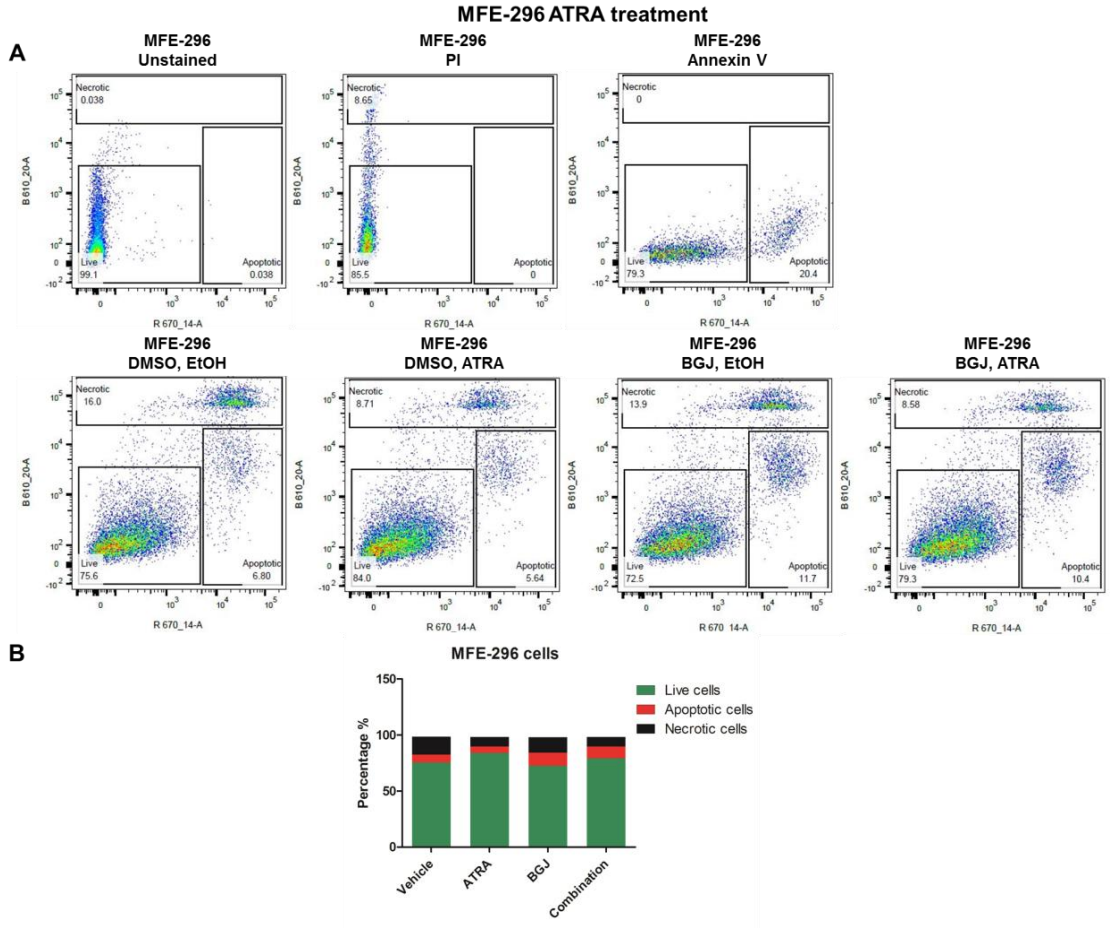

Figure 5.4. ATRA protects from cell death in absence of BGJ in endometrial cancer cells.
Endometrial MFE-296 cancer cells were cultured for 72h in 6-well plates in the presence of either 1µM ATRA, 1.5µM BGJ or a combination of the two, with respective vehicle controls, DMSO and EtOH. Apoptosis and necrosis were detected by staining cells with Annexin V and PI. Percentages of apoptotic, live and necrotic cells in the different conditions are shown. The experiment was performed once.

SNU-16 cells were sensitive to ATRA and BGJ treatment, with ATRA treatment resulting in higher numbers of apoptotic and necrotic cells **(Figure 5.5)**. Combination treatment potentiated this effect even further, as shown by even higher cell numbers undergoing apoptosis and necrosis compared to ATRA treatment alone and increased apoptosis compared to BGJ treatment alone.

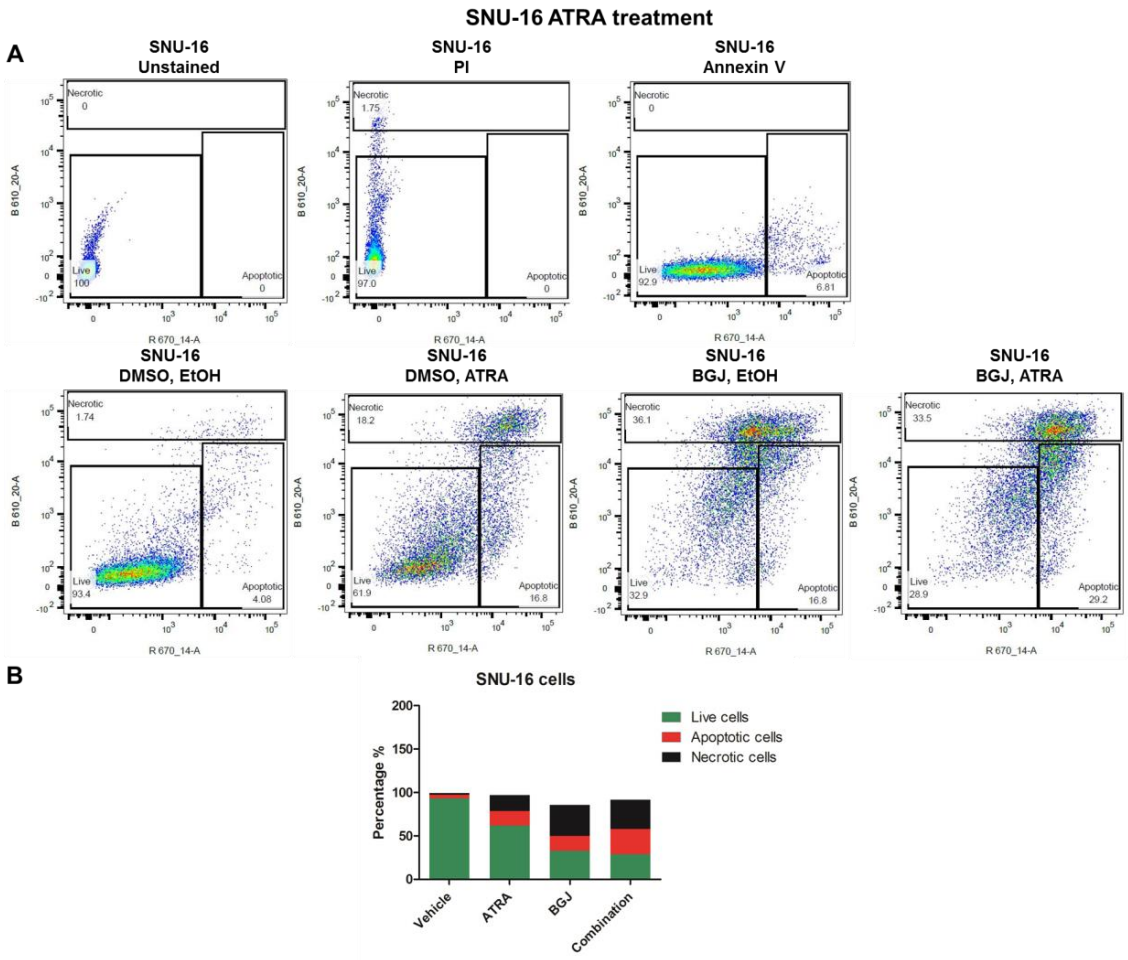

Figure 5.5. Combination treatment may potentiate apoptosis and necrosis in gastric cancer cells. Gastric parental SNU-16 cancer cells were grown in 6-well plates in the presence of either 1μM ATRA or 1.5μM BGJ with respective vehicle controls, DMSO and EtOH and in combination for 72h. Apoptosis and necrosis was detected by staining cells with Annexin V and PI. Percentages of apoptotic, live and necrotic cells in the different conditions are shown. The experiment was performed once.

BGJ-resistant SNU-16 cells did not respond to retinoic acid treatment and apoptotic and necrotic cell numbers were unchanged in BGJ and combination treated cells **(Figure 5.6)**. This could indicate that SNU-16^{BGJR} cells are not only resistant to BGJ but also ATRA.

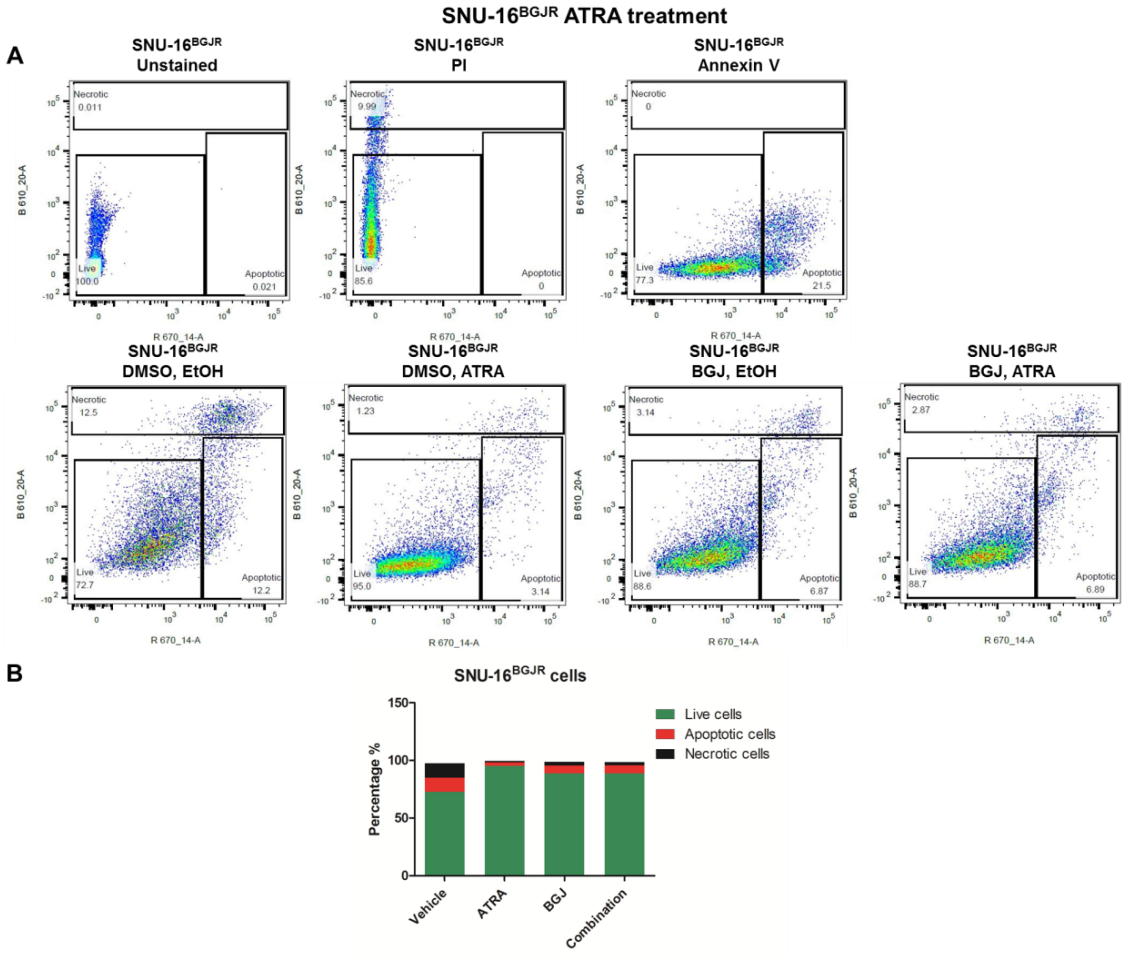

Figure 5.6. BGJ-resistant gastric cancer cells are insensitive to retinoic acid.
Gastric BGJ-resistant SNU-16 cancer cells were grown in 6-well plates in the presence of either 1μM ATRA or 1.5μM BGJ with respective vehicle controls, DMSO and EtOH and in combination for 72h. Apoptosis and necrosis was detected by staining cells with Annexin V and PI. Percentages of apoptotic, live and necrotic cells in the different conditions are shown. The experiment was performed once.

5.3 Sucrose and starch metabolism pathway

The sucrose metabolism pathway plays an important role in proliferation and growth and was one of the pathways significantly upregulated in the BGJ-resistant SNU-16 dataset generated in 3D. The main genes appearing to drive this pathway in cancer cells were *SI* and *ALDOB* **(Figure 5.7)**. *SI* was the top upregulated gene and encodes a glucosidase enzyme specific to the intestinal brush border, which functions in enzymatic cleavage of sucrose or maltose into glucose that is further used to generate energy in the form of ATP (Sim et al., 2010). After extensive literature search and discussion, one hypothesis was that the end product of the enzymatic reaction glucose could drive drug resistance in SNU-16 cells.

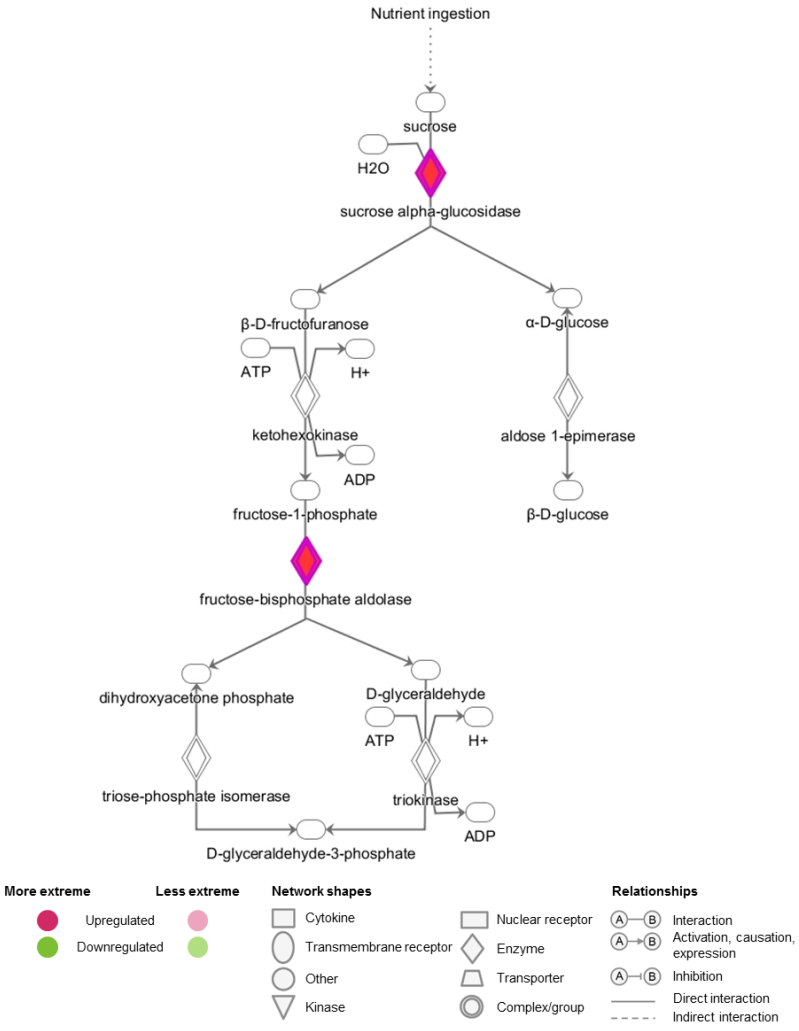

Figure 5.7. SI and ALDOB are significantly upregulated in the sucrose degradation pathway. Sucrose alpha-glucosidase (SI) and fructose-bisphosphate aldolase (ALDOB) are upregulated in SNU-16^{BGJR} cells generated in 3D causing an upregulation of the sucrose and starch degradation pathway.

If resistant cells upregulate glucose production, this would also mean that glucose transportation is increased. Therefore, expression of glucose transporter 1 (GLUT1) was measured with qPCR analysis in parental gastric cancer cells, SNU-16 treated with BGJ, and BGJ-resistant cancer cells. GLUT1 is encoded by *SLC2A1* and facilitates the transport of glucose across the plasma membrane. It is increased upon lower BGJ concentrations and dramatically increased in resistant cells **(Figure 5.8).**

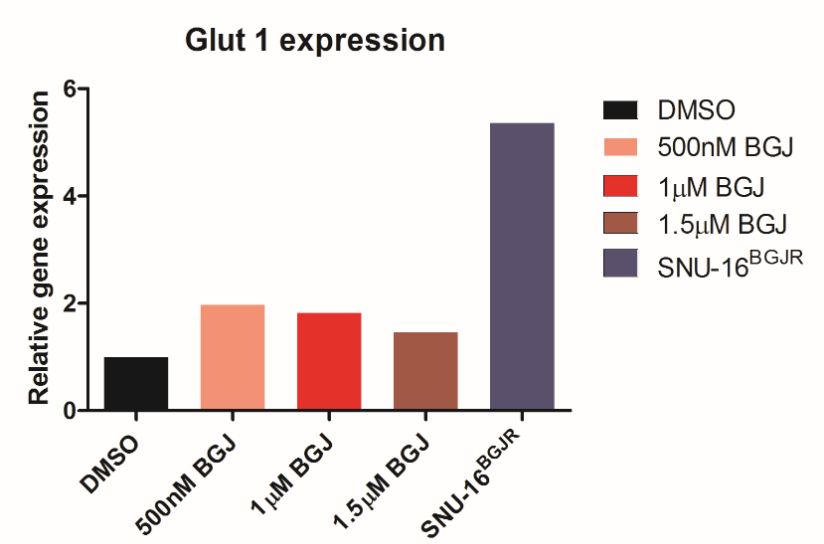

Figure 5.8. Glucose transport is elevated in drug-resistant gastric cancer cells.
RNA was harvested from SNU-16 treated with 500nM, 1μM and 1.5μM BGJ or treated with vehicle DMSO and SNU-16^{BGJR} kept in 1.5μM BGJ and reverse transcribed into cDNA, followed by qPCR analysis according to manufacturer's instructions.

In order to investigate a potential effect of glucose on the generation of resistant cells, medium without glucose supplements was purchased. First of all, cells were grown in normal medium and medium without glucose and cell numbers were counted using a light microscope **(Figure 5.9)**. SNU-16^{BGJR} cells generally proliferate faster than parental SNU-16 cells and growing the cells in medium without glucose had a more dramatic effect in parental SNU-16 cells compared to drug-resistant cells.

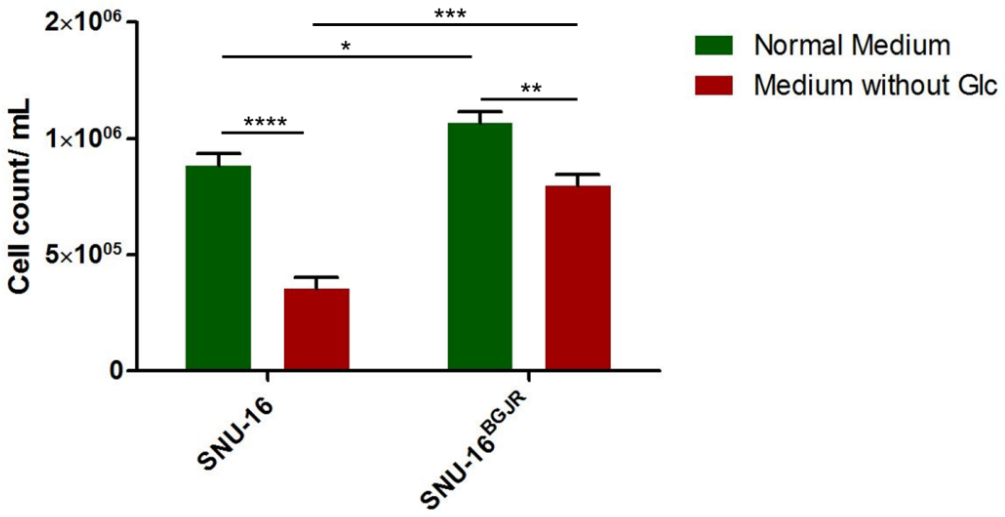

Figure 5.9. SNU-16^{BGJR} cells have a growth advantage in medium without glucose relative to parental cells.
Parental SNU-16 and SNU-16^{BGJR} cells were grown in medium with and without glucose. Cells were harvested after 3 days and counted with a haemocytometer. The experiment was run in biological triplicate. The error bars indicate SEM. Red bars indicate parental SNU-16 cell and green bars SNU-16^{BGJR} cells. Statistical analysis was performed using one-way ANOVA, $p<0.05$=*, $p<0.01$=**, $p<0.005$=***, $p<0.001$=****.

Cells were then exposed to different glucose concentrations by controlled addition of glucose to the medium, based on literature search for a low concentration (1g/L) and a high concentration (4g/L) (Huang and Xiong, 2015; Weil et al., 2009). The normal glucose concentration in complete growth medium (CM) is 2g/L and as a control also a condition without any glucose addition was included (0g/L). Cell growth was measured by cell counting. MFE-296 cells and SNU-16 cells were furthermore treated with different concentrations of BGJ (500nM, 1μM and 1.5μM). After growing the cells in medium with different glucose levels, cells were harvested and stained with DAPI or PI and cell cycle analysis was performed.

MFE-296 cells showed clearly distinct and uniform subpopulations **(Figure 5.10)**. In absence of glucose, the G2 subpopulation was generally smaller and increased upon increasing glucose concentration. Also, a shift towards the right on the horizontal axis with a larger S phase population in 1g/L and 2g/L glucose was observed. When BGJ was added to the cells, a decrease in cell counts of cells in G2 phase was observed. Upon glucose addition to the medium, cells proliferated more in drug compared to

without drug. Additionally, increased numbers of cells in G2 phase were counted, however the proportion did not increase significantly when adding a higher glucose concentration. SNU-16 cells tend to be more heterogeneous and subpopulations are not clearly defined, especially upon adding BGJ **(Appendix Figure 8.49)**. The same was also done with SNU-16^{BGJR} cells, however BGJ was kept at the final concentration used to generate drug-resistant cells (1.5μM). In drug-resistant cells, altering glucose concentration did not have an influence on cells in G1, S or G2 phase, however cell death was reduced in medium containing glucose compared to medium without glucose **(Figure 5.11)**. Therefore, it can be concluded that addition of glucose increases the number of proliferating cells, as seen in MFE-296 cells, and potentially reduces cell death in BGJ resistant cells. SNU-16 cells seem to perform better under higher glucose concentrations, however no clear conclusions can be drawn as different populations cannot be separated due to their heterogeneity upon glucose and inhibitor treatment.

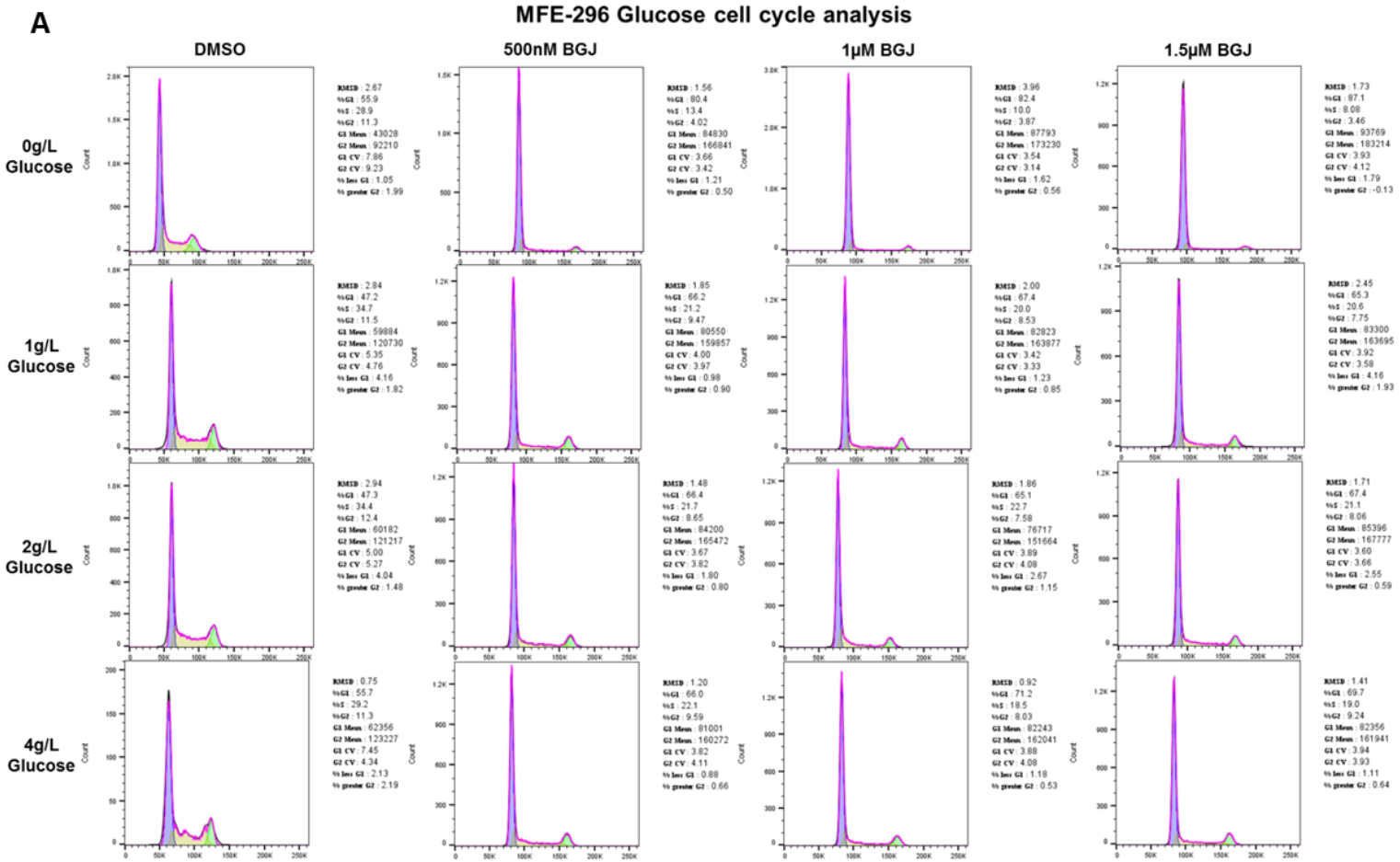

Figure 5.10. MFE-296 cells proliferate best under normal glucose concentrations.
MFE-296 cells were seeded into 6 well-plates and grown in medium with either no glucose, 1, 2 or 4g/L glucose and either 500nM, 1μM and 1.5μM BGJ or vehicle control DMSO. After 72h cells were fixed in 70% Ethanol, followed by PI staining and cell cycle analysis using flow cytometry. The histograms show the cell counts as peaks demonstrating the distinct subpopulations **(A)**.

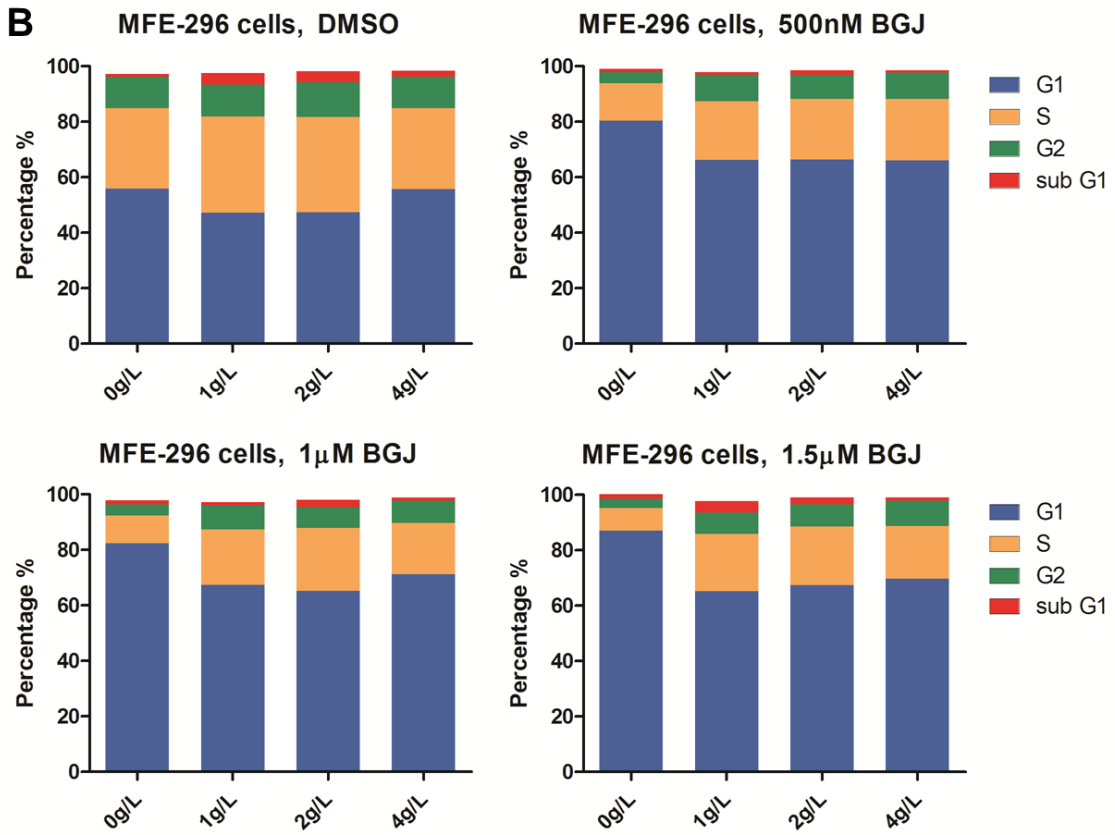

Average proportion of cells in the different phases were calculated with GraphPad Prism 5 (G1=blue, S=yellow, G2=green, sub G1=red) **(B)**. This experiment was performed once.

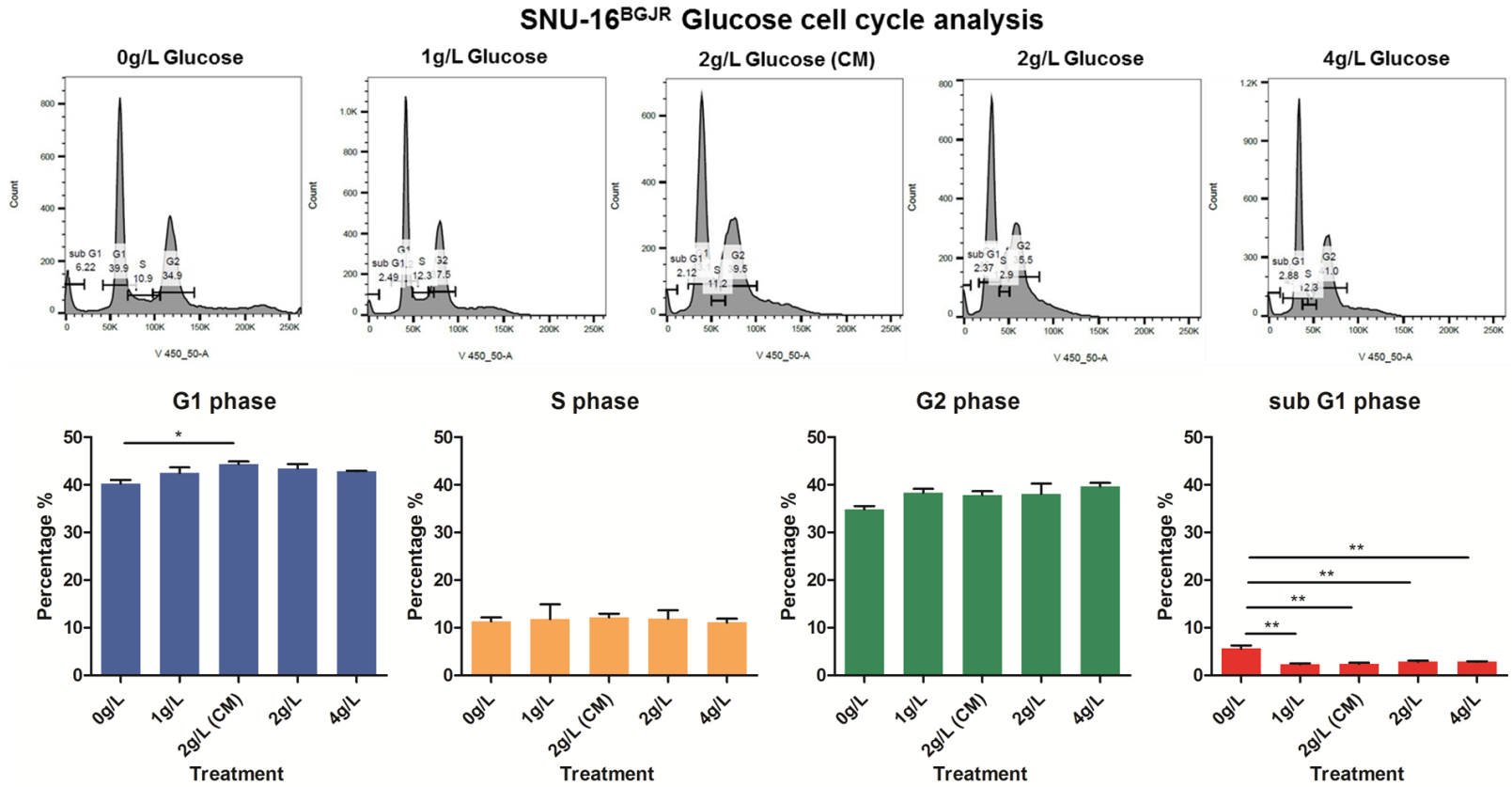

Figure 5.11. Glucose supplementation reduces SNU-16^{BGJR} cell death.
BGJ-resistant cells were seeded in medium without glucose and supplemented with 0, 1, 2 and 4g/L glucose and 1.5µM BGJ. As a control a condition was included were cells were grown in normal complete growth medium (CM). After 72h cells were fixed in 70% Ethanol, followed by PI staining and cell cycle analysis using flow cytometry. This figure is a representation of three individual experiments **(Appendix Figure 8.50)** with error bars indicating SEM. The histogram shows the values indicating the average proportion of cells in the different phases (G1=blue, S=yellow, G2=green, sub G1=red). Statistical analysis was performed using one-way ANOVA, $p<0.05$=*, $p<0.01$=**, $p<0.005$=***.

SNU-16 cells grown in different glucose concentrations were analysed by Western blot **(Figure 5.12)**. No bands were observed for p-AKT, which was however observed previously with this cell type. Interestingly, p-ERK signalling was dramatically reduced at 2g/L and 4g/L glucose concentrations compared to low glucose concentrations.

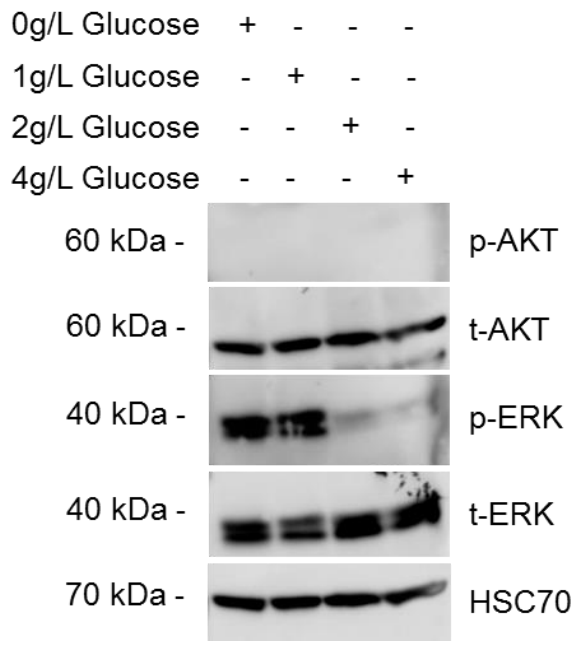

Figure 5.12. MAPK signalling is increased in low glucose concentrations compared to higher glucose levels.
SNU-16 cells were grown in medium with different glucose concentrations and without glucose and grown for 72h followed by Western blot analysis. p-AKT signalling could not be measured however p-ERK signalling was reduced in SNU-16 cells grown in medium supplemented with 2 and 4g/L glucose.

Increasing glucose concentration did increase proliferation significantly, and was not strongly indicative for an involvement in drug resistance. Therefore, instead of adding glucose, which is the final product of the enzymatic cleavage through SI, to the cells, it was hypothesised that addition of the substrate of SI (sucrose) might affect resistance. As before, different concentrations were used; adding no sucrose, 1g/L, 2g/L and 4g/L sucrose to the medium and counting cells and also FACS analysis for Annexin V, to measure apoptosis and necrosis in cells.

In normal medium containing glucose, resistant cells appeared to proliferate more with higher sucrose concentration **(Figure 5.13).** Adding 1g/L sucrose to the medium doubled cell numbers, whereas further addition of sucrose increased cell numbers only slightly more. Compared to resistant cells, parental cells seem to show no indicative trait in respect to sucrose concentration **(Figure 5.14)**. When parental cells were treated with an FGFR inhibitor however, cells performed better with higher sucrose concentrations in the medium, as shown by a steady increase in cell number **(Figure 5.14)**.

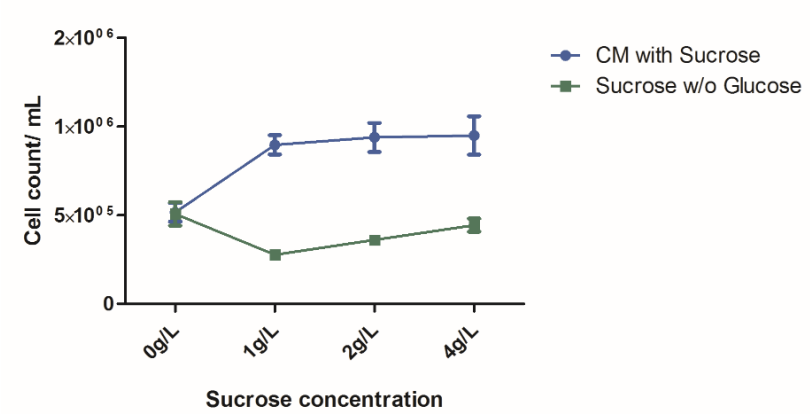

Figure 5.13. BGJ-resistant cells perform better in medium with glucose and sucrose.
Drug-resistant SNU-16 cells were grown in 6-well plates in medium with and without glucose and exposed to 0, 1, 2 or 4g/L sucrose in absence of glucose in the medium. After 72h cells were harvested and counted with Trypan blue and a haemocytometer with a light microscope. The graph represents three biological replicates. The error bars indicate SEM. CM=complete growth medium.

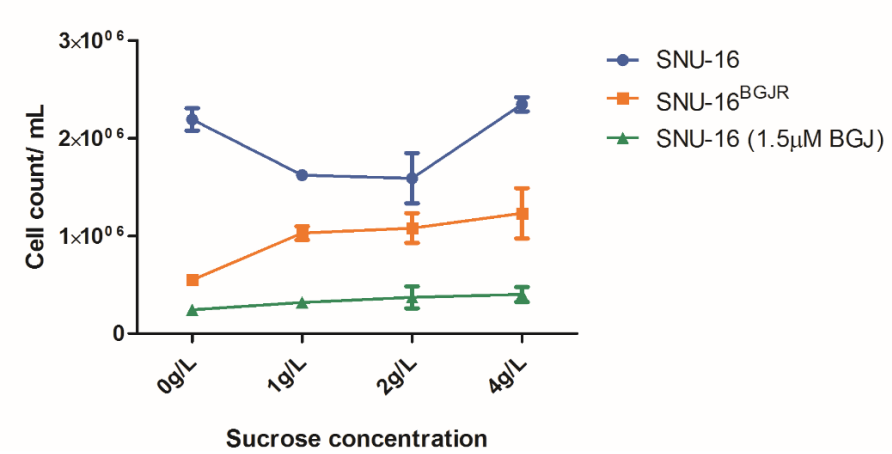

Figure 5.14. SNU-16 cells and SNU-16^{BGJR} cells proliferate more in high Sucrose levels.
Parental and drug-resistant SNU-16 cells were grown in 6-well plates and exposed to 0, 1, 2 or 4g/L sucrose. Additionally parental cells were exposed to 1.5µM BGJ and drug-resistant SNU-16 cells were kept in 1.5µM BGJ. After 72h cells were harvested and counted with Trypan blue and a haemocytometer with a light microscope. The graph represents three biological replicates with error bars indicating SEM.

Parental cells were then treated with different concentrations of BGJ in the presence of sucrose and cell growth was compared **(Figure 5.15)**. Treating cells with BGJ decreased cells numbers in all three drug concentrations (500nM, 1μM and 1.5μM) and increasing sucrose concentration in BGJ-treated cells resulted in higher cell counts. In the vehicle-treated condition, cell growth increased with higher sucrose concentration, except for the highest concentration, possibly due to overcrowding of cells and insufficient nutrient supply.

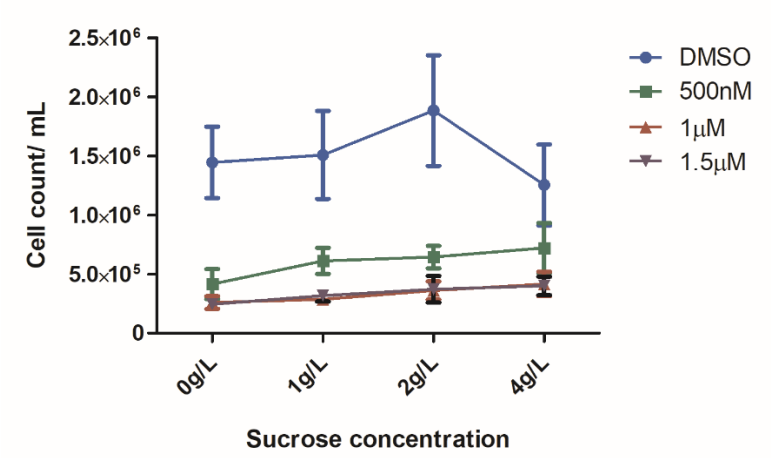

Figure 5.15. SNU-16 cells treated with BGJ survive better with higher sucrose levels.
SNU-16 cells were grown in 6-well plates and treated with 500nM, 1μM or 1.5μM BGJ or vehicle control DMSO. After 72h cells were harvested and cell numbers were counted with trypan blue and a haemocytometer with a light microscope. The graph represents biological triplicate and error bars indicate SEM.

SNU-16 cells were grown in the presence of different sucrose concentrations and protein expression was measured by Western blot **(Appendix Figure 8.51)**. p-ERK levels were unchanged with different sucrose concentrations, however p-AKT levels dropped at higher sucrose levels. Simultaneously, SNU-16 parental and BGJ-resistant cells were run on the same gel to compare protein expression **(Figure 5.16)**. Compared to parental cells, p-AKT signalling was increased in resistant cells and did not decrease with increased sucrose levels, in contrast to the parental cells. However, p-ERK signalling in SNU-16^{BGJR} cells was reduced compared to parental cells.

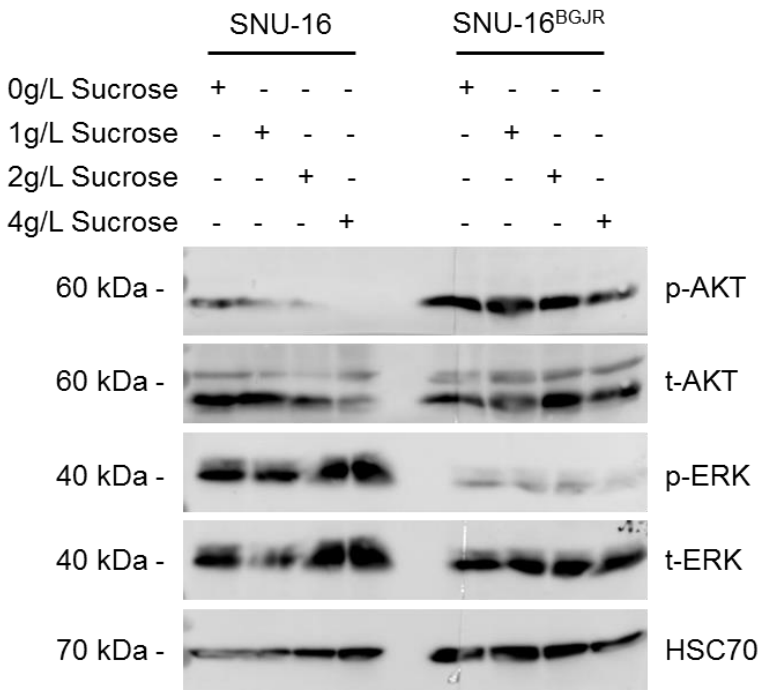

Figure 5.16. Signalling in SNU-16 and SNU-16^{BGJR} cells grown in medium containing different levels of sucrose.
Parental and BGJ-resistant SNU-16 cells were exposed to medium containing 0, 1, 2 and 4g/L sucrose and grown for 72h followed by Western blot analysis. Protein expression of p-AKT, t-AKT, p-ERK, t-ERK and HSC70 was analysed.

The effects on cell numbers in SNU-16 and SNU-16^{BGJR} cells raised the question if it is caused by upregulation of SI and if upregulation actually results in increased activity. As SI is involved in sucrose degradation, and hence generation of glucose, the effects of SI inhibition were investigated. There are no specific SI inhibitors available, however acarbose has been previously described to inhibit the sucrase subunit of the enzyme with reduced activity towards the isomaltase subunit. Acarbose is a pseudo-tetrasaccharide with an amine group instead of a hydroxyl group and competitively interacts with SI and therefore inhibits the generation of glucose by inhibition of the enzymatic cleavage of sucrose **(Figure 5.17)**. It was therefore anticipated that acarbose treatment of cells would have an effect on sensitivity of cancer cells when treating with kinase inhibitors such as BGJ. Cells were exposed to 14μM acarbose, based on the literature (Lee et al., 2012; Mohan et al., 2014). Combination of sucrose and acarbose treatment of SNU-16 cells resulted in lower cell numbers in high sucrose concentrations compared to growing cancer cells in sucrose alone **(Figure 5.18)**. Simultaneously, cell viability of parental SNU-16 and drug-resistant SNU-16 cells to

acarbose was assessed, exhibiting a minor reduction in cell viability with increasing acarbose concentration **(Appendix Figure 8.52)**. The same was also observed in H520 lung cancer cells **(Appendix Figure 8.53)**.

When treating parental SNU-16 cells with different acarbose concentrations, a reduction in cell number was observed in cells grown in medium without glucose but different sucrose concentrations **(Figure 5.19)**.

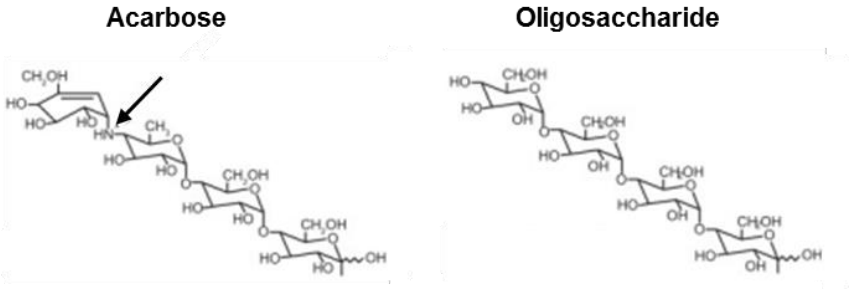

Figure 5.17. Acarbose competitively inhibits α-glucosidase SI.
Acarbose is a pseudotetrasaccharide and is structurally similar to oligosaccharides. Acarbose however harbours an amine group whereas oligosaccharides have an extra ether group. It competitively inhibits α-glucosidases such as SI that are located in the brush border of the small intestine and therefore delaying glucose absorption by decreasing the breakdown of complex carbohydrates (Rosak and Mertes, 2012).

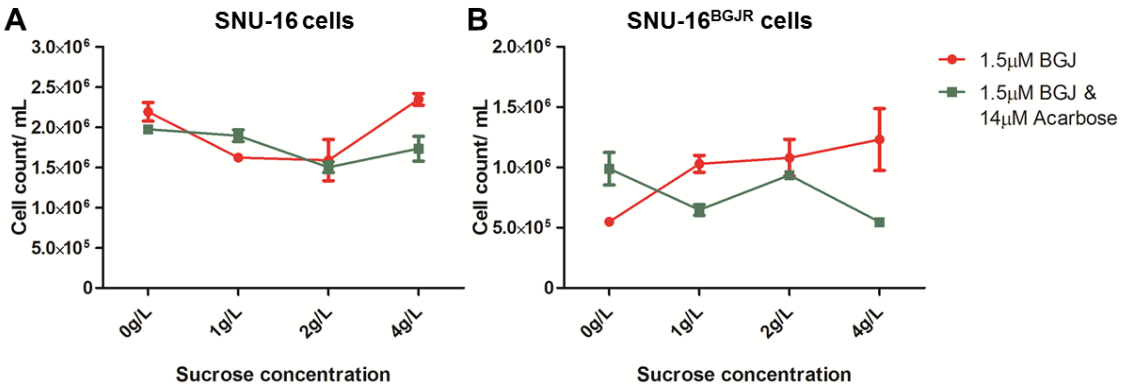

Figure 5.18. Acarbose decreases cell number of parental and drug-resistant cells in high sucrose levels.
Parental **(A)** and drug-resistant SNU-16 **(B)** cells were grown in 6-well plates and exposed to 0, 1, 2 or 4g/L sucrose with and without 14µM Acarbose supplemented in the medium. After 72h cells were harvested and counted with Trypan blue and a haemocytometer with a light microscope. The graph represents three biological replicates. The error bars indicate SEM.

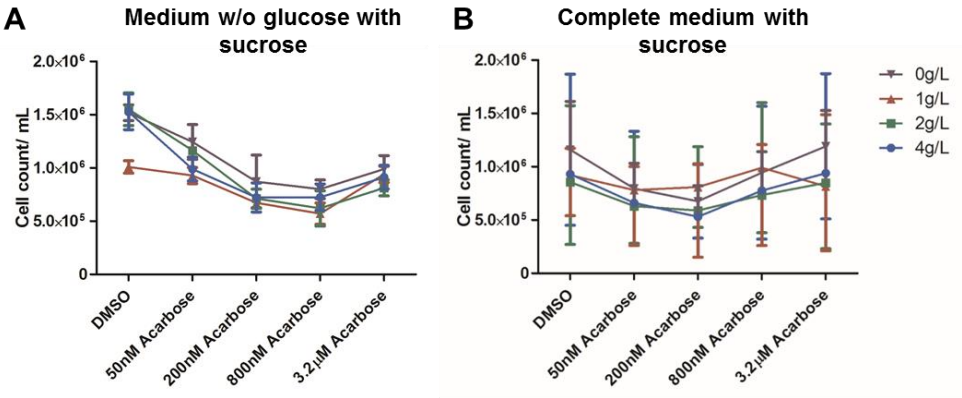

Figure 5.19. Acarbose treatment of SNU-16 cells reduces cell numbers in medium without glucose with increasing sucrose levels.
Parental SNU-16 cells were grown in 6-well plates and exposed to 0, 1, 2 or 4g/L sucrose with either 50nM, 200nM, 800nM or 3.2µM Acarbose in medium without glucose **(A)** or complete growth medium **(B)**. After 72h cells were harvested and counted with Trypan blue and a haemocytoemter with a light microscope. The graphs represent three biological replicates with error bars indicating SEM.

To investigate if acarbose can inhibit SI and therefore inhibit drug-resistant SNU-16 cells, live, apoptotic and necrotic cells were counted by FACS **(Figure 5.20)**. The same drug concentrations as with the parental SNU-16 cells were used. Treatment of cells with different acarbose concentrations however did not result in a higher number of apoptotic and necrotic cells. As acarbose inhibits SI by competitive inhibition of the intestinal enzymatic hydrolysis of oligosaccharides, it was hypothesised that sucrose needs to be present to see an effect in SI inhibition. Thus, cells were also grown in sucrose and acarbose together to see if they influence each other and again apoptosis and necrosis were measured **(Figure 5.22)**. In parental SNU-16 cells, combining sucrose and acarbose resulted in a slight decrease in apoptotic and necrotic cells with high sucrose levels. However, this effect was also observed in vehicle-treated cells **(Figure 5.21).** In drug-resistant cells, acarbose treatment resulted in higher apoptotic and necrotic cells in low sucrose levels and also slightly more in high sucrose levels **(Figure 5.22)**. Low acarbose levels increased apoptotic cells, whereas high acarbose concentration lowered apoptotic cells counts but increased necrosis.

Analysis of SI protein expression was performed with the research group of Dr. Hassan Naim (University of Veterinary Medicine Hannover), who developed an antibody against SI, as other SI antibodies are not highly specific, however no clear bands could be observed **(Appendix Figure 8.54)**.

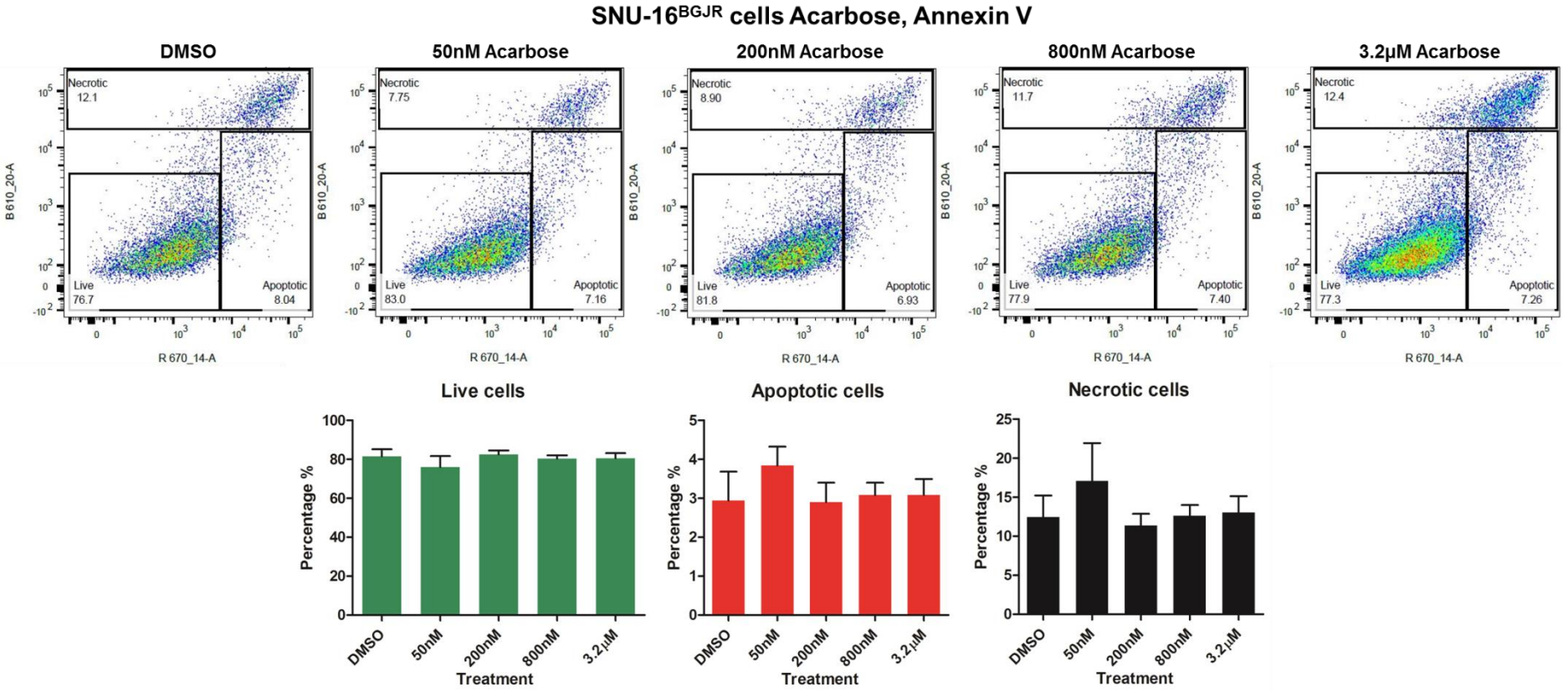

Figure 5.20. Acarbose treatment of SNU-16^{BGJR} cells does not induce apoptosis.
BGJ-resistant cells were seeded into 6-well plates in medium containing different sucrose concentrations and treated with 50nM, 200nM, 800nMm or 32µM acarbose or vehicle and grown for 72h followed by fixation and Annexin V staining. The graphs show representative images of the scatter plots of three individual experiments **(Appendix Figure 8.55)**. Live, apoptotic and necrotic cells are shown as a histogram with error bars indicating SEM.

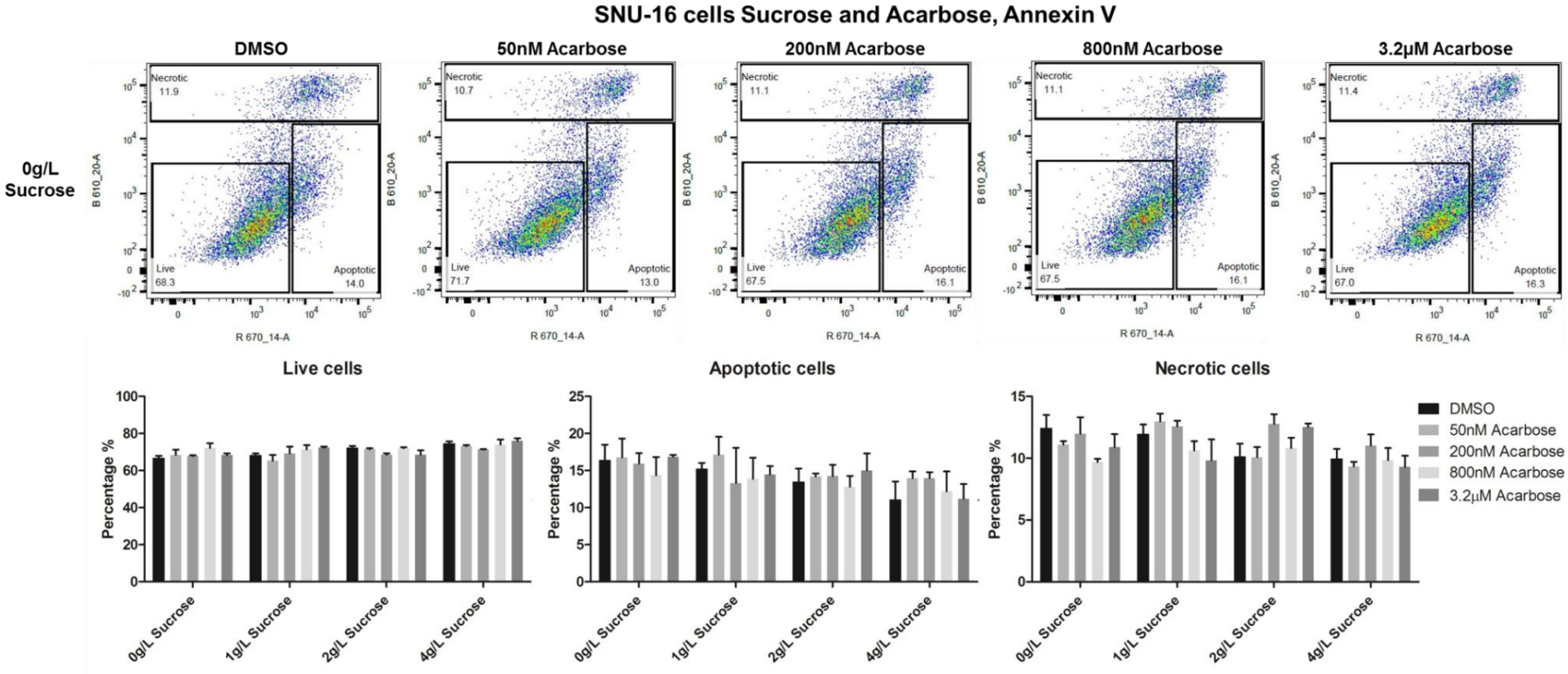

Figure 5.21. High sucrose levels reduce cell death in parental gastric cancer cells.
Parental cells were seeded into 6-well plates in medium containing different sucrose concentrations and treated with 50nM, 200nM, 800nMm or 32µM acarbose or vehicle and grown for 72h followed by fixation and Annexin V staining. The graphs show representative images of the scatter plots of three individual experiments of the condition without sucrose (the rest of the sucrose concentrations are in the appendix) **(Appendix Figure 8.56-Appendix Figure 8.58)**. Live, apoptotic and necrotic cells are shown as a histogram with error bars indicating SEM.

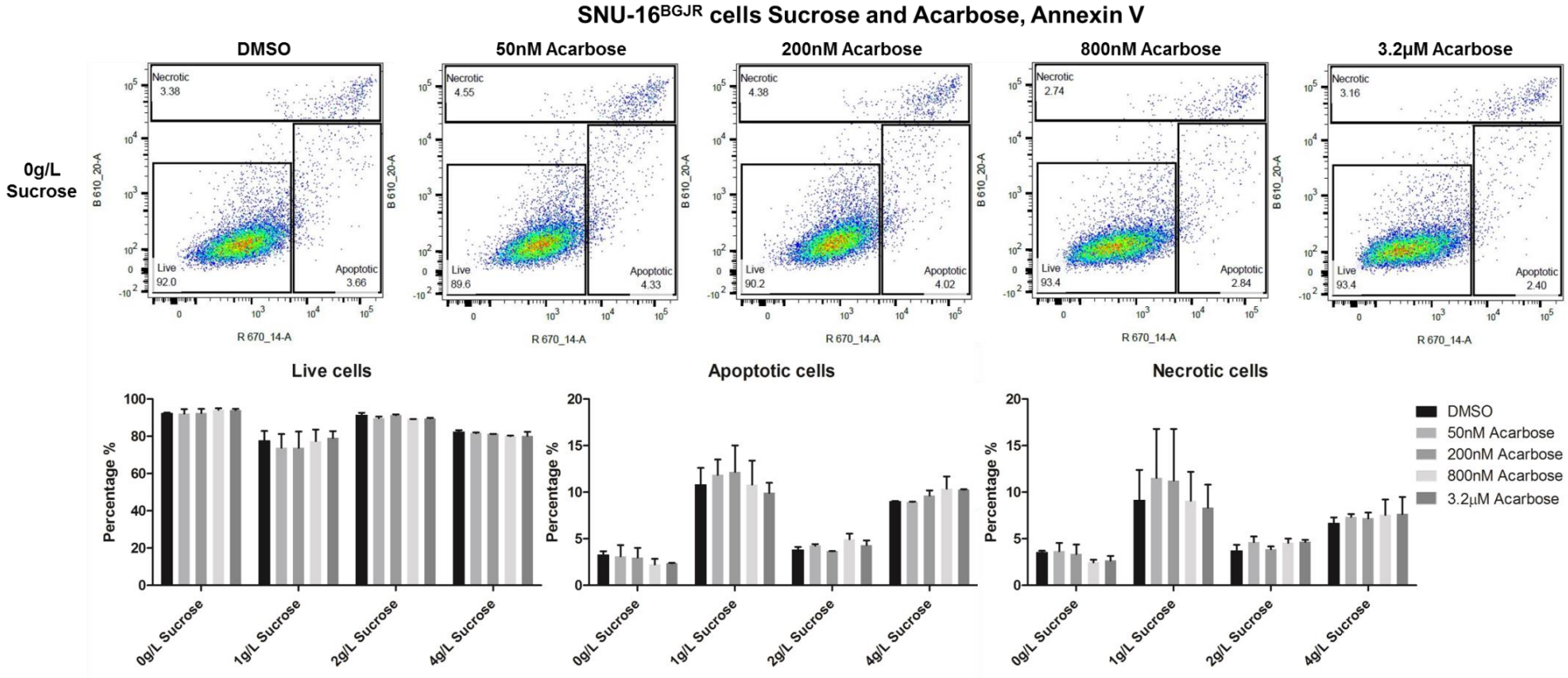

Figure 5.22. Drug-resistant SNU-16 cells are more sensitive at low sucrose levels.
BGJ-resistant cells were seeded into 6-well plates in medium containing different sucrose concentrations and treated with 50nM, 200nM, 800nMm or 32µM acarbose or vehicle and grown for 72h followed by fixation and Annexin V staining. The graphs show representative images of the scatter plots of two individual experiments of the scatter plots of the condition without sucrose (the rest of the sucrose concentrations are in the appendix) **(Appendix Figure 8.59)**. Live, apoptotic and necrotic cells are shown as a histogram with error bars indicating SEM.

In addition to upregulation of *SI*, *ALDOB* was also upregulated significantly and the second most upregulated gene in drug-resistant gastric cancer cells without stromal support. As SI is upregulated it could be that ALDOB has to be upregulated subsequently to break down fructose at a similar pace as SI breaks down sucrose, so that it does not have toxic effects on cells. Therefore, I hypothesised that ALDOB blockade would lead to accumulation of fructose-1-phosphate (F-1-P), which is toxic for cells (Ali et al., 1998; Tran, 2017). TDZD-8, a selective non-ATP competitive inhibitor of glycogen synthase kinase 3 (GSK 3β), was used to treat cancer cells to inhibit ALDOB activity (Grandjean et al., 2016). Inhibition of ALDOB would therefore lead to a block in the transformation of fructose into glyceraldehyde and dihydroxyacetone phosphate (DHAP), resulting in the accumulation of F-1-P, which is highly toxic for cells resulting in cell death **(Figure 5.23)**.

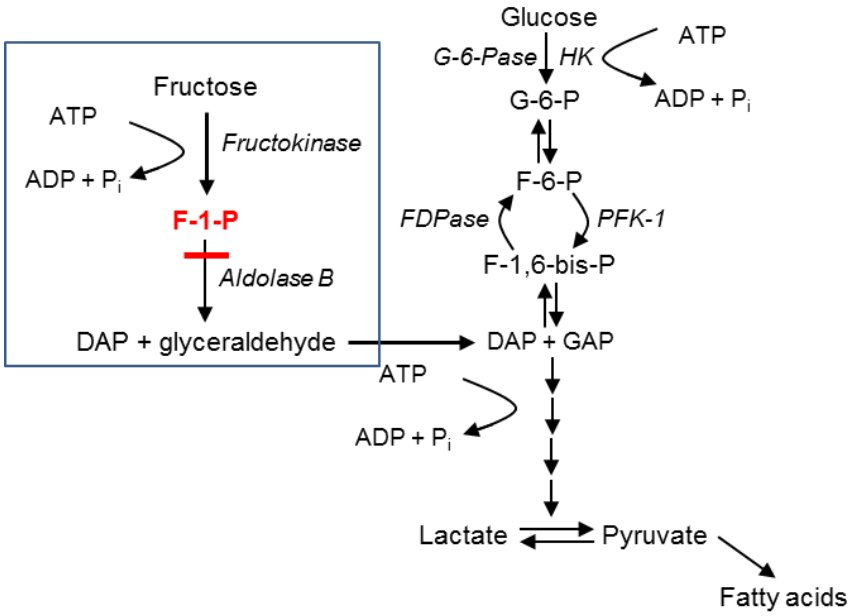

Figure 5.23. F-1-P accumulation in the fructose metabolism results in cell death.
Fructose is phosphorylated to fructose-1-phosphate (F-1-P) by fructokinase. F-1-P then undergoes hydrolysis by aldolase B (ALDOB) to form dihydroxyacetone phosphate (DHAP) and glyceraldehyde. These trioses then either enter the gluconeogenic pathway for glycogen replenishment or the complete metabolism in the fructolytic pathway to pyruvate, which enters the Krebs cycle, and is converted to citrate and subsequently directed toward *de novo* synthesis of fatty acids. The absence of ALDOB results in the accumulation of F-1-P, which following fructose ingestion inhibits glycogenolysis and gluconeogenesis resulting in fatal liver failure. Inhibition of ALDOB therefore results in less available glucose (adpated from Charrez et al., 2015).

When treating cells with TDZD-8, BGJ-resistant cells appeared to be more sensitive towards the drug compared to parental SNU-16 cells **(Figure 5.24)**. Cell viability decreased more in drug-resistant gastric cancer cells as TDZD-8 concentration increased.

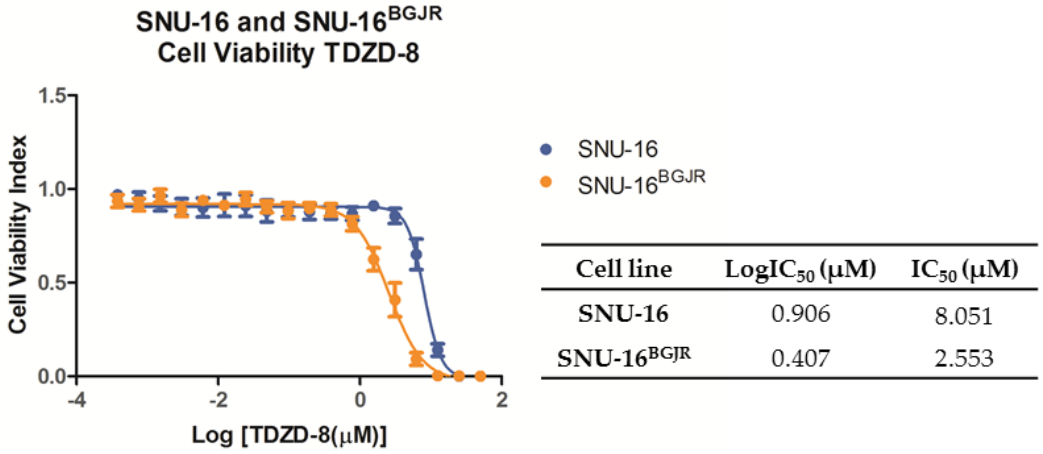

Cell line	LogIC$_{50}$ (μM)	IC$_{50}$ (μM)
SNU-16	0.906	8.051
SNU-16^{BGJR}	0.407	2.553

Figure 5.24. Drug-resistant SNU-16 cells are more sensitive to TDZD-8 than parental cells.

Parental and BGJ-resistant SNU-16 gastric cancer cells were plated in triplicate into 96-well plates and exposed to TDZD-8 concentrations ranging from 0.38nM to 50μM. Control cells were treated with DMSO and as a background control 1% Staurosporine was added to wells containing cells. After 72h the cell viability index was measured and values plotted on a graph. The curves represent an average of 6 biological replicates per cell line with error bars indicating SEM. LogIC$_{50}$ and IC$_{50}$ values were calculated in GraphPad Prism 5.

To determine whether TDZD-8 induces cancer cell death, cells were subjected to Annexin V staining followed by flow cytometry analysis. Proportions of cells undergoing apoptosis and necrosis were similar between parental and drug-resistant cells **(Appendix Figure 8.60, Appendix Figure 8.61)**. At the highest TDZD-8 concentration, in SNU-16^{BGJR}, a slight increase in apoptotic cells was observed, whereas in parental cells no change was observed.

To investigate if there is a synergistic effect of inhibition of SI and ALDOB, acarbose and TDZD-8 were combined and BGJ-resistant cells were treated with a range of concentrations followed by cell viability analysis **(Figure 5.25)**. The curves however look quite similar and there is no evident shift, although it could be hinted at the combination treatment rendering cells slightly more sensitive.

As before also apoptosis and necrosis was investigated in drug-resistant cells treated with either sucrose or acarbose in conjunction with TDZD-8. However as with cell viability, no clear effect can be seen in combination treated cells.

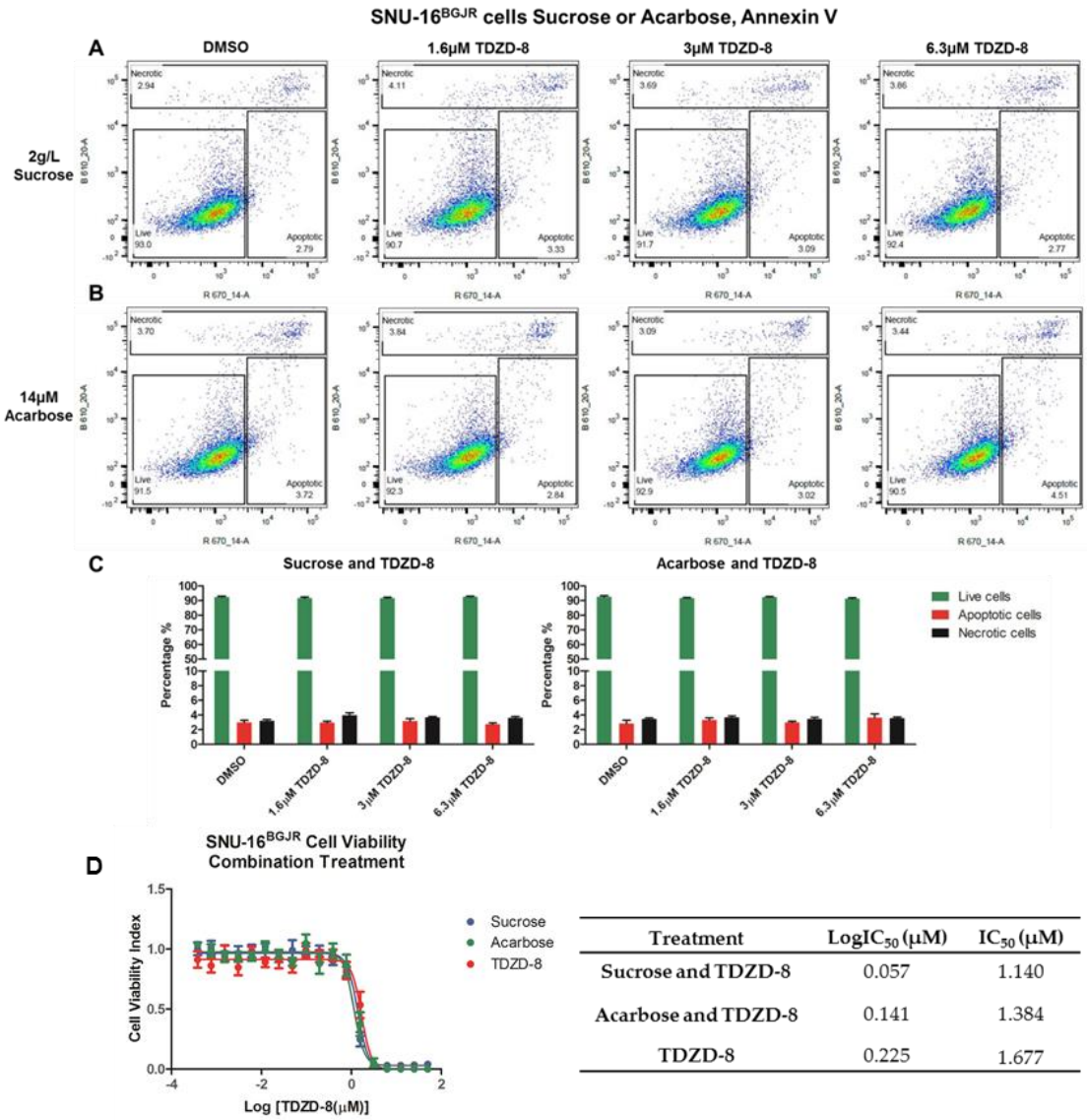

Treatment	LogIC$_{50}$ (µM)	IC$_{50}$ (µM)
Sucrose and TDZD-8	0.057	1.140
Acarbose and TDZD-8	0.141	1.384
TDZD-8	0.225	1.677

Figure 5.25. Drug-resistant SNU-16 cells cannot be efficiently killed using combination treatment. SNU-16^{BGJR} cells were seeded into 6-well plates in medium containing either 2g/L sucrose **(A)** or 14 µM acarbose **(B)** and treated with 1.6µM, 3µM, 6,3µM or vehicle. Apoptosis and necrosis was investigated by staining cells with Annexin V and PI and analysed using flow cytometry. The graphs represent three individual experiments. Apoptotic, live and necrotic cells are displayed as histograms with error bars indicating SEM **(C)**. Drug-resistant SNU-16 cells were either treated with sucrose (2g/L) or acarbose (14µM) and a range of TDZD-8 concentrations. The experiments were performed in biological triplicate **(Appendix Figure 8.62)**.

5.4 PIWIL1 overexpression potentially resensitises drug-resistant gastric cancer cells

PIWIL1 was the gene that was downregulated the most in the SNU-16 dataset and is also among the most downregulated genes in drug-resistant co-culture cells. Reduced PIWIL1 expression has been associated with worse prognosis and PIWIL1 proteins have been linked to hallmarks of cancer such as deregulated cell proliferation, altered apoptosis, genomic instability, invasion, and metastasis (Tan et al., 2015). PIWIL1 was extensively studied and through literature search a research group was identified who generously provided an overexpression plasmid containing PIWIL1 (Lim et al., 2014). PIWIL1 was inserted into the KOZAK cassette of a pcDNA3.1 plasmid **(Appendix Figure 8.63)**. Cells were transfected with the plasmid containing PIWIL1 and SNU-16^{BGJR} transfected with PIWIL1 exhibited a tendency to reduce cell numbers compared to SNU-16^{BGJR} cells transfected with the control empty vector **(Figure 5.26)**.

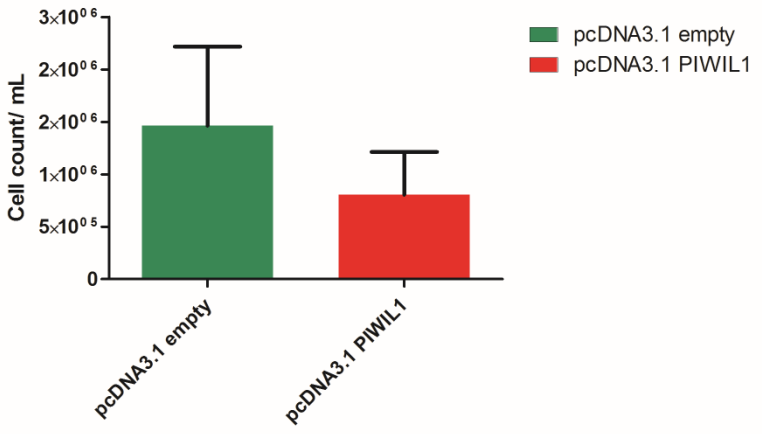

Figure 5.26. PIWIL1 overexpression shows a tendency to reduce cell numbers.
Drug-resistant cells were seeded into 6-well plates and transfected with either pcDNA3.1 with an empty vector or pcDNA3.1 containing PIWIL1. Cells were then counted using a light microscope. Error bars indicate SEM and the experiment was performed in biological triplicate.

Therefore it was investigated if PIWIL1 overexpression would induce apoptosis in cells and the proportion of cells undergoing apoptosis and necrosis was investigated **(Figure 5.27)**. PIWIL1 transfection did not alter apoptotic and necrotic cell counts.

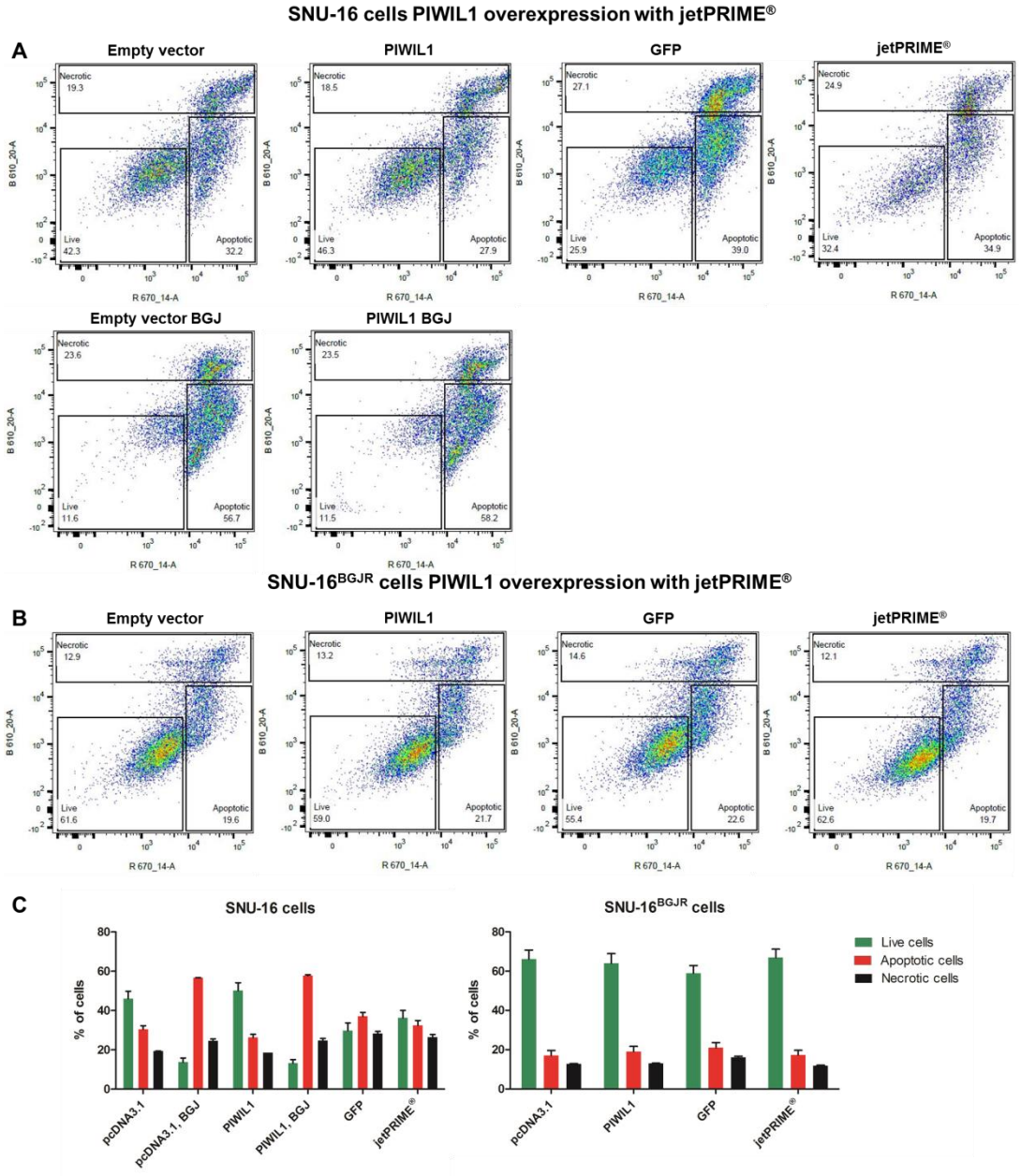

Figure 5.27. PIWIL1 overexpression does not induce apoptosis in drug-resistant cells.
Parental SNU-16 **(A)** and SNU-16^{BGJR} **(B)** cells were seeded into 6-well plates and transfected with plasmids containing an empty vector or PIWIL1 and as a control for transfection with a plasmid containing GFP and with the transfection reagent only. Apoptosis and necrosis was investigated by staining cells with Annexin V and PI and analysed using flow cytometry. The graphs represent three individual experiments. Apoptotic, live and necrotic cells are displayed as histograms **(C)** with error bars indicating SEM. PIWIL1 was also transfected with Lipofectamine® in another experiment **(Appendix Figure 8.64)**.

5.5 *REG1A* and *collagen* genes potentially influence drug resistance in co-culture cells

REG1A was the most upregulated gene in drug-resistant co-culture cells. REG1A is a growth factor involved in tissue regeneration and proliferation in the mucosa of the gastrointestinal tract. It is known to affect pancreatic β cells and has been observed in various malignant tumours (Geng et al., 2017; Hayashi et al., 2008; Kimura et al., 1992; W.-S. Lee et al., 2008; Minamiya et al., 2008; Motoyama et al., 2006; Sasaki et al., 2008; Sekikawa et al., 2008; Yoshino et al., 2005).

Sections from the 3D resistance RNA-Seq experiment were stained with REG1A antibody **(Appendix Figure 8.65)**. Sections with the drug-resistant co-culture possibly reveal a stronger REG1A staining compared to vehicle-treated co-culture cells. To investigate the importance of REG1A in drug-resistant cells, REG1A was knocked-down lentivirally using shRNAs both in drug-resistant SNU-16 and HFF2 cells. Knockdown of REG1A was analysed with Western blot **(Appendix Figure 8.66, Appendix Figure 8.67)** and FACS **(Appendix Figure 8.68)**. With the REG1A antibody however, no bands appeared at the expected size and no significant differences in cell counts were measured.

REG1A knocked down BGJ-resistant SNU-16 and HFF2 cells were then also seeded into Alvetex® scaffolds and grown for one week in presence of BGJ, followed by fixation, H&E staining **(Appendix Figure 8.69)** and REG1A antibody staining **(Appendix Figure 8.70)**. The cells in the scaffolds were also imaged with a fluorescence confocal microscopy and Z-Stacks were rendered with imaris and cell volumes of SNU-16^{BGJR} cells with REG1A knockdown and HFF2 cells with REG1A knockdown were compared **(Appendix Figure 8.71)**. With this, a basis for further experiments involving investigation of the role of REG1A in drug resistance in co-culture was set.

Interestingly, a great number of collagen-associated genes were upregulated in co-culture cells. An initial experiment was to stain Alvetex® scaffolds with Oil Red O to stain triglycerides and lipids **(Appendix Figure 8.72)**.

5.6 Findings in 2D are not representative in 3D

Comparing gene expression in 2D *versus* 3D, it was found that in 2D, gene expression could behave very differently, with several genes regulated in the opposite direction than in 3D cultures **(Figure 5.28)**. REG1A however, is also upregulated in drug-resistant cells in 2D. To compare, gene expression was also analysed in MFE-296 cells, where it is known that PHLDA1 is downregulated in FGFRi-resistant MFE-296 cells **(Figure 5.29)**. In SNU-16^{BGJR} cells however, PHLDA1 was upregulated, in contrast to the downregulation in the RNA-Seq data in 3D **(Figure 5.30)**.

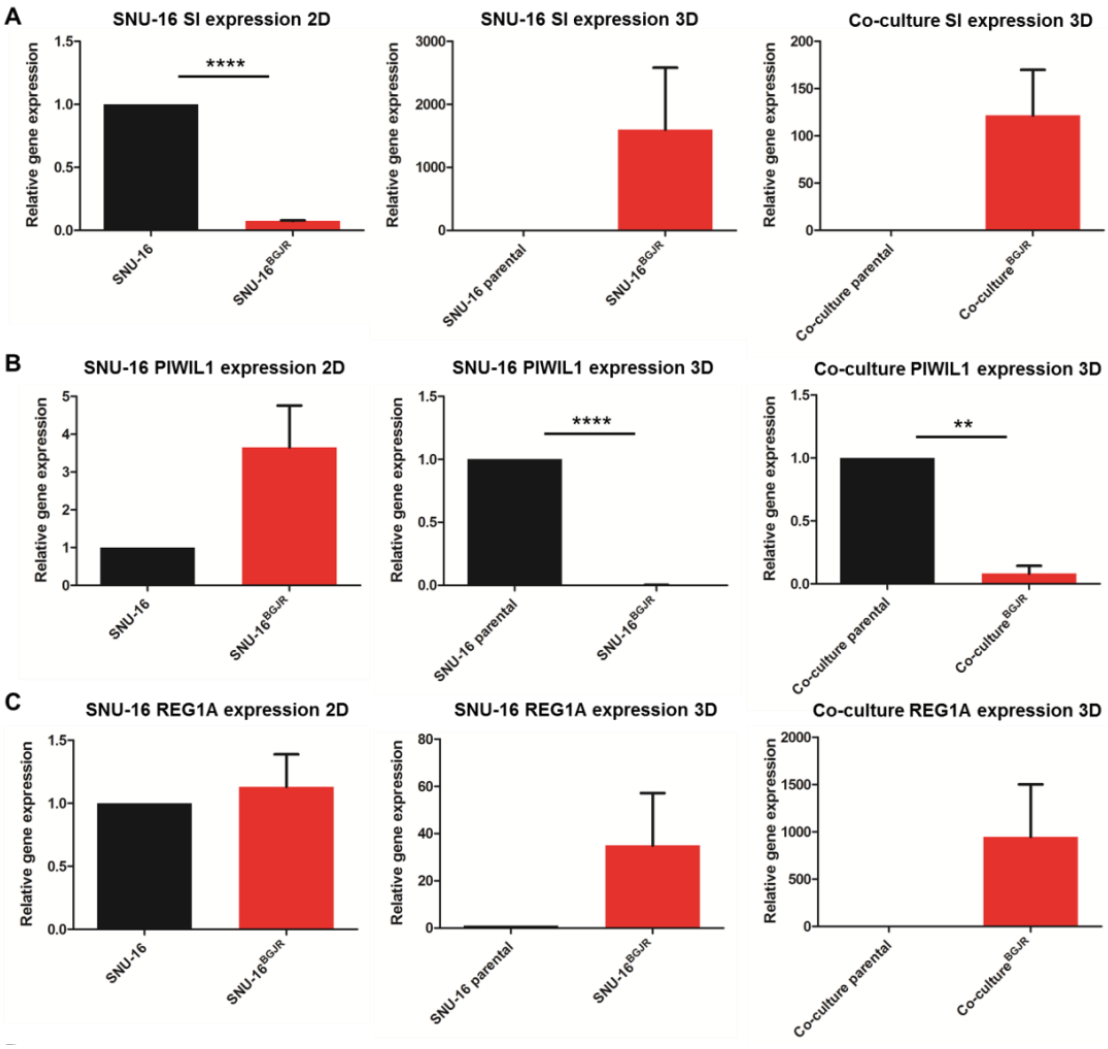

Figure 5.28. Relative gene expression levels of targets.
Gene expression levels of SNU-16 *versus* SNU-16^{BGJR} cells in 2D and 3D and co-culture cells in 3D. Comparison of SI gene expression **(A)**, PIWIL1 expression **(B)** and REG1A expression **(C)**. The experiments were performed in biological triplicate. **p<0.01, ****p<0.001.

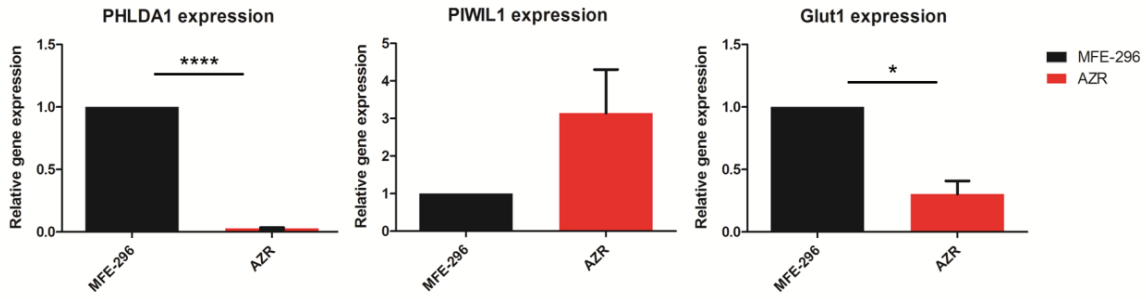

Figure 5.29. Expression of targets in MFE-296 cells and AZD-resistant MFE-296 cells.
Parental MFE-296 and AZD-resistant MFE-296 cells were harvested and RNA extracted, which was reverse transcribed into cDNA. Gene expression was then assessed using qPCR for PHLDA1, PIWIL1 and GLUT1. *p<0.05, ****p<0.001.

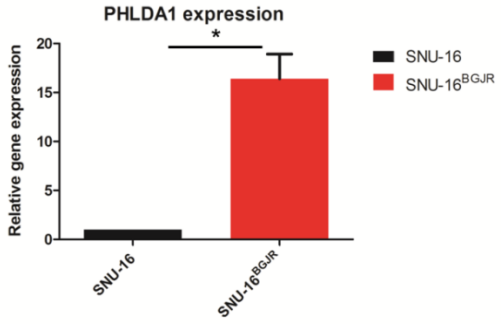

Figure 5.30. PHLDA1 expression in SNU-16 and SNU-16^{BGJR} cells.
Parental SNU-16 and BGJ-resistant SNU-16 cells were harvested and RNA extracted, which was reverse transcribed into cDNA. Gene expression was then assessed using qPCR for PHLDA1. *p<0.05.

PHLDA1 upregulation in BGJ-resistant SNU-16 cells was also confirmed by Western blot **(Figure 5.31)**.

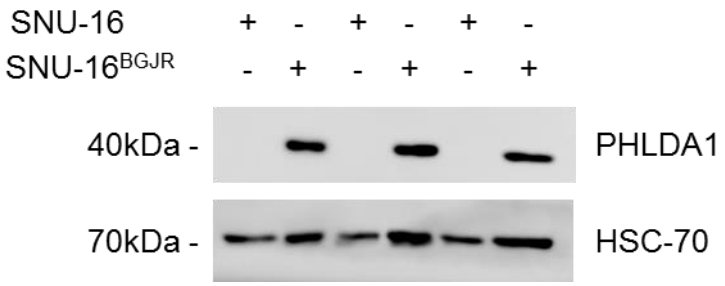

Figure 5.31. PHLDA1 expression in SNU-16 and BGJ-resistant SNU-16 cells.
Protein was extracted from parental SNU-16 and SNU-16^{BGJR} cells and 10µg was loaded into each lane and Western blot analysis was performed probing for PHLDA1 and HSC70. The experiment was performed in biological triplicate.

5.7 Comparison of common gene expression between datasets

5.7.1 MFE-296 microarray

The differential gene expression levels of parental SNU-16 and BGJ-resistant SNU-16 and co-culture cells were also compared to gene expression of AZD-resistant endometrial cancer line MFE-296, which was performed previously in the group (Fearon et al., 2018).

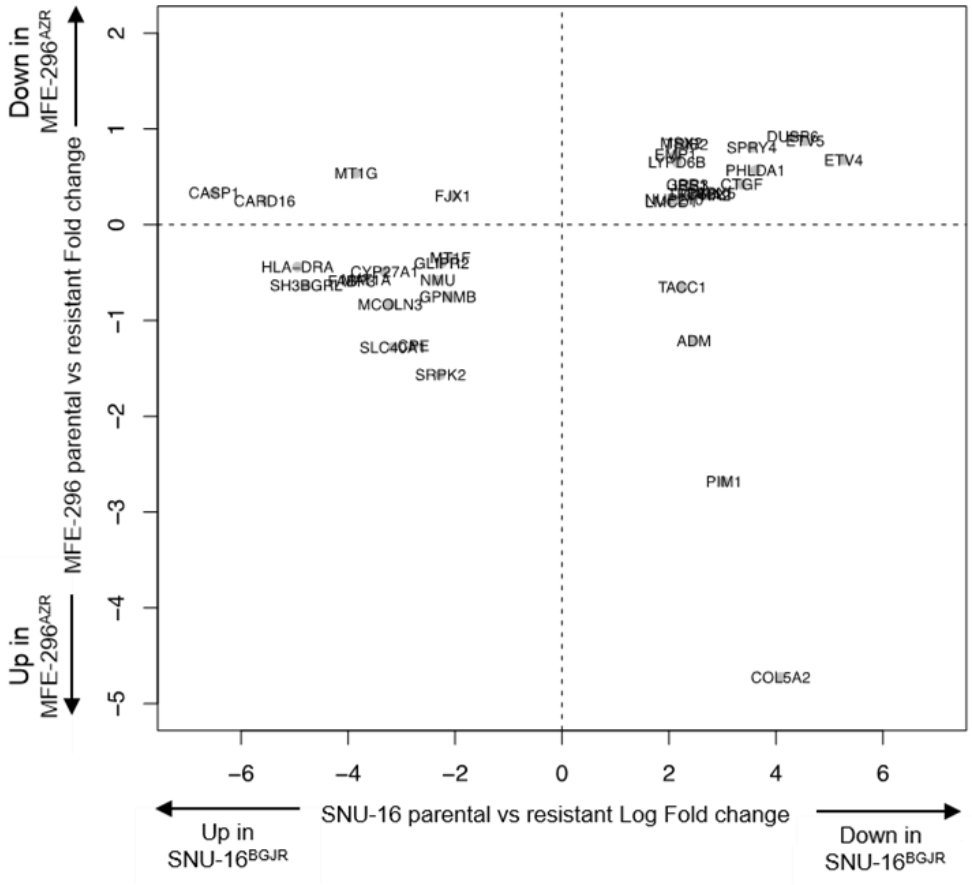

Figure 5.32. Comparing expression of genes between MFE-296 resistant to PD and SNU-16 cells resistant to BGJ.
The top right corner indicates genes that are downregulated in drug-resistant MFE-296 and SNU-16 cells. The MFE-296 data was generated in 2D, while SNU-16 drug-resistant cells were generated in 3D.

Table 5.1. Comparison of the SNU-16 dataset to the MFE-296 dataset.
Cut off at correlation >2. Endometrial cancer cell line MFE-296 was made resistant to AZD and microarray analysis was performed.

Gene name	Description	Correlation	Regulation in drug resistant cells
DUSP6	dual specificity phosphatase 6	15.809	Down
PHLDA1	Pleckstrin homology-like domain family A member 1	14.532	Down
ETV5	ets variant 5	13.638	Down
ETV4	ets variant 4	8.554	Down
SPRY4	sprouty RTK signalling antagonist 4	8.404	Down
MSX2	msh homeobox 2	6.193	Down
TRIB2	tribbles pseudokinase 2	6.151	Down
EMP1	epithelial membrane protein 1	4.035	Down
SLC40A1	solute carrier family 40, member 1	3.760	Up
SH3BGRL	SH3 domain binding glutamate-rich protein like	3.378	Up
CPE	carboxypeptidase E	3.271	Up
LYPD6B	LY6/PLAUR domain containing 6B	3.267	Down
SRPK2	SRSF protein kinase 2	3.087	Up
MCOLN3	mucolipin 3	2.805	Up
CTGF	connective tissue growth factor	2.666	Down
FABP3	fatty acid binding protein 3, muscle and heart	2.629	Up
HLA-DRA	major histocompatibility complex, class II, DR alpha	2.599	Up
MAT1A	methionine adenosyltransferase I, alpha	2.405	Up

From previous work in our group, PHLDA1 has been identified to play a role in drug resistance in endometrial cancer cells and PHDLA1 is downregulated in AZD-resistant MFE-296 cells **(Appendix Figure 8.73)**. PHLDA1 was also significantly

downregulated in BGJ-resistant SNU-16 cells in 3D using Alvetex®, however not in co-culture cells **(Figure 5.33)**.

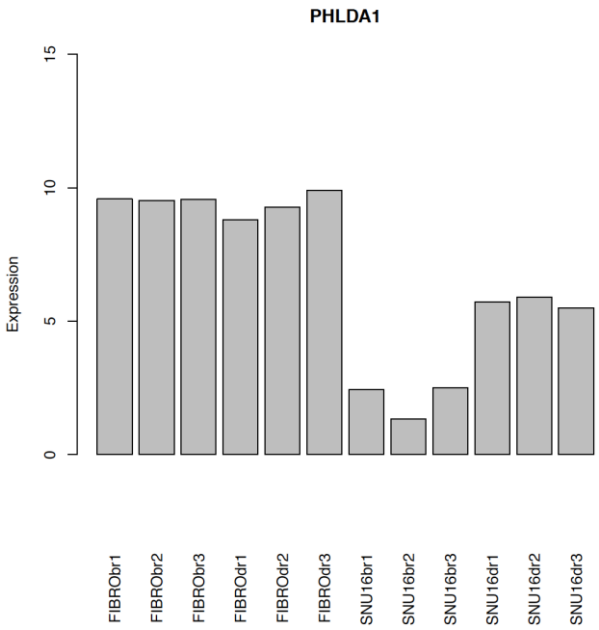

Figure 5.33. PHLDA1 expression in 3D resistance gene expression comparison.
PHLDA1 gene expression was compared between all samples and was significantly down in BGJ-resistant SNU-16 cells. SNU-16d = DMSO-treated SNU-16 cells, SNU-16b = BGJ-treated SNU-16 cells, FIBROd = DMSO-treated co-culture cells, FIBROb = BGJ-treated co-culture cells, r=repeat.

When comparing genes regulated in the same direction, in addition to PHLDA1 also DUSP6 was shown and expression was also analysed in SNU-16 cells using Western blot **(Figure 5.34)**. Again, in contrast to the RNA-Seq data, DUSP6 was also upregulated in SNU-16^{BGJR} cells.

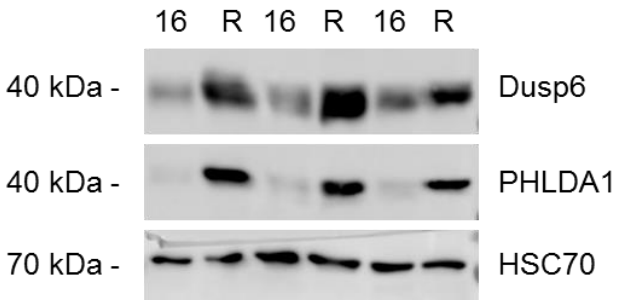

Figure 5.34. DUSP6 and PHLDA1 expression in SNU-16 and SNU-16^{BGJR} cells.
Protein of parental and drug-resistant SNU-16 was extracted and subjected to Western blot analysis probing for DUSP6, PHLDA1 and HSC70 as a loading control. The blots represent three individual experiments. Further blots are in the appendix **(Appendix Figure 8.74)**.

5.7.2 Effect of PI3K and MEK inhibitors on MFE-296 cells

PHLDA1 expression was further investigated by inhibition of FGFR2 downstream pathways. MFE-296 cells were treated with MEK inhibitor U0126 (1μM) and PI3K ZSTK (1μM) and PHLDA1, p-AKT and p-ERK levels were compared to total AKT and ERK, as well as HSC70 levels **(Figure 5.35)**. Phosphorylated AKT and PHLDA1 were both reduced upon PI3K inhibitor treatment. While p-ERK was dowregulated in cells treated with the MEK inhibitor.

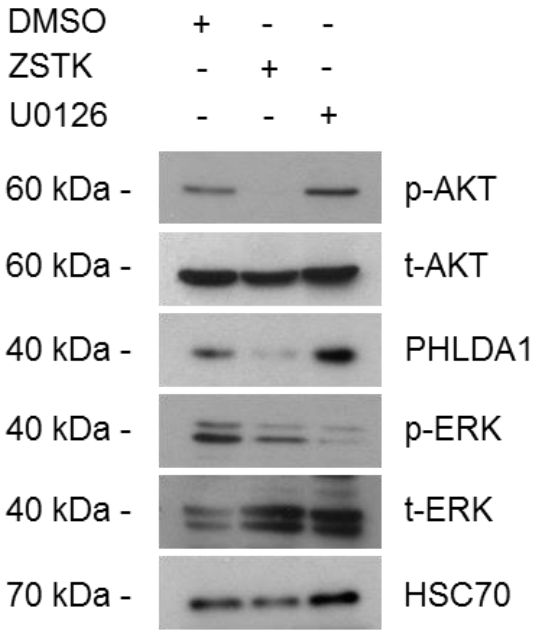

Figure 5.35. Treatment of MFE-296 cells with PI3K inhibitor ZSTK inhibits both p-AKT and PHLDA1. MFE-296 cells were exposed to 1μM ZSTK and 1μM U0126 and cells were harvested after 72h and analysed by Western blot probing for p-AKT, PHDLA1, p-ERK and HSC70 as a loading control. The blots are representative of three individual experiments **(Appendix Figure 8.75)**.

PHLDA1 expression levels were also investigated in AN3CA cells over a time span of 24 hours with exposure to AZD for 1, 4, 8 and 24 hours, revealing loss of PHLDA1 expression after 24 hours. Upon addition of the FGFR inhibitor also p-ERK levels were slightly reduced **(Figure 5.36)**. The same was also done for MFE-296 cells with PD and AZD. PHLDA1 levels were initially reduced in PD and AZD-treated MFE-296 cells, which returned to basal levels after 24 hours for PD-treated cells and already after four hours for AZD-treated cells. Phosphorylation of ERK was dramatically reduced in FGFR inhibitor treated MFE-296 cells **(Figure 5.37).**

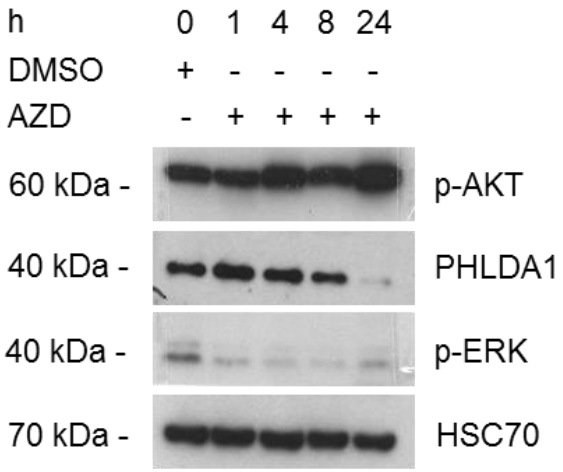

Figure 5.36. After 24h AZD treatment PHLDA1 levels are down in AN3CA cells.
AN3CA cells were exposed to 1μM AZD and cells were harvested after 1, 4, 8, and 24 and analysed by Western blot probing for p-AKT, PHDLA1, p-ERK and HSC70 as a loading control. The blots are representative of two individual experiments **(Appendix Figure 8.76)**.

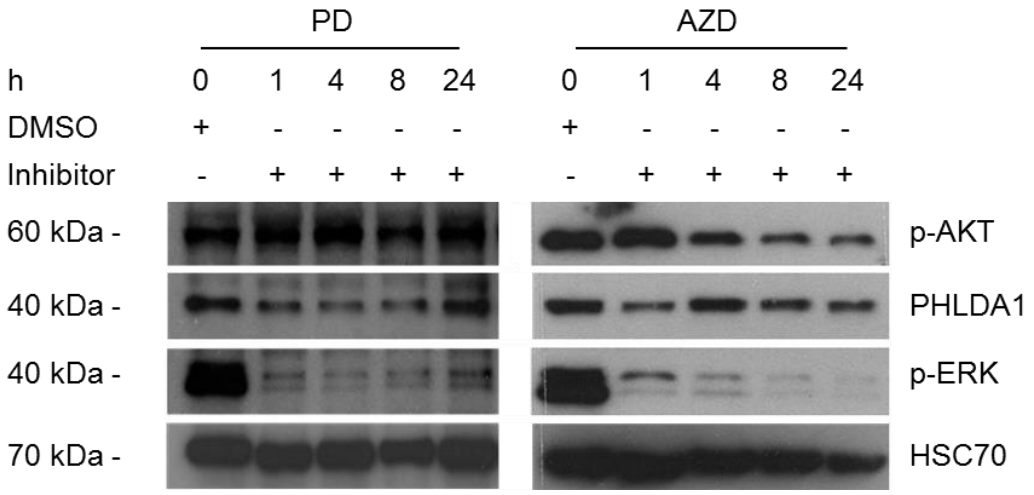

Figure 5.37. PHLDA1 expression returns to basal levels after 24h in *FGFR2*-mutated endometrial cancer cells.
MFE-296 cells were exposed to 5μM PD and 1μM AZD and cells were harvested after 1, 4, 8, and 24 and analysed by Western blot probing for p-AKT, PHDLA1, p-ERK and HSC70 as a loading control. The blots are representative of three individual experiments **(Appendix Figure 8.77, Appendix Figure 8.78)**.

5.7.2.1 Long-term FGFR inhibitor treatment of AN3CA cells

After short-term treatment of AN3CA cells with FGFR inhibitors such as PD or AZD, PHLDA1 levels were decreased **(Figure 5.36)**. Next, we also wanted to probe PHLDA1 and AKT and ERK signalling after long-term drug treatment. Cells were treated with PD at a concentration of 1μM for 7 days. Medium with the drug was exchanged every two days. There was no effect observable in PHLDA1 or p-AKT. However p-ERK levels were decreased in drug-treated cells after 7 days.

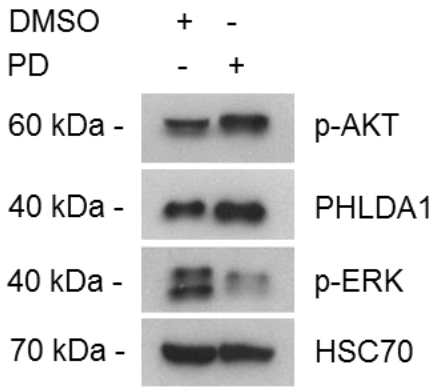

Figure 5.38. After 7 days PD treatment PHLDA1 levels are back to normal in AN3CA cells.
PHLDA1 and p-AKT levels are reversed to basal levels of AN3CA cells after 7 days PD treatment. PHLDA1 levels and p-AKT levels are unchanged after treatment of cells for 7 days with FGFR inhibitor PD. However p-ERK levels are decreased in 7 days treated cells. This image is representative of three individual experiments **(Appendix Figure 8.79)**.

PHLDA1 was knocked down in MFE-296 cells with three different shRNAs, which was confirmed with Western blot **(Appendix Figure 8.80)**. MFE-296 cells with PHLDA1 knockdowns were then grown in Alvetex® and treated with PD and AZD, which did not reduce cell numbers in MFE-296 cells. This confirmed findings that PHLDA1 knockdown confers resistance to FGFR inhibition **(Appendix Figure 8.81)**.

Gene expression levels were also compared to other datasets found on the Gene Expression Omnibus (GEO) database. The gene with the highest correlation between the SNU-16 and MFE-296 dataset (Fearon et al., 2018) was *dual specificity phosphatase 6* (*DUSP6*). Also *PHLDA1*, which was discussed previously, was the second common downregulated gene. Gene expression signature of drug-resistant SNU-16 cells was further compared to to *FGFR1*-amplifed DMS114 small cell lung cancer cell line made resistant to BGJ (3μM) (Accession: GSE92651) and *FGFR3*-mutated urothelial

carcinoma cell line RT112 also made resistant to BGJ (5μM) (Accession: GSE92651) **(Table 5.2, Table 5.3)**. In the comparison between MFE-296 and SNU-16 and RT112 and SNU-16 two genes were shared such as epithelial membrane protein (EMP1) and DUSP6. Whereas BGJ-resistant DMS114 compared to drug-resistant SNU-16 cells did not share genes with the MFE-296 and RT112 datasets.

Table 5.2. DMS114 dataset compared to SNU-16 dataset.
Small cell lung cancer cell line DMS114 was made resistant to BGJ at a concentration of 3μM.

Gene name	Description	Correlation	Regulation in drug resistant cells
FLRT3	fibronectin leucine rich transmembrane protein 3	8.605	Down
IFITM3	interferon induced transmembrane protein 3	6.077	Down
NRIP1	nuclear receptor interacting protein 1	5.550	Up
EYA1	EYA transcriptional coactivator and phosphatase 1	5.005	Up
ETV1	ets variant 1	4.712	Down
SOX4	SRY-box 4	3.536	Up
DCN	decorin	3.286	Up
TBX2	T-box 2	2.760	Up
HMOX1	heme oxygenase 1	2.144	Up
FSTL1	follistatin like 1	2.009	Up
MAP1B	microtubule associated protein 1B	1.889	Up
TXNIP	thioredoxin interacting protein	1.824	Down
CNKSR2	connector enhancer of kinase suppressor of RAS 2	1.488	Up
ID2	inhibitor of DNA binding 2, dominant negative helix-loop-helix protein	1.354	Up
COTL1	coactosin-like F-actin binding protein 1	1.230	Up
CYR61	cysteine-rich, angiogenic inducer, 61	1.028	Up
EDIL3	EGF-like repeats and discoidin I-like domains 3	0.918	Down
MAGI1	membrane associated guanylate kinase, WW and PDZ domain containing 1	0.847	Up
TMEM170B	transmembrane protein 170B	0.825	Up
RCN1	reticulocalbin 1	0.645	Up
TCF12	transcription factor 12	0.306	Up
ASNA1	arsA arsenite transporter, ATP-binding, homolog 1 (bacterial)	0.214	Down
TPD52	tumour protein D52	0.186	Up
RSU1	RAS suppressor protein 1	0.172	Up
S1PR1	sphingosine-1-phosphate receptor 1	0.165	Up

Table 5.3. RT112 dataset compared to SNU-16 dataset.
Urothelial cancer cell line RT112 was made resistant to BGJ at a concentration of 5μM.

Gene name	Description	Correlation	Regulation in drug resistant cells
LGALS1	lectin, galactoside-binding, soluble, 1	20.730	Down
DUSP6	dual specificity phosphatase 6	18.230	Down
PLAT	plasminogen activator, tissue	15.322	Down
NRCAM	neuronal cell adhesion molecule	10.927	Up
AGR2	anterior gradient 2, protein disulphide isomerase family member	6.774	Down
EMP1	epithelial membrane protein 1	5.373	Down
CEACAM1	carcinoembryonic antigen-related cell adhesion molecule 1 (biliary glycoprotein)	4.060	Down
LRP1	LDL receptor related protein 1	3.604	Down
PODXL	podocalyxin-like	2.333	Up
SEL1L3	sel-1 suppressor of lin-12-like 3 (C. elegans)	1.970	Up
ASNS	asparagine synthetase (glutamine-hydrolyzing)	1.437	Up
GSTM4	glutathione S-transferase mu 4	1.394	Up
SLC1A3	solute carrier family 1 (glial high affinity glutamate transporter), member 3	0.594	Down
GSTM3	glutathione S-transferase mu 3 (brain)	0.502	Up
PSAT1	phosphoserine aminotransferase 1	0.340	Up

Taken together, these data have shown that, most importantly, conclusions from 2D data can not be drawn and applied to *in vivo* data or 3D models. Gene expression varied greatly between drug-resistant cells generated in 2D and 3D. It has been shown that retinol and glucose may play a role in drug-resistance, which will be adressed in the discussion. Furthermore, the SNU-16 dataset was compared to other datasets from endometrial, lung and urothelial cancer cells and two FGFR inhibitors such as AZD and BGJ to identify differences and similarities in gene signatures.

5.8 Discussion

5.8.1 Retinol pathway

Vitamin A and its natural derivatives and metabolites such as β-carotene, retinol, retinal, isotetrinoin, ATRA, 9-*cis* retinoic acid, and 13-*cis* retinoic acid have important functions in critical biological processes including cell differentiation, growth, and apoptosis (Theodosiou et al., 2010). Therefore, it was hypothesised that by treating cancer cells with ATRA, cells might be resensitised towards BGJ treatment. As expected, treatment of cells with BGJ induced cell cycle arrest, as shown by an increase of cells in G1 phase and decrease of cells in S and G2 phase. Furthermore, the sub G1 population was increased in drug-treated cells, indicating increased cell death in *FGFR2*-mutated endometrial cells. This however, was not observed in BGJ-resistant gastric cancer cells. In parental SNU-16 cells, the influence of ATRA treatment was not significant and only showed a tendency of a decrease in cells undergoing apoptosis and a slight increase in G1 populations. This effect could be explained by the dual function of retinoic acid and its receptors, as they are not only involved in the classical pathway but play also a role in other essential pathways. Thus, retinoic acids have been shown to regulate *NF-κB, IFN-γ, TGF-β, VEGF* and *MAPK* and also chromatin remodelling (Cras et al., 2012; Dilworth and Chambon, 2001; Papi et al., 2012; Piskunov and Rochette-Egly, 2012; Tang and Gudas, 2011; Ying et al., 2011). RARs and RXRs can form heterodimeric interactions with other receptors, including oestrogen receptor-α, AP-1, peroxisome proliferator-activated receptor (PPAR), liver X receptor (LXR) and vitamin D receptor and therefore influence and regulate these pathways (Hua et al., 2009; Lefebvre et al., 2005; Schug et al., 2007; Wang et al., 2001; Willy et al., 1995). Notably, these pathways often have opposite functions compared to the classical pathway. For example, RA activation of the PPARβ/δ pathway resulted in the induction of pro-survival genes as opposed to the anticipated activity of RARs and RXRs in differentiation (Schug et al., 2007). This could be a potential mechanism how cancer cells not only develop resistance to RA but also overcome drug inhibition.

Another possibility is that the cancer cells have lost receptors necessary for RA to exert its function, by epigenetic regulation of *RAR* genes. *RARβ* has been found to be lost in a number of solid tumours, such as breast cancer (Mehrotra et al., 2004; Sirchia et al., 2000; Widschwendter et al., 1997). Therefore, treatment with ATRA would result in no activation of the classical or non-classical pathway. This could be the case for the cancer cells studied in this work and potentially *RARs* could be reexpressed by using DNA methyltransferase (DNMT) and histone deacetylase (HDAC) inhibitors (Sirchia et al., 2002). Cancer cell proliferation could then possibly be reduced by combination of DNMT or HDAC inhibitors with ATRA and FGFR inhibitors.

However, there may be other mechanisms by which cancer cells affect RARs. It has been reported, that loss of co-activators resulted in upregulated RA metabolism, decreased numbers in RA or reduced RARα signalling (McPherson et al., 2007; Moghal and Neel, 1995; Ren et al., 2005; White et al., 1997). Loss of co-activator AF-2 in lung cancer, for example, resulted in lower RARβ expression. Reduced RARα signalling could negatively influence RARβ activation by lowered activity in chromatin remodelling, which is necessary for RARβ expression. It could also be that cross-talk between RARs and ER, as observed in breast cancer, could allow cancer cells to bypass therapeutic targeted pathways (Ross-Innes et al., 2010).

Most interestingly, upregulated RA metabolism could lead to RA elimination through 4-hydroxylation, 18-hydroxylation and glucuronidation and therefore diminish the biological activity of ATRA. Cytochrome P450, which belongs to the CYP26 family, has been described as an RA metabolising factor, resulting in hydroxylated forms of RA, including 4-OH-RA, 4-oxo-RA, and 18-OH-RA (White et al., 1997). It was also observed that P450 mRNA expression was induced by RA and therefore could demonstrate an auto-regulatory mechanism of RA levels. This could align well with the results from RNA-Seq pathway analysis and associated upregulation of the retinol pathway. When cross-checking in which direction the pathway is driven it can be concluded that the pathway shifted towards hydroxylated metabolites such as 4-OH-RA and, 18-OH-RA and also glucuronidated RA metabolites **(Figure 4.23)**.

Therefore, upregulation of the retinol pathway in the SNU-16 dataset could indicate RA elimination by upregulated retinol metabolism. This finding is also reinforced by the fact that ATRA treatment did not affect apoptosis and necrosis in SNU-16^{BGJR} cells and showed to be insensitive towards the metabolite, whereas parental SNU-16 cells exhibited increased apoptotic and necrotic cells numbers and FGFR inhibitor treatment coupled with retinoic acid treatment could potentiate its effects. Additionally, there could also be a mechanism independent of RARs, such as aberrant c-MYC or p53 expression, which has been implicated in RA resistance in patients with neuroblastoma and oral premalignancies (Lippman et al., 1995; Reynolds et al., 2000). p53 is mutated in SNU-16 cells, however with wildtype expression levels of p53 (Chang et al., 1997; Ku and Park, 2005). C-MYC on the other hand has been found to be overexpressed in SNU-16 cells (Park et al., 1998), which could potentiate the effect of ATRA resistance and insensitivity coupled with ATRA elimination through increased retinol metabolism.

5.8.2 Sucrose and starch pathway and associated genes

Metabolism differs dramatically in cancer cells compared to normal cells, especially energy production, which is dependent on aerobic glycolysis in cancer cells. Other metabolic changes include enhanced fatty acid synthesis and glutamine metabolism. It has been shown previously, that these abnormal metabolic properties in the Warburg effect have been associated with therapeutic resistance in cancer therapy. Inclusion of metabolic targeting in cancer therapy could therefore offer a promising and selective approach to overcome drug resistance in cancer cells. It was already observed in 1959 by Warburg that glycolysis rates were abnormally high in cancer cells and a Warburg effect would indicate that cancer cells prefer a glycolytic breakdown of glucose for energy instead of mitochondrial oxidative phosphorylation (Gatenby and Gillies, 2007; Gillies et al., 2008; Hsu and Sabatini, 2008; Kroemer and Pouyssegur, 2008; Vander Heiden et al., 2009; Warburg, 1956).

Therefore, the Warburg effect describes increased glucose consumption through glycolysis and cancer cells dysregulate metabolism to use the abundant resource available in the body. This mechanism enables cancer cells to be released from the

restraints on growth observed in healthy cells. The starch and sucrose degradation pathway is involved in the degradation of sucrose into glucose and therefore it was hypothesised that upregulation of the starch and sucrose degradation pathway, coupled with upregulation of SI, results in increased glucose concentration in cells. A number of studies have confirmed the connection between obesity and gastric cancer (Abnet et al., 2008; Chow et al., 1998; Ji et al., 1997; Kubo et al., 2005; Yang et al., 2009). Higher serum glucose levels significantly increased gastric cancer incidence and aggressiveness. Altered glucose metabolism could therefore be an important indicator to distinguish gastric cancer cells from normal cells as abnormal glucose metabolism was observed in a number of studies involving gastric cancer (Cai et al., 2010; Hirayama et al., 2009; Hur et al., 2014; Wu et al., 2010). A common explanation for increased glycolysis in cancer is hypoxia resulting from the rapid growth of cancer cells (Daşu et al., 2003) with hypoxia-inducible factor (HIF)-1 being the transcription factor involved in responding to changes in cellular oxygen to help cells in survival in hypoxic microenvironment (Lum et al., 2007; Wang et al., 1995). Positive HIF-1α expression was observed in patients and associated with poor prognosis for patients with gastric cancer. Activation of the RAS-MAPK signal transduction pathway and PI3K-AKT-mTOR signalling, and loss of tumour suppressor proteins, such as PTEN and p53, increased HIF-1α expression (Fukuda et al., 2002; Laughner et al., 2001). HIF-1α directly stimulates glycolysis by activating the expression of glucose transporters and several key glycolytic enzymes, such as hexokinases (HK), Pyruvate kinase isozymes M2 (PKM2) and Lactate dehydrogenase A (LDH-A). The HIF-1α-dependent pathway increases glycolysis and inhibits mitochondrial O_2 consumption, therefore promoting tumour cell survival (Kim et al., 2006). *Myc* is another important proto-oncogene, which plays an important role in glucose metabolism and enhances expression of glycolytic genes including *glucose transporter 1* (*GLUT1*) (Buller et al., 2008). In many cancers also loss of p53 initiates the glycolytic pathway and reduces oxidative phosphorylation (Wu et al., 2014). p53 increases oxidative phosphorylation and decreases glycolysis via downregulation of genes such as *GLUT1* (Watanabe et al., 2010). GLUT1 was found to be upregulated in BGJ-resistant SNU-16 cells, and to a lesser extent GLUT4, upregulation has been associated with endometrial, gastric,

squamous cell carcinoma and ovarian cancers (Abdou et al., 2015; Liu et al., 2015; Ma et al., 2015; van de Nes et al., 2015). Upregulation of GLUT1 in BGJ-resistant cells could indicate that resistant cancer cells transport more glucose and therefore have increased glucose uptake to meet the metabolic demands of drug-resistant cancer cells. Upregulation of GLUT1 in parental cells treated with BGJ could indicate that cancer cells, upon stress, upregulate GLUT1, which has been associated in the regulation of ROS (Andrisse et al., 2014).

Several glycolytic enzymes have been associated with the progression of gastric cancer (Qiu et al., 2011; Rho et al., 2007; Wang et al., 2012). Overexpression of glucose-6-phosphate dehydrogenase (G6PD), which is responsible for the conversion of glucose into ribose-5-phosphate, the first key step in glycolysis, has been associated with progression of gastric cancer. G6PD levels have also been suggested to play a role in NADPH production, which protects cells from DNA damage induced by ROS (Wang et al., 2012).

Similarly, SI could be involved in carcinogenesis and resistance and SI overexpression has been involved as a predictor for Barrett's adenocarcinoma of the gastric cardia (Iannettoni et al., 1996). Due to the importance of SI in cancer and its involvement in the generation of glucose, it was hypothesised that glucose addition could be the driver for drug resistance in gastric cancer cells. Addition of glucose to the cells however mainly resulted in increased proliferation and toxic effects in high concentrations in parental cells. It could be suggested that supplementing the medium with higher glucose concentrations could impact drug sensitivity in parental SNU-16 cells and render them less sensitive to the drug. Further aspects that support this hypothesis are the downregulation of oxidative phosphorylation, as cells use glycolysis instead, and increased fatty acid metabolism, which provides cancer cells with lipids for membrane biogenesis of fast proliferating cells conferring an growth and survival advantage (Pandey et al., 2012). Fatty acid biosynthesis was upregulated in the SNU-16 monoculture dataset, which could further support the hypothesis. Upregulation of both GLUT1 and SI could also explain better tolerance to lack of glucose in drug-resistant cells **(Figure 5.9)**. Parental SNU-16 cells react more

sensitively to glucose absence in the medium than do SNU-16^{BGJR} cells. This indicates that, with the upregulation of GLUT1 and SI, the cells can cope with lack of glucose and use sucrose to generate glucose via SI. MFE-296 cells also showed higher proliferation in medium containing glucose. At high glucose levels however, cells started to proliferate less. SNU-16 cells generally also seemed to perform better with addition of glucose. This suggests that glucose transport is elevated in drug-resistant cells to meet the metabolic needs of cancer cells for growth and signalling.

Interestingly, Western blot analysis of SNU-16 cells exposed to different glucose concentrations revealed a lower p-ERK expression in cells exposed to 2 and 4g/L glucose. This could indicate that cells require glucose, however at higher concentrations it will not further increase proliferation of these cells. In initial studies in *Drosophila*, ERK signalling was found to regulate glucose metabolism to maintan glucose levels in cells. Downregulation of p-ERK could therefore suggest an adaptation to maintain circulating glucose at appropriate levels (Becker et al., 1996; Zhang et al., 2011). Since it is hypothesised that in resistant cells glucose levels are heightened through increased enzymatic activity of SI, it could be explained that there is no effect of glucose addition in BGJ-resistant cells and the effect of sucrose on resistant cells would be more interesting to investigate. Sucrose levels did induce proliferation in SNU-16^{BGJR} cells. In parental cells however, toxic effects were observed at high concentrations, which could be due heightened proliferation and therefore cells overcrowding and not receiving enough nutrients. Interestingly, treating parental cells with BGJ resulted in lower cell numbers as expected, however with increasing sucrose concentration cells performed better and cell numbers increased. Whether SI upregulation leads to increased activity needs to be established. This should be further investigated as there is a long way between activation and maturity including post-translational modification and trafficking/localisation.

AKT signalling does not only play a role in apoptosis, cell proliferation, transcription, and cell migration but also in glucose metabolism. AKT includes three highly similar isoforms, AKT1, AKT2, and AKT3 (Calera et al., 1998), of which AKT2 is involved in the translocation of the glucose transporter GLUT4 to the cell surface, resulting in

insulin-induced glucose uptake into cells (Garofalo et al., 2003). The insulin receptor tyrosine kinase is implicated in the activation of AKT through a pathway involving insulin receptor substrate (IRS), phosphatidylinositol 3 kinase (PI3K), 3-phosphoinositide-dependent protein kinase 1 (PDK1) and AKT (Maarbjerg et al., 2011). Insulin activates this pathway, leading to increased glucose uptake, and insulin generation increases with higher carbohydrate ingestion, including sucrose (Tsuchiya et al., 2014). Dephosphorylation of AKT could therefore indicate that cells are trying to regulate glucose metabolism by inhibiting AKT signalling. Interestingly, comparing p-AKT expression in parental and BGJ-resistant cells, p-AKT expression remains the same in high sucrose concentrations, supporting the hypothesis that cells keep AKT signalling, induced by insulin, at constant level to metabolise more glucose, as opposed to parental cells which regulate glucose metabolism by reducing AKT signalling. Drug-resistant SNU-16 cells therefore rely on glucose metabolism, which gives them an advantage over parental cells. It is therefore crucial to identify the involvement of SI in this process and, if sucrose degradation is inhibited, also insulin-dependent activation of AKT could be reduced together with glucose uptake in cells. Interestingly, p-ERK signalling was reduced in SNU-16^{BGJR} cells, compared to parental cells. ERK signalling has been associated with pyruvate kinase isoenzyme PKM2, which mediates the rate-limiting step of glycolysis through catalysis of phosphoenolpyruvate (PEP) dephosphorylation to produce one molecule of ATP. PKM2 is often upregulated in cancers (Eigenbrodt et al., 1997) and PKM2 knockdown decreased E-Cadherin activity and enhanced EGF/EGFR signalling (Wang et al., 2013), therefore promoting cell migration and invasion. Drug-resistant SNU-16 cells could therefore have lower p-ERK signalling and obtain a more aggressive and migratory phenotype.

Acarbose is used as an anti-diabetic drug and used in the treatment of type-2 diabetes and serves as a blood sugar control method. It works by slowing down glucose digestion and absorption in the small intestine (Gomez-Zubeldia et al., 1993; Krause et al., 1982). Therefore, acarbose was used to inhibit SI activity, as it binds to the enzyme and inhibits it from cleaving further oligosaccharides such as sucrose or maltose to glucose. The concentration of acarbose depends on the concentration of

the SI enzyme, however that is difficult to assess, therefore a range of different concentrations was used to block the SI enzyme. N- (nt) and C-terminus (ct) of SI have different affinities, whereby ctSI can be inhibited with 200nM and ntSI is inhibited using 14µM. In cell counts, addition of acarbose resulted in a decreased number of drug-resistant cells, however no change was observed in apoptosis and necrosis. This indicates that acarbose does influence cell growth in resistant cells, however does not induce apoptosis or necrosis. A similar effect was observed with ALDOB inhibitor TDZD-8, which did not induce changes in apoptosis and necrosis, however did reduce cell counts in gastric cancer cells and more so in drug-resistant cells. This could be connected to TDZD-8 having toxic effects through blockade of ALDOB and therefore an accumulation of F-1-P in cells resulting in lower cell proliferation. Combining acarbose and TDZD-8 however did not induce a dramatic effect in cells, which could be due to the cells opting for other ways to sustain proliferation and survival in cells.

5.8.3 Significantly regulated genes in 3D and comparison to 2D

Initial experiments were conducted with other significantly regulated genes from the RNA-Seq data. PIWIL1 was downregulated the most in drug-resistant monoculture and also among the most significantly downregulated genes in co-culture cells. It is an important member of the Argonaute protein family, and contains evolutionarily conserved PAZ and Piwi motifs that play crucial roles in stem cell proliferation, embryogenesis, growth and development, as well as differentiation an maturation and RNA silencing in multiple organisms (Cox et al., 1998; Liu et al., 2010). Importantly, it may play a role as an intrinsic regulator of the self-renewal capacity of germline and haematopoietic stem cells. It is not clear if PIWIL1 overexpression was efficient in drug-resistant SNU-16 cells as no antibody against PIWIL1 was available, however transfection of SNU-16^{BGJR} cells with the plasmid containing PIWIL1 and therefore bringing PIWIL1 back into cells, reduced cell numbers and therefore growth in resistant cells. This however needs to be further investigated by possibly also knocking PIWIL1 down in parental cells.

First experiments were also performed with REG1A, which was together with REG1B the most upregulated genes in the co-culture condition and was specific for resistant cells with stromal support. REG1A belongs to the calcium-dependent lectin superfamily and encodes five small proteins, secreted by the exocrine pancreas, including REG1A and B. They play important roles in tissue regeneration and in cell proliferation in tumours originating from epithelium and in the mucous of the gastrointestinal tract (Miyaoka et al., 2004; Unno et al., 1992). REG1A downregulation in SNU-16^{BGJR} and HFF2 cells did seem to reduce cell numbers, with some of the shRNAs used. However with others, an increase in cell numbers was observed. Furthermore, knock-down of REG1A in cells could not be confirmed by Western blotting, as the bands and the expected size were not found but at a different size. This could be due to the antibody not being specific enough and therefore downregulation could be tested rather with PCR than Western blotting.

Interestingly, PHLDA1 expression in 2D differed greatly from PHLDA1 expression in 3D. PHLDA1 was identified in drug-resistant endometrial cancer in a microarray, which was however performed in 2D. These experiments, together with the qPCR data highlight the importance to differentiate between 2D *versus* 3D cell culture. Furthermore, this could indicate that PHLDA1 has another function in gastric cancer cells than in endometrial cells. Originally, PHLDA1 was identified as a pro-apoptotic protein associated with T-cell receptor activation-induced apoptosis (Frank et al., 1999; Park et al., 1996). In endometrial cancer cells, PHLDA1 downregulation resulted in resistance by AKT recruitment to free PIP3 sites to maintain cell proliferation and survival upon kinase inhibitor treatment (Fearon et al., 2018). In addition to its function to induce apoptosis, PHLDA1 has also shown to harbour anti-apoptotic properties through insulin-like growth factor 1 (IGF-1) signalling, together with the p38 MAPK pathway in NIH-3T3 cells, and via the PI3K pathway in normal skin fibroblasts (Toyoshima et al., 2004; S. Wu et al., 2010). It was shown that *PHLDA1* downregulation through shRNA increases apoptosis. PHLDA1 was also found to be upregulated in colon cancer and in human intestinal adenoma and carcinoma and *PHLDA1* knockdown inhibited cell migration (Sakthianandeswaren et al., 2011). Also high PHLDA1 expression has been associated with high metastatic potential (Ren et

al., 2015). This suggests that PHLDA1 is tissue-specific and possibly has different roles in different cancers and also in 2D and 3D.

Furthermore, expression levels of other regulated genes were compared and it was shown that a number of genes such as *SI* and *PIWIL1* were in fact downregulated or upregulated in drug-resistant SNU-16 cells generated in 2D as opposed to drug-resistant cancer cells generated in 3D. *SI* was significantly downregulated in drug-resistant SNU-16 cells, whereas *PIWIL1* was upregulated, however not significantly. *REG1A* gene expression was upregulated in monoculture in 2D and 3D and also co-culture in 3D. This suggests that the effects of glucose and sucrose on drug-resistant and parental SNU-16 cells were rather through an SI-independent manner. These findings further highlight the difference in cell signalling between 2D and 3D cell culture and underline the importance to study cancer signalling in 3D.

5.8.4 Comparison to other datasets

The discovery of novel gene/protein targets, but also targetable pathways, is of utmost importance and finding similarities between different cancers can be highly interesting and useful in helping to understand cancer mechanisms such as drug resistance. To compare gene signature to *FGFR2*-amplified drug-resistant SNU-16 cells, three different datasets were used including drug-resistant *FGFR2*-mutant MFE-296, RT112 with *FGFR3* fusion genes and *FGFR1*-amplified DMS114 cells. PD and AZD-resistant MFE-296 cells were generated previously in the group and a microarray was conducted (Fearon et al., 2018). RT112 and DMS114 were both rendered resistant to BGJ and RNA-Seq was performed (Datta et al., 2017) as was done for SNU-16 cells. In BGJ-resistant RT112 and DMS114, drug resistance is induced in an AKT-dependent manner. When comparing the different gene signatures, no genes were shared between all four datasets, however DUSP6 was found downregulated in drug-resistant MFE-296, SNU-16 and RT112 cells and epithelial membrane protein 1 (EMP1) in MFE-296, SNU-16 and DMS114 cells. DUSP6 is a negative regulator of the ERK signalling cascade (Li et al., 2007). Generally, DUSPs are stress-induced negative feedback regulators of MAPK and have been found to be important for the maintenance of cellular homeostasis in response to growth factors.

Loss of DUSP6 through hypermethylation of its promoter in pancreatic cancer leads to a more aggressive and invasive phenotype (Furukawa, 2007; Furukawa et al., 2005, 2003). In lung cancer, DUSP6 could be a growth suppressor whose down-regulation is involved in the progression process of lung cancers (Okudela et al., 2009). EMP1 is associated to tumour metastasis and low EMP1 expression has been associated with increased disease severity (Sun et al., 2014). From this it can be concluded, that gene signatures are relatively distinct and potentially tissue-specific. Comparison of different datasets however, can draw attention to further interesting targets that could play a role in cancer tissues treated with similar drugs or similar origin.

5.8.5 Conclusion

In this chapter, the importance of 3D assays was highlighted and drawing conclusions from 2D data to the *in vivo* state should be done with caution. The importance of glucose for resistance in gastric cancer cells has been validated, however it appeared to be SI-independent in cells from 2D experiments. This could however be different in cells grown in 3D. ALDOB blockade affected cell numbers in drug-resistant cells and potentially slows proliferation of cells, however if ALDOB upregulation induces resistance or if it is through a combination of several pathways needs to be further elucidated.

Chapter VI

Final Discussion

6.1 Overview

Cancer is becoming increasingly prevalent in the world despite attempts in decreasing mortality rates and it is estimated that cancer cases per year will rise to over 20 million by 2025 (Bray and Soerjomataram, 2015). Both lung and gastric cancer are considered two of the major causes for all cancer-related deaths worldwide (Siegel et al., 2012; Torre et al., 2015), whilst endometrial cancer is the main gynaecological cancer type affecting women (Plagens-Rotman et al., 2016). Due to the incidence and importance of these cancers, it is essential to study the different forms of the disease in order to identify them sooner and find successful treatment options for patients suffering from these types of cancers. Cancers can be driven by genetic alterations such as aberrations along the FGF signalling pathway and most commonly affecting the FGF receptor. In gastric cancer, up to 10% and in lung cancer up to 16% of patients were found to harbour *FGFR2* amplifications, while 12% of endometrial cancer patients showed *FGFR2* mutations. FGFs together with their receptors mediate a myriad of cellular processes ranging from embryonic development to differentiation and proliferation (Böttcher and Niehrs, 2005; Feldman et al., 1995; Ghabrial et al., 2003; Polanska et al., 2009; Yamanaka et al., 2010). It is evident, that this pathway with its receptors is often hijacked by cancer cells in order to drive their own proliferation and tumour progression (Tanner and Grose, 2016). Major advances in cancer therapy have led to the invention of small molecule inhibitors that are more effective targeted drug treatments of cancers with specific alterations, which have been applied in a number of different RTK-driven cancers (Byron et al., 2008; Carter et al., 2015). Numerous small molecule inhibitors have shown success in clinical trials (Gavine et al., 2012; Kelly et al., 2018, Pal et al., 2018). One of the main pitfalls however, is the emergence of resistance towards such RTK inhibitors, which presents a major obstacle in successful therapy (Holohan et al., 2013). Signalling alterations induced by the treatment of cancers with small molecule inhibitors often results in compensatory signalling (Holohan et al., 2013). Hence, the effect of such treatments has to be closely studied and monitored and novel approaches have to be applied, which takes into account the alterations acquired upon RTK inhibitor treatment.

6.2 FGFR inhibition and generation of drug-resistant cancer cells in 2D

In this work, one of the main focuses was investigating FGFR-driven gastric cancers. From a panel of gastric cancer cell lines, SNU-16 was chosen as it harbours high levels of *FGFR2* amplifications and exhibited sensitivity towards FGFR inhibitors. By gradually increasing FGFR inhibitor concentration over time, SNU-16 cells could be rendered resistant to the FGFR inhibitor BGJ. Parental SNU-16 cells were highly sensitive to PD, AZD and BGJ compared to SNU-1 cells, which do not harbour any *FGFR2* amplifications. SNU-1 and BGJ-resistant SNU-16 cells showed similar cell viability profiles and protein expression. BGJ-resistant cells also showed cross-resistance towards other FGFR kinase inhibitors such as PD and AZD, as shown with p-ERK expression levels at similar levels as vehicle-treated cells.

Receptor aberrations are associated with sensitivity towards kinase inhibitors, presenting a viable therapeutic target, which could reveal cancers that could be treated with small kinase inhibitors (Brooks et al., 2012; Dieci et al., 2013), however over prolonged treatment such cancers can acquire resistance.

6.3 3D cell modelling and differential gene expression analysis

6.3.1 3D Alvetex® model

Success rates in clinical trials are relatively low, with more than half of all drug trials failing in phase II and III due to a lack of efficacy. A third of all studies then further fail due to safety concerns (Arrowsmith and Miller, 2013). Therefore, it is essential to investigate drug resistance *in vitro* prior to entering clinical trials. Although 2D studies can give valuable initial insights in cancer drug resistance, studying drug resistance in cancers using a 3D setting will present more physiomimetic results and insights (Pampaloni et al., 2007; Ravi et al., 2015). 3D modelling is an accepted tool to perform more *in vivo*-like experiments to address all different kinds of scientific questions, including drug resistance in cancers. Cells grown in 3D structures not only recapitulate their *in vivo* morphology, but also show more representative function, invasion and protein and gene expression as compared to growing cells in traditional 2D models (Baker and Chen, 2012; Chen et al., 1997; Haycock, 2011). Thus, it is of

utmost importance to establish an *in vitro* 3D assay that provides a physiomimetic microenvironment to monitor and recapitulate the tumour-stromal interactions. In order to investigate drug resistance, including cancer signalling in a 3D model, it is important to choose a model where there is no foreign influence that could induce signalling artefact. Organotypic cultures, such as those used in the study of breast and pancreatic cancers (Chioni and Grose, 2012, Coleman et al., 2014), provide a tool capable of assessing the effects of small molecule inhibition in the context of a 3D environment, comprising an ECM-like stromal cell-containing component, however as these cultures comprise of collagen and Matrigel™, this could alter signalling due to animal protein influences and batch to batch variations. In order to study drug resistance in gastric cancer, I developed a novel 3D model using Alvetex® scaffold inserts. One of the great advantages this model has over the organotypic cultures, is the absence of foreign material, and however as it is a scaffold structure many cells fall through the pores, which could be optimised with different pore sizes or other coating methods which enhance attachment. In this project, Alvetex® scaffolds have proven to be valuable tools in order to study cancer resistance in 3D and different cancer cell types were grown successfully in the scaffolds also in conjunction with other cell types such as fibroblasts. I showed that drug-sensitive gastric cancer cells could be rendered resistant in 3D and cancer cells cultured in tandem with fibroblast cells acquired resistance faster than cancer cells alone. This could indicate that fibroblast cells support and promote cancer cells by providing essential growth factors. In a similar study involving lung cancer, it has been found that CAFs aid resistance in lung cancer by secreting proteins that allow the cancer cells to evade apoptosis and therefore become resistant to EGFR inhibitors (Choe et al., 2015). Several studies also discuss the microenvironment as a protective niche for cancers that enables cells to escape the effects of chemotherapy or radiation (Olson and Joyce, 2013; Sung et al., 2007).

Fibroblasts play a major role in tissue repair and the similarity between wound healing and tumour development have been long recognised (Dvorak, 1986). The function of fibroblasts can however change dramatically upon oncogenic transformation and are associated with hallmarks of cancer discussed by Hanahan

and Weinberg (Hanahan and Weinberg, 2000). In prostate and pancreatic cancers, high abundance of fibroblasts in tumours has been associated with an increase in ECM or remodelling of the ECM architecture such as rendering the matrix more rigid and therefore creating a barrier preventing drug dissemination (Feig et al., 2012; Neesse et al., 2011). Potentially, HFF2 cells protected SNU-16 cells from cytotoxic effects of BGJ, by secreting ECM proteins therefore creating a niche for cancer cells to reside and proliferate (Olive et al., 2009).

The Alvetex® 3D model proved highly suitable to study drug resistance in 3D with co-cultures as cells could be grown in scaffolds without influence from other material that could overshadow cell signalling. In addition to this, growing cells over longer periods is one of the great advantages of this model. Ideally, the effects of tumourigenic mutations would be compared to non-malignant cells arising from the same tissue of origin. However, it is extremely difficult to obtain such gastric stromal cells commercially and cells would have to be immortalised in order to use in a 3D model. The use of these cells would further improve the model and provide an even more physiomimetic assay to study drug resistance and paracrine signalling between cancer cells and fibroblasts in gastric cancer.

To visualise the cells in the scaffold and distinguish between the different cell types, cultures were transduced with lentiviral constructs containing fluorescent markers. For RNA-sequencing, RNA from co-culture cells was run combined. Ideally, cancer cells could have been separated from stromal cells by cell sorting with the help of fluorescent markers. Therefore, the influence of stromal cells on cancer cells could be analysed without the gene signature of HFF2 cells in the dataset that complicates the distinction between effects of cancer or stromal cells. Also, a condition with fibroblasts only could have given greater insights and could have allowed distinguishing which gene regulations were driven by fibroblasts. Nevertheless, cell sorting imposes a great amount of cellular stress onto cells, which could alter cell signalling and therefore was decided against. In the future, a variety of different cell types could be included such as immune cells and thus more complex 3D cell culture models could be built to attempt to move even closer to the *in vivo* state.

6.3.2 Dissection of drug resistance mechanisms in 3D using RNA-Seq

After establishing that SNU-16 cells acquire resistance to FGFR inhibitors also in 3D, RNA-Seq was used to gain insight into the differences in the transcriptomes of parental and resistant cells in a global, unbiased manner across all different conditions and changes in cell signalling. Transcriptomic analysis of drug-resistant SNU-16 cells and SNU-16 together with HFF2, showed a distinct gene expression signature common to drug resistant cells, compared to their parental counterparts. The assessment of these differences led to investigations of the potential mechanism underlying the resistance to FGFR inhibition. The main focus was on investigating the difference in cell signalling between gastric cancer cells with and without stromal support, which resulted in interesting observations including upregulation of metabolic pathways. The majority of targets that were found to positively drive drug resistance in cancer cells alone were involved in metabolic processes and pathway analysis revealed that most upregulated pathways have a metabolic function. Metabolomics analysis in addition to RNA-Seq would allow further valuable insights in measuring enriched metabolites stimulated by drug resistance. Serum metabolic profiling has been used previously to identify metabolic mechanisms in gastric cancer (Song et al., 2012). With the identified metabolites, alterations in glycolysis, amino and fatty acid, cholesterol, and nucleotide metabolism in gastric cancer patients could be determined. Thus, this method in conjunction with RNA-Seq could allow insights into metabolic drug resistance mechanisms.

Another interesting aspect from the dataset was the upregulation of a number of genes involved in collagen formation in co-culture cells, which reflects the influence of fibroblasts. The resulting effect of the upregulation could be increased ECM proteins and therefore a more rigid and stiffer matrix, preventing diffusion of inhibitors to reach cells, especially cancer stem cells (Erler et al., 2009; Schrader et al., 2011; Tilghman et al., 2010; Weigelt et al., 2014).

When measuring gene expression levels and protein expression using drug-resistant cells generated in 2D, gene expression often conflicted with data from 3D. This suggests that assumptions cannot be drawn from 2D to 3D or *in vivo* conditions as this can result in highly distinct outcomes. Ideally gene expression analysis would also be performed in human gastric cancer tissue treated with kinase inhibitors.

The datasets were also compared to other datasets that were generated previously in our group or found in published datasets. Comparison of available datasets in respect to similarities and differences will give valuable insights in the cancer type or drug investigated and the emergence of resistance.

6.4 Target validation

What was immediately evident was the involvement of metabolic mechanisms in drug-resistant cancer cells. A number of metabolic pathways were found to be upregulated, most notably the retinol and sucrose degradation pathways. Retinoic acid has already been widely used in the clinic due to its importance in a vast number of biological processes such as development, differentiation, proliferation, and apoptosis (Fanjul et al., 1994; Voigt and Zintl, 2003). Retinoids have been found to suppress carcinogenesis and cells were found to reduce retinol signalling in order to advance carcinogenesis together with a loss of RARβ expression (Widschwendter et al., 1997). On the other hand RA signalling was involved in malignant transformation (Bukhari et al., 2007; Pisano et al., 2007; Shah et al., 2001; Wang et al., 2009). Also, in an ErbB2-induced mammary tumourigenesis model, RARβ expressed by stromal cells was essential for tumourigenesis (Liu et al., 2011). As ATRA did not influence cell death in drug-resistant cells, it was hypothesised that upregulation of the retinol pathway is connected to RA elimination. The effect of retinol addition to SNU-16 and SNU-16^{BGJR} cells therefore needs to be further elucidated and, especially, also the expression of retinoic acid receptors such as RARβ, which could give more insights in the role of retinol signalling in drug resistance. Additionally, RA receptors could be inhibited with shRNAs to investigate the effect on cancer cells and treatment with a FGFR inhibitor could potentiate the effect.

The sucrose degradation pathway belongs to metabolic pathways as well and glucose has been found to fuel carcinogenesis by providing increased energy in the form of ATP (Hsu and Sabatini, 2008). Altering sucrose concentrations has shown initial interesting data and could display a potential mechanism to influence cancer proliferation and survival. It has to be further elucidated what role SI plays, or if the effects are independent of SI and ALDOB. Acarbose is used to treat diabetic patients by blocking alpha glucosidase, which is an enzyme needed to digest carbohydrates (Campbell et al., 1996). Treatment of cells with acarbose, did not show dramatic effects and therefore it is hypothesised that the effect is SI-independent. Notably, upregulation of the sucrose degradation pathway and upregulation of SI could not only be associated with glucose generation, it could also allow cells to generate intermediates in glycolysis such as NADPH, or making ribose, serine or glycine (Israelsen et al., 2013). However, treatment of cells with TDZD-8, which arrests the pathway in the F-1-P state, was associated with a reduction in drug-resistant cell number, without increasing cell death, indicating that TDZD-8 slows down cell proliferation. TDZD-8 together with an FGFR inhibitor could therefore block cell proliferation effectively. It would also be valuable to study further regulated pathways from the dataset such as the fatty acid pathway. However, when investigating the different regulated pathways, it is clear that they are interconnected and this could therefore indicate that multiple pathways should be targeted, to overcome redundancy.

Initial experiments with REG1A and PIWIL1 were promising and need further investigation. PIWIL1 overexpression did show a reduction in cell numbers in drug-resistant cells. In addition, PIWIL1 knockdown in parental SNU-16 cells could potentially render cells resistant to FGFR inhibitors. The implications of REG1A knockdown in co-culture are less evident. It can be assumed that REG1A knockdown reduces cell numbers but further experiments are needed to identify if REG1A is important in stromal or cancer cells.

Analysis of RNA-Seq data of gastric FGFRi-resistant cells grown in 3D and target validation has led in different directions. Few of the traditional FGFR targets have

been identified and potentially there are indirect mechanisms driving drug resistance in these cancers rather than directly through reactivation of FGF signalling. A number of genes, such as upregulation of *CYP* and *UGT*, and thus upregulation of cytochrome P450 and upregulation of the retinol pathway and downregulation of oxidative phosphorylation, were identified that are connected to drug resistance in cancers in general to protect them from cellular damage and to promote drug detoxification. The switch in metabolic activity by upregulation of SI and ALDOB and pathways associated with glucose generation, such as sucrose and starch degeneration, glycolysis I and fatty acid biosynthesis pathways, might be an indirect resistance mechanism, independent from FGF signalling and merely a way to cope with limited nutrition or building block availability and protection of cells from oxidative stress. From Ingenuity pathway analysis, signalling through FGFs was downregulated in drug-resistant cells grown in 3D. Cells potentially bypassed dependency on FGF signalling by co-opting other kinases such as Met, through upregulation of HGF. Downstream of FGF signalling, PI3K/AKT signalling was upregulated, as observed with other FGFR-driven cancer types following use of FGFR inhibitors previously (Baselga et al., 2012; Hu et al., 2014; Datta et al., 2017). The PI3K/AKT pathway is an essential pathway in regulating cell behaviour. In *FGFR2*-amplified gastric cancer cells glucose metabolism was elevated, possibly increasing production of insulin and IGF, which in turn activate the PI3K/AKT pathway (Manning and Toker, 2017). This effect could also be separate from glucose concentration in cells through amplification induced, ligand-independent, activation of FGF signalling and thus activation of downstream PI3K/AKT signalling. Further downstream, this could result activation of CREB or mTOR signalling, thus stimulating cell growth and proliferation. Targeting a combination of the pathways discussed, such as those associated with glucose generation and the PI3K pathway, to inhibit glycolysis, gluconeogenesis and proliferation, could therefore potentially resensitise FGFRi-drug-resistant cells. Thus, through improved understanding of the diversity of resistance pathways in cells, independent of the initial oncogenic driver, we can try to exploit novel therapies to target drug resistant cancers.

6.5 Concluding remarks

Using a novel defined 3D model system and RNA-Seq in combination with biochemical methods and microscopy, differential signalling in FGFR2-driven gastric cancer cells has been elucidated, in a more physiological manner. RNA-Seq proved to be a powerful tool to assess differential gene expression. Potential pathways and genes have been analysed and several possible mechanisms postulated how gastric cancer cells acquire drug resistance in 3D.

From differential genes expression and pathway analysis, it can be concluded that a multitude of mechanisms play a role in drug resistance. Metabolic pathways play a substantial role, such as energy production and cytoprotective mechanisms. Whether this phenomenon is specific to gastric cancer or could be applied to other cancer types needs to be further elucidated and was partially studied using *FGFR*-altered endometrial and lung cancer cell lines. Differential gene expression comparisons across datasets from the GEO database and from data generated in the group have been performed. This needs to be extended to further data that are available, to identify patterns and reveal similarities and differences.

Further investigations using Alvetex® and comparing to expression in 2D and also *in vivo* would provide essential information, allowing comparison between them to delineate similarities and differences to generate a more predictable 3D model. Furthermore, additional cell types could be included such as immune cells to generate a model that resembles the *in vivo* state even more closely. Manipulation of altered pathways in drug-resistant cells should be also performed in Alvetex®, as differential gene expression analysis was performed with cells grown in 3D. Combination treatments could be the way forward and in recent years a number of combination trials are underway (Bayat Mokhtari et al., 2017; Chao et al., 2018; Kelly et al., 2018; Li et al., 2012; Mahipal et al., 2018; Sun et al., 2016).

A substantial proportion of patients do not respond to the targeted therapies that are currently available, which requires better patient selection and personalised targeted therapy. However, no clinically validated and robust biomarkers exist as of now to

select suitable patients for targeted therapy. Therefore the use of combination therapies could aid enhancing the effect of targeted therapies by not only targeting FGF signalling but also other aspects of tumourigenesis such as inhibiting angiogenesis, blocking immune evasion and enhancing anti-tumour immunity (Katoh, 2016). About 40% of combination trials involve programmed death (PD)-1 and Pembrolizumab (Keytruda) targeting immune checkpoints (Harris et al., 2016). Immune checkpoints such as PD-1 and cytotoxic T lymphocyte antigen (CTLA)-4 were shown to be effective targets in cancer therapy (Chang et al., 2018; Pardoll, 2012; Robert et al., 2014; Topalian, 2017; Topalian et al., 2012). Immune checkpoint inhibitors such as Pembrolizumab are monoclonal antibodies that block the PD-1 receptor located on lymphocytes and inhibit interaction with its ligands PD-L1 and PD-L2. This then results in the activation of T-cell mediated immune responses towards cancer cells (McDermott and Jimeno, 2015; Raedler, 2015). However, long term data are still awaited to confirm the benefits of combinatorial use of drugs targeting different pathways. Investigations into neuroblastoma and glioma, amongst others, suggest the use of MK2206 (an AKT inhibitor) together with other small molecule inhibitors and chemotherapeutics, indicating an advantage in causing cancer cell death (Agarwal et al., 2013; Cheng et al., 2012; Li et al., 2012). The use of multiple small molecule compounds targeting specific oncogenic pathways, together with checkpoint inhibitors to re-awaken the immune response could represent a viable method to overcome drug resistance in FGFR-driven cancers.

Chapter VII

References

References

Abdou, A.G., Eldien, M.M.S., Elsakka, D., 2015. GLUT-1 Expression in Cutaneous Basal and Squamous Cell Carcinomas. Int. J. Surg. Pathol. 23, 447–453. https://doi.org/10.1177/1066896915589968

Abeloff's Clinical Oncology - 4th Edition [WWW Document], n.d. URL https://www.elsevier.com/books/abeloffs-clinical-oncology/abeloff/978-0-443-06694-8 (accessed 7.11.18).

Abnet, C.C., Freedman, N.D., Hollenbeck, A.R., Fraumeni, J.F., Leitzmann, M., Schatzkin, A., 2008. A prospective study of BMI and risk of oesophageal and gastric adenocarcinoma. Eur. J. Cancer Oxf. Engl. 1990 44, 465–471. https://doi.org/10.1016/j.ejca.2007.12.009

Aboshanif, M., Kawasaki, Y., Omori, Y., Suzuki, S., Honda, K., Motoyama, S., Ishikawa, K., 2016. Prognostic role of regenerating gene-I in patients with stage-IV head and neck squamous cell carcinoma. Diagn. Pathol. 11, 79. https://doi.org/10.1186/s13000-016-0526-y

Acker, H., Carlsson, J., Mueller-Klieser, W., Sutherland, R.M., 1987. Comparative pO2 measurements in cell spheroids cultured with different techniques. Br. J. Cancer 56, 325–327.

Adnane, J., Gaudray, P., Dionne, C.A., Crumley, G., Jaye, M., Schlessinger, J., Jeanteur, P., Birnbaum, D., Theillet, C., 1991. BEK and FLG, two receptors to members of the FGF family, are amplified in subsets of human breast cancers. Oncogene 6, 659–663.

Affo, S., Yu, L.-X., Schwabe, R.F., 2017. The Role of Cancer-Associated Fibroblasts and Fibrosis in Liver Cancer. Annu. Rev. Pathol. 12, 153–186. https://doi.org/10.1146/annurev-pathol-052016-100322

Agarwal, E., Brattain, M.G., Chowdhury, S., 2013. Cell survival and metastasis regulation by Akt signaling in colorectal cancer. Cell. Signal. 25, 1711–1719. https://doi.org/10.1016/j.cellsig.2013.03.025

Ahmad, I., Iwata, T., Leung, H.Y., 2012. Mechanisms of FGFR-mediated carcinogenesis. Biochim. Biophys. Acta 1823, 850–860. https://doi.org/10.1016/j.bbamcr.2012.01.004

Ahmed, Z., Schüller, A.C., Suhling, K., Tregidgo, C., Ladbury, J.E., 2008. Extracellular point mutations in FGFR2 elicit unexpected changes in intracellular signalling. Biochem. J. 413, 37–49. https://doi.org/10.1042/BJ20071594

Ahn, S.Y., Kim, J., Kim, M.A., Choi, J., Kim, W.H., 2017. Increased HGF Expression Induces Resistance to c-MET Tyrosine Kinase Inhibitors in Gastric Cancer. Anticancer Res. 37, 1127–1138. https://doi.org/10.21873/anticanres.11426

Alavanja, M.C., Brownson, R.C., Benichou, J., 1996. Estimating the effect of dietary fat on the risk of lung cancer in nonsmoking women. Lung Cancer Amst. Neth. 14 Suppl 1, S63-74.

Alberg, A.J., Yung, R.C., Strickland, P., Nelson, J., 2002. Respiratory cancer and exposure to arsenic, chromium, nickel, and polycyclic aromatic hydrocarbons. Clin. Occup. Environ. Med. 2, 779–801. https://doi.org/10.1016/S1526-0046(02)00056-0

Albrengues, J., Bertero, T., Grasset, E., Bonan, S., Maiel, M., Bourget, I., Philippe, C., Herraiz Serrano, C., Benamar, S., Croce, O., Sanz-Moreno, V., Meneguzzi, G., Feral, C.C., Cristofari, G., Gaggioli, C., 2015. Epigenetic switch drives the conversion of fibroblasts into proinvasive cancer-associated fibroblasts. Nat. Commun. 6. https://doi.org/10.1038/ncomms10204

Alessi, D.R., James, S.R., Downes, C.P., Holmes, A.B., Gaffney, P.R., Reese, C.B., Cohen, P., 1997. Characterization of a 3-phosphoinositide-dependent protein kinase which phosphorylates and activates protein kinase Balpha. Curr. Biol. CB 7, 261–269.

Alfarouk, K.O., Stock, C.-M., Taylor, S., Walsh, M., Muddathir, A.K., Verduzco, D., Bashir, A.H.H., Mohammed, O.Y., Elhassan, G.O., Harguindey, S., Reshkin, S.J., Ibrahim, M.E., Rauch, C., 2015. Resistance to cancer chemotherapy: failure in drug response from ADME to P-gp. Cancer Cell Int. 15, 71. https://doi.org/10.1186/s12935-015-0221-1

Ali, M., Rellos, P., Cox, T.M., 1998. Hereditary fructose intolerance. J. Med. Genet. 35, 353–365.

Allison, D.B., Cui, X., Page, G.P., Sabripour, M., 2006. Microarray data analysis: from disarray to consolidation and consensus. Nat. Rev. Genet. 7, 55–65. https://doi.org/10.1038/nrg1749

Altucci, L., Leibowitz, M.D., Ogilvie, K.M., de Lera, A.R., Gronemeyer, H., 2007. RAR and RXR modulation in cancer and metabolic disease. Nat. Rev. Drug Discov. 6, 793–810. https://doi.org/10.1038/nrd2397

Amann, A., Zwierzina, M., Gamerith, G., Bitsche, M., Huber, J.M., Vogel, G.F., Blumer, M., Koeck, S., Pechriggl, E.J., Kelm, J.M., Hilbe, W., Zwierzina, H., 2014. Development of an innovative 3D cell culture system to study tumour--stroma interactions in non-small cell lung cancer cells. PloS One 9, e92511. https://doi.org/10.1371/journal.pone.0092511

Amano, Y., Mandai, M., Yamaguchi, K., Matsumura, N., Kharma, B., Baba, T., Abiko, K., Hamanishi, J., Yoshioka, Y., Konishi, I., 2015. Metabolic alterations caused by HNF1β expression in ovarian clear cell carcinoma contribute to cell survival. Oncotarget 6, 26002–26017.

Amant, F., Moerman, P., Neven, P., Timmerman, D., Van Limbergen, E., Vergote, I., 2005. Endometrial cancer. Lancet Lond. Engl. 366, 491–505. https://doi.org/10.1016/S0140-6736(05)67063-8

Anderson, D., Koch, C.A., Grey, L., Ellis, C., Moran, M.F., Pawson, T., 1990. Binding of SH2 domains of phospholipase C gamma 1, GAP, and Src to activated growth factor receptors. Science 250, 979–982.

Anderson, W.F., Camargo, M.C., Fraumeni, J.F., Correa, P., Rosenberg, P.S., Rabkin, C.S., 2010. Age-specific trends in incidence of noncardia gastric cancer in US adults. JAMA 303, 1723–1728. https://doi.org/10.1001/jama.2010.496

André, F., Bachelot, T., Campone, M., Dalenc, F., Perez-Garcia, J.M., Hurvitz, S.A., Turner, N., Rugo, H., Smith, J.W., Deudon, S., Shi, M., Zhang, Y., Kay, A., Porta, D.G., Yovine, A., Baselga, J., 2013. Targeting FGFR with dovitinib (TKI258): preclinical and clinical data in breast cancer. Clin. Cancer Res. Off. J. Am. Assoc. Cancer Res. 19, 3693–3702. https://doi.org/10.1158/1078-0432.CCR-13-0190

Andrisse, S., Koehler, R.M., Chen, J.E., Patel, G.D., Vallurupalli, V.R., Ratliff, B.A., Warren, D.E., Fisher, J.S., 2014. Role of GLUT1 in regulation of reactive oxygen species. Redox Biol. 2, 764–771. https://doi.org/10.1016/j.redox.2014.03.004

Ang, D., Ballard, M., Beadling, C., Warrick, A., Schilling, A., O'Gara, R., Pukay, M., Neff, T.L., West, R.B., Corless, C.L., Troxell, M.L., 2015. Novel mutations in neuroendocrine carcinoma of the breast: possible therapeutic targets. Appl. Immunohistochem. Mol. Morphol. AIMM Off. Publ. Soc. Appl. Immunohistochem. 23, 97–103. https://doi.org/10.1097/PDM.0b013e3182a40fd1

Antonescu, C.R., Besmer, P., Guo, T., Arkun, K., Hom, G., Koryotowski, B., Leversha, M.A., Jeffrey, P.D., Desantis, D., Singer, S., Brennan, M.F., Maki, R.G., DeMatteo, R.P., 2005. Acquired resistance to imatinib in gastrointestinal stromal tumor occurs through secondary gene mutation. Clin. Cancer Res. Off. J. Am. Assoc. Cancer Res. 11, 4182–4190. https://doi.org/10.1158/1078-0432.CCR-04-2245

Aprelikova, O., Palla, J., Hibler, B., Yu, X., Greer, Y.E., Yi, M., Stephens, R., Maxwell, G.L., Jazaeri, A., Risinger, J.I., Rubin, J.S., Niederhuber, J., 2013. Silencing of miR-148a in cancer-associated fibroblasts results in WNT10B-mediated stimulation of tumor cell motility. Oncogene 32, 3246–3253. https://doi.org/10.1038/onc.2012.351

Arai, Y., Totoki, Y., Hosoda, F., Shirota, T., Hama, N., Nakamura, H., Ojima, H., Furuta, K., Shimada, K., Okusaka, T., Kosuge, T., Shibata, T., 2014. Fibroblast growth factor receptor 2 tyrosine kinase fusions define a unique molecular subtype of cholangiocarcinoma. Hepatol. Baltim. Md 59, 1427–1434. https://doi.org/10.1002/hep.26890

Arnold, S.A., Rivera, L.B., Miller, A.F., Carbon, J.G., Dineen, S.P., Xie, Y., Castrillon, D.H., Sage, E.H., Puolakkainen, P., Bradshaw, A.D., Brekken, R.A., 2010. Lack of host SPARC enhances vascular function and tumor spread in an orthotopic murine model of pancreatic carcinoma. Dis. Model. Mech. 3, 57–72. https://doi.org/10.1242/dmm.003228

Arrowsmith, J., Miller, P., 2013. Trial watch: phase II and phase III attrition rates 2011-2012. Nat. Rev. Drug Discov. 12, 569. https://doi.org/10.1038/nrd4090

Asaka, M., Kimura, T., Nishikawa, S., Miyazuki, T., Alpert, E., 1988. Decreased serum aldolase B levels in patients with malignant tumors. Cancer 62, 2554–2557.

Asano, N., Hampel, U., Garreis, F., Schröder, A., Schicht, M., Hammer, C.M., Paulsen, F., 2018. Differentiation Patterns of Immortalized Human Meibomian Gland Epithelial Cells in Three-Dimensional Culture. Invest. Ophthalmol. Vis. Sci. 59, 1343–1353. https://doi.org/10.1167/iovs.17-23266

Ashkenazi, A., Dixit, V.M., 1998. Death receptors: signaling and modulation. Science 281, 1305–1308.

Assinder, S.J., Beniamen, D., Lovicu, F.J., 2015. Cosuppression of Sprouty and Sprouty-Related Negative Regulators of FGF Signalling in Prostate Cancer: A Working Hypothesis. BioMed Res. Int. 2015, e827462. https://doi.org/10.1155/2015/827462

Astrosini, C., Roeefzaad, C., Dai, Y.-Y., Dieckgraefe, B.K., Jöns, T., Kemmner, W., 2008. REG1A expression is a prognostic marker in colorectal cancer and

associated with peritoneal carcinomatosis. Int. J. Cancer 123, 409–413. https://doi.org/10.1002/ijc.23466

Atsma, F., Bartelink, M.-L.E.L., Grobbee, D.E., van der Schouw, Y.T., 2006. Postmenopausal status and early menopause as independent risk factors for cardiovascular disease: a meta-analysis. Menopause N. Y. N 13, 265–279. https://doi.org/10.1097/01.gme.0000218683.97338.ea

Azuma, K., Kawahara, A., Sonoda, K., Nakashima, K., Tashiro, K., Watari, K., Izumi, H., Kage, M., Kuwano, M., Ono, M., Hoshino, T., 2014. FGFR1 activation is an escape mechanism in human lung cancer cells resistant to afatinib, a pan-EGFR family kinase inhibitor. Oncotarget 5, 5908–5919.

Baca, S.C., Prandi, D., Lawrence, M.S., Mosquera, J.M., Romanel, A., Drier, Y., Park, K., Kitabayashi, N., MacDonald, T.Y., Ghandi, M., Van Allen, E., Kryukov, G.V., Sboner, A., Theurillat, J.-P., Soong, T.D., Nickerson, E., Auclair, D., Tewari, A., Beltran, H., Onofrio, R.C., Boysen, G., Guiducci, C., Barbieri, C.E., Cibulskis, K., Sivachenko, A., Carter, S.L., Saksena, G., Voet, D., Ramos, A.H., Winckler, W., Cipicchio, M., Ardlie, K., Kantoff, P.W., Berger, M.F., Gabriel, S.B., Golub, T.R., Meyerson, M., Lander, E.S., Elemento, O., Getz, G., Demichelis, F., Rubin, M.A., Garraway, L.A., 2013. Punctuated evolution of prostate cancer genomes. Cell 153, 666–677. https://doi.org/10.1016/j.cell.2013.03.021

Backer, J.M., 2008. The regulation and function of Class III PI3Ks: novel roles for Vps34. Biochem. J. 410, 1–17. https://doi.org/10.1042/BJ20071427

Bai, A., Meetze, K., Vo, N.Y., Kollipara, S., Mazsa, E.K., Winston, W.M., Weiler, S., Poling, L.L., Chen, T., Ismail, N.S., Jiang, J., Lerner, L., Gyuris, J., Weng, Z., 2010. GP369, an FGFR2-IIIb-specific antibody, exhibits potent antitumor activity against human cancers driven by activated FGFR2 signaling. Cancer Res. 70, 7630–7639. https://doi.org/10.1158/0008-5472.CAN-10-1489

Baker, B.M., Chen, C.S., 2012. Deconstructing the third dimension: how 3D culture microenvironments alter cellular cues. J. Cell Sci. 125, 3015–3024. https://doi.org/10.1242/jcs.079509

Balla, T., 2013. Phosphoinositides: Tiny Lipids With Giant Impact on Cell Regulation. Physiol. Rev. 93, 1019–1137. https://doi.org/10.1152/physrev.00028.2012

Bao, W., Gao, M., Cheng, Y., Lee, H.J., Zhang, Q., Hemingway, S., Luo, Z., Krol, A., Yang, G., An, J., 2015. Biomodification of PCL Scaffolds with Matrigel, HA, and SR1 Enhances De Novo Ectopic Bone Marrow Formation Induced by rhBMP-2. BioResearch Open Access 4, 298–306. https://doi.org/10.1089/biores.2015.0020

Baraniak, P.R., McDevitt, T.C., 2012. Scaffold-free culture of mesenchymal stem cell spheroids in suspension preserves multilineage potential. Cell Tissue Res. 347, 701–711. https://doi.org/10.1007/s00441-011-1215-5

Barbieri, C.E., Baca, S.C., Lawrence, M.S., Demichelis, F., Blattner, M., Theurillat, J.-P., White, T.A., Stojanov, P., Van Allen, E., Stransky, N., Nickerson, E., Chae, S.-S., Boysen, G., Auclair, D., Onofrio, R.C., Park, K., Kitabayashi, N., MacDonald, T.Y., Sheikh, K., Vuong, T., Guiducci, C., Cibulskis, K., Sivachenko, A., Carter, S.L., Saksena, G., Voet, D., Hussain, W.M., Ramos, A.H., Winckler, W., Redman, M.C., Ardlie, K., Tewari, A.K., Mosquera, J.M., Rupp, N., Wild, P.J., Moch, H., Morrissey, C., Nelson, P.S., Kantoff, P.W.,

Gabriel, S.B., Golub, T.R., Meyerson, M., Lander, E.S., Getz, G., Rubin, M.A., Garraway, L.A., 2012. Exome sequencing identifies recurrent SPOP, FOXA1 and MED12 mutations in prostate cancer. Nat. Genet. 44, 685–689. https://doi.org/10.1038/ng.2279

Barouch-Bentov, R., Sauer, K., 2011. Mechanisms of Drug-Resistance in Kinases. Expert Opin. Investig. Drugs 20, 153–208. https://doi.org/10.1517/13543784.2011.546344

Barretina, J., Taylor, B.S., Banerji, S., Ramos, A.H., Lagos-Quintana, M., Decarolis, P.L., Shah, K., Socci, N.D., Weir, B.A., Ho, A., Chiang, D.Y., Reva, B., Mermel, C.H., Getz, G., Antipin, Y., Beroukhim, R., Major, J.E., Hatton, C., Nicoletti, R., Hanna, M., Sharpe, T., Fennell, T.J., Cibulskis, K., Onofrio, R.C., Saito, T., Shukla, N., Lau, C., Nelander, S., Silver, S.J., Sougnez, C., Viale, A., Winckler, W., Maki, R.G., Garraway, L.A., Lash, A., Greulich, H., Root, D.E., Sellers, W.R., Schwartz, G.K., Antonescu, C.R., Lander, E.S., Varmus, H.E., Ladanyi, M., Sander, C., Meyerson, M., Singer, S., 2010. Subtype-specific genomic alterations define new targets for soft-tissue sarcoma therapy. Nat. Genet. 42, 715–721. https://doi.org/10.1038/ng.619

Baselga, J., Campone, M., Piccart, M., Burris, H.A., Rugo, H.S., Sahmoud, T., Noguchi, S., Gnant, M., Pritchard, K.I., Lebrun, F., Beck, J.T., Ito, Y., Yardley, D., Deleu, I., Perez, A., Bachelot, T., Vittori, L., Xu, Z., Mukhopadhyay, P., Lebwohl, D., Hortobagyi, G.N., 2012. Everolimus in postmenopausal hormone-receptor-positive advanced breast cancer. N. Engl. J. Med. 366, 520–529. https://doi.org/10.1056/NEJMoa1109653

Bayat Mokhtari, R., Homayouni, T.S., Baluch, N., Morgatskaya, E., Kumar, S., Das, B., Yeger, H., 2017. Combination therapy in combating cancer. Oncotarget 8, 38022–38043. https://doi.org/10.18632/oncotarget.16723

Beadsmoore, C.J., Screaton, N.J., 2003. Classification, staging and prognosis of lung cancer. Eur. J. Radiol. 45, 8–17.

Becker, A., Schlöder, P., Steele, J.E., Wegener, G., 1996. The regulation of trehalose metabolism in insects. Experientia 52, 433–439.

Beenken, A., Mohammadi, M., 2009. The FGF family: biology, pathophysiology and therapy. Nat. Rev. Drug Discov. 8, 235–253. https://doi.org/10.1038/nrd2792

Bellosta, P., Iwahori, A., Plotnikov, A.N., Eliseenkova, A.V., Basilico, C., Mohammadi, M., 2001. Identification of Receptor and Heparin Binding Sites in Fibroblast Growth Factor 4 by Structure-Based Mutagenesis. Mol. Cell. Biol. 21, 5946–5957. https://doi.org/10.1128/MCB.21.17.5946-5957.2001

Berg, J.M., Tymoczko, J.L., Stryer, L., Berg, J.M., Tymoczko, J.L., Stryer, L., 2002. Biochemistry, 5th ed. W H Freeman.

Bernfield, M., Götte, M., Park, P.W., Reizes, O., Fitzgerald, M.L., Lincecum, J., Zako, M., 1999. Functions of cell surface heparan sulfate proteoglycans. Annu. Rev. Biochem. 68, 729–777. https://doi.org/10.1146/annurev.biochem.68.1.729

Berry, D.C., Noy, N., 2009. All-trans-retinoic acid represses obesity and insulin resistance by activating both peroxisome proliferation-activated receptor beta/delta and retinoic acid receptor. Mol. Cell. Biol. 29, 3286–3296. https://doi.org/10.1128/MCB.01742-08

Bertuccio, P., Chatenoud, L., Levi, F., Praud, D., Ferlay, J., Negri, E., Malvezzi, M., La Vecchia, C., 2009. Recent patterns in gastric cancer: a global overview. Int. J. Cancer 125, 666–673. https://doi.org/10.1002/ijc.24290

Bhowmick, N.A., Chytil, A., Plieth, D., Gorska, A.E., Dumont, N., Shappell, S., Washington, M.K., Neilson, E.G., Moses, H.L., 2004. TGF-beta signaling in fibroblasts modulates the oncogenic potential of adjacent epithelia. Science 303, 848–851. https://doi.org/10.1126/science.1090922

Bi, L., Okabe, I., Bernard, D.J., Wynshaw-Boris, A., Nussbaum, R.L., 1999. Proliferative defect and embryonic lethality in mice homozygous for a deletion in the p110alpha subunit of phosphoinositide 3-kinase. J. Biol. Chem. 274, 10963–10968.

Bialkowska, A.B., Yang, V.W., 2012. High-throughput screening strategies for targeted identification of therapeutic compounds in colorectal cancer. Future Oncol. Lond. Engl. 8, 259–272. https://doi.org/10.2217/fon.12.19

Bissell, M.J., Hall, H.G., Parry, G., 1982. How does the extracellular matrix direct gene expression? J. Theor. Biol. 99, 31–68.

Bissell, M.J., Kenny, P.A., Radisky, D.C., 2005. Microenvironmental regulators of tissue structure and function also regulate tumor induction and progression: the role of extracellular matrix and its degrading enzymes. Cold Spring Harb. Symp. Quant. Biol. 70, 343–356. https://doi.org/10.1101/sqb.2005.70.013

Bissell, M.J., Rizki, A., Mian, I.S., 2003. Tissue architecture: the ultimate regulator of breast epithelial function. Curr. Opin. Cell Biol. 15, 753–762.

Black, M.H., Watanabe, R.M., 2011. A Principal Components-Based Clustering Method to Identify Variants Associated with Complex Traits. Hum. Hered. 71, 50–58. https://doi.org/10.1159/000323567

Bockorny, B., Rusan, M., Chen, W., Liao, R.G., Li, Y., Piccioni, F., Wang, J., Tan, L., Thorner, A.R., Li, T., Zhang, Y., Miao, C., Ovesen, T., Shapiro, G.I., Kwiatkowski, D.J., Gray, N.S., Meyerson, M., Hammerman, P.S., Bass, A.J., 2018. RAS-MAPK Reactivation Facilitates Acquired Resistance in FGFR1-Amplified Lung Cancer and Underlies a Rationale for Upfront FGFR-MEK Blockade. Mol. Cancer Ther. 17, 1526–1539. https://doi.org/10.1158/1535-7163.MCT-17-0464

Bokhari, M., Carnachan, R.J., Cameron, N.R., Przyborski, S.A., 2007a. Culture of HepG2 liver cells on three dimensional polystyrene scaffolds enhances cell structure and function during toxicological challenge. J. Anat. 211, 567–576. https://doi.org/10.1111/j.1469-7580.2007.00778.x

Bokhari, M., Carnachan, R.J., Cameron, N.R., Przyborski, S.A., 2007b. Novel cell culture device enabling three-dimensional cell growth and improved cell function. Biochem. Biophys. Res. Commun. 354, 1095–1100. https://doi.org/10.1016/j.bbrc.2007.01.105

Bokhari, M., Carnachan, R.J., Przyborski, S.A., Cameron, N.R., 2007c. Emulsion-templated porous polymers as scaffolds for three dimensional cell culture: effect of synthesis parameters on scaffold formation and homogeneity. J. Mater. Chem. 17, 4088–4094. https://doi.org/10.1039/B707499A

Bono, F., De Smet, F., Herbert, C., De Bock, K., Georgiadou, M., Fons, P., Tjwa, M., Alcouffe, C., Ny, A., Bianciotto, M., Jonckx, B., Murakami, M., Lanahan, A.A., Michielsen, C., Sibrac, D., Dol-Gleizes, F., Mazzone, M., Zacchigna, S.,

Herault, J.-P., Fischer, C., Rigon, P., Ruiz de Almodovar, C., Claes, F., Blanc, I., Poesen, K., Zhang, J., Segura, I., Gueguen, G., Bordes, M.-F., Lambrechts, D., Broussy, R., van de Wouwer, M., Michaux, C., Shimada, T., Jean, I., Blacher, S., Noel, A., Motte, P., Rom, E., Rakic, J.-M., Katsuma, S., Schaeffer, P., Yayon, A., Van Schepdael, A., Schwalbe, H., Gervasio, F.L., Carmeliet, G., Rozensky, J., Dewerchin, M., Simons, M., Christopoulos, A., Herbert, J.-M., Carmeliet, P., 2013. Inhibition of tumor angiogenesis and growth by a small-molecule multi-FGF receptor blocker with allosteric properties. Cancer Cell 23, 477–488. https://doi.org/10.1016/j.ccr.2013.02.019

Böttcher, R.T., Niehrs, C., 2005. Fibroblast growth factor signaling during early vertebrate development. Endocr. Rev. 26, 63–77. https://doi.org/10.1210/er.2003-0040

Branford, S., Rudzki, Z., Walsh, S., Grigg, A., Arthur, C., Taylor, K., Herrmann, R., Lynch, K.P., Hughes, T.P., 2002. High frequency of point mutations clustered within the adenosine triphosphate-binding region of BCR/ABL in patients with chronic myeloid leukemia or Ph-positive acute lymphoblastic leukemia who develop imatinib (STI571) resistance. Blood 99, 3472–3475.

Braun, A.C., Olayioye, M.A., 2015. Rho regulation: DLC proteins in space and time. Cell. Signal. 27, 1643–1651. https://doi.org/10.1016/j.cellsig.2015.04.003

Bray, F., Soerjomataram, I., 2015. The Changing Global Burden of Cancer: Transitions in Human Development and Implications for Cancer Prevention and Control, in: Gelband, H., Jha, P., Sankaranarayanan, R., Horton, S. (Eds.), Cancer: Disease Control Priorities, Third Edition (Volume 3). The International Bank for Reconstruction and Development / The World Bank, Washington (DC).

Brennan, C.W., Verhaak, R.G.W., McKenna, A., Campos, B., Noushmehr, H., Salama, S.R., Zheng, S., Chakravarty, D., Sanborn, J.Z., Berman, S.H., Beroukhim, R., Bernard, B., Wu, C.-J., Genovese, G., Shmulevich, I., Barnholtz-Sloan, J., Zou, L., Vegesna, R., Shukla, S.A., Ciriello, G., Yung, W.K., Zhang, W., Sougnez, C., Mikkelsen, T., Aldape, K., Bigner, D.D., Van Meir, E.G., Prados, M., Sloan, A., Black, K.L., Eschbacher, J., Finocchiaro, G., Friedman, W., Andrews, D.W., Guha, A., Iacocca, M., O'Neill, B.P., Foltz, G., Myers, J., Weisenberger, D.J., Penny, R., Kucherlapati, R., Perou, C.M., Hayes, D.N., Gibbs, R., Marra, M., Mills, G.B., Lander, E., Spellman, P., Wilson, R., Sander, C., Weinstein, J., Meyerson, M., Gabriel, S., Laird, P.W., Haussler, D., Getz, G., Chin, L., TCGA Research Network, 2013. The somatic genomic landscape of glioblastoma. Cell 155, 462–477. https://doi.org/10.1016/j.cell.2013.09.034

Brennecke, J., Aravin, A.A., Stark, A., Dus, M., Kellis, M., Sachidanandam, R., Hannon, G.J., 2007. Discrete small RNA-generating loci as master regulators of transposon activity in Drosophila. Cell 128, 1089–1103. https://doi.org/10.1016/j.cell.2007.01.043

Brenner, S., Johnson, M., Bridgham, J., Golda, G., Lloyd, D.H., Johnson, D., Luo, S., McCurdy, S., Foy, M., Ewan, M., Roth, R., George, D., Eletr, S., Albrecht, G., Vermaas, E., Williams, S.R., Moon, K., Burcham, T., Pallas, M., DuBridge, R.B., Kirchner, J., Fearon, K., Mao, J., Corcoran, K., 2000. Gene expression analysis by massively parallel signature sequencing (MPSS) on microbead arrays. Nat. Biotechnol. 18, 630–634. https://doi.org/10.1038/76469

Breslin, S., O'Driscoll, L., 2013. Three-dimensional cell culture: the missing link in drug discovery. Drug Discov. Today 18, 240–249. https://doi.org/10.1016/j.drudis.2012.10.003

Brito, L.P., Ribeiro, T.C., Almeida, M.Q., Jorge, A.A. de L., Soares, I.C., Latronico, A.C., Mendonca, B.B., Fragoso, M.C.B.V., Lerario, A.M., 2012. The role of fibroblast growth factor receptor 4 overexpression and gene amplification as prognostic markers in pediatric and adult adrenocortical tumors. Endocr. Relat. Cancer 19, L11-13. https://doi.org/10.1530/ERC-11-0231

Broekaert, D., Eyckerman, S., Lavens, D., Verhee, A., Waelput, W., Vandekerckhove, J., Tavernier, J., 2002. Comparison of leptin- and interleukin-6-regulated expression of the rPAP gene family: evidence for differential co-regulatory signals. Eur. Cytokine Netw. 13, 78–85.

Brooks, A.N., Kilgour, E., Smith, P.D., 2012. Molecular pathways: fibroblast growth factor signaling: a new therapeutic opportunity in cancer. Clin. Cancer Res. Off. J. Am. Assoc. Cancer Res. 18, 1855–1862. https://doi.org/10.1158/1078-0432.CCR-11-0699

Brown, A.P., Courtney, C.L., King, L.M., Groom, S.C., Graziano, M.J., 2005. Cartilage dysplasia and tissue mineralization in the rat following administration of a FGF receptor tyrosine kinase inhibitor. Toxicol. Pathol. 33, 449–455. https://doi.org/10.1080/01926230590961845

Buday, L., Warne, P.H., Downward, J., 1995. Downregulation of the Ras activation pathway by MAP kinase phosphorylation of Sos. Oncogene 11, 1327–1331.

Bukhari, M.H., Qureshi, S.S., Niazi, S., Asef, M., Naheed, M., Khan, S.A., Chaudhry, N.A., Tayyab, M., Hasan, M., 2007. Chemotherapeutic/chemopreventive role of retinoids in chemically induced skin carcinogenesis in albino mice. Int. J. Dermatol. 46, 1160–1165. https://doi.org/10.1111/j.1365-4632.2007.03425.x

Buller, C.L., Loberg, R.D., Fan, M.-H., Zhu, Q., Park, J.L., Vesely, E., Inoki, K., Guan, K.-L., Brosius, F.C., 2008. A GSK-3/TSC2/mTOR pathway regulates glucose uptake and GLUT1 glucose transporter expression. Am. J. Physiol. Cell Physiol. 295, C836-843. https://doi.org/10.1152/ajpcell.00554.2007

Burgess, W.H., Dionne, C.A., Kaplow, J., Mudd, R., Friesel, R., Zilberstein, A., Schlessinger, J., Jaye, M., 1990. Characterization and cDNA cloning of phospholipase C-gamma, a major substrate for heparin-binding growth factor 1 (acidic fibroblast growth factor)-activated tyrosine kinase. Mol. Cell. Biol. 10, 4770–4777.

Bushue, N., Wan, Y.-J.Y., 2010. Retinoid Pathway and Cancer Therapeutics. Adv. Drug Deliv. Rev. 62, 1285–1298. https://doi.org/10.1016/j.addr.2010.07.003

Byron, S.A., Chen, H., Wortmann, A., Loch, D., Gartside, M.G., Dehkhoda, F., Blais, S.P., Neubert, T.A., Mohammadi, M., Pollock, P.M., 2013. The N550K/H mutations in FGFR2 confer differential resistance to PD173074, dovitinib, and ponatinib ATP-competitive inhibitors. Neoplasia N. Y. N 15, 975–988.

Byron, S.A., Gartside, M.G., Wellens, C.L., Mallon, M.A., Keenan, J.B., Powell, M.A., Goodfellow, P.J., Pollock, P.M., 2008. Inhibition of activated fibroblast growth factor receptor 2 in endometrial cancer cells induces cell death despite PTEN abrogation. Cancer Res. 68, 6902–6907. https://doi.org/10.1158/0008-5472.CAN-08-0770

Byron, S.A., Pollock, P.M., 2009. FGFR2 as a molecular target in endometrial cancer. Future Oncol. Lond. Engl. 5, 27–32. https://doi.org/10.2217/14796694.5.1.27

Cai, Z., Zhao, J.-S., Li, J.-J., Peng, D.-N., Wang, X.-Y., Chen, T.-L., Qiu, Y.-P., Chen, P.-P., Li, W.-J., Xu, L.-Y., Li, E.-M., Tam, J.P.M., Qi, R.Z., Jia, W., Xie, D., 2010. A combined proteomics and metabolomics profiling of gastric cardia cancer reveals characteristic dysregulations in glucose metabolism. Mol. Cell. Proteomics MCP 9, 2617–2628. https://doi.org/10.1074/mcp.M110.000661

Calera, M.R., Martinez, C., Liu, H., Jack, A.K., Birnbaum, M.J., Pilch, P.F., 1998. Insulin increases the association of Akt-2 with Glut4-containing vesicles. J. Biol. Chem. 273, 7201–7204.

Callahan, R., Smith, G.H., 2000. MMTV-induced mammary tumorigenesis: gene discovery, progression to malignancy and cellular pathways. Oncogene 19, 992–1001. https://doi.org/10.1038/sj.onc.1203276

Camargo, M.C., Anderson, W.F., King, J.B., Correa, P., Thomas, C.C., Rosenberg, P.S., Eheman, C.R., Rabkin, C.S., 2011. Divergent trends for gastric cancer incidence by anatomical subsite in US adults. Gut 60, 1644–1649. https://doi.org/10.1136/gut.2010.236737

Campbell, L.K., White, J.R., Campbell, R.K., 1996. Acarbose: its role in the treatment of diabetes mellitus. Ann. Pharmacother. 30, 1255–1262. https://doi.org/10.1177/106002809603001110

Cancer Genome Atlas Network, 2012. Comprehensive molecular portraits of human breast tumours. Nature 490, 61–70. https://doi.org/10.1038/nature11412

Cancer Genome Atlas Research Network, 2014a. Comprehensive molecular characterization of urothelial bladder carcinoma. Nature 507, 315–322. https://doi.org/10.1038/nature12965

Cancer Genome Atlas Research Network, 2014b. Comprehensive molecular characterization of gastric adenocarcinoma. Nature 513, 202–209. https://doi.org/10.1038/nature13480

Cancer Genome Atlas Research Network, 2014c. Comprehensive molecular profiling of lung adenocarcinoma. Nature 511, 543–550. https://doi.org/10.1038/nature13385

Cancer Genome Atlas Research Network, 2013. Comprehensive molecular characterization of clear cell renal cell carcinoma. Nature 499, 43–49. https://doi.org/10.1038/nature12222

Cancer Genome Atlas Research Network, 2012. Comprehensive genomic characterization of squamous cell lung cancers. Nature 489, 519–525. https://doi.org/10.1038/nature11404

Cancer Genome Atlas Research Network, 2011. Integrated genomic analyses of ovarian carcinoma. Nature 474, 609–615. https://doi.org/10.1038/nature10166

Cancer Genome Atlas Research Network, Kandoth, C., Schultz, N., Cherniack, A.D., Akbani, R., Liu, Y., Shen, H., Robertson, A.G., Pashtan, I., Shen, R., Benz, C.C., Yau, C., Laird, P.W., Ding, L., Zhang, W., Mills, G.B., Kucherlapati, R., Mardis, E.R., Levine, D.A., 2013. Integrated genomic characterization of endometrial carcinoma. Nature 497, 67–73. https://doi.org/10.1038/nature12113

Cancer Statistics [WWW Document], n.d. . Natl. Cancer Inst. URL https://www.cancer.gov/about-cancer/understanding/statistics (accessed 7.10.18).

Cao, J., Xu, G., Lan, J., Huang, Q., Tang, Z., Tian, L., 2016. High expression of piwi-like RNA-mediated gene silencing 1 is associated with poor prognosis via regulating transforming growth factor-β receptors and cyclin-dependent kinases in breast cancer. Mol. Med. Rep. 13, 2829–2835. https://doi.org/10.3892/mmr.2016.4842

Cappellen, D., De Oliveira, C., Ricol, D., de Medina, S., Bourdin, J., Sastre-Garau, X., Chopin, D., Thiery, J.P., Radvanyi, F., 1999. Frequent activating mutations of FGFR3 in human bladder and cervix carcinomas. Nat. Genet. 23, 18–20. https://doi.org/10.1038/12615

Carlsson, J., Acker, H., 1988. Relations between pH, oxygen partial pressure and growth in cultured cell spheroids. Int. J. Cancer 42, 715–720.

Carneiro, B.A., Elvin, J.A., Kamath, S.D., Ali, S.M., Paintal, A.S., Restrepo, A., Berry, E., Giles, F.J., Johnson, M.L., 2015. FGFR3–TACC3: A novel gene fusion in cervical cancer. Gynecol. Oncol. Rep. 13, 53–56. https://doi.org/10.1016/j.gore.2015.06.005

Carpenter, G., Ji, Q. s, 1999. Phospholipase C-gamma as a signal-transducing element. Exp. Cell Res. 253, 15–24. https://doi.org/10.1006/excr.1999.4671

Carpenter, T.O., Imel, E.A., Ruppe, M.D., Weber, T.J., Klausner, M.A., Wooddell, M.M., Kawakami, T., Ito, T., Zhang, X., Humphrey, J., Insogna, K.L., Peacock, M., 2014. Randomized trial of the anti-FGF23 antibody KRN23 in X-linked hypophosphatemia. J. Clin. Invest. 124, 1587–1597. https://doi.org/10.1172/JCI72829

Carracedo, A., Ma, L., Teruya-Feldstein, J., Rojo, F., Salmena, L., Alimonti, A., Egia, A., Sasaki, A.T., Thomas, G., Kozma, S.C., Papa, A., Nardella, C., Cantley, L.C., Baselga, J., Pandolfi, P.P., 2008. Inhibition of mTORC1 leads to MAPK pathway activation through a PI3K-dependent feedback loop in human cancer. J. Clin. Invest. 118, 3065–3074. https://doi.org/10.1172/JCI34739

Carter, E.P., Fearon, A.E., Grose, R.P., 2015. Careless talk costs lives: fibroblast growth factor receptor signalling and the consequences of pathway malfunction. Trends Cell Biol. 25, 221–233. https://doi.org/10.1016/j.tcb.2014.11.003

Carter, J.H., Cottrell, C.E., McNulty, S.N., Vigh-Conrad, K.A., Lamp, S., Heusel, J.W., Duncavage, E.J., 2017. FGFR2 amplification in colorectal adenocarcinoma. Cold Spring Harb. Mol. Case Stud. 3. https://doi.org/10.1101/mcs.a001495

Casciari, J.J., Sotirchos, S.V., Sutherland, R.M., 1992. Variations in tumor cell growth rates and metabolism with oxygen concentration, glucose concentration, and extracellular pH. J. Cell. Physiol. 151, 386–394. https://doi.org/10.1002/jcp.1041510220

Castañeda, F., Kinne, R.K., 2000. Short exposure to millimolar concentrations of ethanol induces apoptotic cell death in multicellular HepG2 spheroids. J. Cancer Res. Clin. Oncol. 126, 305–310.

Catasús, L., Matias-Guiu, X., Machin, P., Muñoz, J., Prat, J., 1998. BAX somatic frameshift mutations in endometrioid adenocarcinomas of the endometrium: evidence for a tumor progression role in endometrial carcinomas with microsatellite instability. Lab. Investig. J. Tech. Methods Pathol. 78, 1439–1444.

Cavard, C., Terris, B., Grimber, G., Christa, L., Audard, V., Radenen-Bussiere, B., Simon, M.-T., Renard, C.-A., Buendia, M.-A., Perret, C., 2006. Overexpression of regenerating islet-derived 1 alpha and 3 alpha genes in human primary

liver tumors with beta-catenin mutations. Oncogene 25, 599–608. https://doi.org/10.1038/sj.onc.1208860

Cha, J.Y., Maddileti, S., Mitin, N., Harden, T.K., Der, C.J., 2009. Aberrant receptor internalization and enhanced FRS2-dependent signaling contribute to the transforming activity of the fibroblast growth factor receptor 2 IIIb C3 isoform. J. Biol. Chem. 284, 6227–6240. https://doi.org/10.1074/jbc.M803998200

Chang, J., Park, K., Bang, Y.J., Kim, W.S., Kim, D., Kim, S.J., 1997. Expression of transforming growth factor beta type II receptor reduces tumorigenicity in human gastric cancer cells. Cancer Res. 57, 2856–2859.

Chang, L.-S., Barroso-Sousa, R., Tolaney, S.M., Hodi, F.S., Kaiser, U.B., Min, L., 2018. Endocrine toxicity of cancer immunotherapy targeting immune checkpoints. Endocr. Rev. https://doi.org/10.1210/er.2018-00006

Chantry, D., Vojtek, A., Kashishian, A., Holtzman, D.A., Wood, C., Gray, P.W., Cooper, J.A., Hoekstra, M.F., 1997. p110delta, a novel phosphatidylinositol 3-kinase catalytic subunit that associates with p85 and is expressed predominantly in leukocytes. J. Biol. Chem. 272, 19236–19241.

Chao, A., Lin, C.-Y., Wu, R.-C., Lee, Y.-S., Lee, L.-Y., Tsai, C.-L., Yang, L.-Y., Liu, H., Chen, S.-J., Wang, T.-H., Lai, C.-H., 2018. The combination of everolimus and terameprocol exerts synergistic antiproliferative effects in endometrial cancer: molecular role of insulin-like growth factor binding protein 2. J. Mol. Med. Berl. Ger. https://doi.org/10.1007/s00109-018-1699-5

Charrez, B., Qiao, L., Hebbard, L., 2015. The role of fructose in metabolism and cancer. Horm. Mol. Biol. Clin. Investig. 22, 79–89. https://doi.org/10.1515/hmbci-2015-0009

Chaudhry, P., Asselin, E., 2009. Resistance to chemotherapy and hormone therapy in endometrial cancer. Endocr. Relat. Cancer 16, 363–380. https://doi.org/10.1677/ERC-08-0266

Chell, V., Balmanno, K., Little, A.S., Wilson, M., Andrews, S., Blockley, L., Hampson, M., Gavine, P.R., Cook, S.J., 2013. Tumour cell responses to new fibroblast growth factor receptor tyrosine kinase inhibitors and identification of a gatekeeper mutation in FGFR3 as a mechanism of acquired resistance. Oncogene 32, 3059–3070. https://doi.org/10.1038/onc.2012.319

Chen, C.S., Mrksich, M., Huang, S., Whitesides, G.M., Ingber, D.E., 1997. Geometric control of cell life and death. Science 276, 1425–1428.

Chen, J., Lee, B.H., Williams, I.R., Kutok, J.L., Mitsiades, C.S., Duclos, N., Cohen, S., Adelsperger, J., Okabe, R., Coburn, A., Moore, S., Huntly, B.J.P., Fabbro, D., Anderson, K.C., Griffin, J.D., Gilliland, D.G., 2005. FGFR3 as a therapeutic target of the small molecule inhibitor PKC412 in hematopoietic malignancies. Oncogene 24, 8259–8267. https://doi.org/10.1038/sj.onc.1208989

Chen, J.L.-Y., Lucas, J.E., Schroeder, T., Mori, S., Wu, J., Nevins, J., Dewhirst, M., West, M., Chi, J.-T., 2008. The genomic analysis of lactic acidosis and acidosis response in human cancers. PLoS Genet. 4, e1000293. https://doi.org/10.1371/journal.pgen.1000293

Chen, L., Li, D., Li, C., Engel, A., Deng, C.-X., 2003. A Ser252Trp [corrected] substitution in mouse fibroblast growth factor receptor 2 (Fgfr2) results in craniosynostosis. Bone 33, 169–178.

Chen, W.-J., Ho, C.-C., Chang, Y.-L., Chen, H.-Y., Lin, C.-A., Ling, T.-Y., Yu, S.-L., Yuan, S.-S., Chen, Y.-J.L., Lin, C.-Y., Pan, S.-H., Chou, H.-Y.E., Chen, Y.-J., Chang, G.-C., Chu, W.-C., Lee, Y.-M., Lee, J.-Y., Lee, P.-J., Li, K.-C., Chen, H.-W., Yang, P.-C., 2014. Cancer-associated fibroblasts regulate the plasticity of lung cancer stemness via paracrine signalling. Nat. Commun. 5, 3472. https://doi.org/10.1038/ncomms4472

Chen, Y., Tian, T., Mao, M.-J., Deng, W.-Y., Li, H., 2018. CRBP-1 over-expression is associated with poor prognosis in tongue squamous cell carcinoma. BMC Cancer 18. https://doi.org/10.1186/s12885-018-4249-1

Chen, Z., Che, Q., He, X., Wang, F., Wang, H., Zhu, M., Sun, J., Wan, X., 2015. Stem cell protein Piwil1 endowed endometrial cancer cells with stem-like properties via inducing epithelial-mesenchymal transition. BMC Cancer 15, 811. https://doi.org/10.1186/s12885-015-1794-8

Cheng, J.K., Alper, H.S., 2014. The genome editing toolbox: a spectrum of approaches for targeted modification. Curr. Opin. Biotechnol. 30, 87–94. https://doi.org/10.1016/j.copbio.2014.06.005

Cheng, Y., Zhang, Y., Zhang, L., Ren, X., Huber-Keener, K.J., Liu, X., Zhou, L., Liao, J., Keihack, H., Yan, L., Rubin, E., Yang, J.-M., 2012. MK-2206, a novel allosteric inhibitor of Akt, synergizes with gefitinib against malignant glioma via modulating both autophagy and apoptosis. Mol. Cancer Ther. 11, 154–164. https://doi.org/10.1158/1535-7163.MCT-11-0606

Chioni, A.-M., Grose, R., 2012. FGFR1 cleavage and nuclear translocation regulates breast cancer cell behavior. J. Cell Biol. 197, 801–817. https://doi.org/10.1083/jcb.201108077

Chiu, H.-J., Fischman, D.A., Hammerling, U., 2008. Vitamin A depletion causes oxidative stress, mitochondrial dysfunction, and PARP-1-dependent energy deprivation. FASEB J. Off. Publ. Fed. Am. Soc. Exp. Biol. 22, 3878–3887. https://doi.org/10.1096/fj.08-112375

Cho, J.Y., Guo, C., Torello, M., Lunstrum, G.P., Iwata, T., Deng, C., Horton, W.A., 2004. Defective lysosomal targeting of activated fibroblast growth factor receptor 3 in achondroplasia. Proc. Natl. Acad. Sci. U. S. A. 101, 609–614. https://doi.org/10.1073/pnas.2237184100

Choe, C., Shin, Y.-S., Kim, C., Choi, S.-J., Lee, J., Kim, S.Y., Cho, Y.B., Kim, J., 2015. Crosstalk with cancer-associated fibroblasts induces resistance of non-small cell lung cancer cells to epidermal growth factor receptor tyrosine kinase inhibition. OncoTargets Ther. 8, 3665–3678. https://doi.org/10.2147/OTT.S89659

Chon, S.-H., Berlth, F., Plum, P.S., Herbold, T., Alakus, H., Kleinert, R., Moenig, S.P., Bruns, C.J., Hoelscher, A.H., Meyer, H.-J., 2017. Gastric cancer treatment in the world: Germany. Transl. Gastroenterol. Hepatol. 2. https://doi.org/10.21037/tgh.2017.05.07

Chow, W.H., Blot, W.J., Vaughan, T.L., Risch, H.A., Gammon, M.D., Stanford, J.L., Dubrow, R., Schoenberg, J.B., Mayne, S.T., Farrow, D.C., Ahsan, H., West, A.B., Rotterdam, H., Niwa, S., Fraumeni, J.F., 1998. Body mass index and risk of adenocarcinomas of the esophagus and gastric cardia. J. Natl. Cancer Inst. 90, 150–155.

Christoforidis, S., Miaczynska, M., Ashman, K., Wilm, M., Zhao, L., Yip, S.C., Waterfield, M.D., Backer, J.M., Zerial, M., 1999. Phosphatidylinositol-3-OH kinases are Rab5 effectors. Nat. Cell Biol. 1, 249–252. https://doi.org/10.1038/12075

Chu, J., Cargnello, M., Topisirovic, I., Pelletier, J., 2016. Translation Initiation Factors: Reprogramming Protein Synthesis in Cancer. Trends Cell Biol. 26, 918–933. https://doi.org/10.1016/j.tcb.2016.06.005

Ciriello, G., Miller, M.L., Aksoy, B.A., Senbabaoglu, Y., Schultz, N., Sander, C., 2013. Emerging landscape of oncogenic signatures across human cancers. Nat. Genet. 45, 1127–1133. https://doi.org/10.1038/ng.2762

Cloonan, N., Forrest, A.R.R., Kolle, G., Gardiner, B.B.A., Faulkner, G.J., Brown, M.K., Taylor, D.F., Steptoe, A.L., Wani, S., Bethel, G., Robertson, A.J., Perkins, A.C., Bruce, S.J., Lee, C.C., Ranade, S.S., Peckham, H.E., Manning, J.M., McKernan, K.J., Grimmond, S.M., 2008. Stem cell transcriptome profiling via massive-scale mRNA sequencing. Nat. Methods 5, 613–619. https://doi.org/10.1038/nmeth.1223

Coleman, S.J., Chioni, A.-M., Ghallab, M., Anderson, R.K., Lemoine, N.R., Kocher, H.M., Grose, R.P., 2014. Nuclear translocation of FGFR1 and FGF2 in pancreatic stellate cells facilitates pancreatic cancer cell invasion. EMBO Mol. Med. 6, 467–481. https://doi.org/10.1002/emmm.201302698

Coppock, D., Kopman, C., Gudas, J., Cina-Poppe, D.A., 2000. Regulation of the quiescence-induced genes: quiescin Q6, decorin, and ribosomal protein S29. Biochem. Biophys. Res. Commun. 269, 604–610. https://doi.org/10.1006/bbrc.2000.2324

Corbit, K.C., Trakul, N., Eves, E.M., Diaz, B., Marshall, M., Rosner, M.R., 2003. Activation of Raf-1 signaling by protein kinase C through a mechanism involving Raf kinase inhibitory protein. J. Biol. Chem. 278, 13061–13068. https://doi.org/10.1074/jbc.M210015200

Corley, D.A., Kubo, A., 2004. Influence of site classification on cancer incidence rates: an analysis of gastric cardia carcinomas. J. Natl. Cancer Inst. 96, 1383–1387. https://doi.org/10.1093/jnci/djh265

Correa, P., Shiao, Y.H., 1994. Phenotypic and genotypic events in gastric carcinogenesis. Cancer Res. 54, 1941s-1943s.

Correia, A.L., Bissell, M.J., 2012. The tumor microenvironment is a dominant force in multidrug resistance. Drug Resist. Updat. Rev. Comment. Antimicrob. Anticancer Chemother. 15, 39–49. https://doi.org/10.1016/j.drup.2012.01.006

Cortes, J.E., Kim, D.-W., Pinilla-Ibarz, J., le Coutre, P., Paquette, R., Chuah, C., Nicolini, F.E., Apperley, J.F., Khoury, H.J., Talpaz, M., DiPersio, J., DeAngelo, D.J., Abruzzese, E., Rea, D., Baccarani, M., Müller, M.C., Gambacorti-Passerini, C., Wong, S., Lustgarten, S., Rivera, V.M., Clackson, T., Turner, C.D., Haluska, F.G., Guilhot, F., Deininger, M.W., Hochhaus, A., Hughes, T., Goldman, J.M., Shah, N.P., Kantarjian, H., PACE Investigators, 2013. A phase 2 trial of ponatinib in Philadelphia chromosome-positive leukemias. N. Engl. J. Med. 369, 1783–1796. https://doi.org/10.1056/NEJMoa1306494

Costa, R., Carneiro, B.A., Taxter, T., Tavora, F.A., Kalyan, A., Pai, S.A., Chae, Y.K., Giles, F.J., 2016. FGFR3-TACC3 fusion in solid tumors: mini review. Oncotarget 7, 55924–55938. https://doi.org/10.18632/oncotarget.10482

Coumoul, X., Deng, C.-X., 2003. Roles of FGF receptors in mammalian development and congenital diseases. Birth Defects Res. Part C Embryo Today Rev. 69, 286–304. https://doi.org/10.1002/bdrc.10025

Courjal, F., Cuny, M., Simony-Lafontaine, J., Louason, G., Speiser, P., Zeillinger, R., Rodriguez, C., Theillet, C., 1997. Mapping of DNA amplifications at 15 chromosomal localizations in 1875 breast tumors: definition of phenotypic groups. Cancer Res. 57, 4360–4367.

Cox, D.N., Chao, A., Baker, J., Chang, L., Qiao, D., Lin, H., 1998. A novel class of evolutionarily conserved genes defined by piwi are essential for stem cell self-renewal. Genes Dev. 12, 3715–3727.

Cras, A., Politis, B., Balitrand, N., Darsin-Bettinger, D., Boelle, P.Y., Cassinat, B., Toubert, M.-E., Chomienne, C., 2012. Bexarotene via CBP/p300 induces suppression of NF-κB-dependent cell growth and invasion in thyroid cancer. Clin. Cancer Res. Off. J. Am. Assoc. Cancer Res. 18, 442–453. https://doi.org/10.1158/1078-0432.CCR-11-0510

Creasman, W.T., Odicino, F., Maisonneuve, P., Beller, U., Benedet, J.L., Heintz, A.P., Ngan, H.Y., Sideri, M., Pecorelli, S., 2001. Carcinoma of the corpus uteri. J. Epidemiol. Biostat. 6, 47–86.

Cross, H.S., Quaroni, A., 1991. Inhibition of sucrose-isomaltase expression by EGF in the human colon adenocarcinoma cells Caco-2. Am. J. Physiol. 261, C1173-1183. https://doi.org/10.1152/ajpcell.1991.261.6.C1173

Cross, N.C.P., Reiter, A., 2008. Fibroblast growth factor receptor and platelet-derived growth factor receptor abnormalities in eosinophilic myeloproliferative disorders. Acta Haematol. 119, 199–206. https://doi.org/10.1159/000140631

Cukierman, E., Pankov, R., Stevens, D.R., Yamada, K.M., 2001. Taking cell-matrix adhesions to the third dimension. Science 294, 1708–1712. https://doi.org/10.1126/science.1064829

Cukierman, E., Pankov, R., Yamada, K.M., 2002. Cell interactions with three-dimensional matrices. Curr. Opin. Cell Biol. 14, 633–639.

Curtis, R.K., Oresic, M., Vidal-Puig, A., 2005. Pathways to the analysis of microarray data. Trends Biotechnol. 23, 429–435. https://doi.org/10.1016/j.tibtech.2005.05.011

Cvetković, D., Williams, S.J., Hamilton, T.C., 2003. Loss of cellular retinol-binding protein 1 gene expression in microdissected human ovarian cancer. Clin. Cancer Res. Off. J. Am. Assoc. Cancer Res. 9, 1013–1020.

Dagogo-Jack, I., Shaw, A.T., 2018. Tumour heterogeneity and resistance to cancer therapies. Nat. Rev. Clin. Oncol. 15, 81–94. https://doi.org/10.1038/nrclinonc.2017.166

Dailey, L., Ambrosetti, D., Mansukhani, A., Basilico, C., 2005. Mechanisms underlying differential responses to FGF signaling. Cytokine Growth Factor Rev. 16, 233–247. https://doi.org/10.1016/j.cytogfr.2005.01.007

Dalton, W.S., 2003. The tumor microenvironment: focus on myeloma. Cancer Treat. Rev. 29 Suppl 1, 11–19.

D'Ambrosio, L., Palesandro, E., Moretti, M., Pelosi, G., Fabbri, A., Carnevale Schianca, F., Aglietta, M., Grignani, G., 2017. Alpha-fetoprotein elevation in NUT midline carcinoma: a case report. BMC Cancer 17, 266. https://doi.org/10.1186/s12885-017-3262-0

Darnell, J.E., 1997. STATs and gene regulation. Science 277, 1630–1635.

Das, B.C., Thapa, P., Karki, R., Das, S., Mahapatra, S., Liu, T.-C., Torregroza, I., Wallace, D.P., Kambhampati, S., Van Veldhuizen, P., Verma, A., Ray, S.K., Evans, T., 2014. Retinoic Acid Signaling Pathways in Development and Diseases. Bioorg. Med. Chem. 22, 673–683. https://doi.org/10.1016/j.bmc.2013.11.025

Das, M., Scappini, E., Martin, N.P., Wong, K.A., Dunn, S., Chen, Y.-J., Miller, S.L.H., Domin, J., O'Bryan, J.P., 2007. Regulation of neuron survival through an intersectin-phosphoinositide 3'-kinase C2beta-AKT pathway. Mol. Cell. Biol. 27, 7906–7917. https://doi.org/10.1128/MCB.01369-07

Das Thakur, M., Salangsang, F., Landman, A.S., Sellers, W.R., Pryer, N.K., Levesque, M.P., Dummer, R., McMahon, M., Stuart, D.D., 2013. Modelling vemurafenib resistance in melanoma reveals a strategy to forestall drug resistance. Nature 494, 251–255. https://doi.org/10.1038/nature11814

Daşu, A., Toma-Daşu, I., Karlsson, M., 2003. Theoretical simulation of tumour oxygenation and results from acute and chronic hypoxia. Phys. Med. Biol. 48, 2829–2842.

Datta, J., Damodaran, S., Parks, H., Ocrainiciuc, C., Miya, J., Yu, L., Gardner, E.P., Samorodnitsky, E., Wing, M.R., Bhatt, D., Hays, J., Reeser, J.W., Roychowdhury, S., 2017b. Akt Activation Mediates Acquired Resistance to Fibroblast Growth Factor Receptor Inhibitor BGJ398. Mol. Cancer Ther. 16, 614–624. https://doi.org/10.1158/1535-7163.MCT-15-1010

David, C.C., Jacobs, D.J., 2014. Principal Component Analysis: A Method for Determining the Essential Dynamics of Proteins. Methods Mol. Biol. Clifton NJ 1084, 193–226. https://doi.org/10.1007/978-1-62703-658-0_11

Davies, H., Bignell, G.R., Cox, C., Stephens, P., Edkins, S., Clegg, S., Teague, J., Woffendin, H., Garnett, M.J., Bottomley, W., Davis, N., Dicks, E., Ewing, R., Floyd, Y., Gray, K., Hall, S., Hawes, R., Hughes, J., Kosmidou, V., Menzies, A., Mould, C., Parker, A., Stevens, C., Watt, S., Hooper, S., Wilson, R., Jayatilake, H., Gusterson, B.A., Cooper, C., Shipley, J., Hargrave, D., Pritchard-Jones, K., Maitland, N., Chenevix-Trench, G., Riggins, G.J., Bigner, D.D., Palmieri, G., Cossu, A., Flanagan, A., Nicholson, A., Ho, J.W.C., Leung, S.Y., Yuen, S.T., Weber, B.L., Seigler, H.F., Darrow, T.L., Paterson, H., Marais, R., Marshall, C.J., Wooster, R., Stratton, M.R., Futreal, P.A., 2002. Mutations of the BRAF gene in human cancer. Nature 417, 949–954. https://doi.org/10.1038/nature00766

Day, E.K., Sosale, N.G., Lazzara, M.J., 2016. Cell Signaling Regulation by Protein Phosphorylation: A Multivariate, Heterogeneous, and Context-dependent Process. Curr. Opin. Biotechnol. 40, 185–192. https://doi.org/10.1016/j.copbio.2016.06.005

de Martel, C., Forman, D., Plummer, M., 2013. Gastric cancer: epidemiology and risk factors. Gastroenterol. Clin. North Am. 42, 219–240. https://doi.org/10.1016/j.gtc.2013.01.003

De Moerlooze, L., Spencer-Dene, B., Revest, J.M., Hajihosseini, M., Rosewell, I., Dickson, C., 2000. An important role for the IIIb isoform of fibroblast growth factor receptor 2 (FGFR2) in mesenchymal-epithelial signalling during mouse organogenesis. Dev. Camb. Engl. 127, 483–492.

De Stefani, E., Deneo-Pellegrini, H., Mendilaharsu, M., Carzoglio, J.C., Ronco, A., 1997. Dietary fat and lung cancer: a case-control study in Uruguay. Cancer Causes Control CCC 8, 913–921.

De Wever, O., Mareel, M., 2003. Role of tissue stroma in cancer cell invasion. J. Pathol. 200, 429–447. https://doi.org/10.1002/path.1398

Degner, J.F., Marioni, J.C., Pai, A.A., Pickrell, J.K., Nkadori, E., Gilad, Y., Pritchard, J.K., 2009. Effect of read-mapping biases on detecting allele-specific expression from RNA-sequencing data. Bioinforma. Oxf. Engl. 25, 3207–3212. https://doi.org/10.1093/bioinformatics/btp579

del Carmen, M.G., Birrer, M., Schorge, J.O., 2012. Uterine papillary serous cancer: a review of the literature. Gynecol. Oncol. 127, 651–661. https://doi.org/10.1016/j.ygyno.2012.09.012

Del Carmen, M.G., Boruta, D.M., Schorge, J.O., 2011. Recurrent endometrial cancer. Clin. Obstet. Gynecol. 54, 266–277. https://doi.org/10.1097/GRF.0b013e318218c6d1

Denko, N.C., 2008. Hypoxia, HIF1 and glucose metabolism in the solid tumour. Nat. Rev. Cancer 8, 705–713. https://doi.org/10.1038/nrc2468

Dennis, G., Sherman, B.T., Hosack, D.A., Yang, J., Gao, W., Lane, H.C., Lempicki, R.A., 2003. DAVID: Database for Annotation, Visualization, and Integrated Discovery. Genome Biol. 4, R60.

Desai, A., Adjei, A.A., 2016. FGFR Signaling as a Target for Lung Cancer Therapy. J. Thorac. Oncol. Off. Publ. Int. Assoc. Study Lung Cancer 11, 9–20. https://doi.org/10.1016/j.jtho.2015.08.003

Devesa, S.S., Blot, W.J., Fraumeni, J.F., 1998. Changing patterns in the incidence of esophageal and gastric carcinoma in the United States. Cancer 83, 2049–2053.

Devic, S., 2016. Warburg Effect - a Consequence or the Cause of Carcinogenesis? J. Cancer 7, 817–822. https://doi.org/10.7150/jca.14274

Dhillon, A.S., Hagan, S., Rath, O., Kolch, W., 2007. MAP kinase signalling pathways in cancer. Oncogene 26, 3279–3290. https://doi.org/10.1038/sj.onc.1210421

Dhiman, H.K., Ray, A.R., Panda, A.K., 2005. Three-dimensional chitosan scaffold-based MCF-7 cell culture for the determination of the cytotoxicity of tamoxifen. Biomaterials 26, 979–986. https://doi.org/10.1016/j.biomaterials.2004.04.012

Di Fiore, F., Blanchard, F., Charbonnier, F., Le Pessot, F., Lamy, A., Galais, M.P., Bastit, L., Killian, A., Sesboüé, R., Tuech, J.J., Queuniet, A.M., Paillot, B., Sabourin, J.C., Michot, F., Michel, P., Frebourg, T., 2007. Clinical relevance of KRAS mutation detection in metastatic colorectal cancer treated by Cetuximab plus chemotherapy. Br. J. Cancer 96, 1166–1169. https://doi.org/10.1038/sj.bjc.6603685

Didkowska, J., Wojciechowska, U., Mańczuk, M., Łobaszewski, J., 2016. Lung cancer epidemiology: contemporary and future challenges worldwide. Ann. Transl. Med. 4. https://doi.org/10.21037/atm.2016.03.11

Dieci, M.V., Arnedos, M., Andre, F., Soria, J.C., 2013. Fibroblast growth factor receptor inhibitors as a cancer treatment: from a biologic rationale to medical perspectives. Cancer Discov. 3, 264–279. https://doi.org/10.1158/2159-8290.CD-12-0362

Dilworth, F.J., Chambon, P., 2001. Nuclear receptors coordinate the activities of chromatin remodeling complexes and coactivators to facilitate initiation of transcription. Oncogene 20, 3047–3054. https://doi.org/10.1038/sj.onc.1204329

Ding, L., Getz, G., Wheeler, D.A., Mardis, E.R., McLellan, M.D., Cibulskis, K., Sougnez, C., Greulich, H., Muzny, D.M., Morgan, M.B., Fulton, L., Fulton, R.S., Zhang, Q., Wendl, M.C., Lawrence, M.S., Larson, D.E., Chen, K., Dooling, D.J., Sabo, A., Hawes, A.C., Shen, H., Jhangiani, S.N., Lewis, L.R., Hall, O., Zhu, Y., Mathew, T., Ren, Y., Yao, J., Scherer, S.E., Clerc, K., Metcalf, G.A., Ng, B., Milosavljevic, A., Gonzalez-Garay, M.L., Osborne, J.R., Meyer, R., Shi, X., Tang, Y., Koboldt, D.C., Lin, L., Abbott, R., Miner, T.L., Pohl, C., Fewell, G., Haipek, C., Schmidt, H., Dunford-Shore, B.H., Kraja, A., Crosby, S.D., Sawyer, C.S., Vickery, T., Sander, S., Robinson, J., Winckler, W., Baldwin, J., Chirieac, L.R., Dutt, A., Fennell, T., Hanna, M., Johnson, B.E., Onofrio, R.C., Thomas, R.K., Tonon, G., Weir, B.A., Zhao, X., Ziaugra, L., Zody, M.C., Giordano, T., Orringer, M.B., Roth, J.A., Spitz, M.R., Wistuba, I.I., Ozenberger, B., Good, P.J., Chang, A.C., Beer, D.G., Watson, M.A., Ladanyi, M., Broderick, S., Yoshizawa, A., Travis, W.D., Pao, W., Province, M.A., Weinstock, G.M., Varmus, H.E., Gabriel, S.B., Lander, E.S., Gibbs, R.A., Meyerson, M., Wilson, R.K., 2008. Somatic mutations affect key pathways in lung adenocarcinoma. Nature 455, 1069–1075. https://doi.org/10.1038/nature07423

Dirami, G., Massaro, G.D., Clerch, L.B., Ryan, U.S., Reczek, P.R., Massaro, D., 2004. Lung retinol storing cells synthesize and secrete retinoic acid, an inducer of alveolus formation. Am. J. Physiol. Lung Cell. Mol. Physiol. 286, L249-256. https://doi.org/10.1152/ajplung.00140.2003

do Amaral, J.B., Rezende-Teixeira, P., Freitas, V.M., Machado-Santelli, G.M., 2011. MCF-7 cells as a three-dimensional model for the study of human breast cancer. Tissue Eng. Part C Methods 17, 1097–1107. https://doi.org/10.1089/ten.tec.2011.0260

Dodé, C., Levilliers, J., Dupont, J.-M., De Paepe, A., Le Dû, N., Soussi-Yanicostas, N., Coimbra, R.S., Delmaghani, S., Compain-Nouaille, S., Baverel, F., Pêcheux, C., Le Tessier, D., Cruaud, C., Delpech, M., Speleman, F., Vermeulen, S., Amalfitano, A., Bachelot, Y., Bouchard, P., Cabrol, S., Carel, J.-C., Delemarre-van de Waal, H., Goulet-Salmon, B., Kottler, M.-L., Richard, O., Sanchez-Franco, F., Saura, R., Young, J., Petit, C., Hardelin, J.-P., 2003. Loss-of-function mutations in FGFR1 cause autosomal dominant Kallmann syndrome. Nat. Genet. 33, 463–465. https://doi.org/10.1038/ng1122

Doldo, E., Costanza, G., Ferlosio, A., Pompeo, E., Agostinelli, S., Bellezza, G., Mazzaglia, D., Giunta, A., Sidoni, A., Orlandi, A., 2015. High expression of cellular retinol binding protein-1 in lung adenocarcinoma is associated with poor prognosis. Genes Cancer 6, 490–502.

Doll, R., Hill, A.B., 1950. Smoking and Carcinoma of the Lung. Br. Med. J. 2, 739–748.

Doll, R., Peto, R., Boreham, J., Sutherland, I., 2005. Mortality from cancer in relation to smoking: 50 years observations on British doctors. Br. J. Cancer 92, 426–429. https://doi.org/10.1038/sj.bjc.6602359

Donner, A., 2012. Drug resistance: the stroma's contribution. Nat. Chem. Biol. 8, 739. https://doi.org/10.1038/nchembio.1055

Duggan, B.D., Felix, J.C., Muderspach, L.I., Tourgeman, D., Zheng, J., Shibata, D., 1994. Microsatellite instability in sporadic endometrial carcinoma. J. Natl. Cancer Inst. 86, 1216–1221.

Durkin, M.E., Ullmannova, V., Guan, M., Popescu, N.C., 2007. Deleted in liver cancer 3 (DLC-3), a novel Rho GTPase-activating protein, is downregulated in cancer and inhibits tumor cell growth. Oncogene 26, 4580–4589. https://doi.org/10.1038/sj.onc.1210244

Dusetti, N.J., Frigerio, J.M., Fox, M.F., Swallow, D.M., Dagorn, J.C., Iovanna, J.L., 1994. Molecular cloning, genomic organization, and chromosomal localization of the human pancreatitis-associated protein (PAP) gene. Genomics 19, 108–114. https://doi.org/10.1006/geno.1994.1019

Dutt, A., Salvesen, H.B., Chen, T.-H., Ramos, A.H., Onofrio, R.C., Hatton, C., Nicoletti, R., Winckler, W., Grewal, R., Hanna, M., Wyhs, N., Ziaugra, L., Richter, D.J., Trovik, J., Engelsen, I.B., Stefansson, I.M., Fennell, T., Cibulskis, K., Zody, M.C., Akslen, L.A., Gabriel, S., Wong, K.-K., Sellers, W.R., Meyerson, M., Greulich, H., 2008. Drug-sensitive FGFR2 mutations in endometrial carcinoma. Proc. Natl. Acad. Sci. U. S. A. 105, 8713–8717. https://doi.org/10.1073/pnas.0803379105

Dvorak, H.F., 1986. Tumors: wounds that do not heal. Similarities between tumor stroma generation and wound healing. N. Engl. J. Med. 315, 1650–1659. https://doi.org/10.1056/NEJM198612253152606

Ebong, S., Yu, C.-R., Carper, D.A., Chepelinsky, A.B., Egwuagu, C.E., 2004. Activation of STAT signaling pathways and induction of suppressors of cytokine signaling (SOCS) proteins in mammalian lens by growth factors. Invest. Ophthalmol. Vis. Sci. 45, 872–878.

Edgren, H., Murumagi, A., Kangaspeska, S., Nicorici, D., Hongisto, V., Kleivi, K., Rye, I.H., Nyberg, S., Wolf, M., Borresen-Dale, A.-L., Kallioniemi, O., 2011. Identification of fusion genes in breast cancer by paired-end RNA-sequencing. Genome Biol. 12, R6. https://doi.org/10.1186/gb-2011-12-1-r6

Edmondson, R., Broglie, J.J., Adcock, A.F., Yang, L., 2014. Three-dimensional cell culture systems and their applications in drug discovery and cell-based biosensors. Assay Drug Dev. Technol. 12, 207–218. https://doi.org/10.1089/adt.2014.573

Eigenbrodt, E., Basenau, D., Holthusen, S., Mazurek, S., Fischer, G., 1997. Quantification of tumor type M2 pyruvate kinase (Tu M2-PK) in human carcinomas. Anticancer Res. 17, 3153–3156.

Ellis, J.A., Jackman, M.R., Luzio, J.P., 1992. The post-synthetic sorting of endogenous membrane proteins examined by the simultaneous purification of apical and basolateral plasma membrane fractions from Caco-2 cells. Biochem. J. 283 (Pt 2), 553–560.

Engelman, J.A., Zejnullahu, K., Mitsudomi, T., Song, Y., Hyland, C., Park, J.O., Lindeman, N., Gale, C.-M., Zhao, X., Christensen, J., Kosaka, T., Holmes, A.J., Rogers, A.M., Cappuzzo, F., Mok, T., Lee, C., Johnson, B.E., Cantley, L.C., Jänne, P.A., 2007. MET amplification leads to gefitinib resistance in lung cancer by activating ERBB3 signaling. Science 316, 1039–1043. https://doi.org/10.1126/science.1141478

Erler, J.T., Bennewith, K.L., Cox, T.R., Lang, G., Bird, D., Koong, A., Le, Q.-T., Giaccia, A.J., 2009. Hypoxia-induced lysyl oxidase is a critical mediator of bone marrow cell recruitment to form the premetastatic niche. Cancer Cell 15, 35–44. https://doi.org/10.1016/j.ccr.2008.11.012

Eser, S., Schnieke, A., Schneider, G., Saur, D., 2014. Oncogenic KRAS signalling in pancreatic cancer. Br. J. Cancer 111, 817–822. https://doi.org/10.1038/bjc.2014.215

Esteller, M., Guo, M., Moreno, V., Peinado, M.A., Capella, G., Galm, O., Baylin, S.B., Herman, J.G., 2002. Hypermethylation-associated Inactivation of the Cellular Retinol-Binding-Protein 1 Gene in Human Cancer. Cancer Res. 62, 5902–5905.

Eswarakumar, V.P., Horowitz, M.C., Locklin, R., Morriss-Kay, G.M., Lonai, P., 2004. A gain-of-function mutation of Fgfr2c demonstrates the roles of this receptor variant in osteogenesis. Proc. Natl. Acad. Sci. U. S. A. 101, 12555–12560. https://doi.org/10.1073/pnas.0405031101

Eswarakumar, V.P., Lax, I., Schlessinger, J., 2005. Cellular signaling by fibroblast growth factor receptors. Cytokine Growth Factor Rev. 16, 139–149. https://doi.org/10.1016/j.cytogfr.2005.01.001

Facchinetti, V., Ouyang, W., Wei, H., Soto, N., Lazorchak, A., Gould, C., Lowry, C., Newton, A.C., Mao, Y., Miao, R.Q., Sessa, W.C., Qin, J., Zhang, P., Su, B., Jacinto, E., 2008. The mammalian target of rapamycin complex 2 controls folding and stability of Akt and protein kinase C. EMBO J. 27, 1932–1943. https://doi.org/10.1038/emboj.2008.120

Fang, J.S., Gillies, R.D., Gatenby, R.A., 2008. Adaptation to hypoxia and acidosis in carcinogenesis and tumor progression. Semin. Cancer Biol. 18, 330–337. https://doi.org/10.1016/j.semcancer.2008.03.011

Fang, J.Y., Tan, S.-J., Wu, Y.-C., Yang, Z., Hoang, B.X., Han, B., 2016. From competency to dormancy: a 3D model to study cancer cells and drug responsiveness. J. Transl. Med. 14. https://doi.org/10.1186/s12967-016-0798-8

Fang, M., Yuan, J., Peng, C., Li, Y., 2014. Collagen as a double-edged sword in tumor progression. Tumour Biol. 35, 2871–2882. https://doi.org/10.1007/s13277-013-1511-7

Fanjul, A., Dawson, M.I., Hobbs, P.D., Jong, L., Cameron, J.F., Harlev, E., Graupner, G., Lu, X.P., Pfahl, M., 1994. A new class of retinoids with selective inhibition of AP-1 inhibits proliferation. Nature 372, 107–111. https://doi.org/10.1038/372107a0

Faria, T.N., Mendelsohn, C., Chambon, P., Gudas, L.J., 1999. The targeted disruption of both alleles of RARbeta(2) in F9 cells results in the loss of retinoic acid-associated growth arrest. J. Biol. Chem. 274, 26783–26788.

Fearon, A.E., Carter, E.P., Clayton, N.S., Wilkes, E.H., Baker, A.-M., Kapitonova, E., Bakhouche, B.A., Tanner, Y., Wang, J., Gadaleta, E., Chelala, C., Moore, K.M., Marshall, J.F., Chupin, J., Schmid, P., Jones, J.L., Lockley, M., Cutillas, P.R., Grose, R.P., 2018. PHLDA1 Mediates Drug Resistance in Receptor Tyrosine Kinase-Driven Cancer. Cell Rep. 22, 2469–2481. https://doi.org/10.1016/j.celrep.2018.02.028

Fearon, A.E., Grose, R.P., 2014. Grb-ing receptor activation by the tail. Nat. Struct. Mol. Biol. 21, 113–114. https://doi.org/10.1038/nsmb.2767

Feig, C., Gopinathan, A., Neesse, A., Chan, D.S., Cook, N., Tuveson, D.A., 2012. The pancreas cancer microenvironment. Clin. Cancer Res. Off. J. Am. Assoc. Cancer Res. 18, 4266–4276. https://doi.org/10.1158/1078-0432.CCR-11-3114

Feldman, B., Poueymirou, W., Papaioannou, V.E., DeChiara, T.M., Goldfarb, M., 1995. Requirement of FGF-4 for postimplantation mouse development. Science 267, 246–249.

Ferlay, J., Shin, H.-R., Bray, F., Forman, D., Mathers, C., Parkin, D.M., 2010. Estimates of worldwide burden of cancer in 2008: GLOBOCAN 2008. Int. J. Cancer 127, 2893–2917. https://doi.org/10.1002/ijc.25516

Ferlay, J., Soerjomataram, I., Dikshit, R., Eser, S., Mathers, C., Rebelo, M., Parkin, D.M., Forman, D., Bray, F., 2015. Cancer incidence and mortality worldwide: sources, methods and major patterns in GLOBOCAN 2012. Int. J. Cancer 136, E359-386. https://doi.org/10.1002/ijc.29210

Fernández-Medarde, A., Santos, E., 2011. Ras in cancer and developmental diseases. Genes Cancer 2, 344–358. https://doi.org/10.1177/1947601911411084

Flaherty, K.T., Puzanov, I., Kim, K.B., Ribas, A., McArthur, G.A., Sosman, J.A., O'Dwyer, P.J., Lee, R.J., Grippo, J.F., Nolop, K., Chapman, P.B., 2010. Inhibition of mutated, activated BRAF in metastatic melanoma. N. Engl. J. Med. 363, 809–819. https://doi.org/10.1056/NEJMoa1002011

Fluegen, G., Avivar-Valderas, A., Wang, Y., Padgen, M.R., Williams, J.K., Nobre, A.R., Calvo, V., Cheung, J.F., Bravo-Cordero, J.J., Entenberg, D., Castracane, J., Verkhusha, V., Keely, P.J., Condeelis, J., Aguirre-Ghiso, J.A., 2017. Phenotypic heterogeneity of disseminated tumour cells is preset by primary tumour hypoxic microenvironments. Nat. Cell Biol. 19, 120–132. https://doi.org/10.1038/ncb3465

Fong, C.W., Leong, H.F., Wong, E.S.M., Lim, J., Yusoff, P., Guy, G.R., 2003. Tyrosine phosphorylation of Sprouty2 enhances its interaction with c-Cbl and is crucial for its function. J. Biol. Chem. 278, 33456–33464. https://doi.org/10.1074/jbc.M301317200

Foty, R., 2011. A simple hanging drop cell culture protocol for generation of 3D spheroids. J. Vis. Exp. JoVE. https://doi.org/10.3791/2720

Fox, B.C., Devonshire, A.S., Schutte, M.E., Foy, C.A., Minguez, J., Przyborski, S., Maltman, D., Bokhari, M., Marshall, D., 2010. Validation of reference gene stability for APAP hepatotoxicity studies in different in vitro systems and identification of novel potential toxicity biomarkers. Toxicol. Vitro Int. J. Publ. Assoc. BIBRA 24, 1962–1970. https://doi.org/10.1016/j.tiv.2010.08.007

Francavilla, C., Rigbolt, K.T.G., Emdal, K.B., Carraro, G., Vernet, E., Bekker-Jensen, D.B., Streicher, W., Wikström, M., Sundström, M., Bellusci, S., Cavallaro, U., Blagoev, B., Olsen, J.V., 2013. Functional proteomics defines the molecular switch underlying FGF receptor trafficking and cellular outputs. Mol. Cell 51, 707–722. https://doi.org/10.1016/j.molcel.2013.08.002

Frank, D., Mendelsohn, C.L., Ciccone, E., Svensson, K., Ohlsson, R., Tycko, B., 1999. A novel pleckstrin homology-related gene family defined by Ipl/Tssc3, TDAG51, and Tih1: tissue-specific expression, chromosomal location, and parental imprinting. Mamm. Genome Off. J. Int. Mamm. Genome Soc. 10, 1150–1159.

Franke, T.F., Yang, S.I., Chan, T.O., Datta, K., Kazlauskas, A., Morrison, D.K., Kaplan, D.R., Tsichlis, P.N., 1995. The protein kinase encoded by the Akt proto-oncogene is a target of the PDGF-activated phosphatidylinositol 3-kinase. Cell 81, 727–736.

Freemantle, S.J., Spinella, M.J., Dmitrovsky, E., 2003. Retinoids in cancer therapy and chemoprevention: promise meets resistance. Oncogene 22, 7305–7315. https://doi.org/10.1038/sj.onc.1206936

Freier, K., Schwaenen, C., Sticht, C., Flechtenmacher, C., Mühling, J., Hofele, C., Radlwimmer, B., Lichter, P., Joos, S., 2007. Recurrent FGFR1 amplification and high FGFR1 protein expression in oral squamous cell carcinoma (OSCC). Oral Oncol. 43, 60–66. https://doi.org/10.1016/j.oraloncology.2006.01.005

Froeling, F.E.M., Feig, C., Chelala, C., Dobson, R., Mein, C.E., Tuveson, D.A., Clevers, H., Hart, I.R., Kocher, H.M., 2011. Retinoic acid-induced pancreatic stellate cell quiescence reduces paracrine Wnt-β-catenin signaling to slow tumor progression. Gastroenterology 141, 1486–1497, 1497.e1–14. https://doi.org/10.1053/j.gastro.2011.06.047

Froeling, F.E.M., Mirza, T.A., Feakins, R.M., Seedhar, A., Elia, G., Hart, I.R., Kocher, H.M., 2009. Organotypic culture model of pancreatic cancer demonstrates that stromal cells modulate E-cadherin, beta-catenin, and Ezrin expression in tumor cells. Am. J. Pathol. 175, 636–648. https://doi.org/10.2353/ajpath.2009.090131

Fruman, D.A., Meyers, R.E., Cantley, L.C., 1998. Phosphoinositide kinases. Annu. Rev. Biochem. 67, 481–507. https://doi.org/10.1146/annurev.biochem.67.1.481

Fukuda, R., Hirota, K., Fan, F., Jung, Y.D., Ellis, L.M., Semenza, G.L., 2002. Insulin-like growth factor 1 induces hypoxia-inducible factor 1-mediated vascular endothelial growth factor expression, which is dependent on MAP kinase and phosphatidylinositol 3-kinase signaling in colon cancer cells. J. Biol. Chem. 277, 38205–38211. https://doi.org/10.1074/jbc.M203781200

Fulda, S., Gorman, A.M., Hori, O., Samali, A., 2010. Cellular stress responses: cell survival and cell death. Int. J. Cell Biol. 2010, 214074. https://doi.org/10.1155/2010/214074

Furdui, C.M., Lew, E.D., Schlessinger, J., Anderson, K.S., 2006. Autophosphorylation of FGFR1 kinase is mediated by a sequential and precisely ordered reaction. Mol. Cell 21, 711–717. https://doi.org/10.1016/j.molcel.2006.01.022

Furukawa, T., 2007. Molecular genetics of intraductal papillary-mucinous neoplasms of the pancreas. J. Hepatobiliary. Pancreat. Surg. 14, 233–237. https://doi.org/10.1007/s00534-006-1167-4

Furukawa, T., Fujisaki, R., Yoshida, Y., Kanai, N., Sunamura, M., Abe, T., Takeda, K., Matsuno, S., Horii, A., 2005. Distinct progression pathways involving the dysfunction of DUSP6/MKP-3 in pancreatic intraepithelial neoplasia and intraductal papillary-mucinous neoplasms of the pancreas. Mod. Pathol. Off. J. U. S. Can. Acad. Pathol. Inc 18, 1034–1042. https://doi.org/10.1038/modpathol.3800383

Furukawa, T., Sunamura, M., Motoi, F., Matsuno, S., Horii, A., 2003. Potential tumor suppressive pathway involving DUSP6/MKP-3 in pancreatic cancer. Am. J. Pathol. 162, 1807–1815. https://doi.org/10.1016/S0002-9440(10)64315-5

Fusenig, N.E., Breitkreutz, D., Dzarlieva, R.T., Boukamp, P., Bohnert, A., Tilgen, W., 1983. Growth and differentiation characteristics of transformed keratinocytes from mouse and human skin in vitro and in vivo. J. Invest. Dermatol. 81, 168s–75s.

Gaggioli, C., Hooper, S., Hidalgo-Carcedo, C., Grosse, R., Marshall, J.F., Harrington, K., Sahai, E., 2007. Fibroblast-led collective invasion of carcinoma cells with differing roles for RhoGTPases in leading and following cells. Nat. Cell Biol. 9, 1392–1400. https://doi.org/10.1038/ncb1658

Gähwiler, B.H., 1988. Organotypic cultures of neural tissue. Trends Neurosci. 11, 484–489.

Gähwiler, B.H., 1981a. Morphological differentiation of nerve cells in thin organotypic cultures derived from rat hippocampus and cerebellum. Proc. R. Soc. Lond. B Biol. Sci. 211, 287–290.

Gähwiler, B.H., 1981b. Organotypic monolayer cultures of nervous tissue. J. Neurosci. Methods 4, 329–342.

Gaidarov, I., Smith, M.E., Domin, J., Keen, J.H., 2001. The class II phosphoinositide 3-kinase C2alpha is activated by clathrin and regulates clathrin-mediated membrane trafficking. Mol. Cell 7, 443–449.

Gainor, J.F., Chabner, B.A., 2015. Ponatinib: Accelerated Disapproval. The Oncologist 20, 847–848. https://doi.org/10.1634/theoncologist.2015-0253

Gallego Romero, I., Pai, A.A., Tung, J., Gilad, Y., 2014. RNA-seq: impact of RNA degradation on transcript quantification. BMC Biol. 12, 42. https://doi.org/10.1186/1741-7007-12-42

Galluzzi, L., Kroemer, G., 2008. Necroptosis: a specialized pathway of programmed necrosis. Cell 135, 1161–1163. https://doi.org/10.1016/j.cell.2008.12.004

Galmarini, F.C., Galmarini, C.M., Sarchi, M.I., Abulafia, J., Galmarini, D., 2000. Heterogeneous distribution of tumor blood supply affects the response to chemotherapy in patients with head and neck cancer. Microcirc. N. Y. N 1994 7, 405–410.

Gambarini, A.G., Miyamoto, C.A., Lima, G.A., Nader, H.B., Dietrich, C.P., 1993. Mitogenic activity of acidic fibroblast growth factor is enhanced by highly sulfated oligosaccharides derived from heparin and heparan sulfate. Mol. Cell. Biochem. 124, 121–129.

Garofalo, R.S., Orena, S.J., Rafidi, K., Torchia, A.J., Stock, J.L., Hildebrandt, A.L., Coskran, T., Black, S.C., Brees, D.J., Wicks, J.R., McNeish, J.D., Coleman, K.G., 2003. Severe diabetes, age-dependent loss of adipose tissue, and mild growth deficiency in mice lacking Akt2/PKB beta. J. Clin. Invest. 112, 197–208. https://doi.org/10.1172/JCI16885

Gartside, M.G., Chen, H., Ibrahimi, O.A., Byron, S.A., Curtis, A.V., Wellens, C.L., Bengston, A., Yudt, L.M., Eliseenkova, A.V., Ma, J., Curtin, J.A., Hyder, P., Harper, U.L., Riedesel, E., Mann, G.J., Trent, J.M., Bastian, B.C., Meltzer, P.S., Mohammadi, M., Pollock, P.M., 2009. Loss-of-Function Fibroblast Growth Factor Receptor-2 Mutations in Melanoma. Mol. Cancer Res. MCR 7, 41–54. https://doi.org/10.1158/1541-7786.MCR-08-0021

Gasperino, J., 2011. Gender is a risk factor for lung cancer. Med. Hypotheses 76, 328–331. https://doi.org/10.1016/j.mehy.2010.10.030

Gasperino, J., Rom, W.N., 2004. Gender and lung cancer. Clin. Lung Cancer 5, 353–359. https://doi.org/10.3816/CLC.2004.n.013

Gatenby, R.A., Gillies, R.J., 2007. Glycolysis in cancer: a potential target for therapy. Int. J. Biochem. Cell Biol. 39, 1358–1366. https://doi.org/10.1016/j.biocel.2007.03.021

Gatenby, R.A., Smallbone, K., Maini, P.K., Rose, F., Averill, J., Nagle, R.B., Worrall, L., Gillies, R.J., 2007. Cellular adaptations to hypoxia and acidosis during somatic evolution of breast cancer. Br. J. Cancer 97, 646–653. https://doi.org/10.1038/sj.bjc.6603922

Gavine, P.R., Mooney, L., Kilgour, E., Thomas, A.P., Al-Kadhimi, K., Beck, S., Rooney, C., Coleman, T., Baker, D., Mellor, M.J., Brooks, A.N., Klinowska, T., 2012. AZD4547: an orally bioavailable, potent, and selective inhibitor of the fibroblast growth factor receptor tyrosine kinase family. Cancer Res. 72, 2045–2056. https://doi.org/10.1158/0008-5472.CAN-11-3034

Geng, J., Fan, J., Wang, P., Fang, Z.J., Xia, G.W., Jiang, H.W., Chen, G., Ding, Q., 2009. REG1A predicts recurrence in stage Ta/T1 bladder cancer. Eur. J. Surg. Oncol. J. Eur. Soc. Surg. Oncol. Br. Assoc. Surg. Oncol. 35, 852–857. https://doi.org/10.1016/j.ejso.2008.12.007

Geng, J., Fan, J., Wang, Q., Zhang, X.-P., Kang, L., Li, Q.-Y., Xu, Y.-F., Peng, B., Zheng, J.-H., Yao, X.-D., 2017. Decreased REG1α expression suppresses growth, invasion and angiogenesis of bladder cancer. Eur. J. Surg. Oncol. J. Eur. Soc. Surg. Oncol. Br. Assoc. Surg. Oncol. 43, 837–846. https://doi.org/10.1016/j.ejso.2017.01.013

Gerlinger, M., Rowan, A.J., Horswell, S., Math, M., Larkin, J., Endesfelder, D., Gronroos, E., Martinez, P., Matthews, N., Stewart, A., Tarpey, P., Varela, I., Phillimore, B., Begum, S., McDonald, N.Q., Butler, A., Jones, D., Raine, K., Latimer, C., Santos, C.R., Nohadani, M., Eklund, A.C., Spencer-Dene, B., Clark, G., Pickering, L., Stamp, G., Gore, M., Szallasi, Z., Downward, J., Futreal, P.A., Swanton, C., 2012. Intratumor heterogeneity and branched evolution revealed by multiregion sequencing. N. Engl. J. Med. 366, 883–892. https://doi.org/10.1056/NEJMoa1113205

Ghabrial, A., Luschnig, S., Metzstein, M.M., Krasnow, M.A., 2003. Branching morphogenesis of the Drosophila tracheal system. Annu. Rev. Cell Dev. Biol. 19, 623–647. https://doi.org/10.1146/annurev.cellbio.19.031403.160043

Ghajar, C.M., Bissell, M.J., 2010. Tumor engineering: the other face of tissue engineering. Tissue Eng. Part A 16, 2153–2156. https://doi.org/10.1089/ten.TEA.2010.0135

Ghoreschi, K., Laurence, A., O'Shea, J.J., 2009. Janus kinases in immune cell signaling. Immunol. Rev. 228, 273–287. https://doi.org/10.1111/j.1600-065X.2008.00754.x

Ghyselinck, N.B., Båvik, C., Sapin, V., Mark, M., Bonnier, D., Hindelang, C., Dierich, A., Nilsson, C.B., Håkansson, H., Sauvant, P., Azaïs-Braesco, V., Frasson, M., Picaud, S., Chambon, P., 1999. Cellular retinol-binding protein I is essential for vitamin A homeostasis. EMBO J. 18, 4903–4914. https://doi.org/10.1093/emboj/18.18.4903

Giaccone, null, Pinedo, null, 1996. Drug Resistance. The Oncologist 1, 82–87.

Giese, A., Kluwe, L., Laube, B., Meissner, H., Berens, M.E., Westphal, M., 1996. Migration of human glioma cells on myelin. Neurosurgery 38, 755–764.

Gillies, R.J., Robey, I., Gatenby, R.A., 2008. Causes and consequences of increased glucose metabolism of cancers. J. Nucl. Med. Off. Publ. Soc. Nucl. Med. 49 Suppl 2, 24S-42S. https://doi.org/10.2967/jnumed.107.047258

Girard, A., Sachidanandam, R., Hannon, G.J., Carmell, M.A., 2006. A germline-specific class of small RNAs binds mammalian Piwi proteins. Nature 442, 199–202. https://doi.org/10.1038/nature04917

Girard, N., Lou, E., Azzoli, C.G., Reddy, R., Robson, M., Harlan, M., Orlow, I., Yatabe, Y., Nafa, K., Ladanyi, M., Viale, A., Kris, M.G., Riely, G., Miller, V., Klein, R.J., Matsuo, K., Pao, W., 2010. Analysis of genetic variants in never-smokers with lung cancer facilitated by an Internet-based blood collection protocol: a preliminary report. Clin. Cancer Res. Off. J. Am. Assoc. Cancer Res. 16, 755–763. https://doi.org/10.1158/1078-0432.CCR-09-2437

Glatz, J.F., van der Vusse, G.J., 1996. Cellular fatty acid-binding proteins: their function and physiological significance. Prog. Lipid Res. 35, 243–282.

Gligorijevic, B., Bergman, A., Condeelis, J., 2014. Multiparametric Classification Links Tumor Microenvironments with Tumor Cell Phenotype. PLOS Biol. 12, e1001995. https://doi.org/10.1371/journal.pbio.1001995

Glueck, D.H., Mandel, J., Karimpour-Fard, A., Hunter, L., Muller, K.E., 2008. Exact Calculations of Average Power for the Benjamini-Hochberg Procedure. Int. J. Biostat. 4. https://doi.org/10.2202/1557-4679.1103

Gnanamony, M., Gondi, C.S., 2017. Chemoresistance in pancreatic cancer: Emerging concepts. Oncol. Lett. 13, 2507–2513. https://doi.org/10.3892/ol.2017.5777

Goetz, R., Mohammadi, M., 2013. Exploring mechanisms of FGF signalling through the lens of structural biology. Nat. Rev. Mol. Cell Biol. 14, 166–180. https://doi.org/10.1038/nrm3528

Goltsov, A., Faratian, D., Langdon, S.P., Bown, J., Goryanin, I., Harrison, D.J., 2011. Compensatory effects in the PI3K/PTEN/AKT signaling network following receptor tyrosine kinase inhibition. Cell. Signal. 23, 407–416. https://doi.org/10.1016/j.cellsig.2010.10.011

Goltsov, A., Faratian, D., Langdon, S.P., Mullen, P., Harrison, D.J., Bown, J., 2012. Features of the reversible sensitivity-resistance transition in PI3K/PTEN/AKT signalling network after HER2 inhibition. Cell. Signal. 24, 493–504. https://doi.org/10.1016/j.cellsig.2011.09.030

Gomez-Roman, N., Stevenson, K., Gilmour, L., Hamilton, G., Chalmers, A.J., 2017. A novel 3D human glioblastoma cell culture system for modeling drug and radiation responses. Neuro-Oncol. 19, 229–241. https://doi.org/10.1093/neuonc/now164

Gomez-Zubeldia, M.A., Ropero, F., Sanchez-Casas, P., Tormo, M.A., Blazquez, E., Campillo, J.E., 1993. The effect of acarbose on the intestinal metabolism of glucose in vitro. Acta Diabetol. 30, 85–88.

Gorringe, K.L., Jacobs, S., Thompson, E.R., Sridhar, A., Qiu, W., Choong, D.Y.H., Campbell, I.G., 2007. High-resolution single nucleotide polymorphism array analysis of epithelial ovarian cancer reveals numerous microdeletions and amplifications. Clin. Cancer Res. Off. J. Am. Assoc. Cancer Res. 13, 4731–4739. https://doi.org/10.1158/1078-0432.CCR-07-0502

Gotoh, N., 2008. Regulation of growth factor signaling by FRS2 family docking/scaffold adaptor proteins. Cancer Sci. 99, 1319–1325. https://doi.org/10.1111/j.1349-7006.2008.00840.x

Gottesman, M.M., 2002. Mechanisms of cancer drug resistance. Annu. Rev. Med. 53, 615–627. https://doi.org/10.1146/annurev.med.53.082901.103929

Goubran, H.A., Kotb, R.R., Stakiw, J., Emara, M.E., Burnouf, T., 2014. Regulation of Tumor Growth and Metastasis: The Role of Tumor Microenvironment. Cancer Growth Metastasis 7, 9–18. https://doi.org/10.4137/CGM.S11285

Gounder, M.M., Maki, R.G., 2011. Molecular basis for primary and secondary tyrosine kinase inhibitor resistance in gastrointestinal stromal tumor. Cancer Chemother. Pharmacol. 67 Suppl 1, S25-43. https://doi.org/10.1007/s00280-010-1526-3

Goyal, L., Saha, S.K., Liu, L.Y., Siravegna, G., Leshchiner, I., Ahronian, L.G., Lennerz, J.K., Vu, P., Deshpande, V., Kambadakone, A., Mussolin, B., Reyes, S., Henderson, L., Sun, J.E., Van Seventer, E.E., Gurski, J.M., Baltschukat, S., Schacher-Engstler, B., Barys, L., Stamm, C., Furet, P., Ryan, D.P., Stone, J.R., Iafrate, A.J., Getz, G., Porta, D.G., Tiedt, R., Bardelli, A., Juric, D., Corcoran, R.B., Bardeesy, N., Zhu, A.X., 2017. Polyclonal Secondary FGFR2 Mutations Drive Acquired Resistance to FGFR Inhibition in Patients with FGFR2 Fusion-Positive Cholangiocarcinoma. Cancer Discov. 7, 252–263. https://doi.org/10.1158/2159-8290.CD-16-1000

Grandjean, G., De Jong, P., James, B., Koh, M.Y., Lemos, R., Kingston, J., Aleshin, A., Bankston, L.A., Miller, C.P., Cho, E.J., Edupuganti, R., Devkota, A., Stancu, G., Liddington, R.C., Dalby, K., Powis, G., 2016. Definition of a novel feed-forward mechanism for glycolysis-HIF1α signaling in hypoxic tumors highlights adolase A as a therapeutic target. Cancer Res. 76, 4259–4269. https://doi.org/10.1158/0008-5472.CAN-16-0401

Grant, S., 2008. Cotargeting survival signaling pathways in cancer. J. Clin. Invest. 118, 3003–3006. https://doi.org/10.1172/JCI36898

Grasso, C.S., Wu, Y.-M., Robinson, D.R., Cao, X., Dhanasekaran, S.M., Khan, A.P., Quist, M.J., Jing, X., Lonigro, R.J., Brenner, J.C., Asangani, I.A., Ateeq, B., Chun, S.Y., Siddiqui, J., Sam, L., Anstett, M., Mehra, R., Prensner, J.R., Palanisamy, N., Ryslik, G.A., Vandin, F., Raphael, B.J., Kunju, L.P., Rhodes, D.R., Pienta, K.J., Chinnaiyan, A.M., Tomlins, S.A., 2012. The mutational landscape of lethal castration-resistant prostate cancer. Nature 487, 239–243. https://doi.org/10.1038/nature11125

Greulich, H., Pollock, P.M., 2011. Targeting mutant fibroblast growth factor receptors in cancer. Trends Mol. Med. 17, 283–292. https://doi.org/10.1016/j.molmed.2011.01.012

Griffith, L.G., Swartz, M.A., 2006. Capturing complex 3D tissue physiology in vitro. Nat. Rev. Mol. Cell Biol. 7, 211–224. https://doi.org/10.1038/nrm1858

Grignani, F., De Matteis, S., Nervi, C., Tomassoni, L., Gelmetti, V., Cioce, M., Fanelli, M., Ruthardt, M., Ferrara, F.F., Zamir, I., Seiser, C., Grignani, F., Lazar, M.A., Minucci, S., Pelicci, P.G., 1998. Fusion proteins of the retinoic acid receptor-alpha recruit histone deacetylase in promyelocytic leukaemia. Nature 391, 815–818. https://doi.org/10.1038/35901

Grivna, S.T., Beyret, E., Wang, Z., Lin, H., 2006. A novel class of small RNAs in mouse spermatogenic cells. Genes Dev. 20, 1709–1714. https://doi.org/10.1101/gad.1434406

Grygielewicz, P., Dymek, B., Bujak, A., Gunerka, P., Stanczak, A., Lamparska-Przybysz, M., Wieczorek, M., Dzwonek, K., Zdzalik, D., 2016. Epithelial-mesenchymal transition confers resistance to selective FGFR inhibitors in SNU-16 gastric cancer cells. Gastric Cancer Off. J. Int. Gastric Cancer Assoc. Jpn. Gastric Cancer Assoc. 19, 53–62. https://doi.org/10.1007/s10120-014-0444-1

Guagnano, V., Furet, P., Spanka, C., Bordas, V., Le Douget, M., Stamm, C., Brueggen, J., Jensen, M.R., Schnell, C., Schmid, H., Wartmann, M., Berghausen, J., Drueckes, P., Zimmerlin, A., Bussiere, D., Murray, J., Graus Porta, D., 2011. Discovery of 3-(2,6-dichloro-3,5-dimethoxy-phenyl)-1-{6-[4-(4-ethyl-piperazin-1-yl)-phenylamino]-pyrimidin-4-yl}-1-methyl-urea (NVP-BGJ398), a potent and selective inhibitor of the fibroblast growth factor receptor family of receptor tyrosine kinase. J. Med. Chem. 54, 7066–7083. https://doi.org/10.1021/jm2006222

Gual, P., Giordano, S., Anguissola, S., Parker, P.J., Comoglio, P.M., 2001. Gab1 phosphorylation: a novel mechanism for negative regulation of HGF receptor signaling. Oncogene 20, 156–166. https://doi.org/10.1038/sj.onc.1204047

Gubbay, O., Rae, M.T., McNeilly, A.S., Donadeu, F.X., Zeleznik, A.J., Hillier, S.G., 2006. cAMP response element-binding (CREB) signalling and ovarian surface epithelial cell survival. J. Endocrinol. 191, 275–285. https://doi.org/10.1677/joe.1.06928

Gudernova, I., Vesela, I., Balek, L., Buchtova, M., Dosedelova, H., Kunova, M., Pivnicka, J., Jelinkova, I., Roubalova, L., Kozubik, A., Krejci, P., 2016. Multikinase activity of fibroblast growth factor receptor (FGFR) inhibitors SU5402, PD173074, AZD1480, AZD4547 and BGJ398 compromises the use of small chemicals targeting FGFR catalytic activity for therapy of short-stature syndromes. Hum. Mol. Genet. 25, 9–23. https://doi.org/10.1093/hmg/ddv441

Gunawardane, L.S., Saito, K., Nishida, K.M., Miyoshi, K., Kawamura, Y., Nagami, T., Siomi, H., Siomi, M.C., 2007. A slicer-mediated mechanism for repeat-associated siRNA 5′ end formation in Drosophila. Science 315, 1587–1590. https://doi.org/10.1126/science.1140494

Guo, G., Sun, X., Chen, C., Wu, S., Huang, P., Li, Z., Dean, M., Huang, Y., Jia, W., Zhou, Q., Tang, A., Yang, Z., Li, X., Song, P., Zhao, Xiaokun, Ye, R., Zhang, S., Lin, Zhao, Qi, M., Wan, S., Xie, L., Fan, F., Nickerson, M.L., Zou, X., Hu, X., Xing, L., Lv, Z., Mei, H., Gao, S., Liang, C., Gao, Z., Lu, J., Yu, Y., Liu, C., Li, L., Fang, X., Jiang, Z., Yang, J., Li, C., Zhao, Xin, Chen, J., Zhang, F., Lai, Y., Lin, Zheguang, Zhou, F., Chen, H., Chan, H.C., Tsang, S., Theodorescu, D., Li, Y., Zhang, X., Wang, Jian, Yang, H., Gui, Y., Wang, Jun, Cai, Z., 2013. Whole-genome and whole-exome sequencing of bladder cancer identifies frequent alterations in genes involved in sister chromatid cohesion and segregation. Nat. Genet. 45, 1459–1463. https://doi.org/10.1038/ng.2798

Gupta, P.B., Fillmore, C.M., Jiang, G., Shapira, S.D., Tao, K., Kuperwasser, C., Lander, E.S., 2011. Stochastic state transitions give rise to phenotypic equilibrium in

populations of cancer cells. Cell 146, 633–644. https://doi.org/10.1016/j.cell.2011.07.026

Guttman, M., Garber, M., Levin, J.Z., Donaghey, J., Robinson, J., Adiconis, X., Fan, L., Koziol, M.J., Gnirke, A., Nusbaum, C., Rinn, J.L., Lander, E.S., Regev, A., 2010. Ab initio reconstruction of cell type-specific transcriptomes in mouse reveals the conserved multi-exonic structure of lincRNAs. Nat. Biotechnol. 28, 503–510. https://doi.org/10.1038/nbt.1633

Hacohen, N., Kramer, S., Sutherland, D., Hiromi, Y., Krasnow, M.A., 1998. sprouty Encodes a Novel Antagonist of FGF Signaling that Patterns Apical Branching of the Drosophila Airways. Cell 92, 253–263. https://doi.org/10.1016/S0092-8674(00)80919-8

Hammerman, P.S., Jänne, P.A., Johnson, B.E., 2009. Resistance to Epidermal Growth Factor Receptor Tyrosine Kinase Inhibitors in Non-Small Cell Lung Cancer. Clin. Cancer Res. Off. J. Am. Assoc. Cancer Res. 15, 7502–7509. https://doi.org/10.1158/1078-0432.CCR-09-0189

Han, J.-I., Huang, N.-N., Kim, D.-U., Kehrl, J.H., 2006. RGS1 and RGS13 mRNA silencing in a human B lymphoma line enhances responsiveness to chemoattractants and impairs desensitization. J. Leukoc. Biol. 79, 1357–1368. https://doi.org/10.1189/jlb.1105693

Hanada, M., Feng, J., Hemmings, B.A., 2004. Structure, regulation and function of PKB/AKT--a major therapeutic target. Biochim. Biophys. Acta 1697, 3–16. https://doi.org/10.1016/j.bbapap.2003.11.009

Hanafusa, H., Torii, S., Yasunaga, T., Nishida, E., 2002. Sprouty1 and Sprouty2 provide a control mechanism for the Ras/MAPK signalling pathway. Nat. Cell Biol. 4, 850–858. https://doi.org/10.1038/ncb867

Hanahan, D., Weinberg, R.A., 2011. Hallmarks of cancer: the next generation. Cell 144, 646–674. https://doi.org/10.1016/j.cell.2011.02.013

Hanahan, D., Weinberg, R.A., 2000. The hallmarks of cancer. Cell 100, 57–70.

Hanchen, L., Xueli, F., JeanMarie, H., 2007. Tumor microenvironment: The role of the tumor stroma in cancer. J. Cell. Biochem. 101, 805–815. https://doi.org/10.1002/jcb.21159

Hanusch, M., Stahl, W., Schulz, W.A., Sies, H., 1995. Induction of gap junctional communication by 4-oxoretinoic acid generated from its precursor canthaxanthin. Arch. Biochem. Biophys. 317, 423–428. https://doi.org/10.1006/abbi.1995.1184

Hara, K., Fukui, H., Sun, C., Kitayama, Y., Eda, H., Yamasaki, T., Kondo, T., Tomita, T., Oshima, T., Watari, J., Fujimori, T., Miwa, H., 2015. Effect of REG Iα protein on angiogenesis in gastric cancer tissues. Oncol. Rep. 33, 2183–2189. https://doi.org/10.3892/or.2015.3878

Harbers, M., Carninci, P., 2005. Tag-based approaches for transcriptome research and genome annotation. Nat. Methods 2, 495–502. https://doi.org/10.1038/nmeth768

Harding, T.C., Long, L., Palencia, S., Zhang, H., Sadra, A., Hestir, K., Patil, N., Levin, A., Hsu, A.W., Charych, D., Brennan, T., Zanghi, J., Halenbeck, R., Marshall, S.A., Qin, M., Doberstein, S.K., Hollenbaugh, D., Kavanaugh, W.M., Williams, L.T., Baker, K.P., 2013. Blockade of nonhormonal fibroblast growth factors by

FP-1039 inhibits growth of multiple types of cancer. Sci. Transl. Med. 5, 178ra39. https://doi.org/10.1126/scitranslmed.3005414

Harris, R.E., Zang, E.A., Anderson, J.I., Wynder, E.L., 1993. Race and sex differences in lung cancer risk associated with cigarette smoking. Int. J. Epidemiol. 22, 592–599.

Harris, S.J., Brown, J., Lopez, J., Yap, T.A., 2016. Immuno-oncology combinations: raising the tail of the survival curve. Cancer Biol. Med. 13, 171–193. https://doi.org/10.20892/j.issn.2095-3941.2016.0015

Hartupee, J.C., Zhang, H., Bonaldo, M.F., Soares, M.B., Dieckgraefe, B.K., 2001. Isolation and characterization of a cDNA encoding a novel member of the human regenerating protein family: Reg IV. Biochim. Biophys. Acta 1518, 287–293.

Haugsten, E.M., Wiedlocha, A., Olsnes, S., Wesche, J., 2010. Roles of fibroblast growth factor receptors in carcinogenesis. Mol. Cancer Res. MCR 8, 1439–1452. https://doi.org/10.1158/1541-7786.MCR-10-0168

Hauw, J.J., Berger, B., Escourolle, R., 1972. [Presence of synapses in organotypic culture in vitro of human cerebellum]. Comptes Rendus Hebd. Seances Acad. Sci. Ser. Sci. Nat. 274, 264–266.

Hayashi, K., Motoyama, S., Sugiyama, T., Izumi, J., Anbai, A., Nanjo, H., Watanabe, H., Maruyama, K., Minamiya, Y., Koyota, S., Koizumi, Y., Takasawa, S., Murata, K., Ogawa, J., 2008. REG Ialpha is a reliable marker of chemoradiosensitivity in squamous cell esophageal cancer patients. Ann. Surg. Oncol. 15, 1224–1231. https://doi.org/10.1245/s10434-008-9810-8

Haycock, J.W., 2011. 3D cell culture: a review of current approaches and techniques. Methods Mol. Biol. Clifton NJ 695, 1–15. https://doi.org/10.1007/978-1-60761-984-0_1

Hayden, E.C., 2012. RNA studies under fire. Nature 484, 428. https://doi.org/10.1038/484428a

Hayman, M.W., Smith, K.H., Cameron, N.R., Przyborski, S.A., 2005. Growth of human stem cell-derived neurons on solid three-dimensional polymers. J. Biochem. Biophys. Methods 62, 231–240. https://doi.org/10.1016/j.jbbm.2004.12.001

Hayman, M.W., Smith, K.H., Cameron, N.R., Przyborski, S.A., 2004. Enhanced neurite outgrowth by human neurons grown on solid three-dimensional scaffolds. Biochem. Biophys. Res. Commun. 314, 483–488.

Hazlehurst, L.A., Enkemann, S.A., Beam, C.A., Argilagos, R.F., Painter, J., Shain, K.H., Saporta, S., Boulware, D., Moscinski, L., Alsina, M., Dalton, W.S., 2003. Genotypic and phenotypic comparisons of de novo and acquired melphalan resistance in an isogenic multiple myeloma cell line model. Cancer Res. 63, 7900–7906.

He, J., Jin, Y., Chen, Y., Yao, H.-B., Xia, Y.-J., Ma, Y.-Y., Wang, W., Shao, Q.-S., 2016. Downregulation of ALDOB is associated with poor prognosis of patients with gastric cancer. OncoTargets Ther. 9, 6099–6109. https://doi.org/10.2147/OTT.S110203

Heinrich, M.C., Corless, C.L., Demetri, G.D., Blanke, C.D., von Mehren, M., Joensuu, H., McGreevey, L.S., Chen, C.-J., Van den Abbeele, A.D., Druker, B.J., Kiese, B., Eisenberg, B., Roberts, P.J., Singer, S., Fletcher, C.D.M., Silberman, S.,

Dimitrijevic, S., Fletcher, J.A., 2003. Kinase mutations and imatinib response in patients with metastatic gastrointestinal stromal tumor. J. Clin. Oncol. Off. J. Am. Soc. Clin. Oncol. 21, 4342–4349. https://doi.org/10.1200/JCO.2003.04.190

Heinrich, M.C., Maki, R.G., Corless, C.L., Antonescu, C.R., Harlow, A., Griffith, D., Town, A., McKinley, A., Ou, W.-B., Fletcher, J.A., Fletcher, C.D.M., Huang, X., Cohen, D.P., Baum, C.M., Demetri, G.D., 2008. Primary and secondary kinase genotypes correlate with the biological and clinical activity of sunitinib in imatinib-resistant gastrointestinal stromal tumor. J. Clin. Oncol. Off. J. Am. Soc. Clin. Oncol. 26, 5352–5359. https://doi.org/10.1200/JCO.2007.15.7461

Heinzle, C., Sutterlüty, H., Grusch, M., Grasl-Kraupp, B., Berger, W., Marian, B., 2011. Targeting fibroblast-growth-factor-receptor-dependent signaling for cancer therapy. Expert Opin. Ther. Targets 15, 829–846. https://doi.org/10.1517/14728222.2011.566217

Heist, R.S., Mino-Kenudson, M., Sequist, L.V., Tammireddy, S., Morrissey, L., Christiani, D.C., Engelman, J.A., Iafrate, A.J., 2012. FGFR1 amplification in squamous cell carcinoma of the lung. J. Thorac. Oncol. Off. Publ. Int. Assoc. Study Lung Cancer 7, 1775–1780. https://doi.org/10.1097/JTO.0b013e31826aed28

Hengartner, M.O., 2000. The biochemistry of apoptosis. Nature 407, 770–776. https://doi.org/10.1038/35037710

Henson, B., Li, F., Coatney, D.D., Carey, T.E., Mitra, R.S., Kirkwood, K.L., D'Silva, N.J., 2007. An orthotopic floor-of-mouth model for locoregional growth and spread of human squamous cell carcinoma. J. Oral Pathol. Med. Off. Publ. Int. Assoc. Oral Pathol. Am. Acad. Oral Pathol. 36, 363–370. https://doi.org/10.1111/j.1600-0714.2007.00549.x

Heppner, G.H., 1984. Tumor heterogeneity. Cancer Res. 44, 2259–2265.

Herbert, C., Schieborr, U., Saxena, K., Juraszek, J., De Smet, F., Alcouffe, C., Bianciotto, M., Saladino, G., Sibrac, D., Kudlinzki, D., Sreeramulu, S., Brown, A., Rigon, P., Herault, J.-P., Lassalle, G., Blundell, T.L., Rousseau, F., Gils, A., Schymkowitz, J., Tompa, P., Herbert, J.-M., Carmeliet, P., Gervasio, F.L., Schwalbe, H., Bono, F., 2016. Molecular Mechanism of SSR128129E, an Extracellularly Acting, Small-Molecule, Allosteric Inhibitor of FGF Receptor Signaling. Cancer Cell 30, 176–178. https://doi.org/10.1016/j.ccell.2016.06.015

Herbert, C., Schieborr, U., Saxena, K., Juraszek, J., De Smet, F., Alcouffe, C., Bianciotto, M., Saladino, G., Sibrac, D., Kudlinzki, D., Sreeramulu, S., Brown, A., Rigon, P., Herault, J.-P., Lassalle, G., Blundell, T.L., Rousseau, F., Gils, A., Schymkowitz, J., Tompa, P., Herbert, J.-M., Carmeliet, P., Gervasio, F.L., Schwalbe, H., Bono, F., 2013. Molecular mechanism of SSR128129E, an extracellularly acting, small-molecule, allosteric inhibitor of FGF receptor signaling. Cancer Cell 23, 489–501. https://doi.org/10.1016/j.ccr.2013.02.018

Heyn, P., Kalinka, A.T., Tomancak, P., Neugebauer, K.M., 2015. Introns and gene expression: Cellular constraints, transcriptional regulation, and evolutionary consequences. Bioessays 37, 148–154. https://doi.org/10.1002/bies.201400138

Hirata, H., Tatsumi, H., Sokabe, M., 2007. Dynamics of actin filaments during tension-dependent formation of actin bundles. Biochim. Biophys. Acta 1770, 1115–1127. https://doi.org/10.1016/j.bbagen.2007.03.010

Hirayama, A., Kami, K., Sugimoto, M., Sugawara, M., Toki, N., Onozuka, H., Kinoshita, T., Saito, N., Ochiai, A., Tomita, M., Esumi, H., Soga, T., 2009. Quantitative metabolome profiling of colon and stomach cancer microenvironment by capillary electrophoresis time-of-flight mass spectrometry. Cancer Res. 69, 4918–4925. https://doi.org/10.1158/0008-5472.CAN-08-4806

Hodis, E., Watson, I.R., Kryukov, G.V., Arold, S.T., Imielinski, M., Theurillat, J.-P., Nickerson, E., Auclair, D., Li, L., Place, C., Dicara, D., Ramos, A.H., Lawrence, M.S., Cibulskis, K., Sivachenko, A., Voet, D., Saksena, G., Stransky, N., Onofrio, R.C., Winckler, W., Ardlie, K., Wagle, N., Wargo, J., Chong, K., Morton, D.L., Stemke-Hale, K., Chen, G., Noble, M., Meyerson, M., Ladbury, J.E., Davies, M.A., Gershenwald, J.E., Wagner, S.N., Hoon, D.S.B., Schadendorf, D., Lander, E.S., Gabriel, S.B., Getz, G., Garraway, L.A., Chin, L., 2012. A landscape of driver mutations in melanoma. Cell 150, 251–263. https://doi.org/10.1016/j.cell.2012.06.024

Hoffmann, D., Hoffmann, I., 1997. The changing cigarette, 1950-1995. J. Toxicol. Environ. Health 50, 307–364. https://doi.org/10.1080/009841097160393

Holgado-Madruga, M., Emlet, D.R., Moscatello, D.K., Godwin, A.K., Wong, A.J., 1996. A Grb2-associated docking protein in EGF- and insulin-receptor signalling. Nature 379, 560–564. https://doi.org/10.1038/379560a0

Holohan, C., Van Schaeybroeck, S., Longley, D.B., Johnston, P.G., 2013. Cancer drug resistance: an evolving paradigm. Nat. Rev. Cancer 13, 714–726. https://doi.org/10.1038/nrc3599

Horikawa, Y., Enya, M., Mabe, H., Fukushima, K., Takubo, N., Ohashi, M., Ikeda, F., Hashimoto, K.-I., Watada, H., Takeda, J., 2018. NEUROD1-deficient diabetes (MODY6): Identification of the first cases in Japanese and the clinical features. Pediatr. Diabetes 19, 236–242. https://doi.org/10.1111/pedi.12553

Hossain, G.S., van Thienen, J.V., Werstuck, G.H., Zhou, J., Sood, S.K., Dickhout, J.G., de Koning, A.B.L., Tang, D., Wu, D., Falk, E., Poddar, R., Jacobsen, D.W., Zhang, K., Kaufman, R.J., Austin, R.C., 2003. TDAG51 is induced by homocysteine, promotes detachment-mediated programmed cell death, and contributes to the cevelopment of atherosclerosis in hyperhomocysteinemia. J. Biol. Chem. 278, 30317–30327. https://doi.org/10.1074/jbc.M212897200

Housman, G., Byler, S., Heerboth, S., Lapinska, K., Longacre, M., Snyder, N., Sarkar, S., 2014. Drug Resistance in Cancer: An Overview. Cancers 6, 1769–1792. https://doi.org/10.3390/cancers6031769

Howes, A.L., Chiang, G.G., Lang, E.S., Ho, C.B., Powis, G., Vuori, K., Abraham, R.T., 2007. The phosphatidylinositol 3-kinase inhibitor, PX-866, is a potent inhibitor of cancer cell motility and growth in three-dimensional cultures. Mol. Cancer Ther. 6, 2505–2514. https://doi.org/10.1158/1535-7163.MCT-06-0698

Hsiao, A.Y., Tung, Y.-C., Qu, X., Patel, L.R., Pienta, K.J., Takayama, S., 2012. 384 hanging drop arrays give excellent Z-factors and allow versatile formation of co-culture spheroids. Biotechnol. Bioeng. 109, 1293–1304. https://doi.org/10.1002/bit.24399

Hsu, P.P., Sabatini, D.M., 2008. Cancer cell metabolism: Warburg and beyond. Cell 134, 703–707. https://doi.org/10.1016/j.cell.2008.08.021

Hu, B., El Hajj, N., Sittler, S., Lammert, N., Barnes, R., Meloni-Ehrig, A., 2012. Gastric cancer: Classification, histology and application of molecular pathology. J. Gastrointest. Oncol. 3, 251–261. https://doi.org/10.3978/j.issn.2078-6891.2012.021

Hu, Y., Lu, H., Zhang, Jinchao, Chen, J., Chai, Z., Zhang, Jingxin, 2014. Essential role of AKT in tumor cells addicted to FGFR. Anticancer. Drugs 25, 183–188. https://doi.org/10.1097/CAD.0000000000000034

Hua, S., Kittler, R., White, K.P., 2009. Genomic antagonism between retinoic acid and estrogen signaling in breast cancer. Cell 137, 1259–1271. https://doi.org/10.1016/j.cell.2009.04.043

Huang, D.W., Sherman, B.T., Lempicki, R.A., 2009a. Bioinformatics enrichment tools: paths toward the comprehensive functional analysis of large gene lists. Nucleic Acids Res. 37, 1–13. https://doi.org/10.1093/nar/gkn923

Huang, D.W., Sherman, B.T., Lempicki, R.A., 2009b. Systematic and integrative analysis of large gene lists using DAVID bioinformatics resources. Nat. Protoc. 4, 44–57. https://doi.org/10.1038/nprot.2008.211

Huang, Y., Xiong, Z.-G., 2015. Choosing an appropriate glucose concentration according to different cell types and experimental purposes is very important. Cell Stress Chaperones 20, 1–2. https://doi.org/10.1007/s12192-014-0547-y

Hughes, C.C.W., 2008. Endothelial-stromal interactions in angiogenesis. Curr. Opin. Hematol. 15, 204–209. https://doi.org/10.1097/MOH.0b013e3282f97dbc

Huh, D., Hamilton, G.A., Ingber, D.E., 2011. From 3D cell culture to organs-on-chips. Trends Cell Biol. 21, 745–754. https://doi.org/10.1016/j.tcb.2011.09.005

Hur, H., Paik, M.J., Xuan, Y., Nguyen, D.-T., Ham, I.-H., Yun, J., Cho, Y.K., Lee, G., Han, S.-U., 2014. Quantitative measurement of organic acids in tissues from gastric cancer patients indicates increased glucose metabolism in gastric cancer. PloS One 9, e98581. https://doi.org/10.1371/journal.pone.0098581

Hwang, R.F., Moore, T., Arumugam, T., Ramachandran, V., Amos, K.D., Rivera, A., Ji, B., Evans, D.B., Logsdon, C.D., 2008. Cancer-associated stromal fibroblasts promote pancreatic tumor progression. Cancer Res. 68, 918–926. https://doi.org/10.1158/0008-5472.CAN-07-5714

Hynes, R.O., 2009. Extracellular matrix: not just pretty fibrils. Science 326, 1216–1219. https://doi.org/10.1126/science.1176009

Iannettoni, M.D., Lee, S.S., Bonnell, M.R., Sell, T.L., Whyte, R.I., Orringer, M.B., Beer, D.G., 1996. Detection of Barrett's adenocarcinoma of the gastric cardia with sucrase isomaltase and p53. Ann. Thorac. Surg. 62, 1460–1465; discussion 1465-1466. https://doi.org/10.1016/0003-4975(96)00749-7

Ibrahimi, O.A., Eliseenkova, A.V., Plotnikov, A.N., Yu, K., Ornitz, D.M., Mohammadi, M., 2001. Structural basis for fibroblast growth factor receptor 2 activation in Apert syndrome. Proc. Natl. Acad. Sci. U. S. A. 98, 7182–7187. https://doi.org/10.1073/pnas.121183798

Ibrahimi, O.A., Zhang, F., Eliseenkova, A.V., Linhardt, R.J., Mohammadi, M., 2004. Proline to arginine mutations in FGF receptors 1 and 3 result in Pfeiffer and Muenke craniosynostosis syndromes through enhancement of FGF binding affinity. Hum. Mol. Genet. 13, 69–78. https://doi.org/10.1093/hmg/ddh011

Igney, F.H., Krammer, P.H., 2002. Death and anti-death: tumour resistance to apoptosis. Nat. Rev. Cancer 2, 277–288. https://doi.org/10.1038/nrc776

Iliev, R., Stanik, M., Fedorko, M., Poprach, A., Vychytilova-Faltejskova, P., Slaba, K., Svoboda, M., Fabian, P., Pacik, D., Dolezel, J., Slaby, O., 2016. Decreased expression levels of PIWIL1, PIWIL2, and PIWIL4 are associated with worse survival in renal cell carcinoma patients. OncoTargets Ther. 9, 217–222. https://doi.org/10.2147/OTT.S91295

Imielinski, M., Berger, A.H., Hammerman, P.S., Hernandez, B., Pugh, T.J., Hodis, E., Cho, J., Suh, J., Capelletti, M., Sivachenko, A., Sougnez, C., Auclair, D., Lawrence, M.S., Stojanov, P., Cibulskis, K., Choi, K., de Waal, L., Sharifnia, T., Brooks, A., Greulich, H., Banerji, S., Zander, T., Seidel, D., Leenders, F., Ansén, S., Ludwig, C., Engel-Riedel, W., Stoelben, E., Wolf, J., Goparju, C., Thompson, K., Winckler, W., Kwiatkowski, D., Johnson, B.E., Jänne, P.A., Miller, V.A., Pao, W., Travis, W.D., Pass, H.I., Gabriel, S.B., Lander, E.S., Thomas, R.K., Garraway, L.A., Getz, G., Meyerson, M., 2012. Mapping the hallmarks of lung adenocarcinoma with massively parallel sequencing. Cell 150, 1107–1120. https://doi.org/10.1016/j.cell.2012.08.029

Inukai, M., Toyooka, S., Ito, S., Asano, H., Ichihara, S., Soh, J., Suehisa, H., Ouchida, M., Aoe, K., Aoe, M., Kiura, K., Shimizu, N., Date, H., 2006. Presence of epidermal growth factor receptor gene T790M mutation as a minor clone in non-small cell lung cancer. Cancer Res. 66, 7854–7858. https://doi.org/10.1158/0008-5472.CAN-06-1951

Ishiwata, T., Matsuda, Y., Yamamoto, T., Uchida, E., Korc, M., Naito, Z., 2012. Enhanced expression of fibroblast growth factor receptor 2 IIIc promotes human pancreatic cancer cell proliferation. Am. J. Pathol. 180, 1928–1941. https://doi.org/10.1016/j.ajpath.2012.01.020

Israelsen, W.J., Dayton, T.L., Davidson, S.M., Fiske, B.P., Hosios, A.M., Bellinger, G., Li, J., Yu, Y., Sasaki, M., Horner, J.W., Burga, L.N., Xie, J., Jurczak, M.J., DePinho, R.A., Clish, C.B., Jacks, T., Kibbey, R.G., Wulf, G.M., Di Vizio, D., Mills, G.B., Cantley, L.C., Vander Heiden, M.G., 2013. PKM2 isoform-specific deletion reveals a differential requirement for pyruvate kinase in tumor cells. Cell 155, 397–409. https://doi.org/10.1016/j.cell.2013.09.025

Itano, N., Okamoto, S., Zhang, D., Lipton, S.A., Ruoslahti, E., 2003. Cell spreading controls endoplasmic and nuclear calcium: A physical gene regulation pathway from the cell surface to the nucleus. Proc. Natl. Acad. Sci. 100, 5181–5186. https://doi.org/10.1073/pnas.0531397100

Iyer, G., Al-Ahmadie, H., Schultz, N., Hanrahan, A.J., Ostrovnaya, I., Balar, A.V., Kim, P.H., Lin, O., Weinhold, N., Sander, C., Zabor, E.C., Janakiraman, M., Garcia-Grossman, I.R., Heguy, A., Viale, A., Bochner, B.H., Reuter, V.E., Bajorin, D.F., Milowsky, M.I., Taylor, B.S., Solit, D.B., 2013. Prevalence and co-occurrence of actionable genomic alterations in high-grade bladder cancer. J. Clin. Oncol. Off. J. Am. Soc. Clin. Oncol. 31, 3133–3140. https://doi.org/10.1200/JCO.2012.46.5740

Jackson, C.C., Medeiros, L.J., Miranda, R.N., 2010. 8p11 myeloproliferative syndrome: a review. Hum. Pathol. 41, 461–476. https://doi.org/10.1016/j.humpath.2009.11.003

Jackson, E.L., Willis, N., Mercer, K., Bronson, R.T., Crowley, D., Montoya, R., Jacks, T., Tuveson, D.A., 2001. Analysis of lung tumor initiation and progression

using conditional expression of oncogenic K-ras. Genes Dev. 15, 3243–3248. https://doi.org/10.1101/gad.943001

Jacobson, M.D., Weil, M., Raff, M.C., 1997. Programmed cell death in animal development. Cell 88, 347–354.

Jacquemier, J., Adelaide, J., Parc, P., Penault-Llorca, F., Planche, J., deLapeyriere, O., Birnbaum, D., 1994. Expression of the FGFR1 gene in human breast-carcinoma cells. Int. J. Cancer 59, 373–378.

Jain, R.K., Au, P., Tam, J., Duda, D.G., Fukumura, D., 2005. Engineering vascularized tissue. Nat. Biotechnol. 23, 821–823. https://doi.org/10.1038/nbt0705-821

Jang, J.H., Shin, K.H., Park, J.G., 2001. Mutations in fibroblast growth factor receptor 2 and fibroblast growth factor receptor 3 genes associated with human gastric and colorectal cancers. Cancer Res. 61, 3541–3543.

Januchowski, R., Świerczewska, M., Sterzyńska, K., Wojtowicz, K., Nowicki, M., Zabel, M., 2016. Increased Expression of Several Collagen Genes is Associated with Drug Resistance in Ovarian Cancer Cell Lines. J. Cancer 7, 1295–1310. https://doi.org/10.7150/jca.15371

Japanese Gastric Cancer Association, null, 1998. Japanese Classification of Gastric Carcinoma - 2nd English Edition -. Gastric Cancer Off. J. Int. Gastric Cancer Assoc. Jpn. Gastric Cancer Assoc. 1, 10–24. https://doi.org/10.1007/s101209800016

Jaskoll, T., Abichaker, G., Witcher, D., Sala, F.G., Bellusci, S., Hajihosseini, M.K., Melnick, M., 2005. FGF10/FGFR2b signaling plays essential roles during in vivo embryonic submandibular salivary gland morphogenesis. BMC Dev. Biol. 5, 11. https://doi.org/10.1186/1471-213X-5-11

Javidi-Sharifi, N., Traer, E., Martinez, J., Gupta, A., Taguchi, T., Dunlap, J., Heinrich, M.C., Corless, C.L., Rubin, B.P., Druker, B.J., Tyner, J.W., 2015. Crosstalk between KIT and FGFR3 Promotes Gastrointestinal Stromal Tumor Cell Growth and Drug Resistance. Cancer Res. 75, 880–891. https://doi.org/10.1158/0008-5472.CAN-14-0573

Jebar, A.H., Hurst, C.D., Tomlinson, D.C., Johnston, C., Taylor, C.F., Knowles, M.A., 2005. FGFR3 and Ras gene mutations are mutually exclusive genetic events in urothelial cell carcinoma. Oncogene 24, 5218–5225. https://doi.org/10.1038/sj.onc.1208705

Jemal, A., Center, M.M., Ward, E., 2009. The convergence of lung cancer rates between blacks and whites under the age of 40, United States. Cancer Epidemiol. Biomark. Prev. Publ. Am. Assoc. Cancer Res. Cosponsored Am. Soc. Prev. Oncol. 18, 3349–3352. https://doi.org/10.1158/1055-9965.EPI-09-0740

Jemal, A., Thun, M.J., Ries, L.A.G., Howe, H.L., Weir, H.K., Center, M.M., Ward, E., Wu, X.-C., Eheman, C., Anderson, R., Ajani, U.A., Kohler, B., Edwards, B.K., 2008. Annual report to the nation on the status of cancer, 1975-2005, featuring trends in lung cancer, tobacco use, and tobacco control. J. Natl. Cancer Inst. 100, 1672–1694. https://doi.org/10.1093/jnci/djn389

Jerónimo, C., Henrique, R., Oliveira, J., Lobo, F., Pais, I., Teixeira, M.R., Lopes, C., 2004. Aberrant cellular retinol binding protein 1 (CRBP1) gene expression and promoter methylation in prostate cancer. J. Clin. Pathol. 57, 872–876. https://doi.org/10.1136/jcp.2003.014555

Jessup, J.M., Lavin, P.T., Andrews, C.W., Loda, M., Mercurio, A., Minsky, B.D., Mies, C., Cukor, B., Bleday, R., Steele, G., 1995. Sucrase-isomaltase is an independent prognostic marker for colorectal carcinoma. Dis. Colon Rectum 38, 1257–1264. https://doi.org/10.1007/BF02049149

Ji, B.T., Chow, W.H., Yang, G., McLaughlin, J.K., Gao, R.N., Zheng, W., Shu, X.O., Jin, F., Fraumeni, J.F., Gao, Y.T., 1997. Body mass index and the risk of cancers of the gastric cardia and distal stomach in Shanghai, China. Cancer Epidemiol. Biomark. Prev. Publ. Am. Assoc. Cancer Res. Cosponsored Am. Soc. Prev. Oncol. 6, 481–485.

Jiao, Y., Pawlik, T.M., Anders, R.A., Selaru, F.M., Streppel, M.M., Lucas, D.J., Niknafs, N., Guthrie, V.B., Maitra, A., Argani, P., Offerhaus, G.J.A., Roa, J.C., Roberts, L.R., Gores, G.J., Popescu, I., Alexandrescu, S.T., Dima, S., Fassan, M., Simbolo, M., Mafficini, A., Capelli, P., Lawlor, R.T., Ruzzenente, A., Guglielmi, A., Tortora, G., de Braud, F., Scarpa, A., Jarnagin, W., Klimstra, D., Karchin, R., Velculescu, V.E., Hruban, R.H., Vogelstein, B., Kinzler, K.W., Papadopoulos, N., Wood, L.D., 2013. Exome sequencing identifies frequent inactivating mutations in BAP1, ARID1A and PBRM1 in intrahepatic cholangiocarcinomas. Nat. Genet. 45, 1470–1473. https://doi.org/10.1038/ng.2813

Jiménez-Lara, A.M., Clarke, N., Altucci, L., Gronemeyer, H., 2004. Retinoic-acid-induced apoptosis in leukemia cells. Trends Mol. Med. 10, 508–515. https://doi.org/10.1016/j.molmed.2004.08.006

Johannessen, C.M., Boehm, J.S., Kim, S.Y., Thomas, S.R., Wardwell, L., Johnson, L.A., Emery, C.M., Stransky, N., Cogdill, A.P., Barretina, J., Caponigro, G., Hieronymus, H., Murray, R.R., Salehi-Ashtiani, K., Hill, D.E., Vidal, M., Zhao, J.J., Yang, X., Alkan, O., Kim, S., Harris, J.L., Wilson, C.J., Myer, V.E., Finan, P.M., Root, D.E., Roberts, T.M., Golub, T., Flaherty, K.T., Dummer, R., Weber, B.L., Sellers, W.R., Schlegel, R., Wargo, J.A., Hahn, W.C., Garraway, L.A., 2010. COT drives resistance to RAF inhibition through MAP kinase pathway reactivation. Nature 468, 968–972. https://doi.org/10.1038/nature09627

Johnson, L.M., Price, D.K., Figg, W.D., 2013. Treatment-induced secretion of WNT16B promotes tumor growth and acquired resistance to chemotherapy: implications for potential use of inhibitors in cancer treatment. Cancer Biol. Ther. 14, 90–91. https://doi.org/10.4161/cbt.22636

Jung, Eun-Jung, Jung, Eun-Ji, Min, S.Y., Kim, M.A., Kim, W.H., 2012. Fibroblast growth factor receptor 2 gene amplification status and its clinicopathologic significance in gastric carcinoma. Hum. Pathol. 43, 1559–1566. https://doi.org/10.1016/j.humpath.2011.12.002

Junttila, M.R., de Sauvage, F.J., 2013. Influence of tumour micro-environment heterogeneity on therapeutic response. Nature 501, 346–354. https://doi.org/10.1038/nature12626

Kagan, L., Dreifinger, T., Mager, D.E., Hoffman, A., 2010. Role of p-glycoprotein in region-specific gastrointestinal absorption of talinolol in rats. Drug Metab. Dispos. Biol. Fate Chem. 38, 1560–1566. https://doi.org/10.1124/dmd.110.033019

Kalinina, J., Dutta, K., Ilghari, D., Beenken, A., Goetz, R., Eliseenkova, A.V., Cowburn, D., Mohammadi, M., 2012. The alternatively spliced acid box region plays a

key role in FGF receptor autoinhibition. Struct. Lond. Engl. 1993 20, 77–88. https://doi.org/10.1016/j.str.2011.10.022

Kalluri, R., 2016. The biology and function of fibroblasts in cancer. Nat. Rev. Cancer 16, 582–598. https://doi.org/10.1038/nrc.2016.73

Kan, S., Elanko, N., Johnson, D., Cornejo-Roldan, L., Cook, J., Reich, E.W., Tomkins, S., Verloes, A., Twigg, S.R.F., Rannan-Eliya, S., McDonald-McGinn, D.M., Zackai, E.H., Wall, S.A., Muenke, M., Wilkie, A.O.M., 2002. Genomic screening of fibroblast growth-factor receptor 2 reveals a wide spectrum of mutations in patients with syndromic craniosynostosis. Am. J. Hum. Genet. 70, 472–486. https://doi.org/10.1086/338758

Kanwal, R., Gupta, S., 2012. Epigenetic modifications in cancer. Clin. Genet. 81, 303–311. https://doi.org/10.1111/j.1399-0004.2011.01809.x

Kapse-Mistry, S., Govender, T., Srivastava, R., Yergeri, M., 2014. Nanodrug delivery in reversing multidrug resistance in cancer cells. Front. Pharmacol. 5. https://doi.org/10.3389/fphar.2014.00159

Karimi, P., Islami, F., Anandasabapathy, S., Freedman, N.D., Kamangar, F., 2014. Gastric cancer: descriptive epidemiology, risk factors, screening, and prevention. Cancer Epidemiol. Biomark. Prev. Publ. Am. Assoc. Cancer Res. Cosponsored Am. Soc. Prev. Oncol. 23, 700–713. https://doi.org/10.1158/1055-9965.EPI-13-1057

Katoh, M., 2016. FGFR inhibitors: Effects on cancer cells, tumor microenvironment and whole-body homeostasis (Review). Int. J. Mol. Med. 38, 3–15. https://doi.org/10.3892/ijmm.2016.2620

Katoh, M., 2010. Genetic alterations of FGF receptors: an emerging field in clinical cancer diagnostics and therapeutics. Expert Rev. Anticancer Ther. 10, 1375–1379. https://doi.org/10.1586/era.10.128

Katoh, Y., Katoh, M., 2009. FGFR2-related pathogenesis and FGFR2-targeted therapeutics (Review). Int. J. Mol. Med. 23, 307–311.

Kaunas, R., Nguyen, P., Usami, S., Chien, S., 2005. Cooperative effects of Rho and mechanical stretch on stress fiber organization. Proc. Natl. Acad. Sci. U. S. A. 102, 15895–15900. https://doi.org/10.1073/pnas.0506041102

Kaur, A., Webster, M.R., Marchbank, K., Behera, R., Ndoye, A., Kugel, C.H., Dang, V.M., Appleton, J., O'Connell, M.P., Cheng, P., Valiga, A.A., Morissette, R., McDonnell, N.B., Ferrucci, L., Kossenkov, A.V., Meeth, K., Tang, H.-Y., Yin, X., Wood, W.H., Lehrmann, E., Becker, K.G., Flaherty, K.T., Frederick, D.T., Wargo, J.A., Cooper, Z.A., Tetzlaff, M.T., Hudgens, C., Aird, K.M., Zhang, R., Xu, X., Liu, Q., Bartlett, E., Karakousis, G., Eroglu, Z., Lo, R.S., Chan, M., Menzies, A.M., Long, G.V., Johnson, D.B., Sosman, J., Schilling, B., Schadendorf, D., Speicher, D.W., Bosenberg, M., Ribas, A., Weeraratna, A.T., 2016. sFRP2 in the aged microenvironment drives melanoma metastasis and therapy resistance. Nature 532, 250–254. https://doi.org/10.1038/nature17392

Kawase, T., Ohki, R., Shibata, T., Tsutsumi, S., Kamimura, N., Inazawa, J., Ohta, T., Ichikawa, H., Aburatani, H., Tashiro, F., Taya, Y., 2009. PH domain-only protein PHLDA3 is a p53-regulated repressor of Akt. Cell 136, 535–550. https://doi.org/10.1016/j.cell.2008.12.002

Kelly, C.M., Shoushtari, A.N., Qin, L.-X., D'Angelo, S.P., Dickson, M.A., Gounder, M.M., Keohan, M.L., Mcfadyen, C., Sjoberg, A., Singer, S., DeMatteo, R.P.,

Hwang, S., Heinemann, M.H., Francis, J.H., Antonescu, C.R., Chi, P., Tap, W.D., 2018. A phase Ib study of BGJ398, a pan-FGFR kinase inhibitor in combination with imatinib in patients with advanced gastrointestinal stromal tumor. Invest. New Drugs. https://doi.org/10.1007/s10637-018-0648-z

Kelm, J.M., Timmins, N.E., Brown, C.J., Fussenegger, M., Nielsen, L.K., 2003. Method for generation of homogeneous multicellular tumor spheroids applicable to a wide variety of cell types. Biotechnol. Bioeng. 83, 173–180. https://doi.org/10.1002/bit.10655

Khaitan, D., Chandna, S., Dwarakanath, S.B., 2009. Short-term exposure of multicellular tumor spheroids of a human glioma cell line to the glycolytic inhibitor 2-deoxy-D-glucose is more toxic than continuous exposure. J. Cancer Res. Ther. 5 Suppl 1, S67-73. https://doi.org/10.4103/0973-1482.55147

Kharaziha, P., Rodriguez, P., Li, Q., Rundqvist, H., Björklund, A.-C., Augsten, M., Ullén, A., Egevad, L., Wiklund, P., Nilsson, S., Kroemer, G., Grander, D., Panaretakis, T., 2012. Targeting of distinct signaling cascades and cancer-associated fibroblasts define the efficacy of Sorafenib against prostate cancer cells. Cell Death Dis. 3, e262. https://doi.org/10.1038/cddis.2012.1

Kiaris, H., Chatzistamou, I., Kalofoutis, C., Koutselini, H., Piperi, C., Kalofoutis, A., 2004. Tumour-stroma interactions in carcinogenesis: basic aspects and perspectives. Mol. Cell. Biochem. 261, 117–122.

Kim, J., Tchernyshyov, I., Semenza, G.L., Dang, C.V., 2006. HIF-1-mediated expression of pyruvate dehydrogenase kinase: a metabolic switch required for cellular adaptation to hypoxia. Cell Metab. 3, 177–185. https://doi.org/10.1016/j.cmet.2006.02.002

Kim, J.K., Diehl, J.A., 2009. Nuclear cyclin D1: an oncogenic driver in human cancer. J. Cell. Physiol. 220, 292–296. https://doi.org/10.1002/jcp.21791

Kim, P.H., Cha, E.K., Sfakianos, J.P., Iyer, G., Zabor, E.C., Scott, S.N., Ostrovnaya, I., Ramirez, R., Sun, A., Shah, R., Yee, A.M., Reuter, V.E., Bajorin, D.F., Rosenberg, J.E., Schultz, N., Berger, M.F., Al-Ahmadie, H.A., Solit, D.B., Bochner, B.H., 2015. Genomic predictors of survival in patients with high-grade urothelial carcinoma of the bladder. Eur. Urol. 67, 198–201. https://doi.org/10.1016/j.eururo.2014.06.050

Kimura, N., Yonekura, H., Okamoto, H., Nagura, H., 1992. Expression of human regenerating gene mRNA and its product in normal and neoplastic human pancreas. Cancer 70, 1857–1863.

Klemm, F., Joyce, J.A., 2015. Microenvironmental regulation of therapeutic response in cancer. Trends Cell Biol. 25, 198–213. https://doi.org/10.1016/j.tcb.2014.11.006

Klint, P., Claesson-Welsh, L., 1999. Signal transduction by fibroblast growth factor receptors. Front. Biosci. J. Virtual Libr. 4, D165-177.

Knight, E., Murray, B., Carnachan, R., Przyborski, S., 2011. Alvetex®: polystyrene scaffold technology for routine three dimensional cell culture. Methods Mol. Biol. Clifton NJ 695, 323–340. https://doi.org/10.1007/978-1-60761-984-0_20

Knights, V., Cook, S.J., 2010. De-regulated FGF receptors as therapeutic targets in cancer. Pharmacol. Ther. 125, 105–117. https://doi.org/10.1016/j.pharmthera.2009.10.001

Kobrin, M.S., Yamanaka, Y., Friess, H., Lopez, M.E., Korc, M., 1993. Aberrant expression of type I fibroblast growth factor receptor in human pancreatic adenocarcinomas. Cancer Res. 53, 4741–4744.

Kodaki, T., Woscholski, R., Hallberg, B., Rodriguez-Viciana, P., Downward, J., Parker, P.J., 1994. The activation of phosphatidylinositol 3-kinase by Ras. Curr. Biol. CB 4, 798–806.

Kodzius, R., Kojima, M., Nishiyori, H., Nakamura, M., Fukuda, S., Tagami, M., Sasaki, D., Imamura, K., Kai, C., Harbers, M., Hayashizaki, Y., Carninci, P., 2006. CAGE: cap analysis of gene expression. Nat. Methods 3, 211–222. https://doi.org/10.1038/nmeth0306-211

Kole, T.P., Tseng, Y., Jiang, I., Katz, J.L., Wirtz, D., 2005. Intracellular Mechanics of Migrating Fibroblasts. Mol. Biol. Cell 16, 328–338. https://doi.org/10.1091/mbc.E04-06-0485

Kondoh, E., Mori, S., Yamaguchi, K., Baba, T., Matsumura, N., Cory Barnett, J., Whitaker, R.S., Konishi, I., Fujii, S., Berchuck, A., Murphy, S.K., 2010. Targeting slow-proliferating ovarian cancer cells. Int. J. Cancer 126, 2448–2456. https://doi.org/10.1002/ijc.24919

Konecny, G.E., Kolarova, T., O'Brien, N.A., Winterhoff, B., Yang, G., Qi, J., Qi, Z., Venkatesan, N., Ayala, R., Luo, T., Finn, R.S., Kristof, J., Galderisi, C., Porta, D.G., Anderson, L., Shi, M.M., Yovine, A., Slamon, D.J., 2013. Activity of the fibroblast growth factor receptor inhibitors dovitinib (TKI258) and NVP-BGJ398 in human endometrial cancer cells. Mol. Cancer Ther. 12, 632–642. https://doi.org/10.1158/1535-7163.MCT-12-0999

Kopanska, K.S., Alcheikh, Y., Staneva, R., Vignjevic, D., Betz, T., 2016. Tensile Forces Originating from Cancer Spheroids Facilitate Tumor Invasion. PloS One 11, e0156442. https://doi.org/10.1371/journal.pone.0156442

Korc, M., Friesel, R.E., 2009. The role of fibroblast growth factors in tumor growth. Curr. Cancer Drug Targets 9, 639–651.

Kosaka, T., Yamaki, E., Mogi, A., Kuwano, H., 2011. Mechanisms of resistance to EGFR TKIs and development of a new generation of drugs in non-small-cell lung cancer. J. Biomed. Biotechnol. 2011, 165214. https://doi.org/10.1155/2011/165214

Kouhara, H., Hadari, Y.R., Spivak-Kroizman, T., Schilling, J., Bar-Sagi, D., Lax, I., Schlessinger, J., 1997. A lipid-anchored Grb2-binding protein that links FGF-receptor activation to the Ras/MAPK signaling pathway. Cell 89, 693–702.

Kovalenko, D., Yang, X., Nadeau, R.J., Harkins, L.K., Friesel, R., 2003. Sef Inhibits Fibroblast Growth Factor Signaling by Inhibiting FGFR1 Tyrosine Phosphorylation and Subsequent ERK Activation. J. Biol. Chem. 278, 14087–14091. https://doi.org/10.1074/jbc.C200606200

Krause, H.P., Keup, U., Puls, W., 1982. Inhibition of disaccharide digestion in rat intestine by the alpha-glucosidase inhibitor acarbose (BAY g 5421). Digestion 23, 232–238. https://doi.org/10.1159/000198755

Krauthammer, M., Kong, Y., Ha, B.H., Evans, P., Bacchiocchi, A., McCusker, J.P., Cheng, E., Davis, M.J., Goh, G., Choi, M., Ariyan, S., Narayan, D., Dutton-Regester, K., Capatana, A., Holman, E.C., Bosenberg, M., Sznol, M., Kluger, H.M., Brash, D.E., Stern, D.F., Materin, M.A., Lo, R.S., Mane, S., Ma, S., Kidd, K.K., Hayward, N.K., Lifton, R.P., Schlessinger, J., Boggon, T.J., Halaban, R.,

2012. Exome sequencing identifies recurrent somatic RAC1 mutations in melanoma. Nat. Genet. 44, 1006–1014. https://doi.org/10.1038/ng.2359

Kreso, A., O'Brien, C.A., van Galen, P., Gan, O.I., Notta, F., Brown, A.M.K., Ng, K., Ma, J., Wienholds, E., Dunant, C., Pollett, A., Gallinger, S., McPherson, J., Mullighan, C.G., Shibata, D., Dick, J.E., 2013. Variable clonal repopulation dynamics influence chemotherapy response in colorectal cancer. Science 339, 543–548. https://doi.org/10.1126/science.1227670

Kristensen, L.S., Nielsen, H.M., Hansen, L.L., 2009. Epigenetics and cancer treatment. Eur. J. Pharmacol. 625, 131–142. https://doi.org/10.1016/j.ejphar.2009.10.011

Kroemer, G., Pouyssegur, J., 2008. Tumor cell metabolism: cancer's Achilles' heel. Cancer Cell 13, 472–482. https://doi.org/10.1016/j.ccr.2008.05.005

Ku, J.-L., Park, J.-G., 2005. Biology of SNU Cell Lines. Cancer Res. Treat. Off. J. Korean Cancer Assoc. 37, 1–19. https://doi.org/10.4143/crt.2005.37.1.1

Kubo, M., Sano, T., Fukagawa, T., Katai, H., Sasako, M., 2005. Increasing body mass index in Japanese patients with gastric cancer. Gastric Cancer Off. J. Int. Gastric Cancer Assoc. Jpn. Gastric Cancer Assoc. 8, 39–41. https://doi.org/10.1007/s10120-004-0304-5

Kunii, K., Davis, L., Gorenstein, J., Hatch, H., Yashiro, M., Di Bacco, A., Elbi, C., Lutterbach, B., 2008. FGFR2-amplified gastric cancer cell lines require FGFR2 and Erbb3 signaling for growth and survival. Cancer Res. 68, 2340–2348. https://doi.org/10.1158/0008-5472.CAN-07-5229

Kuperwasser, C., Chavarria, T., Wu, M., Magrane, G., Gray, J.W., Carey, L., Richardson, A., Weinberg, R.A., 2004. Reconstruction of functionally normal and malignant human breast tissues in mice. Proc. Natl. Acad. Sci. U. S. A. 101, 4966–4971. https://doi.org/10.1073/pnas.0401064101

Kuppumbatti, Y.S., Bleiweiss, I.J., Mandeli, J.P., Waxman, S., Mira-Y-Lopez, R., 2000. Cellular retinol-binding protein expression and breast cancer. J. Natl. Cancer Inst. 92, 475–480.

Kuppumbatti, Y.S., Rexer, B., Nakajo, S., Nakaya, K., Mira-y-Lopez, R., 2001. CRBP suppresses breast cancer cell survival and anchorage-independent growth. Oncogene 20, 7413–7419. https://doi.org/10.1038/sj.onc.1204749

Kurita, A., Miyauchi, Y., Ikushiro, S., Mackenzie, P.I., Yamada, H., Ishii, Y., 2017. Comprehensive Characterization of Mouse UDP-Glucuronosyltransferase (Ugt) Belonging to the Ugt2b Subfamily: Identification of Ugt2b36 as the Predominant Isoform Involved in Morphine Glucuronidation. J. Pharmacol. Exp. Ther. 361, 199–208. https://doi.org/10.1124/jpet.117.240382

Lai, L., Bohnsack, B.L., Niederreither, K., Hirschi, K.K., 2003. Retinoic acid regulates endothelial cell proliferation during vasculogenesis. Dev. Camb. Engl. 130, 6465–6474. https://doi.org/10.1242/dev.00887

Langley, R.R., Fidler, I.J., 2011. The seed and soil hypothesis revisited--the role of tumor-stroma interactions in metastasis to different organs. Int. J. Cancer 128, 2527–2535. https://doi.org/10.1002/ijc.26031

Larsen, J.E., Minna, J.D., 2011. Molecular biology of lung cancer: clinical implications. Clin. Chest Med. 32, 703–740. https://doi.org/10.1016/j.ccm.2011.08.003

Lau, H.-Y., Chen, Y.-J., Yen, M.-S., Chao, K.-C., Chen, R.-F., Yeh, S.-O., Twu, N.-F., 2014. Clinicopathological features and survival in young Taiwanese women

with endometrial carcinoma. Int. J. Gynecol. Cancer Off. J. Int. Gynecol. Cancer Soc. 24, 1015–1020. https://doi.org/10.1097/IGC.0000000000000193

Laughner, E., Taghavi, P., Chiles, K., Mahon, P.C., Semenza, G.L., 2001. HER2 (neu) signaling increases the rate of hypoxia-inducible factor 1alpha (HIF-1alpha) synthesis: novel mechanism for HIF-1-mediated vascular endothelial growth factor expression. Mol. Cell. Biol. 21, 3995–4004. https://doi.org/10.1128/MCB.21.12.3995-4004.2001

Lax, I., Wong, A., Lamothe, B., Lee, A., Frost, A., Hawes, J., Schlessinger, J., 2002. The Docking Protein FRS2α Controls a MAP Kinase-Mediated Negative Feedback Mechanism for Signaling by FGF Receptors. Mol. Cell 10, 709–719. https://doi.org/10.1016/S1097-2765(02)00689-5

Lee, B.-H., Eskandari, R., Jones, K., Reddy, K.R., Quezada-Calvillo, R., Nichols, B.L., Rose, D.R., Hamaker, B.R., Pinto, B.M., 2012. Modulation of starch digestion for slow glucose release through "toggling" of activities of mucosal α-glucosidases. J. Biol. Chem. 287, 31929–31938. https://doi.org/10.1074/jbc.M112.351858

Lee, G.Y., Kenny, P.A., Lee, E.H., Bissell, M.J., 2007. Three-dimensional culture models of normal and malignant breast epithelial cells. Nat. Methods 4, 359–365. https://doi.org/10.1038/nmeth1015

Lee, J., Cuddihy, M.J., Kotov, N.A., 2008. Three-dimensional cell culture matrices: state of the art. Tissue Eng. Part B Rev. 14, 61–86. https://doi.org/10.1089/teb.2007.0150

Lee, W.-S., Seo, G., Shin, H.J., Yun, S.H., Yun, H., Choi, N., Lee, J., Son, D., Cho, J., Kim, J., Cho, Y.B., Chun, H.-K., Lee, W.Y., 2008. Identification of differentially expressed genes in microsatellite stable HNPCC and sporadic colon cancer. J. Surg. Res. 144, 29–35. https://doi.org/10.1016/j.jss.2007.02.005

Lefebvre, P., Martin, P.J., Flajollet, S., Dedieu, S., Billaut, X., Lefebvre, B., 2005. Transcriptional activities of retinoic acid receptors. Vitam. Horm. 70, 199–264. https://doi.org/10.1016/S0083-6729(05)70007-8

Lefèvre, G., Babchia, N., Calipel, A., Mouriaux, F., Faussat, A.-M., Mrzyk, S., Mascarelli, F., 2009. Activation of the FGF2/FGFR1 autocrine loop for cell proliferation and survival in uveal melanoma cells. Invest. Ophthalmol. Vis. Sci. 50, 1047–1057. https://doi.org/10.1167/iovs.08-2378

Leith, C.P., Kopecky, K.J., Chen, I.M., Eijdems, L., Slovak, M.L., McConnell, T.S., Head, D.R., Weick, J., Grever, M.R., Appelbaum, F.R., Willman, C.L., 1999. Frequency and clinical significance of the expression of the multidrug resistance proteins MDR1/P-glycoprotein, MRP1, and LRP in acute myeloid leukemia: a Southwest Oncology Group Study. Blood 94, 1086–1099.

Levental, K.R., Yu, H., Kass, L., Lakins, J.N., Egeblad, M., Erler, J.T., Fong, S.F.T., Csiszar, K., Giaccia, A., Weninger, W., Yamauchi, M., Gasser, D.L., Weaver, V.M., 2009. Matrix crosslinking forces tumor progression by enhancing integrin signaling. Cell 139, 891–906. https://doi.org/10.1016/j.cell.2009.10.027

Li, C., Scott, D.A., Hatch, E., Tian, X., Mansour, S.L., 2007. Dusp6 (Mkp3) is a negative feedback regulator of FGF-stimulated ERK signaling during mouse development. Dev. Camb. Engl. 134, 167–176. https://doi.org/10.1242/dev.02701

Li, H., Fan, X., Houghton, J., 2007. Tumor microenvironment: the role of the tumor stroma in cancer. J. Cell. Biochem. 101, 805–815. https://doi.org/10.1002/jcb.21159

Li, H.-H., Chen, R., Hyduke, D.R., Williams, A., Frötschl, R., Ellinger-Ziegelbauer, H., O'Lone, R., Yauk, C.L., Aubrecht, J., Fornace, A.J., 2017. Development and validation of a high-throughput transcriptomic biomarker to address 21st century genetic toxicology needs. Proc. Natl. Acad. Sci. U. S. A. 114, E10881–E10889. https://doi.org/10.1073/pnas.1714109114

Li, J., Chen, J., Kirsner, R., 2007. Pathophysiology of acute wound healing. Clin. Dermatol. 25, 9–18. https://doi.org/10.1016/j.clindermatol.2006.09.007

Li, X.-Y., Zhan, X.-R., Liu, X.-M., Wang, X.-C., 2011. CREB is a regulatory target for the protein kinase Akt/PKB in the differentiation of pancreatic ductal cells into islet β-cells mediated by hepatocyte growth factor. Biochem. Biophys. Res. Commun. 404, 711–716. https://doi.org/10.1016/j.bbrc.2010.12.048

Li, Z., Yan, S., Attayan, N., Ramalingam, S., Thiele, C.J., 2012. Combination of an allosteric Akt Inhibitor MK-2206 with etoposide or rapamycin enhances the antitumor growth effect in neuroblastoma. Clin. Cancer Res. Off. J. Am. Assoc. Cancer Res. 18, 3603–3615. https://doi.org/10.1158/1078-0432.CCR-11-3321

Li, Z.-W., Dalton, W.S., 2006. Tumor microenvironment and drug resistance in hematologic malignancies. Blood Rev. 20, 333–342. https://doi.org/10.1016/j.blre.2005.08.003

Liang, D., Chen, Q., Guo, Y., Zhang, T., Guo, W., 2017. Insight into resistance mechanisms of AZD4547 and E3810 to FGFR1 gatekeeper mutation via theoretical study. Drug Des. Devel. Ther. 11, 451–461. https://doi.org/10.2147/DDDT.S129991

Liao, Y., Hung, M.-C., 2010. Physiological regulation of Akt activity and stability. Am. J. Transl. Res. 2, 19–42.

Lietzke, S.E., Bose, S., Cronin, T., Klarlund, J., Chawla, A., Czech, M.P., Lambright, D.G., 2000. Structural basis of 3-phosphoinositide recognition by pleckstrin homology domains. Mol. Cell 6, 385–394.

Lièvre, A., Bachet, J.-B., Le Corre, D., Boige, V., Landi, B., Emile, J.-F., Côté, J.-F., Tomasic, G., Penna, C., Ducreux, M., Rougier, P., Penault-Llorca, F., Laurent-Puig, P., 2006. KRAS mutation status is predictive of response to cetuximab therapy in colorectal cancer. Cancer Res. 66, 3992–3995. https://doi.org/10.1158/0008-5472.CAN-06-0191

Lim, S.L., Ricciardelli, C., Oehler, M.K., Tan, I.M.D.D.A., Russell, D., Grützner, F., 2014. Overexpression of piRNA pathway genes in epithelial ovarian cancer. PloS One 9, e99687. https://doi.org/10.1371/journal.pone.0099687

Lin, H.-Y., Chin, Y.-T., Yang, Y.-C.S.H., Lai, H.-Y., Wang-Peng, J., Liu, L.F., Tang, H.-Y., Davis, P.J., 2016. Thyroid Hormone, Cancer, and Apoptosis. Compr. Physiol. 6, 1221–1237. https://doi.org/10.1002/cphy.c150035

Lindahl, U., Höök, M., 1978. Glycosaminoglycans and their binding to biological macromolecules. Annu. Rev. Biochem. 47, 385–417. https://doi.org/10.1146/annurev.bi.47.070178.002125

Liongue, C., O'Sullivan, L.A., Trengove, M.C., Ward, A.C., 2012. Evolution of JAK-STAT pathway components: mechanisms and role in immune system

development. PloS One 7, e32777. https://doi.org/10.1371/journal.pone.0032777
Liotta, L.A., Kohn, E.C., 2001. The microenvironment of the tumour-host interface. Nature 411, 375–379. https://doi.org/10.1038/35077241
Lippman, S.M., Shin, D.M., Lee, J.J., Batsakis, J.G., Lotan, R., Tainsky, M.A., Hittelman, W.N., Hong, W.K., 1995. p53 and retinoid chemoprevention of oral carcinogenesis. Cancer Res. 55, 16–19.
Lister, R., O'Malley, R.C., Tonti-Filippini, J., Gregory, B.D., Berry, C.C., Millar, A.H., Ecker, J.R., 2008. Highly integrated single-base resolution maps of the epigenome in Arabidopsis. Cell 133, 523–536. https://doi.org/10.1016/j.cell.2008.03.029
Lito, P., Rosen, N., Solit, D.B., 2013. Tumor adaptation and resistance to RAF inhibitors. Nat. Med. 19, 1401–1409. https://doi.org/10.1038/nm.3392
Litwin, M., Szczepańska-Buda, A., Michałowska, D., Grzegrzółka, J., Piotrowska, A., Gomułkiewicz, A., Wojnar, A., Dzięgiel, P., Witkiewicz, W., 2018. Aberrant Expression of PIWIL1 and PIWIL2 and Their Clinical Significance in Ductal Breast Carcinoma. Anticancer Res. 38, 2021–2030. https://doi.org/10.21873/anticanres.12441
Liu, J., Wen, D., Fang, X., Wang, X., Liu, T., Zhu, J., 2015. p38MAPK Signaling Enhances Glycolysis Through the Up-Regulation of the Glucose Transporter GLUT-4 in Gastric Cancer Cells. Cell. Physiol. Biochem. Int. J. Exp. Cell. Physiol. Biochem. Pharmacol. 36, 155–165. https://doi.org/10.1159/000374060
Liu, S.-H., Lin, C.-Y., Peng, S.-Y., Jeng, Y.-M., Pan, H.-W., Lai, P.-L., Liu, C.-L., Hsu, H.-C., 2002. Down-regulation of annexin A10 in hepatocellular carcinoma is associated with vascular invasion, early recurrence, and poor prognosis in synergy with p53 mutation. Am. J. Pathol. 160, 1831–1837. https://doi.org/10.1016/S0002-9440(10)61129-7
Liu, W.-K., Jiang, X.-Y., Zhang, Z.-X., 2010. Expression of PSCA, PIWIL1 and TBX2 and its correlation with HPV16 infection in formalin-fixed, paraffin-embedded cervical squamous cell carcinoma specimens. Arch. Virol. 155, 657–663. https://doi.org/10.1007/s00705-010-0635-y
Liu, X., Nugoli, M., Laferrière, J., Saleh, S.M., Rodrigue-Gervais, I.G., Saleh, M., Park, M., Hallett, M.T., Muller, W.J., Giguère, V., 2011. Stromal retinoic acid receptor beta promotes mammary gland tumorigenesis. Proc. Natl. Acad. Sci. U. S. A. 108, 774–779. https://doi.org/10.1073/pnas.1011845108
Liu, X., Sun, Y., Guo, J., Ma, H., Li, J., Dong, B., Jin, G., Zhang, J., Wu, J., Meng, L., Shou, C., 2006. Expression of hiwi gene in human gastric cancer was associated with proliferation of cancer cells. Int. J. Cancer 118, 1922–1929. https://doi.org/10.1002/ijc.21575
Liu, Y., Gao, F., Song, W., 2017. Periostin contributes to arsenic trioxide resistance in hepatocellular carcinoma cells under hypoxia. Biomed. Pharmacother. Biomedecine Pharmacother. 88, 342–348. https://doi.org/10.1016/j.biopha.2017.01.052
Liu, Z., Wei, Z., Liu, Y., Wang, Z., Fu, Z., Liu, S., Shen, J., Hu, Z., 2017. [Role and mechanism of stromal cell derived factor 1 on proliferation of vascular endothelial cells]. Zhongguo Xiu Fu Chong Jian Wai Ke Za Zhi Zhongguo

Xiufu Chongjian Waike Zazhi Chin. J. Reparative Reconstr. Surg. 31, 91–97. https://doi.org/10.7507/1002-1892.201609071

Liu, Z., Zhang, Yuehong, Xie, J., Li, C., Wang, X., Shen, J., Zhang, Yiqiang, Wang, S., Cheng, N., 2015. Regenerating gene 1B silencing inhibits colon cancer cell HCT116 proliferation and invasion. Int. J. Biol. Markers 30, e217-225. https://doi.org/10.5301/jbm.5000133

Lohr, J.G., Stojanov, P., Carter, S.L., Cruz-Gordillo, P., Lawrence, M.S., Auclair, D., Sougnez, C., Knoechel, B., Gould, J., Saksena, G., Cibulskis, K., McKenna, A., Chapman, M.A., Straussman, R., Levy, J., Perkins, L.M., Keats, J.J., Schumacher, S.E., Rosenberg, M., Getz, G., Golub, T.R., Anderson, K.C., Richardson, P., Krishnan, A., Lonial, S., Kaufman, J., Siegel, D.S., Vesole, D.H., Roy, V., Rivera, C.E., Rajkumar, S.V., Kumar, S., Fonseca, R., Ahmann, G.J., Bergsagel, P.L., Stewart, A.K., Hofmeister, C.C., Efebera, Y.A., Jagannath, S., Chari, A., Trudel, S., Reece, D., Wolf, J., Martin, T., Zimmerman, T., Rosenbaum, C., Jakubowiak, A.J., Lebovic, D., Vij, R., Stockerl-Goldstein, K., 2014. Widespread Genetic Heterogeneity in Multiple Myeloma: Implications for Targeted Therapy. Cancer Cell 25, 91–101. https://doi.org/10.1016/j.ccr.2013.12.015

Lojda, Z., Fric, P., 1996. Sucrase-isomaltase and other brush border glycosidases in colorectal tumors. Acta Histochem. 98, 285–293. https://doi.org/10.1016/S0065-1281(96)80021-3

Longley, D.B., Johnston, P.G., 2005. Molecular mechanisms of drug resistance. J. Pathol. 205, 275–292. https://doi.org/10.1002/path.1706

Longo-Sorbello, G.S., Bertino, J.R., 2001. Current understanding of methotrexate pharmacology and efficacy in acute leukemias. Use of newer antifolates in clinical trials. Haematologica 86, 121–127.

López-Knowles, E., Hernández, S., Malats, N., Kogevinas, M., Lloreta, J., Carrato, A., Tardón, A., Serra, C., Real, F.X., 2006. PIK3CA mutations are an early genetic alteration associated with FGFR3 mutations in superficial papillary bladder tumors. Cancer Res. 66, 7401–7404. https://doi.org/10.1158/0008-5472.CAN-06-1182

Luca, A.C., Mersch, S., Deenen, R., Schmidt, S., Messner, I., Schäfer, K.-L., Baldus, S.E., Huckenbeck, W., Piekorz, R.P., Knoefel, W.T., Krieg, A., Stoecklein, N.H., 2013. Impact of the 3D Microenvironment on Phenotype, Gene Expression, and EGFR Inhibition of Colorectal Cancer Cell Lines. PLoS ONE 8. https://doi.org/10.1371/journal.pone.0059689

Ludovini, V., Bianconi, F., Pistola, L., Chiari, R., Minotti, V., Colella, R., Giuffrida, D., Tofanetti, F.R., Siggillino, A., Flacco, A., Baldelli, E., Iacono, D., Mameli, M.G., Cavaliere, A., Crinò, L., 2011. Phosphoinositide-3-kinase catalytic alpha and KRAS mutations are important predictors of resistance to therapy with epidermal growth factor receptor tyrosine kinase inhibitors in patients with advanced non-small cell lung cancer. J. Thorac. Oncol. Off. Publ. Int. Assoc. Study Lung Cancer 6, 707–715. https://doi.org/10.1097/JTO.0b013e31820a3a6b

Lum, J.J., Bui, T., Gruber, M., Gordan, J.D., DeBerardinis, R.J., Covello, K.L., Simon, M.C., Thompson, C.B., 2007. The transcription factor HIF-1alpha plays a critical role in the growth factor-dependent regulation of both aerobic and

anaerobic glycolysis. Genes Dev. 21, 1037–1049. https://doi.org/10.1101/gad.1529107

Lv, Z., Xu, Q., Yuan, Y., 2017. A systematic review and meta-analysis of the association between long non-coding RNA polymorphisms and cancer risk. Mutat. Res. 771, 1–14. https://doi.org/10.1016/j.mrrev.2016.10.002

Ma, S., Dai, Y., 2011. Principal component analysis based methods in bioinformatics studies. Brief. Bioinform. 12, 714–722. https://doi.org/10.1093/bib/bbq090

Ma, X., Hui, Y., Lin, L., Wu, Y., Zhang, X., Liu, P., 2015. Clinical significance of COX-2, GLUT-1 and VEGF expressions in endometrial cancer tissues. Pak. J. Med. Sci. 31, 280–284. https://doi.org/10.12669/pjms.312.6604

Ma, Y., Feng, Q., Sekula, D., Diehl, J.A., Freemantle, S.J., Dmitrovsky, E., 2005. Retinoid targeting of different D-type cyclins through distinct chemopreventive mechanisms. Cancer Res. 65, 6476–6483. https://doi.org/10.1158/0008-5472.CAN-05-0370

Maarbjerg, S.J., Sylow, L., Richter, E.A., 2011. Current understanding of increased insulin sensitivity after exercise - emerging candidates. Acta Physiol. Oxf. Engl. 202, 323–335. https://doi.org/10.1111/j.1748-1716.2011.02267.x

Machida, S., Saga, Y., Takei, Y., Mizuno, I., Takayama, T., Kohno, T., Konno, R., Ohwada, M., Suzuki, M., 2005. Inhibition of peritoneal dissemination of ovarian cancer by tyrosine kinase receptor inhibitor SU6668 (TSU-68). Int. J. Cancer 114, 224–229. https://doi.org/10.1002/ijc.20751

Mahipal, A., Tella, S.H., Kommalapati, A., Goyal, G., Soares, H., Neuger, A., Copolla, D., Kim, J., Kim, R., 2018. Phase 1 trial of enzalutamide in combination with gemcitabine and nab-paclitaxel for the treatment of advanced pancreatic cancer. Invest. New Drugs. https://doi.org/10.1007/s10637-018-0676-8

Majewski, I.J., Mittempergher, L., Davidson, N.M., Bosma, A., Willems, S.M., Horlings, H.M., de Rink, I., Greger, L., Hooijer, G.K.J., Peters, D., Nederlof, P.M., Hofland, I., de Jong, J., Wesseling, J., Kluin, R.J.C., Brugman, W., Kerkhoven, R., Nieboer, F., Roepman, P., Broeks, A., Muley, T.R., Jassem, J., Niklinski, J., van Zandwijk, N., Brazma, A., Oshlack, A., van den Heuvel, M., Bernards, R., 2013. Identification of recurrent FGFR3 fusion genes in lung cancer through kinome-centred RNA sequencing. J. Pathol. 230, 270–276. https://doi.org/10.1002/path.4209

Makker, A., Goel, M.M., Mahdi, A.A., 2014. PI3K/PTEN/Akt and TSC/mTOR signaling pathways, ovarian dysfunction, and infertility: an update. J. Mol. Endocrinol. 53, R103-118. https://doi.org/10.1530/JME-14-0220

Malecki, M.T., Jhala, U.S., Antonellis, A., Fields, L., Doria, A., Orban, T., Saad, M., Warram, J.H., Montminy, M., Krolewski, A.S., 1999. Mutations in NEUROD1 are associated with the development of type 2 diabetes mellitus. Nat. Genet. 23, 323–328. https://doi.org/10.1038/15500

Maltman, D.J., Przyborski, S.A., 2010. Developments in three-dimensional cell culture technology aimed at improving the accuracy of in vitro analyses. Biochem. Soc. Trans. 38, 1072–1075. https://doi.org/10.1042/BST0381072

Malumbres, M., Barbacid, M., 2009. Cell cycle, CDKs and cancer: a changing paradigm. Nat. Rev. Cancer 9, 153–166. https://doi.org/10.1038/nrc2602

Manning, B.D., Toker, A., 2017. AKT/PKB Signaling: Navigating the Network. Cell 169, 381–405. https://doi.org/10.1016/j.cell.2017.04.001

Mansson, P.E., Adams, P., Kan, M., McKeehan, W.L., 1989. Heparin-binding growth factor gene expression and receptor characteristics in normal rat prostate and two transplantable rat prostate tumors. Cancer Res. 49, 2485–2494.

Manzano, J.L., Layos, L., Bugés, C., de los Llanos Gil, M., Vila, L., Martínez-Balibrea, E., Martínez-Cardús, A., 2016. Resistant mechanisms to BRAF inhibitors in melanoma. Ann. Transl. Med. 4. https://doi.org/10.21037/atm.2016.06.07

Marek, L., Ware, K.E., Fritzsche, A., Hercule, P., Helton, W.R., Smith, J.E., McDermott, L.A., Coldren, C.D., Nemenoff, R.A., Merrick, D.T., Helfrich, B.A., Bunn, P.A., Heasley, L.E., 2009. Fibroblast growth factor (FGF) and FGF receptor-mediated autocrine signaling in non-small-cell lung cancer cells. Mol. Pharmacol. 75, 196–207. https://doi.org/10.1124/mol.108.049544

Marin, J.J.G., Al-Abdulla, R., Lozano, E., Briz, O., Bujanda, L., Banales, J.M., Macias, R.I.R., 2016. Mechanisms of Resistance to Chemotherapy in Gastric Cancer. Anticancer Agents Med. Chem. 16, 318–334.

Marioni, J.C., Mason, C.E., Mane, S.M., Stephens, M., Gilad, Y., 2008. RNA-seq: an assessment of technical reproducibility and comparison with gene expression arrays. Genome Res. 18, 1509–1517. https://doi.org/10.1101/gr.079558.108

Marusyk, A., Polyak, K., 2010. Tumor heterogeneity: causes and consequences. Biochim. Biophys. Acta 1805, 105–117. https://doi.org/10.1016/j.bbcan.2009.11.002

Mason, J.M., Morrison, D.J., Bassit, B., Dimri, M., Band, H., Licht, J.D., Gross, I., 2004. Tyrosine Phosphorylation of Sprouty Proteins Regulates Their Ability to Inhibit Growth Factor Signaling: A Dual Feedback Loop. Mol. Biol. Cell 15, 2176–2188. https://doi.org/10.1091/mbc.E03-07-0503

Matsui, J., Yamamoto, Y., Funahashi, Y., Tsuruoka, A., Watanabe, T., Wakabayashi, T., Uenaka, T., Asada, M., 2008. E7080, a novel inhibitor that targets multiple kinases, has potent antitumor activities against stem cell factor producing human small cell lung cancer H146, based on angiogenesis inhibition. Int. J. Cancer 122, 664–671. https://doi.org/10.1002/ijc.23131

Matsuo, I., Kimura-Yoshida, C., 2013. Extracellular modulation of Fibroblast Growth Factor signaling through heparan sulfate proteoglycans in mammalian development. Curr. Opin. Genet. Dev. 23, 399–407. https://doi.org/10.1016/j.gde.2013.02.004

Mauchamp, J., Mirrione, A., Alquier, C., André, F., 1998. Follicle-like structure and polarized monolayer: role of the extracellular matrix on thyroid cell organization in primary culture. Biol. Cell 90, 369–380.

Mauro, M.J., 2006. Defining and managing imatinib resistance. Hematol. Am. Soc. Hematol. Educ. Program 219–225. https://doi.org/10.1182/asheducation-2006.1.219

McBeath, R., Pirone, D.M., Nelson, C.M., Bhadriraju, K., Chen, C.S., 2004. Cell shape, cytoskeletal tension, and RhoA regulate stem cell lineage commitment. Dev. Cell 6, 483–495.

McCubrey, J.A., Steelman, L.S., Chappell, W.H., Abrams, S.L., Wong, E.W.T., Chang, F., Lehmann, B., Terrian, D.M., Milella, M., Tafuri, A., Stivala, F., Libra, M., Basecke, J., Evangelisti, C., Martelli, A.M., Franklin, R.A., 2007. Roles of the Raf/MEK/ERK pathway in cell growth, malignant transformation and drug

resistance. Biochim. Biophys. Acta 1773, 1263–1284. https://doi.org/10.1016/j.bbamcr.2006.10.001

McDermott, J., Jimeno, A., 2015. Pembrolizumab: PD-1 inhibition as a therapeutic strategy in cancer. Drugs Today Barc. Spain 1998 51, 7–20. https://doi.org/10.1358/dot.2015.51.1.2250387

McDowell, L.M., Frazier, B.A., Studelska, D.R., Giljum, K., Chen, J., Liu, J., Yu, K., Ornitz, D.M., Zhang, L., 2006. Inhibition or activation of Apert syndrome FGFR2 (S252W) signaling by specific glycosaminoglycans. J. Biol. Chem. 281, 6924–6930. https://doi.org/10.1074/jbc.M512932200

McPherson, L.A., Woodfield, G.W., Weigel, R.J., 2007. AP2 transcription factors regulate expression of CRABPII in hormone responsive breast carcinoma. J. Surg. Res. 138, 71–78. https://doi.org/10.1016/j.jss.2006.07.002

Meads, M.B., Gatenby, R.A., Dalton, W.S., 2009. Environment-mediated drug resistance: a major contributor to minimal residual disease. Nat. Rev. Cancer 9, 665–674. https://doi.org/10.1038/nrc2714

Mehdawi, L.M., Prasad, C.P., Ehrnström, R., Andersson, T., Sjölander, A., 2016. Non-canonical WNT5A signaling up-regulates the expression of the tumor suppressor 15-PGDH and induces differentiation of colon cancer cells. Mol. Oncol. 10, 1415–1429. https://doi.org/10.1016/j.molonc.2016.07.011

Mehra, R., Serebriiskii, I.G., Dunbrack, R.L., Robinson, M.K., Burtness, B., Golemis, E.A., 2011. Protein-intrinsic and signaling network-based sources of resistance to EGFR- and ErbB family-targeted therapies in head and neck cancer. Drug Resist. Updat. Rev. Comment. Antimicrob. Anticancer Chemother. 14, 260–279. https://doi.org/10.1016/j.drup.2011.08.002

Mehrotra, J., Vali, M., McVeigh, M., Kominsky, S.L., Fackler, M.J., Lahti-Domenici, J., Polyak, K., Sacchi, N., Garrett-Mayer, E., Argani, P., Sukumar, S., 2004. Very high frequency of hypermethylated genes in breast cancer metastasis to the bone, brain, and lung. Clin. Cancer Res. Off. J. Am. Assoc. Cancer Res. 10, 3104–3109.

Mehta, G., Hsiao, A.Y., Ingram, M., Luker, G.D., Takayama, S., 2012. Opportunities and challenges for use of tumor spheroids as models to test drug delivery and efficacy. J. Control. Release Off. J. Control. Release Soc. 164, 192–204. https://doi.org/10.1016/j.jconrel.2012.04.045

Memarzadeh, S., Xin, L., Mulholland, D.J., Mansukhani, A., Wu, H., Teitell, M.A., Witte, O.N., 2007. Enhanced paracrine FGF10 expression promotes formation of multifocal prostate adenocarcinoma and an increase in epithelial androgen receptor. Cancer Cell 12, 572–585. https://doi.org/10.1016/j.ccr.2007.11.002

Merlot, A.M., Kalinowski, D.S., Richardson, D.R., 2014. Unraveling the mysteries of serum albumin—more than just a serum protein. Front. Physiol. 5. https://doi.org/10.3389/fphys.2014.00299

Mewes, A., Franke, H., Singer, D., 2012. Organotypic brain slice cultures of adult transgenic P301S mice--a model for tauopathy studies. PloS One 7, e45017. https://doi.org/10.1371/journal.pone.0045017

Micallef, L., Vedrenne, N., Billet, F., Coulomb, B., Darby, I.A., Desmoulière, A., 2012. The myofibroblast, multiple origins for major roles in normal and pathological tissue repair. Fibrogenesis Tissue Repair 5, S5. https://doi.org/10.1186/1755-1536-5-S1-S5

Mignatti, P., Morimoto, T., Rifkin, D.B., 1992. Basic fibroblast growth factor, a protein devoid of secretory signal sequence, is released by cells via a pathway independent of the endoplasmic reticulum-Golgi complex. J. Cell. Physiol. 151, 81–93. https://doi.org/10.1002/jcp.1041510113

Minamiya, Y., Kawai, H., Saito, H., Ito, M., Hosono, Y., Motoyama, S., Katayose, Y., Takahashi, N., Ogawa, J.-I., 2008. REG1A expression is an independent factor predictive of poor prognosis in patients with non-small cell lung cancer. Lung Cancer Amst. Neth. 60, 98–104. https://doi.org/10.1016/j.lungcan.2007.09.012

Missiaglia, E., Selfe, J., Hamdi, M., Williamson, D., Schaaf, G., Fang, C., Koster, J., Summersgill, B., Messahel, B., Versteeg, R., Pritchard-Jones, K., Kool, M., Shipley, J., 2009. Genomic imbalances in rhabdomyosarcoma cell lines affect expression of genes frequently altered in primary tumors: an approach to identify candidate genes involved in tumor development. Genes. Chromosomes Cancer 48, 455–467. https://doi.org/10.1002/gcc.20655

Miyaoka, Y., Kadowaki, Y., Ishihara, S., Ose, T., Fukuhara, H., Kazumori, H., Takasawa, S., Okamoto, H., Chiba, T., Kinoshita, Y., 2004. Transgenic overexpression of Reg protein caused gastric cell proliferation and differentiation along parietal cell and chief cell lineages. Oncogene 23, 3572–3579. https://doi.org/10.1038/sj.onc.1207333

Mo, A., Jackson, S., Varma, K., Carpino, A., Giardina, C., Devers, T.J., Rosenberg, D.W., 2016. Distinct Transcriptional Changes and Epithelial-Stromal Interactions Are Altered in Early-Stage Colon Cancer Development. Mol. Cancer Res. MCR 14, 795–804. https://doi.org/10.1158/1541-7786.MCR-16-0156

Moghal, N., Neel, B.G., 1995. Evidence for impaired retinoic acid receptor-thyroid hormone receptor AF-2 cofactor activity in human lung cancer. Mol. Cell. Biol. 15, 3945–3959.

Mohammadi, M., Dikic, I., Sorokin, A., Burgess, W.H., Jaye, M., Schlessinger, J., 1996. Identification of six novel autophosphorylation sites on fibroblast growth factor receptor 1 and elucidation of their importance in receptor activation and signal transduction. Mol. Cell. Biol. 16, 977–989.

Mohammadi, M., Froum, S., Hamby, J.M., Schroeder, M.C., Panek, R.L., Lu, G.H., Eliseenkova, A.V., Green, D., Schlessinger, J., Hubbard, S.R., 1998. Crystal structure of an angiogenesis inhibitor bound to the FGF receptor tyrosine kinase domain. EMBO J. 17, 5896–5904. https://doi.org/10.1093/emboj/17.20.5896

Mohammadi, M., Honegger, A.M., Rotin, D., Fischer, R., Bellot, F., Li, W., Dionne, C.A., Jaye, M., Rubinstein, M., Schlessinger, J., 1991. A tyrosine-phosphorylated carboxy-terminal peptide of the fibroblast growth factor receptor (Flg) is a binding site for the SH2 domain of phospholipase C-gamma 1. Mol. Cell. Biol. 11, 5068–5078.

Mohan, S., Eskandari, R., Pinto, B.M., 2014. Naturally occurring sulfonium-ion glucosidase inhibitors and their derivatives: a promising class of potential antidiabetic agents. Acc. Chem. Res. 47, 211–225. https://doi.org/10.1021/ar400132g

Mok, T.S., Wu, Y.-L., Thongprasert, S., Yang, C.-H., Chu, D.-T., Saijo, N., Sunpaweravong, P., Han, B., Margono, B., Ichinose, Y., Nishiwaki, Y., Ohe, Y., Yang, J.-J., Chewaskulyong, B., Jiang, H., Duffield, E.L., Watkins, C.L.,

Armour, A.A., Fukuoka, M., 2009. Gefitinib or carboplatin-paclitaxel in pulmonary adenocarcinoma. N. Engl. J. Med. 361, 947–957. https://doi.org/10.1056/NEJMoa0810699

Mokarram, P., Kumar, K., Brim, H., Naghibalhossaini, F., Saberi-firoozi, M., Nouraie, M., Green, R., Lee, E., Smoot, D.T., Ashktorab, H., 2009. Distinct high-profile methylated genes in colorectal cancer. PloS One 4, e7012. https://doi.org/10.1371/journal.pone.0007012

Mongan, N.P., Gudas, L.J., 2007. Diverse actions of retinoid receptors in cancer prevention and treatment. Differ. Res. Biol. Divers. 75, 853–870. https://doi.org/10.1111/j.1432-0436.2007.00206.x

Montagut, C., Sharma, S.V., Shioda, T., McDermott, U., Ulman, M., Ulkus, L.E., Dias-Santagata, D., Stubbs, H., Lee, D.Y., Singh, A., Drew, L., Haber, D.A., Settleman, J., 2008. Elevated CRAF as a potential mechanism of acquired resistance to BRAF inhibition in melanoma. Cancer Res. 68, 4853–4861. https://doi.org/10.1158/0008-5472.CAN-07-6787

Montgomery, S.B., Sammeth, M., Gutierrez-Arcelus, M., Lach, R.P., Ingle, C., Nisbett, J., Guigo, R., Dermitzakis, E.T., 2010. Transcriptome genetics using second generation sequencing in a Caucasian population. Nature 464, 773–777. https://doi.org/10.1038/nature08903

Moran, M.F., Koch, C.A., Anderson, D., Ellis, C., England, L., Martin, G.S., Pawson, T., 1990. Src homology region 2 domains direct protein-protein interactions in signal transduction. Proc. Natl. Acad. Sci. U. S. A. 87, 8622–8626.

Morice, P., Leary, A., Creutzberg, C., Abu-Rustum, N., Darai, E., 2016. Endometrial cancer. Lancet Lond. Engl. 387, 1094–1108. https://doi.org/10.1016/S0140-6736(15)00130-0

Morin, R., Bainbridge, M., Fejes, A., Hirst, M., Krzywinski, M., Pugh, T., McDonald, H., Varhol, R., Jones, S., Marra, M., 2008. Profiling the HeLa S3 transcriptome using randomly primed cDNA and massively parallel short-read sequencing. BioTechniques 45, 81–94. https://doi.org/10.2144/000112900

Mortazavi, A., Williams, B.A., McCue, K., Schaeffer, L., Wold, B., 2008. Mapping and quantifying mammalian transcriptomes by RNA-Seq. Nat. Methods 5, 621–628. https://doi.org/10.1038/nmeth.1226

Motoyama, S., Sugiyama, T., Ueno, Y., Okamoto, H., Takasawa, S., Nanjo, H., Watanabe, H., Maruyama, K., Okuyama, M., Ogawa, J.-I., 2006. REG I expression predicts long-term survival among locally advanced thoracic squamous cell esophageal cancer patients treated with neoadjuvant chemoradiotherapy followed by esophagectomy. Ann. Surg. Oncol. 13, 1724–1731. https://doi.org/10.1245/s10434-006-9075-z

Moyano, M., Stefani, G., 2015. piRNA involvement in genome stability and human cancer. J. Hematol. Oncol.J Hematol Oncol 8, 38. https://doi.org/10.1186/s13045-015-0133-5

Mroue, R., Bissell, M.J., 2013. Three-dimensional cultures of mouse mammary epithelial cells. Methods Mol. Biol. Clifton NJ 945, 221–250. https://doi.org/10.1007/978-1-62703-125-7_14

Mueller, M.M., Fusenig, N.E., 2002. Tumor-stroma interactions directing phenotype and progression of epithelial skin tumor cells. Differ. Res. Biol. Divers. 70, 486–497. https://doi.org/10.1046/j.1432-0436.2002.700903.x

Muenke, M., Schell, U., Hehr, A., Robin, N.H., Losken, H.W., Schinzel, A., Pulleyn, L.J., Rutland, P., Reardon, W., Malcolm, S., 1994. A common mutation in the fibroblast growth factor receptor 1 gene in Pfeiffer syndrome. Nat. Genet. 8, 269–274. https://doi.org/10.1038/ng1194-269

Mukaida, N., Sasaki, S., 2016. Fibroblasts, an inconspicuous but essential player in colon cancer development and progression. World J. Gastroenterol. 22, 5301–5316. https://doi.org/10.3748/wjg.v22.i23.5301

Mumenthaler, S.M., Foo, J., Choi, N.C., Heise, N., Leder, K., Agus, D.B., Pao, W., Michor, F., Mallick, P., 2015. The Impact of Microenvironmental Heterogeneity on the Evolution of Drug Resistance in Cancer Cells. Cancer Inform. 14, 19–31. https://doi.org/10.4137/CIN.S19338

Murata, T., Sato, T., Kamoda, T., Moriyama, H., Kumazawa, Y., Hanada, N., 2014. Differential susceptibility to hydrogen sulfide-induced apoptosis between PHLDA1-overexpressing oral cancer cell lines and oral keratinocytes: role of PHLDA1 as an apoptosis suppressor. Exp. Cell Res. 320, 247–257. https://doi.org/10.1016/j.yexcr.2013.10.023

Nagalakshmi, U., Wang, Z., Waern, K., Shou, C., Raha, D., Gerstein, M., Snyder, M., 2008. The Transcriptional Landscape of the Yeast Genome Defined by RNA Sequencing. Science 320, 1344–1349. https://doi.org/10.1126/science.1158441

Nakamura, W., Inada, K., Hirano, K., Tsukamoto, T., Inoue, H., Kito, K., Yoshikawa, A., Nakamura, S., Tatematsu, M., 1998. Increased Expression of Sucrase and Intestinal-type Alkaline Phosphatase in Human Gastric Carcinomas with Progression. Jpn. J. Cancer Res. Gann 89, 186–191. https://doi.org/10.1111/j.1349-7006.1998.tb00547.x

Nandan, M.O., Yang, V.W., 2011. An Update on the Biology of RAS/RAF Mutations in Colorectal Cancer. Curr. Colorectal Cancer Rep. 7, 113–120. https://doi.org/10.1007/s11888-011-0086-1

Napoli, J.L., 1999. Interactions of retinoid binding proteins and enzymes in retinoid metabolism. Biochim. Biophys. Acta 1440, 139–162.

Nath, S., Devi, G.R., 2016. Three-Dimensional Culture Systems in Cancer Research: Focus on Tumor Spheroid Model. Pharmacol. Ther. 163, 94–108. https://doi.org/10.1016/j.pharmthera.2016.03.013

Nathanson, A.I., Aladé, F., Sharp, M.L., Rasmussen, E.E., Christy, K., 2014. The relation between television exposure and executive function among preschoolers. Dev. Psychol. 50, 1497–1506. https://doi.org/10.1037/a0035714

Nazarian, R., Shi, H., Wang, Q., Kong, X., Koya, R.C., Lee, H., Chen, Z., Lee, M.-K., Attar, N., Sazegar, H., Chodon, T., Nelson, S.F., McArthur, G., Sosman, J.A., Ribas, A., Lo, R.S., 2010. Melanomas acquire resistance to B-RAF(V600E) inhibition by RTK or N-RAS upregulation. Nature 468, 973–977. https://doi.org/10.1038/nature09626

Neef, R., Kuske, M.A., Pröls, E., Johnson, J.P., 2002. Identification of the human PHLDA1/TDAG51 gene: down-regulation in metastatic melanoma contributes to apoptosis resistance and growth deregulation. Cancer Res. 62, 5920–5929.

Neesse, A., Michl, P., Frese, K.K., Feig, C., Cook, N., Jacobetz, M.A., Lolkema, M.P., Buchholz, M., Olive, K.P., Gress, T.M., Tuveson, D.A., 2011. Stromal biology

and therapy in pancreatic cancer. Gut 60, 861–868. https://doi.org/10.1136/gut.2010.226092

Nelson, C.M., Bissell, M.J., 2006. Of extracellular matrix, scaffolds, and signaling: tissue architecture regulates development, homeostasis, and cancer. Annu. Rev. Cell Dev. Biol. 22, 287–309. https://doi.org/10.1146/annurev.cellbio.22.010305.104315

Neofytou, E.A., Chang, E., Patlola, B., Joubert, L.-M., Rajadas, J., Gambhir, S.S., Cheng, Z., Robbins, R.C., Beygui, R.E., 2011. Adipose tissue-derived stem cells display a proangiogenic phenotype on 3D scaffolds. J. Biomed. Mater. Res. A 98, 383–393. https://doi.org/10.1002/jbm.a.33113

Netti, P.A., Berk, D.A., Swartz, M.A., Grodzinsky, A.J., Jain, R.K., 2000. Role of extracellular matrix assembly in interstitial transport in solid tumors. Cancer Res. 60, 2497–2503.

Neuville, P., Geinoz, A., Benzonana, G., Redard, M., Gabbiani, F., Ropraz, P., Gabbiani, G., 1997. Cellular retinol-binding protein-1 is expressed by distinct subsets of rat arterial smooth muscle cells in vitro and in vivo. Am. J. Pathol. 150, 509–521.

Ng, K.W., Anderson, C., Marshall, E.A., Minatel, B.C., Enfield, K.S.S., Saprunoff, H.L., Lam, W.L., Martinez, V.D., 2016. Piwi-interacting RNAs in cancer: emerging functions and clinical utility. Mol. Cancer 15, 5. https://doi.org/10.1186/s12943-016-0491-9

Nguyen, T.V., Sleiman, M., Moriarty, T., Herrick, W.G., Peyton, S.R., 2014. Sorafenib resistance and JNK signaling in carcinoma during extracellular matrix stiffening. Biomaterials 35, 5749–5759. https://doi.org/10.1016/j.biomaterials.2014.03.058

Nicholson, K.M., Anderson, N.G., 2002. The protein kinase B/Akt signalling pathway in human malignancy. Cell. Signal. 14, 381–395.

Nilsson, E.M., Brokken, L.J.S., Härkönen, P.L., 2010. Fibroblast growth factor 8 increases breast cancer cell growth by promoting cell cycle progression and by protecting against cell death. Exp. Cell Res. 316, 800–812. https://doi.org/10.1016/j.yexcr.2009.11.019

Nitsche, U., Stangel, D., Pan, Z., Schlitter, A.M., Esposito, I., Regel, I., Raulefs, S., Friess, H., Kleeff, J., Erkan, M., 2016. Periostin and tumor-stroma interactions in non-small cell lung cancer. Oncol. Lett. 12, 3804–3810. https://doi.org/10.3892/ol.2016.5132

Nogova, L., Sequist, L.V., Perez Garcia, J.M., Andre, F., Delord, J.-P., Hidalgo, M., Schellens, J.H.M., Cassier, P.A., Camidge, D.R., Schuler, M., Vaishampayan, U., Burris, H., Tian, G.G., Campone, M., Wainberg, Z.A., Lim, W.-T., LoRusso, P., Shapiro, G.I., Parker, K., Chen, X., Choudhury, S., Ringeisen, F., Graus-Porta, D., Porter, D., Isaacs, R., Buettner, R., Wolf, J., 2017. Evaluation of BGJ398, a Fibroblast Growth Factor Receptor 1-3 Kinase Inhibitor, in Patients With Advanced Solid Tumors Harboring Genetic Alterations in Fibroblast Growth Factor Receptors: Results of a Global Phase I, Dose-Escalation and Dose-Expansion Study. J. Clin. Oncol. Off. J. Am. Soc. Clin. Oncol. 35, 157–165. https://doi.org/10.1200/JCO.2016.67.2048

Nogueira, V., Park, Y., Chen, C.-C., Xu, P.-Z., Chen, M.-L., Tonic, I., Unterman, T., Hay, N., 2008. Akt determines replicative senescence and oxidative or

oncogenic premature senescence and sensitizes cells to oxidative apoptosis. Cancer Cell 14, 458–470. https://doi.org/10.1016/j.ccr.2008.11.003

Nord, H., Segersten, U., Sandgren, J., Wester, K., Busch, C., Menzel, U., Komorowski, J., Dumanski, J.P., Malmström, P.-U., Díaz de Ståhl, T., 2010. Focal amplifications are associated with high grade and recurrences in stage Ta bladder carcinoma. Int. J. Cancer 126, 1390–1402. https://doi.org/10.1002/ijc.24954

Norsworthy, K.J., Hernandez, D., Su, M., 2015. RAR-alpha targeting compounds overcome bone marrow (BM) stromal protection of AML by CYP26. Blood 126, 2474.

Noy, N., 2010. Between death and survival: retinoic acid in regulation of apoptosis. Annu. Rev. Nutr. 30, 201–217. https://doi.org/10.1146/annurev.nutr.28.061807.155509

Noy, N., 2000. Retinoid-binding proteins: mediators of retinoid action. Biochem. J. 348, 481–495.

Nyström, M., Thomas, G., Stone, M., Mackenzie, I., Hart, I., Marshall, J., 2005. Development of a quantitative method to analyse tumour cell invasion in organotypic culture. J. Pathol. 205, 468–475. https://doi.org/10.1002/path.1716

Oberst, A., Bender, C., Green, D.R., 2008. Living with death: The evolution of the mitochondrial pathway of apoptosis in animals. Cell Death Differ. 15, 1139–1146. https://doi.org/10.1038/cdd.2008.65

O'Byrne, S.M., Blaner, W.S., 2013. Retinol and retinyl esters: biochemistry and physiology. J. Lipid Res. 54, 1731–1743. https://doi.org/10.1194/jlr.R037648

Oh, H.J., Bae, J.M., Wen, X.-Y., Cho, N.-Y., Kim, J.H., Kang, G.H., 2017. Overexpression of POSTN in Tumor Stroma Is a Poor Prognostic Indicator of Colorectal Cancer. J. Pathol. Transl. Med. 51, 306–313. https://doi.org/10.4132/jptm.2017.01.19

Ohki, R., Saito, K., Chen, Y., Kawase, T., Hiraoka, N., Saigawa, R., Minegishi, M., Aita, Y., Yanai, G., Shimizu, H., Yachida, S., Sakata, N., Doi, R., Kosuge, T., Shimada, K., Tycko, B., Tsukada, T., Kanai, Y., Sumi, S., Namiki, H., Taya, Y., Shibata, T., Nakagama, H., 2014. PHLDA3 is a novel tumor suppressor of pancreatic neuroendocrine tumors. Proc. Natl. Acad. Sci. U. S. A. 111, E2404-2413. https://doi.org/10.1073/pnas.1319962111

Okudela, K., Yazawa, T., Woo, T., Sakaeda, M., Ishii, J., Mitsui, H., Shimoyamada, H., Sato, H., Tajiri, M., Ogawa, N., Masuda, M., Takahashi, T., Sugimura, H., Kitamura, H., 2009. Down-Regulation of DUSP6 Expression in Lung Cancer —Its Mechanism and Potential Role in Carcinogenesis. Am. J. Pathol. 175, 867–881. https://doi.org/10.2353/ajpath.2009.080489

Olive, K.P., Jacobetz, M.A., Davidson, C.J., Gopinathan, A., McIntyre, D., Honess, D., Madhu, B., Goldgraben, M.A., Caldwell, M.E., Allard, D., Frese, K.K., Denicola, G., Feig, C., Combs, C., Winter, S.P., Ireland-Zecchini, H., Reichelt, S., Howat, W.J., Chang, A., Dhara, M., Wang, L., Rückert, F., Grützmann, R., Pilarsky, C., Izeradjene, K., Hingorani, S.R., Huang, P., Davies, S.E., Plunkett, W., Egorin, M., Hruban, R.H., Whitebread, N., McGovern, K., Adams, J., Iacobuzio-Donahue, C., Griffiths, J., Tuveson, D.A., 2009. Inhibition of Hedgehog signaling enhances delivery of chemotherapy in a mouse model of

pancreatic cancer. Science 324, 1457–1461. https://doi.org/10.1126/science.1171362

Olsburgh, J., Harnden, P., Weeks, R., Smith, B., Joyce, A., Hall, G., Poulsom, R., Selby, P., Southgate, J., 2003. Uroplakin gene expression in normal human tissues and locally advanced bladder cancer. J. Pathol. 199, 41–49. https://doi.org/10.1002/path.1252

Olsen, S.K., Garbi, M., Zampieri, N., Eliseenkova, A.V., Ornitz, D.M., Goldfarb, M., Mohammadi, M., 2003. Fibroblast growth factor (FGF) homologous factors share structural but not functional homology with FGFs. J. Biol. Chem. 278, 34226–34236. https://doi.org/10.1074/jbc.M303183200

Olson, O.C., Joyce, J.A., 2013. Microenvironment-mediated resistance to anticancer therapies. Cell Res. 23, 179–181. https://doi.org/10.1038/cr.2012.123

Ong, S.H., Lim, Y.P., Low, B.C., Guy, G.R., 1997. SHP2 associates directly with tyrosine phosphorylated p90 (SNT) protein in FGF-stimulated cells. Biochem. Biophys. Res. Commun. 238, 261–266. https://doi.org/10.1006/bbrc.1997.7272

Onuigbo, W.I., 1975. Human model for studying seed-soil factors in blood-borne metastasis. Arch. Pathol. 99, 342–343.

Orlandi, A., Ferlosio, A., Ciucci, A., Francesconi, A., Lifschitz-Mercer, B., Gabbiani, G., Spagnoli, L.G., Czernobilsky, B., 2006. Cellular retinol binding protein-1 expression in endometrial hyperplasia and carcinoma: diagnostic and possible therapeutic implications. Mod. Pathol. Off. J. U. S. Can. Acad. Pathol. Inc 19, 797–803. https://doi.org/10.1038/modpathol.3800586

Ornitz, D.M., 2000. FGFs, heparan sulfate and FGFRs: complex interactions essential for development. BioEssays News Rev. Mol. Cell. Dev. Biol. 22, 108–112. https://doi.org/10.1002/(SICI)1521-1878(200002)22:2<108::AID-BIES2>3.0.CO;2-M

Ornitz, D.M., Itoh, N., 2015. The Fibroblast Growth Factor signaling pathway. Wiley Interdiscip. Rev. Dev. Biol. 4, 215–266. https://doi.org/10.1002/wdev.176

Ornitz, D.M., Itoh, N., 2001. Fibroblast growth factors. Genome Biol. 2, REVIEWS3005.

Oronsky, B.T., Oronsky, N., Fanger, G.R., Parker, C.W., Caroen, S.Z., Lybeck, M., Scicinski, J.J., 2014. Follow the ATP: tumor energy production: a perspective. Anticancer Agents Med. Chem. 14, 1187–1198.

O'Shea, J.J., Gadina, M., Schreiber, R.D., 2002. Cytokine signaling in 2002: new surprises in the Jak/Stat pathway. Cell 109 Suppl, S121-131.

Ota, S., Zhou, Z.-Q., Link, J.M., Hurlin, P.J., 2009. The role of senescence and prosurvival signaling in controlling the oncogenic activity of FGFR2 mutants associated with cancer and birth defects. Hum. Mol. Genet. 18, 2609–2621. https://doi.org/10.1093/hmg/ddp195

Page, H., Flood, P., Reynaud, E.G., 2013. Three-dimensional tissue cultures: current trends and beyond. Cell Tissue Res. 352, 123–131. https://doi.org/10.1007/s00441-012-1441-5

Page-McCaw, A., Ewald, A.J., Werb, Z., 2007. Matrix metalloproteinases and the regulation of tissue remodelling. Nat. Rev. Mol. Cell Biol. 8, 221–233. https://doi.org/10.1038/nrm2125

Paget, S., 1989. The distribution of secondary growths in cancer of the breast. 1889. Cancer Metastasis Rev. 8, 98–101.

Pal, S.K., Rosenberg, J.E., Hoffman-Censits, J.H., Berger, R., Quinn, D.I., Galsky, M.D., Wolf, J., Dittrich, C., Keam, B., Delord, J.-P., Schellens, J.H.M., Gravis, G., Medioni, J., Maroto, P., Sriuranpong, V., Charoentum, C., Burris, H.A., Grünwald, V., Petrylak, D., Vaishampayan, U., Gez, E., De Giorgi, U., Lee, J.-L., Voortman, J., Gupta, S., Sharma, S., Mortazavi, A., Vaughn, D.J., Isaacs, R., Parker, K., Chen, X., Yu, K., Porter, D., Graus Porta, D., Bajorin, D.F., 2018. Efficacy of BGJ398, a Fibroblast Growth Factor Receptor 1-3 Inhibitor, in Patients with Previously Treated Advanced Urothelial Carcinoma with FGFR3 Alterations. Cancer Discov. 8, 812–821. https://doi.org/10.1158/2159-8290.CD-18-0229

Pampaloni, F., Reynaud, E.G., Stelzer, E.H.K., 2007. The third dimension bridges the gap between cell culture and live tissue. Nat. Rev. Mol. Cell Biol. 8, 839–845. https://doi.org/10.1038/nrm2236

Pan, Q., Shai, O., Lee, L.J., Frey, B.J., Blencowe, B.J., 2008. Deep surveying of alternative splicing complexity in the human transcriptome by high-throughput sequencing. Nat. Genet. 40, 1413–1415. https://doi.org/10.1038/ng.259

Pandey, P.R., Liu, W., Xing, F., Fukuda, K., Watabe, K., 2012. Anti-cancer drugs targeting fatty acid synthase (FAS). Recent Patents Anticancer Drug Discov. 7, 185–197.

Pao, W., Wang, T.Y., Riely, G.J., Miller, V.A., Pan, Q., Ladanyi, M., Zakowski, M.F., Heelan, R.T., Kris, M.G., Varmus, H.E., 2005. KRAS Mutations and Primary Resistance of Lung Adenocarcinomas to Gefitinib or Erlotinib. PLoS Med. 2. https://doi.org/10.1371/journal.pmed.0020017

Papi, A., Guarnieri, T., Storci, G., Santini, D., Ceccarelli, C., Taffurelli, M., De Carolis, S., Avenia, N., Sanguinetti, A., Sidoni, A., Orlandi, M., Bonafé, M., 2012. Nuclear receptors agonists exert opposing effects on the inflammation dependent survival of breast cancer stem cells. Cell Death Differ. 19, 1208–1219. https://doi.org/10.1038/cdd.2011.207

Paraiso, K.H.T., Smalley, K.S.M., 2013. Fibroblast-mediated drug resistance in cancer. Biochem. Pharmacol. 85, 1033–1041. https://doi.org/10.1016/j.bcp.2013.01.018

Pardo, O.E., Latigo, J., Jeffery, R.E., Nye, E., Poulsom, R., Spencer-Dene, B., Lemoine, N.R., Stamp, G.W., Aboagye, E.O., Seckl, M.J., 2009. The fibroblast growth factor receptor inhibitor PD173074 blocks small cell lung cancer growth in vitro and in vivo. Cancer Res. 69, 8645–8651. https://doi.org/10.1158/0008-5472.CAN-09-1576

Pardoll, D.M., 2012. The blockade of immune checkpoints in cancer immunotherapy. Nat. Rev. Cancer 12, 252–264. https://doi.org/10.1038/nrc3239

Park, C.G., Lee, S.Y., Kandala, G., Lee, S.Y., Choi, Y., 1996. A novel gene product that couples TCR signaling to Fas(CD95) expression in activation-induced cell death. Immunity 4, 583–591.

Park, I.C., Park, M.J., Lee, S.H., Choe, T.B., Jang, J.J., Hong, S.I., 1998. Increased susceptibility of the c-Myc overexpressing cell line, SNU-16, to TNF-alpha. Cancer Lett. 125, 17–23.

Park, J.B., Lee, C.S., Jang, J.-H., Ghim, J., Kim, Y.-J., You, S., Hwang, D., Suh, P.-G., Ryu, S.H., 2012. Phospholipase signalling networks in cancer. Nat. Rev. Cancer 12, 782–792. https://doi.org/10.1038/nrc3379

Parker, B.C., Annala, M.J., Cogdell, D.E., Granberg, K.J., Sun, Y., Ji, P., Li, X., Gumin, J., Zheng, H., Hu, L., Yli-Harja, O., Haapasalo, H., Visakorpi, T., Liu, X., Liu, C.-G., Sawaya, R., Fuller, G.N., Chen, K., Lang, F.F., Nykter, M., Zhang, W., 2013. The tumorigenic FGFR3-TACC3 gene fusion escapes miR-99a regulation in glioblastoma. J. Clin. Invest. 123, 855–865. https://doi.org/10.1172/JCI67144

Parker, B.C., Zhang, W., 2013. Fusion genes in solid tumors: an emerging target for cancer diagnosis and treatment. Chin. J. Cancer 32, 594–603. https://doi.org/10.5732/cjc.013.10178

Parkin, D.M., 2006. The global health burden of infection-associated cancers in the year 2002. Int. J. Cancer 118, 3030–3044. https://doi.org/10.1002/ijc.21731

Parkin, D.M., Bray, F., Ferlay, J., Pisani, P., 2005. Global cancer statistics, 2002. CA. Cancer J. Clin. 55, 74–108.

Parkinson, H., Kapushesky, M., Kolesnikov, N., Rustici, G., Shojatalab, M., Abeygunawardena, N., Berube, H., Dylag, M., Emam, I., Farne, A., Holloway, E., Lukk, M., Malone, J., Mani, R., Pilicheva, E., Rayner, T.F., Rezwan, F., Sharma, A., Williams, E., Bradley, X.Z., Adamusiak, T., Brandizi, M., Burdett, T., Coulson, R., Krestyaninova, M., Kurnosov, P., Maguire, E., Neogi, S.G., Rocca-Serra, P., Sansone, S.-A., Sklyar, N., Zhao, M., Sarkans, U., Brazma, A., 2009. ArrayExpress update--from an archive of functional genomics experiments to the atlas of gene expression. Nucleic Acids Res. 37, D868-872. https://doi.org/10.1093/nar/gkn889

Paszek, M.J., Zahir, N., Johnson, K.R., Lakins, J.N., Rozenberg, G.I., Gefen, A., Reinhart-King, C.A., Margulies, S.S., Dembo, M., Boettiger, D., Hammer, D.A., Weaver, V.M., 2005. Tensional homeostasis and the malignant phenotype. Cancer Cell 8, 241–254. https://doi.org/10.1016/j.ccr.2005.08.010

Pawson, T., Olivier, P., Rozakis-Adcock, M., McGlade, J., Henkemeyer, M., 1993. Proteins with SH2 and SH3 domains couple receptor tyrosine kinases to intracellular signalling pathways. Philos. Trans. R. Soc. Lond. B. Biol. Sci. 340, 279–285. https://doi.org/10.1098/rstb.1993.0069

Peifer, M., Fernández-Cuesta, L., Sos, M.L., George, J., Seidel, D., Kasper, L.H., Plenker, D., Leenders, F., Sun, R., Zander, T., Menon, R., Koker, M., Dahmen, I., Müller, C., Di Cerbo, V., Schildhaus, H.-U., Altmüller, J., Baessmann, I., Becker, C., de Wilde, B., Vandesompele, J., Böhm, D., Ansén, S., Gabler, F., Wilkening, I., Heynck, S., Heuckmann, J.M., Lu, X., Carter, S.L., Cibulskis, K., Banerji, S., Getz, G., Park, K.-S., Rauh, D., Grütter, C., Fischer, M., Pasqualucci, L., Wright, G., Wainer, Z., Russell, P., Petersen, I., Chen, Y., Stoelben, E., Ludwig, C., Schnabel, P., Hoffmann, H., Muley, T., Brockmann, M., Engel-Riedel, W., Muscarella, L.A., Fazio, V.M., Groen, H., Timens, W., Sietsma, H., Thunnissen, E., Smit, E., Heideman, D.A.M., Snijders, P.J.F., Cappuzzo, F., Ligorio, C., Damiani, S., Field, J., Solberg, S., Brustugun, O.T., Lund-Iversen, M., Sänger, J., Clement, J.H., Soltermann, A., Moch, H., Weder, W., Solomon, B., Soria, J.-C., Validire, P., Besse, B., Brambilla, E., Brambilla, C., Lantuejoul, S., Lorimier, P., Schneider, P.M., Hallek, M., Pao, W., Meyerson, M., Sage, J., Shendure, J., Schneider, R., Büttner, R., Wolf, J., Nürnberg, P., Perner, S., Heukamp, L.C., Brindle, P.K., Haas, S., Thomas, R.K., 2012. Integrative genome analyses identify key somatic driver mutations of small-cell lung cancer. Nat. Genet. 44, 1104–1110. https://doi.org/10.1038/ng.2396

Peiffer, J.A., Kaushik, S., Sakai, H., Arteaga-Vazquez, M., Sanchez-Leon, N., Ghazal, H., Vielle-Calzada, J.-P., Meyers, B.C., 2008. A spatial dissection of the Arabidopsis floral transcriptome by MPSS. BMC Plant Biol. 8, 43. https://doi.org/10.1186/1471-2229-8-43

Peng, J., Wang, Q., Liu, H., Ye, M., Wu, X., Guo, L., 2016. EPHA3 regulates the multidrug resistance of small cell lung cancer via the PI3K/BMX/STAT3 signaling pathway. Tumour Biol. J. Int. Soc. Oncodevelopmental Biol. Med. 37, 11959–11971. https://doi.org/10.1007/s13277-016-5048-4

Peng, S.-Y., Lai, P.-L., Pan, H.-W., Hsiao, L.-P., Hsu, H.-C., 2008. Aberrant expression of the glycolytic enzymes aldolase B and type II hexokinase in hepatocellular carcinoma are predictive markers for advanced stage, early recurrence and poor prognosis. Oncol. Rep. 19, 1045–1053.

Peng, W.-X., Kudo, M., Fujii, T., Teduka, K., Naito, Z., 2014. Altered expression of fibroblast growth factor receptor 2 isoform IIIc: relevance to endometrioid adenocarcinoma carcinogenesis and histological differentiation. Int. J. Clin. Exp. Pathol. 7, 1069–1076.

Peralta, R., Baudis, M., Vazquez, G., Juárez, S., Ortiz, R., Decanini, H., Hernandez, D., Gallegos, F., Valdivia, A., Piña, P., Salcedo, M., 2010. Increased expression of cellular retinol-binding protein 1 in laryngeal squamous cell carcinoma. J. Cancer Res. Clin. Oncol. 136, 931–938. https://doi.org/10.1007/s00432-009-0735-9

Petersen, I., 2011. The morphological and molecular diagnosis of lung cancer. Dtsch. Arzteblatt Int. 108, 525–531. https://doi.org/10.3238/arztebl.2011.0525

Petersen, O.W., Rønnov-Jessen, L., Howlett, A.R., Bissell, M.J., 1992. Interaction with basement membrane serves to rapidly distinguish growth and differentiation pattern of normal and malignant human breast epithelial cells. Proc. Natl. Acad. Sci. U. S. A. 89, 9064–9068.

Phipps, A.I., Buchanan, D.D., Makar, K.W., Win, A.K., Baron, J.A., Lindor, N.M., Potter, J.D., Newcomb, P.A., 2013. KRAS-mutation status in relation to colorectal cancer survival: the joint impact of correlated tumour markers. Br. J. Cancer 108, 1757–1764. https://doi.org/10.1038/bjc.2013.118

Pijnappel, W.W., Hendriks, H.F., Folkers, G.E., van den Brink, C.E., Dekker, E.J., Edelenbosch, C., van der Saag, P.T., Durston, A.J., 1993. The retinoid ligand 4-oxo-retinoic acid is a highly active modulator of positional specification. Nature 366, 340–344. https://doi.org/10.1038/366340a0

Pisano, C., Vesci, L., Foderà, R., Ferrara, F.F., Rossi, C., De Cesare, M., Zuco, V., Pratesi, G., Supino, R., Zunino, F., 2007. Antitumor activity of the combination of synthetic retinoid ST1926 and cisplatin in ovarian carcinoma models. Ann. Oncol. Off. J. Eur. Soc. Med. Oncol. 18, 1500–1505. https://doi.org/10.1093/annonc/mdm195

Piskunov, A., Rochette-Egly, C., 2012. A retinoic acid receptor RARα pool present in membrane lipid rafts forms complexes with G protein αQ to activate p38MAPK. Oncogene 31, 3333–3345. https://doi.org/10.1038/onc.2011.499

Pitteloud, N., Acierno, J.S., Meysing, A.U., Dwyer, A.A., Hayes, F.J., Crowley, W.F., 2005. Reversible kallmann syndrome, delayed puberty, and isolated anosmia occurring in a single family with a mutation in the fibroblast growth factor

receptor 1 gene. J. Clin. Endocrinol. Metab. 90, 1317–1322. https://doi.org/10.1210/jc.2004-1361

Plagens-Rotman, K., Żak, E., Pięta, B., 2016. Odds ratio analysis in women with endometrial cancer. Przegląd Menopauzalny Menopause Rev. 15, 12–19. https://doi.org/10.5114/pm.2016.58767

Plaks, V., Kong, N., Werb, Z., 2015. The cancer stem cell niche: how essential is the niche in regulating stemness of tumor cells? Cell Stem Cell 16, 225–238. https://doi.org/10.1016/j.stem.2015.02.015

Platt, F.M., Hurst, C.D., Taylor, C.F., Gregory, W.M., Harnden, P., Knowles, M.A., 2009. Spectrum of phosphatidylinositol 3-kinase pathway gene alterations in bladder cancer. Clin. Cancer Res. Off. J. Am. Assoc. Cancer Res. 15, 6008–6017. https://doi.org/10.1158/1078-0432.CCR-09-0898

Plotnikov, A.N., Hubbard, S.R., Schlessinger, J., Mohammadi, M., 2000. Crystal structures of two FGF-FGFR complexes reveal the determinants of ligand-receptor specificity. Cell 101, 413–424.

Plotnikov, A.N., Schlessinger, J., Hubbard, S.R., Mohammadi, M., 1999. Structural basis for FGF receptor dimerization and activation. Cell 98, 641–650.

Plummer, M., Franceschi, S., Vignat, J., Forman, D., de Martel, C., 2015. Global burden of gastric cancer attributable to Helicobacter pylori. Int. J. Cancer 136, 487–490. https://doi.org/10.1002/ijc.28999

Polanska, U.M., Duchesne, L., Harries, J.C., Fernig, D.G., Kinnunen, T.K., 2009. N-Glycosylation Regulates Fibroblast Growth Factor Receptor/EGL-15 Activity in Caenorhabditis elegans in Vivo. J. Biol. Chem. 284, 33030–33039. https://doi.org/10.1074/jbc.M109.058925

Polgar, O., Bates, S.E., 2005. ABC transporters in the balance: is there a role in multidrug resistance? Biochem. Soc. Trans. 33, 241–245. https://doi.org/10.1042/BST0330241

Politi, K., Fan, P.-D., Shen, R., Zakowski, M., Varmus, H., 2010. Erlotinib resistance in mouse models of epidermal growth factor receptor-induced lung adenocarcinoma. Dis. Model. Mech. 3, 111–119. https://doi.org/10.1242/dmm.003681

Pollock, P., Gartside, M., Dejeza, L., Powell, M., Mallon, M., Davies, H., Mohammadi, M., Futreal, P., Stratton, M., Trent, J., Goodfellow, P., 2007. Frequent activating FGFR2 mutations in endometrial carcinomas parallel germline mutations associated with craniosynostosis and skeletal dysplasia syndromes. Oncogene 26, 7158–7162. https://doi.org/10.1038/sj.onc.1210529

Ponchio, L., Duma, L., Oliviero, B., Gibelli, N., Pedrazzoli, P., Robustelli della Cuna, G., 2000. Mitomycin C as an alternative to irradiation to inhibit the feeder layer growth in long-term culture assays. Cytotherapy 2, 281–286.

Pop, M., Salzberg, S.L., 2008. Bioinformatics challenges of new sequencing technology. Trends Genet. TIG 24, 142–149. https://doi.org/10.1016/j.tig.2007.12.006

Popovici, C., Adélaïde, J., Ollendorff, V., Chaffanet, M., Guasch, G., Jacrot, M., Leroux, D., Birnbaum, D., Pébusque, M.-J., 1998. Fibroblast growth factor receptor 1 is fused to FIM in stem-cell myeloproliferative disorder with t(8;13)(p12;q12). Proc. Natl. Acad. Sci. U. S. A. 95, 5712–5717.

Posor, Y., Eichhorn-Gruenig, M., Puchkov, D., Schöneberg, J., Ullrich, A., Lampe, A., Müller, R., Zarbakhsh, S., Gulluni, F., Hirsch, E., Krauss, M., Schultz, C., Schmoranzer, J., Noé, F., Haucke, V., 2013. Spatiotemporal control of endocytosis by phosphatidylinositol-3,4-bisphosphate. Nature 499, 233–237. https://doi.org/10.1038/nature12360

Potter, D.S., Galvin, M., Brown, S., Lallo, A., Hodgkinson, C.L., Blackhall, F., Morrow, C.J., Dive, C., 2016. Inhibition of PI3K/BMX Cell Survival Pathway Sensitizes to BH3 Mimetics in SCLC. Mol. Cancer Ther. 15, 1248–1260. https://doi.org/10.1158/1535-7163.MCT-15-0885

Potter, D.S., Kelly, P., Denneny, O., Juvin, V., Stephens, L.R., Dive, C., Morrow, C.J., 2014. BMX acts downstream of PI3K to promote colorectal cancer cell survival and pathway inhibition sensitizes to the BH3 mimetic ABT-737. Neoplasia N. Y. N 16, 147–157. https://doi.org/10.1593/neo.131376

Pradelli, L.A., Bénéteau, M., Ricci, J.-E., 2010. Mitochondrial control of caspase-dependent and -independent cell death. Cell. Mol. Life Sci. CMLS 67, 1589–1597. https://doi.org/10.1007/s00018-010-0285-y

Preusser, M., Berghoff, A.S., Berger, W., Ilhan-Mutlu, A., Dinhof, C., Widhalm, G., Dieckmann, K., Wöhrer, A., Hackl, M., von Deimling, A., Streubel, B., Birner, P., 2014. High rate of FGFR1 amplifications in brain metastases of squamous and non-squamous lung cancer. Lung Cancer Amst. Neth. 83, 83–89. https://doi.org/10.1016/j.lungcan.2013.10.004

Przyborski, S.A., Christie, V.B., Hayman, M.W., Stewart, R., Horrocks, G.M., 2004. Human embryonal carcinoma stem cells: models of embryonic development in humans. Stem Cells Dev. 13, 400–408. https://doi.org/10.1089/scd.2004.13.400

Qian, X., Ba, Y., Zhuang, Q., Zhong, G., 2014. RNA-Seq technology and its application in fish transcriptomics. Omics J. Integr. Biol. 18, 98–110. https://doi.org/10.1089/omi.2013.0110

Qiao, D., Zeeman, A.-M., Deng, W., Looijenga, L.H.J., Lin, H., 2002. Molecular characterization of hiwi, a human member of the piwi gene family whose overexpression is correlated to seminomas. Oncogene 21, 3988–3999. https://doi.org/10.1038/sj.onc.1205505

Qiu, M.-Z., Han, B., Luo, H.-Y., Zhou, Z.-W., Wang, Z.-Q., Wang, F.-H., Li, Y.-H., Xu, R.-H., 2011. Expressions of hypoxia-inducible factor-1α and hexokinase-II in gastric adenocarcinoma: the impact on prognosis and correlation to clinicopathologic features. Tumour Biol. J. Int. Soc. Oncodevelopmental Biol. Med. 32, 159–166. https://doi.org/10.1007/s13277-010-0109-6

Quail, D., Joyce, J., 2013. Microenvironmental regulation of tumor progression and metastasis. Nat. Med. 19, 1423–1437. https://doi.org/10.1038/nm.3394

Raedler, L.A., 2015. Keytruda (Pembrolizumab): First PD-1 Inhibitor Approved for Previously Treated Unresectable or Metastatic Melanoma. Am. Health Drug Benefits 8, 96–100.

Raffioni, S., Thomas, D., Foehr, E.D., Thompson, L.M., Bradshaw, R.A., 1999. Comparison of the intracellular signaling responses by three chimeric fibroblast growth factor receptors in PC12 cells. Proc. Natl. Acad. Sci. U. S. A. 96, 7178–7183.

Rajan, N., Elliott, R., Clewes, O., Mackay, A., Reis-Filho, J.S., Burn, J., Langtry, J., Sieber-Blum, M., Lord, C.J., Ashworth, A., 2011. Dysregulated TRK signalling is a therapeutic target in CYLD defective tumours. Oncogene 30, 4243–4260. https://doi.org/10.1038/onc.2011.133

Rameh, L.E., Rhee, S.G., Spokes, K., Kazlauskas, A., Cantley, L.C., Cantley, L.G., 1998. Phosphoinositide 3-kinase regulates phospholipase Cgamma-mediated calcium signaling. J. Biol. Chem. 273, 23750–23757.

Ramirez, M., Rajaram, S., Steininger, R.J., Osipchuk, D., Roth, M.A., Morinishi, L.S., Evans, L., Ji, W., Hsu, C.-H., Thurley, K., Wei, S., Zhou, A., Koduru, P.R., Posner, B.A., Wu, L.F., Altschuler, S.J., 2016. Diverse drug-resistance mechanisms can emerge from drug-tolerant cancer persister cells. Nat. Commun. 7. https://doi.org/10.1038/ncomms10690

Ravi, M., Paramesh, V., Kaviya, S.R., Anuradha, E., Solomon, F.D.P., 2015. 3D cell culture systems: advantages and applications. J. Cell. Physiol. 230, 16–26. https://doi.org/10.1002/jcp.24683

Reeves, M.E., Firek, M., Chen, S.-T., Amaar, Y.G., 2014. Evidence that RASSF1C stimulation of lung cancer cell proliferation depends on IGFBP-5 and PIWIL1 expression levels. PloS One 9, e101679. https://doi.org/10.1371/journal.pone.0101679

Reifenberger, J., Knobbe, C.B., Sterzinger, A.A., Blaschke, B., Schulte, K.W., Ruzicka, T., Reifenberger, G., 2004. Frequent alterations of Ras signaling pathway genes in sporadic malignant melanomas. Int. J. Cancer 109, 377–384. https://doi.org/10.1002/ijc.11722

Reinartz, J., Bruyns, E., Lin, J.-Z., Burcham, T., Brenner, S., Bowen, B., Kramer, M., Woychik, R., 2002. Massively parallel signature sequencing (MPSS) as a tool for in-depth quantitative gene expression profiling in all organisms. Brief. Funct. Genomic. Proteomic. 1, 95–104.

Reis-Filho, J.S., Simpson, P.T., Turner, N.C., Lambros, M.B., Jones, C., Mackay, A., Grigoriadis, A., Sarrio, D., Savage, K., Dexter, T., Iravani, M., Fenwick, K., Weber, B., Hardisson, D., Schmitt, F.C., Palacios, J., Lakhani, S.R., Ashworth, A., 2006. FGFR1 emerges as a potential therapeutic target for lobular breast carcinomas. Clin. Cancer Res. Off. J. Am. Assoc. Cancer Res. 12, 6652–6662. https://doi.org/10.1158/1078-0432.CCR-06-1164

Reiter, A., Sohal, J., Kulkarni, S., Chase, A., Macdonald, D.H., Aguiar, R.C., Gonçalves, C., Hernandez, J.M., Jennings, B.A., Goldman, J.M., Cross, N.C., 1998. Consistent fusion of ZNF198 to the fibroblast growth factor receptor-1 in the t(8;13)(p11;q12) myeloproliferative syndrome. Blood 92, 1735–1742.

Ren, L., Mendoza, A., Zhu, J., Briggs, J.W., Halsey, C., Hong, E.S., Burkett, S.S., Morrow, J., Lizardo, M.M., Osborne, T., Li, S.Q., Luu, H.H., Meltzer, P., Khanna, C., 2015. Characterization of the metastatic phenotype of a panel of established osteosarcoma cells. Oncotarget 6, 29469–29481. https://doi.org/10.18632/oncotarget.5177

Ren, M., Pozzi, S., Bistulfi, G., Somenzi, G., Rossetti, S., Sacchi, N., 2005. Impaired retinoic acid (RA) signal leads to RARbeta2 epigenetic silencing and RA resistance. Mol. Cell. Biol. 25, 10591–10603. https://doi.org/10.1128/MCB.25.23.10591-10603.2005

Reynolds, C.P., Wang, Y., Melton, L.J., Einhorn, P.A., Slamon, D.J., Maurer, B.J., 2000. Retinoic-acid-resistant neuroblastoma cell lines show altered MYC regulation and high sensitivity to fenretinide. Med. Pediatr. Oncol. 35, 597–602.

Rho, M., Kim, J., Jee, C.D., Lee, Y.M., Lee, H.E., Kim, M.A., Lee, H.S., Kim, W.H., 2007. Expression of type 2 hexokinase and mitochondria-related genes in gastric carcinoma tissues and cell lines. Anticancer Res. 27, 251–258.

Rizki, A., Weaver, V.M., Lee, S.-Y., Rozenberg, G.I., Chin, K., Myers, C.A., Bascom, J.L., Mott, J.D., Semeiks, J.R., Grate, L.R., Mian, I.S., Borowsky, A.D., Jensen, R.A., Idowu, M.O., Chen, F., Chen, D.J., Petersen, O.W., Gray, J.W., Bissell, M.J., 2008. A human breast cell model of preinvasive to invasive transition. Cancer Res. 68, 1378–1387. https://doi.org/10.1158/0008-5472.CAN-07-2225

Robert, C., Ribas, A., Wolchok, J.D., Hodi, F.S., Hamid, O., Kefford, R., Weber, J.S., Joshua, A.M., Hwu, W.-J., Gangadhar, T.C., Patnaik, A., Dronca, R., Zarour, H., Joseph, R.W., Boasberg, P., Chmielowski, B., Mateus, C., Postow, M.A., Gergich, K., Elassaiss-Schaap, J., Li, X.N., Iannone, R., Ebbinghaus, S.W., Kang, S.P., Daud, A., 2014. Anti-programmed-death-receptor-1 treatment with pembrolizumab in ipilimumab-refractory advanced melanoma: a randomised dose-comparison cohort of a phase 1 trial. Lancet Lond. Engl. 384, 1109–1117. https://doi.org/10.1016/S0140-6736(14)60958-2

Roberts, D., Williams, S.J., Cvetkovic, D., Weinstein, J.K., Godwin, A.K., Johnson, S.W., Hamilton, T.C., 2002. Decreased expression of retinol-binding proteins is associated with malignant transformation of the ovarian surface epithelium. DNA Cell Biol. 21, 11–19. https://doi.org/10.1089/10445490252810276

Robin, N.H., Feldman, G.J., Mitchell, H.F., Lorenz, P., Wilroy, R.S., Zackai, E.H., Allanson, J.E., Reich, E.W., Pfeiffer, R.A., Clarke, L.A., 1994. Linkage of Pfeiffer syndrome to chromosome 8 centromere and evidence for genetic heterogeneity. Hum. Mol. Genet. 3, 2153–2158.

Rodriguez-Viciana, P., Warne, P.H., Dhand, R., Vanhaesebroeck, B., Gout, I., Fry, M.J., Waterfield, M.D., Downward, J., 1994. Phosphatidylinositol-3-OH kinase as a direct target of Ras. Nature 370, 527–532. https://doi.org/10.1038/370527a0

Romero-López, M., Trinh, A.L., Sobrino, A., Hatch, M.M.S., Keating, M.T., Fimbres, C., Lewis, D.E., Gershon, P.D., Botvinick, E.L., Digman, M., Lowengrub, J.S., Hughes, C.C.W., 2017. Recapitulating the human tumor microenvironment: Colon tumor-derived extracellular matrix promotes angiogenesis and tumor cell growth. Biomaterials 116, 118–129. https://doi.org/10.1016/j.biomaterials.2016.11.034

Rønnov-Jessen, L., Petersen, O.W., 1993. Induction of alpha-smooth muscle actin by transforming growth factor-beta 1 in quiescent human breast gland fibroblasts. Implications for myofibroblast generation in breast neoplasia. Lab. Investig. J. Tech. Methods Pathol. 68, 696–707.

Rosak, C., Mertes, G., 2012. Critical evaluation of the role of acarbose in the treatment of diabetes: patient considerations. Diabetes Metab. Syndr. Obes. Targets Ther. 5, 357–367. https://doi.org/10.2147/DMSO.S28340

Roscioli, T., Flanagan, S., Kumar, P., Masel, J., Gattas, M., Hyland, V.J., Glass, I.A., 2000. Clinical findings in a patient with FGFR1 P252R mutation and comparison with the literature. Am. J. Med. Genet. 93, 22–28.

Rose, P.G., 1996. Endometrial carcinoma. N. Engl. J. Med. 335, 640–649. https://doi.org/10.1056/NEJM199608293350907

Ross, S.A., McCaffery, P.J., Drager, U.C., De Luca, L.M., 2000. Retinoids in embryonal development. Physiol. Rev. 80, 1021–1054. https://doi.org/10.1152/physrev.2000.80.3.1021

Ross-Innes, C.S., Stark, R., Holmes, K.A., Schmidt, D., Spyrou, C., Russell, R., Massie, C.E., Vowler, S.L., Eldridge, M., Carroll, J.S., 2010. Cooperative interaction between retinoic acid receptor-alpha and estrogen receptor in breast cancer. Genes Dev. 24, 171–182. https://doi.org/10.1101/gad.552910

Rotsch, C., Radmacher, M., 2000. Drug-induced changes of cytoskeletal structure and mechanics in fibroblasts: an atomic force microscopy study. Biophys. J. 78, 520–535.

Roumiantsev, S., Krause, D.S., Neumann, C.A., Dimitri, C.A., Asiedu, F., Cross, N.C.P., Van Etten, R.A., 2004. Distinct stem cell myeloproliferative/T lymphoma syndromes induced by ZNF198-FGFR1 and BCR-FGFR1 fusion genes from 8p11 translocations. Cancer Cell 5, 287–298.

Rozengurt, E., 2014. Mechanistic target of rapamycin (mTOR): a point of convergence in the action of insulin/IGF-1 and G protein-coupled receptor agonists in pancreatic cancer cells. Front. Physiol. 5. https://doi.org/10.3389/fphys.2014.00357

Ruano-Ravina, A., Figueiras, A., Barros-Dios, J.M., 2003. Lung cancer and related risk factors: an update of the literature. Public Health 117, 149–156. https://doi.org/10.1016/S0033-3506(02)00023-9

Ruano-Ravina, A., Figueiras, A., Barros-Dios, J.M., 2000. Diet and lung cancer: a new approach. Eur. J. Cancer Prev. Off. J. Eur. Cancer Prev. Organ. ECP 9, 395–400.

Rupp, C., Scherzer, M., Rudisch, A., Unger, C., Haslinger, C., Schweifer, N., Artaker, M., Nivarthi, H., Moriggl, R., Hengstschläger, M., Kerjaschki, D., Sommergruber, W., Dolznig, H., Garin-Chesa, P., 2015. IGFBP7, a novel tumor stroma marker, with growth-promoting effects in colon cancer through a paracrine tumor-stroma interaction. Oncogene 34, 815–825. https://doi.org/10.1038/onc.2014.18

Rutland, P., Pulleyn, L.J., Reardon, W., Baraitser, M., Hayward, R., Jones, B., Malcolm, S., Winter, R.M., Oldridge, M., Slaney, S.F., 1995. Identical mutations in the FGFR2 gene cause both Pfeiffer and Crouzon syndrome phenotypes. Nat. Genet. 9, 173–176. https://doi.org/10.1038/ng0295-173

Ryan, S.-L., Baird, A.-M., Vaz, G., Urquhart, A.J., Senge, M., Richard, D.J., O'Byrne, K.J., Davies, A.M., 2016. Drug Discovery Approaches Utilizing Three-Dimensional Cell Culture. Assay Drug Dev. Technol. 14, 19–28. https://doi.org/10.1089/adt.2015.670

Sadikot, T., Swink, M., Eskew, J.D., Brown, D., Zhao, H., Kusuma, B.R., Rajewski, R.A., Blagg, B.S.J., Matts, R.L., Holzbeierlein, J.M., Vielhauer, G.A., 2013. Development of a high-throughput screening cancer cell-based luciferase refolding assay for identifying Hsp90 inhibitors. Assay Drug Dev. Technol. 11, 478–488. https://doi.org/10.1089/adt.2012.498

Saito, S., Morishima, K., Ui, T., Hoshino, H., Matsubara, D., Ishikawa, S., Aburatani, H., Fukayama, M., Hosoya, Y., Sata, N., Lefor, A.K., Yasuda, Y., Niki, T., 2015. The role of HGF/MET and FGF/FGFR in fibroblast-derived growth

stimulation and lapatinib-resistance of esophageal squamous cell carcinoma. BMC Cancer 15, 82. https://doi.org/10.1186/s12885-015-1065-8

Saka, H., Kitagawa, C., Kogure, Y., Takahashi, Y., Fujikawa, K., Sagawa, T., Iwasa, S., Takahashi, N., Fukao, T., Tchinou, C., Landers, D., Yamada, Y., 2017. Safety, tolerability and pharmacokinetics of the fibroblast growth factor receptor inhibitor AZD4547 in Japanese patients with advanced solid tumours: a Phase I study. Invest. New Drugs 35, 451–462. https://doi.org/10.1007/s10637-016-0416-x

Sakthianandeswaren, A., Christie, M., D'Andreti, C., Tsui, C., Jorissen, R.N., Li, S., Fleming, N.I., Gibbs, P., Lipton, L., Malaterre, J., Ramsay, R.G., Phesse, T.J., Ernst, M., Jeffery, R.E., Poulsom, R., Leedham, S.J., Segditsas, S., Tomlinson, I.P.M., Bernhard, O.K., Simpson, R.J., Walker, F., Faux, M.C., Church, N., Catimel, B., Flanagan, D.J., Vincan, E., Sieber, O.M., 2011. PHLDA1 expression marks the putative epithelial stem cells and contributes to intestinal tumorigenesis. Cancer Res. 71, 3709–3719. https://doi.org/10.1158/0008-5472.CAN-10-2342

Sala, G., Dituri, F., Raimondi, C., Previdi, S., Maffucci, T., Mazzoletti, M., Rossi, C., Iezzi, M., Lattanzio, R., Piantelli, M., Iacobelli, S., Broggini, M., Falasca, M., 2008. Phospholipase Cgamma1 is required for metastasis development and progression. Cancer Res. 68, 10187–10196. https://doi.org/10.1158/0008-5472.CAN-08-1181

Sanderson, I.R., Ezzell, R.M., Kedinger, M., Erlanger, M., Xu, Z.X., Pringault, E., Leon-Robine, S., Louvard, D., Walker, W.A., 1996. Human fetal enterocytes in vitro: modulation of the phenotype by extracellular matrix. Proc. Natl. Acad. Sci. U. S. A. 93, 7717–7722.

Santiago-Walker, A., Li, L., Haass, N.K., Herlyn, M., 2009. Melanocytes: from morphology to application. Skin Pharmacol. Physiol. 22, 114–121. https://doi.org/10.1159/000178870

Santini, M.T., Rainaldi, G., Indovina, P.L., 2000. Apoptosis, cell adhesion and the extracellular matrix in the three-dimensional growth of multicellular tumor spheroids. Crit. Rev. Oncol. Hematol. 36, 75–87.

Sarbassov, D.D., Guertin, D.A., Ali, S.M., Sabatini, D.M., 2005. Phosphorylation and regulation of Akt/PKB by the rictor-mTOR complex. Science 307, 1098–1101. https://doi.org/10.1126/science.1106148

Sarker, D., Molife, R., Evans, T.R.J., Hardie, M., Marriott, C., Butzberger-Zimmerli, P., Morrison, R., Fox, J.A., Heise, C., Louie, S., Aziz, N., Garzon, F., Michelson, G., Judson, I.R., Jadayel, D., Braendle, E., de Bono, J.S., 2008. A phase I pharmacokinetic and pharmacodynamic study of TKI258, an oral, multitargeted receptor tyrosine kinase inhibitor in patients with advanced solid tumors. Clin. Cancer Res. Off. J. Am. Assoc. Cancer Res. 14, 2075–2081. https://doi.org/10.1158/1078-0432.CCR-07-1466

Sarrazin, S., Lamanna, W.C., Esko, J.D., 2011. Heparan sulfate proteoglycans. Cold Spring Harb. Perspect. Biol. 3. https://doi.org/10.1101/cshperspect.a004952

Sarrouilhe, D., Clarhaut, J., Defamie, N., Mesnil, M., 2015. Serotonin and cancer: what is the link? Curr. Mol. Med. 15, 62–77.

Sarveswaran, K., Kurz, V., Dong, Z., Tanaka, T., Penny, S., Timp, G., 2016. Synthetic Capillaries to Control Microscopic Blood Flow. Sci. Rep. 6. https://doi.org/10.1038/srep21885

Sasaki, A., Taketomi, T., Kato, R., Saeki, K., Nonami, A., Sasaki, M., Kuriyama, M., Saito, N., Shibuya, M., Yoshimura, A., 2003. Mammalian Sprouty4 suppresses Ras-independent ERK activation by binding to Raf1. Nat. Cell Biol. 5, 427–432. https://doi.org/10.1038/ncb978

Sasaki, N., Ishii, T., Kamimura, R., Kajiwara, M., Machimoto, T., Nakatsuji, N., Suemori, H., Ikai, I., Yasuchika, K., Uemoto, S., 2011. Alpha-fetoprotein-producing pancreatic cancer cells possess cancer stem cell characteristics. Cancer Lett. 308, 152–161. https://doi.org/10.1016/j.canlet.2011.04.023

Sasaki, Y., Minamiya, Y., Takahashi, N., Nakagawa, T., Katayose, Y., Ito, A., Saito, H., Motoyama, S., Ogawa, J., 2008. REG1A expression is an independent factor predictive of poor prognosis in patients with breast cancer. Ann. Surg. Oncol. 15, 3244–3251. https://doi.org/10.1245/s10434-008-0137-2

Sato, Y., Marzese, D.M., Ohta, K., Huang, S.K., Sim, M.S., Chong, K., Hoon, D.S., 2013. Epigenetic regulation of REG1A and chemosensitivity of cutaneous melanoma. Epigenetics 8, 1043–1052. https://doi.org/10.4161/epi.25810

Schabath, M.B., Cress, W.D., Muñoz-Antonia, T., 2016. Racial and Ethnic Differences in the Epidemiology of Lung Cancer and the Lung Cancer Genome. Cancer Control J. Moffitt Cancer Cent. 23, 338–346.

Scheid, M.P., Woodgett, J.R., 2003. Unravelling the activation mechanisms of protein kinase B/Akt. FEBS Lett. 546, 108–112.

Schell, U., Hehr, A., Feldman, G.J., Robin, N.H., Zackai, E.H., de Die-Smulders, C., Viskochil, D.H., Stewart, J.M., Wolff, G., Ohashi, H., 1995. Mutations in FGFR1 and FGFR2 cause familial and sporadic Pfeiffer syndrome. Hum. Mol. Genet. 4, 323–328.

Schlessinger, J., Plotnikov, A.N., Ibrahimi, O.A., Eliseenkova, A.V., Yeh, B.K., Yayon, A., Linhardt, R.J., Mohammadi, M., 2000. Crystal structure of a ternary FGF-FGFR-heparin complex reveals a dual role for heparin in FGFR binding and dimerization. Mol. Cell 6, 743–750.

Schmeichel, K.L., Bissell, M.J., 2003. Modeling tissue-specific signaling and organ function in three dimensions. J. Cell Sci. 116, 2377–2388. https://doi.org/10.1242/jcs.00503

Schmidt, K., Moser, C., Hellerbrand, C., Zieker, D., Wagner, C., Redekopf, J., Schlitt, H.J., Geissler, E.K., Lang, S.A., 2015. Targeting Fibroblast Growth Factor Receptor (FGFR) with BGJ398 in a Gastric Cancer Model. Anticancer Res. 35, 6655–6665.

Schrader, J., Gordon-Walker, T.T., Aucott, R.L., van Deemter, M., Quaas, A., Walsh, S., Benten, D., Forbes, S.J., Wells, R.G., Iredale, J.P., 2011. Matrix Stiffness Modulates Proliferation, Chemotherapeutic Response and Dormancy in Hepatocellular Carcinoma Cells. Hepatol. Baltim. Md 53, 1192–1205. https://doi.org/10.1002/hep.24108

Schu, P.V., Takegawa, K., Fry, M.J., Stack, J.H., Waterfield, M.D., Emr, S.D., 1993. Phosphatidylinositol 3-kinase encoded by yeast VPS34 gene essential for protein sorting. Science 260, 88–91.

Schug, T.T., Berry, D.C., Shaw, N.S., Travis, S.N., Noy, N., 2007. Opposing effects of retinoic acid on cell growth result from alternate activation of two different nuclear receptors. Cell 129, 723–733. https://doi.org/10.1016/j.cell.2007.02.050

Schutte, M., Fox, B., Baradez, M.-O., Devonshire, A., Minguez, J., Bokhari, M., Przyborski, S., Marshall, D., 2011. Rat primary hepatocytes show enhanced performance and sensitivity to acetaminophen during three-dimensional culture on a polystyrene scaffold designed for routine use. Assay Drug Dev. Technol. 9, 475–486. https://doi.org/10.1089/adt.2011.0371

Sebens, S., Schafer, H., 2012. The tumor stroma as mediator of drug resistance--a potential target to improve cancer therapy? Curr. Pharm. Biotechnol. 13, 2259–2272.

Seewaldt, V.L., Johnson, B.S., Parker, M.B., Collins, S.J., Swisshelm, K., 1995. Expression of retinoic acid receptor beta mediates retinoic acid-induced growth arrest and apoptosis in breast cancer cells. Cell Growth Differ. Mol. Biol. J. Am. Assoc. Cancer Res. 6, 1077–1088.

Sekikawa, A., Fukui, H., Fujii, S., Ichikawa, K., Tomita, S., Imura, J., Chiba, T., Fujimori, T., 2008. REG Ialpha protein mediates an anti-apoptotic effect of STAT3 signaling in gastric cancer cells. Carcinogenesis 29, 76–83. https://doi.org/10.1093/carcin/bgm250

Sengupta, S., Bolin, J.M., Ruotti, V., Nguyen, B.K., Thomson, J.A., Elwell, A.L., Stewart, R., 2011. Single Read and Paired End mRNA-Seq Illumina Libraries from 10 Nanograms Total RNA. J. Vis. Exp. JoVE. https://doi.org/10.3791/3340

Seo, H.-S., Liu, D.D., Bekele, B.N., Kim, M.-K., Pisters, K., Lippman, S.M., Wistuba, I.I., Koo, J.S., 2008. CREB Overexpression: A Feature Associated with Negative Prognosis in Never-Smokers with NSCLC. Cancer Res. 68, 6065–6073. https://doi.org/10.1158/0008-5472.CAN-07-5376

Sequist, L.V., Cassier, P., Varga, A., Tabernero, J., Schellens, J.H., Delord, J.-P., LoRusso, P., Camidge, D.R., Medina, M.H., Schuler, M., Campone, M., Tian, G.G., Wong, S., Corral, J., Isaacs, R., Sen, S.K., Porta, D.G., Kulkarni, S.G., Lefebvre, C., Wolf, J., 2014. Abstract CT326: Phase I study of BGJ398, a selective pan-FGFR inhibitor in genetically preselected advanced solid tumors. Cancer Res. 74, CT326–CT326. https://doi.org/10.1158/1538-7445.AM2014-CT326

Serra, M., Brito, C., Correia, C., Alves, P.M., 2012. Process engineering of human pluripotent stem cells for clinical application. Trends Biotechnol. 30, 350–359. https://doi.org/10.1016/j.tibtech.2012.03.003

Seshagiri, S., Stawiski, E.W., Durinck, S., Modrusan, Z., Storm, E.E., Conboy, C.B., Chaudhuri, S., Guan, Y., Janakiraman, V., Jaiswal, B.S., Guillory, J., Ha, C., Dijkgraaf, G.J.P., Stinson, J., Gnad, F., Huntley, M.A., Degenhardt, J.D., Haverty, P.M., Bourgon, R., Wang, W., Koeppen, H., Gentleman, R., Starr, T.K., Zhang, Z., Largaespada, D.A., Wu, T.D., de Sauvage, F.J., 2012. Recurrent R-spondin fusions in colon cancer. Nature 488, 660–664. https://doi.org/10.1038/nature11282

Sethakorn, N., Dulin, N.O., 2013. RGS expression in cancer: oncomining the cancer microarray data. J. Recept. Signal Transduct. Res. 33, 166–171. https://doi.org/10.3109/10799893.2013.773450

Shah, R.K., Valdez, T.A., Wang, Z., Shapshay, S.M., 2001. Pulsed-dye laser and retinoic acid delay progression of oral squamous cell carcinoma: a murine model. The Laryngoscope 111, 1203–1208. https://doi.org/10.1097/00005537-200107000-00013

Shankar, D.B., Cheng, J.C., Kinjo, K., Federman, N., Moore, T.B., Gill, A., Rao, N.P., Landaw, E.M., Sakamoto, K.M., 2005. The role of CREB as a proto-oncogene in hematopoiesis and in acute myeloid leukemia. Cancer Cell 7, 351–362. https://doi.org/10.1016/j.ccr.2005.02.018

Shanker, M., Willcutts, D., Roth, J.A., Ramesh, R., 2010. Drug resistance in lung cancer. Lung Cancer Targets Ther. 1, 23–36.

Shanmugam, M., McBrayer, S.K., Rosen, S.T., 2009. Targeting the Warburg Effect in Hematological Malignancies: from PET to Therapy. Curr. Opin. Oncol. 21, 531–536. https://doi.org/10.1097/CCO.0b013e32832f57ec

Shaw, N., Elholm, M., Noy, N., 2003. Retinoic acid is a high affinity selective ligand for the peroxisome proliferator-activated receptor beta/delta. J. Biol. Chem. 278, 41589–41592. https://doi.org/10.1074/jbc.C300368200

Shi, W.-J., Gao, J.-B., 2016. Molecular mechanisms of chemoresistance in gastric cancer. World J. Gastrointest. Oncol. 8, 673–681. https://doi.org/10.4251/wjgo.v8.i9.673

Shields, P.G., 2002. Molecular epidemiology of smoking and lung cancer. Oncogene 21, 6870–6876. https://doi.org/10.1038/sj.onc.1205832

Shin, J.-W., Mooney, D.J., 2016. Extracellular matrix stiffness causes systematic variations in proliferation and chemosensitivity in myeloid leukemias. Proc. Natl. Acad. Sci. U. S. A. 113, 12126–12131. https://doi.org/10.1073/pnas.1611338113

Shiraki, T., Kondo, S., Katayama, S., Waki, K., Kasukawa, T., Kawaji, H., Kodzius, R., Watahiki, A., Nakamura, M., Arakawa, T., Fukuda, S., Sasaki, D., Podhajska, A., Harbers, M., Kawai, J., Carninci, P., Hayashizaki, Y., 2003. Cap analysis gene expression for high-throughput analysis of transcriptional starting point and identification of promoter usage. Proc. Natl. Acad. Sci. U. S. A. 100, 15776–15781. https://doi.org/10.1073/pnas.2136655100

Shirakihara, T., Horiguchi, K., Miyazawa, K., Ehata, S., Shibata, T., Morita, I., Miyazono, K., Saitoh, M., 2011. TGF-β regulates isoform switching of FGF receptors and epithelial–mesenchymal transition. EMBO J. 30, 783–795. https://doi.org/10.1038/emboj.2010.351

Shoji, H., Yamada, Y., Okita, N., Takashima, A., Honma, Y., Iwasa, S., Kato, K., Hamaguchi, T., Shimada, Y., 2015. Amplification of FGFR2 Gene in Patients with Advanced Gastric Cancer Receiving Chemotherapy: Prevalence and Prognostic Significance. Anticancer Res. 35, 5055–5061.

Shukla, N., Ameur, N., Yilmaz, I., Nafa, K., Lau, C.-Y., Marchetti, A., Borsu, L., Barr, F.G., Ladanyi, M., 2012. Oncogene mutation profiling of pediatric solid tumors reveals significant subsets of embryonal rhabdomyosarcoma and neuroblastoma with mutated genes in growth signaling pathways. Clin. Cancer Res. Off. J. Am. Assoc. Cancer Res. 18, 748–757. https://doi.org/10.1158/1078-0432.CCR-11-2056

Siddiqi, S., Matushansky, I., 2012. Piwis and piwi-interacting RNAs in the epigenetics of cancer. J. Cell. Biochem. 113, 373–380. https://doi.org/10.1002/jcb.23363

Siddiqi, S., Terry, M., Matushansky, I., 2012. Hiwi mediated tumorigenesis is associated with DNA hypermethylation. PloS One 7, e33711. https://doi.org/10.1371/journal.pone.0033711

Siegel, R., Naishadham, D., Jemal, A., 2012. Cancer statistics, 2012. CA. Cancer J. Clin. 62, 10–29. https://doi.org/10.3322/caac.20138

Siegel, R.L., Miller, K.D., Jemal, A., 2015. Cancer statistics, 2015. CA. Cancer J. Clin. 65, 5–29. https://doi.org/10.3322/caac.21254

Silva, D.P., DeLuca, H.F., 1982. Metabolism of retinoic acid in vivo in the vitamin A-deficient rat. Biochem. J. 206, 33–41.

Sim, L., Willemsma, C., Mohan, S., Naim, H.Y., Pinto, B.M., Rose, D.R., 2010. Structural Basis for Substrate Selectivity in Human Maltase-Glucoamylase and Sucrase-Isomaltase N-terminal Domains. J. Biol. Chem. 285, 17763–17770. https://doi.org/10.1074/jbc.M109.078980

Simon, R., Richter, J., Wagner, U., Fijan, A., Bruderer, J., Schmid, U., Ackermann, D., Maurer, R., Alund, G., Knönagel, H., Rist, M., Wilber, K., Anabitarte, M., Hering, F., Hardmeier, T., Schönenberger, A., Flury, R., Jäger, P., Fehr, J.L., Schraml, P., Moch, H., Mihatsch, M.J., Gasser, T., Sauter, G., 2001. High-throughput tissue microarray analysis of 3p25 (RAF1) and 8p12 (FGFR1) copy number alterations in urinary bladder cancer. Cancer Res. 61, 4514–4519.

Singh, D., Chan, J.M., Zoppoli, P., Niola, F., Sullivan, R., Castano, A., Liu, E.M., Reichel, J., Porrati, P., Pellegatta, S., Qiu, K., Gao, Z., Ceccarelli, M., Riccardi, R., Brat, D.J., Guha, A., Aldape, K., Golfinos, J.G., Zagzag, D., Mikkelsen, T., Finocchiaro, G., Lasorella, A., Rabadan, R., Iavarone, A., 2012. Transforming fusions of FGFR and TACC genes in human glioblastoma. Science 337, 1231–1235. https://doi.org/10.1126/science.1220834

Singhvi, R., Kumar, A., Lopez, G.P., Stephanopoulos, G.N., Wang, D.I., Whitesides, G.M., Ingber, D.E., 1994. Engineering cell shape and function. Science 264, 696–698.

Sirchia, S.M., Ferguson, A.T., Sironi, E., Subramanyan, S., Orlandi, R., Sukumar, S., Sacchi, N., 2000. Evidence of epigenetic changes affecting the chromatin state of the retinoic acid receptor beta2 promoter in breast cancer cells. Oncogene 19, 1556–1563. https://doi.org/10.1038/sj.onc.1203456

Sirchia, S.M., Ren, M., Pili, R., Sironi, E., Somenzi, G., Ghidoni, R., Toma, S., Nicolò, G., Sacchi, N., 2002. Endogenous reactivation of the RARbeta2 tumor suppressor gene epigenetically silenced in breast cancer. Cancer Res. 62, 2455–2461.

Sleeman, M., Fraser, J., McDonald, M., Yuan, S., White, D., Grandison, P., Kumble, K., Watson, J.D., Murison, J.G., 2001. Identification of a new fibroblast growth factor receptor, FGFR5. Gene 271, 171–182.

Sleijfer, S., Wiemer, E., Seynaeve, C., Verweij, J., 2007. Improved insight into resistance mechanisms to imatinib in gastrointestinal stromal tumors: a basis for novel approaches and individualization of treatment. The Oncologist 12, 719–726. https://doi.org/10.1634/theoncologist.12-6-719

Smith, C.C., Lin, K., Stecula, A., Sali, A., Shah, N.P., 2015. FLT3 D835 mutations confer differential resistance to type II FLT3 inhibitors. Leukemia 29, 2390–2392. https://doi.org/10.1038/leu.2015.165

Smith, I., Haag, M., Ugbode, C., Tams, D., Rattray, M., Przyborski, S., Bithell, A., Whalley, B.J., 2015. Neuronal-glial populations form functional networks in a biocompatible 3D scaffold. Neurosci. Lett. 609, 198–202. https://doi.org/10.1016/j.neulet.2015.10.044

Smyth, E.C., Turner, N.C., Popat, S., Morgan, S., Owen, K., Gillbanks, A., Jain, V.K., Cunningham, D., 2013. FGFR: Proof-of-concept study of AZD4547 in patients with FGFR1 or FGFR2 amplified tumours. ASCO Meet. Abstr. 31, TPS2626.

Soares, C.P., Midlej, V., de Oliveira, M.E.W., Benchimol, M., Costa, M.L., Mermelstein, C., 2012. 2D and 3D-Organized Cardiac Cells Shows Differences in Cellular Morphology, Adhesion Junctions, Presence of Myofibrils and Protein Expression. PLoS ONE 7. https://doi.org/10.1371/journal.pone.0038147

Solaini, G., Harris, D.A., 2005. Biochemical dysfunction in heart mitochondria exposed to ischaemia and reperfusion. Biochem. J. 390, 377–394. https://doi.org/10.1042/BJ20042006

Song, H., Peng, J.-S., Dong-Sheng, Y., Yang, Z.-L., Liu, H.-L., Zeng, Y.-K., Shi, X.-P., Lu, B.-Y., 2012. Serum metabolic profiling of human gastric cancer based on gas chromatography/mass spectrometry. Braz. J. Med. Biol. Res. Rev. Bras. Pesqui. Medicas E Biol. 45, 78–85.

Song, H., Xia, S.-L., Liao, C., Li, Y.-L., Wang, Y.-F., Li, T.-P., Zhao, M.-J., 2004. Genes encoding Pir51, Beclin 1, RbAp48 and aldolase b are up or down-regulated in human primary hepatocellular carcinoma. World J. Gastroenterol. 10, 509–513.

Song, S., Jacobson, K.N., McDermott, K.M., Reddy, S.P., Cress, A.E., Tang, H., Dudek, S.M., Black, S.M., Garcia, J.G.N., Makino, A., Yuan, J.X.-J., 2016. ATP promotes cell survival via regulation of cytosolic [Ca2+] and Bcl-2/Bax ratio in lung cancer cells. Am. J. Physiol. Cell Physiol. 310, C99-114. https://doi.org/10.1152/ajpcell.00092.2015

Soria, J.-C., DeBraud, F., Bahleda, R., Adamo, B., Andre, F., Dienstmann, R., Dientsmann, R., Delmonte, A., Cereda, R., Isaacson, J., Litten, J., Allen, A., Dubois, F., Saba, C., Robert, R., D'Incalci, M., Zucchetti, M., Camboni, M.G., Tabernero, J., 2014. Phase I/IIa study evaluating the safety, efficacy, pharmacokinetics, and pharmacodynamics of lucitanib in advanced solid tumors. Ann. Oncol. Off. J. Eur. Soc. Med. Oncol. 25, 2244–2251. https://doi.org/10.1093/annonc/mdu390

Sparano, J.A., Bernardo, P., Stephenson, P., Gradishar, W.J., Ingle, J.N., Zucker, S., Davidson, N.E., 2004. Randomized phase III trial of marimastat versus placebo in patients with metastatic breast cancer who have responding or stable disease after first-line chemotherapy: Eastern Cooperative Oncology Group trial E2196. J. Clin. Oncol. Off. J. Am. Soc. Clin. Oncol. 22, 4683–4690. https://doi.org/10.1200/JCO.2004.08.054

Spivak-Kroizman, T., Mohammadi, M., Hu, P., Jaye, M., Schlessinger, J., Lax, I., 1994. Point mutation in the fibroblast growth factor receptor eliminates phosphatidylinositol hydrolysis without affecting neuronal differentiation of PC12 cells. J. Biol. Chem. 269, 14419–14423.

Spyratos, D., Zarogoulidis, P., Porpodis, K., Tsakiridis, K., Machairiotis, N., Katsikogiannis, N., Kougioumtzi, I., Dryllis, G., Kallianos, A., Rapti, A., Li, C.,

Zarogoulidis, K., 2013. Occupational exposure and lung cancer. J. Thorac. Dis. 5, S440–S445. https://doi.org/10.3978/j.issn.2072-1439.2013.07.09

Stahelin, R.V., Karathanassis, D., Bruzik, K.S., Waterfield, M.D., Bravo, J., Williams, R.L., Cho, W., 2006. Structural and membrane binding analysis of the Phox homology domain of phosphoinositide 3-kinase-C2alpha. J. Biol. Chem. 281, 39396–39406. https://doi.org/10.1074/jbc.M607079200

Stauber, D.J., DiGabriele, A.D., Hendrickson, W.A., 2000. Structural interactions of fibroblast growth factor receptor with its ligands. Proc. Natl. Acad. Sci. U. S. A. 97, 49–54.

Steele, I.A., Edmondson, R.J., Bulmer, J.N., Bolger, B.S., Leung, H.Y., Davies, B.R., 2001. Induction of FGF receptor 2-IIIb expression and response to its ligands in epithelial ovarian cancer. Oncogene 20, 5878–5887. https://doi.org/10.1038/sj.onc.1204755

Steevens, J., Botterweck, A.A.M., Dirx, M.J.M., van den Brandt, P.A., Schouten, L.J., 2010. Trends in incidence of oesophageal and stomach cancer subtypes in Europe. Eur. J. Gastroenterol. Hepatol. 22, 669–678. https://doi.org/10.1097/MEG.0b013e32832ca091

Steller, H., 1995. Mechanisms and genes of cellular suicide. Science 267, 1445–1449.

Stemmermann, G., Heffelfinger, S.C., Noffsinger, A., Hui, Y.Z., Miller, M.A., Fenoglio-Preiser, C.M., 1994. The molecular biology of esophageal and gastric cancer and their precursors: oncogenes, tumor suppressor genes, and growth factors. Hum. Pathol. 25, 968–981.

Stranger, B.E., Forrest, M.S., Dunning, M., Ingle, C.E., Beazley, C., Thorne, N., Redon, R., Bird, C.P., de Grassi, A., Lee, C., Tyler-Smith, C., Carter, N., Scherer, S.W., Tavaré, S., Deloukas, P., Hurles, M.E., Dermitzakis, E.T., 2007. Relative impact of nucleotide and copy number variation on gene expression phenotypes. Science 315, 848–853. https://doi.org/10.1126/science.1136678

Streb, H., Irvine, R.F., Berridge, M.J., Schulz, I., 1983. Release of Ca2+ from a nonmitochondrial intracellular store in pancreatic acinar cells by inositol-1,4,5-trisphosphate. Nature 306, 67–69.

Sturm, I., Bosanquet, A.G., Hermann, S., Güner, D., Dörken, B., Daniel, P.T., 2003. Mutation of p53 and consecutive selective drug resistance in B-CLL occurs as a consequence of prior DNA-damaging chemotherapy. Cell Death Differ. 10, 477–484. https://doi.org/10.1038/sj.cdd.4401194

Su, M., Alonso, S., Jones, J.W., Yu, J., Kane, M.A., Jones, R.J., Ghiaur, G., 2015. All-Trans Retinoic Acid Activity in Acute Myeloid Leukemia: Role of Cytochrome P450 Enzyme Expression by the Microenvironment. PloS One 10, e0127790. https://doi.org/10.1371/journal.pone.0127790

Suh, D.H., Kim, H.S., Kim, B., Song, Y.S., 2014. Metabolic orchestration between cancer cells and tumor microenvironment as a co-evolutionary source of chemoresistance in ovarian cancer: a therapeutic implication. Biochem. Pharmacol. 92, 43–54. https://doi.org/10.1016/j.bcp.2014.08.011

Sun, G.-G., Wang, Y.-D., Cui, D.-W., Cheng, Y.-J., Hu, W.-N., 2014. Epithelial membrane protein 1 negatively regulates cell growth and metastasis in colorectal carcinoma. World J. Gastroenterol. WJG 20, 4001–4010. https://doi.org/10.3748/wjg.v20.i14.4001

Sun, P., Enslen, H., Myung, P.S., Maurer, R.A., 1994. Differential activation of CREB by Ca2+/calmodulin-dependent protein kinases type II and type IV involves phosphorylation of a site that negatively regulates activity. Genes Dev. 8, 2527–2539.

Sun, W., Sanderson, P., Zheng, W., 2016. Drug combination therapy increases successful drug repositioning. Drug Discov. Today 21, 1189–1195. https://doi.org/10.1016/j.drudis.2016.05.015

Sung, S.-Y., Hsieh, C.-L., Wu, D., Chung, L.W.K., Johnstone, P.A.S., 2007. Tumor microenvironment promotes cancer progression, metastasis, and therapeutic resistance. Curr. Probl. Cancer 31, 36–100. https://doi.org/10.1016/j.currproblcancer.2006.12.002

Sutherland, R.M., Durand, R.E., 1984. Growth and cellular characteristics of multicell spheroids. Recent Results Cancer Res. Fortschritte Krebsforsch. Progres Dans Rech. Sur Cancer 95, 24–49.

Sutherland, R.M., Inch, W.R., McCredie, J.A., Kruuv, J., 1970. A multi-component radiation survival curve using an in vitro tumour model. Int. J. Radiat. Biol. Relat. Stud. Phys. Chem. Med. 18, 491–495.

Sutherland, R.M., McCredie, J.A., Inch, W.R., 1971. Growth of multicell spheroids in tissue culture as a model of nodular carcinomas. J. Natl. Cancer Inst. 46, 113–120.

Suzui, M., Masuda, M., Lim, J.T.E., Albanese, C., Pestell, R.G., Weinstein, I.B., 2002. Growth inhibition of human hepatoma cells by acyclic retinoid is associated with induction of p21(CIP1) and inhibition of expression of cyclin D1. Cancer Res. 62, 3997–4006.

Swanson, C.A., Brown, C.C., Sinha, R., Kulldorff, M., Brownson, R.C., Alavanja, M.C., 1997. Dietary fats and lung cancer risk among women: the Missouri Women's Health Study (United States). Cancer Causes Control CCC 8, 883–893.

Tabernero, J., Bahleda, R., Dienstmann, R., Infante, J.R., Mita, A., Italiano, A., Calvo, E., Moreno, V., Adamo, B., Gazzah, A., Zhong, B., Platero, S.J., Smit, J.W., Stuyckens, K., Chatterjee-Kishore, M., Rodon, J., Peddareddigari, V., Luo, F.R., Soria, J.-C., 2015. Phase I Dose-Escalation Study of JNJ-42756493, an Oral Pan-Fibroblast Growth Factor Receptor Inhibitor, in Patients With Advanced Solid Tumors. J. Clin. Oncol. Off. J. Am. Soc. Clin. Oncol. 33, 3401–3408. https://doi.org/10.1200/JCO.2014.60.7341

Takeda, M., Arao, T., Yokote, H., Komatsu, T., Yanagihara, K., Sasaki, H., Yamada, Y., Tamura, T., Fukuoka, K., Kimura, H., Saijo, N., Nishio, K., 2007. AZD2171 shows potent antitumor activity against gastric cancer over-expressing fibroblast growth factor receptor 2/keratinocyte growth factor receptor. Clin. Cancer Res. Off. J. Am. Assoc. Cancer Res. 13, 3051–3057. https://doi.org/10.1158/1078-0432.CCR-06-2743

Tan, W., Krishnaraj, R., Desai, T.A., 2001. Evaluation of nanostructured composite collagen--chitosan matrices for tissue engineering. Tissue Eng. 7, 203–210. https://doi.org/10.1089/107632701300062831

Tan, Y., Liu, L., Liao, M., Zhang, C., Hu, S., Zou, M., Gu, M., Li, X., 2015. Emerging roles for PIWI proteins in cancer. Acta Biochim. Biophys. Sin. 47, 315–324. https://doi.org/10.1093/abbs/gmv018

Tang, X.-H., Gudas, L.J., 2011. Retinoids, retinoic acid receptors, and cancer. Annu. Rev. Pathol. 6, 345–364. https://doi.org/10.1146/annurev-pathol-011110-130303

Tanizaki, J., Ercan, D., Capelletti, M., Dodge, M.E., Xu, C., Bahcall, M., Tricker, E.M., Butaney, M., Calles, A., Sholl, L.M., Hammerman, P.S., Oxnard, G.R., Wong, K.-K., Janne, P.A., 2015. Identification of oncogenic and drug-sensitizing mutations in the extracellular domain of FGFR2. Cancer Res. https://doi.org/10.1158/0008-5472.CAN-14-3771

Tanner, Y., Grose, R.P., 2016. Dysregulated FGF signalling in neoplastic disorders. Semin. Cell Dev. Biol. 53, 126–135. https://doi.org/10.1016/j.semcdb.2015.10.012

Tao, Q., Yuan, S., Yang, F., Yang, S., Yang, Y., Yuan, J., Wang, Z., Xu, Q., Lin, K., Cai, J., Yu, J., Huang, W., Teng, X., Zhou, C., Wang, F., Sun, S., Zhou, W., 2015. Aldolase B inhibits metastasis through Ten–Eleven Translocation 1 and serves as a prognostic biomarker in hepatocellular carcinoma. Mol. Cancer 14. https://doi.org/10.1186/s12943-015-0437-7

Tarca, A.L., Draghici, S., Khatri, P., Hassan, S.S., Mittal, P., Kim, J., Kim, C.J., Kusanovic, J.P., Romero, R., 2009. A novel signaling pathway impact analysis. Bioinformatics 25, 75–82. https://doi.org/10.1093/bioinformatics/btn577

Tarca, A.L., Romero, R., Draghici, S., 2006. Analysis of microarray experiments of gene expression profiling. Am. J. Obstet. Gynecol. 195, 373–388. https://doi.org/10.1016/j.ajog.2006.07.001

Tarin, D., Croft, C.B., 1969. Ultrastructural features of wound healing in mouse skin. J. Anat. 105, 189–190.

Taylor, J.G., Cheuk, A.T., Tsang, P.S., Chung, J.-Y., Song, Y.K., Desai, K., Yu, Y., Chen, Q.-R., Shah, K., Youngblood, V., Fang, J., Kim, S.Y., Yeung, C., Helman, L.J., Mendoza, A., Ngo, V., Staudt, L.M., Wei, J.S., Khanna, C., Catchpoole, D., Qualman, S.J., Hewitt, S.M., Merlino, G., Chanock, S.J., Khan, J., 2009. Identification of FGFR4-activating mutations in human rhabdomyosarcomas that promote metastasis in xenotransplanted models. J. Clin. Invest. 119, 3395–3407. https://doi.org/10.1172/JCI39703

Tchaicha, J.H., Akbay, E.A., Altabef, A., Mikse, O.R., Kikuchi, E., Rhee, K., Liao, R.G., Bronson, R.T., Sholl, L.M., Meyerson, M., Hammerman, P.S., Wong, K.-K., 2014. Kinase domain activation of FGFR2 yields high-grade lung adenocarcinoma sensitive to a Pan-FGFR inhibitor in a mouse model of NSCLC. Cancer Res. 74, 4676–4684. https://doi.org/10.1158/0008-5472.CAN-13-3218

Terazono, K., Yamamoto, H., Takasawa, S., Shiga, K., Yonemura, Y., Tochino, Y., Okamoto, H., 1988. A novel gene activated in regenerating islets. J. Biol. Chem. 263, 2111–2114.

Theodosiou, M., Laudet, V., Schubert, M., 2010. From carrot to clinic: an overview of the retinoic acid signaling pathway. Cell. Mol. Life Sci. CMLS 67, 1423–1445. https://doi.org/10.1007/s00018-010-0268-z

Thien, C.B.F., Langdon, W.Y., 2001. Cbl: many adaptations to regulate protein tyrosine kinases. Nat. Rev. Mol. Cell Biol. 2, 294–307. https://doi.org/10.1038/35067100

Thisse, B., Thisse, C., 2005. Functions and regulations of fibroblast growth factor signaling during embryonic development. Dev. Biol. 287, 390–402. https://doi.org/10.1016/j.ydbio.2005.09.011

Thorpe, L.M., Yuzugullu, H., Zhao, J.J., 2015. PI3K in cancer: divergent roles of isoforms, modes of activation and therapeutic targeting. Nat. Rev. Cancer 15, 7–24. https://doi.org/10.1038/nrc3860

Thun, M., Peto, R., Boreham, J., Lopez, A.D., 2012. Stages of the cigarette epidemic on entering its second century. Tob. Control 21, 96–101. https://doi.org/10.1136/tobaccocontrol-2011-050294

Tian, Y.-F., Hsieh, P.-L., Lin, C.-Y., Sun, D.-P., Sheu, M.-J., Yang, C.-C., Lin, L.-C., He, H.-L., Solórzano, J., Li, C.-F., Chang, I.-W., 2017. High Expression of Aldolase B Confers a Poor Prognosis for Rectal Cancer Patients Receiving Neoadjuvant Chemoradiotherapy. J. Cancer 8, 1197–1204. https://doi.org/10.7150/jca.18197

Tilghman, R.W., Cowan, C.R., Mih, J.D., Koryakina, Y., Gioeli, D., Slack-Davis, J.K., Blackman, B.R., Tschumperlin, D.J., Parsons, J.T., 2010. Matrix rigidity regulates cancer cell growth and cellular phenotype. PloS One 5, e12905. https://doi.org/10.1371/journal.pone.0012905

Tolan, D.R., Niclas, J., Bruce, B.D., Lebo, R.V., 1987. Evolutionary implications of the human aldolase-A, -B, -C, and -pseudogene chromosome locations. Am. J. Hum. Genet. 41, 907–924.

Tolcher, A.W., Papadopoulos, K.P., Patnaik, A., Wilson, K., Thayer, S., Zanghi, J., Gemo, A.T., Kavanaugh, W.M., Keer, H.N., LoRusso, P.M., 2016. A phase I, first in human study of FP-1039 (GSK3052230), a novel FGF ligand trap, in patients with advanced solid tumors. Ann. Oncol. Off. J. Eur. Soc. Med. Oncol. 27, 526–532. https://doi.org/10.1093/annonc/mdv591

Tomasek, J.J., Gabbiani, G., Hinz, B., Chaponnier, C., Brown, R.A., 2002. Myofibroblasts and mechano-regulation of connective tissue remodelling. Nat. Rev. Mol. Cell Biol. 3, 349–363. https://doi.org/10.1038/nrm809

Topalian, S.L., 2017. Targeting Immune Checkpoints in Cancer Therapy. JAMA 318, 1647–1648. https://doi.org/10.1001/jama.2017.14155

Topalian, S.L., Hodi, F.S., Brahmer, J.R., Gettinger, S.N., Smith, D.C., McDermott, D.F., Powderly, J.D., Carvajal, R.D., Sosman, J.A., Atkins, M.B., Leming, P.D., Spigel, D.R., Antonia, S.J., Horn, L., Drake, C.G., Pardoll, D.M., Chen, L., Sharfman, W.H., Anders, R.A., Taube, J.M., McMiller, T.L., Xu, H., Korman, A.J., Jure-Kunkel, M., Agrawal, S., McDonald, D., Kollia, G.D., Gupta, A., Wigginton, J.M., Sznol, M., 2012. Safety, activity, and immune correlates of anti-PD-1 antibody in cancer. N. Engl. J. Med. 366, 2443–2454. https://doi.org/10.1056/NEJMoa1200690

Torre, L.A., Bray, F., Siegel, R.L., Ferlay, J., Lortet-Tieulent, J., Jemal, A., 2015. Global cancer statistics, 2012. CA. Cancer J. Clin. 65, 87–108. https://doi.org/10.3322/caac.21262

Toyooka, S., Mitsudomi, T., Soh, J., Aokage, K., Yamane, M., Oto, T., Kiura, K., Miyoshi, S., 2011. Molecular oncology of lung cancer. Gen. Thorac. Cardiovasc. Surg. 59, 527–537. https://doi.org/10.1007/s11748-010-0743-3

Toyoshima, Y., Karas, M., Yakar, S., Dupont, J., Lee Helman, null, LeRoith, D., 2004. TDAG51 mediates the effects of insulin-like growth factor I (IGF-I) on cell

survival. J. Biol. Chem. 279, 25898–25904. https://doi.org/10.1074/jbc.M400661200

Tran, C., 2017. Inborn Errors of Fructose Metabolism. What Can We Learn from Them? Nutrients 9. https://doi.org/10.3390/nu9040356

Trapnell, C., Williams, B.A., Pertea, G., Mortazavi, A., Kwan, G., van Baren, M.J., Salzberg, S.L., Wold, B.J., Pachter, L., 2010. Transcript assembly and quantification by RNA-Seq reveals unannotated transcripts and isoform switching during cell differentiation. Nat. Biotechnol. 28, 511–515. https://doi.org/10.1038/nbt.1621

Travis, W.D., 2011. Pathology of lung cancer. Clin. Chest Med. 32, 669–692. https://doi.org/10.1016/j.ccm.2011.08.005

Tsai, J., Lee, J.T., Wang, W., Zhang, J., Cho, H., Mamo, S., Bremer, R., Gillette, S., Kong, J., Haass, N.K., Sproesser, K., Li, L., Smalley, K.S.M., Fong, D., Zhu, Y.-L., Marimuthu, A., Nguyen, H., Lam, B., Liu, J., Cheung, I., Rice, J., Suzuki, Y., Luu, C., Settachatgul, C., Shellooe, R., Cantwell, J., Kim, S.-H., Schlessinger, J., Zhang, K.Y.J., West, B.L., Powell, B., Habets, G., Zhang, C., Ibrahim, P.N., Hirth, P., Artis, D.R., Herlyn, M., Bollag, G., 2008. Discovery of a selective inhibitor of oncogenic B-Raf kinase with potent antimelanoma activity. Proc. Natl. Acad. Sci. U. S. A. 105, 3041–3046. https://doi.org/10.1073/pnas.0711741105

Tsang, M., Friesel, R., Kudoh, T., Dawid, I.B., 2002. Identification of Sef, a novel modulator of FGF signalling. Nat. Cell Biol. 4, 165–169. https://doi.org/10.1038/ncb749

Tseng, C.-H., Tseng, F.-H., 2014. Diabetes and gastric cancer: The potential links. World J. Gastroenterol. WJG 20, 1701–1711. https://doi.org/10.3748/wjg.v20.i7.1701

Tsuchiya, A., Kanno, T., Nishizaki, T., 2014. PI3 kinase directly phosphorylates Akt1/2 at Ser473/474 in the insulin signal transduction pathway. J. Endocrinol. 220, 49–59. https://doi.org/10.1530/JOE-13-0172

Turkington, R.C., Longley, D.B., Allen, W.L., Stevenson, L., McLaughlin, K., Dunne, P.D., Blayney, J.K., Salto-Tellez, M., Van Schaeybroeck, S., Johnston, P.G., 2014. Fibroblast growth factor receptor 4 (FGFR4): a targetable regulator of drug resistance in colorectal cancer. Cell Death Dis. 5, e1046. https://doi.org/10.1038/cddis.2014.10

Turner, M.C., Krewski, D., Pope, C.A., Chen, Y., Gapstur, S.M., Thun, M.J., 2011. Long-term ambient fine particulate matter air pollution and lung cancer in a large cohort of never-smokers. Am. J. Respir. Crit. Care Med. 184, 1374–1381. https://doi.org/10.1164/rccm.201106-1011OC

Turner, N., Grose, R., 2010. Fibroblast growth factor signalling: from development to cancer. Nat. Rev. Cancer 10, 116–129. https://doi.org/10.1038/nrc2780

Ueda, S.M., Kapp, D.S., Cheung, M.K., Shin, J.Y., Osann, K., Husain, A., Teng, N.N., Berek, J.S., Chan, J.K., 2008. Trends in demographic and clinical characteristics in women diagnosed with corpus cancer and their potential impact on the increasing number of deaths. Am. J. Obstet. Gynecol. 198, 218.e1–6. https://doi.org/10.1016/j.ajog.2007.08.075

Ueki, K., Matsuda, S., Tobe, K., Gotoh, Y., Tamemoto, H., Yachi, M., Akanuma, Y., Yazaki, Y., Nishida, E., Kadowaki, T., 1994. Feedback regulation of mitogen-

activated protein kinase kinase kinase activity of c-Raf-1 by insulin and phorbol ester stimulation. J. Biol. Chem. 269, 15756–15761.

Ugbode, C.I., Hirst, W.D., Rattray, M., 2016. Astrocytes Grown in Alvetex(®) Three Dimensional Scaffolds Retain a Non-reactive Phenotype. Neurochem. Res. 41, 1857–1867. https://doi.org/10.1007/s11064-016-1911-3

Unno, M., Itoh, T., Watanabe, T., Miyashita, H., Moriizumi, S., Teraoka, H., Yonekura, H., Okamoto, H., 1992. Islet beta-cell regeneration and reg genes. Adv. Exp. Med. Biol. 321, 61–66; discussion 67-69.

Usami, S., Motoyama, S., Koyota, S., Wang, J., Hayashi-Shibuya, K., Maruyama, K., Takahashi, N., Saito, H., Minamiya, Y., Takasawa, S., Ogawa, J.-I., Sugiyama, T., 2010. Regenerating gene I regulates interleukin-6 production in squamous esophageal cancer cells. Biochem. Biophys. Res. Commun. 392, 4–8. https://doi.org/10.1016/j.bbrc.2009.12.129

Usui, T., Sakurai, M., Kawasaki, H., Ohama, T., Yamawaki, H., Sato, K., 2017. Establishment of a novel three-dimensional primary culture model for hippocampal neurogenesis. Physiol. Rep. 5. https://doi.org/10.14814/phy2.13318

Vaarala, M.H., Porvari, K.S., Kyllönen, A.P., Mustonen, M.V., Lukkarinen, O., Vihko, P.T., 1998. Several genes encoding ribosomal proteins are over-expressed in prostate-cancer cell lines: confirmation of L7a and L37 over-expression in prostate-cancer tissue samples. Int. J. Cancer 78, 27–32.

Vagin, V.V., Sigova, A., Li, C., Seitz, H., Gvozdev, V., Zamore, P.D., 2006. A distinct small RNA pathway silences selfish genetic elements in the germline. Science 313, 320–324. https://doi.org/10.1126/science.1129333

van de Nes, J.A.P., Griewank, K.G., Schmid, K.-W., Grabellus, F., 2015. Immunocytochemical analysis of glucose transporter protein-1 (GLUT-1) in typical, brain invasive, atypical and anaplastic meningioma. Neuropathol. Off. J. Jpn. Soc. Neuropathol. 35, 24–36. https://doi.org/10.1111/neup.12148

Van Glabbeke, M., Verweij, J., Casali, P.G., Le Cesne, A., Hohenberger, P., Ray-Coquard, I., Schlemmer, M., van Oosterom, A.T., Goldstein, D., Sciot, R., Hogendoorn, P.C.W., Brown, M., Bertulli, R., Judson, I.R., 2005. Initial and late resistance to imatinib in advanced gastrointestinal stromal tumors are predicted by different prognostic factors: a European Organisation for Research and Treatment of Cancer-Italian Sarcoma Group-Australasian Gastrointestinal Trials Group study. J. Clin. Oncol. Off. J. Am. Soc. Clin. Oncol. 23, 5795–5804. https://doi.org/10.1200/JCO.2005.11.601

Van Tongelen, A., Loriot, A., De Smet, C., 2017. Oncogenic roles of DNA hypomethylation through the activation of cancer-germline genes. Cancer Lett. 396, 130–137. https://doi.org/10.1016/j.canlet.2017.03.029

Vander Heiden, M.G., Cantley, L.C., Thompson, C.B., 2009. Understanding the Warburg effect: the metabolic requirements of cell proliferation. Science 324, 1029–1033. https://doi.org/10.1126/science.1160809

Vanhaesebroeck, B., Guillermet-Guibert, J., Graupera, M., Bilanges, B., 2010. The emerging mechanisms of isoform-specific PI3K signalling. Nat. Rev. Mol. Cell Biol. 11, 329–341. https://doi.org/10.1038/nrm2882

Velculescu, V.E., Zhang, L., Vogelstein, B., Kinzler, K.W., 1995. Serial analysis of gene expression. Science 270, 484–487.

Vella, F., 1995. Biochemistry: by R H Garrett and C M Grisham. pp 1154. Saunders College Publishing: Harcourt Brace, Orlando, FL. 1995. £19.95. Biochem. Educ. 23, 108. https://doi.org/10.1016/0307-4412(95)90667-3

Vinci, M., Gowan, S., Boxall, F., Patterson, L., Zimmermann, M., Court, W., Lomas, C., Mendiola, M., Hardisson, D., Eccles, S.A., 2012. Advances in establishment and analysis of three-dimensional tumor spheroid-based functional assays for target validation and drug evaluation. BMC Biol. 10, 29. https://doi.org/10.1186/1741-7007-10-29

Vineis, P., Forastiere, F., Hoek, G., Lipsett, M., 2004. Outdoor air pollution and lung cancer: recent epidemiologic evidence. Int. J. Cancer 111, 647–652. https://doi.org/10.1002/ijc.20292

Voigt, A., Zintl, F., 2003. Effects of retinoic acid on proliferation, apoptosis, cytotoxicity, migration, and invasion of neuroblastoma cells. Med. Pediatr. Oncol. 40, 205–213. https://doi.org/10.1002/mpo.10250

Volkomorov, V., Grigoryeva, E., Krasnov, G., Litviakov, N., Tsyganov, M., Karbyshev, M., Zavyalova, M., Afanasyev, S., Cherdyntseva, N., Lisitsyn, N., Beresten, S., 2013. Search for potential gastric cancer markers using miRNA databases and gene expression analysis. Exp. Oncol. 35, 2–7.

von der Mark, K., Gauss, V., von der Mark, H., Müller, P., 1977. Relationship between cell shape and type of collagen synthesised as chondrocytes lose their cartilage phenotype in culture. Nature 267, 531–532.

Vukicevic, S., Luyten, F.P., Kleinman, H.K., Reddi, A.H., 1990. Differentiation of canalicular cell processes in bone cells by basement membrane matrix components: regulation by discrete domains of laminin. Cell 63, 437–445.

Wagle, N., Emery, C., Berger, M.F., Davis, M.J., Sawyer, A., Pochanard, P., Kehoe, S.M., Johannessen, C.M., Macconaill, L.E., Hahn, W.C., Meyerson, M., Garraway, L.A., 2011. Dissecting therapeutic resistance to RAF inhibition in melanoma by tumor genomic profiling. J. Clin. Oncol. Off. J. Am. Soc. Clin. Oncol. 29, 3085–3096. https://doi.org/10.1200/JCO.2010.33.2312

Wakioka, T., Sasaki, A., Kato, R., Shouda, T., Matsumoto, A., Miyoshi, K., Tsuneoka, M., Komiya, S., Baron, R., Yoshimura, A., 2001. Spred is a Sprouty-related suppressor of Ras signalling. Nature 412, 647–651. https://doi.org/10.1038/35088082

Wakita, A., Motoyama, S., Sato, Y., Koyota, S., Usami, S., Yoshino, K., Sasaki, T., Imai, K., Saito, H., Minamiya, Y., 2015. REG Iα activates c-Jun through MAPK pathways to enhance the radiosensitivity of squamous esophageal cancer cells. Tumour Biol. J. Int. Soc. Oncodevelopmental Biol. Med. 36, 5249–5254. https://doi.org/10.1007/s13277-015-3183-y

Wan, X., Li, J., Xie, X., Lu, W., 2007. PTEN augments doxorubicin-induced apoptosis in PTEN-null Ishikawa cells. Int. J. Gynecol. Cancer Off. J. Int. Gynecol. Cancer Soc. 17, 808–812. https://doi.org/10.1111/j.1525-1438.2007.00890.x

Wang, E.T., Sandberg, R., Luo, S., Khrebtukova, I., Zhang, L., Mayr, C., Kingsmore, S.F., Schroth, G.P., Burge, C.B., 2008. Alternative isoform regulation in human tissue transcriptomes. Nature 456, 470–476. https://doi.org/10.1038/nature07509

Wang, G.L., Jiang, B.H., Rue, E.A., Semenza, G.L., 1995. Hypoxia-inducible factor 1 is a basic-helix-loop-helix-PAS heterodimer regulated by cellular O2 tension. Proc. Natl. Acad. Sci. U. S. A. 92, 5510–5514.

Wang, J., Lippman, S.M., Lee, J.J., Yang, H., Khuri, F.R., Kim, E., Lin, J., Chang, D.W., Lotan, R., Hong, W.K., Wu, X., 2010. Genetic variations in regulator of G-protein signaling genes as susceptibility loci for second primary tumor/recurrence in head and neck squamous cell carcinoma. Carcinogenesis 31, 1755–1761. https://doi.org/10.1093/carcin/bgq138

Wang, J., Mikse, O., Liao, R.G., Li, Y., Tan, L., Janne, P.A., Gray, N.S., Wong, K.–., Hammerman, P.S., 2015. Ligand-associated ERBB2/3 activation confers acquired resistance to FGFR inhibition in FGFR3-dependent cancer cells. Oncogene 34, 2167–2177. https://doi.org/10.1038/onc.2014.161

Wang, J., Yuan, W., Chen, Zhikang, Wu, S., Chen, J., Ge, J., Hou, F., Chen, Zihua, 2012. Overexpression of G6PD is associated with poor clinical outcome in gastric cancer. Tumour Biol. J. Int. Soc. Oncodevelopmental Biol. Med. 33, 95–101. https://doi.org/10.1007/s13277-011-0251-9

Wang, J.K., Xu, H., Li, H.C., Goldfarb, M., 1996. Broadly expressed SNT-like proteins link FGF receptor stimulation to activators of Ras. Oncogene 13, 721–729.

Wang, L., Rhodes, C.J., Lawrence, J.C., 2006. Activation of mammalian target of rapamycin (mTOR) by insulin is associated with stimulation of 4EBP1 binding to dimeric mTOR complex 1. J. Biol. Chem. 281, 24293–24303. https://doi.org/10.1074/jbc.M603566200

Wang, L., Rudert, W.A., Loutaev, I., Roginskaya, V., Corey, S.J., 2002. Repression of c-Cbl leads to enhanced G-CSF Jak-STAT signaling without increased cell proliferation. Oncogene 21, 5346–5355. https://doi.org/10.1038/sj.onc.1205670

Wang, L.-Y., Liu, Y.-P., Chen, L.-G., Chen, Y.-L., Tan, L., Liu, J.-J., Jazag, A., Ren, J.-L., Guleng, B., 2013. Pyruvate kinase M2 plays a dual role on regulation of the EGF/EGFR signaling via E-cadherin-dependent manner in gastric cancer cells. PloS One 8, e67542. https://doi.org/10.1371/journal.pone.0067542

Wang, M., Zhao, J., Zhang, L., Wei, F., Lian, Y., Wu, Y., Gong, Z., Zhang, S., Zhou, J., Cao, K., Li, X., Xiong, W., Li, G., Zeng, Z., Guo, C., 2017. Role of tumor microenvironment in tumorigenesis. J. Cancer 8, 761–773. https://doi.org/10.7150/jca.17648

Wang, Q., Lee, D., Sysounthone, V., Chandraratna RAS, null, Christakos, S., Korah, R., Wieder, R., 2001. 1,25-dihydroxyvitamin D3 and retonic acid analogues induce differentiation in breast cancer cells with function- and cell-specific additive effects. Breast Cancer Res. Treat. 67, 157–168.

Wang, W., Kirsch, T., 2002. Retinoic acid stimulates annexin-mediated growth plate chondrocyte mineralization. J. Cell Biol. 157, 1061–1069. https://doi.org/10.1083/jcb.200203014

Wang, W., Li, Q., Yamada, T., Matsumoto, K., Matsumoto, I., Oda, M., Watanabe, G., Kayano, Y., Nishioka, Y., Sone, S., Yano, S., 2009. Crosstalk to stromal fibroblasts induces resistance of lung cancer to epidermal growth factor receptor tyrosine kinase inhibitors. Clin. Cancer Res. Off. J. Am. Assoc. Cancer Res. 15, 6630–6638. https://doi.org/10.1158/1078-0432.CCR-09-1001

Wang, X.-Q., Tang, Z.-X., Yu, D., Cui, S.-J., Jiang, Y.-H., Zhang, Q., Wang, J., Yang, P.-Y., Liu, F., 2016. Epithelial but not stromal expression of collagen alpha-1(III)

is a diagnostic and prognostic indicator of colorectal carcinoma. Oncotarget 7, 8823–8838. https://doi.org/10.18632/oncotarget.6815

Wang, Y., Bao, X., Zhang, Z., Sun, Y., Zhou, X., 2017. FGF2 promotes metastasis of uveal melanoma cells via store-operated calcium entry. OncoTargets Ther. 10, 5317–5328. https://doi.org/10.2147/OTT.S136677

Wang, Y., Wen, W., Yi, Y., Zhang, Z., Lubet, R.A., You, M., 2009. Preventive effects of bexarotene and budesonide in a genetically engineered mouse model of small cell lung cancer. Cancer Prev. Res. Phila. Pa 2, 1059–1064. https://doi.org/10.1158/1940-6207.CAPR-09-0221

Wang, Y., Xiao, R., Yang, F., Karim, B.O., Iacovelli, A.J., Cai, J., Lerner, C.P., Richtsmeier, J.T., Leszl, J.M., Hill, C.A., Yu, K., Ornitz, D.M., Elisseeff, J., Huso, D.L., Jabs, E.W., 2005. Abnormalities in cartilage and bone development in the Apert syndrome FGFR2(+/S252W) mouse. Dev. Camb. Engl. 132, 3537–3548. https://doi.org/10.1242/dev.01914

Wang, Z., Gerstein, M., Snyder, M., 2009. RNA-Seq: a revolutionary tool for transcriptomics. Nat. Rev. Genet. 10, 57–63. https://doi.org/10.1038/nrg2484

Warburg, O., 1956. On the origin of cancer cells. Science 123, 309–314.

Ware, M.J., Colbert, K., Keshishian, V., Ho, J., Corr, S.J., Curley, S.A., Godin, B., 2016. Generation of Homogenous Three-Dimensional Pancreatic Cancer Cell Spheroids Using an Improved Hanging Drop Technique. Tissue Eng. Part C Methods 22, 312–321. https://doi.org/10.1089/ten.TEC.2015.0280

Watanabe, M., Naraba, H., Sakyo, T., Kitagawa, T., 2010. DNA damage-induced modulation of GLUT3 expression is mediated through p53-independent extracellular signal-regulated kinase signaling in HeLa cells. Mol. Cancer Res. MCR 8, 1547–1557. https://doi.org/10.1158/1541-7786.MCR-10-0011

Watanabe, T., Takeda, A., Tsukiyama, T., Mise, K., Okuno, T., Sasaki, H., Minami, N., Imai, H., 2006. Identification and characterization of two novel classes of small RNAs in the mouse germline: retrotransposon-derived siRNAs in oocytes and germline small RNAs in testes. Genes Dev. 20, 1732–1743. https://doi.org/10.1101/gad.1425706

Watanabe, T., Yonekura, H., Terazono, K., Yamamoto, H., Okamoto, H., 1990. Complete nucleotide sequence of human reg gene and its expression in normal and tumoral tissues. The reg protein, pancreatic stone protein, and pancreatic thread protein are one and the same product of the gene. J. Biol. Chem. 265, 7432–7439.

Wegman-Ostrosky, T., Soto-Reyes, E., Vidal-Millán, S., Sánchez-Corona, J., 2015. The renin-angiotensin system meets the hallmarks of cancer. J. Renin-Angiotensin-Aldosterone Syst. JRAAS 16, 227–233. https://doi.org/10.1177/1470320313496858

Wei, T., Zhu, W., Fang, S., Zeng, X., Huang, J., Yang, J., Zhang, J., Guo, L., 2017. miR-495 promotes the chemoresistance of SCLC through the epithelial-mesenchymal transition via Etk/BMX. Am. J. Cancer Res. 7, 628–646.

Wei, Z., Liang, L., Junsong, L., Rui, C., Shuai, C., Guanglin, Q., Shicai, H., Zexing, W., Jin, W., Xiangming, C., Shufeng, W., 2015. The impact of insulin on chemotherapeutic sensitivity to 5-fluorouracil in gastric cancer cell lines SGC7901, MKN45 and MKN28. J. Exp. Clin. Cancer Res. CR 34. https://doi.org/10.1186/s13046-015-0151-8

Weigelt, B., Ghajar, C.M., Bissell, M.J., 2014. The need for complex 3D culture models to unravel novel pathways and identify accurate biomarkers in breast cancer. Adv. Drug Deliv. Rev. 69–70, 42–51. https://doi.org/10.1016/j.addr.2014.01.001

Weil, B.R., Abarbanell, A.M., Herrmann, J.L., Wang, Y., Meldrum, D.R., 2009. High glucose concentration in cell culture medium does not acutely affect human mesenchymal stem cell growth factor production or proliferation. Am. J. Physiol. Regul. Integr. Comp. Physiol. 296, R1735-1743. https://doi.org/10.1152/ajpregu.90876.2008

Wen, S., Niu, Y., Yeh, S., Chang, C., 2015. BM-MSCs promote prostate cancer progression via the conversion of normal fibroblasts to cancer-associated fibroblasts. Int. J. Oncol. 47, 719–727. https://doi.org/10.3892/ijo.2015.3060

Werner, T., 2008. Bioinformatics applications for pathway analysis of microarray data. Curr. Opin. Biotechnol. 19, 50–54. https://doi.org/10.1016/j.copbio.2007.11.005

Westbrook, A.M., Lucks, J.B., 2017. Achieving large dynamic range control of gene expression with a compact RNA transcription–translation regulator. Nucleic Acids Res. 45, 5614–5624. https://doi.org/10.1093/nar/gkx215

Wheeler, D.L., Yarden, Y., 2015. Receptor Tyrosine Kinases: Family and Subfamilies. Springer.

White, J.A., Beckett-Jones, B., Guo, Y.D., Dilworth, F.J., Bonasoro, J., Jones, G., Petkovich, M., 1997. cDNA cloning of human retinoic acid-metabolizing enzyme (hP450RAI) identifies a novel family of cytochromes P450. J. Biol. Chem. 272, 18538–18541.

White, K.E., Cabral, J.M., Davis, S.I., Fishburn, T., Evans, W.E., Ichikawa, S., Fields, J., Yu, X., Shaw, N.J., McLellan, N.J., McKeown, C., Fitzpatrick, D., Yu, K., Ornitz, D.M., Econs, M.J., 2005. Mutations that cause osteoglophonic dysplasia define novel roles for FGFR1 in bone elongation. Am. J. Hum. Genet. 76, 361–367. https://doi.org/10.1086/427956

Whiteside, T.L., 2008. The tumor microenvironment and its role in promoting tumor growth. Oncogene 27, 5904–5912. https://doi.org/10.1038/onc.2008.271

WHO | World Health Statistics 2018 [WWW Document], n.d. . WHO. URL http://www.who.int/gho/publications/world_health_statistics/2018/en/ (accessed 7.12.18).

Widschwendter, M., Berger, J., Daxenbichler, G., Müller-Holzner, E., Widschwendter, A., Mayr, A., Marth, C., Zeimet, A.G., 1997. Loss of retinoic acid receptor beta expression in breast cancer and morphologically normal adjacent tissue but not in the normal breast tissue distant from the cancer. Cancer Res. 57, 4158–4161.

Wilhelm, B.T., Marguerat, S., Watt, S., Schubert, F., Wood, V., Goodhead, I., Penkett, C.J., Rogers, J., Bähler, J., 2008. Dynamic repertoire of a eukaryotic transcriptome surveyed at single-nucleotide resolution. Nature 453, 1239–1243. https://doi.org/10.1038/nature07002

Wilkie, A.O.M., Patey, S.J., Kan, S.-H., van den Ouweland, A.M.W., Hamel, B.C.J., 2002. FGFs, their receptors, and human limb malformations: clinical and molecular correlations. Am. J. Med. Genet. 112, 266–278. https://doi.org/10.1002/ajmg.10775

Williams, S.V., Hurst, C.D., Knowles, M.A., 2013. Oncogenic FGFR3 gene fusions in bladder cancer. Hum. Mol. Genet. 22, 795–803. https://doi.org/10.1093/hmg/dds486

Willy, P.J., Umesono, K., Ong, E.S., Evans, R.M., Heyman, R.A., Mangelsdorf, D.J., 1995. LXR, a nuclear receptor that defines a distinct retinoid response pathway. Genes Dev. 9, 1033–1045.

Witz, I.P., Levy-Nissenbaum, O., 2006. The tumor microenvironment in the post-PAGET era. Cancer Lett. 242, 1–10. https://doi.org/10.1016/j.canlet.2005.12.005

Wolf, G., 2007. Identification of a membrane receptor for retinol-binding protein functioning in the cellular uptake of retinol. Nutr. Rev. 65, 385–388.

Wolf, M.K., 1970. Anatomy of cultured mouse cerebellum. II. Organotypic migration of granule cells demonstrated by silver impregnantion of normal and mutant cultures. J. Comp. Neurol. 140, 281–298. https://doi.org/10.1002/cne.901400304

Wolff, E., 1961. Utilisation de la membrane vitelline de l'oeuf de poule en culture organotypique I. Technique et possibilités. Dev. Biol. 3, 767–786. https://doi.org/10.1016/0012-1606(61)90040-9

Wolff, E., Marin, L., 1960. [On the factors determining the transformation of an organ culture into a tissue culture]. Comptes Rendus Hebd. Seances Acad. Sci. 250, 609–611.

Wolff, E., Marin, L., 1957. [Movements of embryonal liver explants cultivated in vitro]. Comptes Rendus Hebd. Seances Acad. Sci. 244, 2745–2747.

Wong, A., Lamothe, B., Lee, A., Schlessinger, J., Lax, I., Li, A., 2002. FRS2 alpha attenuates FGF receptor signaling by Grb2-mediated recruitment of the ubiquitin ligase Cbl. Proc. Natl. Acad. Sci. U. S. A. 99, 6684–6689. https://doi.org/10.1073/pnas.052138899

Wright, J.D., Fiorelli, J., Kansler, A.L., Burke, W.M., Schiff, P.B., Cohen, C.J., Herzog, T.J., 2009. Optimizing the management of stage II endometrial cancer: the role of radical hysterectomy and radiation. Am. J. Obstet. Gynecol. 200, 419.e1–7. https://doi.org/10.1016/j.ajog.2008.11.003

Wright, P.A., Quirke, P., Attanoos, R., Williams, G.T., 1992. Molecular pathology of gastric carcinoma: progress and prospects. Hum. Pathol. 23, 848–859.

Wu, H., Li, Zongwei, Yang, P., Zhang, L., Fan, Y., Li, Zhuoyu, 2014. PKM2 depletion induces the compensation of glutaminolysis through β-catenin/c-Myc pathway in tumor cells. Cell. Signal. 26, 2397–2405. https://doi.org/10.1016/j.cellsig.2014.07.024

Wu, H., Xue, R., Tang, Z., Deng, C., Liu, T., Zeng, H., Sun, Y., Shen, X., 2010. Metabolomic investigation of gastric cancer tissue using gas chromatography/mass spectrometry. Anal. Bioanal. Chem. 396, 1385–1395. https://doi.org/10.1007/s00216-009-3317-4

Wu, S., Walenkamp, M.J., Lankester, A., Bidlingmaier, M., Wit, J.M., De Luca, F., 2010. Growth hormone and insulin-like growth factor I insensitivity of fibroblasts isolated from a patient with an I{kappa}B{alpha} mutation. J. Clin. Endocrinol. Metab. 95, 1220–1228. https://doi.org/10.1210/jc.2009-1662

Wu, Y.-M., Su, F., Kalyana-Sundaram, S., Khazanov, N., Ateeq, B., Cao, X., Lonigro, R.J., Vats, P., Wang, R., Lin, S.-F., Cheng, A.-J., Kunju, L.P., Siddiqui, J., Tomlins, S.A., Wyngaard, P., Sadis, S., Roychowdhury, S., Hussain, M.H., Feng, F.Y., Zalupski, M.M., Talpaz, M., Pienta, K.J., Rhodes, D.R., Robinson,

D.R., Chinnaiyan, A.M., 2013. Identification of targetable FGFR gene fusions in diverse cancers. Cancer Discov. 3, 636–647. https://doi.org/10.1158/2159-8290.CD-13-0050

Xiao, S., Nalabolu, S.R., Aster, J.C., Ma, J., Abruzzo, L., Jaffe, E.S., Stone, R., Weissman, S.M., Hudson, T.J., Fletcher, J.A., 1998. FGFR1 is fused with a novel zinc-finger gene, ZNF198, in the t(8;13) leukaemia/lymphoma syndrome. Nat. Genet. 18, 84–87. https://doi.org/10.1038/ng0198-84

Xie, L., Su, X., Zhang, Lin, Yin, X., Tang, L., Zhang, Xiuhua, Xu, Y., Gao, Z., Liu, K., Zhou, M., Gao, B., Shen, D., Zhang, Lianhai, Ji, J., Gavine, P.R., Zhang, J., Kilgour, E., Zhang, Xiaolin, Ji, Q., 2013. FGFR2 gene amplification in gastric cancer predicts sensitivity to the selective FGFR inhibitor AZD4547. Clin. Cancer Res. Off. J. Am. Assoc. Cancer Res. 19, 2572–2583. https://doi.org/10.1158/1078-0432.CCR-12-3898

Xie, Z., Geiger, T.R., Johnson, E.N., Nyborg, J.K., Druey, K.M., 2008. RGS13 acts as a nuclear repressor of CREB. Mol. Cell 31, 660–670. https://doi.org/10.1016/j.molcel.2008.06.024

Xiong, S., Zhao, Q., Rong, Z., Huang, G., Huang, Y., Chen, P., Zhang, S., Liu, L., Chang, Z., 2003. hSef inhibits PC-12 cell differentiation by interfering with Ras-mitogen-activated protein kinase MAPK signaling. J. Biol. Chem. 278, 50273–50282. https://doi.org/10.1074/jbc.M306936200

Xu, H., Lee, K.W., Goldfarb, M., 1998. Novel recognition motif on fibroblast growth factor receptor mediates direct association and activation of SNT adapter proteins. J. Biol. Chem. 273, 17987–17990.

Xu, Y., Shi, T., Xu, A., Zhang, L., 2016. 3D spheroid culture enhances survival and therapeutic capacities of MSCs injected into ischemic kidney. J. Cell. Mol. Med. 20, 1203–1213. https://doi.org/10.1111/jcmm.12651

Yadav, V., Zhang, X., Liu, J., Estrem, S., Li, S., Gong, X.-Q., Buchanan, S., Henry, J.R., Starling, J.J., Peng, S.-B., 2012. Reactivation of Mitogen-activated Protein Kinase (MAPK) Pathway by FGF Receptor 3 (FGFR3)/Ras Mediates Resistance to Vemurafenib in Human B-RAF V600E Mutant Melanoma. J. Biol. Chem. 287, 28087–28098. https://doi.org/10.1074/jbc.M112.377218

Yamada, K.M., Cukierman, E., 2007. Modeling tissue morphogenesis and cancer in 3D. Cell 130, 601–610. https://doi.org/10.1016/j.cell.2007.08.006

Yamanaka, Y., Lanner, F., Rossant, J., 2010. FGF signal-dependent segregation of primitive endoderm and epiblast in the mouse blastocyst. Dev. Camb. Engl. 137, 715–724. https://doi.org/10.1242/dev.043471

Yang, P., Zhou, Y., Chen, B., Wan, H.-W., Jia, G.-Q., Bai, H.-L., Wu, X.-T., 2009. Overweight, obesity and gastric cancer risk: results from a meta-analysis of cohort studies. Eur. J. Cancer Oxf. Engl. 1990 45, 2867–2873. https://doi.org/10.1016/j.ejca.2009.04.019

Yang, R.-B., Ng, C.K.D., Wasserman, S.M., Kömüves, L.G., Gerritsen, M.E., Topper, J.N., 2003. A novel interleukin-17 receptor-like protein identified in human umbilical vein endothelial cells antagonizes basic fibroblast growth factor-induced signaling. J. Biol. Chem. 278, 33232–33238. https://doi.org/10.1074/jbc.M305022200

Yashiro, M., Matsuoka, T., 2016. Fibroblast growth factor receptor signaling as therapeutic targets in gastric cancer. World J. Gastroenterol. 22, 2415–2423. https://doi.org/10.3748/wjg.v22.i8.2415

Yayon, A., Klagsbrun, M., Esko, J.D., Leder, P., Ornitz, D.M., 1991. Cell surface, heparin-like molecules are required for binding of basic fibroblast growth factor to its high affinity receptor. Cell 64, 841–848.

Ye, F., Chen, Y., Xia, L., Lian, J., Yang, S., 2018. Aldolase A overexpression is associated with poor prognosis and promotes tumor progression by the epithelial-mesenchymal transition in colon cancer. Biochem. Biophys. Res. Commun. 497, 639–645. https://doi.org/10.1016/j.bbrc.2018.02.123

Ye, Y., Shi, Y., Zhou, Y., Du, C., Wang, C., Zhan, H., Zheng, B., Cao, X., Sun, M.-H., Fu, H., 2010. The fibroblast growth factor receptor-4 Arg388 allele is associated with gastric cancer progression. Ann. Surg. Oncol. 17, 3354–3361. https://doi.org/10.1245/s10434-010-1323-6

Yeramian, A., Moreno-Bueno, G., Dolcet, X., Catasus, L., Abal, M., Colas, E., Reventos, J., Palacios, J., Prat, J., Matias-Guiu, X., 2013. Endometrial carcinoma: molecular alterations involved in tumor development and progression. Oncogene 32, 403–413. https://doi.org/10.1038/onc.2012.76

Ying, M., Wang, S., Sang, Y., Sun, P., Lal, B., Goodwin, C.R., Guerrero-Cazares, H., Quinones-Hinojosa, A., Laterra, J., Xia, S., 2011. Regulation of glioblastoma stem cells by retinoic acid: role for Notch pathway inhibition. Oncogene 30, 3454–3467. https://doi.org/10.1038/onc.2011.58

Yokota, M., Kobayashi, Y., Morita, J., Suzuki, H., Hashimoto, Y., Sasaki, Y., Akiyoshi, K., Moriyama, K., 2014. Therapeutic effect of nanogel-based delivery of soluble FGFR2 with S252W mutation on craniosynostosis. PloS One 9, e101693. https://doi.org/10.1371/journal.pone.0101693

Yoshida, H., Kitamura, K., Tanaka, K., Omura, S., Miyazaki, T., Hachiya, T., Ohno, R., Naoe, T., 1996. Accelerated degradation of PML-retinoic acid receptor alpha (PML-RARA) oncoprotein by all-trans-retinoic acid in acute promyelocytic leukemia: possible role of the proteasome pathway. Cancer Res. 56, 2945–2948.

Yoshino, N., Ishihara, S., Rumi, M. a. K., Ortega-Cava, C.F., Yuki, T., Kazumori, H., Takazawa, S., Okamoto, H., Kadowaki, Y., Kinoshita, Y., 2005. Interleukin-8 regulates expression of Reg protein in Helicobacter pylori-infected gastric mucosa. Am. J. Gastroenterol. 100, 2157–2166. https://doi.org/10.1111/j.1572-0241.2005.41915.x

Young, M.A., Shah, N.P., Chao, L.H., Seeliger, M., Milanov, Z.V., Biggs, W.H., Treiber, D.K., Patel, H.K., Zarrinkar, P.P., Lockhart, D.J., Sawyers, C.L., Kuriyan, J., 2006. Structure of the kinase domain of an imatinib-resistant Abl mutant in complex with the Aurora kinase inhibitor VX-680. Cancer Res. 66, 1007–1014. https://doi.org/10.1158/0008-5472.CAN-05-2788

Yu, K., Herr, A.B., Waksman, G., Ornitz, D.M., 2000. Loss of fibroblast growth factor receptor 2 ligand-binding specificity in Apert syndrome. Proc. Natl. Acad. Sci. U. S. A. 97, 14536–14541.

Yun, B.-R., Lee, M.-J., Kim, J.-H., Kim, I.-H., Yu, G.-R., Kim, D.-G., 2010. Enhancement of parthenolide-induced apoptosis by a PKC-alpha inhibition through heme oxygenase-1 blockage in cholangiocarcinoma cells. Exp. Mol. Med. 42, 787–797. https://doi.org/10.3858/emm.2010.42.11.082

Yusoff, P., Lao, D.-H., Ong, S.H., Wong, E.S.M., Lim, J., Lo, T.L., Leong, H.F., Fong, C.W., Guy, G.R., 2002. Sprouty2 inhibits the Ras/MAP kinase pathway by inhibiting the activation of Raf. J. Biol. Chem. 277, 3195–3201. https://doi.org/10.1074/jbc.M108368200

Zanoni, M., Piccinini, F., Arienti, C., Zamagni, A., Santi, S., Polico, R., Bevilacqua, A., Tesei, A., 2016. 3D tumor spheroid models for in vitro therapeutic screening: a systematic approach to enhance the biological relevance of data obtained. Sci. Rep. 6, 19103. https://doi.org/10.1038/srep19103

Zenilman, M.E., Kim, S., Levine, B.A., Lee, C., Steinberg, J.J., 1997. Ectopic expression of reg protein: A marker of colorectal mucosa at risk for neoplasia. J. Gastrointest. Surg. Off. J. Soc. Surg. Aliment. Tract 1, 194–201; discussion 201-202.

Zhang, D., Fan, D., 2007. Multidrug resistance in gastric cancer: recent research advances and ongoing therapeutic challenges. Expert Rev. Anticancer Ther. 7, 1369–1378. https://doi.org/10.1586/14737140.7.10.1369

Zhang, J., Guo, L., Liu, X., Li, W., Ying, J., 2016. MET overexpression, gene amplification and relevant clinicopathological features in gastric adenocarcinoma. Oncotarget 8, 10264–10273. https://doi.org/10.18632/oncotarget.14382

Zhang, J., Yang, P.L., Gray, N.S., 2009. Targeting cancer with small molecule kinase inhibitors. Nat. Rev. Cancer 9, 28–39. https://doi.org/10.1038/nrc2559

Zhang, J., Zhang, L., Su, X., Li, M., Xie, L., Malchers, F., Fan, S., Yin, X., Xu, Y., Liu, K., Dong, Z., Zhu, G., Qian, Z., Tang, L., Schöttle, J., Zhan, P., Ji, Q., Kilgour, E., Smith, P.D., Brooks, A.N., Thomas, R.K., Gavine, P.R., 2012. Translating the therapeutic potential of AZD4547 in FGFR1-amplified non-small cell lung cancer through the use of patient-derived tumor xenograft models. Clin. Cancer Res. Off. J. Am. Assoc. Cancer Res. 18, 6658–6667. https://doi.org/10.1158/1078-0432.CCR-12-2694

Zhang, L., Zhou, Y., Huang, T., Cheng, A.S.L., Yu, J., Kang, W., To, K.F., 2017. The Interplay of LncRNA-H19 and Its Binding Partners in Physiological Process and Gastric Carcinogenesis. Int. J. Mol. Sci. 18. https://doi.org/10.3390/ijms18020450

Zhang, W., Huang, P., 2011. Cancer-stromal interactions: role in cell survival, metabolism and drug sensitivity. Cancer Biol. Ther. 11, 150–156.

Zhang, W., Thompson, B.J., Hietakangas, V., Cohen, S.M., 2011. MAPK/ERK Signaling Regulates Insulin Sensitivity to Control Glucose Metabolism in Drosophila. PLoS Genet. 7. https://doi.org/10.1371/journal.pgen.1002429

Zhang, Y., Pan, T., Zhong, X., Cheng, C., 2014. Resistance to cetuximab in EGFR-overexpressing esophageal squamous cell carcinoma xenografts due to FGFR2 amplification and overexpression. J. Pharmacol. Sci. 126, 77–83.

Zhang, Z., Castelló, A., 2017. Principal components analysis in clinical studies. Ann. Transl. Med. 5. https://doi.org/10.21037/atm.2017.07.12

Zhao, L., Li, Z., Chen, W., Zhai, W., Pan, J., Pang, H., Li, X., 2017. H19 promotes endometrial cancer progression by modulating epithelial-mesenchymal transition. Oncol. Lett. 13, 363–369. https://doi.org/10.3892/ol.2016.5389

Zhou, S.-F., 2008. Structure, function and regulation of P-glycoprotein and its clinical relevance in drug disposition. Xenobiotica Fate Foreign Compd. Biol. Syst. 38, 802–832. https://doi.org/10.1080/00498250701867889

Zhou, W., Hur, W., McDermott, U., Dutt, A., Xian, W., Ficarro, S.B., Zhang, J., Sharma, S.V., Brugge, J., Meyerson, M., Settleman, J., Gray, N.S., 2010. A structure-guided approach to creating covalent FGFR inhibitors. Chem. Biol. 17, 285–295. https://doi.org/10.1016/j.chembiol.2010.02.007

Zimmermann, W.-H., Melnychenko, I., Wasmeier, G., Didié, M., Naito, H., Nixdorff, U., Hess, A., Budinsky, L., Brune, K., Michaelis, B., Dhein, S., Schwoerer, A., Ehmke, H., Eschenhagen, T., 2006. Engineered heart tissue grafts improve systolic and diastolic function in infarcted rat hearts. Nat. Med. 12, 452–458. https://doi.org/10.1038/nm1394

Zorde Khvalevsky, E., Gabai, R., Rachmut, I.H., Horwitz, E., Brunschwig, Z., Orbach, A., Shemi, Adva, Golan, T., Domb, A.J., Yavin, E., Giladi, H., Rivkin, L., Simerzin, A., Eliakim, R., Khalaileh, A., Hubert, A., Lahav, M., Kopelman, Y., Goldin, E., Dancour, A., Hants, Y., Arbel-Alon, S., Abramovitch, R., Shemi, Amotz, Galun, E., 2013. Mutant KRAS is a druggable target for pancreatic cancer. Proc. Natl. Acad. Sci. U. S. A. 110, 20723–20728. https://doi.org/10.1073/pnas.1314307110

Zucker, S., Wang, M., Sparano, J.A., Gradishar, W.J., Ingle, J.N., Davidson, N.E., Eastern Cooperative Oncology Group, 2006. Plasma matrix metalloproteinases 7 and 9 in patients with metastatic breast cancer treated with marimastat or placebo: Eastern Cooperative Oncology Group trial E2196. Clin. Breast Cancer 6, 525–529.

Zweibaum, A., Triadou, N., Kedinger, M., Augeron, C., Robine-Léon, S., Pinto, M., Rousset, M., Haffen, K., 1983. Sucrase-isomaltase: a marker of foetal and malignant epithelial cells of the human colon. Int. J. Cancer 32, 407–412.

List of Appendix Figures

List of Appendix Tables

Chapter VIII

Appendix Figures and Tables

8.1 Appendix Chapter III Results Part I

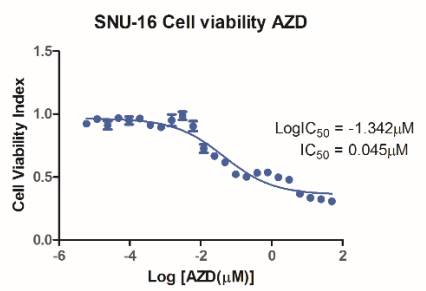

Appendix Figure 8.1. *FGFR2*-amplified gastric cancer cell line SNU-16 treated with AZD.
SNU-16 cells were seeded into 96-well plates and treated with increasing dosages of AZD ranging from 0.006nM to 50μM and control cells were treated with DMSO and as a background control 1% Staurosporine was added to wells containing cells. After 72h incubation, MTS reagent was added and cell viability was measured colorimetrically after 2h. An average of three biological MTS experiments in technical triplicate is shown with error bars indicating SEM. Log IC_{50} and IC_{50} values were calculated with GraphPad Prism 5.

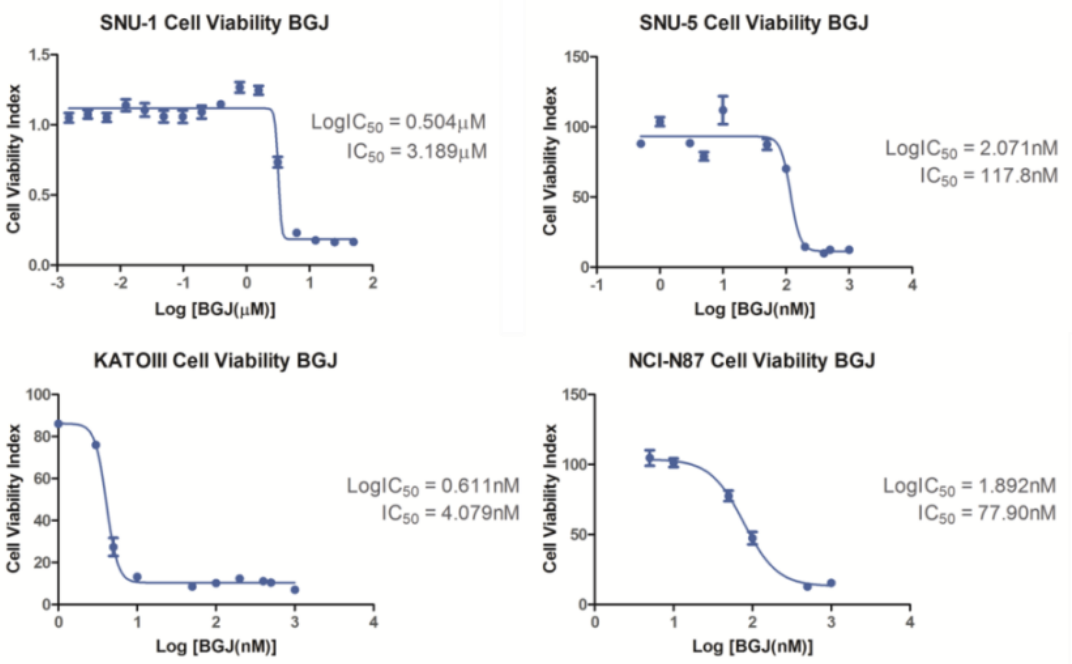

Appendix Figure 8.2. Dose response curves of further gastric cancer cell lines treated with BGJ.
Gastric cancer cell lines were seeded into 96-well plates and exposed to increasing dosages of BGJ ranging from 0.006nM to 50μM and control cells were treated with DMSO and as a background control 1% Staurosporine was added to wells containing cells. After 72h incubation, MTS reagent was added and cell viability was measured colorimetrically after 2h. An average of three biological MTT and MTS experiments in technical triplicate is shown with error bars indicating SEM. Log IC_{50} and IC_{50} values were calculated with GraphPad Prism 5.

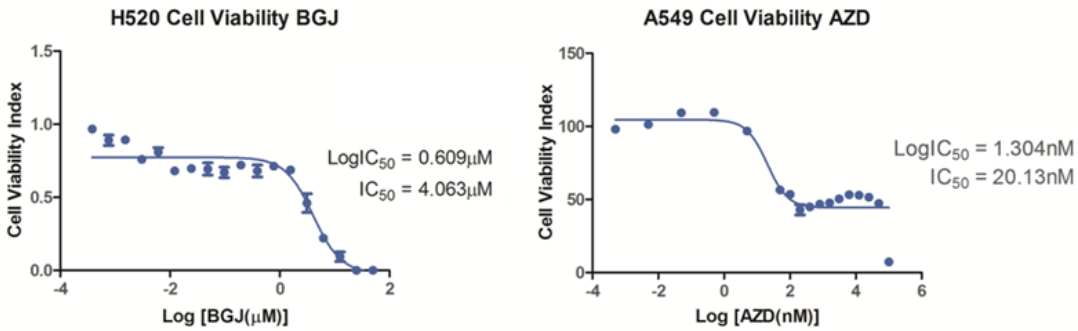

Appendix Figure 8.3. Cell survival of lung cancer cell lines upon FGFR inhibition with AZD or BGJ.
Lung cancer cell lines H520 (*FGFR1*-amplified) and A549 (*FGFR1*-wt) were seeded into 96-well plates and treated with increasing dosages of AZD or BGJ ranging from 0.006nM to 50μM and control cells were treated with DMSO and as a background control 1% Staurosporine was added to wells containing cells. After 72h incubation, MTS reagent was added and cell viability was measured colorimetrically after 2h. An average of three biological MTS experiments in technical triplicate is shown with error bars indicating SEM. Log IC_{50} and IC_{50} values were calculated with GraphPad Prism 5.

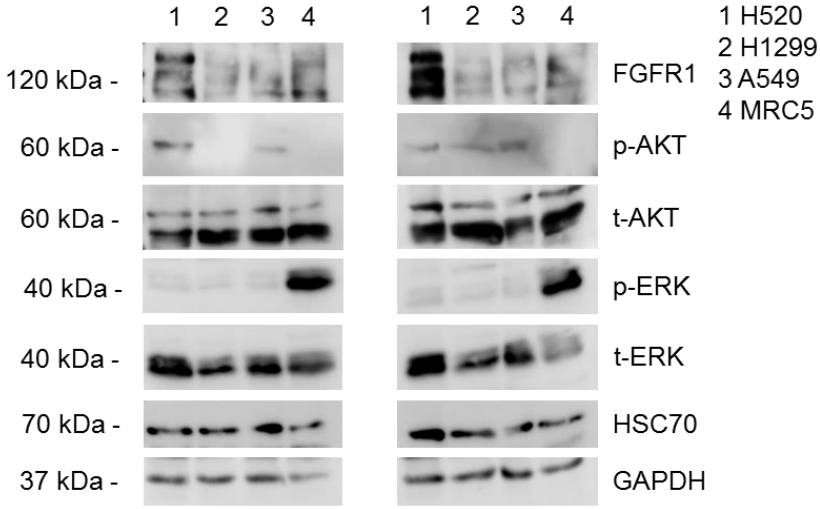

Appendix Figure 8.4. Comparison of lung cancer cell lines and lung fibroblasts.
Additional replicates of cells seeded into 6-well plates and harvested the next day and subjected to Western blot analysis. 1: H520, 2: H1299, 3: A549, 4: MRC-5. H520 cells harbour *FGFR1*-amplifications as shown with the increased FGFR1 expression as compared to other cell lines with wildtype receptor expression. HSC70 and GAPDH served as internal controls.

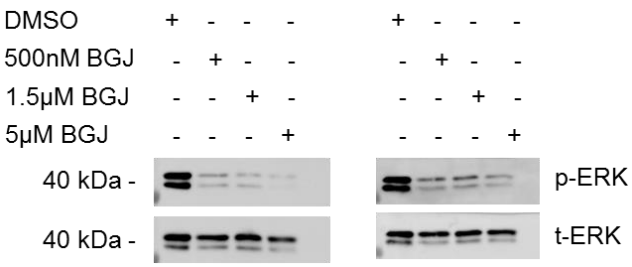

Appendix Figure 8.5. Drug treatments of SNU-16 cells.
Additional replicates of SNU-16 cells treated with increasing concentrations of BGJ. Cells were seeded into 6-well plates and treated with 500nM, 1 or 5μM BGJ. After 72h incubation, cells were harvested and protein was extracted and probed for p-ERK and as an internal control for t-ERK.

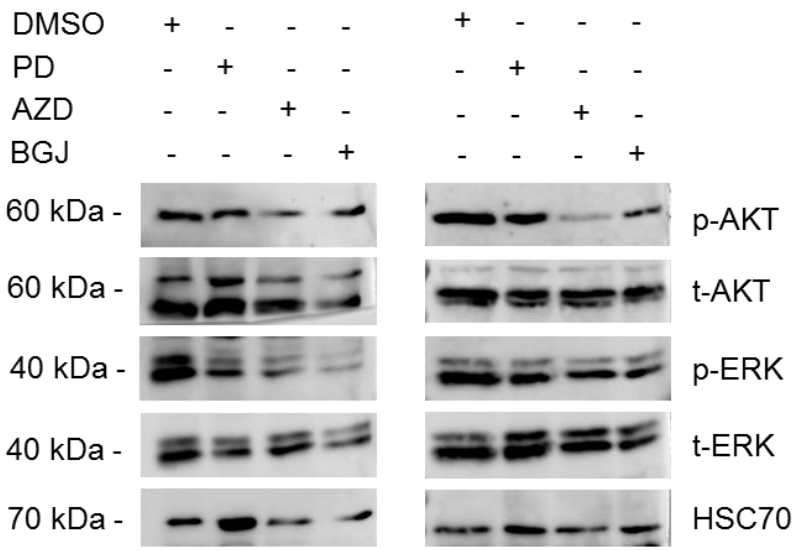

Appendix Figure 8.6. *FGFR1*-amplified lung cancer cells treated with FGFR inhibitors.
Additional replicates of *FGFR1*-amplified lung cancer cells H520 that were seeded into 6-well plates and treated with vehicle or 1μM PD, AZD or 1.5μM BGJ. After 72h, protein was extracted and signalling analysed with Western blot probing for p-AKT, t-AKT, p-ERK, t-ERK and HSC70 as a control.

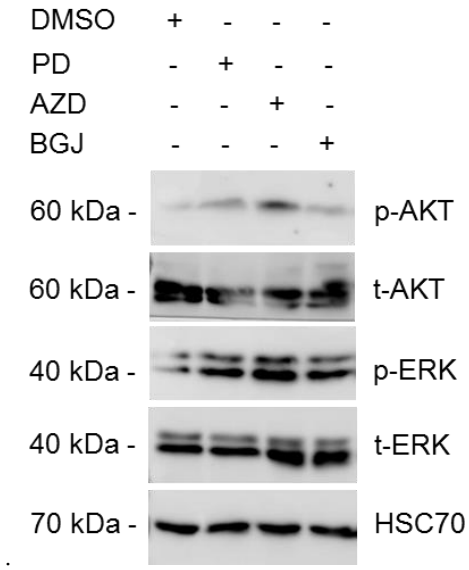

Appendix Figure 8.7. *FGFR1* wildtype lung cancer cells treated with FGFR inhibitors.
Additional replicate of *FGFR1*-wt lung cancer cells H1299 that were seeded into 6-well plates and treated with vehicle or 1μM PD, AZD or 1.5μM BGJ. After 72h, protein was extracted and signalling analysed with Western blot probing for p-AKT, t-AKT, p-ERK, t-ERK and HSC70 as a control.

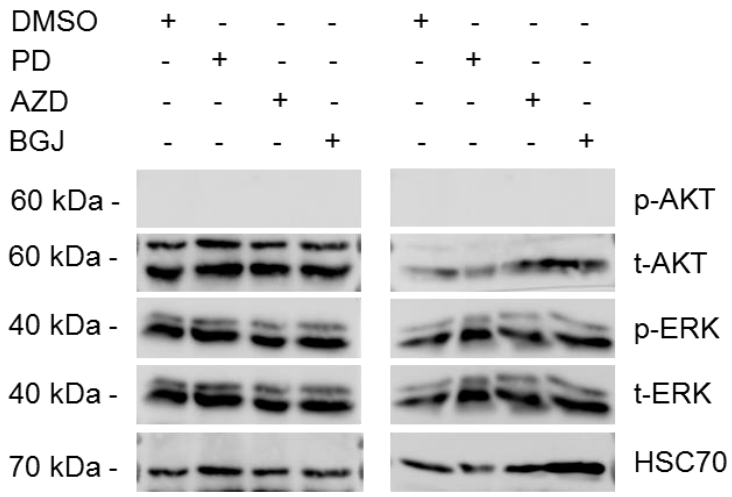

Appendix Figure 8.8. Protein expression levels of MRC-5 cells treated with FGFR inhibitors.
Additional replicates of MRC-5 cells were seeded into 6-well plates and treated with 1µM AZD or PD or 1.5µM BGJ vehicle for 72h. Protein was extracted and Western blot analysis was performed probing for p-AKT, t-AKT, p-ERK, t-ERK and loading control HSC70.

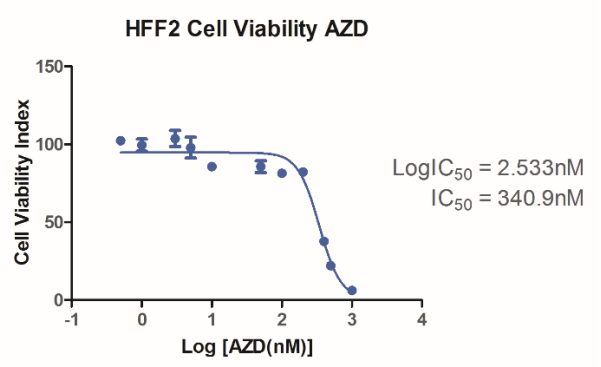

Appendix Figure 8.9. Cell survival of HFF2 cells upon FGFR inhibition with AZD.
HFF2 cells were seeded into 96-well plates and treated with increasing dosages of AZD ranging from 0.006nM to 50µM and control cells were treated with DMSO and as a background control 1% Staurosporine was added to wells containing cells. After 72h incubation, MTT was added to the medium and cell viability was measured colorimetrically after 2h. An average of three biological MTT experiments in technical triplicate is shown with error bars indicating SEM. Log IC_{50} and IC_{50} values were calculated with GraphPad Prism 5.

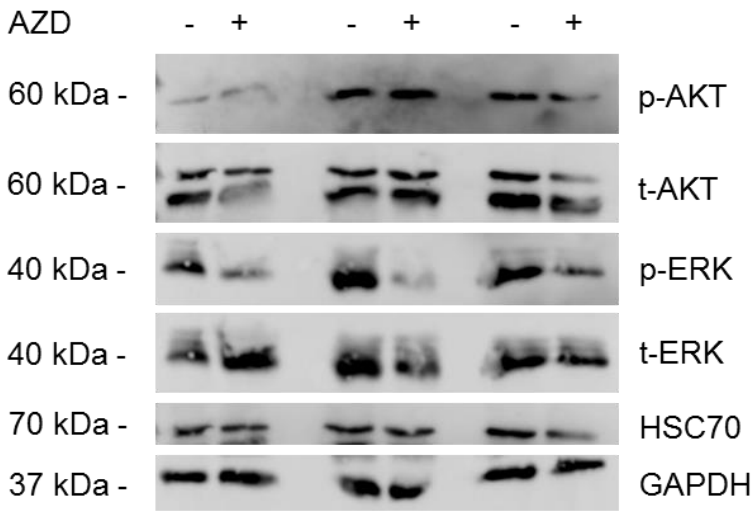

Appendix Figure 8.10. Protein expression levels of HFF2 cells treated with AZD.
HFF2 cells were seeded into 6-well plates and treated with 1µM AZD or vehicle for 72h. Protein was extracted and Western blot analysis was performed probing for p-AKT, t-AKT, p-ERK, t-ERK and loading controls GAPDH and HSC70. The blots represent three biological replicates.

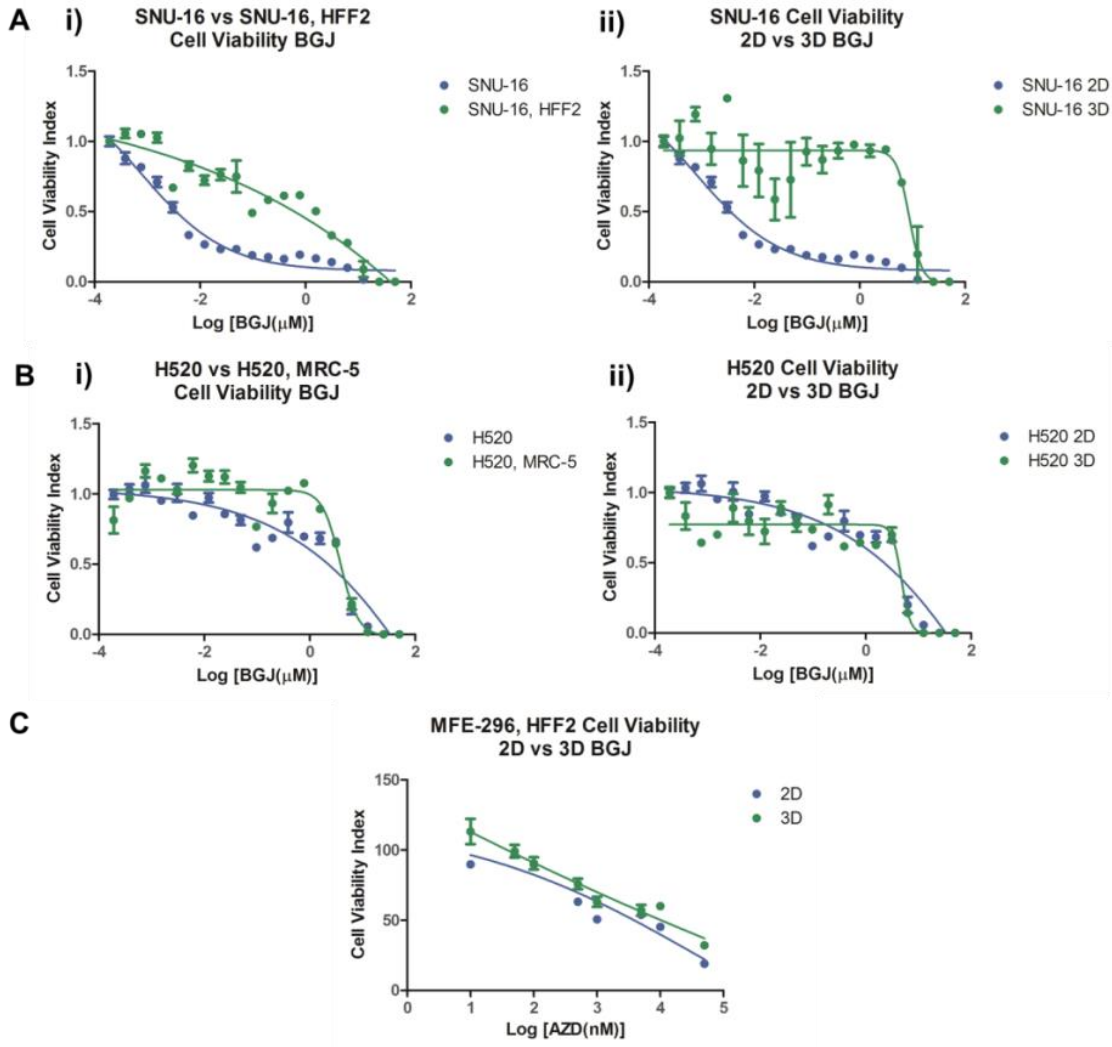

Appendix Figure 8.11. Comparison of cell survival of gastric, endometrial and lung cancer cells grown with and without stromal support and either in 2D or 3D.
Cells were seeded into 96-well plates and treated with increasing dosages of AZD or BGJ ranging from 0.006nM to 50μM and control cells were treated with DMSO and as a background control 1% Staurosporine was added to wells containing cells. After 72h incubation, MTS reagent was added and cell viability was measured colorimetrically after 2h. An average of three biological MTS experiments in technical triplicate is shown with error bars indicating SEM. Cell survival of gastric cancer cells SNU-16 **(A)** were compared to SNU-16 cells co-cultured with HFF2 cells **(i)** and to SNU-16 cells grown in 3D in Alvetex® 96-well plates **(ii)**. Cell survival of lung cancer cells H520 **(A)** were compared to H520cells co-cultured with MRC-5 cells **(i)** and to H520 cells grown in 3D in Alvetex® 96-well plates **(ii)**. Cell survival of co-cultured MFE-296 cells with HFF2 cells in 2D and 3D was compared **(C)**.

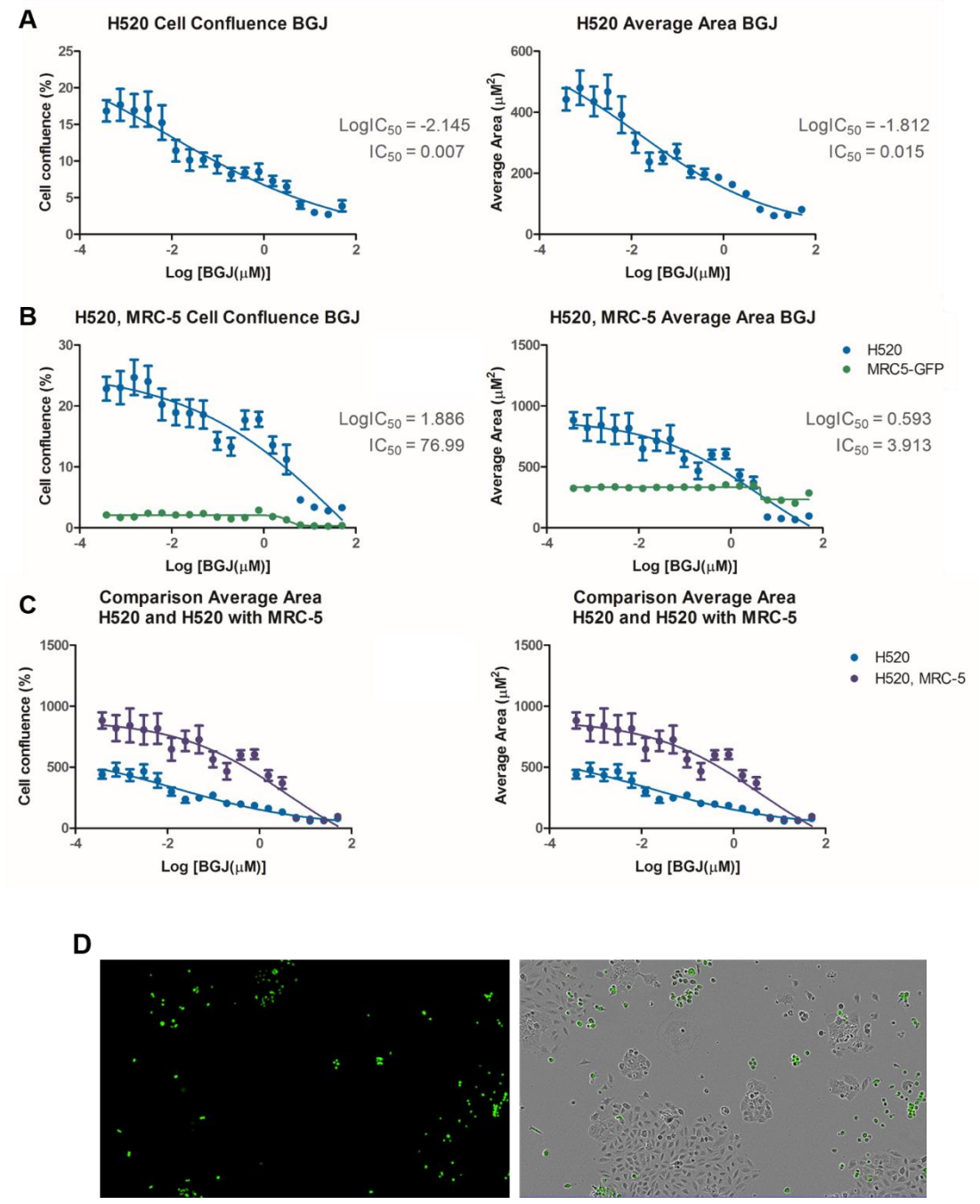

Appendix Figure 8.12. Cell confluence and area measured with IncuCyte™ ZOOM®.
H520 cells were grown alone **(A)** or in co-culture with MRC-5 fibroblasts **(B)** and imaged with IncuCyte™ ZOOM®. Comparison of cell confluence and average area of H520 cells alone, and H520 grown with MRC-5 cells **(C)**. Bright-field and fluorescence microscopy of co-cultured H520 and HFF2 cells **(D)**.

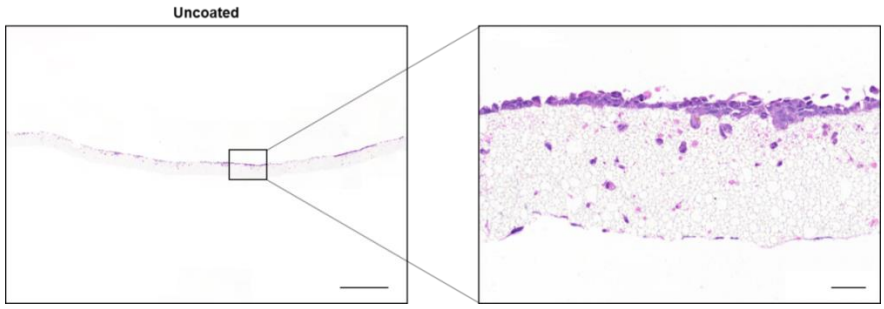

Appendix Figure 8.13. H&E staining of an uncoated 12 well insert Alvetex® Strata scaffold.
MFE-296 cells were seeded into a 12-well Alvetex® Strata insert and grown for one week. The whole scaffold scale bar indicates 2000µm and magnification scale bar indicates 100µm.

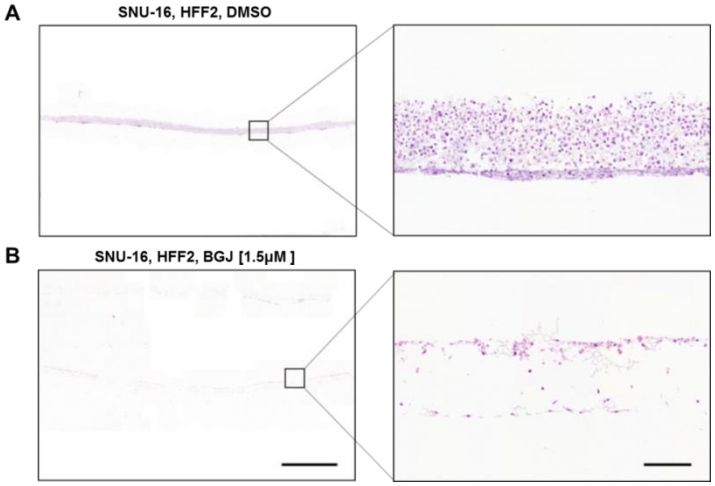

Appendix Figure 8.14. SNU-16 cells co-cultured with HFF2 cells in Alvetex® and treated with BGJ.
Additional replicate of H&E staining of SNU-16 cells co-cultured with HFF2 cells in Alvetex® scaffolds. The whole scaffold scale bar indicates 2000µm and the magnified image scale bar 100µm.

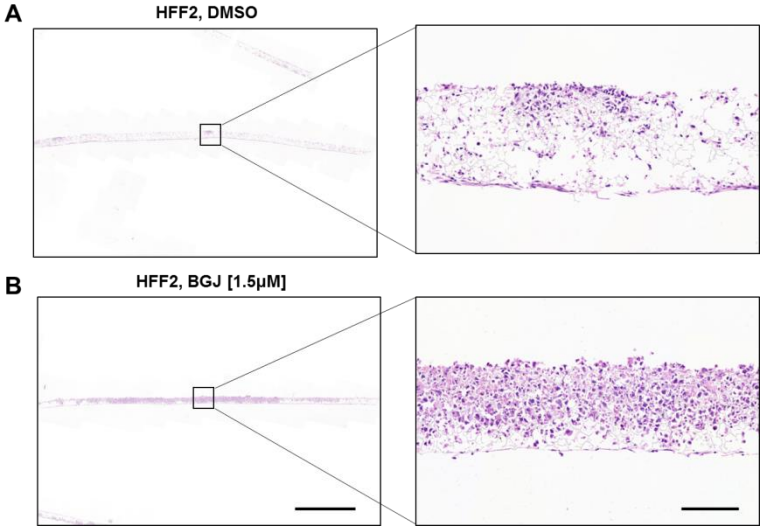

Appendix Figure 8.15. Fibroblasts cultured in Alvetex® and treated with BGJ.
Additional replicate of H&E staining of HFF2 cells in Alvetex® scaffolds. The whole scaffold scale bar indicates 2000µm and the magnified image scale bar 100µm.

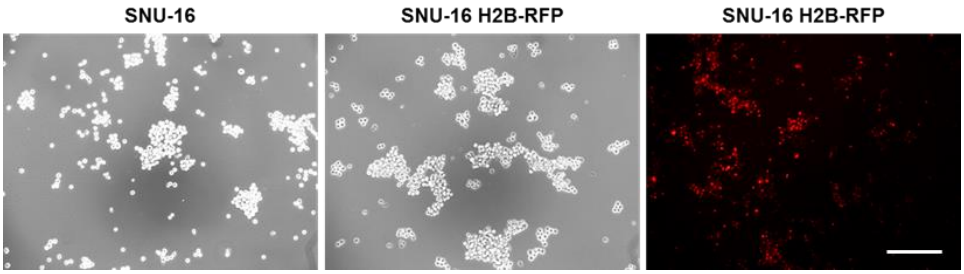

Appendix Figure 8.16. SNU-16 morphology or untreated and fluorescently-tagged SNU-16 cells using H2B-RFP.
SNU-16 cells were transduced with lentiviral particles containing an H2B-RFP tag and imaged with phase and fluorescence microscopy. The scale bar indicates 25µm.

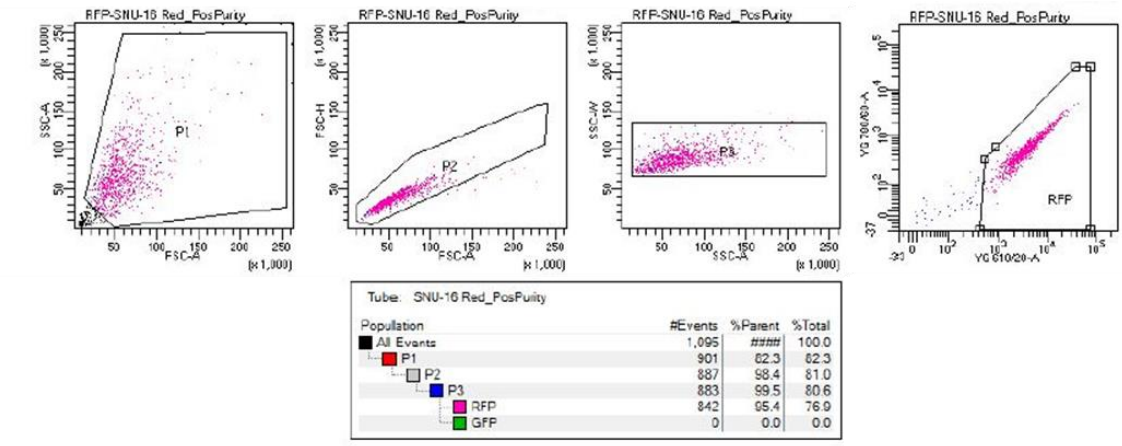

Appendix Figure 8.17. Cell sorting of H2B-positive SNU-16 cells.
H2B-RFP transduced SNU-16 cells were grown for 8 passages followed by cell sorting using FACS. P1 displays the selection of live cells and P2 and P3 were used to discriminate cell doublets. Then H2B-RFP positive cells were selected using channel YG610/20-A to detect RFP signal.

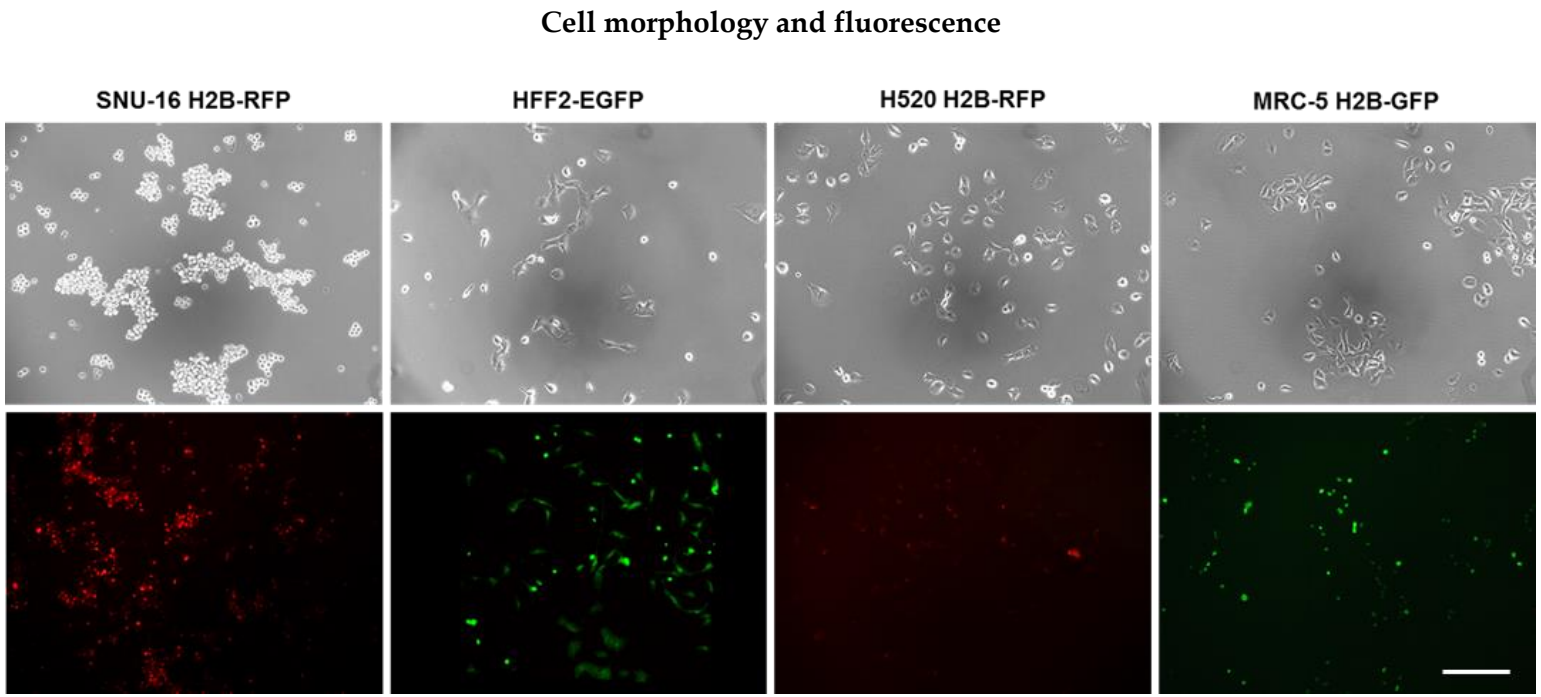

Appendix Figure 8.18. Fluorescent cells used in this thesis.
Cells were transduced with lentiviral supernatant containing the plasmid with the fluorescent markers (see section 2.2.17). For SNU-16 and H520 H2B-RFP and for MRC-5 H2B-GFP was used. For HFF2 cells, EGFP was used to generate fluorescent cells.

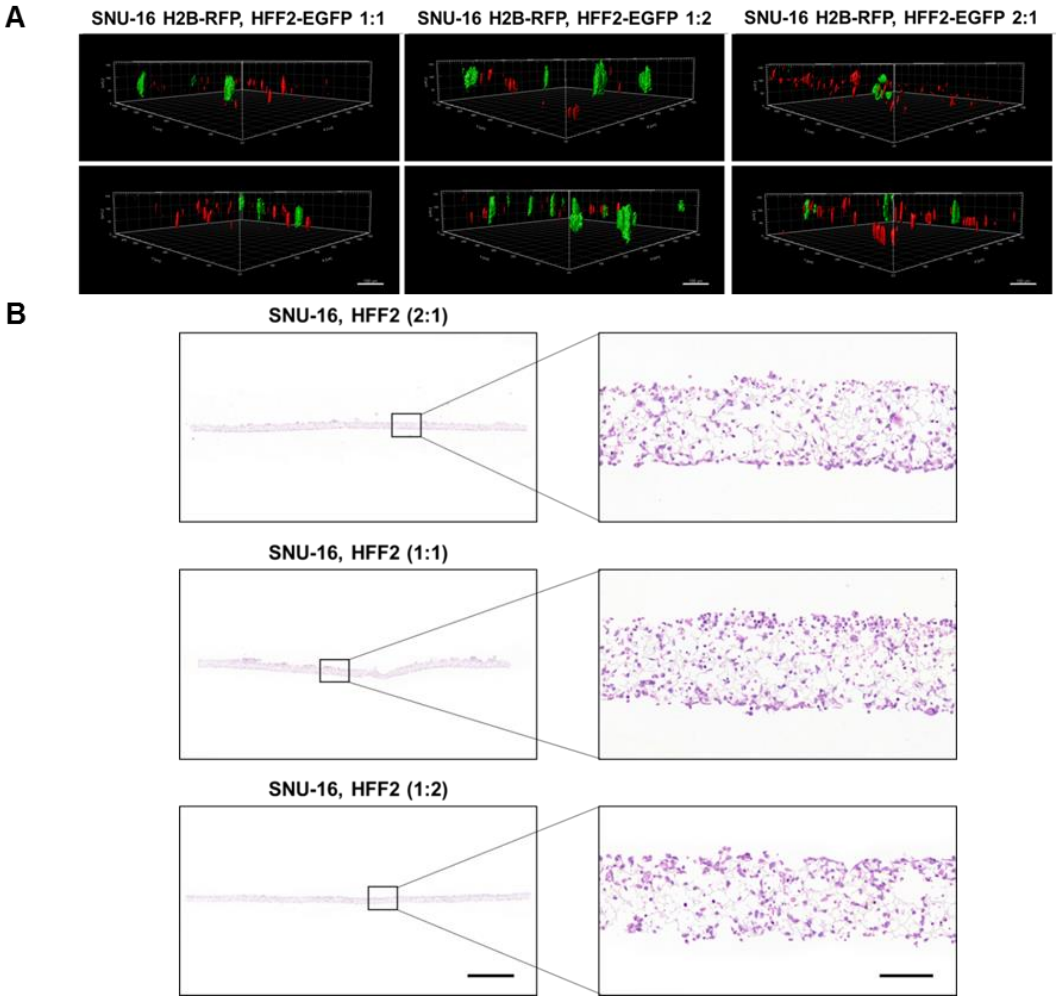

Appendix Figure 8.19. Co-culturing of SNU-16-H2B-RFP and HFF2-EGFP cells in Alvetex®. SNU-16 and HFF2 cells were seeded into 12-well Alvetex® scaffold inserts either 1:1, 1:2 or 2:1 and grown for one week, followed by microscopic image acquisition and 3D image rendering with Imaris **(A)**. The scale bar indicates 100µm. Simultaneouly, scaffolds were also fixed, paraffin-embedded and H&E stained **(B)**. The whole scaffold scale bar indicates 2000µm and the the scale bar in the enlarged image indicates 100µm.

8.2 Appendix Chapter IV Results Part II

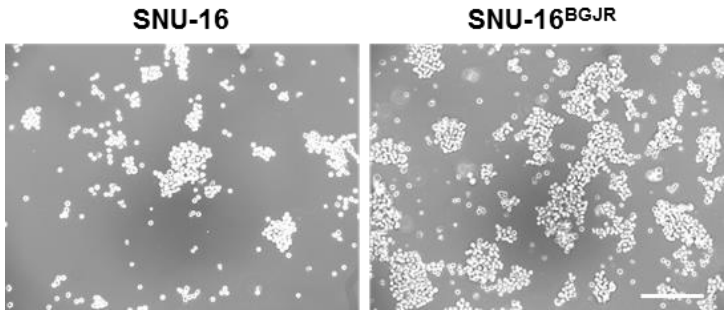

Appendix Figure 8.20. Morphology of parental SNU-16 and SNU-16^{BGJR} cells grown in 2D.
Bright-field acquisition of SNU-16 parental and SNU-16^{BGJR} cells. The scale bar indicates 25µm.

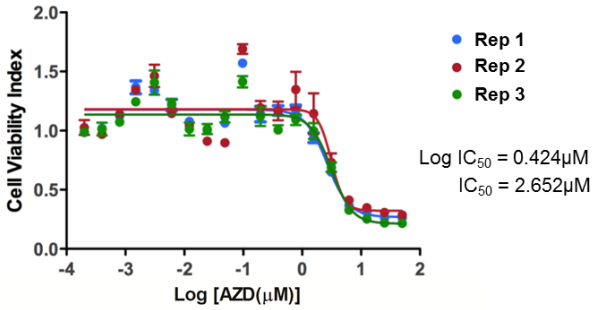

Appendix Figure 8.21. SNU-16^{BGJR} treated with AZD.
SNU-16^{BGJR} cells were seeded into 96-well plates and treated with increasing dosages of AZD ranging from 0.006nM to 50µM and control cells were treated with DMSO and as a background control 1% Staurosporine was added to wells containing cells. After 72h incubation, MTS reagent was added and cell viability was measured colorimetrically after 2h. An average of three biological MTS experiments in technical triplicate is shown with error bars indicating SEM. Log IC_{50} and IC_{50} values were calculated with GraphPad Prism 5.

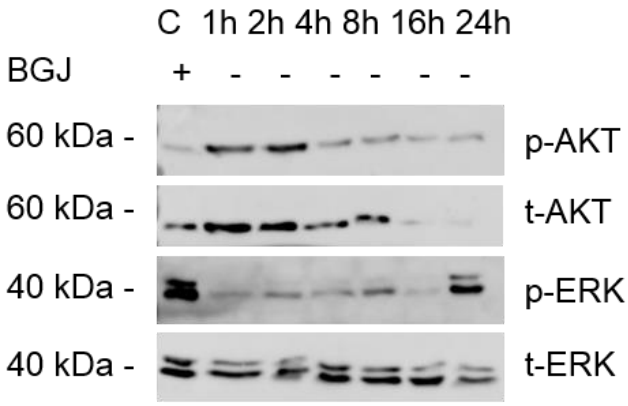

Appendix Figure 8.22. Removing drug from drug-resistant SNU-16 cells suggests cross-talk between ERK and AKT.
Additional replicate of SNU-16^{BGJR} cells were seeded into 6-well plates and drug was removed and cells were harvested after 1, 2, 4, 8, 16 and 24h. As a control cells were kept in medium containing BGJ. Protein was extracted and Western blot analysis was performed probing for p-AKT, t-AKT, p-ERK, and t-ERK.

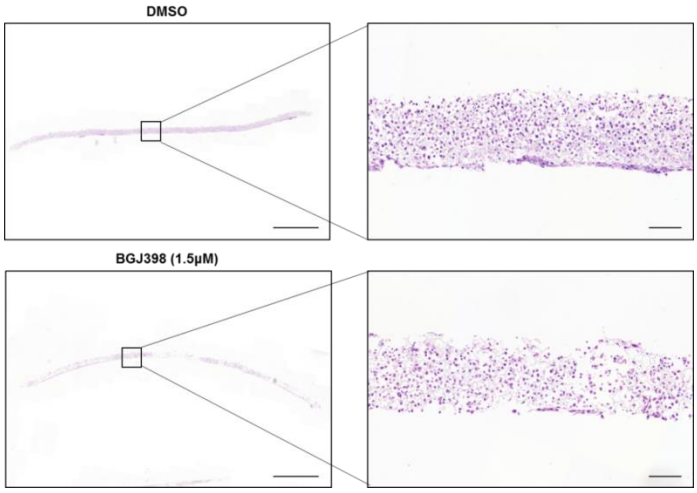

Appendix Figure 8.23. SNU-16^{BGJR} cells alone in Alvetex® grown for 7 days.
Additional replicate of drug-resistant SNU-16 cells seeded into a 12-well Alvetex® scaffolds and treated with 1.5µM BGJ for one week followed by formalin-fixation, paraffin-embedding and H&E staining. Scale bar indicates 1000µm in the left panel and 100µm in the enlarged panel.

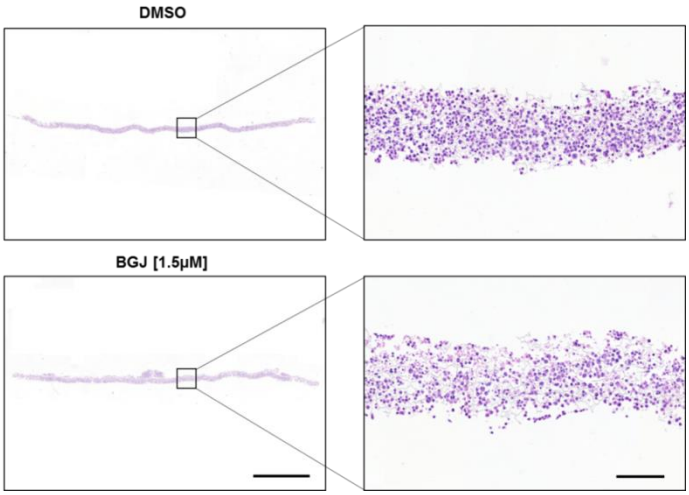

Appendix Figure 8.24. SNU-16^{BGJR} cells alone in Alvetex® grown for 7 days.
Additional replicate of drug-resistant SNU-16 cells seeded into a 12-well Alvetex® scaffolds and treated with 1.5µM BGJ for one week followed by formalin-fixation, paraffin-embedding and H&E staining. Scale bar indicates 1000µm in the left panel and 100µm in the enlarged panel.

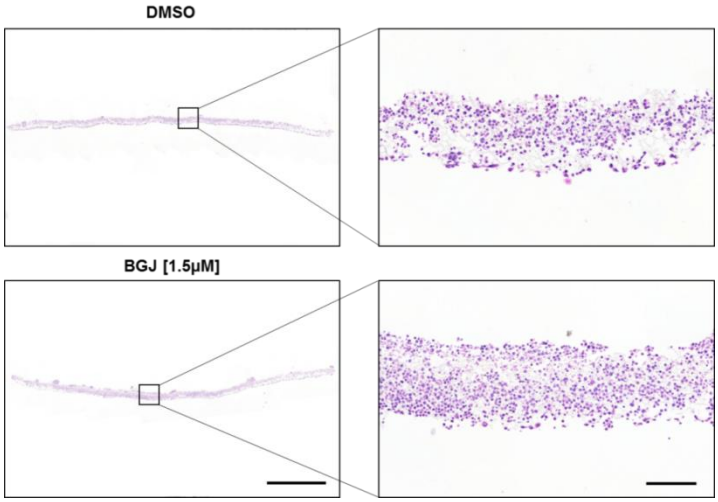

Appendix Figure 8.25. BGJ-resistant cells with fibroblasts.
SNU-16^{BGJR} cells and HFF2 cells were mixed 2:1 and were seeded into 12-well insert Alvetex® scaffolds and incubated overnight. The cells were grown in the scaffolds for 1 week. Medium containing 1.5μM BGJ was fed from below and exchanged every 2 days. The experiment was performed in triplicate. Scale bar indicates 1000μm in the left panel and 100μm in the enlarged panel.

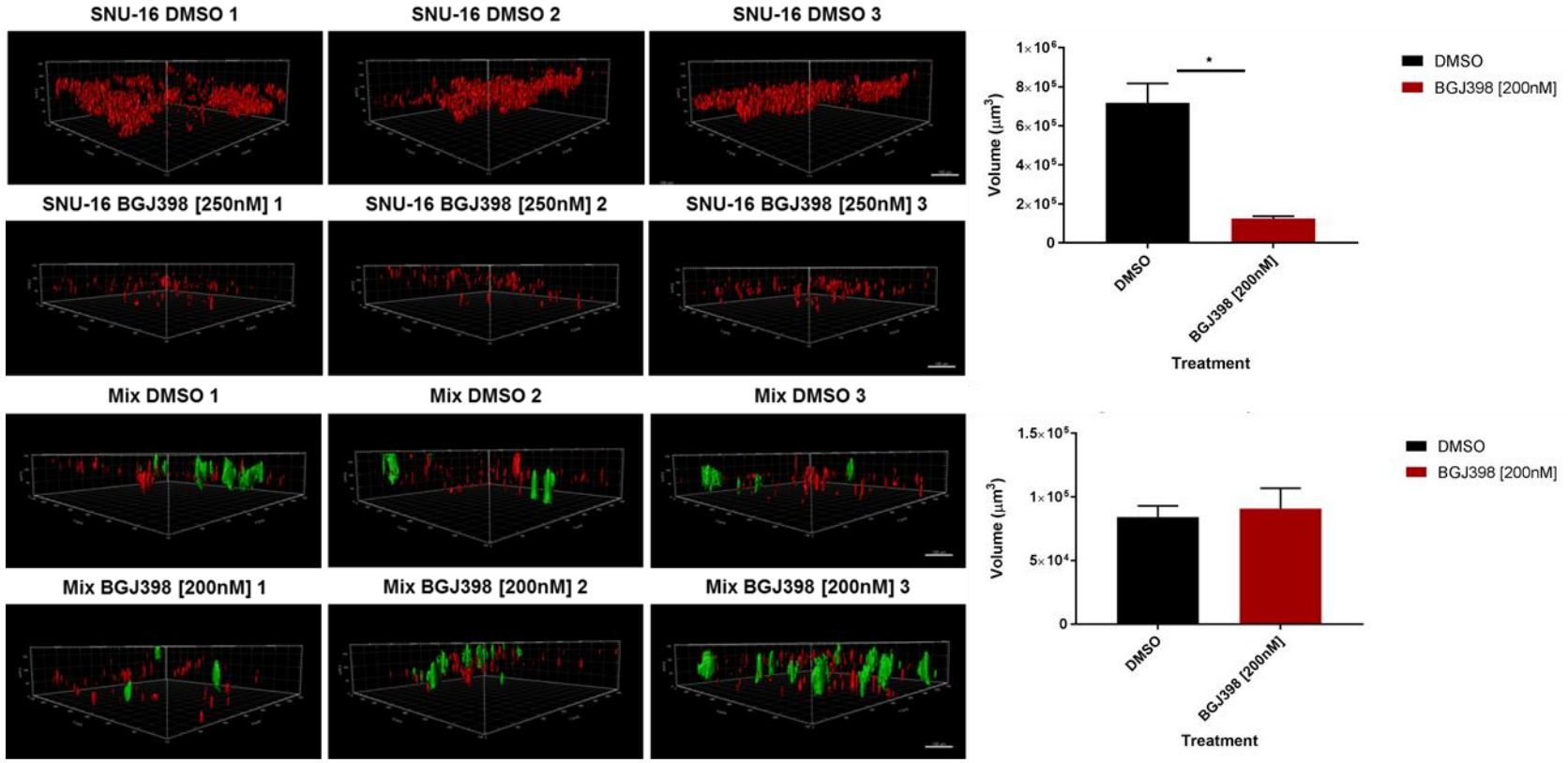

Appendix Figure 8.26. Imaris rendered images of 3D resistance assay in Alvetex® of week 1.
The experiment was performed in biological and technical triplicate. Per condition three images were taken using a confocal microscope. Scale bar indicates 100µm.

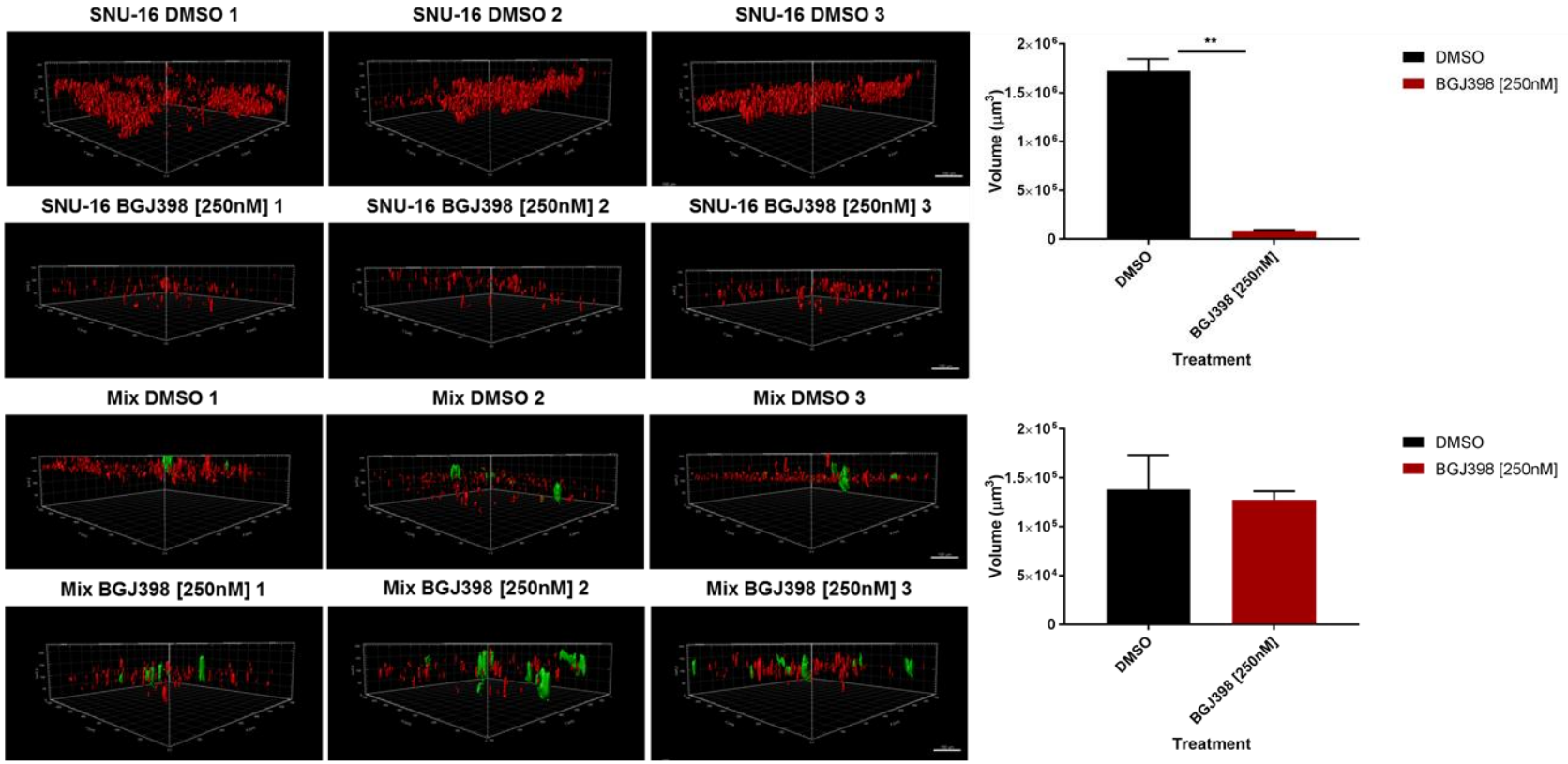

Appendix Figure 8.27. Imaris rendered images of 3D resistance assay in Alvetex® of week 2.
The experiment was performed in biological and technical triplicate. Per condition three images were taken using a confocal microscope. Scale bar indicates 100µm.

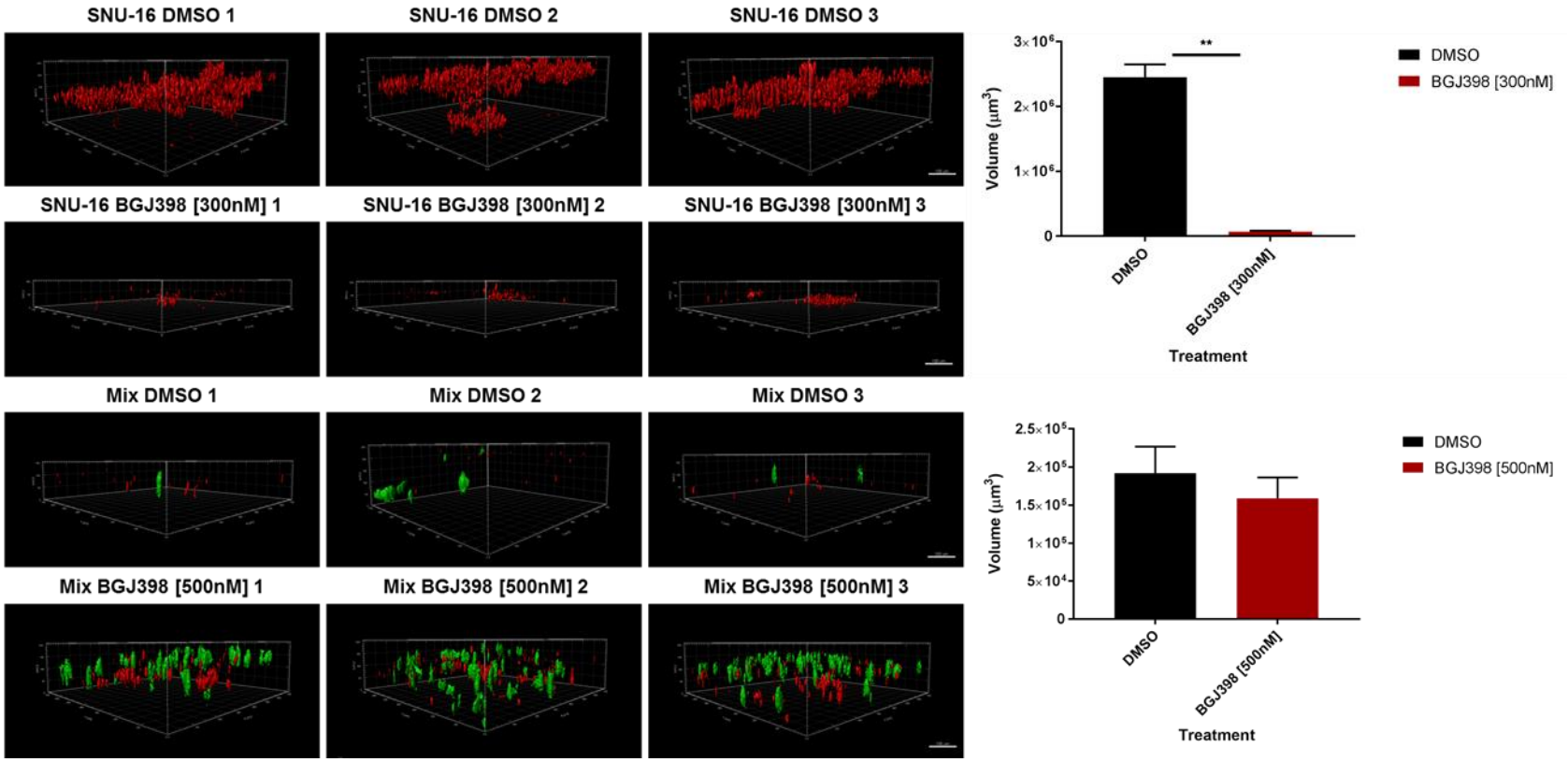

Appendix Figure 8.28. Imaris rendered images of 3D resistance assay in Alvetex® of week 3.
The experiment was performed in biological and technical triplicate. Per condition three images were taken using a confocal microscope. Scale bar indicates 100µm.

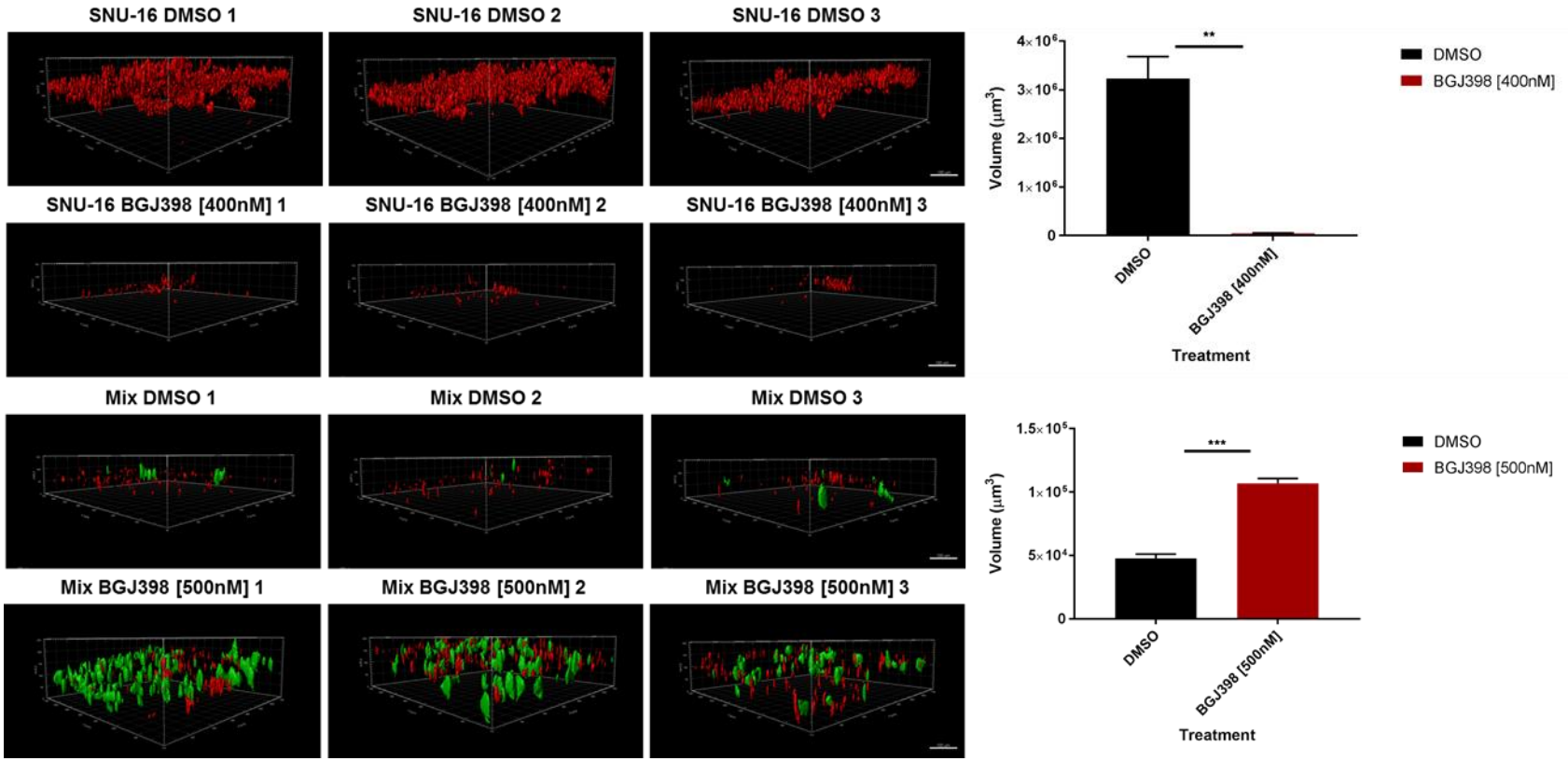

Appendix Figure 8.29. Imaris rendered images of 3D resistance assay in Alvetex® of week 4.
The experiment was performed in biological and technical triplicate. Per condition three images were taken using a confocal microscope. Scale bar indicates 100µm.

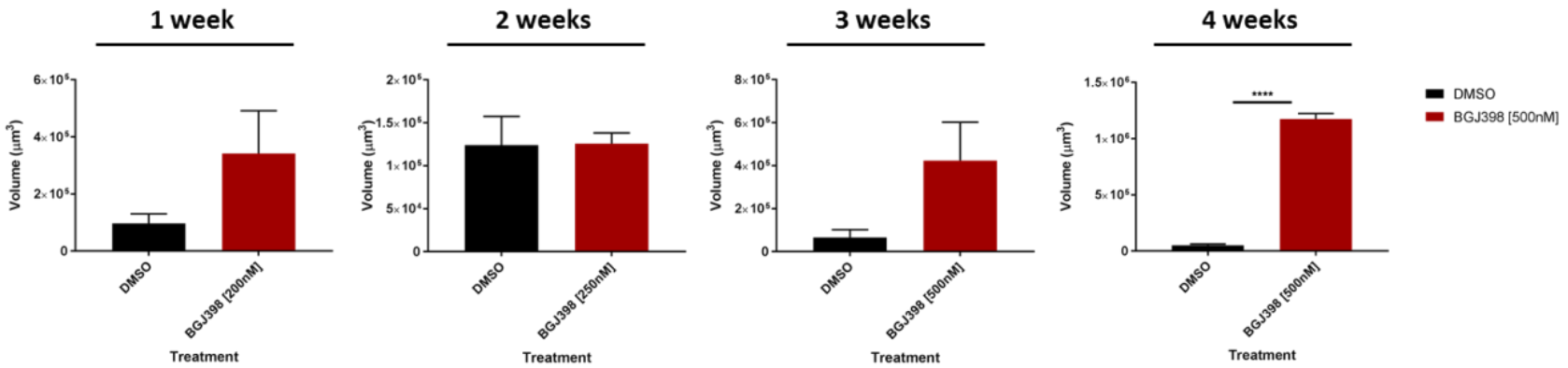

Appendix Figure 8.30. Cell volume measurements of HFF2 cells in co-culture with SNU-16 cells rendered resistant in Alvetex®.
Volume changes of HFF2 cells grown together in co-culture with SNU-16 cells in Alvetex® were measured over four weeks.

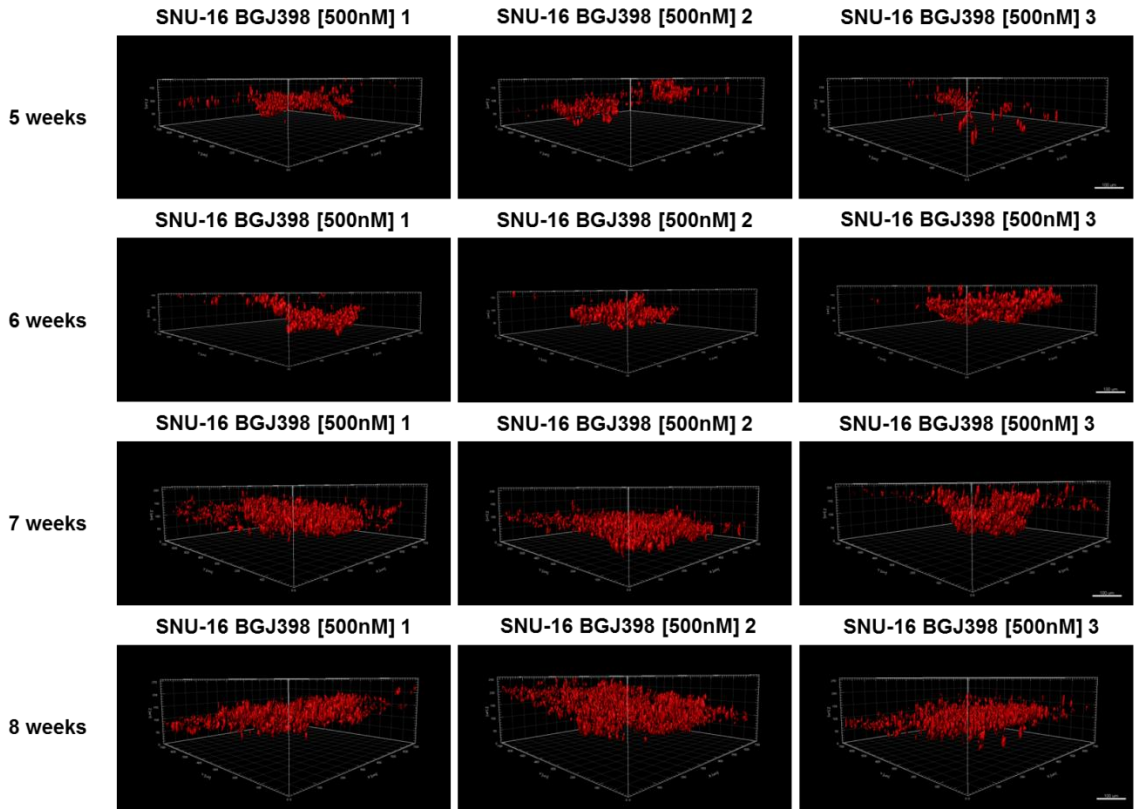

Appendix Figure 8.31. Imaris rendered images of 3D resistance assay in Alvetex® of week 5, 6, 7 and 8.
The experiment was performed in biological and technical triplicate. Per condition three images were taken using a confocal microscope. Scale bar indicates 100µm.

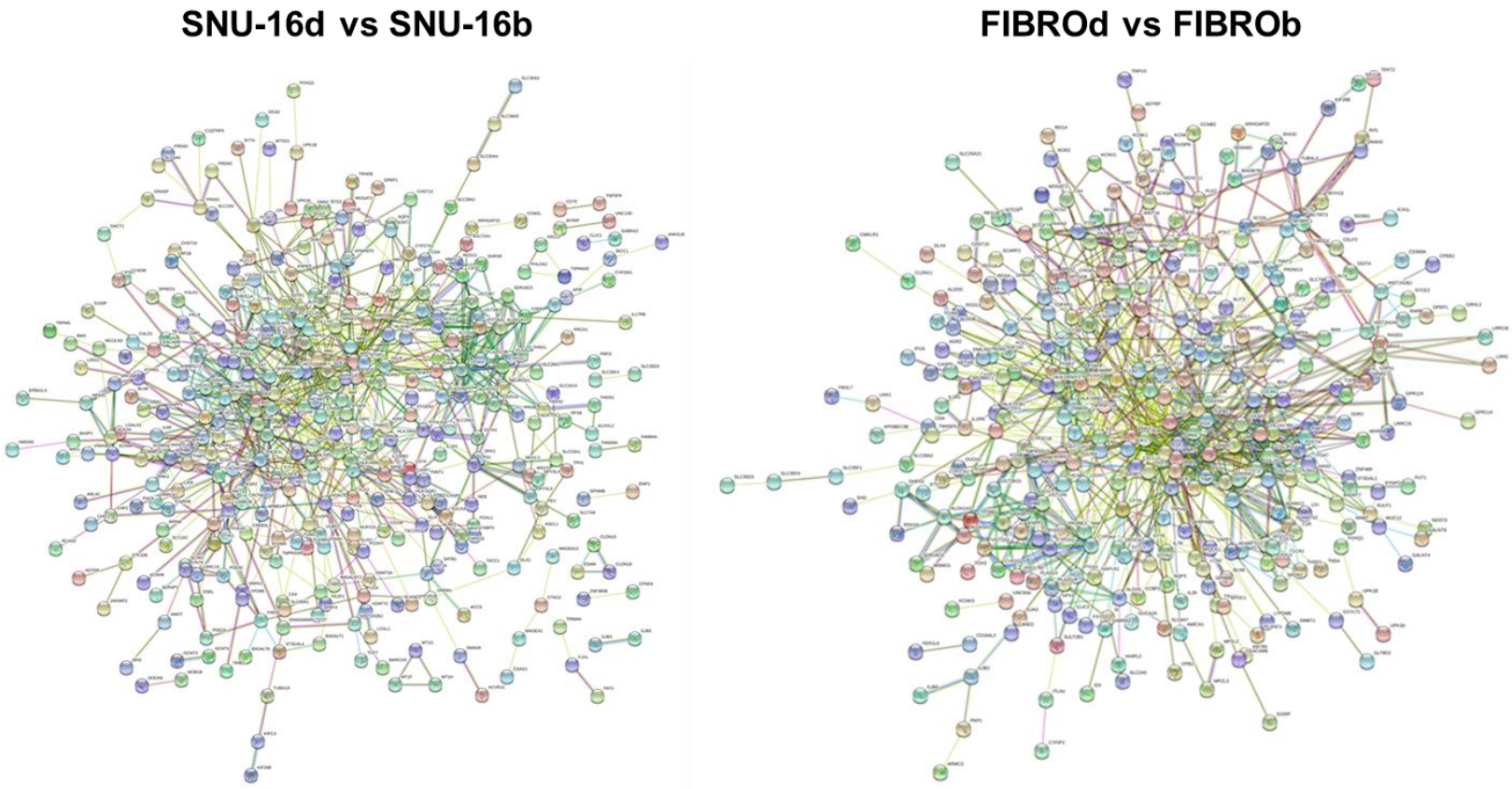

Appendix Figure 8.32. STRING networks ofSNU-16 (SdvsSb) and Co-culture cells (FdvsFb),
Significantly regulated genes (Log fold change >2, <-2) were analysed and network interactions displayed.

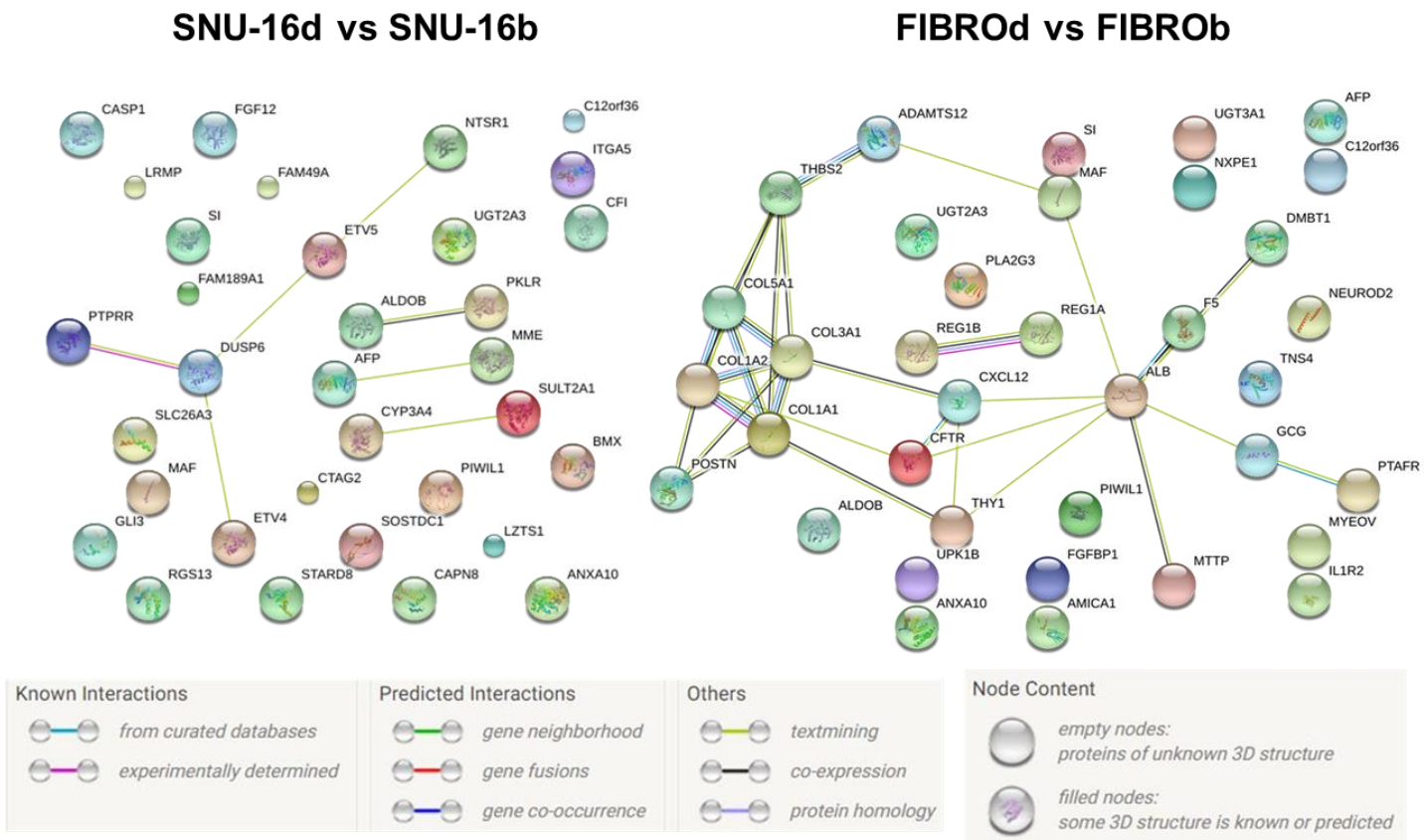

Appendix Figure 8.33. STRING networks.
STRING networks of top 20 up and downregulated genes in SNU-16^{BGJR} compared to parental SNU-16 and Co-culture^{BGJR} compared to parental co-culture cells.

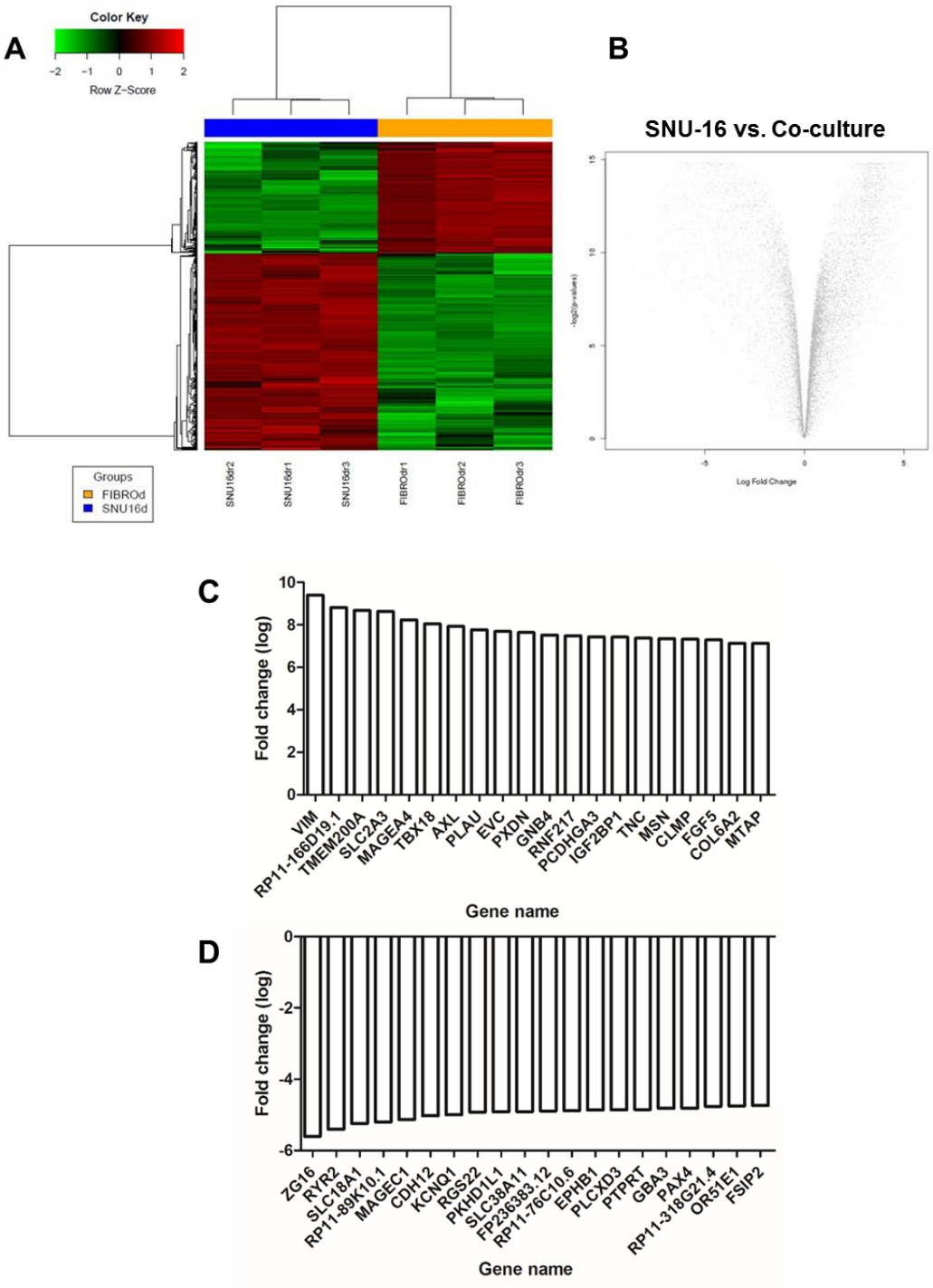

Appendix Figure 8.34. Top 20 targets upregulated in BGJ-resistant co-culture cells compared to BGJ-resistant SNU-16 in Alvetex® (other comparison).
Top 20 targets downregulated in BGJ398-resistant co-culture cells compared to BGJ-resistant SNU-16 in Alvetex®. Among the 2480 genes, 1591 genes were upregulated in SNU16d and 889 genes were upregulated in FIBROd.

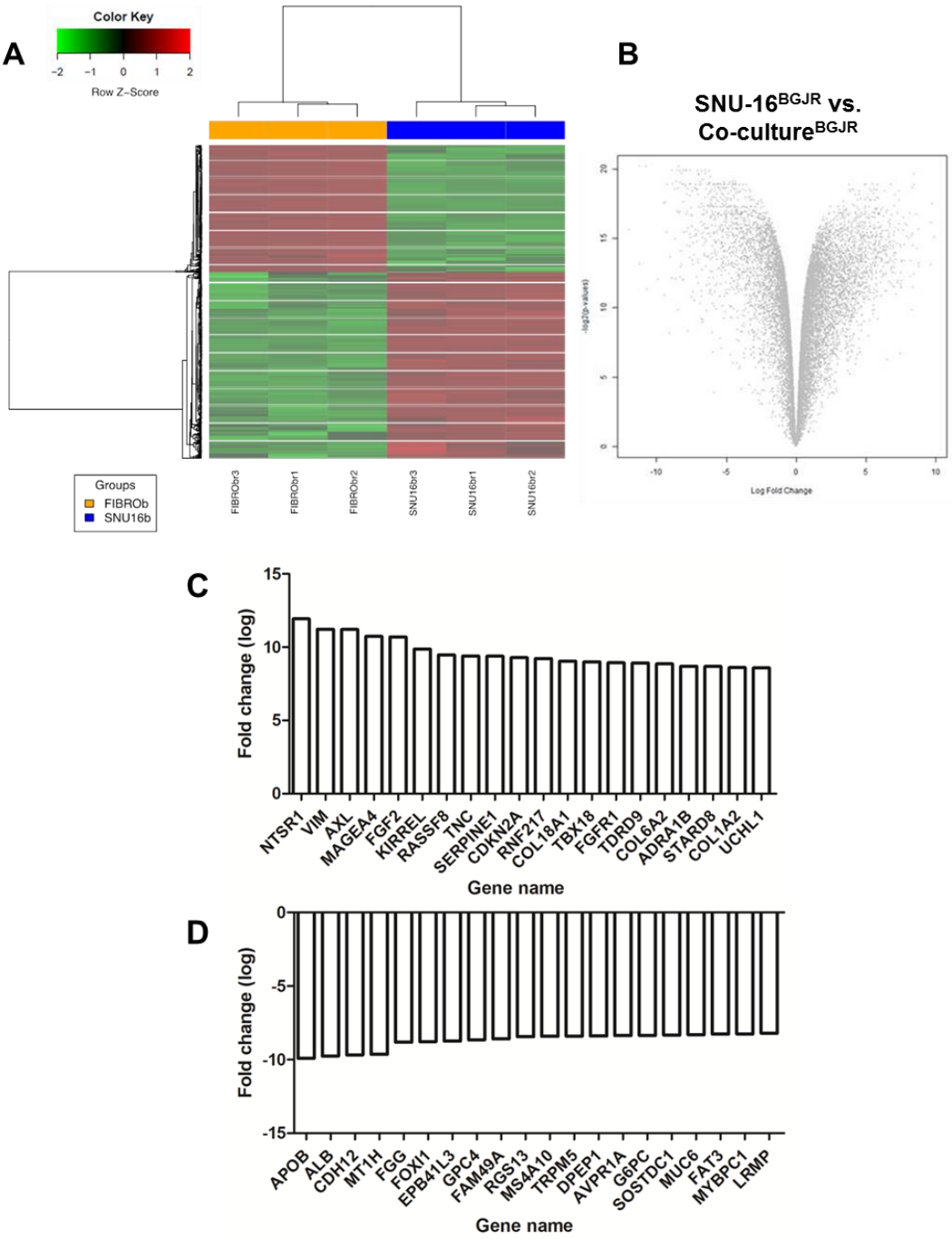

Appendix Figure 8.35. Top 20 target upregulated in SNU-16 gastric cancer cells treated with BGJ over 8 weeks in Alvetex®.

Top 20 targets Downregulated in SNU-16 gastric cancer cells treated with BGJ over 8 weeks in Alvetex®. Among the 3413 genes, 2028 genes were upregulated in SNU16b and 1385 genes were upregulated in FIBRObr.

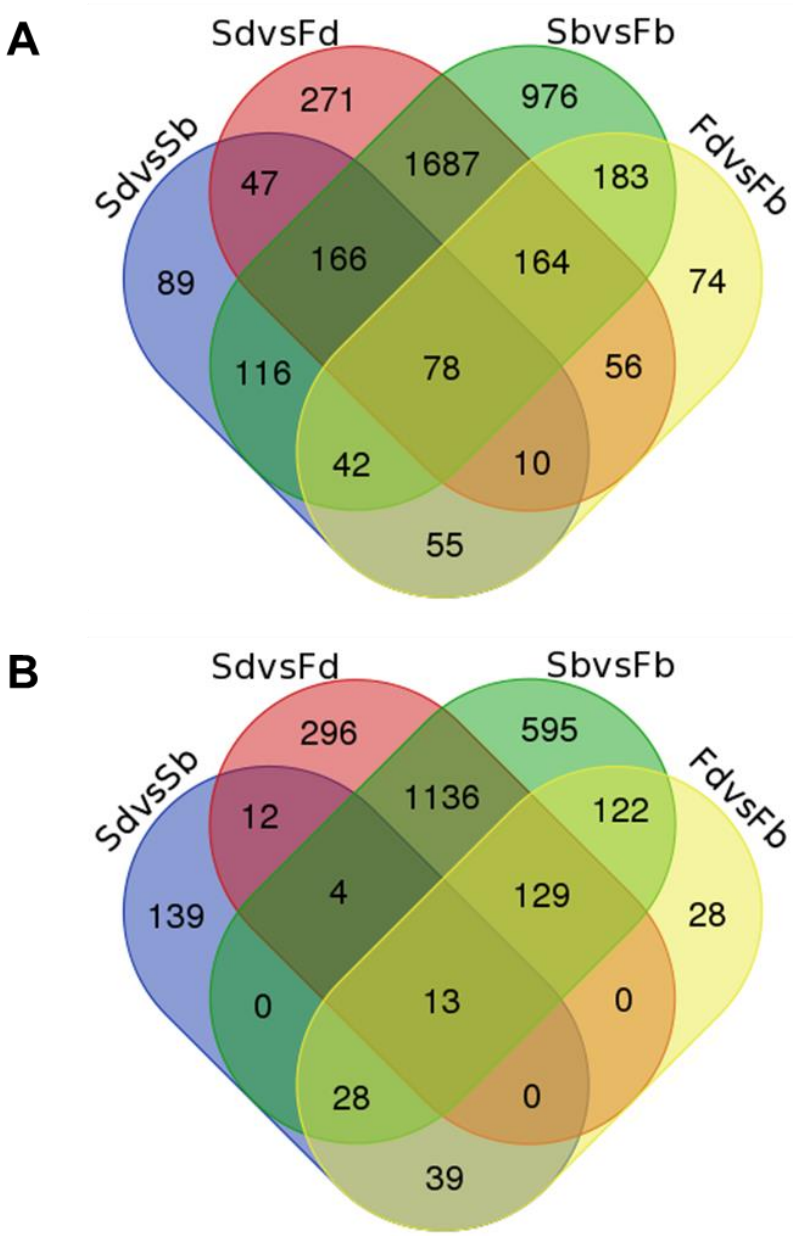

Appendix Figure 8.36. Comparison of all datasets from differential gene expression analysis.
(A) Comparison of all genes from all datasets that were compared to each other, where 78 genes where shared between all datasets. **(B)** Comparison of all significantly regulated genes from all datasets that were compared to each other, where 13 genes where shared between all datasets. SdvsSb = DMSO-treated SNU-16 cells compared to BGJ-treated SNU-16 cells, SdvsFb = DMSO-treated SNU-16 cells compared to BGJ-treated co-culture cells, SbvsFb = BGJ-treated SNU-16 compared to BGJ-treated co-culture cells, FdvsFb = DMSO-treated co-culture cells compared to BGJ-treated co-culture cells.

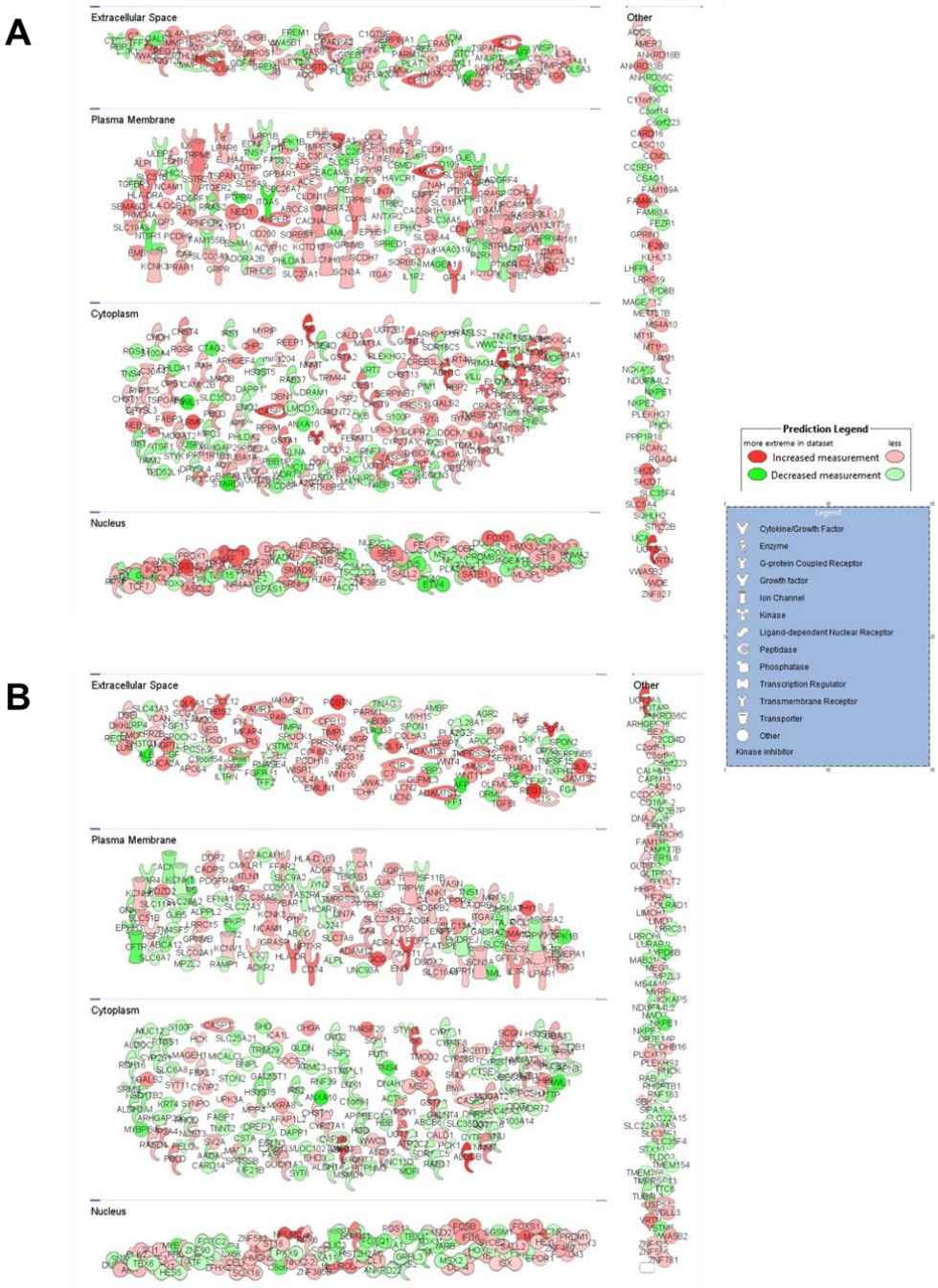

Appendix Figure 8.37. Spatial information of up- and downregulated genes.
(A) Location of significantly regulated genes of SNU-16^{BGJR} cells compared to parental cells. **(B)** Location of significantly regulated genes of co-culture^{BGJR} cells compared to parental cells. Red indicates upregulation and green downregulation. The intensity of the colour represents the extent of regulation. The shape of the protein depicts the different classes of proteins to which the genes belong.

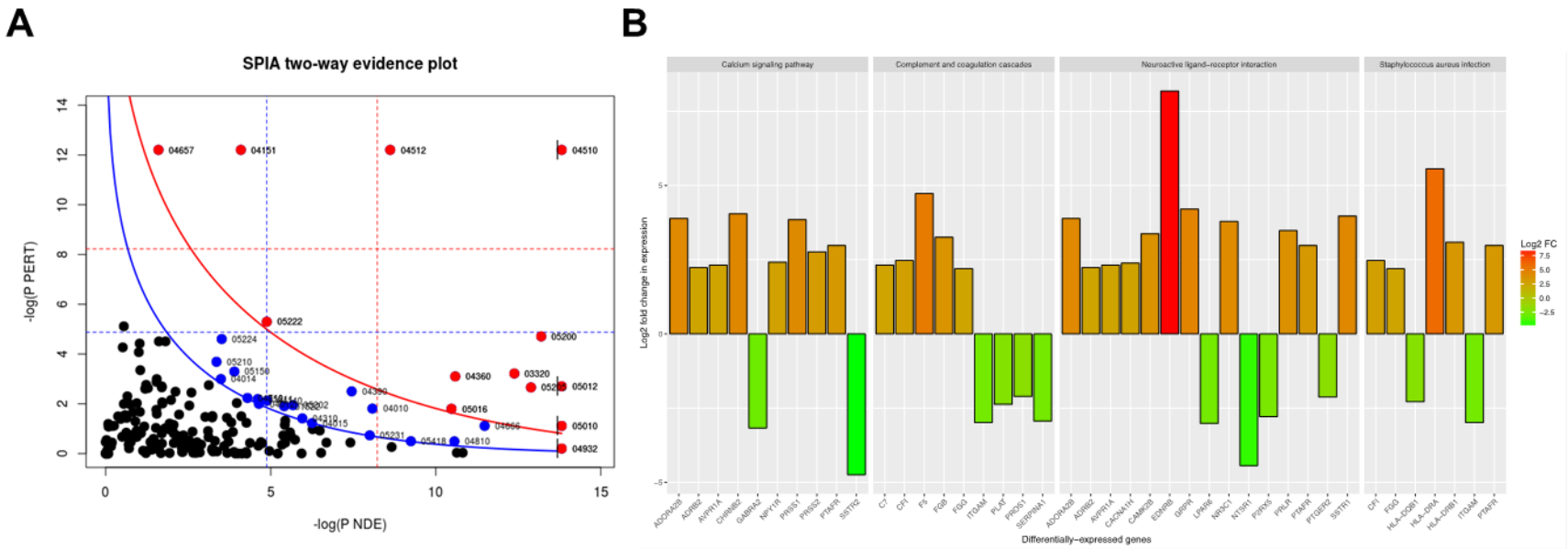

Appendix Figure 8.38. SPIA plot of regulated pathways and differential gene expression analysis.
Pathway analysis was also performed with Signaling Pathway Impact Analysis (SPIA) using a Bioconductor package in R, showing significantly regulated pathways ($p<0.05$, red line). This method combines the evidence obtained from classical enrichment analysis with a novel type of evidence, which includes the actual perturbation on a given pathway under a given condition (Tarca et al., 2009).

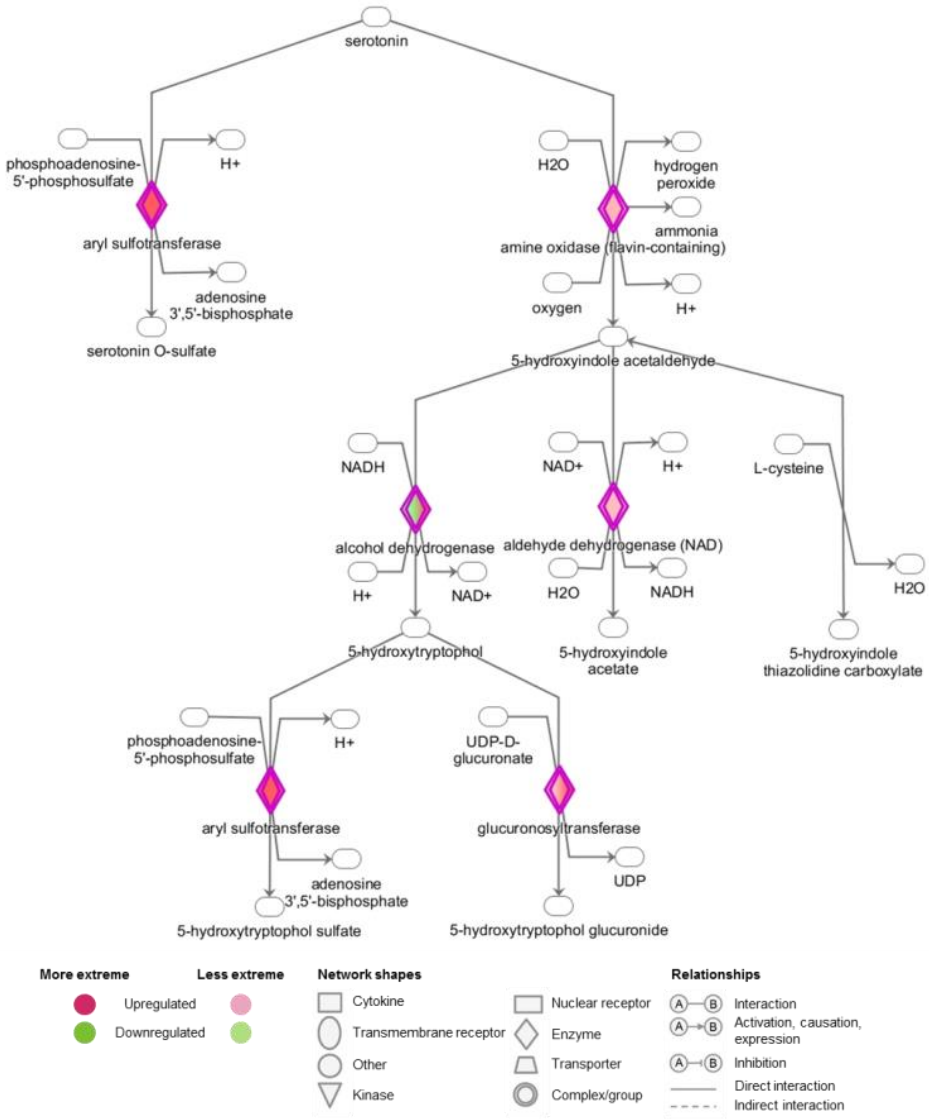

Appendix Figure 8.39. Serotonin degradation in SNU-16 and co-culture cells.
The serotonin pathway is driven by the upregulation of aryl sulfotransferase, amine oxidase, aldehyde dehydrogenase and glucuronyltransferase.

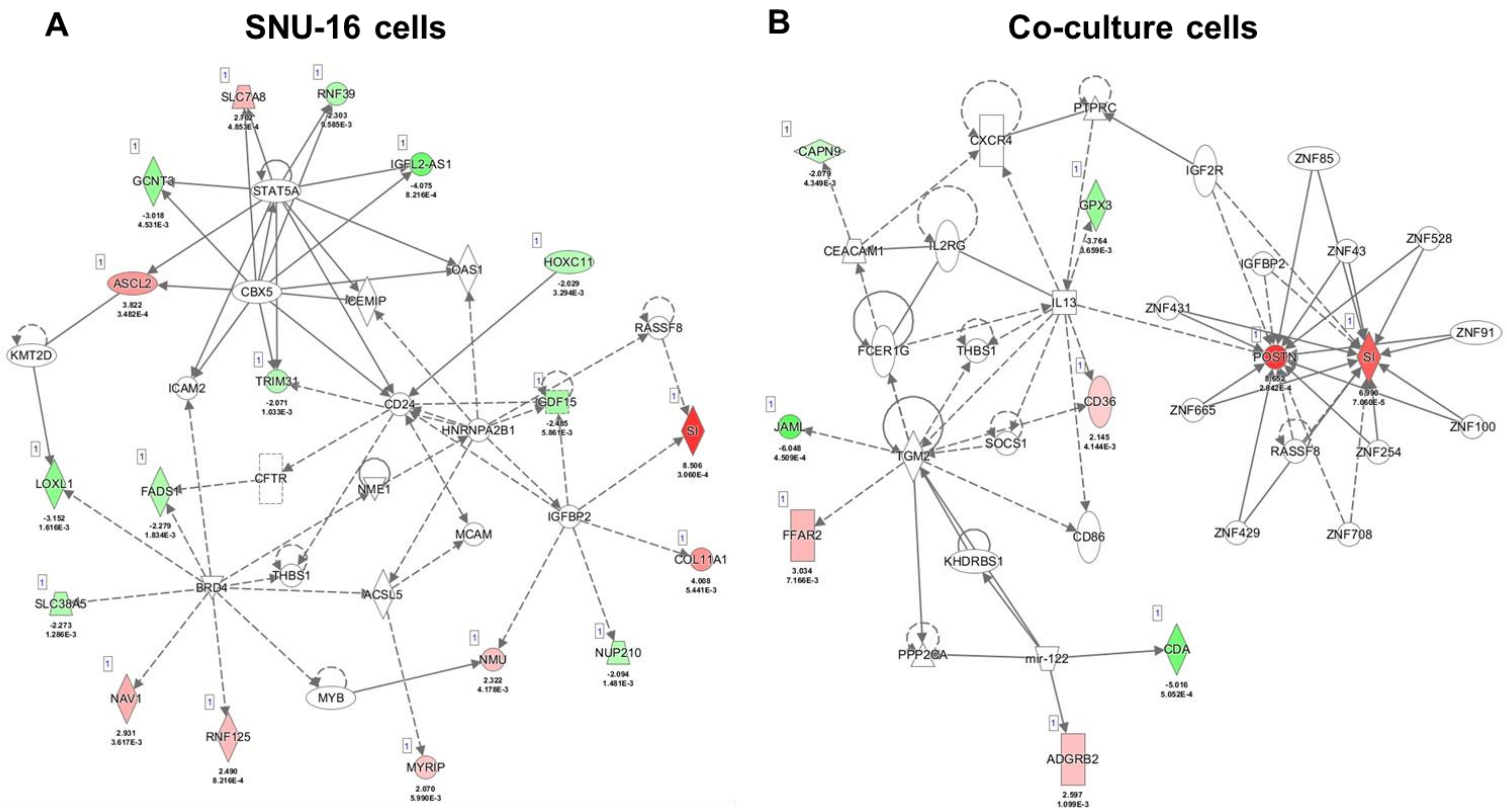

Appendix Figure 8.40. SI interaction network in SNU-16^{BGJR} cells compared to parental SNU-16 cells.
From the significantly regulated genes in the gene expression analysis of SNU-16 cells against SNU-16^{BGJR} generated in Alvetex®, SI was isolated and an interaction map created using IPA. The shape of the protein categorises the gene into functional classes and the strength of the colour indicates up- (red) or downregulation (green).

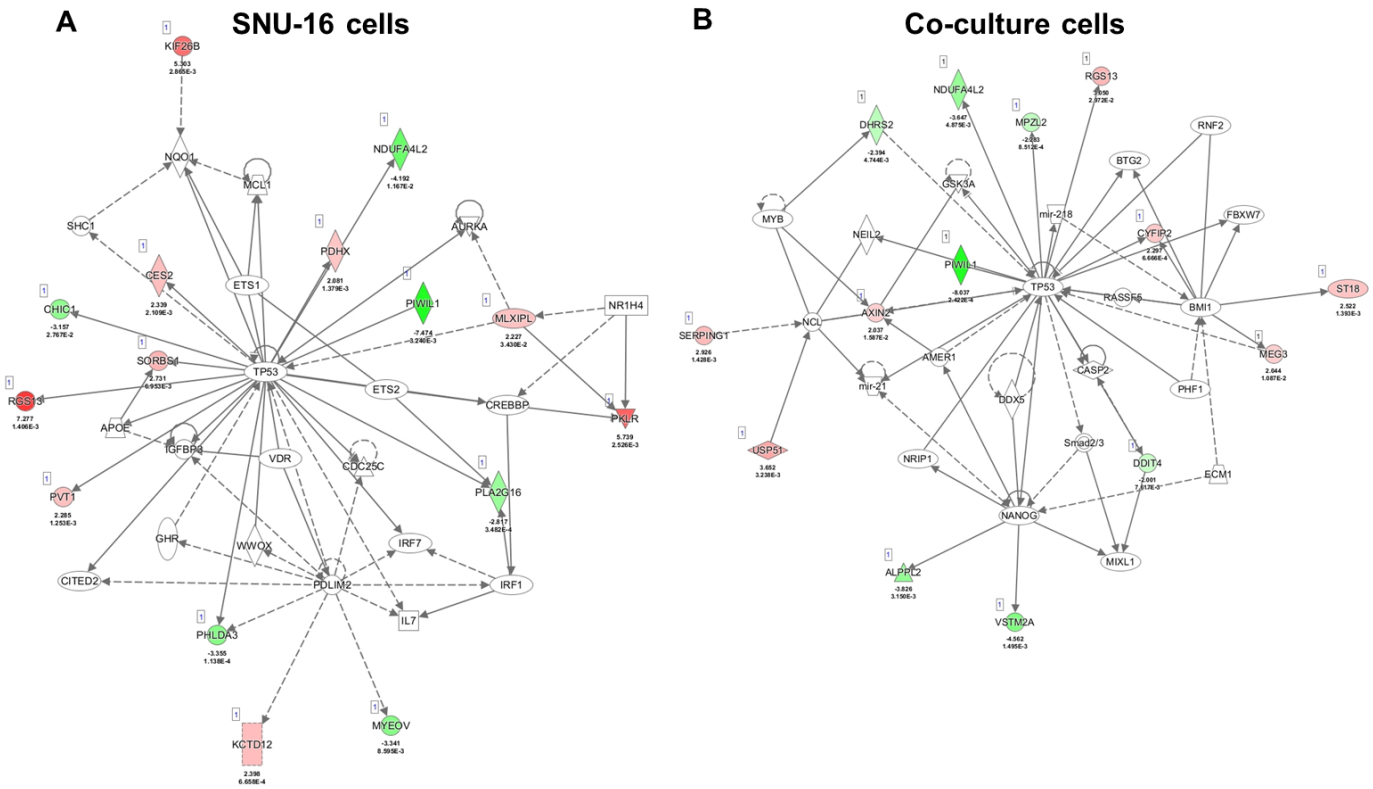

Appendix Figure 8.41. PIWIL1 interaction network in SNU-16BGJR cells compared to parental SNU-16 cells.
From the significantly regulated genes in the gene expression analysis of SNU-16 cells against SNU-16^{BGJR} generated in Alvetex®, PIWIL1 was isolated and an interaction map created using IPA. The shape of the protein categorises the gene into functional classes and the strength of the colour indicates up- (red) or downregulation (green).

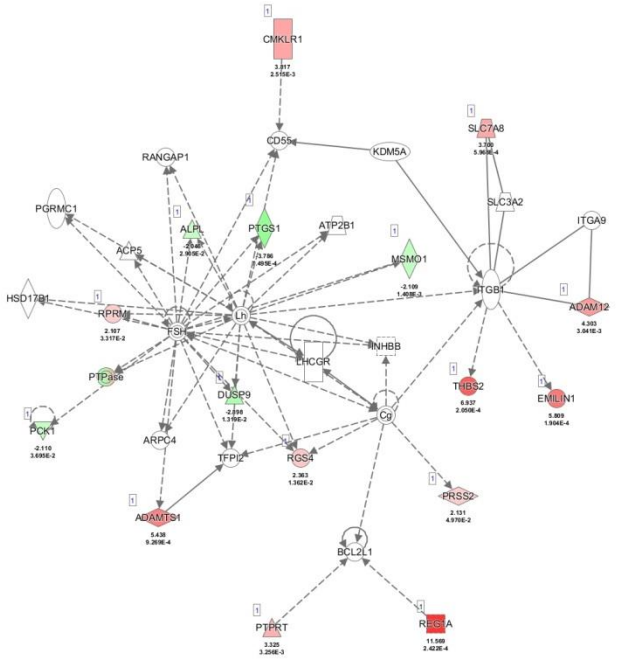

Appendix Figure 8.42. REG1A interaction network in co-culture cells.
From the significantly regulated genes in the gene expression analysis of SNU-16 cells against SNU-16^{BGJR} generated in Alvetex®, REG1A was isolated and an interaction map created using IPA. The shape of the protein categorises the gene into functional classes and the strength of the colour indicates up- (red) or downregulation (green).

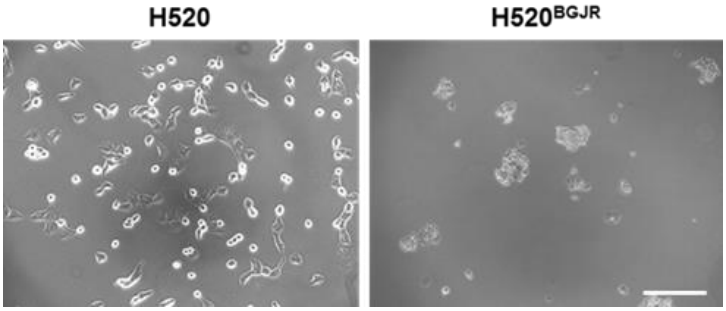

Appendix Figure 8.43. *FGFR1*-amplified lung cancer.
Phase contrast image of H520 cells untreated, with lentiviral transfection and BGJ-resistant H520 cells. The scale bar indicates 25µm.

Appendix Table 8.1. Count files of RNA-Seq reads mapped to hg38.
Paired end reads and alignment and percentage of reads for gene quantification.
FIBROb=Co-culture treated with BGJ, FIBROd=Co-culture treated with DMSO, SNU16b=SNU-16 treated with BGJ, SNU16d=SNU-16 treated with DMSO.

	Total number paired end reads	Number of paired-end reads uniquely aligned to gene features	Percentage of reads used for gene quantification
FIBRObr1	32249015	24296659	75.34
FIBRObr2	31648117	20705563	65.42
FIBRObr3	28494183	18771410	65.88
FIBROdr1	39770923	26322042	66.18
FIBROdr2	36439322	23520509	64.55
FIBROdr3	40377416	26462316	65.54
SNU16br1	37497647	24093113	64.25
SNU16br2	36080060	21702294	60.15
SNU16br3	31914026	21417907	67.11
SNU16dr1	32216061	21156983	65.67
SNU16dr2	32371589	22055306	68.13
SNU16dr3	35026685	23163878	66.13

Appendix Table 8.2. Gene names, aliases and function of the top 5 upregulated targets of SNU-16 cells treated with BGJ.

Gene name	Aliases	Function
SI	Sucrase isomaltase	• Expressed in foetal life • Glucosidase enzyme (breaking down carbohydrates) ultimately leading to ATP • Type II transmembrane glycoprotein (C-term in lumen) • Intestinal enzyme located on brush border of small intestine • Not expressed in normal gastric mucosa, SI mutations in CLL • Colon oncofoetal antigen → enterocytic differentiation (Cross and Quaroni, 1991; Ellis et al., 1992; Iannettoni et al., 1996; Lojda and Fric, 1996; Mehdawi et al., 2016)
ALDOB	Aldolase, Fructose-Bisphosphate B	• Conversion of fructose-1,6-bisphosphate to glyceraldehydes-3-phosphate • Plays a key role in both glycolysis and gluconeogenesis. (Glucose → pyruvate) • Cancer 200 fold glycolytic rates (He et al., 2016; Peng et al., 2008; Tao et al., 2015)
BMX	Cytoplasmic tyrosine-protein kinase BMX	• Non-receptor tyrosine kinase, which may play a role in the growth and differentiation of hematopoietic cells • Transfer a phosphate group from ATP to a protein • Induce activation of the Stat signalling pathway • Anti-apoptotic downstream effector of PI3K (Peng et al., 2016; Potter et al., 2016, 2014; Wei et al., 2017)
UGT2A3	UDP glucuronosyltransferase family 2 member A3	• Catalyse phase II biotransformation reactions in which lipophilic substrates are conjugated with glucuronic acid to increase water solubility and enhance excretion • Elimination of potentially toxic xenobiotics and endogenous compounds (Kurita et al., 2017)
RGS13	Regulator of G-Protein 13	• Suppresses the immunoglobulin E-mediated allergic responses • Accelerate GTPase activity of G protein alpha-subunits, thereby driving G protein into their inactive GDP-bound form, thus negatively regulating G protein signalling • Nuclear repressor of CREB (Han et al., 2006; Sethakorn and Dulin, 2013; Wang et al., 2010; Xie et al., 2008)

Appendix Table 8.3. Gene names, aliases and function of the top 5 downregulated targets of SNU-16 cells treated with BGJ.

Gene name	Full name	Function
PIWIL1	Piwi-like RNA-mediated gene silencing 1	• PIWI subfamily of Argonaute proteins • Containing both PAZ and Piwi motifs that play important roles in stem cell self-renewal, RNA silencing, and translational regulation in diverse organisms • Intrinsic regulator of the self-renewal capacity of germline and hematopoietic stem cells (Cao et al., 2016; Chen et al., 2015; Iliev et al., 2016; Van Tongelen et al., 2017)
H19	Imprinted maternally expressed transcript	• Long non-coding RNA • Role in negative regulation of body weight and cell proliferation • Only transcribed from maternally inherited allele (Lv et al., 2017; Zhang et al., 2017; Zhao et al., 2017)
AFP	Alpha-fetoprotein	• Glycoprotein, plasma protein in yolk sac and liver • Foetal form of serum albumin • Binds copper, nickel, fatty acids, bilirubin (D'Ambrosio et al., 2017; Sasaki et al., 2011)
STARD8	StAR related lipid transfer domain containing 8	• Rho GTPase-activating protein (GAP) • Expression inhibits the growth of human breast and prostate cancer cells in culture • Protein is expressed in tissues throughout the body, but is absent or reduced in many kinds of tumour cells (Braun and Olayioye, 2015; Durkin et al., 2007; Mokarram et al., 2009)
FGF12	Fibroblast growth factor 12	• Broad mitogenic and cell survival activities, and are involved in a variety of biological processes, including embryonic development, cell growth, morphogenesis, tissue repair, tumour growth, and invasion (Volkomorov et al., 2013)

Appendix Table 8.4. Gene names, aliases and function of the top 5 upregulated targets of co-culture cells treated with BGJ.

Gene name	Full name	Function
REG1A	Lithostathine-1-alpha also known as islet cells regeneration factor (ICRF) or islet of Langerhans regenerating protein (REG)	• multi protein family grouped into four subclasses, types I, II, III and IV based on the primary structures of the proteins • secreted by exocrine pancreas • contain a C-lectin domain (Aboshanif et al., 2016; Geng et al., 2017; Hara et al., 2015; Wakita et al., 2015)
REG1B	Lithostathine-1-alpha also known as islet cells regeneration factor (ICRF) or islet of Langerhans regenerating protein (REG)	type I subclass of the REG family of genes (Liu et al., 2015; Usami et al., 2010)
ALDOB	See above	
COL3A1	Collagen alpha-1(III) chain	• precursor to collagen III • connected to Ehlers-Danlos syndrome and aortic arterial aneruysms (Januchowski et al., 2016; Wang et al., 2016)
POSTN	Periostin	• ligand for alpha-V/beta-3 and alpha-V/beta-5 integrins to support adhesion and migration of epithelial cells • secreted extracellular matrix protein • from the mesenchymal lineage • EMT • binds to integrins on cancer cells, activating the AKT/PKB-and FAK-mediated signalling pathways (Liu et al., 2017; Nitsche et al., 2016; Oh et al., 2017)

Appendix Table 8.5 Gene names, aliases and function of the top 5 downregulated targets of co-culture cells treated with BGJ.

Gene name	Full name	Function
AFP	alpha-fetoprotein See above	
ALB	Albumin	• in human blood • produced in liver • transports hormones, fatty acids and other compounds, buffer pH and maintains oncotic pressure • transports drugs as well • down-regulated in inflammatory state (Alfarouk et al., 2015; Merlot et al., 2014)
ANXA10	Annexin A10	• calcium-dependent phospholipid-binding proteins • associated with vascular invasion (Liu et al., 2002)
PIWIL1	See above	
UPK1B	Uroplakin 1B	• transmembrane 4 superfamily, also known as the tetraspanin family • cell-surface proteins (Olsburgh et al., 2003)

Appendix Table 8.6. Diseases identified with the DAVID database using OMI.
Significantly regulated genes (>-2, >2), **(A)** SNU-16 cells and **(B)** co-culture cells.

A

Diseases term	Genes	p-value
Diabetes mellitus, noninsulin-dependent	4 (0.7%)	0.004
Multiple sclerosis, susceptibility to, 1	2 (0.4%)	0.055
Pancreatitis, hereditary	2 (0.4%)	0.055
Hypofibrinogenemia, congenital	2 (0.4%)	0.055
Dysfibrinogenemia, congenital	2 (0.4%)	0.081
Afibrinogenemia, congenital	2 (0.4%)	0.081
Fraser syndrome	2 (0.4%)	0.081

B

Diseases term	Genes	p-value
Diabetes mellitus, noninsulin-dependent	3 (0.5%)	0.039
Osteogenesis imperfecta, type II	2 (0.3%)	0.052
Osteogenesis imperfecta, type IV	2 (0.3%)	0.052
Multiple sclerosis, susceptibility, to1	2 (0.3%)	0.052
Osteogenesis imperfecta, type III	2 (0.3%)	0.052

Appendix Table 8.7. Diseases identified with the DAVID database using all genes in the datasets.
SNU-16 cells and **(B)** co-culture cells.

A

Diseases term	Genes	p-value
Mitochondrial complex I deficiency	16 (0.1%)	0.003
Mitochondrial complex I deficiency	9 (0.1%)	0.033
Leukaemia, acute myeloid	11 (0.1%)	0.036
Gastric cancer, somatic	8 (0.1%)	0.056
Breast cancer susceptibility	8 (0.1%)	0.056
Colorectal cancer, somatic	13 (0.1%)	0.072

B

Diseases term	Genes	p-value
Mitochondrial complex I deficiency	16 (0.1%)	0.003
Mitochondrial complex IV deficiency	9 (0.1%)	0.033
Leukaemia, acute myeloid	11 (0.1%)	0.036
Breast cancer	8 (0.1%)	0.056
Gastric cancer (somatic)	8 (0.1%)	0.056
Colorectal cancer (somatic)	13 (0.1%)	0.072

Appendix Table 8.8. KEGG in DAVID looking at all genes of SNU-16 cells alone and co-culture cells.

Pathway name	Genes	p-value
Metabolic pathways	986 (7%)	<0.001
Cell cycle	120 (0.8%)	<0.001
Spliceosome	126 (0.9%)	<0.001
Endocytosis	225 (1.6%)	<0.001
Protein processing in endoplasmic reticulum	154 (1.1%)	<0.001
Ubiquitin mediated proteolysis	126 (0.9%)	<0.001
Ribosome	124 (0.9%)	<0.001
Biosynthesis of antibiotics	180 (1.3%)	<0.001
Lysosome	109 (0.8%)	<0.001
Pancreatic cancer	63 (0.4%)	<0.001

8.3 Appendix chapter IX Results part III

8.3.1 Retinol pathway

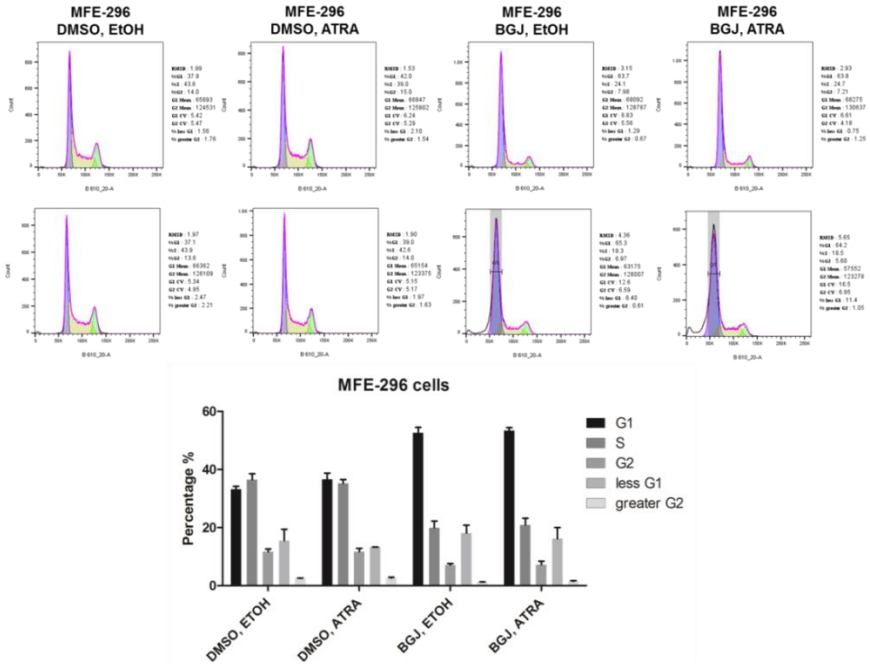

Appendix Figure 8.44. MFE-296 cells treated with ATRA and BGJ.
Additional replicates and inclusion of all cells in the analysis. The error bars indicate SEM.

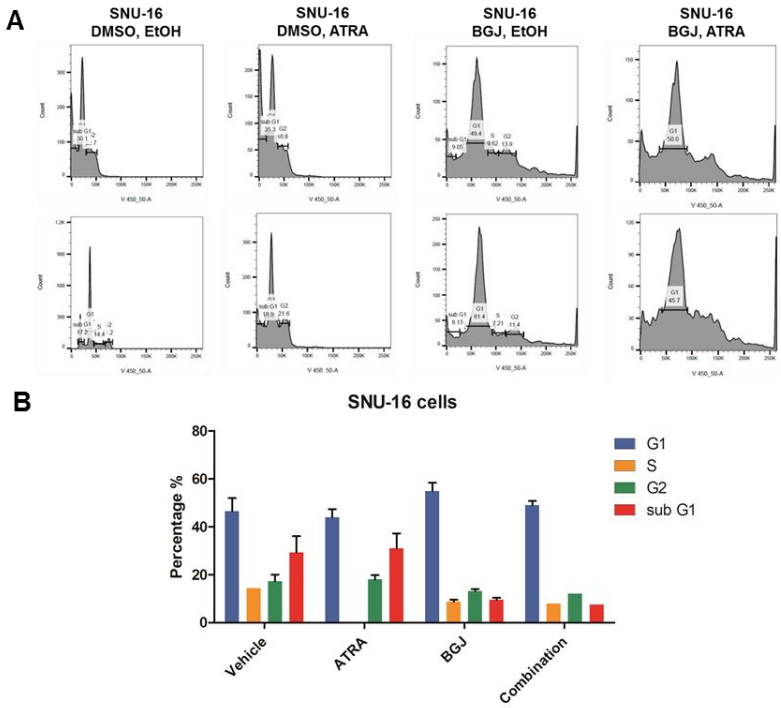

Appendix Figure 8.45. SNU-16 cells treated with ATRA.
SNU-16 cells were seeded into 6 well-plates and and treated with vehicle, ATRA, BGJ or a combination of ATRA and BGJ. After 72h cells were harvested and stained with DAPI and cell cycle was analysed using FACS. The error bars indicate SEM.

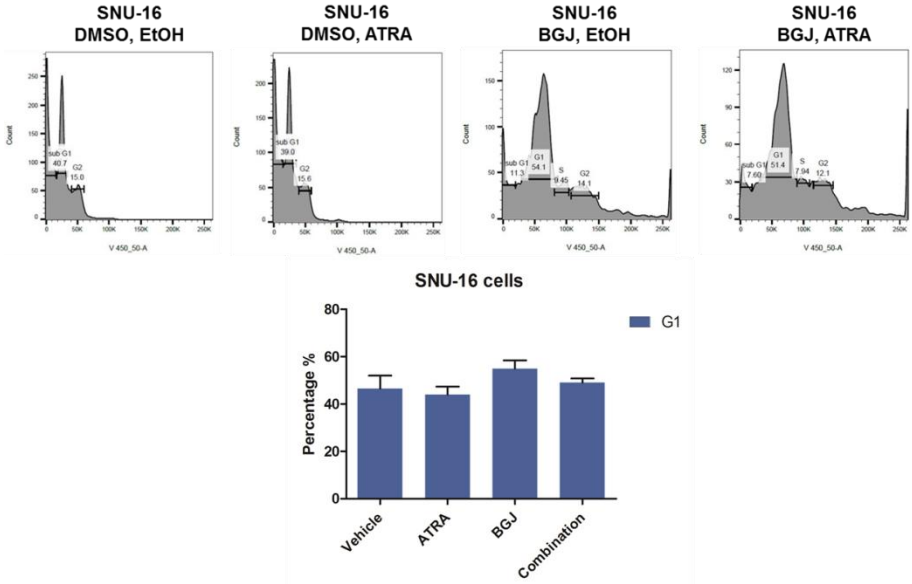

Appendix Figure 8.46. ATRA in SNU-16 potentially induces a decrease in G1 subpopulations.
Gastric SNU-16 cancer cells were plated into 6-well plates and treated with 1µM ATRA and 1.5µM BGJ and corresponding vehicle controls. After 72h cells were fixed in 70% Ethanol, followed by DAPI staining and cell cycle analysis using flow cytometry. Typical cell cycle profiles are shown for one of three individual biological replicates. The histogram shows the values indicating the average proportion of cells in G1 phase with y-axis indicating cell counts and x-axis DAPI staining. The error bars indicate SEM.

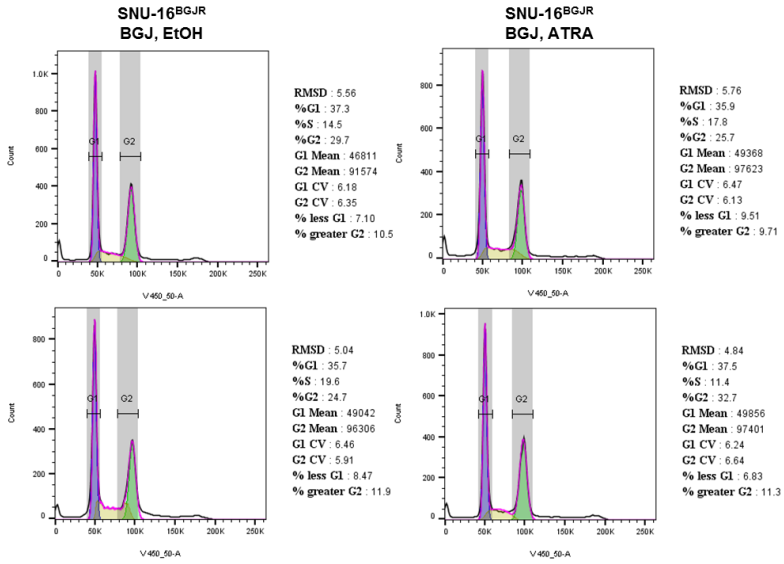

Appendix Figure 8.47. SNU-16^{BGJR} cells treated with ATRA.
Additonal replicates of drug-resistant cells treated eith ATRA or in combination with BGJ, followed by cell cycle analysis with FACS.

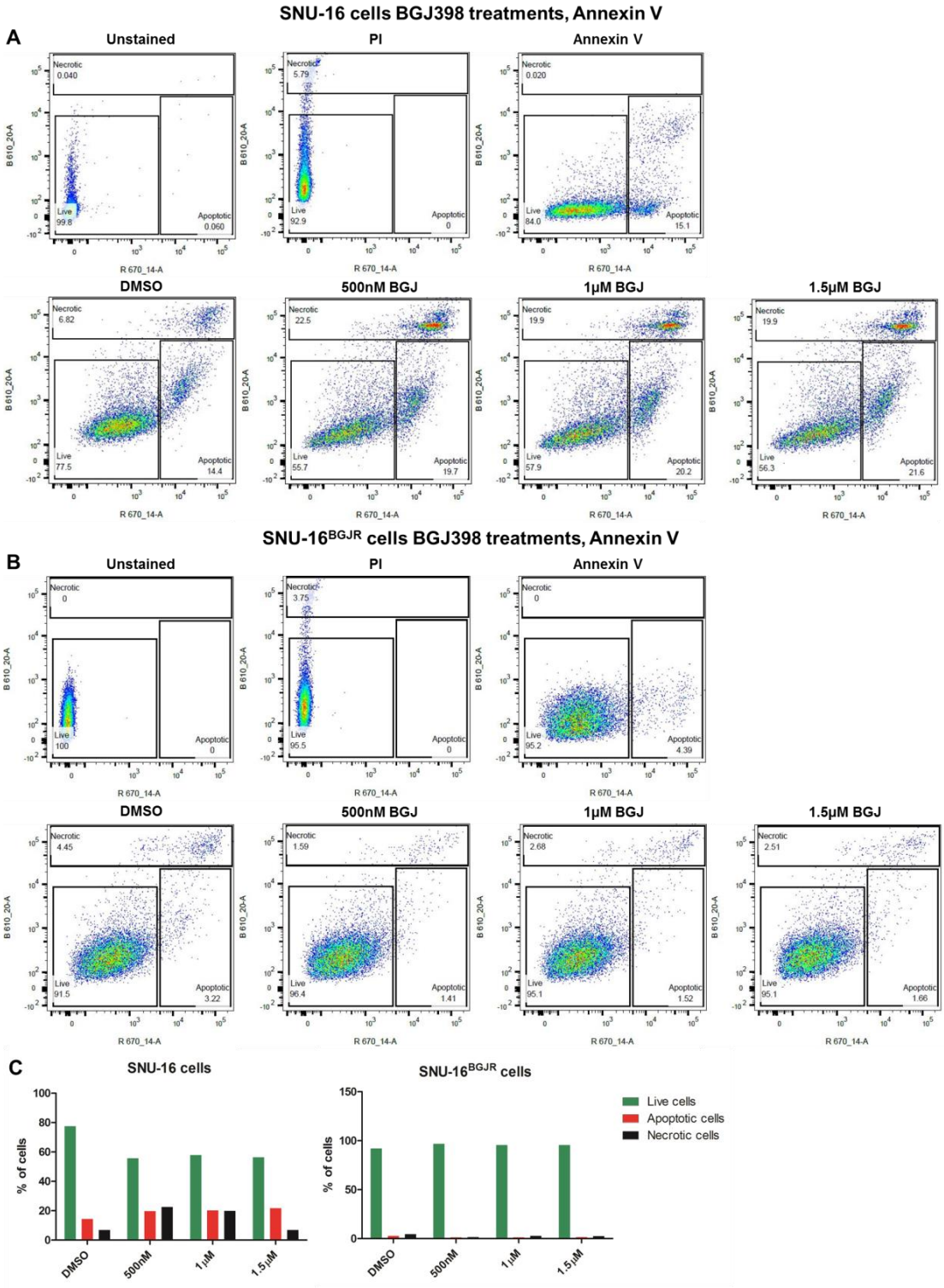

Appendix Figure 8.48. SNU-16 cells undergo apoptosis upon BGJ treatment.
SNU-16 and SNU-18BGJR cells were seeded into 6-well plates and treated with 500nM, 1μM, 1.5μM and DMSO. After 72h cells were stained with Annexin V and PI to measure apoptosis and necrosis in cells using flow cytometry in SNU-16 **(A)** and SNU-16^{BGJR} **(B)** cells with the corresponding analysis **(C)**. The experiment was performed once.

8.3.2 Sucrose and starch pathway

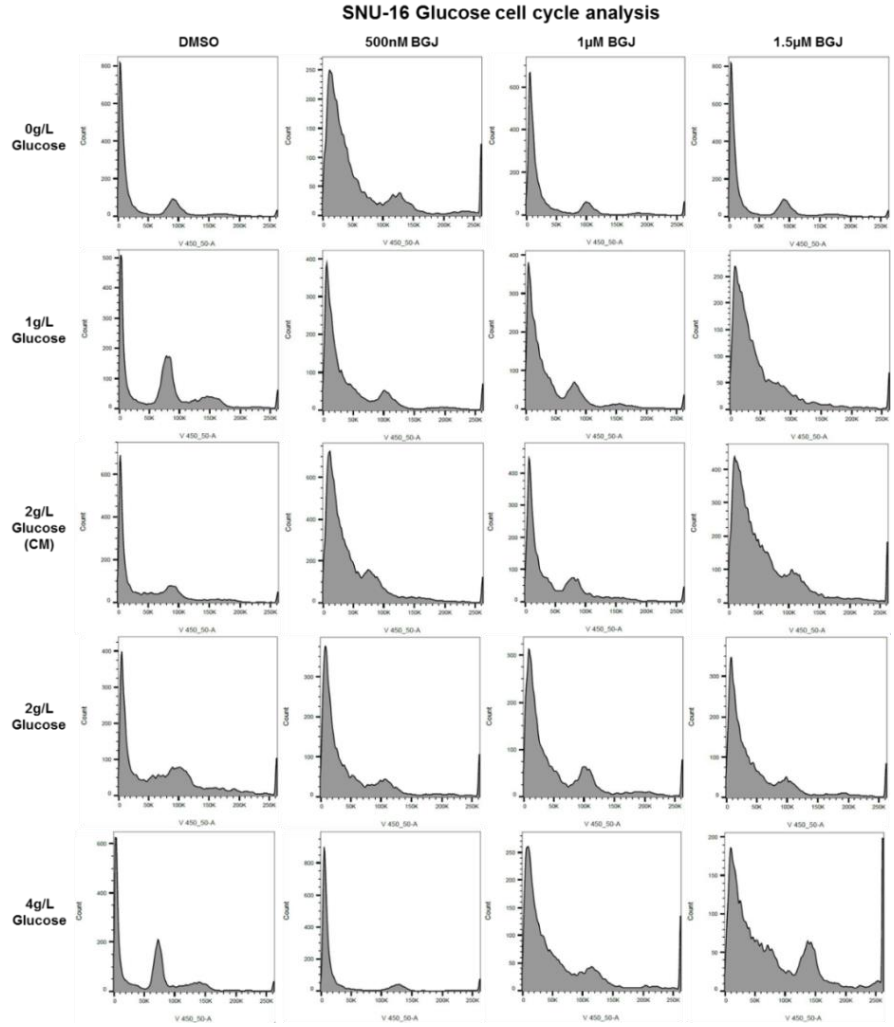

Appendix Figure 8.49. SNU-16 cells are highly heterogeneous in cell populations.
SNU-16 cells were seeded into 6 well-plates and grown in medium with either no glucose, 1, 2 or 4g/L glucose and either 500nM, 1µM and 1.5µM BGJ or vehicle control DMSO. After 72h cells were fixed in 70% Ethanol, followed by PI staining and cell cycle analysis using flow cytometry.

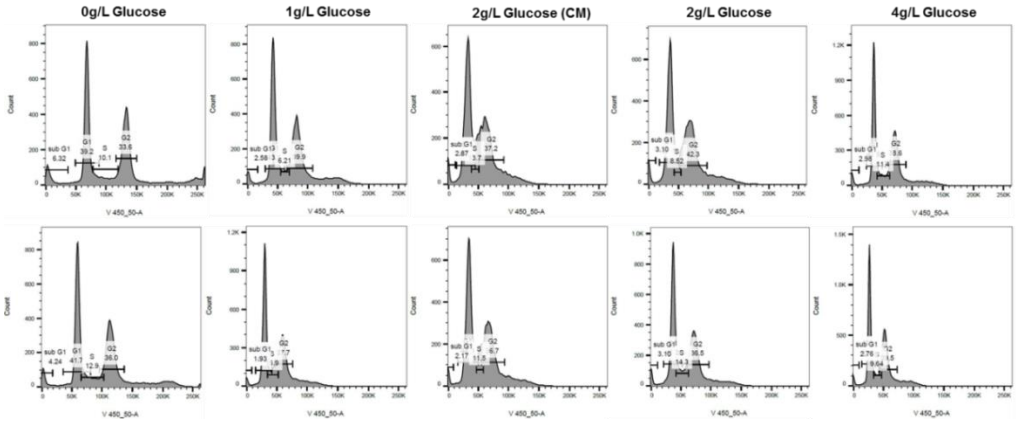

Appendix Figure 8.50. SNU-16^{BGJR} cell cycle analysis treated with different glucose concentrations.
Additional replicates.

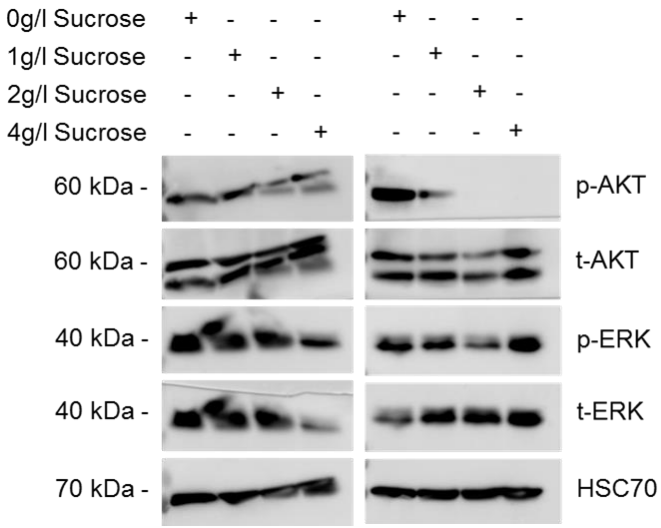

Appendix Figure 8.51. SNU-16 cells have a reduced AKT phosphorylation with higher sucrose concentrations.
SNU-16 cells were exposed to medium containing 0, 1, 2 and 4g/L sucrose and grown for 72h followed by Western blot analysis. Protein expression of p-AKT, t-AKT, p-ERK, t-ERK and housekeeping gene HSC70 was analysed. This blot is representative of two individual experiments.

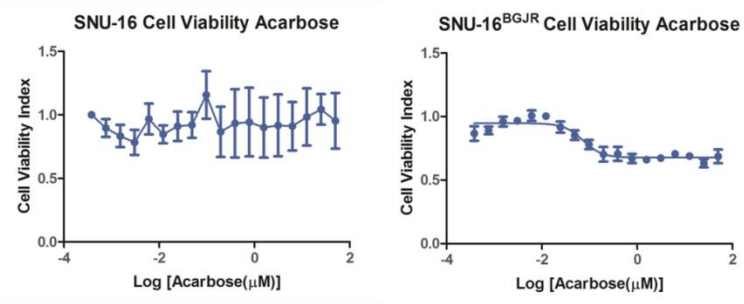

Appendix Figure 8.52. SNU-16 cells and SNU-16^{BGJR} cells treated with Acarbose.
SNU-16 and SNU-16^{BGJR} cells were seeded into 96-well plates and treated with increasing dosages of acarbose ranging from 0.006nM to 50μM and control cells were treated with DMSO and as a background control 1% Staurosporine was added to wells containing cells. After 72h incubation, MTS reagent was added and cell viability was measured colorimetrically after 2h. An average of three biological MTS experiments in technical triplicate is shown with error bars indicating SEM.

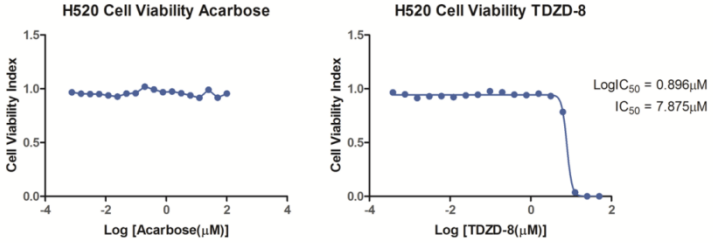

Appendix Figure 8.53. BGJ, Acarbose and TDZD-8 treatment of H520 cells.
H520 cells were seeded into 96-well plates and treated with increasing dosages of acarbose and TDZD-8 ranging from 0.006nM to 50μM and control cells were treated with DMSO and as a background control 1% Staurosporine was added to wells containing cells. After 72h incubation, MTS reagent was added and cell viability was measured colorimetrically after 2h. An average of three biological MTS experiments in technical triplicate is shown with error bars indicating SEM.

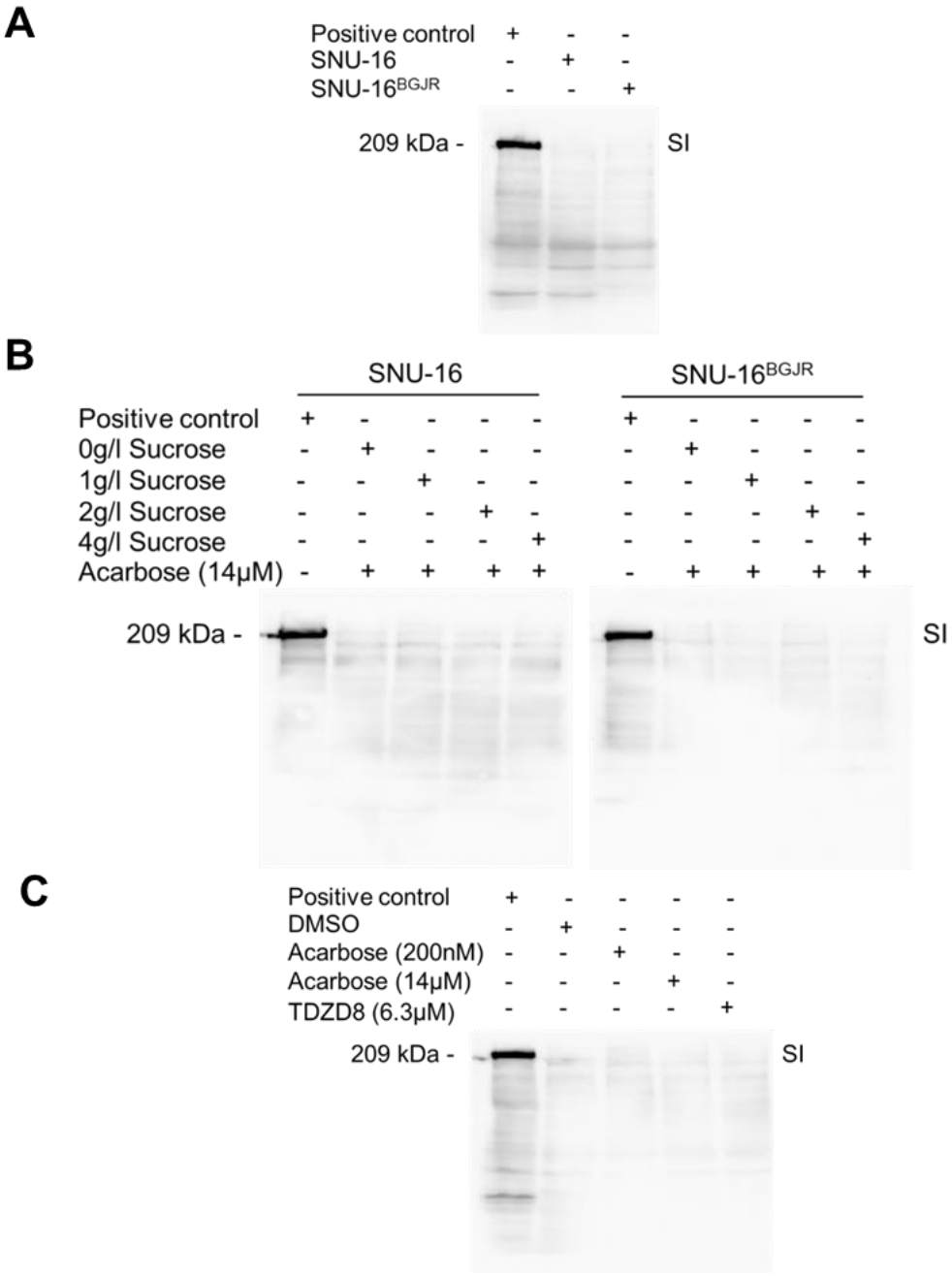

Appendix Figure 8.54. SI expression in SNU-16 and SNU-16^{BGJR} cells grown in medium with altered Sucrose levels and treated with Acarbose.
As a positive control, protein lysates from Caco-2 cells were used, which express high SI levels.

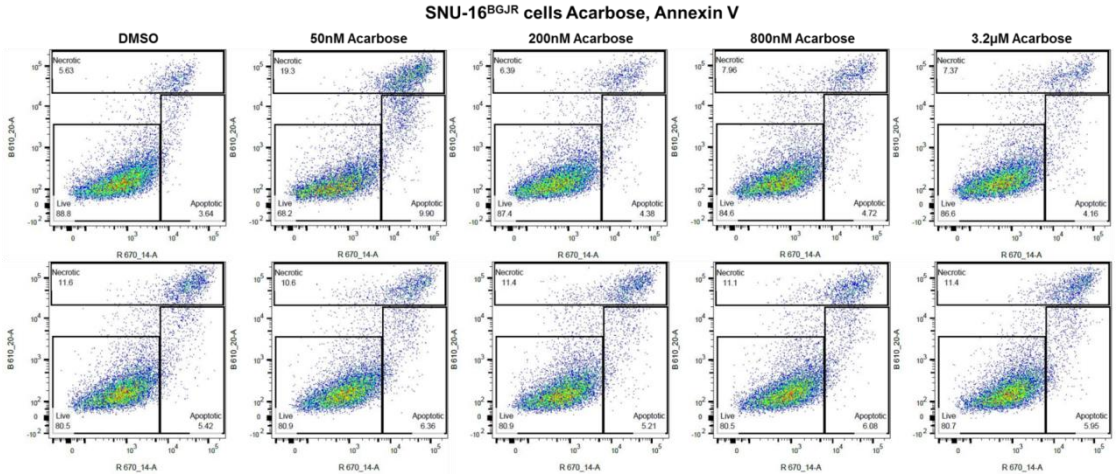

Appendix Figure 8.55. Acarbose treatment of BGJ-resistant SNU-16 cells.
Additional replicates.

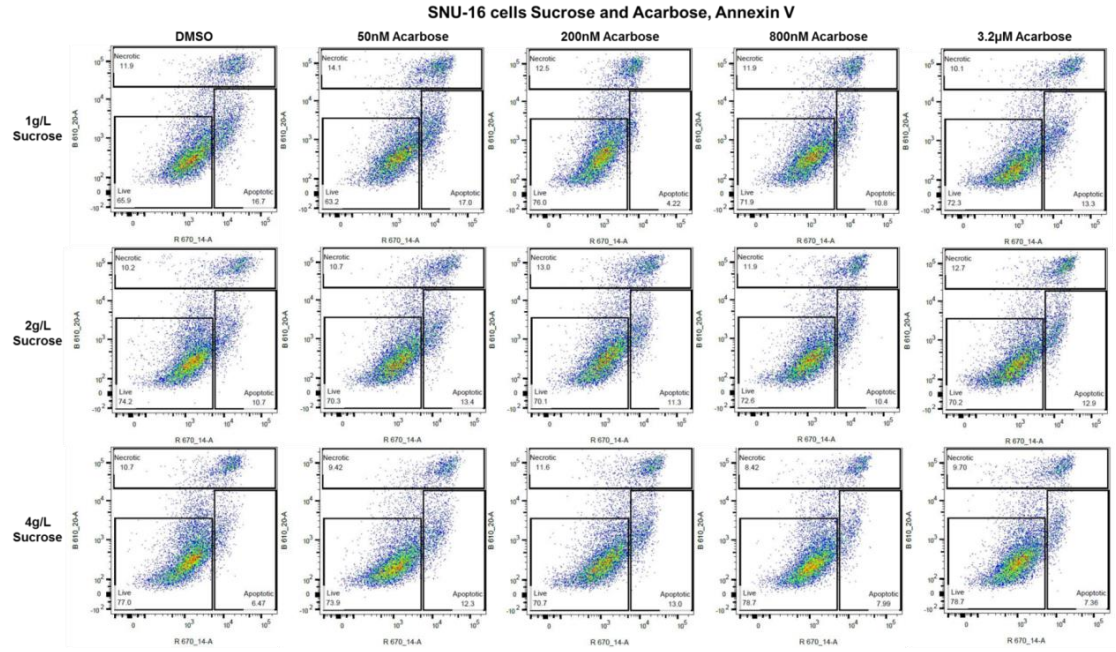

Appendix Figure 8.56. Additonal sucrose concentrations of parental SNU-16 cells treated with sucrose and acarbose.

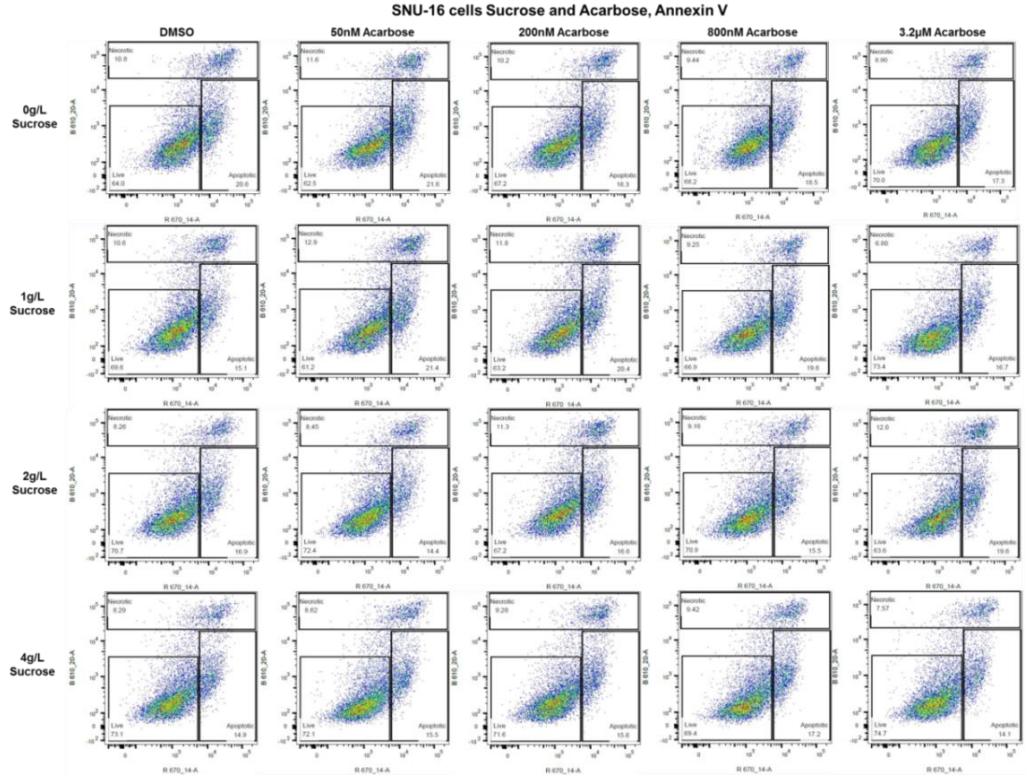

Appendix Figure 8.57. Additonal replicates of parental SNU-16 cells treated with sucrose and acarbose.

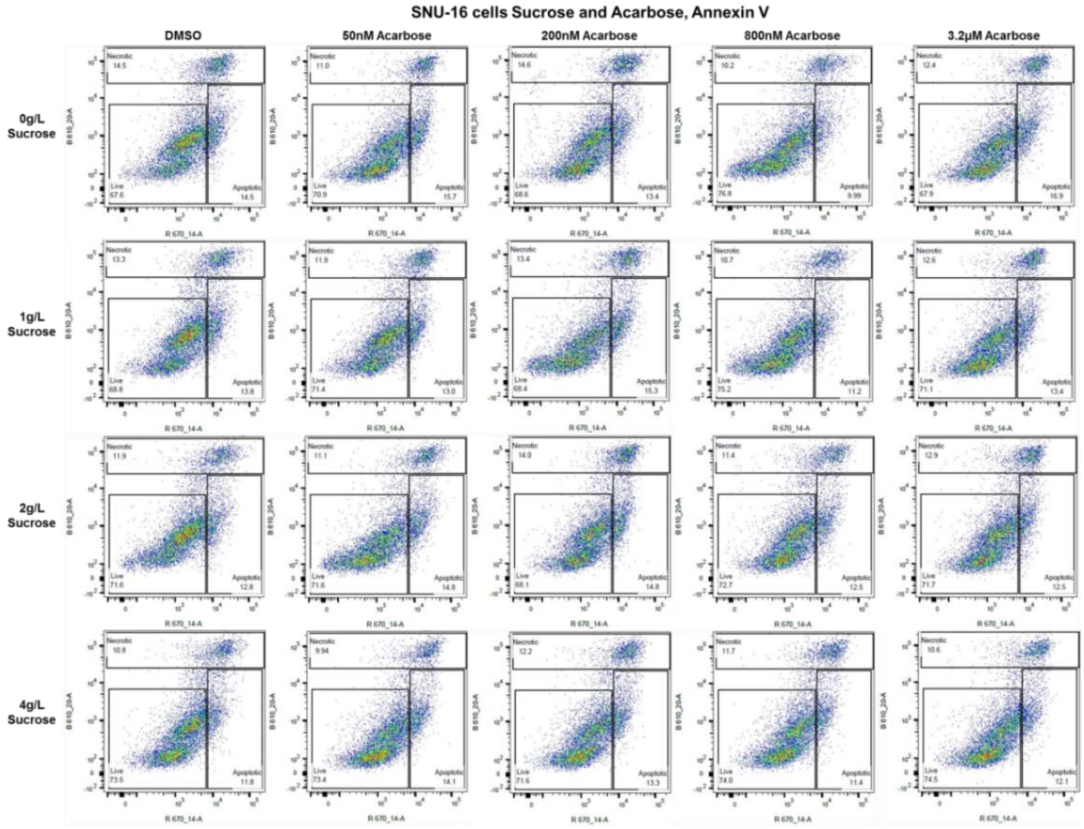

Appendix Figure 8.58. Additonal replicates of parental SNU-16 cells treated with sucrose and acarbose.

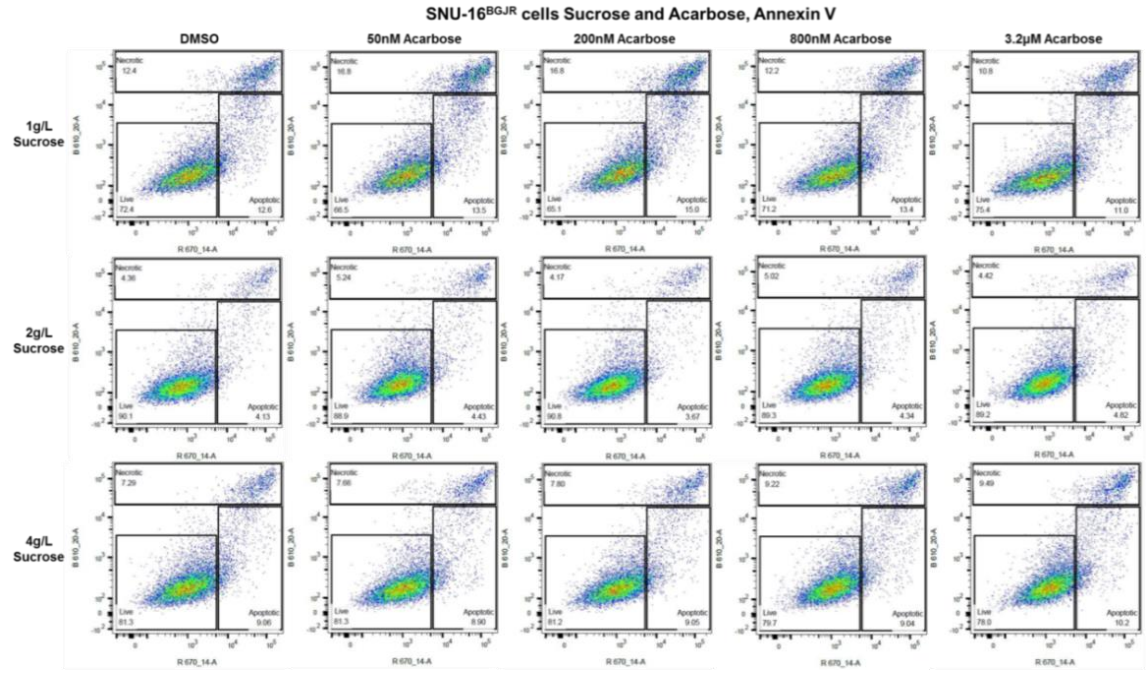

Appendix Figure 8.59. Additional sucrose concentrations for Annexin V staining of SNU-16^{BGJR} cells.

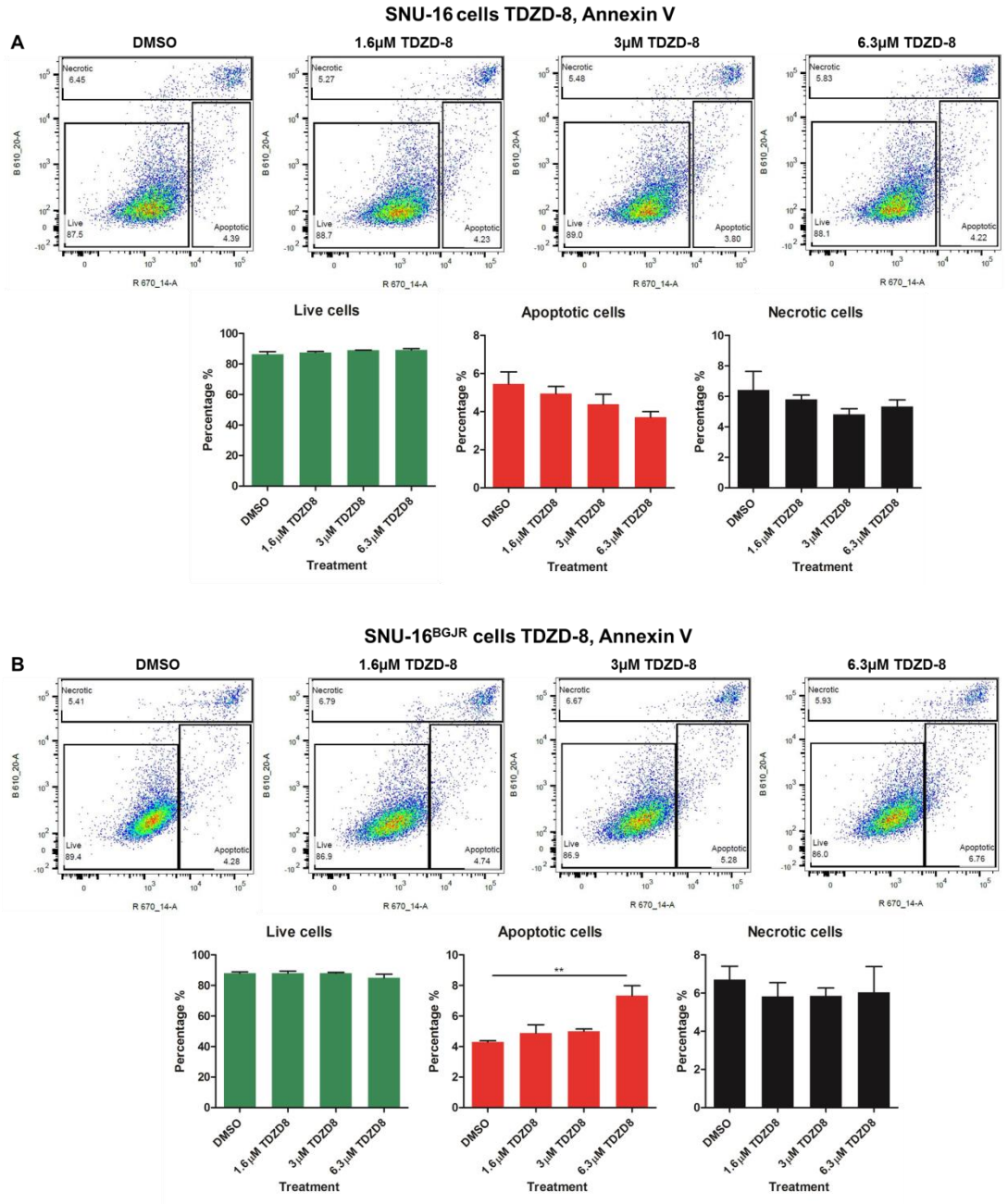

Appendix Figure 8.60. TDZD-8 treatment of parental and BGJ-resistant cells does not affect apoptosis or necrosis.

Parental and drug-resistant SNU-16 cells were plated into 6-well plates and grown in presence of 1.6, 3 and 6.3μM TDZD-8 for 72h followed by fixation in 70% Ethanol. Apoptotic and necrotic cells were identified by staining with Annexin V and PI. Error bars indicate SEM. The experiment was performed in biological triplicate.

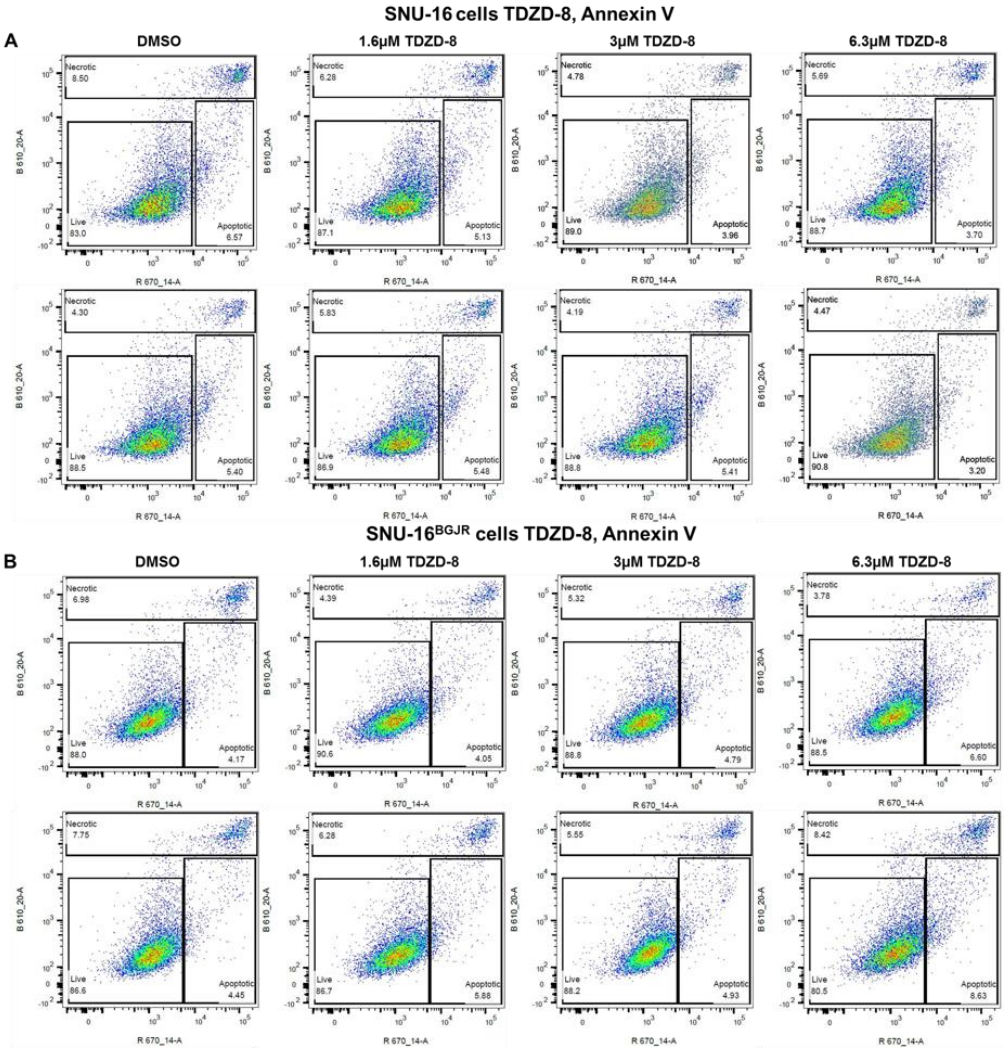

Appendix Figure 8.61. Additonal replicates of gastric cancer cells treated with TDZD-8.

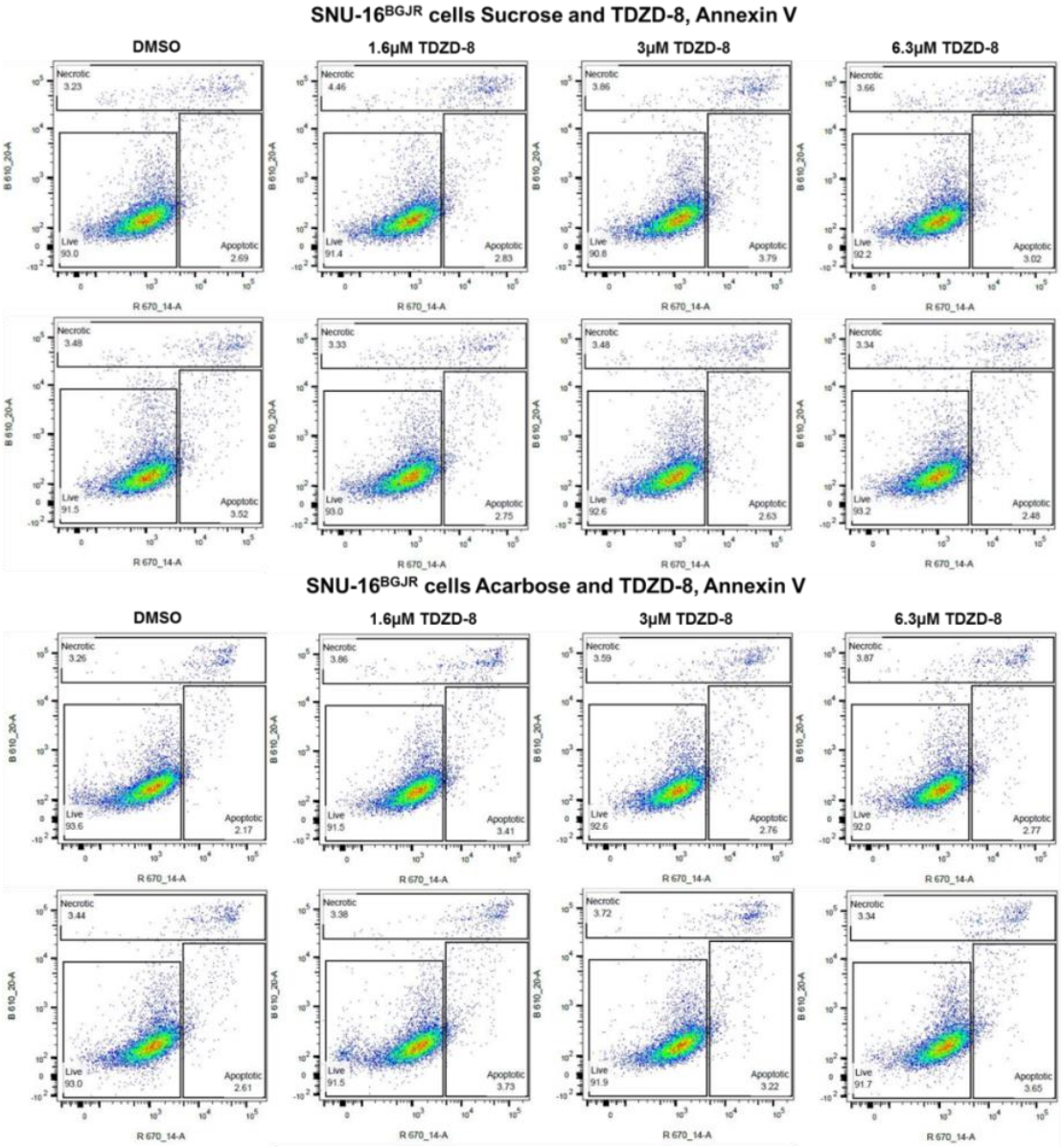

Appendix Figure 8.62. Additional replicates of BGJ-resistant cells treated with Acarbose or Sucrose and TDZD-8.

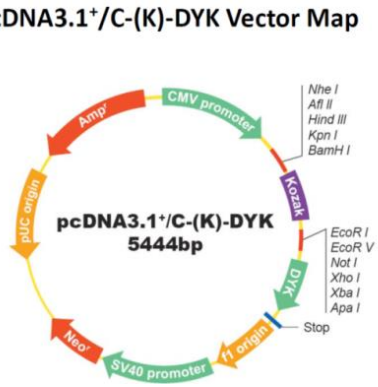

Appendix Figure 8.63. Plasmid sequence map with KOZAK cassette containing PIWIL1.

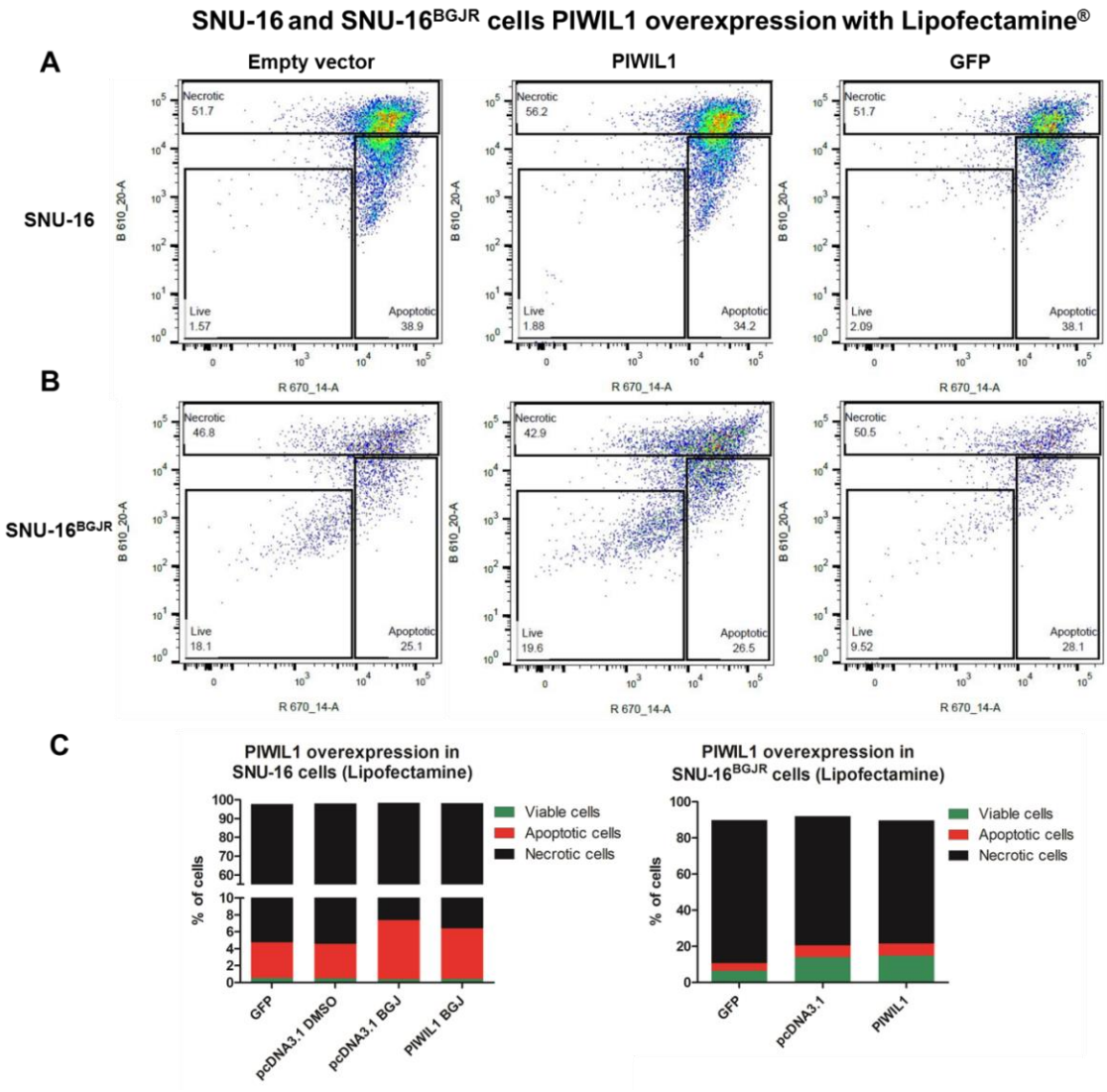

Appendix Figure 8.64. PIWIL1 overexpression in SNU-16 and SNU-16^{BGJR} cells with Lipofectamine®.

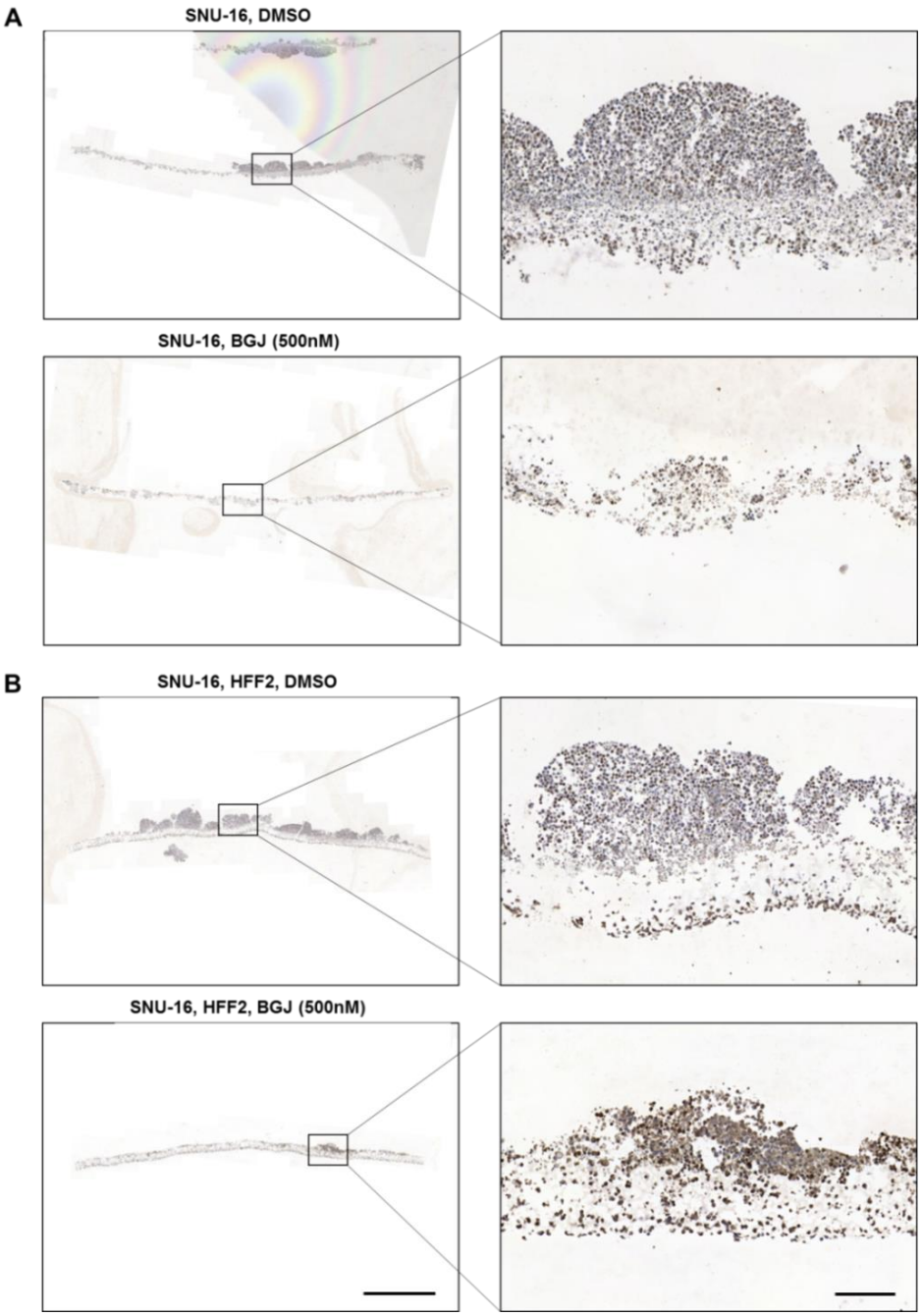

Appendix Figure 8.65. REG1A staining of Alvetex® sections.
Alvetex® scaffold sections of SNU-16 cells and SNU-16 cells co-cultured with HFF2 cells and either treated with vehicle or rendered resistant to BGJ were stained with REG1A antibody and the slides were imaged. Scale bar on the left indicates 1000µm and on the right 100µm.

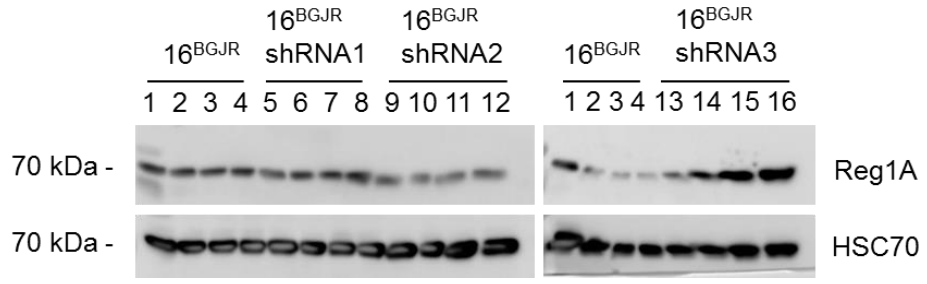

Appendix Figure 8.66. REG1A knockdown of SNU-16^{BGJR} cells.
Cells were seeded into 30mm dishes and transfected with lentiviral particles containing plasmids with REG1A shRNAs and grown in puromycin to select for cells containing the plasmid. Cells were then seeded into 6-well plates protein was extracted to perform Western blot analysis loading 20µM protein in each lane.

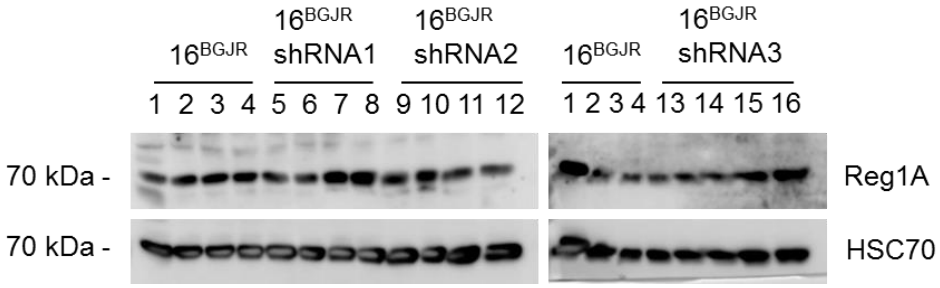

Appendix Figure 8.67. REG1A knockdown in SNU-16^{BGJR} cells.
Cells were seeded into 30mm dishes and transfected with lentiviral particles containing plasmids with REG1A shRNAs and grown in puromycin to select for cells containing the plasmid. Cells were then seeded into 6-well plates protein was extracted to perform Western blot analysis loading 20µM protein in each lane. The blots were tested with a REG1A antibody from Tanja Crnogorac-Jurcevic's group.

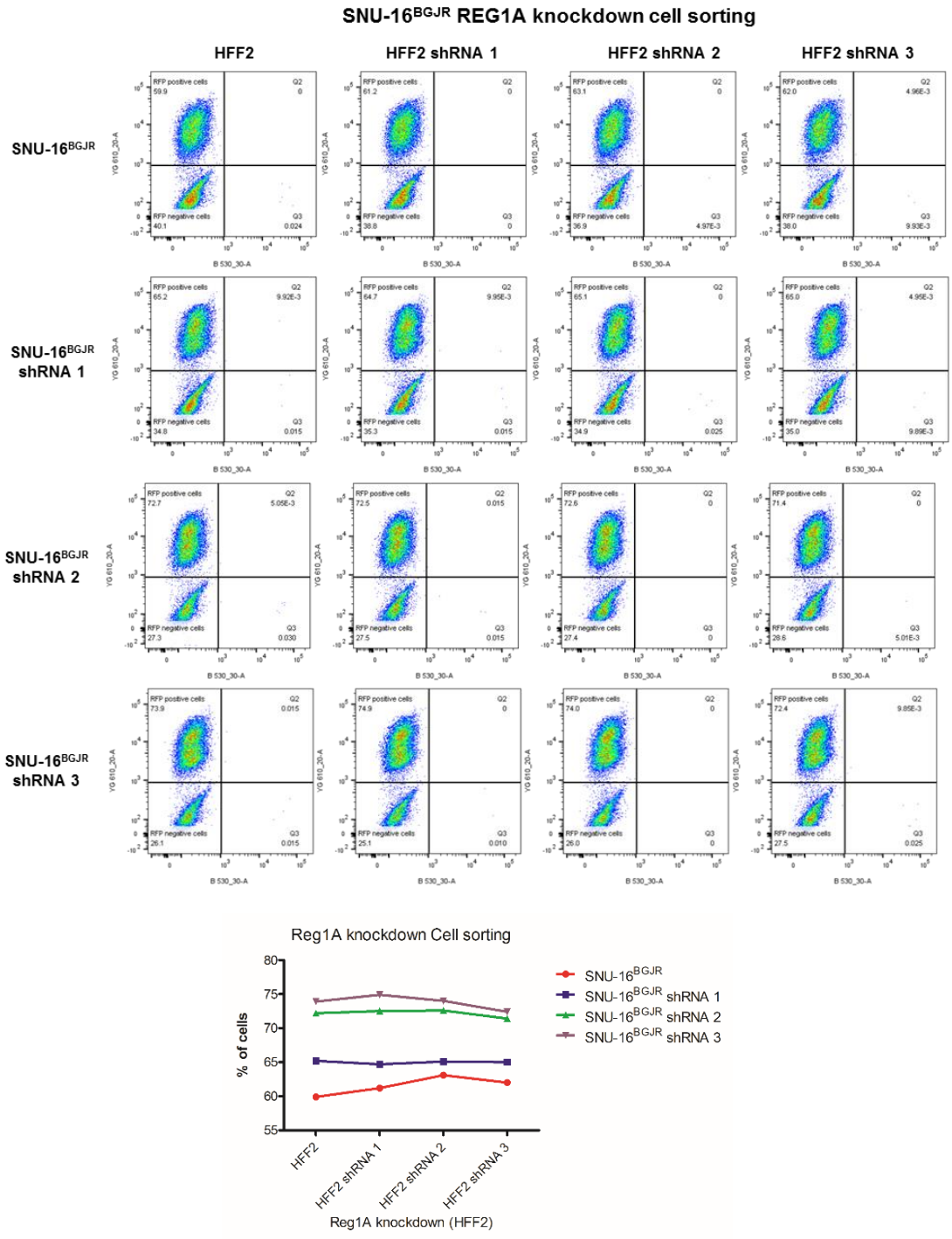

Appendix Figure 8.68. FACS sorting of drug-resistant cells with REG1A knock-down.
Drug-resistant gastric cancer cells and fibroblasts treated with different shRNAs were seeded into Alvetex® scaffolds and grown for one week following cell extraction from scaffolds. Cells were the sorted into RFP and GFP-positive cells and percentages of cells in the samples of untreated and shRNA treated cells were compared.

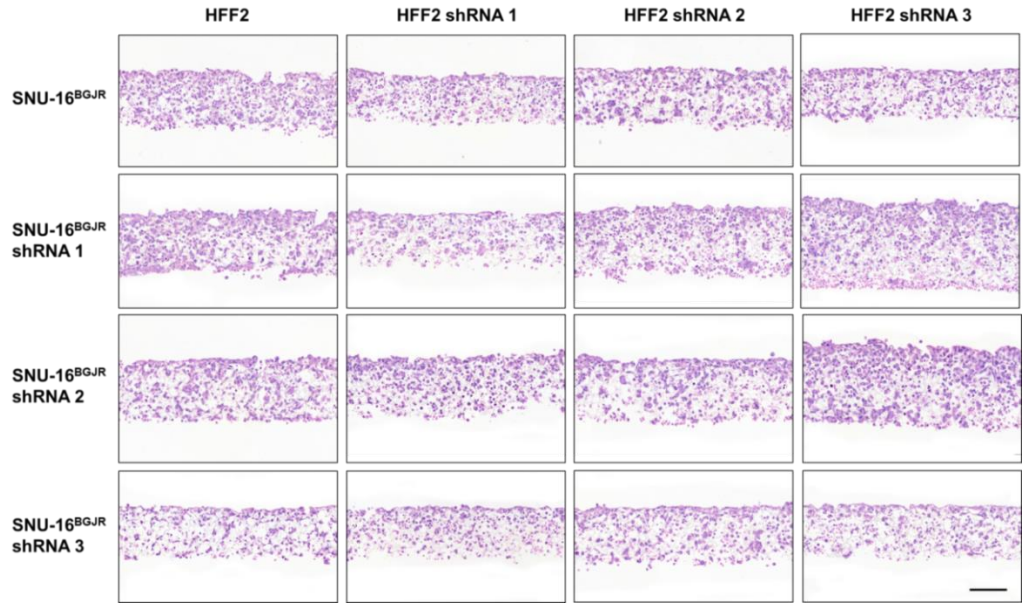

Appendix Figure 8.69. REG1A shRNA knockdown in SNU-16^{BGJR} cells and HFF2.
SNU-16^{BGJR} and HFF2 cells were transfected with three different shRNAs for REG1A and grown in Alvetex® scaffolds, followed by H&E staining prior to scanning of the sections. Scale bar indicates 100μm.

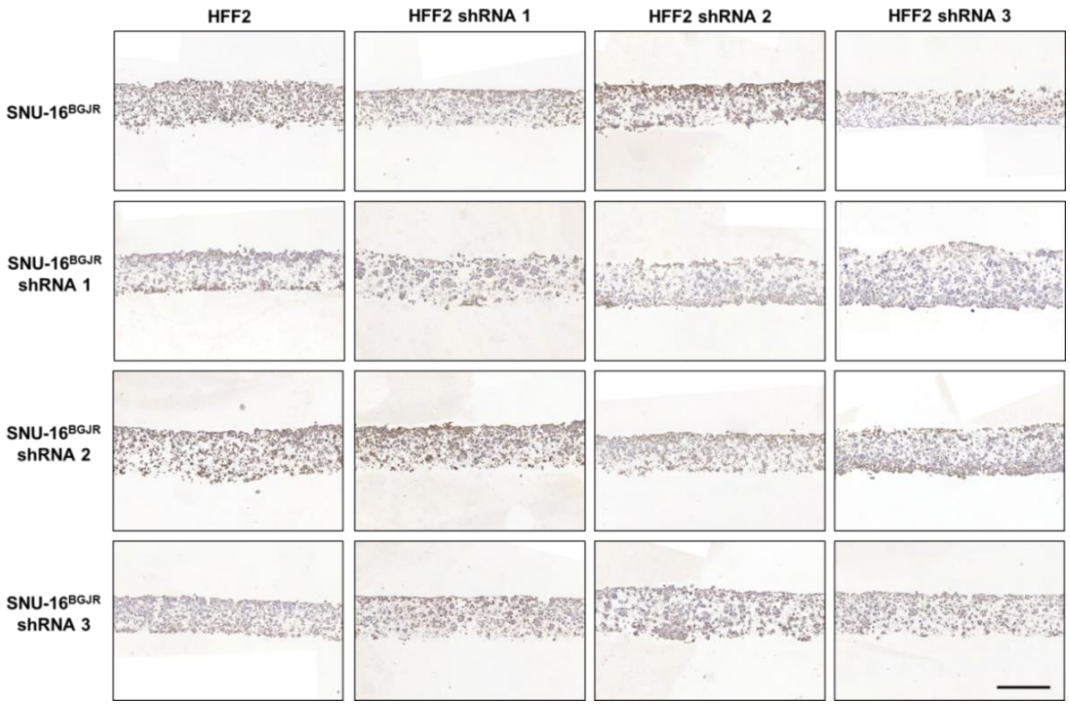

Appendix Figure 8.70. REG1A staining of SNU-16^{BGJR} cells together with fibroblasts REG1A shRNA knockdown.
SNU-16^{BGJR} and HFF2 cells were transfected with three different shRNAs for REG1A and grown in Alvetex® scaffolds, followed by REG1A staining prior to scanning of the sections. Scale bar indicates 100μm.

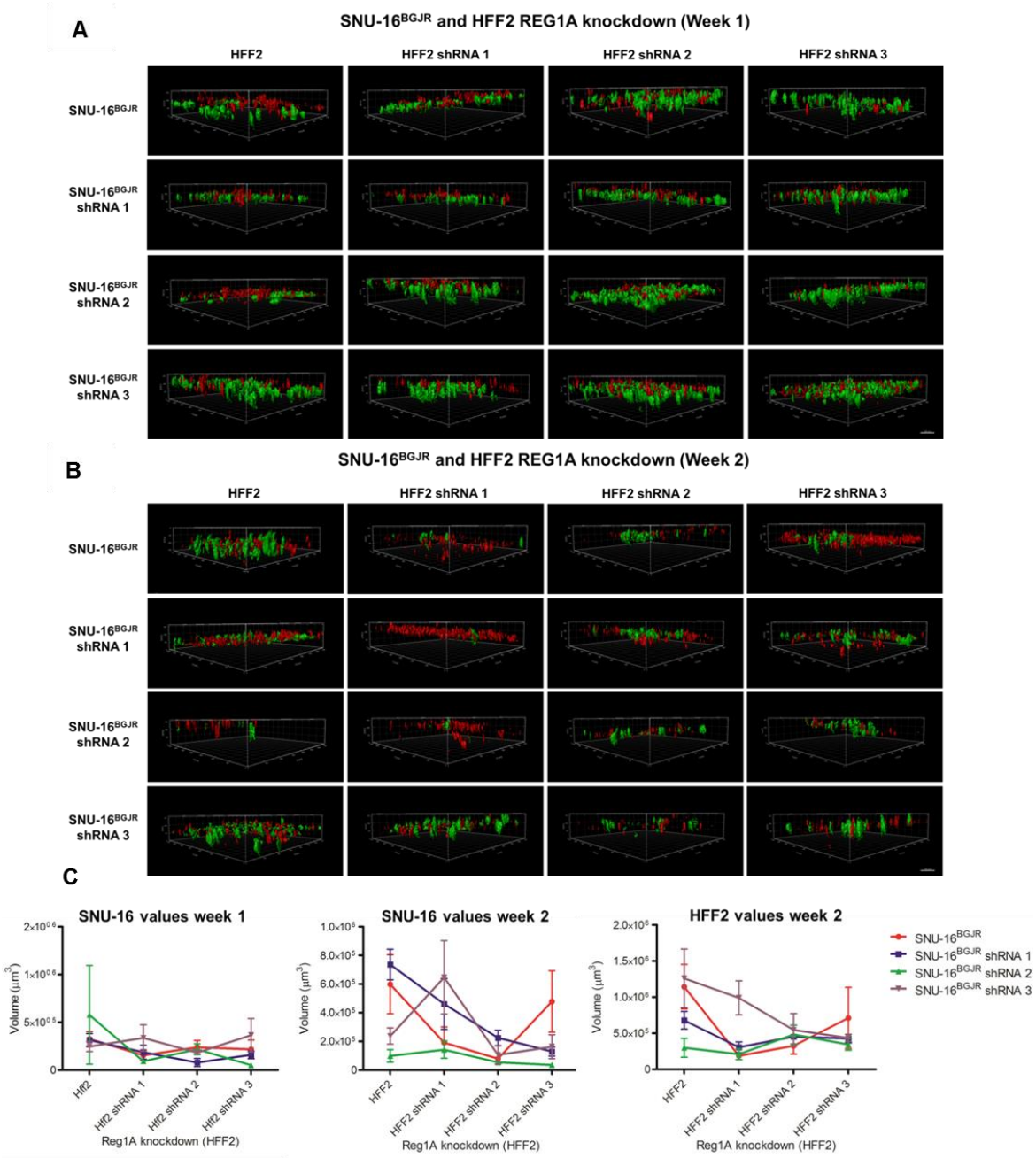

Appendix Figure 8.71. REG1A knockdown in SNU-16^{BGJR} and HFF2 cells in Alvetex®.
SNU-16^{BGJR} and HFF2 cells with three different shRNA knockdowns were seeded into Alvetex® scaffolds 2:1 and grown with microscopic acquisition and Imaris analysis at week 1 **(A)** and week 2 **(B)**. Three microscopic images per scaffold were acquired with 50 Z-stacks per image. Scale bar indicates 100µm. From the Imaris images, cell volumes were plotted and SNU-16 cell volume values were compared from week 1 (**Ci**) to values from week 2 **(Cii).** Additionally cell volumes of HFF2 cells at week 2 were plotted **(Cii).** Error bars indicate SEM. The scale bar indicates 100µm.

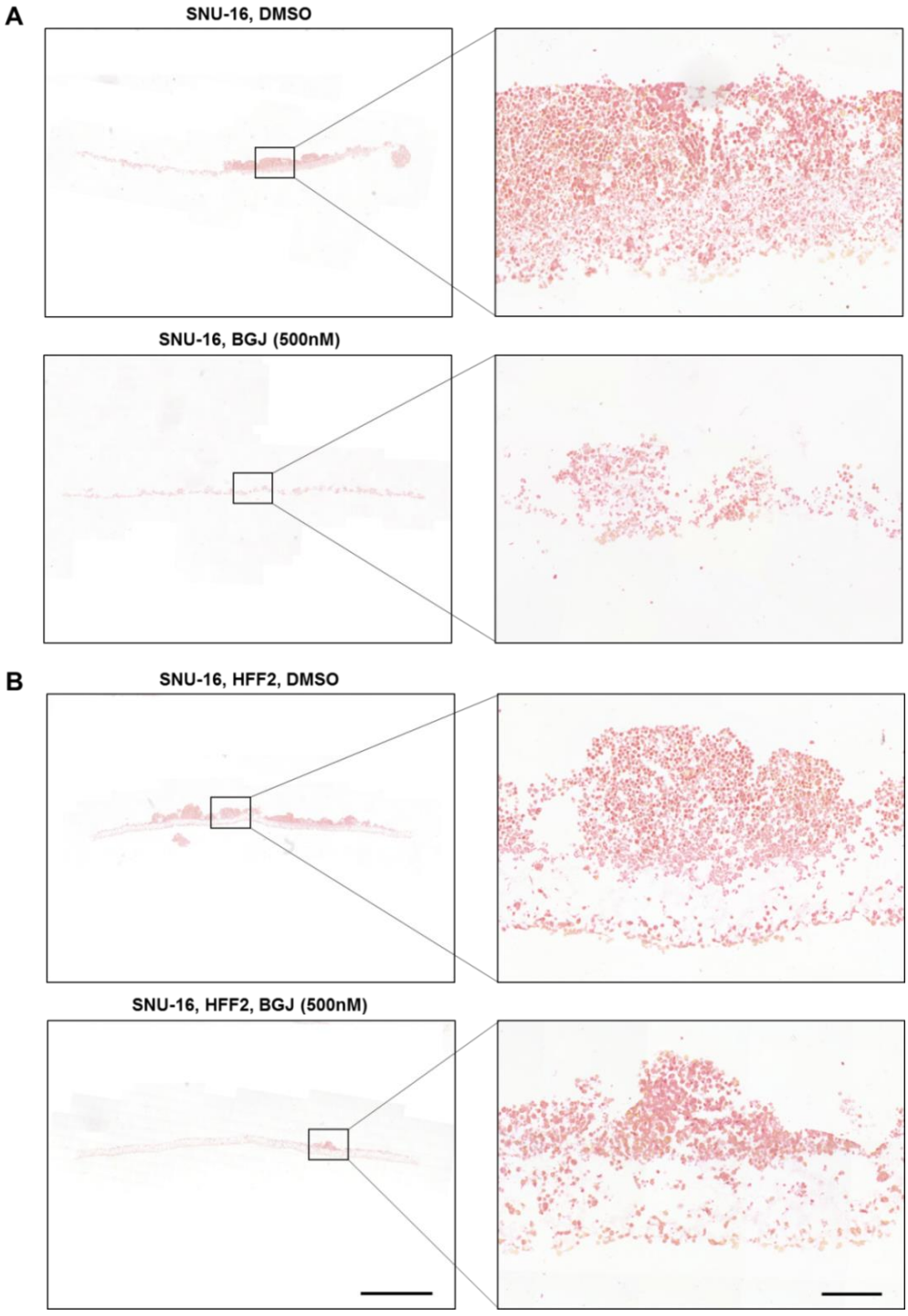

Appendix Figure 8.72. Drug-resistant co-culture cells do not show increased lipid deposits.
SNU-16 cells were grown alone **(A)** or in co-culture with HFF2 cells **(B)** and either treated with vehicle or made resistant to BGJ. Once resistant cell populations were observed with live cell imaging, scaffolds were fixed, paraffin-embedded and sectioned. The sections were then stained with Oil red O to stain lipid deposits. Scale bar on the left indicates 2000µm and on the right 100µm.

8.3.3 Additonal regulated genes in mono- and co-culture cells

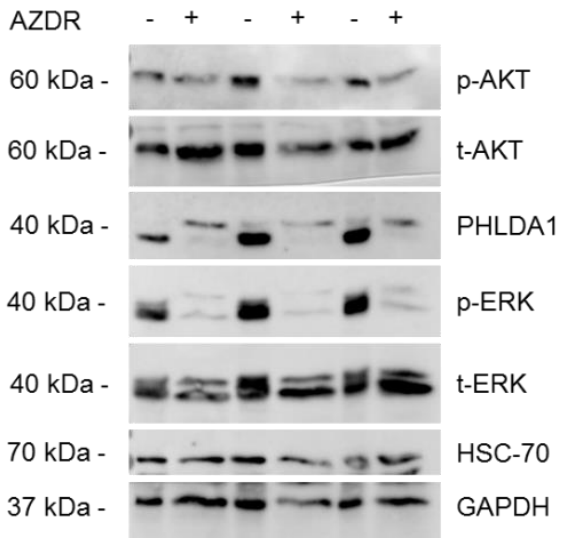

Appendix Figure 8.73. PHLDA1 expression is decreased in AZD-resistant endometrial cancer cells. MFE-296 or MFE-296^{AZDR} cells were seeded into 6-well plates and incubated for 72h. Protein was extracted and Western blot analysis was performed probing for PHLDA1, p-AKT, t-AKT, p-ERK, t-ERK and GAPDH and HSC70 as loading controls. The blots represent three biological replicates.

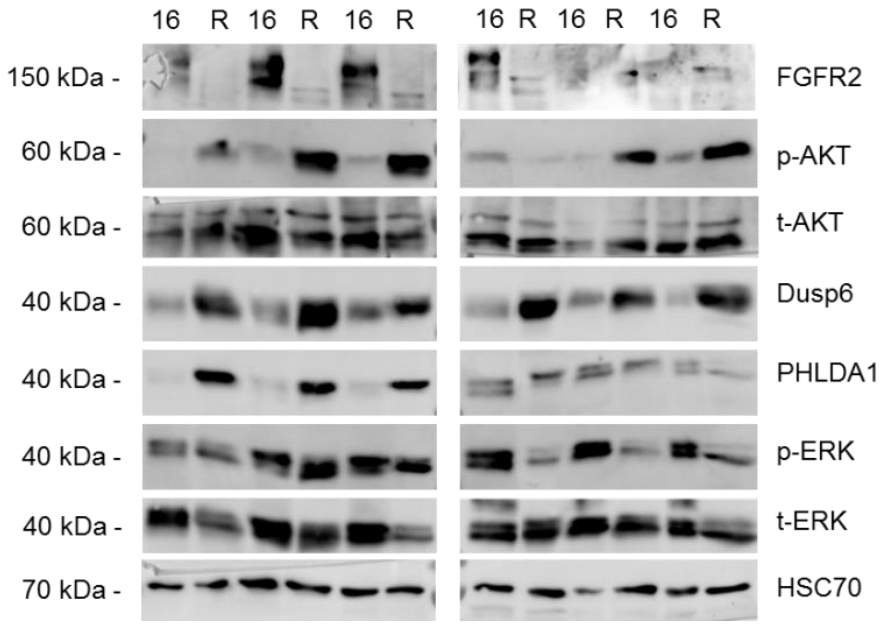

Appendix Figure 8.74. Protein expression levels of parental and drug-resistant SNU-16 cells. Protein of parental and drug-resistant SNU-16 cells was extracted and probed for, FGFR2, p-AKT, t-AKT, DUSP6, PHLDA1, p-ERK, t-ERK and HSC70 as a loading control. The blots represent three individual experiments.

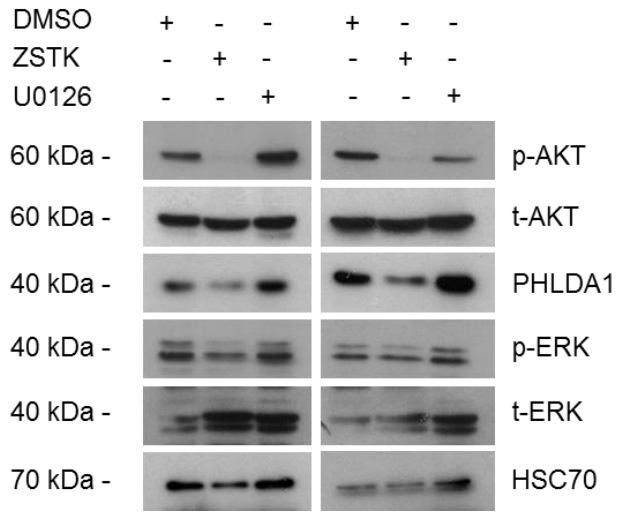

Appendix Figure 8.75. ERK and PI3K inhibitor treatment of MFE-296 cells.
Additional replicates of Western blots of endometrial MFE-296 cells treated with PI3K inhibitor ZSTK, ERK inhibitor U0126 or vehicle for 72h. Protein was extracted and probed for PHLDA1, p-AKT, t-AKT, p-ERK, t-ERK and HSC70 as a loading control.

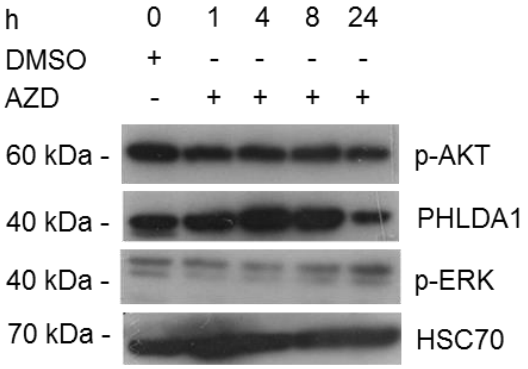

Appendix Figure 8.76. AN3CA 24h AZD.
AN3CA cells were seeded into 6-well plates and treated with vehicle or AZD. Cells were harvested after 1, 4, 8, or 24 hours. Protein was extracted and expression levels were measured for p-AKT, PHLDA1, p-ERK and HSC70 as a loading control.

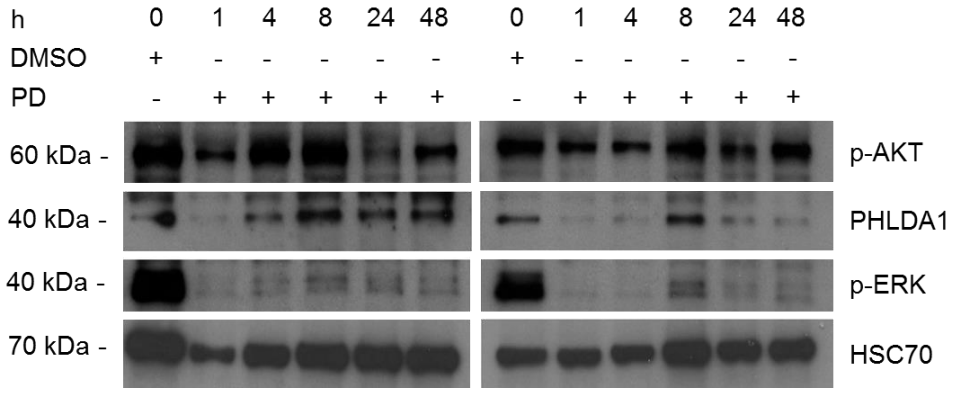

Appendix Figure 8.77. Time course of MFE-296 cells treated with PD.
MFE-296 cells were seeded into 6-well plates and treated with vehicle or PD. Cells were harvested after 1, 4, 8, 24 and 48 hours. Protein was extracted and expression levels were measured for p-AKT, PHLDA1, p-ERK and HSC70 as a loading control.

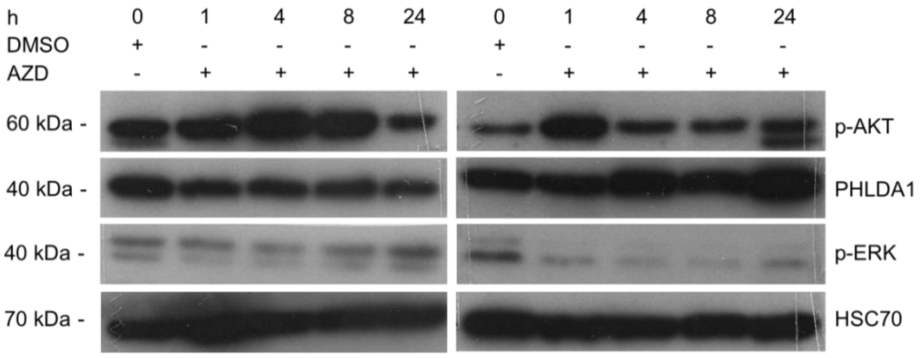

Appendix Figure 8.78. Time course of MFE-296 cells treated with AZD.
MFE-296 cells were seeded into 6-well plates and treated with vehicle or AZD. Cells were harvested after 1, 4, 8 or 24 hours. Protein was extracted and expression levels were measured for p-AKT, PHLDA1, p-ERK and HSC70 as a loading control.

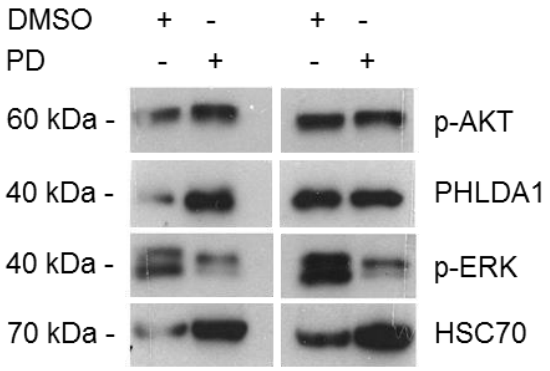

Appendix Figure 8.79. PHLDA1 reappears after one week FGFR inhibition.
Additional replicates of endometrial AN3CA cancer cells treated with FGFR inhibitor PD for one week. Protein was extracted and probed for p-AKT, PHLDA1, p-ERK or HSC70 as a loading control.

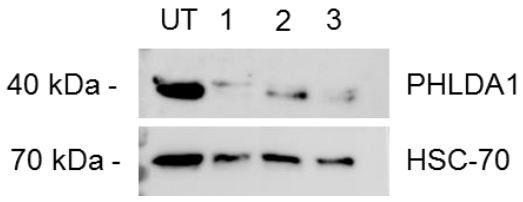

Appendix Figure 8.80. PHLDA1 knockdown in MFE-296 cells
PHLDA1 was knocked down in *FGFR2*-mutated lung cancer cells MFE-296 using three different shRNAs towards PHLDA1. As a control, cells were transduced with a scrambled shRNA (UT). Protein was extracted and expression levels of PHLDA1, and HSC70 as a control, were measured.

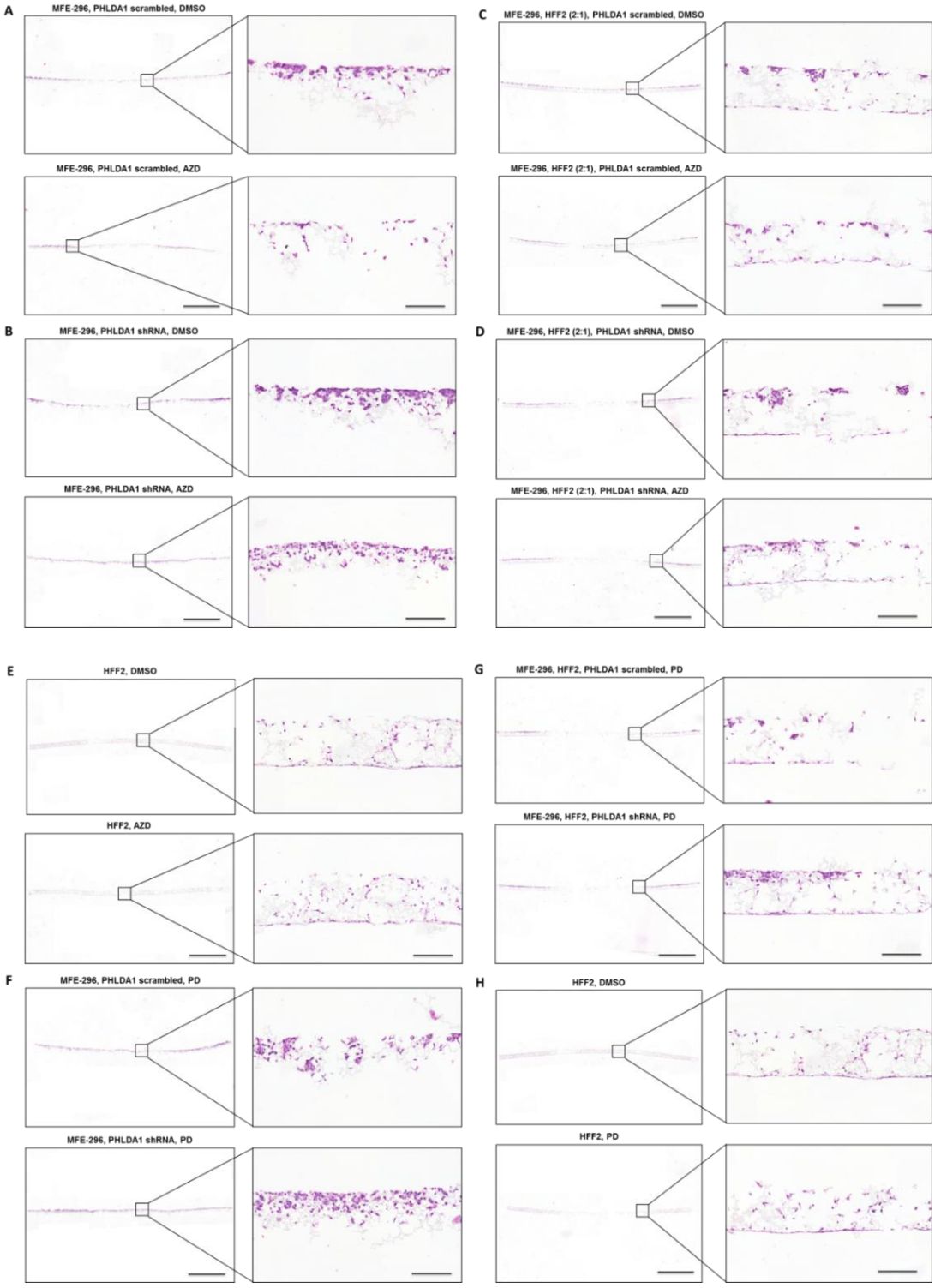

Appendix Figure 8.81. PHLDA1 knockdown in MFE-296 cells confers resistance towards kinase inhibitors.

MFE-296 cells with PHLDA1 scrambled treated with 1μM AZD and vehicle. (**B)** MFE-296 cells with PHLDA1 shRNA knockdown treated with 1μM AZD and vehicle. **(C)** MFE-296 and HFF2 cells with PHLDA1 scrambled treated with 1μM AZD and vehicle. **(D)** MFE-296 and HFF2 cells with PHLDA1 knockdown treated with 1μM AZD and vehicle. **(E)** HFF2 cells treated with vehicle and AZD. **(F)** MFE-296 cells with PHLDA1 scrambled or PHLDA1 knockdown and treated with 1μM PD. **(G)** MFE-296 and HFF2 cells with PHLDA1 scrambled or PHLDA1 knockdown and treated with 1μM PD. **(H)** HFF2 cells treated with vehicle and PD. Scale bar on the whole scaffold image indicates 2000μm and on the magnified image 100μm.